istituto nazionale di fisica nucleare
laboratori nazionali di frascati

2011

ANNUAL REPORT

Scientific Editor
D. Babusci

Technical Editor
D. Bifaretti

Cover artwork
C. Federici

FOREWORD

Laboratori Nazionali di Frascati-Frascati National Laboratories (LNF)
Present and Future

For the scientific activities of the INFN Frascati National Laboratories 2011 has been basically a year of steady continuation of successful programs already on the floor. In fact, as you will read in the various sections of this report and just to cite major activities, Frascati groups have given their much appreciated contributions to the fantastic exploitation of LHC at Cern, to the preparation of the upgraded programs at Jlab in the USA and Fair in Germany and to the data analysis of the CDF experiment at FNAL; on site constructions for the rare kaon experiment NA62 continued steadily allowing this challenging experiment to respect its schedule that aims a beginning of data taking with a technical run at the end of 2012. The exploitation of the in-house e^+e^- collider Dafne was slowed down due to a serious failure that affected the electron gun but important machine optimizations have been nevertheless carried out preparing the ground for high luminosity future operation.

2011 has been very important for the future high-luminosity SuperB Flavor Factory: in fact the project has been approved by the Italian Government as one of the "Flagship Projects" inside the newly approved Italian National Research Plan and at the end of the year the legal entity that will follow the construction of the accelerator has been formed by the two partners, INFN and Tor Vergata University, with a prominent role of the Frascati Laboratory in the management. Organization of the Consortium, named "Nicola Cabibbo Laboratory", is ongoing aiming to an agressive schedule for the completion of the constructions.

With regard to the activities of the SPARC group during 2011, they continued the experiments with the Free Electron Laser (FEL). The FEL operation in the Single Spike mode, investigated for the first time in the world at SPARC this year, has been the most relevant result in 2011; in fact the capability to produce short electron bunches with the original technique named “velocity bunching” combined with the possibility of varying the intensity of the SPARC undulator magnetic field (Tapering), has enabled SPARC to produce radiation pulses with a reduced spectral width compared to the SASE regime. It has been also launched a new facility, named SPARC_LAB (Sources for Plasma Accelerators and Radiation Compton with Lasers and Beams), born from the union of two existing infrastructures at LNF: SPARC and the TW class laser FLAME. With the mission to coordinate and harmonize all the activities making use of the high intensity electrons and photons beams, SPARC_LAB will become operational in 2012 and will be an interdisciplinary laboratory dedicated to the study of new techniques for particles acceleration (electrons, protons, ions) and the development and application of advanced radiation sources (FEL, THz, Compton-Thomson).

The skills of accelerator scientists in Frascati also contributed to the R&D for future large elctron-positron high energy colliders and to the construction of the first Italian facility for hadrotherapy, CNAO (Centro Nazionale di Adroterapia Oncologica); for CNAO Frascati has been a major stakeholder in the design and construction of the synchrotron for Carbon-ion and during 2011 the machine has been successfully commissioned allowing, at the end of the year, to start with the phase involving patients.

The LNF still host a running gravitational wave antenna that exhibits unprecedented sensitivity at its resonance frequency; the possibility of continuing to take data during the upgrade period of the Virgo and Ligo interferometers, albeit in a narrower frequency band, is an important fueature since it would be a pity to miss the detection of a gravitational wave due to the contemporary unavailability of running detectors!

The Frascati laboratories also in 2011 have continued the improvements of its other facilities like, just to mention some, the synchrotron radiation beam lines, whose exploitation is embedded in an European coordination, the Beam Test Facility, a recognized state-of-the-art testing facility with exotic characteristics, the X-lab and the laboratory for testing space borne detectors. Still very active is the R&D work for novel radiation detectors, both for High Energy Physics utilization and for other applications, like medical or energy.

Finally, 2011 has been yet another year that has seen the usual enthusiasm in opening the lab to the general public, schools and school teachers continuing the dissemination process that is very important for our society. In this spirit in December 2011 we have celebrated with a "scientific twinning" between the towns of Frascati and Orsay (France) the 50th year from the birth of the first e^+e^- machine in the world, AdA (Anello di Accumulazione), stemming from the genius of Bruno Touschek.

All this work, only briefly summarized here and discussed at length in the rest of the document, is continuing with some pain since the external conditions are becoming more severe: budget constraints and more importantly limitations in the hiring possibilities are seriously threatening the beauty of the Frascati laboratories, a jewel in the crown of the Italian research.

Umberto Dosselli

Director

ATLAS

A. Annovi, M. Antonelli(Resp.), M.M. Beretta, H. Bilokon,
E. Capitolo(Tech.), A. Castegnaro(Laur.), F. Cerutti, V. Chiarella, M. Curatolo,
R. Di Nardo(Ass. Ric.), M. Dreucci, B. Esposito(Resp.), M. Gatta (Tech.), C. Gatti, P.F. Laurelli,
G. Maccarrone, A. Martini, G. Nicoletti, G. Pileggi (Tech.),
B. Ponzio(Tech.), V. Russo(Tech.), A. Sansoni,
M. Testa (Ass.Ric.), T. Vassilieva (Tech.), E. Vilucchi, G. Volpi.

In collaboration with:
Centro di Calcolo:
M. Pistoni, C. Soprano, D. Spigone

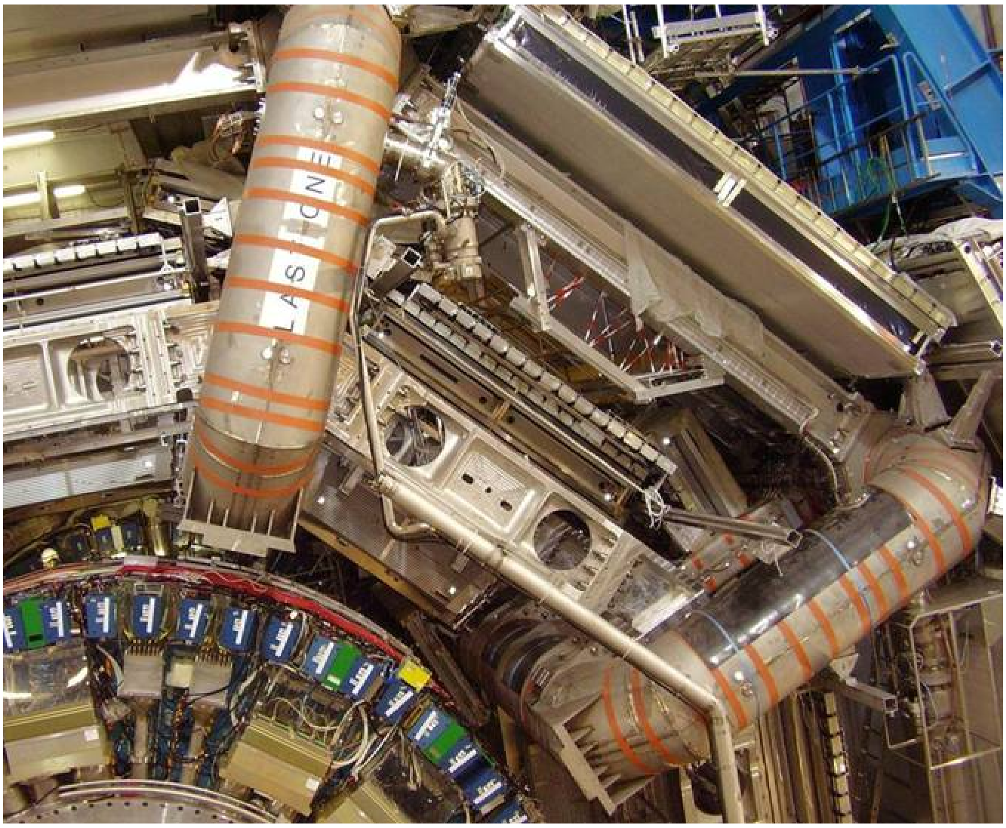

1 Introduction

After more than 20 years of continuous work the ATLAS experiment started data taking at the Large Hadron Collider (CERN) from November 2009. In the 2011 data taking ATLAS collected proton-proton collisions at 7 TeV center of mass energy corresponding to an integrated luminosity of about 5 fb^{-1}.
These data samples allows for the first time to extend the higgs searches sensitivity in unexplored domains.
The Frascati group is involved in the study of the performances and the optimization of the muons, of the $\not\!\!E_T$reconstruction and is focusing the analysis activity in the Higgs boson searches in the WW and ZZ channels. Additional analysis activity has been devoted to Z$\rightarrow \mu\mu$, W$\rightarrow \mu\nu$, $Z' \rightarrow \mu\mu$, the inclusive muon cross section, and the study of the J/Ψ and Z production in Pb-Pb collisions.
The activity of our group is also focused on the operation of the computing resources of the Frascati Proto-Tier2 and the development of the Fast Track (FTK) proposal for the upgrade of the trigger system. In the following sections a brief description of these activities is reported.

2 Measurement of the muon momentum resolution with 2011 collision data

The physics program of the ATLAS experiment at the LHC includes investigations of many processes with final state muons. The ATLAS detector is equipped with a Muon Spectrometer (MS) optimized to provide a momentum measurement with a relative resolution designed to be better than 3% over a wide p_T range and 10% at $p_T = 1$ TeV, where p_T is the muon momentum component in the plane transverse to the beam axis. The momentum in the MS is measured from the deflection of the muon trajectory in the magnetic field generated by a system of air-core toroid coils. The MS track is reconstructed using three layers of precision drift tube (MDT) chambers in the pseudorapidity range $|\eta| < 2.0$ and two layers of MDT chambers behind one layer of cathode strip chambers (CSC) for $2.0 < |\eta| < 2.7$. Large and small MDT and CSC chambers alternate to cover the full angle in the transverse plane, ϕ, following the azimuthal segmentation of the toroid magnet system. Three layers of resistive plate chambers (RPC) in the barrel region ($|\eta| < 1.05$) and three layers of thin gap chambers (TGC) in the end-caps ($1.0 < |\eta| < 2.4$) provide fast response to select events with muons in the final state in real-time, forming the ATLAS level-1 muon trigger. The trigger chambers also measure the muon trajectory in the non-bending (longitudinal) plane of the spectrometer magnets. An additional determination of the muon momentum is provided by the Inner Detector (ID) for $|\eta| < 2.5$. The ID is composed of three detectors providing coordinate measurements for track reconstruction inside a solenoidal magnetic field of 2 T. A silicon pixel detector is mounted close to the interaction point and is surrounded by a silicon strip detector (SCT). The outermost part is a transition radiation straw tube tracker (TRT) whose full coverage is given up to $|\eta| = 1.9$ in pseudorapidity. Muons considered for this analysis are reconstructed as combined muons. The underlying muon identification relies on the principle that first separate tracks are measured in ID and MS before the two tracks are reconstructed as a single trajectory with higher momentum resolution than each of the individual tracks could achieve. First momentum calibration has been obtained with the first data collected in 2010, corresponding to an integrated luminosity of 40 pb^{-1} [1].
Additional data from 2011 allows to bring the spectrometer perfomances close to the design.
The relative resolution on the momentum measurement, $\sigma(p)/p$, is dictated by different effects related to the amount of material that the muon traverses, the accuracy of the magnetic field description, the spatial resolution of the individual track points and the degree of internal alignment of the two subsystems. The MS is designed to provide a uniform momentum resolution as a function of the pseudorapidity. For a given value of η, the resolution can be parametrized in

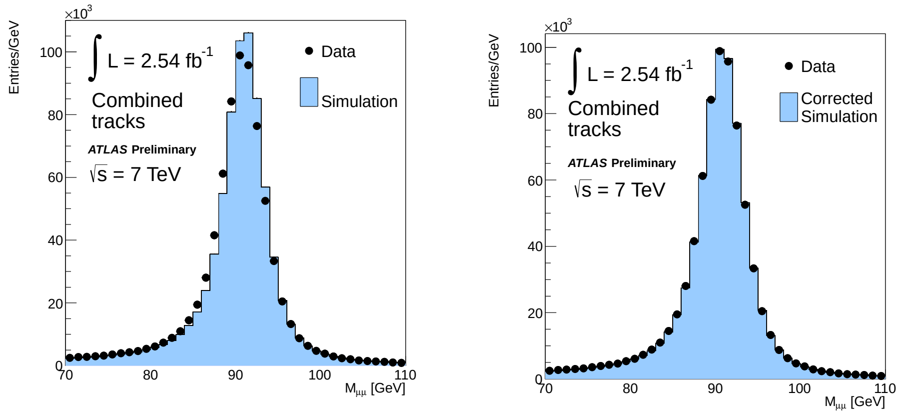

Figure 1: *Z candidates di-Muon invariant mass distribution for data and Monte Carlo (left) and corrected Monte carlo (right).*

the following way as a function of the transverse component p_T:

$$\frac{\sigma(p)}{p} = \frac{p_0^{MS}}{p_T} \oplus p_1^{MS} \oplus p_2^{MS} \times p_T \tag{1}$$

where p_0^{MS}, p_1^{MS} and p_2^{MS} are the energy loss in the calorimeter material, multiple scattering and intrinsic resolution terms, respectively. For the ID a similar parametrization can be found. In this case the curvature measurement depends on the track length of the muon in the active material, which is reduced close to the edge of the TRT fiducial volume. This translates into a uniform response in the central part and a rapidly worsening resolution beyond this region. The following approximate parametrization of the resolution is used:

$$\frac{\sigma(p)}{p} = p_1^{ID} \oplus p_2^{ID} \times p_T \tag{2}$$

for $\eta < 1.9$. For $\eta > 1.9$

$$\frac{\sigma(p)}{p} = p_1^{ID} \oplus p_2^{ID} \times p_T \times \frac{1}{\tan^2(\theta)} \tag{3}$$

where $\eta = -\log(\tan(\theta/2))$ and θ the muon polar angle.
Four regions of pseudorapidity are distinguished for which we expect to have different resolutions in the ID and MS:

- *barrel* – covering $0 < |\eta| < 1.05$,
- *transition region* – covering $1.05 < |\eta| < 1.7$,
- *end-caps* – covering $1.7 < |\eta| < 2.0$ and
- *CSC/no TRT:* – covering $2.0 < |\eta| < 2.5$.

The measurement of the MS and ID momentum resolution are obtained using a Monte Carlo template technique: additional momentum smearing is added to the Monte Carlo momenta to reproduce the data distributions. External information coming from alignment with straight tracks and from the estimation of amount of material in the ID are used to constrain the fit result. The resolution parameters in Eq. 2 and 3 are determined for the four η regions.
The additional momentum smearing measured in this way is added at analysis level. The good data-MC agreement obtained after this correction for the Z invariant mass distribution is shown in Fig. 1. It can be seen a considerble improvement with respect to 2010 data.

3 Reconstruction of the missing transverse energy

The reconstruction and calibration of the missing transverse energy ($\not{E}_T$) developed in ATLAS makes use of the full event reconstruction and of a calibration based on reconstructed physics objects (refined calibration).
Calorimeter cells are associated with a parent reconstructed and identified high-p_{T} object in a chosen order: electrons, photons, hadronically decaying τ-leptons, jets and muons.
Cells belonging to topologically formed clusters (topoclusters) not associated with any such objects are also taken into account in the $\not{E}_T$ calculation.
Once the cells are associated with a category of object as described above and calibrated accordingly, $\not{E}_T$ is calculated as follows:

$$E_{x(y)}^{\mathrm{miss,calo}} = E_{x(y)}^{\mathrm{miss},e} + E_{x(y)}^{\mathrm{miss},\gamma} + E_{x(y)}^{\mathrm{miss},\tau} + E_{x(y)}^{\mathrm{miss,jets}} + E_{x(y)}^{\mathrm{miss,softjets}} + E_{x(y)}^{\mathrm{miss,calo},\mu} + E_{x(y)}^{\mathrm{miss,CellOut}} \quad (4)$$

where each term is calculated from the negative sum of calibrated cell energies inside the corresponding objects:

- $E_{x(y)}^{\mathrm{miss},e}$, $E_{x(y)}^{\mathrm{miss},\gamma}$, $E_{x(y)}^{\mathrm{miss},\tau}$ are reconstructed from cells in electrons, photons and taus, respectively
- $E_{x(y)}^{\mathrm{miss,jets}}$ is reconstructed from cells in jets with $p_{\mathrm{T}} > 20$ GeV
- $E_{x(y)}^{\mathrm{miss,softjets}}$ is reconstructed from cells in jets with 7 GeV $< p_{\mathrm{T}} < 20$ GeV
- $E_{x(y)}^{\mathrm{miss,calo},\mu}$ is the contribution to $\not{E}_T$ originating from the energy lost by muons in the calorimeter
- the $E_{x(y)}^{\mathrm{miss,CellOut}}$ term is calculated from the cells in topoclusters which are not included in the reconstructed objects. For the calculation of this term an energy flow algorithm is used.

The final $E_{x(y)}^{\mathrm{miss}}$ is then calculated adding the $E_{x(y)}^{\mathrm{miss},\mu}$ term.
The $\not{E}_T$ muon term is calculated from the momenta of muon tracks reconstructed with $|\eta| < 2.7$: $E_{x(y)}^{\mathrm{miss},\mu} = -\sum_{\mathrm{selected\ muons}} p_{x(y)}^{\mu}$
In the region $|\eta| < 2.5$, only well reconstructed muons in the muon spectrometer with a matched track in the inner detector are considered.
In order to deal appropriately with the energy deposited by the muon in calorimeters, the muon term is calculated differently for isolated and non-isolated muons.
This algorithm, allowing to calibrate cells separately and independently according to the object to which they belong, has the best performances in terms of linearity and resolution of the $\not{E}_T$ for events containing electrons, photons, taus and muons.
The $\not{E}_T$ reconstruction, especially the low-pt contribution $E_{x(y)}^{\mathrm{miss,CellOut}}$ and $E_{x(y)}^{\mathrm{miss,softjets}}$, is strongly affected by the increasing of pile-up. For several analyses involving $\not{E}_T$ measurements is essential a precise modeling of pile-up in simulation. Moreover the systematic uncertainty due to the pile-up is an issue for several important analyses concerning Higgs searches (see Sec. 5.2).
The systematic uncertainty induced by the pileup can be determined in situ by exploiting the balance between the soft-terms and the total transverse momentum of the hard objects in $Z/\gamma^* \to \mu^+\mu^-$ events. In figure 2 the mean and the resolution of soft-terms as function of the number of vertices is shown. The overall systematic uncertainty on the $\not{E}_T$ including all contribution in Eq. 4 is shown in figure 3 for $W \to e\nu$ events. and is on on average 3%.
Also the determination of the absolute $E_{\mathrm{T}}^{\mathrm{miss}}$ scale is important in a range of analyses involving $E_{\mathrm{T}}^{\mathrm{miss}}$ measurements, ranging from precision measurements to searches for new physics. The

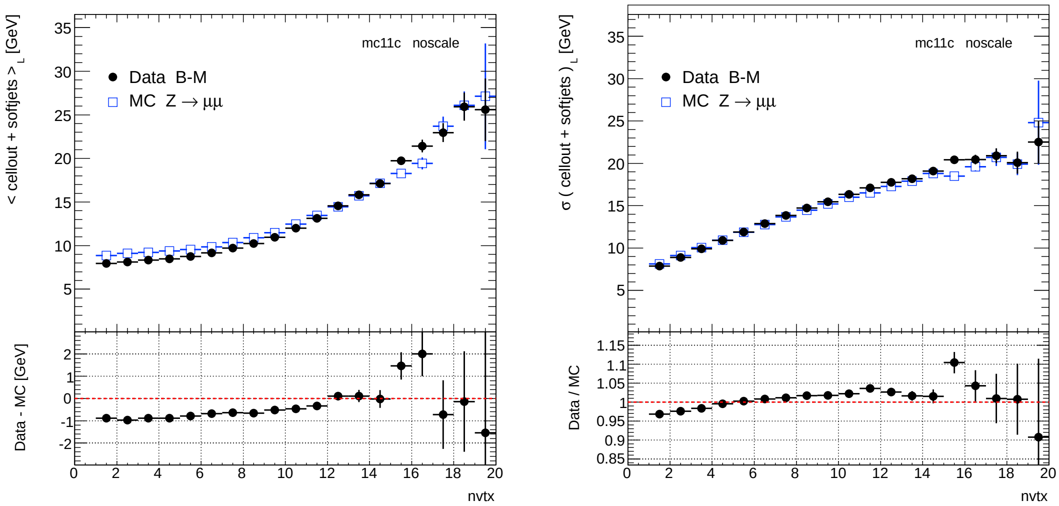

Figure 2: Mean (left) and resolution (right) of the longitudinal component of the soft-terms as a function of the number of vertices in the event for data (black points) and MonteCarlo (blue points).

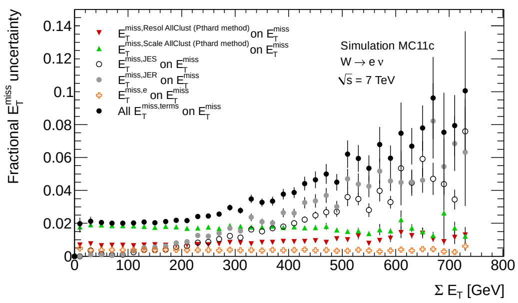

Figure 3: Fractional systematic uncertainty on different $E_{\mathrm{T}}^{\mathrm{miss}}$ terms as a function of respective $\sum E_{\mathrm{T}}{}^{\mathrm{term}}$

overall $\not{E}_T$ scale has been determined in situ through fit to the distribution of transverse mass, mT, of the lepton $\not{E}_T$ system (Figure 4) in $W \to \mu\nu$ events. The uncertainty on the scale is about 2% with 36 pb^{-1}. With the full statistics collcted by ATLAS an uncertainty on the $\not{E}_T$ scale of about 200 MeV can be reached.

4 PileUp suppression

In 2012, when about 30 mean interaction per bunch crossing are expected, pileup suppression will be an issue especially for the $\not{E}_T$ reconstruction. Degradation of $\not{E}_T$ performances are mostly due to the soft-terms contribution, $E_T^{\mathrm{miss,CellOut}}$ and $E_T^{\mathrm{miss,SoftJets}}$ term. Several techniques have been studied, mostly exploiting the tracks pointing at the primary vertex to reduce the dependence on

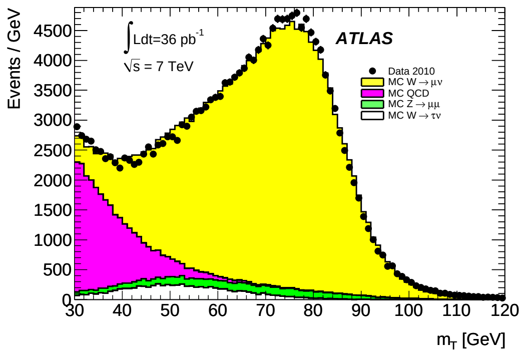

Figure 4: Fit to m_T distribution for $W \to \mu\nu$ events

the $\not{E}_T$ performances the number of reconstructed vertices. The aim of the algorithm should ideally to improve resolution without affecting the linearity of the $\not{E}_T$. A trade-off between the two effects should be found. In Fig. 5(right) the $\not{E}_T$ resolution as a function of the number of vertices is shown for several methods. In Fig. 5(left) the effect on the calibration in $Z/\gamma^* \to \mu^+\mu^-$ events, is also shown. The best compromise is obtained when only jets containing at least one primary track or jets with pt>5 GeV not contenting any primary track are retained.

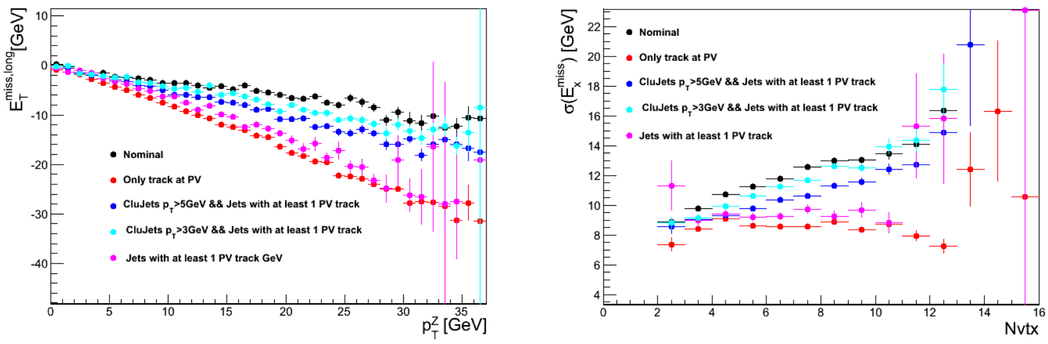

Figure 5:

5 SM Higgs Boson search

One of the main LHC physics goals is the understanding of Standard Model (SM) electroweak symmetry breaking mechanism, that requires the existence of a scalar Higgs boson to provide mass terms to fermions and gauge bosons.
The main SM Higgs boson production process at the LHC is the Higgs boson is the gluon fusion ($gg \rightarrow H$) due to the large gluon density, although vector boson fusion ($qq \rightarrow qqH$) is also important. Moreover, for $m_H \leq$ 135 GeV the associated production of Higgs bosons (WH, ZH) contributes more than 4% to the total production rate.
Direct searches at LEP the set a limit on the Higgs boson mass mH > 114.4 GeV at 95% confidence level (CL). While precision electroweak data constrain the mass of the SM Higgs boson to be less than 152 GeV at 95% CL. The SM Higgs boson is excluded at 95% CL by the Tevatron experiments in the mass range 147-179 GeV and 100-106 GeV, and by the ATLAS experiment in the mass ranges 145-206, 214-224, 340-450 GeV.

5.1 Search for the Higgs boson in the $H \rightarrow ZZ^{(*)} \rightarrow 4l$ decay channel

The $H \rightarrow ZZ^{(*)} \rightarrow l^+l^-l'^+l'^-$ with l, l'=e or μ decay channel provide a good sensitivity for the SM Higgs boson search over a wide mass range. The main advantages for this channel are the purity (S/B∼1) and the possibility to fully reconstruct the invariant mass of the Higgs boson. In particular three finale state (4μ, $4e$, $2e2\mu$) are considered. The latest results on this analysis uses all the data collected in 2011 corresponding to an integrated luminosity of 4.8 fb^{-1}. The data are selected using single-lepton with an high-p_T threshold or di-lepton triggers (p_T =10 GeV threshold for di-muon trigger and E_T=12 GeV for di-electron trigger). The experimental signature for this analysis corresponds to two same-flavour, opposite-sign lepton pairs in an event. The main background for this channel are:

- the $(Z^{(*)}/\gamma^*)(Z^{(*)}/\gamma^*)$ irreducible continuum background
- the $Z + jets$ and $t\bar{t}$ production for m_H, where the additional charged lepton candidates come either from decays of hadrons with b-quark or c-quark content or from misidentification of jets.

All the four leptons have to satisfy p_T>7 GeV with at least two leptons with p_T>20 GeV and be reconstructed in $|\eta|$< 2.47 for electrons and $|\eta|$< 2.7 for muons. The invariant mass of the same-flavour and opposite-sign lepton pair closest to the Z boson mass (m_Z) is denoted by m_{12} and $|m_Z - m_{12}| < 15$ GeV is required. The invariant mass of the remaining same-flavour and opposite-sign lepton pair, m_{34} , is required to be $m_{34} > 15 - 60$ GeV depending on the reconstructed four lepton invariant mass. Isolation criteria are applied to the four leptons to reduce the $Z + jets$ and $t\bar{t}$ contamination. Additional cut on the transverse impact parameter significance of the leptons are required. The signal reconstruction and selection efficiencies for m_H= 130 GeV and m_H= 360 GeV are summarized in table 1 Data driven methods have been

	4μ channel	$4e$ channel	$2e2\mu$ channel
m_H=130	27%	14%	18%
m_H=360	60%	45%	52%

Table 1: Signal reconstruction and selection combined efficiencies for m_H= 130 GeV and m_H= 360 GeV.

used to extract the normalization of the background MC estimation for $Z + jets$ and $t\bar{t}$ processes

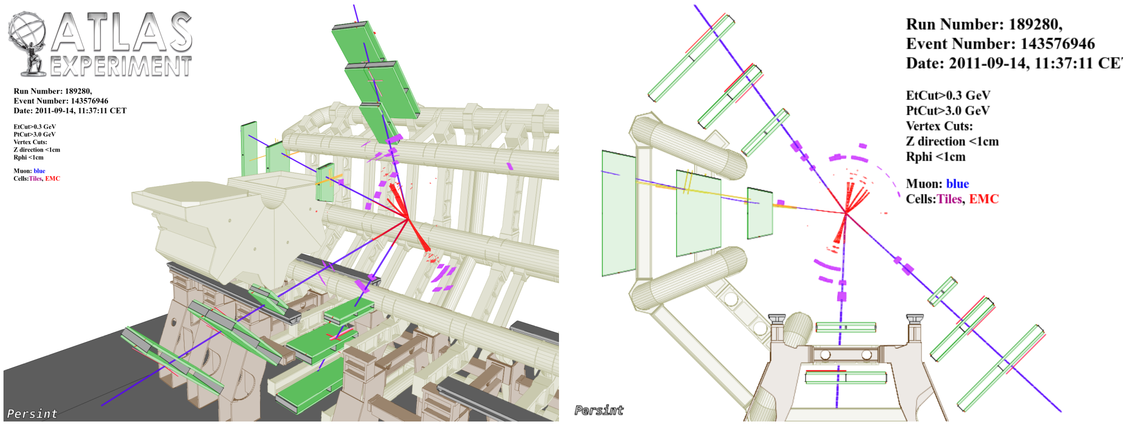

Figure 6: Event display of a 4μ candidate event with m_{4l}=124.6 GeV. The masses of the lepton pairs are 89.7 GeV and 24.6 GeV.

while for the ZZ^* background the MC simulation has been normalized to the theoretical cross section. The main systematic uncertainties for this channel are:

- the Higgs boson production cross section ($\sim$ 15%). This is due to the parton distribution function (PDF) uncertainty , α_s uncertainty and due to the choice of QCD scale
- electron reconstruction efficiencies ($\sim$ 2-8 %)
- ZZ^* background theoretical estimation ($\sim$ 15%)
- $Z + jets$ background normalization ($\sim$ 45%) that takes into account for the statistical

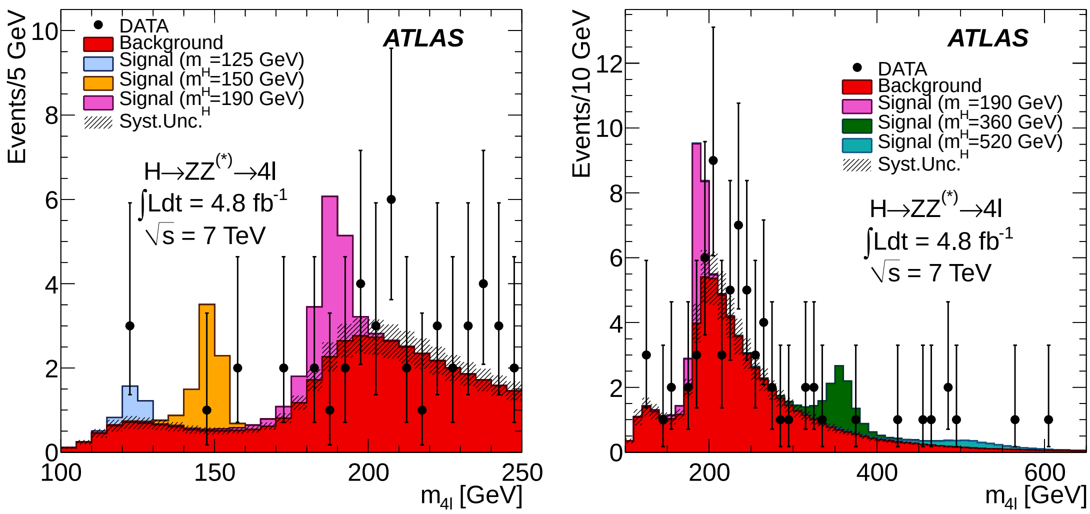

Figure 7: m_{4l} distribution of the selected candidates compared to background expectation for 100 GeV $< m_{4l} <$ 250 GeV (left) and 100 GeV $< m_{4l} <$ 600 GeV (right). Signal expectation for various m$_{\mathrm{H}}$hypotheses is also shown.

uncertainty in the yield and the composition of the control sample and the uncertainty on the MC-based extrapolation to the signal region.

At the end of the cut flow, 71 candidate events (24 4μ, 30 $2e2\mu$ and 17 $4e$) are selected by the analysis. The background expectation is 62 ± 9 events (18.6 ± 2.8 4μ, 29.7 ± 4.5 $2e2\mu$, 13.4 ± 2.0 4e). An event display of a 4μ candidate event with m_{4l} = 124.6 GeV and with the masses of the lepton pairs m_{12} and m_{34} is shown in figure 6. Figure 7 shows the expected m_{4l} distribution for the total background and different signal hypotheses compared to data. Figure 8 shows the observed and expected 95% CL cross section upper limits as a function of $\mathrm{m_H}$. The mass ranges 134-156 GeV, 182-233 GeV, 256-265 GeV and 268-415 GeV are excluded at the 95% confidence level. Deviations from the background-only hypothesis are observed for Higgs boson masses of 125 GeV, 244 GeV and 500 GeV with a local significances of 2.1, 2.2 and 2.1 standard deviations. The SM Higgs

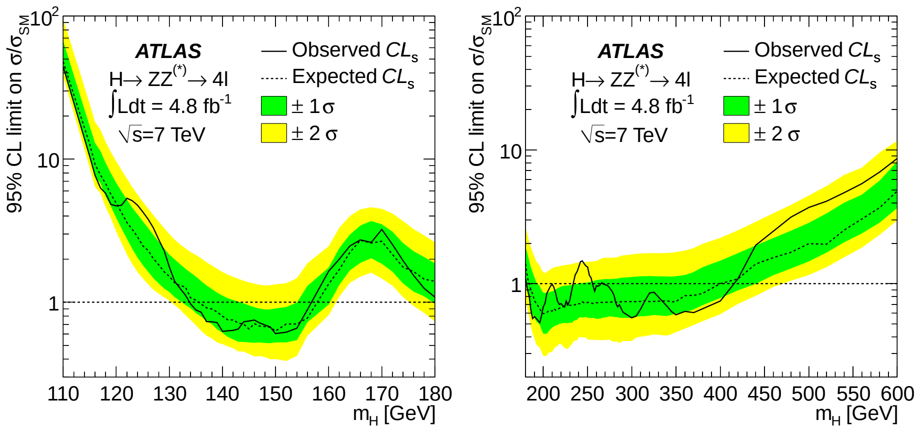

Figure 8: The expected (dashed) and observed (full line) 95% CL upper limits on the Standard Model Higgs boson production cross section as a function of $\mathrm{m_H}$, divided by the expected SM Higgs boson cross section. The dark (green) and light (yellow) bands indicate the expected limits with $\pm 1\ \sigma$ and $\pm 2\ \sigma$fluctuations.

5.2 Search for the Higgs boson in the $H \to WW^{(*)} \to l\nu l\nu$ decay channel

For a SM Higgs boson with a mass greater than 135 GeV, the $H \to WW^{(*)}$ is the dominant decay mode and in the region around $\mathrm{m_H}$= 160 GeV the purely leptonic mode $H \to WW^{(*)} \to l\nu l\nu$ is the most sensitive channel. The experimental signature for this channel consists of two opposite sign, isolated and with high transverse momentum leptons (e or μ) and large missing transverse energy, $\not{E}_T$, due to the undetected neutrino. The main backgrounds for this channel, after the two leptons requirement, are the Drell-Yan and $Z + jets$ processes, tt and single top ($tW/tb/tqb$), WW , other diboson processes ($WZ/ZZ/W\gamma$), and $W + jets$ where a jet is misidentified as a lepton. The full 2011 data sample has been used for this analysis corresponding to an integrated luminosity of 4.7 fb^{-1}. Data are subdivided into $H +$ 0-jet, $H +$ 1-jet, and $H +$ 2-jet channel in order to maximise the sensitivity by applying further selection criteria that depend on the jet multiplicity. The event are selected by using a single lepton trigger requiring a high-p_T electron or muon. The selection criteria for this analysis are the following:

- exactly two isolated opposite-sign leptons (p_T> 25,15 GeV). This requirement reduces mostly the QCD and the $W + jets$ backgrounds.

- large missing energy requirement and Z mass veto cut, used to suppress the Drell-Yan and the $Z + jets$ contamination. In particular the quantity $E_{\mathrm{T,rel}}^{\mathrm{miss}}$ is used in this analysis defined as $E_{\mathrm{T,rel}}^{\mathrm{miss}} = \not{E}_T \sin(\Delta\phi_{min})$ with $\Delta\phi_{min} = \min\ (\Delta\phi, \pi/2)$ and $\Delta\phi$ defined as the absolute azimuthal angular difference between the $\not{E}_T$ vector and the nearest candidate lepton or jet with $p_{\mathrm{T}} > 25$ GeV.

- b-jet veto is used to suppress the tt background.

- topological cuts ($\Delta\phi_{ll}$ <1.8 and m_{ll} <50 GeV) are used to reduce the SM WW contamination exploiting the spin correlations in the $WW^{(*)}$ system arising from the spin-0 nature of the Higgs boson.

- cuts on p_{T}^{ll} (0-jet channel) or p_{T}^{tot} [1] (1-jet and 2-jet channel) are used to further suppress Drell-Yan and soft-jets backgrounds.

The crucial aspects for this analysis are

- the understanding of the $\not{E}_T$(real or fake). In fact $\not{E}_T$ spectrum and resolution are very sensitive to pile-up and with an higher pileup environment an increase of resolution is expected with the results that one have to tighten the cut on $E_{\mathrm{T,rel}}^{\mathrm{miss}}$ with a signal loss. Understanding of sources on data-MC disagreement on $\not{E}_T$ distribution (especially with high pileup) and improvements in additional Drell- Yan suppression are fundamental for this channel, in particular for the same-flavour channels. Figure 9 shows the $E_{\mathrm{T,rel}}^{\mathrm{miss}}$ distribution of the $\mu\mu$ channel (left) and $e\mu$ channel (right) with the minimum lepton p_{T} cut applied. and with the signal that is shown for $\mathrm{m_H} = 125$ GeV.

[1]defined as the magnitude of the vector $\overrightarrow{p_{\mathrm{T}}^{tot}}$ where $\overrightarrow{p_{\mathrm{T}}^{tot}}$ is the vector sum of the transverse momenta of the jet, the two leptons and the $\not{E}_T$ vector

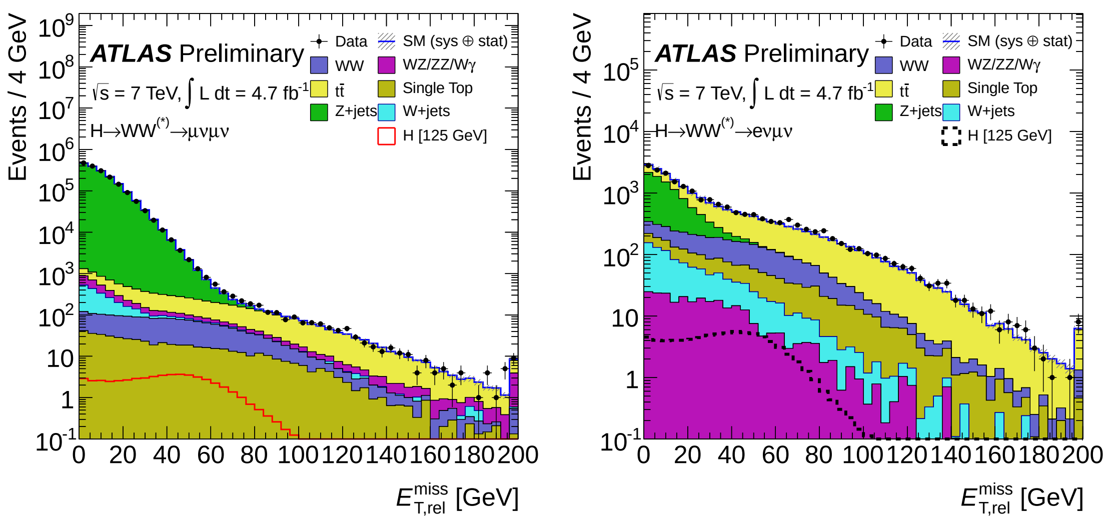

Figure 9: The $E_{\mathrm{T,rel}}^{\mathrm{miss}}$ distribution in the $\mu\mu$ channel (left) and $e\mu$ channel (right) with the minimum lepton p_{T} cut applied. The signal is shown for $\mathrm{m_H} = 125$ GeV.

- an excellent understanding of the background in the signal region. Signal free control region are used in data to constrain MC expectations in order to use MC simulation to extrapolate to the signal region. The $W + jets$ background contribution has been estimated using a control sample of events from data where one of the two leptons satisfies the identification and isolation criteria and the other lepton fails these criteria while satisfying a loosened selection. The $Z + jets$ background is normalized using a Z control sample ($|m_{ll} - M_Z| < 15$ GeV) correcting for mismodeling of $\not{E}_T$ tails. The top background prediction is normalized to the data using a control sample defined by reversing the b-jet veto and removing the requirements on m_{ll} and $\Delta\phi_{ll}$. The SM WW background, which represent the 65% of the total background, is normalized using an high-m_{ll} control region. The remaining backgrounds from di-bosons are estimated using MC simulation.

The transverse mass variable, m_T, is used in this analysis to test for the presence of a signal. This variable is defined as:

$$m_\mathrm{T} = \sqrt{(E_\mathrm{T}^\mathrm{ll} + E_\mathrm{T}^\mathrm{miss})^2 - |\mathbf{p}_T^{ll} + \mathbf{p}_T^{miss}|} \qquad (5)$$

Figure 10 shows the distributions of the transverse mass for events satisfying all criteria in the $H +$ 0-jet (left) and $H +$ 1-jet (right) analyses with a superimposed signal shown for $\mathrm{m_H} = 125$ GeV. Table 2 shows the expected number and observed events for each lepton channel at the end of the cutflow without a m_T cut applied. Figure 11 shows, as a function of $\mathrm{m_H}$, the observed and expected cross section upper limits at 95% CL, for the combined $H +$ 0-jet, $H +$ 1-jet and $H +$ 2-jet analyses. No significant excess of events over the expected background is observed over the entire mass range. A Standard Model Higgs boson with a mass in the range from 130 GeV to

Lepton Channels	0-jet ee	0-jet $\mu\mu$	0-jet $e\mu$	1-jet ee	1-jet $\mu\mu$	1-jet $e\mu$
Total bkg.	58±5	114±10	257±13	21±3	37±5	76±6
Signal	3.8±0.1	9.0±0.1	25±0.2	1.1±0.1	2.3±0.1	6.0±0.1
Observed	52	138	237	19	36	90

Table 2: Expected number and observed events for each lepton channel at the end of the cutflow without a m_T cut applied

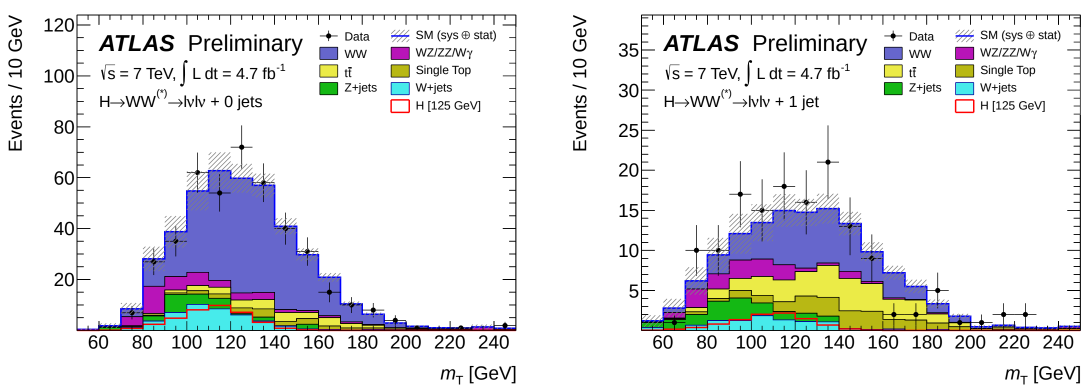

Figure 10: Transverse mass after all selection criteria in the $H + 0 - jet$ (left) and $H + 1 - jet$ (right) analyses for all lepton flavours combined.The superimposed signal shown is for mH = 125 GeV.

260 GeV is excluded at 95% CL with this channel while the expected exclusion range is 127 GeV $\leq$ $m_H \leq$ 234 GeV.

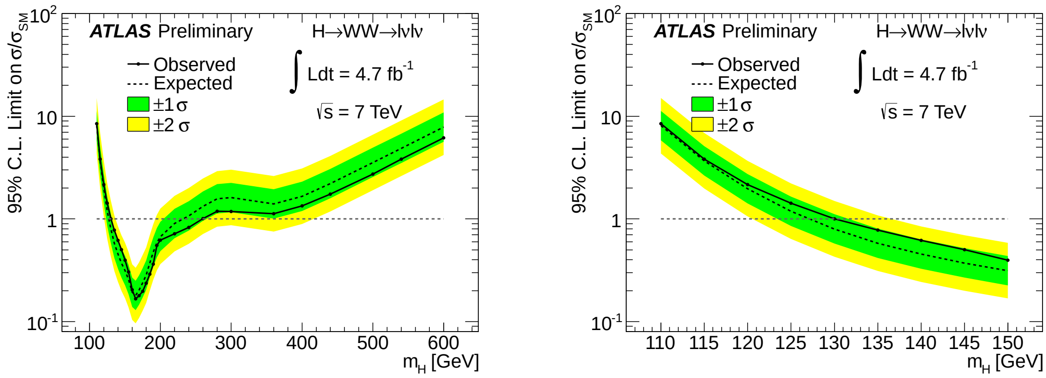

Figure 11: Expected (dashed) and observed (solid) 95% C.L. upper limits on the cross section, normalised to the SM cross section, as a function of m_H. The green and yellow regions indicate the $\pm1\sigma$ and $\pm2\sigma$ uncertainty bands on the expected limit, respectively. On the left the expected (dashed) and observed (solid) 95% C.L. upper limits on the cross section are shown for $m_H <$ 150 GeV.

6 Tier-2

The LNF ATLAS Tier 2 was approved in September 2011 after a long period in which, although not officially approved by INFN, however, covered the role of an ATLAS Tier2, performing all the activities provided by the experiment, beeing part of the Italian Federation of ATLAS Tier2 [9]. Part of the main work is to follow production and analysis jobs (user analysis and group analysis) run in the site, in order to assure the maximum efficiency, and the data transfer (automatic transfer of popular data for analysis and user subscribed data) [A. Andreazza et al, Computing infrastructure for ATLAS data analysis in the Italian Grid cloud, J. Phys.: Conf. Ser. 331 (2011) 052001, Proc of CHEP 2010, Taiwan 2010.]. The effort made by the ATLAS LNF group was significant and showed that the Tier2's farm is able to reach the highest levels of performance and reliability, both in the activities of Monte Carlo production and data analysis, as shown by figure 1, where an histogram shows the efficiency of all jobs run in the four ATLAS Italian Tier2 during all the 2011. From fig.12 we can see that Frascati's Tier2 efficiency is close to 90% and between the highest of the Italian federation.
In addition, the site is continuosly submitted to centralized tests, to verify its effciency; it is always very high, so it receive the greatest share of data consistent with its size. In addition, the personnel involved in the Tier2 management gave full support to the analysis activities of the local ATLAS group; providing users of servers to access grid resources, a local farm for interactive jobs and local storage space for download data. Among these activities, the ATLAS LNF group started a collaboration with Cern developers to setup a new analysis tool for local and grid computing clusters: Proof on Demand (PoD), a tool to perform the last steps of the user analysis. This activity implied the setup of a local farm for testing of parallel proof jobs and the implementation of new protocols for access to grid data; tests on gLite framework are ongoing and the collaboration is open, at the moment, to the other ATLAS Italian Tier2.
The size of the Tier2 farm, in terms of computing power and disk space, increased in the last

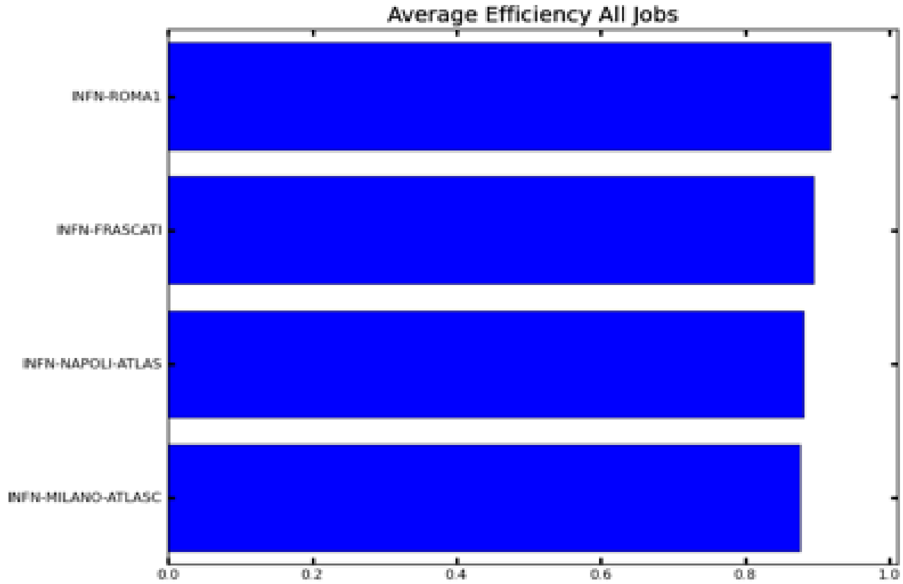

Figure 12: Efficeincies for the italians Tier-2

months, also thanks to the collaboration with the LNF SuperB group, which included in the Tier 2 cluster some computing nodes to be used in share between the two experiments. This shared use of computing resources will lead to a more efficient use of both computing and uman resources. In the Fig.13 we can see the evolution of the computing power starting from 2008.

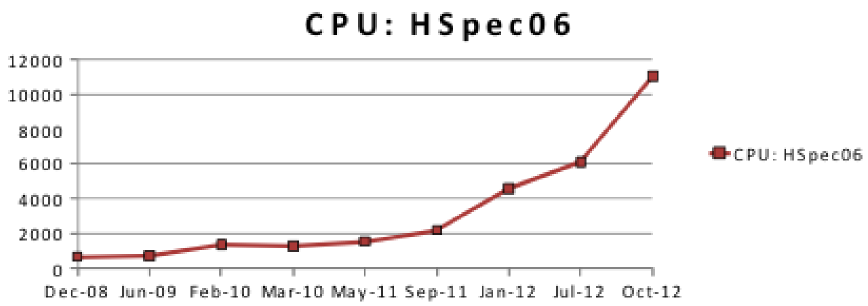

Figure 13: Evolution of the computing power starting from 2008.

The last increment after July 2012 will be a consequence of the acquisition of seventy disused server from Cern Tdaq. They will be partially devoted to central production activity and partially to setup a Proof on Demand farm for the local group (results will be presented in the next Cehp 2012 conference).

7 FTK

The trigger is a fundamental part of any experiment at hadron colliders. It is needed to select on-line the interesting low cross-section physics from the huge QCD background.
Experience at high luminosity hadron collider experiments shows that controlling trigger rates at high instantaneous luminosity can be extremely challenging. As the luminosity increases, physics goals change in response to new discoveries, and detector aging. It is thus essential that the trigger system be flexible and robust, and redundant and significant operating margin. Providing high quality track reconstruction over the full ATLAS Inner Detector by the start of processing in the level-2 computer farm can be an important element in achieving these goals.
With the goal to improve and make more robust the ATLAS trigger, during summer 2007 the group joined the Fast-Track (FTK) proposal for "A hardware track finder for the ATLAS trigger". This is a proposal to build a hardware track finder as an upgrade to the ATLAS trigger. It will provide global reconstruction of tracks above 1 GeV/c in the silicon detectors, with high quality helix parameters, by the beginning of level-2 trigger processing. FTK can be particularly important for the selection of 3rd-generation fermions (b and τ). These have enormous background from QCD jets, which can be quickly rejected in level-2 if reconstructed tracks are available early. This R&D proposal was completed with the submission of the FTK Technical Proposal that was finally approved by the ATLAS collaboration meeting in June 2011. We are continuing the design and prototyping R&D aiming to prepare the FastTrack Technical Design Report in 2 years.
The FTK processor performs pattern recognition with a custom device called the Associative Memory (AM). It is an array of VLSI chips that stores pre-calculated trajectories for a ultra-fast comparison with data. The first way to reduce the combinatorial at high luminosity is to work with better resolution in the AM. In order to do that, we will need a new AM chip with a high density of patterns, so that all possible tracks with a thinner resolution can be stored in the AM. Even with better resolution the number of candidate tracks that the AM will find at these high instantaneous luminosities will be very large. For this reason we redesigned the FTK architecture to increase the internal parallelism and data-flow to accommodate a larger flux of data.
For this purpose it was essential a new ideas. The efficiency curves for patterns is slowly increasing for efficiencies above 70%. This is due to the fact that many low probability patterns are needed to gain the missing efficiency. This is a consequence of the fact that the AM performs pattern recognition with a fixed resolution. We developed the idea of variable resolution patterns that increases the equivalent number of pattern per AMchip by a factor 3-5 with a corresponding reduction in hardware size [10].
In 2011 we completed the R&D of the new AM chip in collaboration with Pisa, Milano and Fermilab. The AMchip04 was submitted for prototyping in January 2012. This is a very challenging task because we need to increase the pattern per chip with respect to the current AM chip designed for the SVT upgrade at CDF by a factor 30 with similar power consumption running at 100 MHz clock speed instead of 40 MHz. In order to achieve these goals we need several separate improvements: better technology 65 nm instead of 180 nm, design full custom cell that implements the core AM logic, a specific optimization of the global logic, and possibly implement a 3D silicon device to increase the available area. Frascati and Milano worked on the design of the full custom AM cell. This work is the critical element of this project because advanced techniques are required to meet the density and power consumption goals. This element will require intensive simulation to verify functionality under all conditions. Based on FTK simulation results, the 65nm AM cell was designed to work with at least 3 (and up to 6) don't care bits per layer.
The Frascati group studied a hardware-implementable clustering algorithm for the pixel detector.

Clustering in the pixel detector is a non trivial computational problem because of the 2D nature of the pixel detectors and of the huge amount of data involved. The pixel detector's RODs deliver data over 132 S-Link fibers each with a 1.2 Gbps bandwidth. The clustering algorithm must identify and cluster hits as well as calculate the center of the cluster. In 2011 we built the first prototypes of mezzanine card (FTK_IM) that will implement the clustering algorithm. The card is shown in figure 14. The card was successfully tested and integrated with the EDRO board in the Pisa test stand. The firmware to receive SLink data from the detector has been written and it was successfully tested. The card is now included in the FTK test stand.

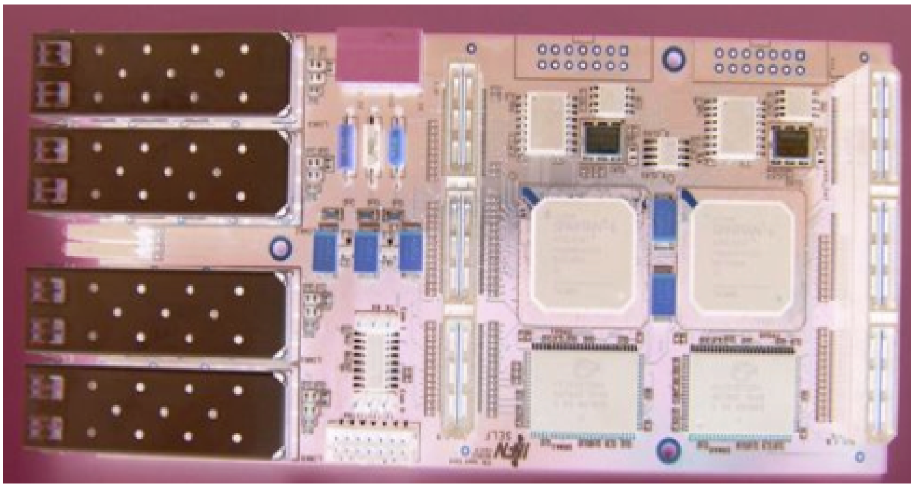

Figure 14: First prototype of the FTK input mezzanine (FTK_IM).

We collaborated on the integration of the FTK vertical slice. A full high-rate test must be performed before the FTK vertical slice can be used for parasitic data taking. A working setup has been build in fall 2011 with existing EDRO (V1) and AM boards (SLIM V1). We are currently working to integrate the new version of the prototypes: EDRO (V2) with FTK specific firmware and AM boards (SLIM V2).
Guido Volpi coordinated the simulation activity of the Fast-Tracker collaboration. The simulation activity was essential to define the specifications for the AMchip design, including the variable resolution presented at the ANIMMA 2011 conference. It was essential to find an affordable configuration for FTK at high luminosity $3*10^{34}$ and 10^{35} cm^{-2}s^{-1}. The proof-of-principle was then integrated into the current FTKSim package. A new and important branch of activity emerged: the integration of the standalone FTK simulation within the ATLAS software and production frameworks. we worked in close contact with the ATLAS experts at CERN and this new activity is now half completed. This is already beyond the needed schedule because the FTK studies for the Technical Design Report can be completed with the standalone simulation, but it will allow a wider application of the FTK simulation inside the Atlas collaboration.

References

1. ATLAS Collaboration, "ATLAS muon momentum resolution in the first pass reconstruction of the 2010 pp collision data at $\sqrt{s} = 7$ TeV", ATL-CONF-2011-046.

2. ATLAS Collaboration, "Performance of missing transverse momentum reconstruction in proton-proton collisions at 7 TeV with ATLAS", EPJC 72 (2012), arXiv:1108.5602 [hep-ex]

3. ATLAS Collaboration, "A measurement of the total $W^{\pm}$ and Z/γ^{*} cross sections in the e and μ decay channels and of their ratios in pp collisions at $\sqrt{s} = 7$ TeV with the ATLAS detector", ATL-CONF-2011-041.

4. ATLAS Collaboration, "Search for the Standard Model Higgs boson in the decay channel $H \to ZZ^{(*)} \to 4l$ with 4.8 fb^{-1}of pp collision data at $\sqrt{s} = 7$ TeV with ATLAS",submitted to Physics Letters B, arXiv:1202.1415v3 [hep-ex]

5. ATLAS Collaboration, "Search for the Standard Model Higgs boson in the $H \to WW^{(*)} \to l\nu l\nu$ decay mode with 4.7 fb^{-1}of ATLAS data at $\sqrt{s} = 7$ TeV"ATLAS-CONF-2012-012

6. "$\not{E}_T$ Studies for the $H \to WW^{(*)} \to l\nu l\nu$ search", ATL-COM-PHYS-2011-1757

7. "Monte Carlo generators and theoretical aspects for the search of the Higgs boson in the $H \to WW^{(*)} \to l\nu l\nu$ decay mode using 4.7 fb^{-1}of data collected with the ATLAS detector at $\sqrt{s} = 7$ TeV" ATL-COM-PHYS-2011-1726

8. ATLAS Collaboration, "Measurement of the centrality dependence of J/ψ yields and observation of Z production in lead-lead collisions with the ATLAS detector at the LHC," Phys. Lett. B **697**, 294 (2011) [arXiv:1012.5419 [hep-ex]].

9. LNF 11/11(IR),
http://www.lnf.infn.it/sis/preprint/pdf/getfile.php?filename=LNF-11-11(IR).pdf

10. A new Variable Resolution Associative Memory for High Energy Physics
Presented by G. Volpi at the Second International Conference on Advancements in Nuclear Instrumentation, Measurement Methods and their Applications, ANIMMA, 6-9 June, 2011, Ghent, Belgium

11. The Fast Tracker Real Time Processor
Presented by A. Annovi at the ACES workshop, 9-11 March 2011, CERN - Geneva, Switzerland

12. Associative Memory design for the Fast TracKer processor (FTK) at ATLAS
Presented by M. Beretta at TWEPP 2011 Topical Workshop on Electronics for Particle Physics, 26-30 September 2011, Vienna

13. The EDRO board connected to the Associative Memory: a "Baby" FastTracKer processor for the ATLAS experiment ATL-DAQ-PROC-2011-018
https://cdsweb.cern.ch/record/1382040/, to be published on NIM A.

14. Associative Memory Design for the FastTrack Processor (FTK) at ATLAS
ATL-DAQ-PROC-2011-045 https://cdsweb.cern.ch/record/1402465?ln=en, to be published on IEEE 2011 Conference records.

15. The FastTrack Real Time Processor and Its Impact on Muon Isolation, Tau and b-Jet Online Selections at ATLAS, Accepted for publication on IEEE Transactions on Nuclear Science

16. A new Variable Resolution Associative Memory for High Energy Physics
ATL-UPGRADE-PROC-2011-004 https://cdsweb.cern.ch/record/1352152, to be published on IEEE Conference Proceedings

17. ATLAS FTK: Fast Track Trigger ATL-DAQ-PROC-2011-022
https://cdsweb.cern.ch/record/1383885, to be published on NIM A.

BABAR

A. Calcaterra, R. de Sangro, G. Finocchiaro, P. Patteri,
I. Peruzzi (Resp.), M. Piccolo, M. Rama, A. Zallo

1 Introduction

The *BABAR* experiment has been running at the PEP-II asymmetric B factory of the SLAC National Laboratory (Stanford, USA) from 2001 to 2008, collecting a data sample corresponding to approximately $0.5\,\mathrm{ab}^{-1}$. The data were collected mostly at the CM energy corresponding to the $\Upsilon(4S)$ mass; large data sample were also obtained at the CM energy corresponding to the $\Upsilon(2S)$ and $\Upsilon(3S)$ resonances. The experiment has produced a wealth of important physics results, ranging from measurements of all three angles of the Unitarity triangle, to the discovery of the $D-\bar{D}$ mixing, the discovery of the η_b, the discovery of several interesting charm and charmonium states. The study of the ISR events, also pursued at *BABAR* has produced many important results in the energy range down hadron threshold production. To date the *BABAR* analysis effort has resulted in about 500 publications in Phys. Rev. Lett. or Phys. Rev. D. After the end of data taking the complete data set was reprocessed, and large amount of Monte Carlo events were generated and fully reconstructed. During 2011 the intense analysis period has not yet slowed down.

The preparation of a “Physics of the B-factories” book, in collaboration with the Belle group, to illustrate the analysis strategies and the physics results of the B-factories is near completion. The main activity of the LNF group in 2011 has been the analysis of $B \rightarrow D^{*+}D^{*-}$ selected with a partial reconstruction technique, described in the next section.

2 Measurement of $\sin 2\beta$ with partial reconstruction of B mesons to the $D^{*+}D^{*-}$ decay

In 2011 this analysis has been finalized for publication. The parameters S, C are extracted from the CP and tag side vertices time difference Δt distribution of events selected using event topology and kinematic cuts. In fig. 1 we show the recoil mass distribution of real data from RUN 1 through

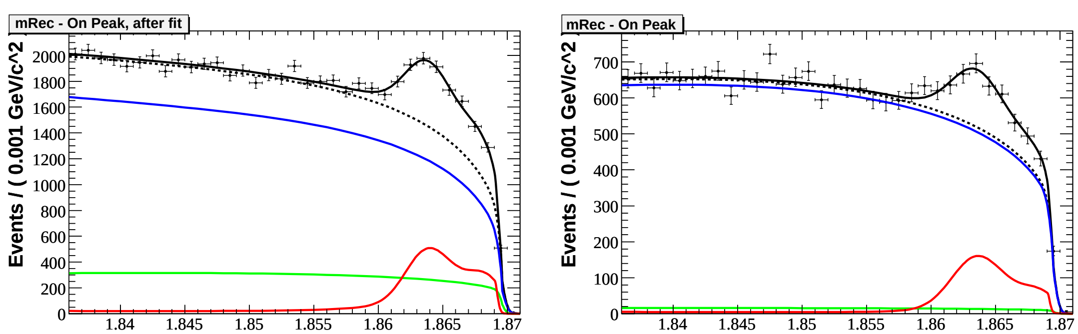

Figure 1: Missing mass for $B \rightarrow D^{*\pm}\pi^{\mp}(X)$ for kaon (left) and lepton (right) tagged events. The curves represent the probability distribution functions (p.d.f.) for signal (red), continuum background (green), $B\bar{B}$ background (blue) and their sum (black).

6 (black crosses), corresponding to $\approx 435\ fb^{-1}$ of integrated luminosity. The presence of an excess of events in the signal region is evident. We fit the data with a PDF (black curve), made of a signal component (red) plus a continuum (green) and $B\bar{B}$ (blue) combinatorial background component. We find a total of 3843 ± 397 (1128 ± 218) events in the kaon (lepton) sample. We fit the time

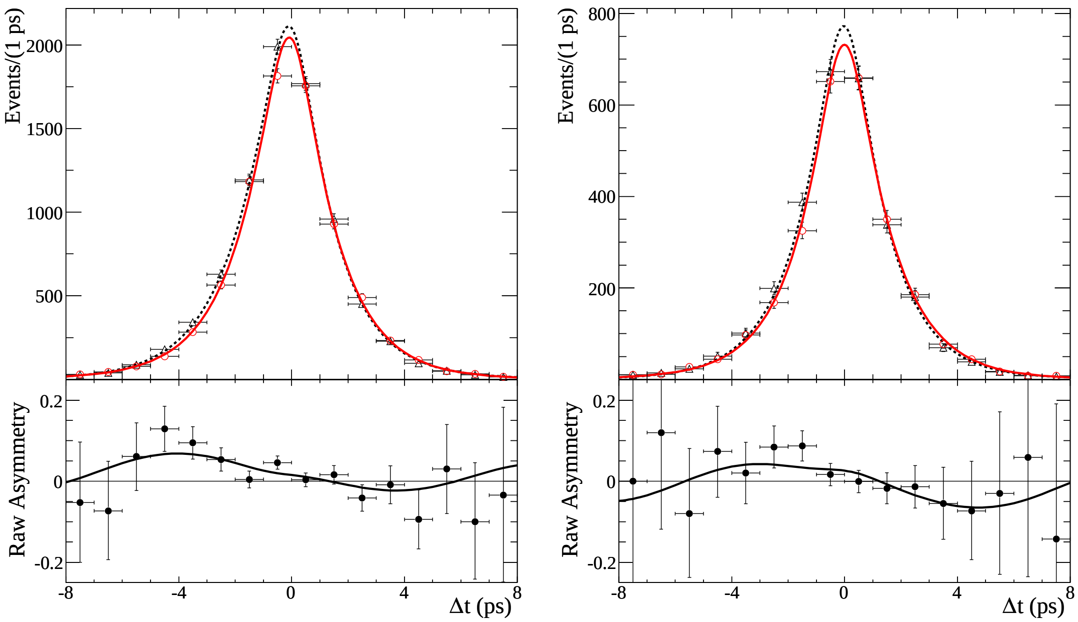

Figure 2: Top: Δt distribution for the B^0 (black, dashed) and $\overline{B}^0$ (red, solid) kaon(left) and lepton(right) tags. Bottom: respective raw time-dependent CP asymmetries.

distribution in the data, whose result we show in fig. 2 where we plot the time difference distribution of all data events for the full collected sample, and the corrisponding raw CP asymmetry for the lepton and kaon tag samples.

Following the preliminary review stage, the analysis was allowed to be unblinded at the end of the year, and is now in the final stage of the process leading to publication. As the results are not official yet, we can only summarize here the statistical errors obtained from the fit. We find:

$$\begin{array}{ll} \delta C = \pm 0.11 & \\ \delta S = \pm 0.16 & \end{array} \quad \text{kaon tags,}$$

$$\begin{array}{ll} \delta C = \pm 0.15 & \\ \delta S = \pm 0.20. & \end{array} \quad \text{lepton tags.}$$

The combined statistical and systematic errors are:

$$\delta C = \pm 0.09 \pm 0.05 \qquad (1)$$

$$\delta S = \pm 0.12 \pm 0.09, \qquad (2)$$

This measurement reduces the error of the previous BaBar measurement performed with fully reconstructed $D^{*+}D^{*-}$final states by $\approx 25\%$.

A full description of this analysis and its results has been included in the B-Factories legacy book.

3 Physics of the B-factories book

Over the last decade BaBar and Belle have studied the physics of bottom and charm mesons, tau leptons, heavy quarkonium states, etc. that were produced at the PEP-II and KEKB e+e- storage rings. The two collaborations contiuously developed more and more sophisticated techniques for extracting the maximum amount of information from data. A project is ongoing to document all these techniques in a book, named "Physics of the B-Factories". The book will provide descriptions of all of the techniques developed by the experiments and a comprehensive overview of the measurements. The publication of the book is currently expected to happen in 2012. One member of our group is co-editor of the chapter on the measurement of the angle γ of the Unitarity Triangle.

References

1. J. P. Lees *et al.* [The BABAR Collaboration], Phys. Rev. D **85** (2012) 011102 [arXiv:1110.6005 [hep-ex]].
2. J. P. Lees *et al.* [The BaBar Collaboration], Phys. Rev. D **85** (2012) 011101 [arXiv:1110.5600 [hep-ex]].
3. J. P. Lees *et al.* [BABAR Collaboration], Phys. Rev. D **85** (2012) 031102 [arXiv:1109.1527 [hep-ex]].
4. J. P. Lees *et al.* [BaBar Collaboration], Phys. Rev. D **84** (2011) 092007 [arXiv:1109.0143 [hep-ex]].
5. J. P. Lees *et al.* [BABAR Collaboration], Phys. Rev. D **84** (2011) 092003 [arXiv:1108.5874 [hep-ex]].
6. J. P. Lees *et al.* [BABAR Collaboration], Phys. Rev. Lett. **107** (2011) 221803 [arXiv:1108.3549 [hep-ex]].
7. J. P. Lees *et al.* [BABAR Collaboration], Phys. Rev. D **84** (2011) 071102 [Phys. Rev. D **85** (2012) 039903] [arXiv:1108.3211 [hep-ex]].
8. J. P. Lees *et al.* [The BABAR Collaboration], Phys. Rev. D **84** (2011) 112007 [arXiv:1107.5751 [hep-ex]].
9. J. P. Lees *et al.* [The BABAR Collaboration], Phys. Rev. D **84** (2011) 072006 [arXiv:1107.4465 [hep-ex]].
10. J. P. Lees *et al.* [The BABAR Collaboration], Phys. Rev. D **84** (2011) 012001 [arXiv:1105.5159 [hep-ex]].
11. J. P. Lees *et al.* [BABAR Collaboration], Phys. Rev. D **84** (2011) 011104 [arXiv:1105.4234 [hep-ex]].
12. J. P. Lees *et al.* [The BABAR Collaboration], Phys. Rev. D **84** (2011) 031103 [arXiv:1105.4410 [hep-ex]].
13. P. del Amo Sanchez *et al.* [BABAR Collaboration], Phys. Rev. D **83** (2011) 071103 [arXiv:1011.5477 [hep-ex]].
14. J. P. Lees [The BABAR Collaboration], Phys. Rev. D **83** (2011) 112010 [arXiv:1105.0125 [hep-ex]].

15. J. P. Lees *et al.* [The BABAR Collaboration], Phys. Rev. D **84** (2011) 072002 [Phys. Rev. D **84** (2011) 099901] [arXiv:1104.5254 [hep-ex]].

16. J. P. Lees *et al.* [The BABAR Collaboration], Phys. Rev. D **84** (2011) 012002 [arXiv:1104.4472 [hep-ex]].

17. P. del Amo Sanchez *et al.* [The BABAR Collaboration], Phys. Rev. D **84** (2011) 012004 [arXiv:1103.3971 [hep-ex]].

18. J. P. Lees *et al.* [The BABAR Collaboration], Phys. Rev. D **83** (2011) 072003 [arXiv:1103.2675 [hep-ex]].

19. J. P. Lees *et al.* [The BABAR Collaboration], Phys. Rev. D **84** (2011) 091101 [arXiv:1102.4565 [hep-ex]].

20. P. del Amo Sanchez *et al.* [BABAR Collaboration], Phys. Rev. D **83** (2011) 091101 [arXiv:1101.3830 [hep-ex]].

21. P. del Amo Sanchez *et al.* [BABAR Collaboration], Phys. Rev. D **84** (2011) 052001 [arXiv:1101.1142 [hep-ex]].

22. P. del Amo Sanchez *et al.* [The BABAR Collaboration], Phys. Rev. D **83** (2011) 031103 [arXiv:1012.5031 [hep-ex]].

23. P. del Amo Sanchez *et al.* [BABAR Collaboration], Phys. Rev. D **83** (2011) 051101 [arXiv:1012.4044 [hep-ex]].

24. P. del Amo Sanchez *et al.* [The BABAR Collaboration], Phys. Rev. Lett. **107** (2011) 041804 [arXiv:1012.4158 [hep-ex]].

25. P. del Amo Sanchez *et al.* [The BABAR Collaboration], Phys. Rev. D **83** (2011) 072001 [arXiv:1012.1810 [hep-ex]].

26. P. del Amo Sanchez *et al.* [The BABAR Collaboration], Phys. Rev. D **83** (2011) 052001 [arXiv:1011.4190 [hep-ex]].

27. P. del Amo Sanchez *et al.* [The BaBar Collaboration], Phys. Rev. D **83** (2011) 032002 [arXiv:1011.3917 [hep-ex]].

28. P. del Amo Sanchez *et al.* [The BABAR Collaboration], Phys. Rev. D **83** (2011) 032004 [arXiv:1011.3929 [hep-ex]].

29. P. del Amo Sanchez *et al.* [The BABAR Collaboration], Phys. Rev. D **83** (2011) 032006 [arXiv:1010.2229 [hep-ex]].

30. P. del Amo Sanchez *et al.* [BABAR Collaboration], Phys. Rev. D **83** (2011) 052011 [arXiv:1010.0987 [hep-ex]].

31. P. del Amo Sanchez *et al.* [BaBar Collaboration], Phys. Rev. Lett. **107** (2011) 021804 [arXiv:1007.4646 [hep-ex]].

32. P. del Amo Sanchez *et al.* [BABAR Collaboration], Phys. Rev. D **83** (2011) 032007 [arXiv:1005.3288 [hep-ex]].

BESIII

M. Anelli (Tecn.), R. Baldini Ferroli, M. Bertani (Resp.), A. Calcaterra,
S. Pacetti (Ass.), D. Pierluigi (Tecn.), R. Rosellini (Tecn.), A. Russo (Tecn.),
S. Stucci (Laur.), A. Zallo, A. Zossi (Tecn.)

1 The BESIII experiment

The BESIII experiment is running at the Beijing Electron Positron Collider BEPC-II, a major upgrade of the previous BEPC, at the Beijing Institute of High Energy Physics, IHEP. The BESIII detector, a scheme is shown in fig. 1, is designed to study the τ-charm physics. The first physics event was observed on July 19, 2008.

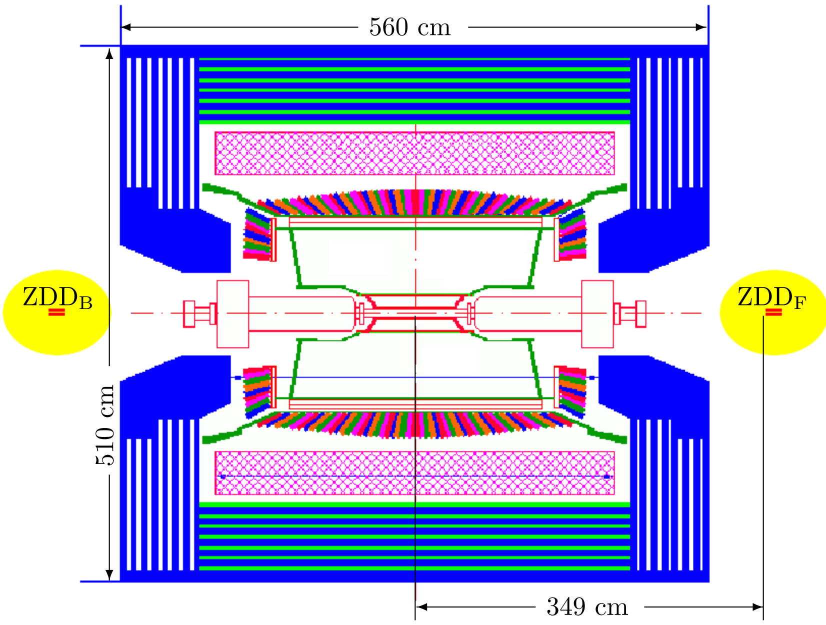

Figure 1: Overview of BESIII with ZDD detector installed. The ZDD stations, in the forward and backward region, are shown in red, highlighted by yellow ovals. All components are drawn to scale.

So far BESIII collected the world largest collections of charmonia, in particular 225 million of J/ψ, 106 million of ψ', 2.9 fb^{-1} at the $\psi(3770)$ and 0.5 fb^{-1} at the $\psi(4040)$. The actual total integrated luminosity amounts to 4 fb^{-1} with a maximum instantaneous value of 0.6×10^{33} cm^{-2} s^{-1} (April 2011).
The LNF group started work on BESIII at the end of 2009. Our interest within this collaboration is twofold:

- physics analyses of processes mainly involving nucleons or light hadrons;
- design, construction and installation of a new detector for zero-degree photon tagging.

In 2010 the CSN1 (Commissione Scientifica Nazionale 1) has approved the BESIII activity within INFN and funded the proposed detector. In 2011 a group from the University and INFN section of Torino joined the BESIII Collaboration and started to work in this project.

2 The zero degree detector: physics, design and construction

2.1 The initial state radiation technique

At τ-charm and b factories e^+e^- annihilation processes to hadrons can be investigated by means of the so-called initial state radiation technique (ISR). Such a technique consists in measuring the reaction $e^+e^- \to H\gamma$, where H is a hadronic final state and the photon is emitted by one of the initial leptons. The differential cross section for this process is proportional to the direct $e^+e^- \to H$ cross section. The proportionality factor is the *radiator* function, it gives the probability for the initial photon emission and can be computed to an accuracy better than 1%.
The angular distribution of the ISR photon in the center of mass (CoM) frame is peaked at small angles. Indeed the fraction of photons hitting the main detector, which has a typical geometrical acceptance $20^o \leq \theta \leq 160^o$, is lower than 20%. The possibility of measuring the small-angle photons, even in a few milliradians cone around the beam line would largely increase the ISR acceptance (almost a factor of two).

2.2 The ZDD

At the BEPC-II facility there is the possibility to install two small calorimeters ($\sim$ 50 cm^2 of cross-section each) along the beam line, about 3 m away from the BESIII detector, that can cover the very-forward and very-backward region. Such a detection device, called zero-degree detector, **ZDD**, can be used to tag the forward-backward ISR photons.

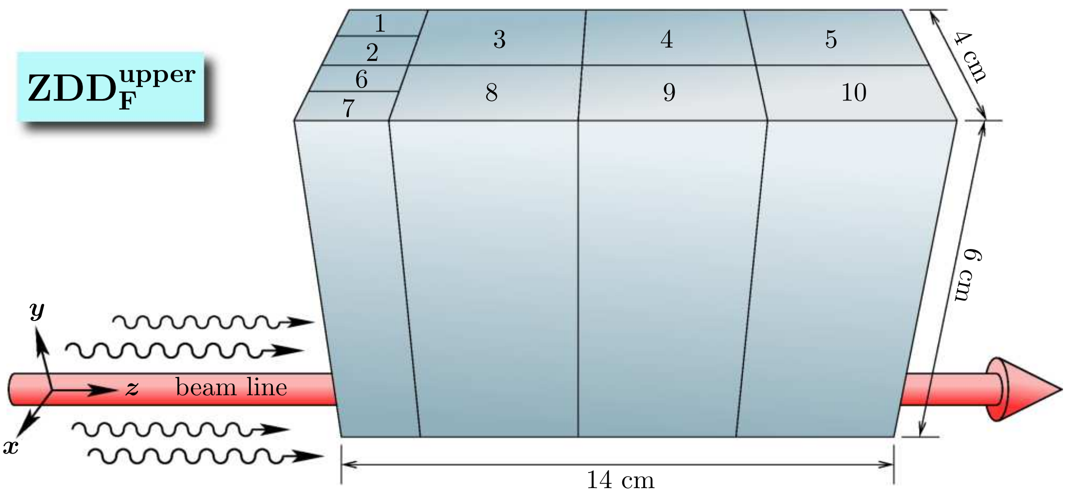

Figure 2: Upper forward module of the ZDD detector. The segmentation on the upper face indicates the ten reading sectors. The red arrow shows the ideal beam direction.

Moreover, this detector is destined to replace the present BESIII luminometer. In fact, it can furnish a fast measurement of beam-to-beam relative BESIII luminosity via instantaneous rates of appropriate sums of channels.

2.3 Design

The proposed ZDD is made of two identical stations, $\mathrm{ZDD_F}$ and $\mathrm{ZDD_B}$ in the forward and backward direction, located along the ideal z-axis, i.e. the beam direction in the e^+e^- CoM, see fig. 1 and 2. Furthermore, to avoid the severe background due to Bremsstrahlung photons produced in the process $e^+e^- \to e^+e^-\gamma$, which populate the very small-angle regions, each ZDD station is divided in two parts, upper and lower module ($\mathrm{ZDD}_{\mathrm{F,B}}^{\mathrm{upper,lower}}$), by an empty 10 mm-wide slot, along the x axis, between $y = -5$ mm and $y = +5$ mm. In this way, by leaving inactive the slot region, there is a geometrical separation of the two effects: ISR, our signal, and Bremsstrahlung, the main background.
Figure 2 shows a perspective view of the upper forward module, $\mathrm{ZDD}_{\mathrm{F}}^{\mathrm{upper}}$. The beam line runs between $\mathrm{ZDD}_{\mathrm{F}}^{\mathrm{upper}}$ and $\mathrm{ZDD}_{\mathrm{F}}^{\mathrm{lower}}$, not shown in fig. 2, and the photons hit the left face of the module.
The modules are $4 \times 6 \times 14$ cm^3 arrays of scintillating fibers, 60% of the volume, embedded in lead. The fibers are lined up along the y axis so that the signal is read out from the upper (lower) face of each upper (lower) module.
They are segmented, in the xz plane, in ten reading sectors, as shown in fig. 2. A thinner segmentation has been adopted for the first layer (2 cm wide) to have a better y-resolution.
The light signal is extracted from each module and channeled to the photomultipliers through ten bundles of clear optical fibers, 2 m long, one for each sector (see fig. 2 and fig. 3).

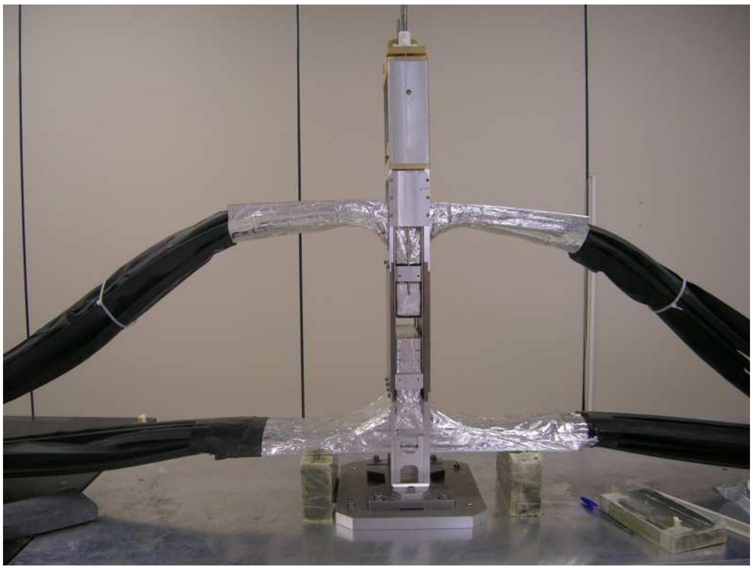

Figure 3: The ZDD forward station completely assembled at LNF.

The clear optical fibers, a novelty introduced with this detector, have been preferred over more classical solutions, typically solid lucite light guides, for two reasons:

1. their flexibility is of great help in transporting the light out of a space region very crowded with magnets and electronic equipment. Projecting and realizing a solid light guide of very complex form would have been complicated, and errors would have implied the greatest difficulties in installing the setup in the correct position.

2. Solid light guides lose signal according to the ratio of output vs. input area, but this effect is practically absent for clear optical fibers that have a constant cross section.

2.4 Readout electronics

The clear optical fibers carry the scintillating light to 16 phototubes Hamamatsu H10828, characterized by a very fast response, and expressly selected to have uniform gains of $\sim 10^6$ at 1500 V. The signals from the photomultipliers are fed into preamplifiers ($\times 2$) located close to the experimental area and sent, via RG58 cables 20 m long, to shaper, splitter and discriminator circuitry located in the BESIII DAQ crates.
There, the 16 signals are further amplified by two and stretched to match the FlashADC sampling frequency of 500 MHz. The output is then split in three: one for the FlashADC, one to a local exit for monitoring purposes, and one for constant-fraction discriminators for time measurements. The DAQ electronics, located in VME, is composed by FlashADC's CAEN V1721 and TDC CAEN V1190. Moreover, analog sums of 4 channels are available for luminosity measurements.
The preamplifiers, as well as the readout electronics, are a project and realization of the "SELF" group of the LNF.

2.5 Test with cosmic rays

One complete ZDD station (upper and lower modules) was completely built and assembled during the first six months of 2011, allowing tests with cosmic rays and at the Beam Test Facility at LNF. The ZDD has been tested with cosmic rays. The configuration used is sketched in fig. 4. A module of the ZDD has been placed with the exposed face turned upwards. The signal is triggered by the coincidence of two scintillators. A "finger" scintillator $11 \times 5 \times 50$ mm^3 on top and a "paddle" scintillator on the bottom. In this configuration the trigger rate was $5 - 10$ mHz.
Two types of data taking have been considered: integrated charge (QDC) and line-shape (flash ADC). The QDC data allowed for: inter-channel calibration, absolute scale setting and resolution studies. The line-shape data have been used to calibrate the released energy/voltage (MeV/mV). The absolute scale, i.e. the amount of charge per unit of energy released by the passing tracks has been estimated as 11 pC/MeV.
The measured energy resolution is in agreement with Monte Carlo (MC) simulation and it is $\sigma_E/E = 11\%$. No shower fluctuation has been observed.
The number of photoelectrons per cosmic ray track has been measured as $N_{\mathrm{pe}} = 443$. By using the MC simulation to estimate the total amount of released energy, we obtain that the number of photoelectrons per unit of energy is $N_{\mathrm{pe}}/E_{\mathrm{released}} = 28/\mathrm{MeV}$.

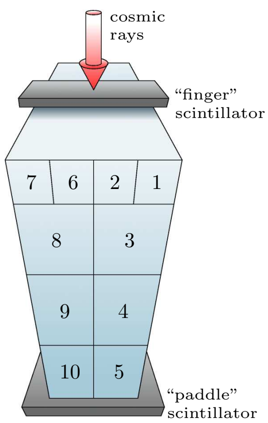

Figure 4: Cosmic rays test configuration.

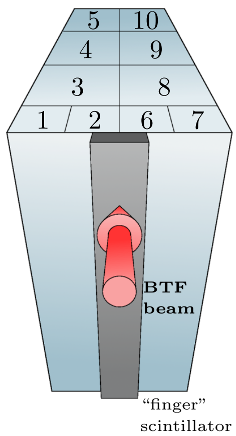

Figure 5: Setup at the BTF.

2.6 Test at the Frascati Beam Test Facility

The test at the Frascati Beam Test Facility (BTF) has been done using the configuration shown in fig. 5. The exposed face is vertical and a finger $11 \times 4 \times 60$ mm^3 scintillator is placed in front of it to trigger the incoming electrons in coincidence with the beam radio frequency. The beam consists of bunches of 0 to 3 electrons pulsed at a frequency of 50 Hz.

The main purpose of this test is to study the response of the ZDD to single electrons of different energies and hence compare the results to those obtained with cosmic rays. The number of photoelectrons for a 450 MeV incoming electron is $N_{\text{pe}} = 1600$ and, since, according to the MC simulation, the amount of released energy is 12%, this means $N_{\text{pe}}/E_{\text{released}} = 30/\text{MeV}$, in agreement with the cosmic-rays result.

The measured energy resolution is $\sigma_{450\,\text{MeV}}/(450\,\text{MeV}) = 12.4\%$.

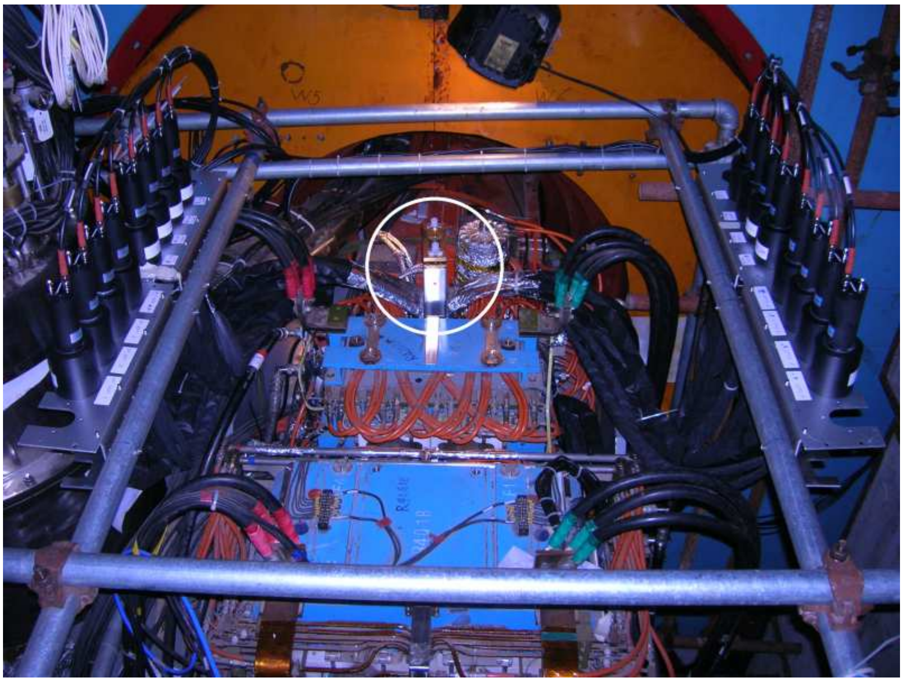

Figure 6: The ZDD, highlighted by the white circle, installed at BEPC-II.

2.7 Installation at BEPC-II and first cosmic rays data

In August 2011 the first station (upper and lower modules) of the ZDD has been successfully installed as a stand-alone detector, in the East side region of BESIII detector, fig 6. A first test in situ has been performed with cosmic rays and using an "auto-generated" trigger. The correct functioning of each channel has been verified. In the first months of 2012 the ZDD readout will be incorporated into the BESIII general data acquisition system.

3 Physics

3.1 The measurement of $J/\psi \to p\overline{p}$ and $J/\psi \to n\overline{n}$ breaching fractions

The decay of the J/ψ meson to a nucleon-antinucleon pair represents a good testbed for studying perturbative QCD. The $J/\psi \to N\overline{N}$ amplitude has a strong (QCD) and an electromagnetic (EM) contribution. The strong amplitude accounts for the lowest order QCD diagram where the decay is mediated by three gluons that produce the $N\overline{N}$ final state via single gluon-quark-antiquark vertices. The EM amplitude, instead, describes the $N\overline{N}$ production though one-photon exchange. Since the J/ψ meson has isospin zero, the strong amplitudes for decays in $p\overline{p}$ and $n\overline{n}$ should be the same. The EM amplitudes for protons and neutrons scale with the magnetic moments that are almost opposite ($\mu_p = 2.973$ and $\mu_n = -1.91$ in units of Bohr magneton). If all amplitudes are real (in phase), as it is expected at that energy, the interference terms between strong and EM part in case of $p\overline{p}$ and $n\overline{n}$ production have opposite sign so that we expect $\Gamma(J/\psi \to n\overline{n}) : \Gamma(J/\psi \to p\overline{p}) \simeq 1 : 2$. The branching fractions, measured by BESIII with a sample of 225 million J/ψ, are

$$\begin{array}{l} \Gamma(J/\psi \to n\overline{n}) = (2.07 \pm 0.17) \times 10^{-3} \\[2ex] \Gamma(J/\psi \to p\overline{p}) = (2.11 \pm 0.03) \times 10^{-3} \end{array} \quad \Rightarrow \quad \frac{\Gamma(J/\psi \to n\overline{n})}{\Gamma(J/\psi \to p\overline{p})} = 0.98 \pm 0.08\,.$$

These results, that represent significant improvements over previous measurements, strongly support almost orthogonal EM and strong amplitudes. This means that, contrary to the expectation, there should be a relative phase of about 90 degrees between these amplitudes, *i.e.*: if one is real the other must be purely imaginary. The origin of this unexpected phase is still under investigation.

3.2 Proposal to measure the phase between J/ψ strong and electromagnetic decay amplitudes by means of a resonance scan

We have submitted to the BESIII Collaboration a proposal to measure the phase difference between EM and strong J/ψ decay amplitudes in a model independent way. The procedure consists in looking for an interference pattern, in all possible channels, between the resonant amplitude and the non resonant one, by means of an energy scan of the J/ψ.
More in detail, this study requires setting a continuum reference at ∼100 MeV below the J/ψ and then measuring the decay rate at four different energies lying between this reference point and the J/ψ mass.
The choice of these energy points and the computation of the necessary integrated luminosity have been done to maximize the capability to discriminate between the extreme cases, *i.e.* relative phase equal to zero, maximum interference, and 90 degrees, no interference.
The BESIII Collaboration has accepted our proposal, by allocating to this study five days of data taking in 2012.

4 List of Conference Talks by LNF Authors in 2011

1. M. Bertani, "BESIII: stato e risultati" (IFAE2011), Perugia, Italy.
   Il Nuovo Cimento, Vol. 34C, N.6, 146.

2. A. Zallo, "Time-like Baryon Form Factors near Threshold Status and Perspectives", (Hadron Structure 2011), Tatranská Štrba, Slovak Republic.
   Nucl. Phys. Proc. Suppl. **219-220** (2011) 32.

3. R. Baldini Ferroli, "Baryon Form Factors at threshold", (PHIPSI11), Novosibirsk, Russia.
   To be published in Nucl. Phys. B (Proc. Suppl.).

5 Publications

1. The BESIII Collaboration, Phys. Rev. D **83**, 012006 (2011).
2. The BESIII Collaboration, Phys. Rev. D **83**, 012003 (2011).
3. The BESIII Collaboration, Phys. Rev. Lett. **106**, 072002 (2011).
4. The BESIII Collaboration, Phys. Rev. D **83**, 032003 (2011).
5. The BESIII Collaboration, Phys. Rev. D **83**, 112005 (2011).
6. The BESIII Collaboration, Phys. Rev. Lett. **107**, 092001 (2011).
7. The BESIII Collaboration, Phys. Rev. D **84**, 032006 (2011).
8. The BESIII Collaboration, Phys. Rev. Lett. **107**, 182001 (2011).
9. The BESIII Collaboration, Phys. Rev. D **84**, 091102 (2011).
10. The BESIII Collaboration, Phys. Rev. D **84**, 092006 (2011).

Report of the Frascati CDF-II group activities for the year 2011

A. Annovi, M. Cordelli (Resp.), P. Giromini, F. Happacher

1 Introduction

The Tevatron, with a $p\bar{p}$ collision energy of 1.96 TeV in the center of mass system, is running with a record instantaneous luminosity, L, delivered to the experiments of 450×10^{30} $cm^{-2}s^{-1}$ ($vs.$ $\sim 10^{31}$ of Run I). At the end of year 2010, the Tevatron has delivered to the experiments more than $\sim$ 11 fb^{-1}; CDF experiment has collected on tape $\sim$ 10 fb^{-1} (see Figure 1 and 2); during the whole Run I we collected $\sim$ 109 pb^{-1}. The Tevatron and CDF have been shut down on September 30, 2011.

The CDF group of Frascati has built the central hadronic calorimeter (the iron-scintillator based calorimeter in the central and end-wall region, CHA and WHA) and is responsible for the hardware maintenance and for the energy scale calibration.

The analysis interest of the Frascati group focused on the measurements of b quark production cross sections and vetor Bosons production.

Indeed, the bottom quark production at the Fermilab Tevatron has been called one of the few instances in which experimental results appear to challenge the ability of perturbative QCD to accurately predict absolute rates in hadronic collisions. We repeated the most significant b quark cross section measurements from Run I in order to clarify the current situation.

The discrepancy between Run I annd Run II events seems to be due to the presence of an additional background that has been suppressed when making the tight SVX requirements on the muon tracks. This background has been studied in detail and can be characterized by the presence of two back-to-back cones containing an anomalousely high number of muons.

Analysis searching for SM production of heavy boson pair in the lepton neutrino jet jet channel, that is sensitive to the WW and WZ processes together, is interesting since these events have the same signature of low mass SM Higgs events. This analysis is a very interesting results since it shows a discrepancy between data and prediction in the distribution of the invarinat mass of the two jets associated to a W boson in the region 145 GeV/c^2 with a statistical significance of 3.5 σ.

2 Calibration of the central hadron calorimeter

The Frascati group played a leading role in the calibration of the central hadron calorimeters, CHA/WHA.

For the WHA calorimeter the original Run I ^{137}Cs Sources system is fully working and therefore it can be used to set the absolute energy scale for all the towers; we have taken two ^{137}Cs Source runs during 2007 and we have accordingly computed a set of Linear Energy Response:

$$LER = \frac{^{137}Cs(test - beam)e^{-\Delta t/\tau}}{^{137}Cs(today)}$$

that have been downloaded in the front end electronics to correct the raw ADMEM counts. This system effectively probes the behavior of the calorimeter since the source runs in front of the inner scintillator plane of the wedges thus irradiating few of the scintillator/absorber layers of the

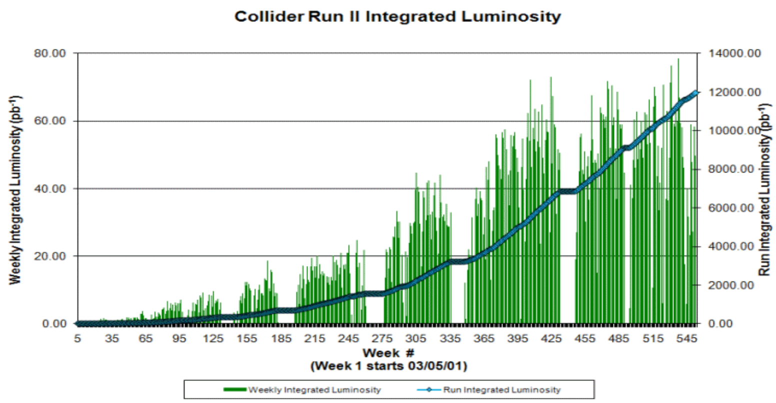

Figure 1: Integrated Luminosity vs time

calorimeter. In this way we monitor aging phenomena of the scintillator together with PM gain variations.

We calibrate the CHA calorimeter looking at the energy deposition of Minimum Ionizing Particles (i.e. muons from J/Ψ decays).

We briefly recall the procedure to set the absolute calorimeter energy scale using Mip's. Looking at μ's from the $\sim$ 81 pb^{-1} dimuon trigger sample collected in Run Ib, we determined the necessary statistics to determine the peaks of μ's hadronic energy, HadE, distributions with enough precision per every CHA tower. With a statistics of $\sim$ 40 pb^{-1} we find that the tower by tower peak is determined with a precision of $\sim$ 1.5%. The LER's correction factors are derived comparing tower by tower the HadE deposition for Run I and Run II mips every 30-40 pb^{-1} of data; the LER at a given time time t are defined as the previous set of LER (t-1) multiplied by the observed ratio of the Mip's at a time t and in Run I:

$$LER(t) = LER^{t-1} \times \frac{MIP(RunI)}{MIP(t)}$$

We look at Mip's peaks response every $\sim$ 100 pb^{-1} and the typical response shows a tiny 1.5% gain variations on average and few channels that drift more than 5%.

The laser system represents a quick tool to follow the trend of the PM's gains. We have continuously acquired laser runs since year 2003 to monitor the gain variations of each photomultiplier; the CHA is stable within $\sim$ 2%.

2.1 ONLINE-OFFLINE energy scale calibration

At CDF with the current luminosity the data are being processed through the OFFLINE reconstruction every couple of months. Before producing the fully reconstructed events from the raw information of the detector we first produce small dedicated calibration samples to derive the calibrations constants for all the sub detectors. Every 6-8 weeks we run an executable called CalibExe which produces all the data ntuples for different data sets, including the dimuon trigger data sample where we reconstruct J/Ψ events; then the various calibrators use these samples to derive the calibrations. We made all this procedure automatic during the year 2006.

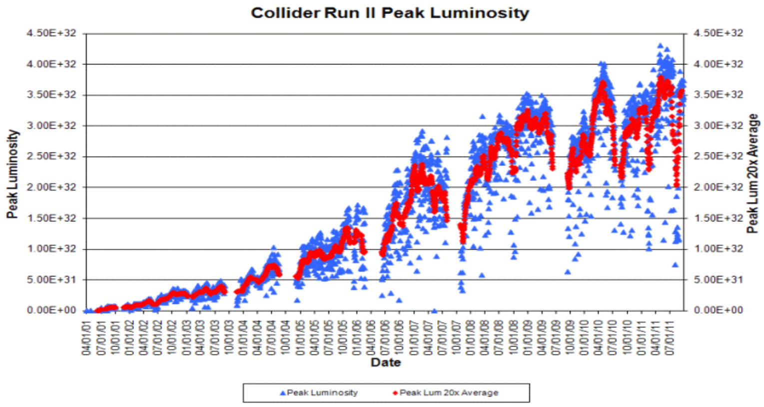

Figure 2: Peak Luminosity vs time

Usually for the Hadron calorimeters we produce two set of calibrations: ONLINE calibrations are directly downloaded in the ADMEM electronics and are intended to correct the energy response for data that have to be acquired afterward; the OFFLINE calibrations attempts to propagate back to the data already acquired the needed corrections. The calibration constants are then filled in appropriate ORACLE data base tables called CHALINERESPONSE and CHAOFFLER. To validate the OFFLINE calibrations, the same data sets are reconstructed again picking the right calibration tables for every run range they have been produced for and the calibrators have to repeat their analysis to check that the calibrations are correct.

With this procedure the calorimeter response is kept constant at $\sim 2\%$ level over the running period.

3 An additional study of multi-muon events produced in $p\bar{p}$ collisions at $\sqrt{s} = 1.96$ TeV

This study reports on one additional test on the possible origin of multi-muon events observed at the Tevatron. These events were identified in a study of a data set acquired with two central ($|\eta| < 0.7$) primary (or trigger) muons, each with transverse momentum $p_T \geq 3$ GeV/c, and with invariant mass larger than 5 GeV/c^2 and smaller than 80 GeV/c^2. That study shows that many long-standing inconsistencies between measured and predicted properties of the correlated $b\bar{b}$ production and semileptonic decay at hadron colliders could be explained by the presence of a relevant source of muons which appear to be mostly produced beyond the beam pipe of radius 1.5 cm (this contribution is whimsically referred to as ghost events because they were unnoticed or ignored by previous measurements). Within the large uncertainty of the prediction, mostly based on simulations, the observed rate of ghost events is found to be consistent with being produced by muons arising from in-flight-decays of pions and kaons, or punchthrough of hadronic prongs from K^0_S or hyperon decays. However, a search in ghost events for additional muons with $p_T \geq 2$ GeV/c and $|\eta| \leq 1.1$ and contained in a $\cos\theta \geq 0.8$ cone around the direction of a primary muon selects a small but significant fraction of events with a large content of muon candidates that appears difficult to account for in terms of known sources with the present understanding of the CDF II detector, trigger, and event reconstruction.

A more recent study by the CDF collaboration has improved the estimate of the contribution of ordinary sources to ghost events. This study addresses in particular the contribution from pion and kaon in-flight-decays. In 1426 pb^{-1} of data, there are 54437 ± 14171 ghost events and 12169 ± 1319 ghost events with three or more muons which cannot yet be accounted for with ordinary sources.

In this analysis, we investigate the distribution of the azimuthal angle ($\delta\phi$) between the two primary muons in events in which both primary muons are accompanied by at least one (or two) additional muon candidates in a $\cos\theta \geq 0.8$ cone around their direction, and compare it to those for all QCD sources known to produce dimuon events: $b\bar{b}$, $c\bar{c}$, and Υ production or events in which one trigger muon is due to hadrons misidentified as muons (cosmic rays are removed from the data sample and the contribution of secondary interactions in the detector volume is negligible. Known QCD sources produce a handful of events with four and none with six muon candidates. However, if the unaccounted multi-muon events were generated by a gross underestimate of the number of additional muons mimicked by hadrons in ordinary QCD events, the $\delta\phi$ distribution of primary muons in multi-muon events would be similar to that of ordinary QCD events in which the large contribution of next-to-leading order (NLO) terms due to initial and final state radiation results in a broader $\delta\phi$ distribution than that predicted by the Born (LO) approximation. In fact, the $\delta\phi$ distribution of pairs of b hadrons or jets is traditionally used to determine the relative contribution of NLO to LO terms. This type of comparison was also suggested by R. Barbieri *et al.,* (J. Phys. G **36**, 115008 (2009)), in which the excess of multi-muon events is modeled with the decay of two colorless particles produced through the exchange of a heavy object. In such a hypothetical case, their deviation from the back-to-back configuration in the azimuthal angle ($\delta\phi = \pi$) is only caused by initial state radiation of the incoming quarks and is expected to be small.

The study presented here uses a dimuon data set corresponding to an integrated luminosity of 3.9 fb^{-1}. High precision charged particle tracking is provided by a large central drift chamber surrounding a trio of silicon tracking devices composed of eight layers of silicon microstrip detectors ranging in radius from 1.5 to 28 cm in the pseudorapidity region $|\eta| < 1$. The tracking detectors are inside a 1.4 T solenoid which in turn is surrounded by electromagnetic and hadronic calorimeters. Outside the calorimeters, drift chambers in the region $|\eta| \leq 1.1$ provide muon identification. We search events for additional muons using tracks with $p_T \geq 2$ GeV/c and $|\eta| \leq 1.1$. The rate of additional muons mimicked by hadronic punchthrough is estimated with a probability per track derived by using kaons and pions from $D^{*\pm} \rightarrow \pi^{\pm} D^0$ with $D^0 \rightarrow K^+\pi^-$ decays. The difference between observed additional muons and predicted misidentifications is referred to as real muons.

The $\delta\phi$ distribution for all 3.9 M events is shown in Fig. 3. Figure 4 compares to the corresponding heavy flavor simulations the $\delta\phi$ distribution of trigger muons due to $b\bar{b}$ and $c\bar{c}$ production. This figure is reproduced from the study that has measured $\sigma_{b\rightarrow\mu,\bar{b}\rightarrow\mu}$ and $\sigma_{c\rightarrow\mu,\bar{c}\rightarrow\mu}$ in a dimuon data set corresponding to a luminosity of 742 pb^{-1}. In the $b\bar{b}$ case, the distribution has an average of 2.5 with a rms deviation of 0.8 rad. The long and important tail extending to $\delta\phi = 0$ is due to NLO terms and the non-perturbative fragmentation function of b quarks. In $c\bar{c}$ events, because of the smaller quark mass, NLO terms are approximately a factor of three larger and the fragmentation function is much softer. Accordingly, the $\delta\phi$ distribution has a smaller average (2.4 rad) and a larger rms deviation (0.9 rad).

The azimuthal-angle distribution for primary muons produced by $\Upsilon(1S)$ decays is expected to be similar to those for heavy flavors because the final state contains a bleaching gluon recoiling against the Υ meson. This distribution, shown in Fig. 5, is constructed using muon pairs with invariant mass in the range $9.28 - 9.6$ GeV/c^2. The combinatorial background under the $\Upsilon(1S)$ signal is removed with a sideband subtraction technique. A similar $\delta\phi$ distribution is also expected for those cases in which one muon is mimicked by a track in the jet recoiling against a muon due to a heavy-quark semileptonic decay. Figure 5 shows the $\delta\phi$ distribution of primary muons when

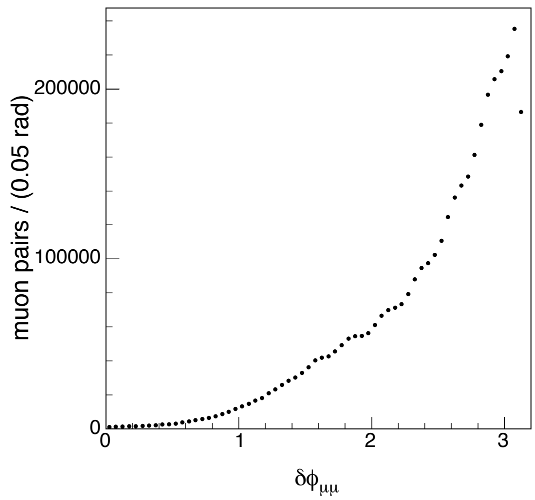

Figure 3: Distribution of the azimuthal angle $\delta\phi$ between the two trigger muons for all events.

one of them is mimicked by pions produced by K^0_S decays. We select $K^0_S \to \pi^+\pi^-$ with a $\pi \to \mu$ misidentification by combining primary muons with tracks of opposite charge and $p_T \geq 0.5$ GeV/c. We select pairs consistent to those arising from a common three-dimensional vertex. We also take advantage of the K^0_S long lifetime to suppress the combinatorial background. We further require that the distance between the K^0_S vertex and the event primary vertex, corrected by the K^0_S Lorentz boost, corresponds to $ct > 0.1$ cm. We select K^0_S candidates with invariant mass in the range $0.47 - 0.52$ GeV/c^2 and remove the combinatorial background with a sideband subtraction technique.

In summary, the $\delta\phi$ distributions of primary muons produced by known QCD processes peak at $\delta\phi \simeq \pi$, and exhibit a significant tail extending to $\delta\phi = 0$. Depending on the production mechanism, the mean and rms deviation of these distributions are in the range of $2.4-2.5$ rad and $0.7 - 0.9$ rad, respectively.

The $\delta\phi$ distributions in the subset of events in which each trigger muon is accompanied by at least one or at least two additional real muons are shown in Fig. 6. These $\delta\phi$ distributions, with mean of 2.9 rad and rms deviation of 0.2 rad and without any tail below $\delta\phi = 2.5$ rad, are different from those of primary muons due to all known QCD sources.

In conclusion, as mentioned earlier, within our present understanding of the CDF-detector response no known sources produce events in which each $\cos\theta \geq 0.8$ angular cone around a primary muon contain at least two additional real muons. Had the additional muons been produced by a subtle failure of our method to evaluate the fake-muon contribution, the resulting $\delta\phi$ distribution of primary muons would have been found consistent with those typical of ordinary QCD processes.

4 Study of the invariant mass distribution of jet pairs produced in association with a W boson

We started in 2009 an analysis searching for SM pair production of heavy boson pairs in the lepton neutrino jet jet channel, that is sensitive to the WW and WZ processes together, that was published

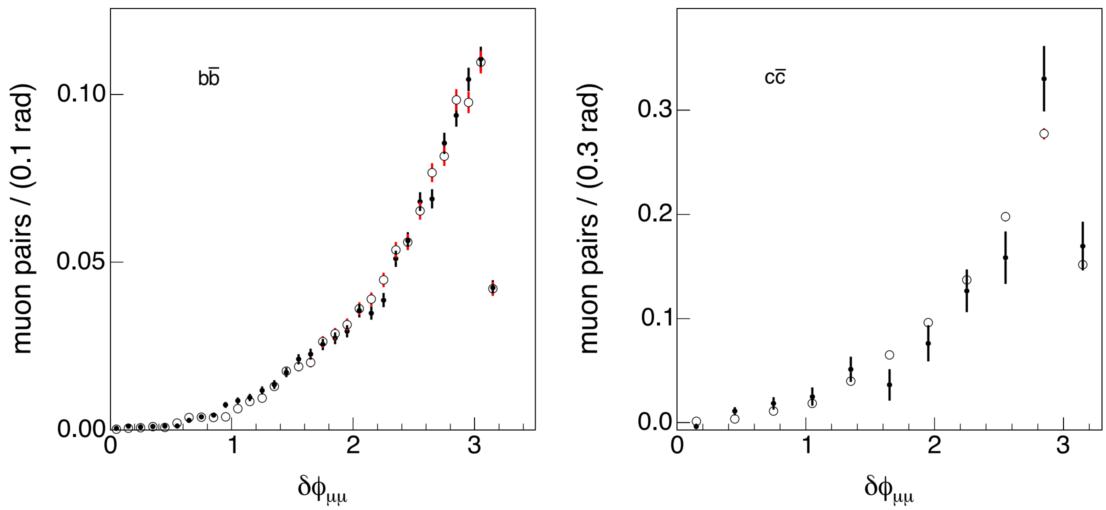

Figure 4: The distributions (•) of the azimuthal angle $\delta\phi$ between trigger muons due to (left) $b\bar{b}$ and (right) $c\bar{c}$ production are compared to the corresponding heavy flavor simulations (∘). Distributions are normalized to unit area.

in [1]. We then further studied this data sample to investigate the properties of an excess of events at a dijet invariant mass of about 150 GeV as seen in figure 7. This work was done in collaboration with Viviana Cavaliere (University of Siena and INFN Pisa, and now with University of Illinois at Urbana-Champaign) and Pierluigi Catastini (Fermilab, and now with University of Harvard).

In this new analysis, we increase the jet E_T threshold to 30 GeV motivated by the interest in a higher invariant mass range. After this selection, which improves the experimental accuracy for jet measurement and reduces the theoretical uncertanties, the excess at 150 GeV becomes more significant. We investigate the modeling of each background component and found that all backgrounds appear well modeled in the control samples. After considering systematics for non-W event modeling, Jet Energy Scale and renormalization/factorization scale for the main W+jets background, we still observe a significant excess in the 120-160 GeV/c^2 region, see figure 8.

We try to model the excess with an additional Gaussian peak and perform a $\Delta\chi^2$ test of this hypothesis. The Gaussian is chosen as the simplest hypothesis compatible with the assumption of a two jet decay of a narrow resonance with definite mass. The width of the Gaussian is fixed to the expected dijet mass resolution by scaling the width of the W peak in the same spectrum: $\sigma_{\text{resolution}} = \sigma_W \sqrt{\frac{M_{jj}}{M_W}} = 14.3$ GeV/c^2, where σ_W and M_W are the resolution and the average dijet invariant mass for the hadronic W in the WW simulations respectively, and M_{jj} is the dijet mass where the Gaussian template is centered. We take the difference between the χ^2 of the two fits ($\Delta\chi^2$), with and without the additional Gaussian structure to assess the significance of the excess. Assuming only background contributions, and systematic errors, the probability to observe an excess larger than in the data is 7.6×10^{-4} corresponding to a significance of 3.2 standard deviations for a Gaussian distribution. A full description of this analysis is available in Ref. [3)].

The excess observed by CDF has been searched by the D0 collaboration in data sample

[1] T. Aaltonen et al. (CDF Collaboration), Phys.Rev.Lett. 104, 101801 (2010). arXiv:0911.4449

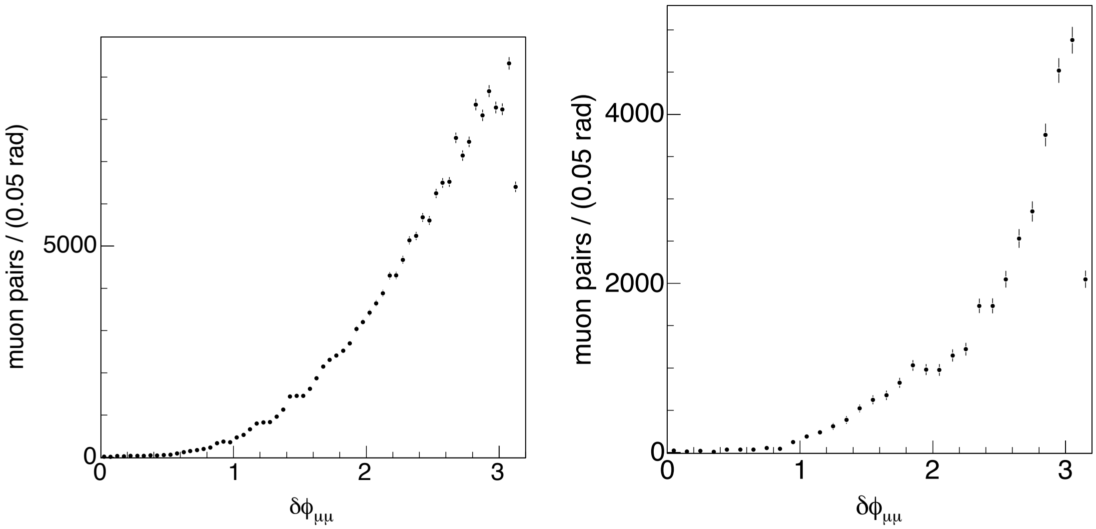

Figure 5: Distribution of the azimuthal angle $\delta\phi$ between the two trigger muons produced by Υ decays (left) and for events (right) in which one primary muon is mimicked by a pion produced by an identified K_S^0 decay. The combinatorial background underneath the Υ and K_S^0 signals has been removed with a sideband subtraction method.

of 4.3 fb^{-1}, as published in [2]. The data is found to be in agreement with the SM background expectations. While some differences are present between the two analyses and the treatment of systematic uncertainties, one can proceed to make a direct comparison on the cross section estimated using an acceptance and efficiency from a MC sample of WH with a Higgs mass of 150 GeV, and using the same luminosity. The cross sections are 0.4 ± 0.8 pb and 3.1 ± 0.8 pb , respectively for D0 and CDF, leading to a difference between the two experiments of approximately 2.5 standard deviations using gaussian approximation for the errors. In conclusion, the D0 analysis doesn‘t confirm the CDF excess. The results of the two experiments show a tension at the level of approximately 2.5 standard deviations.

[2] V. M. Abazov et al. (D0 Collaboration), Phys.Rev.Lett. 107, 011804 (2011). arXiv:1106.1921

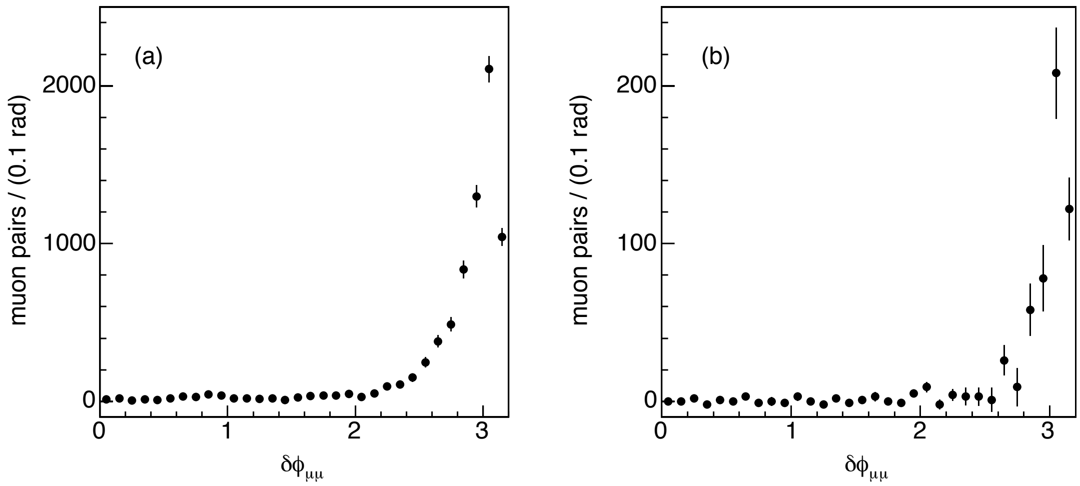

Figure 6: Distribution of the azimuthal angle $\delta\phi$ between the two trigger muons accompanied by at least (a) one or (b) two additional real muons in a 36.8^{deg} cone around their direction.

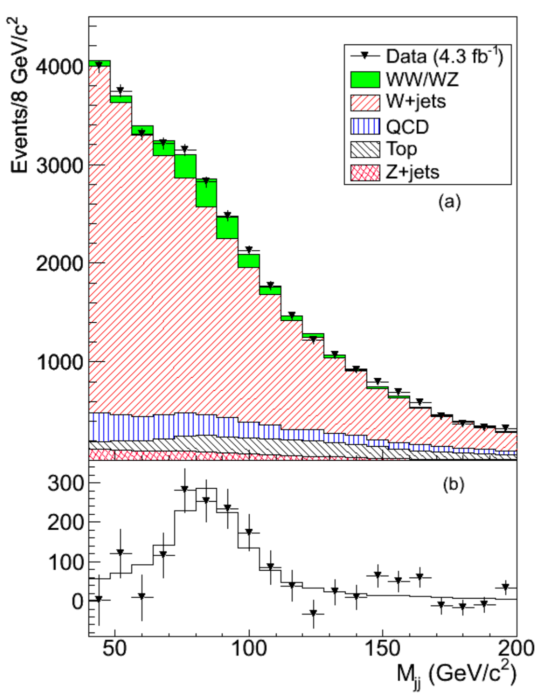

Figure 7: Sum of the electron and muon fit along with background subtracted plot.

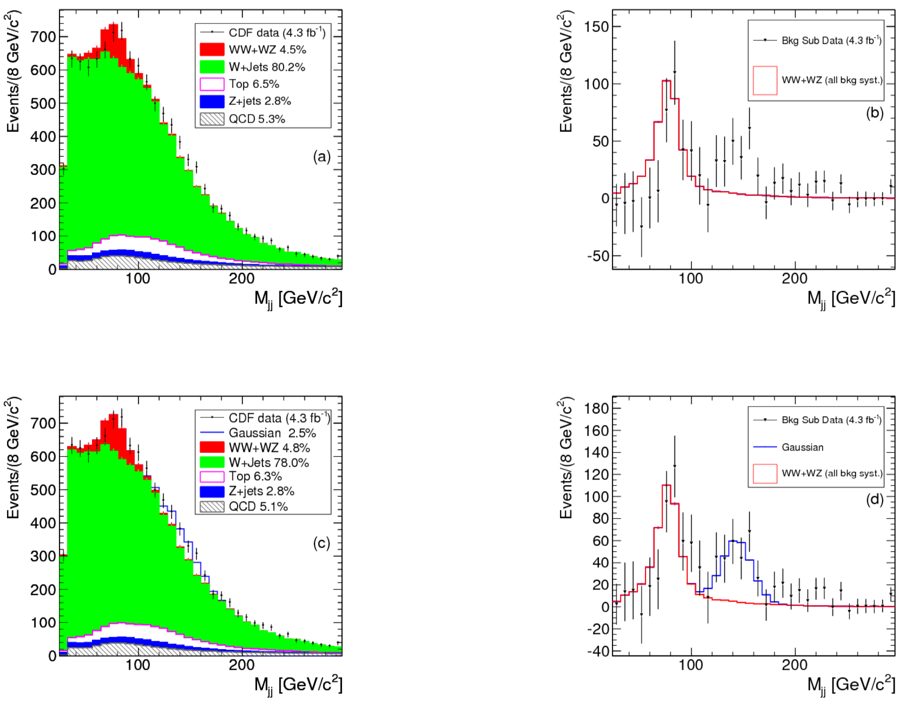

Figure 8: The dijet invariant mass distribution. The sum of electron and muon events is plotted. In the left plots we show the fits for known processes only (a) and with the addition of a hypothetical Gaussian component (c). On the right plots we show, by subtraction, only the resonant contribution to M_{jj} including WW and WZ production (b) and the hypothesized narrow Gaussian contribution (d). In plot (b) and (d) data points differ because the normalization of the background changes between the two fits. The band in the subtracted plots represents the sum of all background shape systematic uncertainties described in the text. The distributions are shown with a 8 GeV/c^2 binning while the actual fit is performed using a 4 GeV/c^2 bin size.

Conferences 2011

- A. Annovi, BSM Results from Tevatron; Presented at Lepton Photon 22-27 August 2011, Mumbai, India

Publications 2011

1. T. Aaltonen *et al.,*[CDF Collaboration] arXiv:1111.5242 An additional study of multi-muon events produced in $p\bar{p}$ collisions at $\sqrt{s} = 1.96$ TeV.
2. T. Aaltonen *et al.,* Eur. Phys. J. C **71**,1720 (2011). Improved determination of the sample composition of dimuon events produced in $p\bar{p}$ collisions at $\sqrt{s} = 1.96$ TeV.
3. T. Aaltonen *et al.* [CDF Collaboration], “Invariant Mass Distribution of Jet Pairs Produced in Association with a W boson in $p\bar{p}$ Collisions at $\sqrt{s} = 1.96$ TeV,” Phys.Rev.Lett. 106 (2011) 171801, arXiv:1104.0699 [hep-ex].

CMS

L. Benussi, S. Bianco (Resp.), M.A. Caponero (Ass.)
S. Colafranceschi (Dott.), F.L. Fabbri (Ass.), F. Felli (Ass.), M. Ferrini (Ass.)
M. Giardoni (Ass.), M. Pallotta(Ass.), M. Parvis (Ass.), L. Passamonti (Tecn.), D. Piccolo
D. Pierluigi (Tecn.), A. Russo (Tecn.), G. Saviano (Ass.), C. Vendittozzi (Dott.)

In collaboration with:
B.Dulach (SPECAS), D.Orecchini (SPECAS),

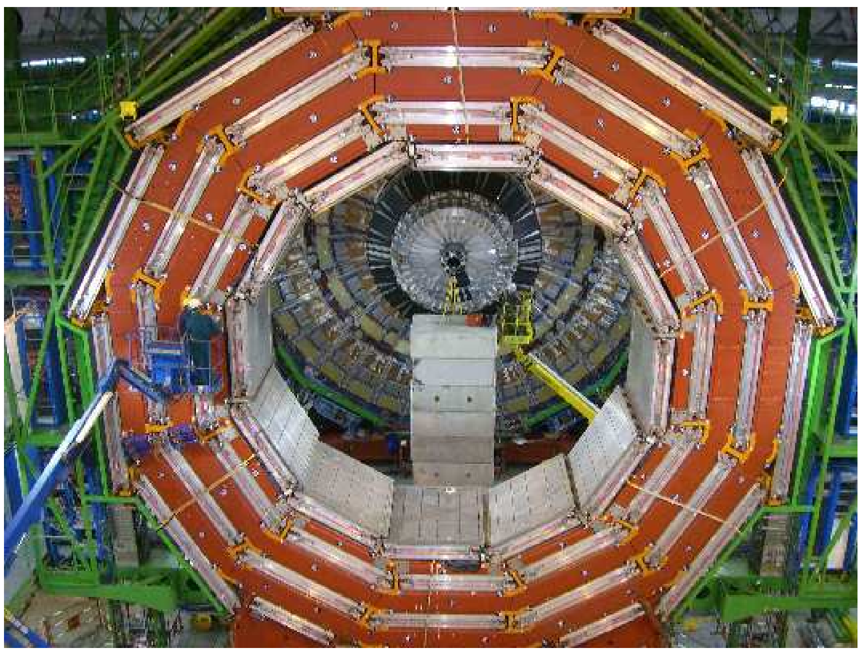

The Compact Muon Solenoid (CMS) experiment [1] will search for the missing block of Nature - the Higgs boson - and for new exotic elementary particles that are predicted by theory and by cosmological observations. The CMS detector uses Resistive Plate Chambers (RPC) as muon detectors, coupled to Drift Tubes in the barrel region, and to Cathode Strip Chambers in the endcaps. The activity of the CMS Frascati groups is centered on various responsibilities in the construction,operating and monitoring the RPC detector, as well as in the quality control of data and physical data analysis.

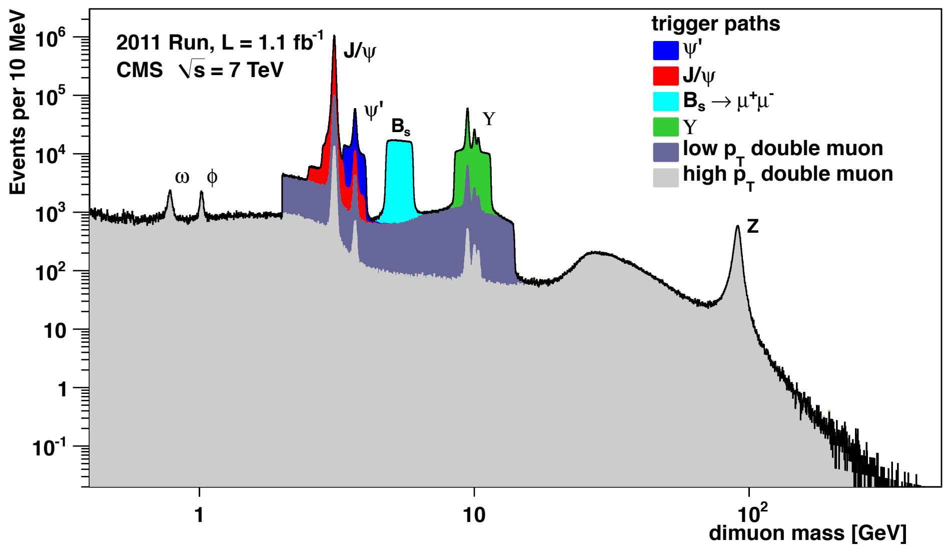

Figure 1: Dimuon spectrum from CMS for a 1 fb^{-1} integrated luminosity.

1 Status of the CMS experiment and the RPC muon detector

The CMS experiment has started data taking in December 2009 and continued successfully over 2010 and 2011. LHC delivered so far 4 fb^{-1} useful for reliable operations and CMS recorded with an overall data taking efficiency larger than 92%, and more than 85% recorded with all subdetectors in perfect conditions. All subdetectors have at least 98% of all channels operational.

CMS published a lot of physics results which are available at

`https://twiki.cern.ch/twiki/bin/view/CMSPublic/PhysicsResults`

Topics covered so far are heavy ions, jet production, HQ production, vector boson production, Higgs searches (Fig.2), searches for supersimmetry(Fig.3), exotic signatures (Fig.4) . For a total of 120 physics analyses approved so far based on 2011 data, 45 papers completed (published, submitted, or close to submission), 29 papers in preparation, 25 analyses to be approved soon.

The excellent performance of the muon system is shown by the dimuon spectrum (Fig.1) which contains very clean signals from all known resonances.

The RPC barrel and endcap systems, which were fully characterized during year 2009 by participating at the CMS global cosmic ray events runs, performed up to specifications in 2010 and 2011. The detector efficiency was measured for each chamber with a resolution of about 100 cm^2, showing a very uniform distribution and an average value above 96% in both the barrel and endcaps region.

The 2011 data-taking was very successfully for both the RPC detector and trigger. The RPC system ran very smoothly in 2011, showing an excellent stability and very high data-taking efficiency.

Thanks to the high LHC luminosity and to the corresponding high number of muons impinging on the muon system, the RPC community had, for the first time, the possibility to calibrate

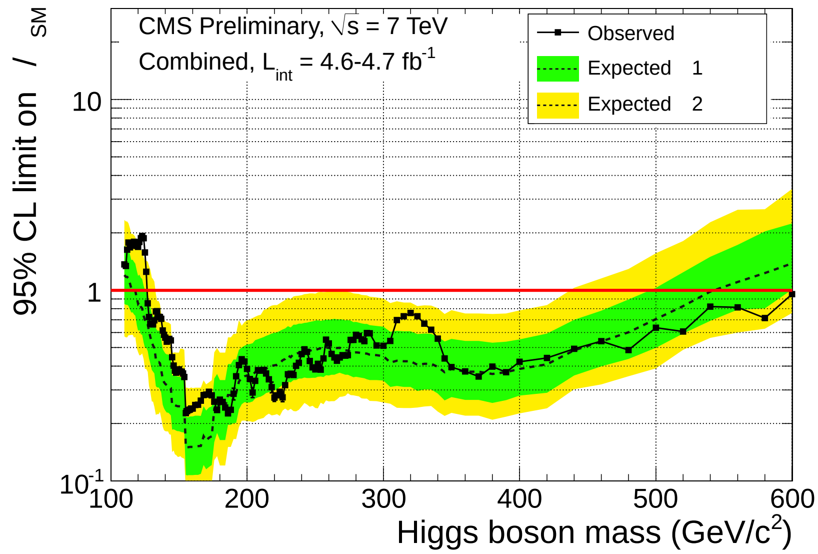

Figure 2: Limits on Higgs searches.

every single detector element (roll) already in the first part of the 2011. In March 2011 9 calibration runs at different HV point were taken, which corresponding to 7 milion of events. The main goal of the RPC calibration was to study the detector parameters as a function of high-voltage working points. Efficiency, cluster size and noise rate were the parameters measured for each roll at different high-voltage values. All these parameters were taking into account to determine the "best" working point (WP), which must sit be in a stable region of the efficiency plateau (pressure variation in one year generates a shifts of the working point up to 200 V). The experimental "plateau curve" was fit with a sigmoid function in order to determine the "best" high-voltage working point for each single roll. In addition the working point should allow to keep the streamer probability and cluster size low in order to not spoil the trigger performances. The 2011 working point (WP) has been defined as the HV voltage at 95% efficiency + 150 V in the endcap region and as WP at 95% efficiency +100 V in the barrel region. The extrapolated average efficiency at WP was greater than 95% and average cluster size was about 1.6. The high-voltage working point is corrected, chamber-by-chamber, for atmospheric pressure variation since July 2011. in order to reduce the efficiency fluctuation. This correction produced a decrease in the fluctuation from 3.5% to 1.5%. Corrections are applied at PVSS level during the stand-by mode (no collision) and are not changed until the next fill. The detector calibration by the HV scan and the pressure correction described before were very important steps towards fine-tuning the stability of the RPC performances.

Detector and trigger configuration and monitoring tools: During 2011, the number of disconnected chambers increased from six to eight corresponding to 0.8% of the full system, while the single-gap-mode chambers increased from 28 to 31. Most of the problematic chambers are due to bad high-voltage connection and electronic failures that can be solved only during the 2013-2014 Long Shutdown. 98.4% of the electronic channels were operational. Two major updates have been made in the RPC PAC trigger. The muon candidate in the barrel is generated if at least three layers out of the six available are fired (four layers were required in 2010). This modification

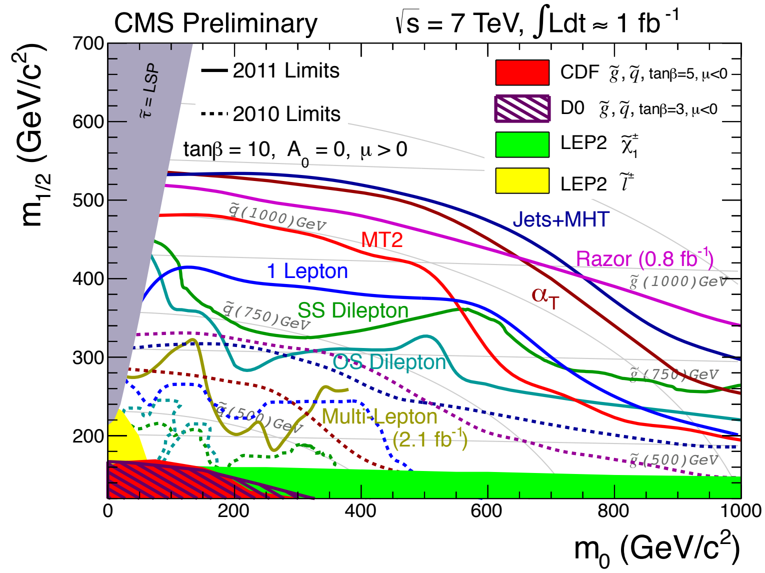

Figure 3: Limits for SUSY particles in the Minimal Supersymmetric Standard Model.

increased the RPC PAC trigger efficiency in the barrel by a few percent. The goal of the second modification of the algorithm (applied at the end of May 2011) is to allow the triggering of "slow" particles (like heavy stable charged particles), which reach the muon system in the next BX. The PAC now looks for the coincidence of hits in two consecutive BXes (the RPC chamber hits inside the PAC are extended to one additional BX). Another important improvement has been the development of a new procedure to configure the electronic front-end boards. All the thresholds and widths are now loaded automatically by the database and provide a very easy way to fine-tune the thresholds and improve the speed of the configuration. This was the last step to have the full RPC detector automatically configured and further reduce dead time. A new version of the RPC web-based monitoring (WBM) has been released in October. It includes many new summary plots and results about the dark current, background and environmental parameters that help us a lot in monitoring our system.

The average detection efficiency in 2011 was about 95%, and the average cluster size was about 1.6. Those values confirm the ones obtained during measured during the HV scan done at the beginning of the 2011 data-taking and the stability of the system all over the year. Data loss for RPC was about 0.37%, corresponding to 19 pb^{-1}. Efficiency has been monitored run-by-run, with DQM and dedicated offline analysis in order to study the stability of the system.. The rate of background and of the detector current has been shown in 2011 a linear dependence of on luminosity. The maximum values of these correlated quantities are 1.3 Hz/cm^2 and 10 mA per chamber and are mostly in the external disks of the endcap region. Average intrinsic noise, measured without beam, is stable at 0.1 Hz/cm^2 and dark current (no beam) is still around 1 mA. The extrapolation of the rate and of the current at 10^{34} cm^{-2}s^{-1} has shown that all the chambers are still far away from the theoretical limit of 100 mA and 100 Hz/cm^2.

Activity is in progress for the RPC upgrade. CMS was designed to have six concentric layers of chambers in the barrel part and four layers for the each end caps to cover a rapidity

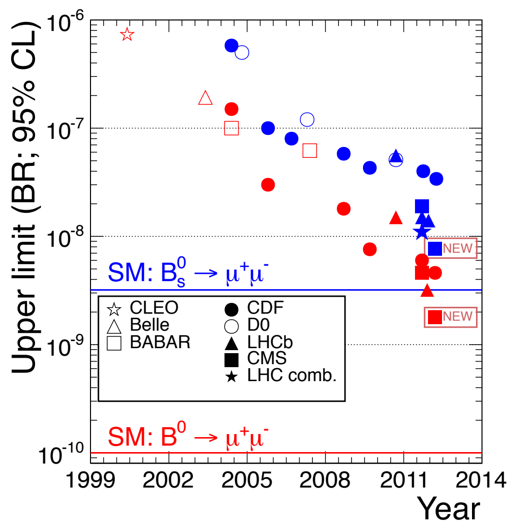

Figure 4: Limits for rare decay of B meson to dimuon.

up to $\|\eta\| = 2.1$. Due to insufficient funding availability, only 3 layers were built in the endcap which provided a limited rapidity coverage up to $\|\eta\| = 1.6$. The completion of the forward RPC system to 4 layers per end cap is therefore a priority for the shutdown 2013-2014. The 4th layer is composed of two concentric rings (RE4/2 and RE4/3) of RPC chambers. The new RPC chambers will be of the standard CMS forward design. The total number of chambers needed is 144 (plus spares). In 2011 the project, his organization and time schedule was completely defined. The Engineering Design Review (EDR) was held on November 24th. The feedback from both CMS and external referees was very positive. The project is on schedule. The first set of bakelite sheets were produced in Italy, qualified by the Pavia group, and delivered to Korea, which will produce all the 660 gaps, at the end of 2011. The Korean gap production site was completed in middle of 2011 and the plan is to have 30 gaps produced in March 2012 and sent to the three test sites (Ghent, Mumbai/Chandigarh and CERN). Production of on-detector electronics (Front-end boards, control boards and adapter boards) started in Pakistan. In 2011 all components ordered and test bench prepared. Concerning the off-detector electronics the design of link system (link between front-end and readout electronics) was reviewed to house the voltage regulators on the new link and control boards in order to protect them from possibly spike signal from power system.The design and production is under INFN responsibility.

The monitoring of gas system, the gas gain monitoring system and purifier studies are responsibilities of the Frascati group. The CMS RPC muon detector uses a huge volume of expensive gas mixture. This has demanded the need for a gas recirculation system (Closed Loop) with filters for gas purification. The CL system has been in operation since years with performance meeting specifications. All modules of the gas system (primary supply, mixer, purifier module I e II, humidifier, pump, pre-distribution and distribution) have been operational in closed loop mode since mid 2008. The clean mix fraction is about 10%. The system is integrated in DCS PVSS. Both IR analyzer for isobutane and $O_2 + H_2O$ analyzer have been installed and are operational. The gas quality monitoring system (gas cromatograph and electrodes) are operational and routinely used to check the mix composition and presence of major pollutants. The gas system is stable and no currents increase have been observed due to closed loop mode. During year 2011 the activity at the scaled-down closed loop system in the ISR test area has continued for full characterization of purifiers. The CL system ran smoothly during the collision runs over the entire 2011.

2 Activity of the CMS Frascati group in 2011

The Frascati group has joined CMS in the RPC muon detectors at the end of year 2005. The Frascati group contributes to the electroweak studies, namely in the measurement of the Z cross section in the dimuon channel. Frascati is responsible for the Gas Gain Monitoring system, RPC materials studies, and the test of the Closed Loop recirculation system for characterization of gas purifiers.

Frascati has rapidly harmonized with the RPC group, and the quality of work provided was rapidly recognized by the RPC collaboration which, during 2011, decided to ask members of the Frascati group to cover L2 responsibilities such as DPG coordinator and Run coordinator. Such responsibilities were crucial for both the successful running of the RPC detector during the data taking, and for the quality of data collected. Prime tasks managed by Frascati physicists during operation and data quality monitoring were the HV feedback, the determination of efficiencies via systematic HV scans, and monitoring of working point via the GGM system.

2.1 Physics analysis

The Frascati group completed the CMS Electroweak Analysis group and is involved in the study of the measurement of inclusive $Z \to \mu^+\mu^-$ cross section. This process is characterized by a clear signature in an almost free background environment and has been studied since the arrival of the first colliding beams.

The work has been focused on the development of methods to select events and measure reconstruction and trigger efficiencies directly from data. An original method has been proposed which consists in five different categories of Z candidates according to the way the muons have been reconstructed (tracker track, standalone muon detector system, combined track+standalone muon) and trigger topologies.

A fit of Z production yield, reconstruction and trigger efficiency is then performed simultaneously on the five categories, thus allowing to extract all the needed information in a single step. This method has been showed to be very robust in handling also a low statistical sample as could be expected in case of few $\mathrm{pb}^{-}1$ of integrated luminosity collected.

2.2 Gas Gain Monitoring System

The Gas Gain Monitoring (GGM) system of RPC detectors in CMS monitors the changes in working point due to gas variations, by means of monitoring of anodic charge in small RPC gaps in a cosmic ray telescope. The system is composed of three subsystem of RPC single gaps, readout by 45cm x 45cm pads in a cosmic ray telescope located in the SGX5 gas building. Each subsystem is flushed with a different gas. The Reference subsystem is flushed with fresh open loop gas mixture. The MonitorOut subsystem is flushed with CL gas downstream of CMS RPCs. The MonitorIn subsystem is flushed with CL gas upstream of CMS RPCs. Each subsystem is composed of three gaps, whose high voltage is set to the standard working point voltage at the efficiency knee, and to

200 V above and below the knee respectively. Each cosmic ray track therefore provides completely correlated pulses in the three subsystems, allowing one to study the differential response of gaps and by disentangling any effect due to changes in the gas mixture. In case a working point change is detected, an alarm condition is released and the gas quality monitoring system will verify what the change of work point is due to.

The system was located in the SGX5 gas room of CMS in December 2008 and operated before the January 2009 shutdown. During 2008 the GGM was operated at the scaled down closed loop gas system in the ISR test area. The large experience allowed one to determine both sensitivity to working point changes and cancellation algorithms for changes due to environmental variables. Results have been presented at RPC07 and IEEE08. At the end of 2008 the integration of GGM with the CMS DCS-based monitoring has started, with data exchange with PVSS and data save to the OMDS online database. A beta-release control panel was released in December 2008. The system has been integrated during 2009 in the CMS DCS system. Data on operational experience in 2009 have been published. A novel model based on neural networks for the modellization of RPC response was developed on data from the GGM.

The GGM performed up to specifications over the entire 2010, with limited down times due mainly to technical software interventions while finalizing the full integration with the CMS CDS framework. At the end of 2010 one out of twelve chambers showed reduced efficiency, and, while still operated at higher voltage, it was planned to be replaced at the beginning of 2011.

A proposal for PRIN was submitted and approved at the end of 2009. The PRIN will study optical fiber sensors for gas contaminants detection, in collaboration with Politecnico Torino and Sapienza Università di Roma.

3 Activity planned for 2012

The main activity in 2012 will be the physics analysis, participation to data taking shifts and operation of the RPC detector. The test at the scaled down Closed Loop system will continue in at high-radiation environment at the GIF facility. At the GIF, optical sensors for contaminants detection will be developped in the framework of the PRIN project approved and funded.

A new analysis on single-top production will be started, sensitive to new physics contributions. The Frascati group will join the working group for the measurement of the production cross section of single top in the s channel. Top quark production proceeds via W-exchange, with following W decay to top and bottom quarks. The cross section is therefore sensitive to the presence of new physics, such as W' exchange. Furthermore, the measurement is directly related to the CKM matrix element V_{tb}.

Studies for medium and long-term upgrades of the RPC detector have been finalized in collaboration with the SPECAS service of Frascati. A simulation study was performed to verify the possibility of doubling the gaps in the inner layer of the barrel RPC, in order to add an orthogonal coordinate. Work on the option of installing a GEM detector in the forward region was started. Finally, the Frascati group will contribute to the construction and installation of a fourth endcap disk, so far missing (upscope), by installing FBG sensors for temperature, humidity and gas contaminants, participation to design of and testing link boards trigger electronics, upscope of distributors in gas system.

4 Conference Talks by LNF Authors

1. S. Bianco, New results on searches for Supersymmetry and Beyond the Standard Model physics from ATLAS and CMS, presented at LC11, September 30th, 2011, Trento (Italy).

2. M.Caponero et al., Sensors for Temperature monitoring in HEP detectors, TIPP 2011 Chicago IL USA.

3. S. Colafranceschi et al., Construction and Performance of Large-Area Triple-GEM Prototypes for Future Upgrades of the CMS Forward Muon System, 2011 IEEE Nuclear Science Symposium and Medical Imaging Conference, 23-29 October 2011, Valencia, Spain.

4. S. Colafranceschi et al., Construction and Performance of full scale GEM prototypes for future upgrades of the CMS forward Muon system 2011 IEEE Nuclear Science Symposium and Medical Imaging Conference, 23-29 October 2011, Valencia, Spain.

5. S. Bianco, Experiment Summary, plenary talk delivered at HADRON11, Münich, Germany, June 2011.

5 Theses

S. Colafranceschi, Material studies in the CMS RPC muon detectors, Sapienza Università di Roma (2011).

6 Preprints

1. M. Tytgat *et al.*, “Construction and Performance of Large-Area Triple-GEM Prototypes for Future Upgrades of the CMS Forward Muon System,” arXiv:1111.7249 [physics.ins-det].

2. D. Abbaneo *et al.*, “Test beam results of the GE1/1 prototype for a future upgrade of the CMS high-η muon system,” arXiv:1111.4883 [physics.ins-det].

7 Papers

1. For the listing of CMS papers in 2011 see /www.slac.stanford.edu/spires/

2. L.Benussi et al., Modified POF Sensor for Gaseous Hydrogen Fluoride Monitoring in the Presence of Ionizing Radiations Instrumentation and Measurement, IEEE Transactions on Nuclear Science, Volume: PP Issue:99 On page(s): 1 - 8 ISSN: 0018-9456 Digital Object Identifier: 10.1109/TIM.2011.2175821

8 Volumes

L. Benussi, S. Bianco, D. Piccolo and D. Rebuzzi (Eds.), “Heavy quarks and leptons. Proceedings, 10th Nicola Cabibbo International Conference, HQL 2010, Frascati, Italy, October 11-15, 2010” *PoS HQL2010 (2011) nonconsec. pag.*

References

1. CMS Collaboration home page is /cms.cern.ch/.

2. R. Adolphi *et al.* [CMS Collaboration], "The CMS experiment at the CERN LHC," JINST **3** (2008) S08004

3. M. Abbrescia et al., Nucl. Instr. And Meth. A533 (1994) 102-106; M.Abbrescia et al., Nucl. Instr. And Meth. A515 (1993) 342-347.

4. M.Abbrescia et al., HF production in CMS Resistive Plate Chambers, submitted to NIM, presented by R.Guida at the RPC Conference, Seoul (Korea) 2005.

5. M.Abbrescia et al., Proposal for a systematic study of the CERN closed loop gas system used by the RPC muon detectors in CMS, Frascati preprint LNF-06/26(IR).

6. M. Abbrescia *et al.*, "Gas analysis and monitoring systems for the RPC detector of CMS at LHC", presented by S.Bianco at the IEEE 2006, San Diego (USA), arXiv:physics/0701014.

KLOE/KLOE-2

The KLOE/KLOE-2 Collaboration at the LNF

D. Babusci, G. Bencivenni, C. Bloise (Resp.), F. Bossi, P. Campana, G. Capon (Ass.), S. Cerioni (Tecn.), P. Ciambrone, E. Czerwinski (Bors. PD), E. Dane' (Art. 23), E. De Lucia, P. de Simone, D. Domenici (Art. 23), J. Dong (Bors. EU), M. Dreucci (Art. 2222), G. Felici, G. Fortugno (Tecn.), C. Gatti, S. Giovannella, F. Happacher, E. Iarocci (Ass.)*, M. Iannarelli (Tecn.), J. Lee-Franzini (Ass), B. Leverington (Bors. PD), M. Martini (Ass)**, S. Miscetti, V. Patera (Ass.)*, G. Pileggi (Tecn.), B. Ponzio (Tecn.), R. Rosellini (Tecn.), F. Roukoutakis (Bors. EU), P. Santangelo, A. Saputi (Tecn.), I. Sarra (Dott.), F. Sborzacchi (Tecn.), B. Sciascia, A. Sciubba (Ass)*, E. Turri (Tecn.), G. Venanzoni, R. Versaci (Ass. Ric.)

**Also Dipartimento di Energetica, "Sapienza" University, Rome, Italy*

***Also Dipartimento di Scienze e Tecnologie applicate, "Guglielmo Marconi" University, Rome, Italy*

1 Overview of the experimental activities

In year 2011 the KLOE detector has been operated to follow the machine commissioning providing the necessary feedback to DAΦNE in terms of luminosity, background levels, and characterization of the beams in the interaction region (IP1). Unfortunately, for severe faults occurred first in the injection septum of the positron ring, and afterwards in the cathode of the LINAC, the machine commissioning was tremendously delayed avoiding the scheduled data taking. Major progress towards machine commissioning was only achieved in November and December when DAΦNE reached a specific luminosity of $1.4{\cdot}10^{32}$ cm^{-2} s^{-1} and was able to deliver 6/pb/day with circulating currents of 0.9 A of electrons and 0.7 A of positrons. The machine background during injection often was at a rate level of 800 kHz in the low theta region of the calorimeter endcaps.

At least a factor of two in delivered luminosity, a reduction of background levels to countings of 200-300 kHz in the hot region of the endcaps, and the onset of stable operational conditions, are needed for proper data taking at KLOE-2.

The detector operation has required continuos maintenance work in addition to the shifts for data taking and the updating of the procedures for detector calibration and data reconstruction.

A major update of the archiving system was due in order to store (and recall) data to CNAF, because of the contamination by biological agents of the automated library at the LNF. Data move from the contaminated to an old library, properly upgraded, was successfully accomplished in November and December.

The tagger system for γ–γ events has been worked on, studying the response of the LET calorimeters, and measuring the background level in the HET position while progressing in the realization of the final HET stations and readout system.

The construction of the upgrades of the KLOE apparatus has progressed: the first layer of the Inner Tracker (IT) was completed and tested; the design of CCALT has been finalized, the crystals ordered and the mechanics realized at the INFN workshop in Naples; the design of the QCALT PCB boards revised, a first quarter of QCALT components realized, i.e. tiles, fibers and absorbers. A summary of the achievements for the IT construction is given in Sec.5. Sec.6 presents the results of the test–beam for the characterization of the LYSO crystals for the LET stations of the taggers and CCALT, calorimeters at low polar angle.

Besides the publication of the papers in Refs. [1, 2, 3], other analyses have been finalized and presented to the EPS-HEP Conference in Grenoble, namely i) the measurement of the hadronic cross section normalized to radiative di-muon events, summarized in Sec.3 together with recent achievements in the field of γ–γ physics; ii) the results of the searches for the U-boson in the mass range 5–470 MeV, discussed in Sec.4 and iii) a new limit on the CP-violating process, $K_S \to \pi^0\pi^0\pi^0$, reported in Sec.2.

2 Kaon physics: results and prospects

The KLOE experiment has measured most of the decay branching fractions (BR) of K_S, K_L and $K^\pm$ mesons, providing precision results on the CKM parameter V_{us}, and the most sensitive unitarity test of the quark flavor mixing matrix. We are presently finalizing i) the analysis of the BR($K^\pm \to \pi^+\pi^+\pi^-$) that completes the measurements of the kaon dominant BR's, and ii) the update of the upper limit published in year 2005 [4] on the BR($K_S \to 3\pi^0$).

The neutral kaon system offers the unique opportunity to perform tests of CPT invariance and quantum mechanics (QM). In particular, a new analysis of the KLOE data is in progress to test CPT and Lorentz symmetries in the framework of the Standard-Model Extension (SME), exploiting the EPR correlation in the neutral kaon pairs produced at the ϕ-factory. The ongoing analyses and the prospects for further improvements in sensitivity on kaon physics with the KLOE-2 experiment are summarized in the following paragraphs.

2.1 $K^+ \to \pi^+\pi^+\pi^-$

The BR($K^+ \to \pi^+\pi^+\pi^-$) was obtained with 4% relative precision and a new measurement at 0.5% level has an impact on the semileptonic decays (thus on $f_+(0)\,V_{us}$) and on the $\pi\pi$ scattering lengths from the $K^\pm \to \pi^\pm\pi^0\pi^0$ cusp analysis. The ongoing study of the $K^+ \to \pi^+\pi^+\pi^-$ decay is based on i) the selection of K^+ candidates (tagging procedure) by the identification of $K^- \to \pi^-\pi^0$ and $K^- \to \mu^-\nu$ samples, independently treated; ii) the reconstruction of the K^+ path from the kinematical constraints given by the K^- momentum and ϕ momentum (from Bhabha–scattering events); ii) the backward extrapolation of any charged track not belonging to the K^- decay chain; iii) the reconstruction of the track closest-approach point ($\mathbf{CA}_i$) and closest-approach distance (CAd_i) to the K^+ path; iv) the selection of events with at least two tracks with $\mathrm{CAd}_i \leq 3\ cm$ and $\mathbf{CA}_i$ outside the drift chamber (DC) (for a better control of systematics from tagging procedure); v) the measurement of the missing–mass distribution, $M^2_{miss} = \Delta^2\ E_{K^+-\pi\pi}$ - $|\Delta\ \mathbf{P}_{K^+-\pi\pi}|^2$. The tagging procedure affects the selection efficiency of the $K^+ \to \pi^+\pi^+\pi^-$ sample introducing a bias (tag–bias) on the BR measurement that has been evaluated by Monte Carlo simulation and controlled by the comparison of the two tagging channels. A further control of the tag–bias is in progress, by the selection of a third tagging sample based on the K^- identification through the dE/dx measurement in the DC. The selection efficiency of the $K^+ \to \pi^+\pi^+\pi^-$ sample ($\sim 7\%$) is obtained from the study of a control sample of $K^+ \to \pi^- X$. A fit to the missing–mass distribution with the Monte Carlo shapes for signal and residual backgrounds (1% level of contamination by other decays almost uniformly distributed in the M^2_{miss} range of interest) is used for the event counting. From the analysis of a subsample of 174/pb we obtained a relative error on the absolute BR of 0.6% that we are checking to assess the various contributions.

2.2 $K_S \to \pi^0\pi^0\pi^0$

The CP-violating transition $K_S \to \pi^0\pi^0\pi^0$ is expected with a BR of $1.70(2)\times10^{-9}$. KLOE has obtained the upper limit BR($K_S \to 3\pi^0$)$\leq 1.2 \times 10^{-7}$ at 90% C.L. using a sample of 450/pb [4]. The main background source is given by incorrectly reconstructed $K_S \to \pi^0\pi^0$ decays, when the photon-energy deposit in the calorimeter is reconstructed as split clusters, or additional photons from machine background are assigned to the K_S decay. The result, a factor of ten better than the previous upper limit, has allowed KLOE to increase the sensitivity on the CP and CPT parameters using the unitary condition (Bell-Steinberger relation) as explained in Ref. [5]. Since then, further improvements on the clustering procedure to recover erroneously-split photon clusters are proven to reduce contamination by a factor of six while leaving the signal efficiency unaffected. The ongoing analysis proceeds through i) the selection of K_S candidates by the identification of K_L interactions in the calorimeter requiring an energy releaseΔE $_K$ >129 MeV and 0.196< β_K <0.250; ii) the selection of events with six prompt neutral clusters (not connected to any track in the DC and with times compatible with the hypothesis of photons from the interaction region); iii) the χ^2_{evt} evaluation with the measurements of the position, energy and time of each photon constrained by total energy-momentum conservation: the events with χ^2_{evt} >35 are rejected; iv) the evaluation of $\chi^2_{3\pi}$ and $\chi^2_{2\pi}$ with the measurements of the position, energy and time of each photon in the hypothesis of $K_S \to 3\pi^0$, and $K_S \to 2\pi^0$ plus two additional clusters from machine background, respectively. The candidates are those with $\chi^2_{3\pi}$ ≤4.6 and 12≤ $\chi^2_{2\pi}$ ≤60; v) the rejection of events that in the second hypothesis at point iv have a total energy Etot$_{2\pi}$ >(510 MeV - 1.7σ_E); vi) the evaluation of the minimal distance among photon clusters in the event, keeping as candidates those with R$_{min}$ >65 cm. The selection efficiency is obtained from Monte Carlo simulation, $\epsilon_{3\pi} = 0.19(1)$. From the selected sample at point i) the $K_S \to 2\pi^0$ events are also identified ($\epsilon_{2\pi} = 0.660(3)$) and used as normalization for the BR($K_S \to 3\pi^0$) measurement. No candidate survives the analysis selection, and 9.0×10^7 $K_S \to 2\pi^0$ decays are found in the tagged sample. The preliminary result for the upper limit, on 1.7/fb of integrated luminosity, is BR($K_S \to 3\pi^0$) <2.9 10^{-8} at 90% C.L., a factor of 4 better than the previous KLOE result. Studies are in progress to evaluate the increase in acceptance at KLOE-2, with the installation of the crystal calorimeters at low angle [6], and the improvement in tagging efficiency from the addition of K_L decay samples. This is important, together with the background suppression obtained by the ongoing analysis, in the perspective of a first evidence of the process at KLOE-2.

2.3 QM and CPT test with neutral kaon interferometry

Several tests of QM and CPT invariance have been performed at KLOE, where time evolution of the neutral kaon pairs is sensitive to decoherence phenomena, and to the breakdown of CPT symmetry dealt with in the standard Lorentz–symmetry–violating Extension of the Standard Model (SME) [6]. The first evidence of the interference has been obtained in year 2006. Since then, more data have been analyzed and improvements in the analysis procedures have brought the results on decoherence and CPT-violating parameters presented in Ref. [7]. An analysis of the K_S $K_L \to \pi^+\pi^-\pi^+\pi^-$ final state is in progress to improve on the SME parameters, through the measurement of the decay amplitude as a function of the delay between kaon decays, ordered according to the quadrant in the celestial coordinate frame. The reconstruction of events in the region Δt∼0 is crucial for the precision measurement of the interference term and the inner tracker, that is being constructed, will improve the resolution from $\sigma_{\Delta t} \sim \tau_S$ to $\sim 0.3\tau_S$, and the sensitivity to most of the QM and CPT tests by a factor of 2. The physics reach on kaon interferometry at KLOE-2, up to a factor of ten better than present data, is summarized in Ref. [6].

3 Results on hadron physics

The most recent results on hadron physics include the measurement of i) the hadronic cross section normalized to the radiative di-muon events; ii) the rare decays $\eta \to \pi^+\pi^-\gamma$ and $\eta \to e^+e^-e^+e^-$; iii) the single-η and the $\pi^0\pi^0$ production in γ–γ fusion processes.

3.1 Hadronic cross section

In year 2005 and 2008 KLOE published two measurements (labelled KLOE05, KLOE08) of the $\pi^+\pi^-$ cross section with the photon emitted at small angle, and an independent measurement (labelled KLOE10) of the $\pi^+\pi^-$ cross section with the photon at large angle using data at 1 GeV (*i.e.* 20 MeV below the ϕ-peak) was published in year 2011. While such measurements were normalized to the DAΦNE luminosity using large angle Bhabha scattering, a new analysis has been performed which derives the pion form factor directly from measuring the bin-by-bin $\pi^+\pi^-\gamma/\mu^+\mu^-\gamma$ ratio. The preliminary results (labelled KLOE11) on the pion form factor and the related hadronic contribution to the muon anomaly have been presented for the first time at the EPS-HEP Conference in Grenoble, in July 2011.

The anomalous magnetic moment of the muon, a_μ, is one of the best known quantities in particle physics. Recent theoretical evaluations [8] show a 3–σ discrepancy with the value obtained from the g-2 experiment at Brookhaven [9]. A large part of the uncertainty on the theoretical estimate comes from the leading order hadronic contribution $a_\mu^{\rm had,lo}$, which at low energy can not be calculated from perturbative QCD but must be evaluated through the dispersion integral using the precision measurements of the hadronic cross section as input. The radiative events with initial state radiation (ISR) have been used to obtain the hadronic cross section as a function of the momentum transfer at the kaon and B factories that run at fixed energies [10]. The region below 1 GeV, which is accessible with the KLOE experiment, is dominated by the $\pi^+\pi^-$ final state and contributes with $\sim 70\%$ to $a_\mu^{\rm had,lo}$, and $\sim 60\%$ to its uncertainty. Therefore, improved precisions in the $\pi\pi$ cross section result in reduction of the uncertainty on the leading order hadronic contribution to a_μ, and thus on the Standard Model prediction.

The $\pi\pi$ cross section can be extracted from the $\pi^+\pi^-\gamma/\mu^+\mu^-\gamma$ ratio [11]:

$$\sigma_{\pi\pi(\gamma)} = \sigma_{\mu\mu(\gamma)} \frac{{\rm d}\sigma_{\pi\pi\gamma}/{\rm d}s'}{{\rm d}\sigma_{\mu\mu\gamma}/{\rm d}s'} = \frac{4\pi\alpha^2}{3s'}(1+2m_\mu^2/s')\beta_\mu\ \frac{{\rm d}\sigma_{\pi\pi\gamma}/{\rm d}s'}{{\rm d}\sigma_{\mu\mu\gamma}/{\rm d}s'}, \tag{1}$$

where s' is the 4-momentum square of the virtual photon, i.e. the e^+e^-center-of-mass energy squared after ISR emission, m_μ is the muon mass, β_μ, β_π are the muon and pion velocities in the center-of-mass frame, ${\rm d}\sigma_{\pi\pi\gamma}/{\rm d}s'$, ${\rm d}\sigma_{\mu\mu\gamma}/{\rm d}s'$ are the $e^+e^- \to \pi^+\pi^-\gamma$, $e^+e^- \to \mu^+\mu^-\gamma$ differential cross sections. In Eq. (1) Final State Radiation (FSR) terms are neglected, while they are properly taken into account in data analysis. The integrated luminosity and the radiation function completely cancel out in the ratio, as does the vacuum polarisation.

Eq.(1) has been used to extract the pion form factor via a bin-by-bin ratio between the observed pion and muon ISR differential cross sections.

The same sample of 239.2/pb of KLOE08 was analyzed with the small angle photon selection. While the analysis of the $\pi\pi\gamma$ sample is the same for the two measurements, the analysis of the $\mu\mu\gamma$ events is based on i) the separation between $\mu\mu\gamma$ and $\pi\pi\gamma$ obtained assuming as final state two equal–mass (M_{TRK}) charged particles and one photon: the $M_{TRK} < 115$ MeV ($M_{TRK} > 130$ MeV) cut leads to 9×10^5 (3.1×10^6) candidates of $\mu\mu\gamma$ ($\pi\pi\gamma$) events. The selection is controlled via comparison with other criteria, such as kinematic fit or tight cuts on the charged track quality, all bringing to consistent results; ii) trigger, particle identification and tracking efficiencies checked with data control samples. The measurement of the $\mu\mu\gamma$ cross section (KLOE11) has been compared and found in good agreement with the PHOKHARA MonteCarlo [11]. The table in Fig.1 contains the $a_\mu^{\pi\pi}$ predictions using as input the KLOE results. The pion form factor obtained is consistent with the other measurements, as shown in Fig. 1), and confirms the 3–σ discrepancy between the experimental value and the Standard Model prediction of a_μ.

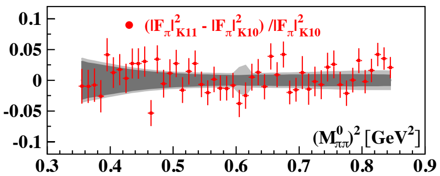

Analysis	$a_\mu^{\pi\pi}(0.35 - 0.85\ \mathrm{GeV}^2) \times 10^{10}$
KLOE11	$376.4 \pm 1.2_{\mathrm{stat}} \pm 4.1_{\mathrm{sys+theo}}$
KLOE10	$376.6 \pm 0.9_{\mathrm{stat}} \pm 3.3_{\mathrm{sys+theo}}$
	$a_\mu^{\pi\pi}(0.35 - 0.95\ \mathrm{GeV}^2) \times 10^{10}$
KLOE11	$384.1 \pm 1.2_{\mathrm{stat}} \pm 4.0_{\mathrm{sys}} \pm 1.2_{\mathrm{theo}}$
KLOE08	$387.2 \pm 0.5_{\mathrm{stat}} \pm 2.4_{\mathrm{sys}} \pm 2.3_{\mathrm{theo}}$

Figure 1: Fractional difference between $|F_\pi|^2$ obtained by $\pi\pi\gamma/\mu\mu\gamma$ ratio (KLOE11) and the previous (KLOE10) analysis and table with the di-pion contribution to a_μ as extracted by all of the KLOE hadronic cross section measurements.

3.2 Rare η decays

The properties of the η meson are being studied through the radiative decay $\phi \to \eta\gamma$. The full KLOE data set contains 10^8 ηs. The $\eta \to \pi^+\pi^-\gamma$, as discussed in the previous LNF Activity Report, proceeds and is sensitive to box anomaly. Both, the branching ratio and the 2–pion invariant mass distribution are of theoretical interest [12]. The most recent results from CLEO show a 2–σ discrepancy with those dating back to 70's. KLOE has obtained the measurement

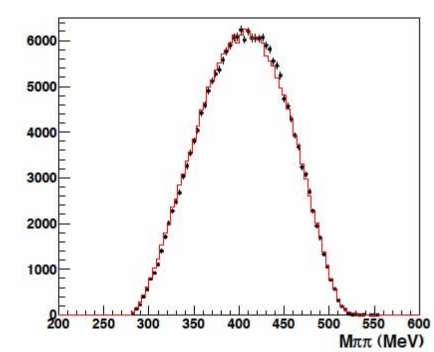

Figure 2: Di–pion invariant mass distribution for the $\eta \to \pi^+\pi^-\gamma$ channel, points: data; histogram: fit function as in Ref. [13].

of the branching ratio normalized to $\eta \to \pi^+\pi^-\pi^0$ on the basis of a sample of 558 pb^{-1}. The analysis has been recently completed, and the final result,$\Gamma(\ \eta \to \pi^+\pi^-\gamma)/\Gamma(\eta \to \pi^+\pi^-\pi^0) = 0.1838 \pm 0.0005 \pm 0.0030$ is in good agreement with CLEO data. The normalization sample is very clean and on the basis of about $1.2{\times}10^6$ events, we can extract a branching fraction, $BR(\eta \to \pi^+\pi^-\pi^0) = (22.41 \pm 0.03 \pm 0.35)\%$, in agreement with the world average, $(22.74 \pm 0.28)\%$. The

$M_{\pi\pi}$ distribution, shown in Fig.2, is well described by the parametrization in Ref. [13].

The decay $\eta \to e^+e^-e^+e^-$ proceeds through two virtual photons intermediate state, with photon conversion to e^+e^-. The theoretical expectation for the branching ratio is about 2.5×10^{-5}. Two upper limits at 90% C.L., based on few events, have been set by the CMD-2 Collaboration, $BR(\eta \to e^+e^-e^+e^-) < 6.9\times10^{-5}$, and by WASA at CELSIUS, $BR(\eta \to e^+e^-e^+e^-) < 9.7\times10^{-5}$. From the analysis of 1.7 fb^{-1} we obtain the first evidence of this decay. The 4–leptons invariant mass has been used for event counting, giving 362$\pm$ 29 events that correspond to the $BR(\eta \to e^+e^-e^+e^-) = (2.4\pm0.2\pm0.1)\times10^{-5}$ [2].

In γ–γ processes, like $e^+e^- \to e^+e^-\gamma^*\gamma^* \to e^+e^-X$, $C = +1$ hadronic states can be produced. If both photons are quasi-real, the event yield evaluated in the Equivalent Photon Approximation is $N_{eeX} = L\int \frac{dF}{dW_{\gamma\gamma}}\sigma_{\gamma\gamma\to X}(W_{\gamma\gamma})dW_{\gamma\gamma}$, where $W_{\gamma\gamma}$ is the $\gamma\gamma$ invariant mass, L is the integrated luminosity and $dF/dW_{\gamma\gamma}$ is the flux function. Final states with one π^0 or η or $\pi\pi$ can be studied at DAΦNE . The latter is interesting for the measurement of the $\sigma(600)$, via the reaction $\gamma\gamma \to \sigma(600) \to \pi\pi$. The off–peak data (250/pb) have been exploited to avoid the large background from ϕ decays.

The cleanest channel is $\gamma\gamma \to \pi^0\pi^0$; events with only four prompt photons have been selected, because scattered leptons escape detection flying along beam line. In fig.3 the distribution of the 4–photons invariant mass is shown; the background has been evaluated according to the expected cross-sections. Work is in progress to extract $\sigma(\gamma\gamma \to \pi^0\pi^0)$. In the same data sample the η meson production has been studied by selecting $\eta \to \pi^+\pi^-\pi^0$ and $\eta \to \pi^0\pi^0\pi^0$. In Fig.3 the missing mass for the charged channel is reported. After background subtraction, 650 events are left, with missing mass distribution shown in Fig.3. In the neutral channel, 921 signal events have been obtained. Work is in progress to extract $\sigma(e^+e^- \to e^+e^-\eta)$. We have also measured the cross–section of

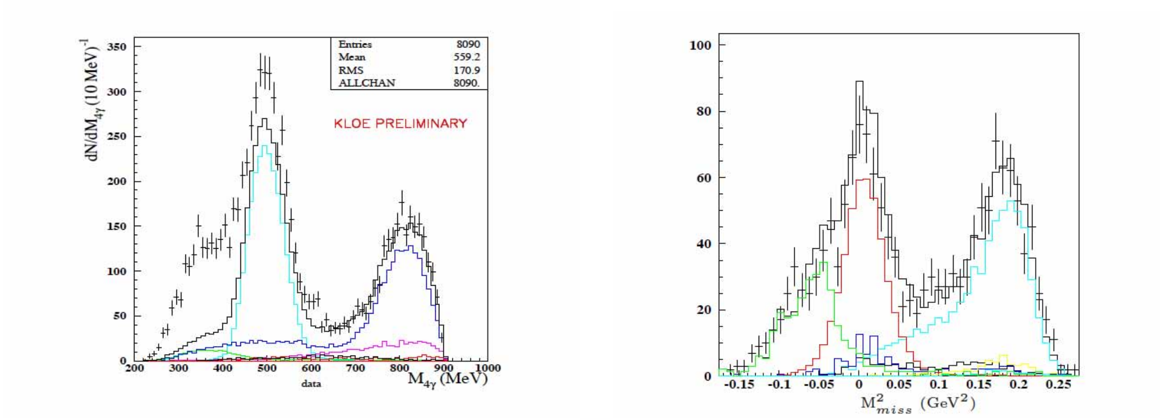

Figure 3: Left - $e^+e^- \to e^+e^-\pi^0\pi^0$: 4–photons invariant mass: points = data, histograms = background from MC. Right - Missing mass in $e^+e^- \to e^+e^-\eta$: points = data, light blue histogram = signal MC.

the main background channel in the γ–γ production of η meson, $\sigma(e^+e^- \to \eta\gamma, \sqrt{s} = 1\ \text{GeV}) = (0.866\pm0.009\pm0.093)$ nb. The KLOE-2 data–taking at the ϕ peak can be used for γ–γ physics thanks to the taggers that detect the scattered leptons, so that the background is largely suppressed and the kinematics of the events closed. A precision measurement of $\sigma(\gamma\gamma \to \pi^0\pi^0)$, to improve on the region of $W_{\gamma\gamma} < 800$ MeV, is feasible [6], together with the π^0 and η 2–photons widths and the transition form factor, $F_{\pi^0\gamma^*\gamma^*}(q_1^2, q_2^2)$, relevant for the calculation of the hadronic light-by-light scattering contribution to the muon anomaly.

4 Searches for U–boson

The existence of a light dark force mediator has been tested with the KLOE detector at DAΦNE. Such an abelian gauge field, the U boson with mass near the GeV scale, couples the secluded sector to the SM through its kinetic mixing with the SM hyper-charge gauge field. The kinetic mixing parameter, ϵ, is expected to be of the order 10^{-4}–10^{-2} [14, 15] so that observable effects can be induced in $\mathcal{O}$(GeV)–energy e^+e^- colliders [15, 16, 17, 18, 19] and fixed target experiments [20, 21, 22, 23].

The U boson can be produced at e^+e^- colliders via different processes: $e^+e^- \to U\gamma$, $e^+e^- \to Uh'$ (h'-strahlung), where h' is a higgs-like particle responsible for the breaking of the hidden symmetry, and $V \to P\gamma$ decays, where V and P are vector and pseudoscalar mesons, respectively. We have studied the process $\phi \to \eta\, U$, using a sample of ϕ mesons produced at the DAΦNE collider. The U boson can be observed by its decay into a lepton pair, while the η can be tagged by one of its main decays. An irreducible background due to the Dalitz decay of the ϕ meson, $\phi \to \eta\, \ell^+\ell^-$, is present. This decay has been studied by the SND and CMD-2 experiments, obtaining a cross section of $\sigma(\phi \to \eta\, \ell^+\ell^-) \sim 0.7$ nb in a di-lepton mass range $M_{\ell\ell} < 470$ MeV. For the signal, the expected cross section is expressed by [17]:

$$\sigma(\phi \to \eta\, U) = \epsilon^2\, |F_{\phi\eta}(m_U^2)|^2\, \frac{\lambda^{3/2}(m_\phi^2, m_\eta^2, m_U^2)}{\lambda^{3/2}(m_\phi^2, m_\eta^2, 0)}\, \sigma(\phi \to \eta\gamma)\,, \tag{2}$$

where $F_{\phi\eta}(m_U^2)$ is the $\phi\eta\gamma^*$ transition form factor evaluated at the U mass while the following term represents the ratio of the kinematic functions of the decays [1]. Using $\epsilon = 10^{-3}$ and $|F_{\phi\eta}(m_U^2)|^2 = 1$, a cross section $\sigma(\phi \to \eta\, U) \sim 40$ fb is obtained. Despite the small ratio between the overall cross section of $\phi \to \eta\, U$ and $\phi \to \eta\, \ell^+\ell^-$, their different di-lepton invariant mass distributions allow to test the ϵ parameter down to 10^{-3} with the KLOE data set.

The best U decay channel to search for the $\phi \to \eta\, U$ process at KLOE is in e^+e^-, since a wider range of U boson masses can be tested and $e^\pm$ are easily identified using time-of-flight (ToF) technique. The η can be tagged by the 3-pions or 2-photons final state which represent $\sim 85\%$ of the total decay rate. We have used the $\eta \to \pi^+\pi^-\pi^0$ decay channel which provides a clean final state with four charged particles and two photons.

The analysis of the decay chain $\phi \to \eta\, U$, $\eta \to \pi^+\pi^-\pi^0$, $U \to e^+e^-$, has been performed on a data sample of 1.5 fb^{-1}, corresponding approximately to 5×10^9 produced ϕ mesons. The Monte Carlo (MC) simulation of the irreducible background $\phi \to \eta\, e^+e^-$, $\eta \to \pi^+\pi^-\pi^0$ has been produced with $d\Gamma(\phi \to \eta\, e^+e^-)/dm_{ee}$ weighted according to the Vector Meson Dominance model with the form factor parametrization from the SND experiment [24]. The MC simulation for the $\phi \to \eta\, U$ decay has been developed according to [17], with a flat distribution in M_{ee}. All MC productions, including all other ϕ decays, take into account changes in DAΦNE operation and background conditions on a run-by-run basis. Data-MC corrections for cluster energies and tracking efficiency, evaluated with radiative Bhabha events and $\phi \to \rho\pi$ samples, respectively, have been applied.

The selection criteria applied and the data set obtained are discussed in the previous LNF Activity Report.

The upper limit on $\phi \to \eta\, U$ signal as a function of M_U is then obtained in the following way:

(a) MC events are divided in sub-samples of 1 MeV width in the range $5 < M_U < 470$ MeV;

(b) for each M_U sub-sample, the average value of the $\phi \to \eta\, e^+e^-$ background, $b(M_{ee})$, is obtained by fitting the reconstructed M_{ee} spectrum with 5 MeV binning, removing five bins centered at M_U;

[1] $\lambda(m_1^2, m_2^2, m_3^2) = [1 + m_3^2/(m_1^2 - m_2^2)]^2 - 4m_1^2 m_3^2/(m_1^2 - m_2^2)^2$.

(c) for each fit, the maximum variation of $b(M_{ee})$ events, $\Delta b(M_{ee})$, is obtained changing by $\pm 1\,\sigma$ the fit parameters;

(d) for each M_U value, the signal hypothesis is tested comparing observed data, $b(M_{ee})$ and MC signal in the five reconstructed bins excluded in (b). The exclusion plot is obtained applying the CLs method [25]. A Gaussian spread of width $\Delta b(M_{ee})$ on the background distribution is applied while evaluating CLs.

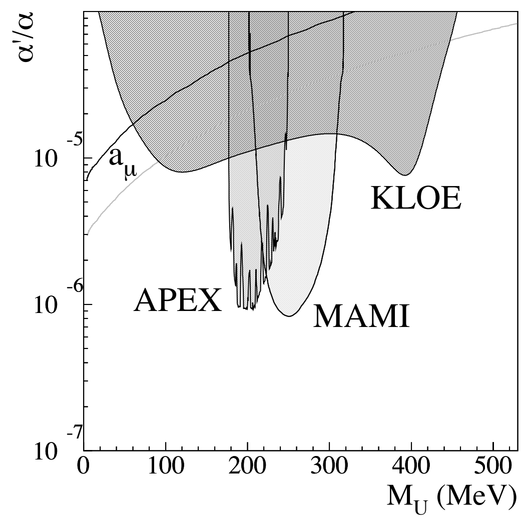

Figure 4: Exclusion plot at 90% C.L. for $\alpha'/\alpha = \epsilon^2$, compared with existing limits in the mass region of interest for KLOE.

Using Eq.(2) and taking into account the analysis efficiency, the exclusion plot at 90 % C.L. is obtained in the plane of parameters $\alpha'/\alpha = \epsilon^2$–$M_U$, where α' is the coupling of the U boson to electrons and α is the fine structure constant. The opening of the $U \to \mu^+\mu^-$ threshold, in the hypothesis that the U boson decays only to lepton pairs and assuming equal coupling to e^+e^- and $\mu^+\mu^-$, is included. In Fig.4 the smoothed exclusion plot at 90% C.L. on α'/α is compared with existing limits from the muon anomalous magnetic moment a_μ [26] and from recent measurements of the MAMI/A1 [27] and APEX [28] experiments. The gray line is where the U boson parameters should lay to account for the observed discrepancy between measured and calculated a_μ values. Our result greatly improves existing limits in a wide mass range, resulting in the upper limit on the α'/α parameter of $\leq 2 \times 10^{-5}$ @ 90% C.L. for $50 < M_U < 420$ MeV, thus covering sizeable part of the expected ϵ range. We exclude that the existing a_μ discrepancy is due to U boson with mass from 90 to 450 MeV.

5 The KLOE-2 inner tracker

In KLOE, tracking is provided by a huge and transparent Drift Chamber [29], filled with He:iC_4H_{10} 90:10. The chamber has a full stereo geometry, with a spatial resolution of $\sigma_{r\varphi} \simeq 150$ μm, $\sigma_z \simeq 2$ mm and a vertex resolution of ~ 6 mm. The resolution on transverse momenta is $\sigma_{p_\perp}/p_\perp \sim 0.4\%$.

The chamber is 4 m long, with a 2 m outer radius and 25 cm inner radius. It is surronded by an electromagnetic calorimeter [30], covering 98% of the solid angle. The calorimeter is composed by lead-scintillating fiber and it provides an energy resolution of $\sigma_E/E = 5.7\%/\sqrt{E(\mathrm{GeV})}$ and a time resolution of $\sigma_t = 54$ ps$/\sqrt{\mathrm{E(GeV)}} \oplus 100$ ps. The whole apparatus is embedded in a superconductive magnet which provides a 0.52 T axial magnetic field.

In order to improve the resolution on the vertices at few cm from the IP, a new tracking detector will be installed in the free space between the Drift Chamber inner wall and the beam pipe, reducing the present track extrapolation length. The Inner Tracker (IT) contribution to the overall material budget has to be kept as low as possible to minimize multiple scattering term to the track momentum resolution and the probability of photon conversion outside the calorimeters. The requirements for the Inner Tracker can be summarized as:

- $\sigma_{r\varphi} \sim 200$ μm and $\sigma_z \sim 500$ μm spatial resolution
- 5 kHz/cm^2 rate capability
- $< 2\% X_0$ material budget

The adopted solution is the Cylindrical-GEM (CGEM), a triple-GEM detector composed by concentric cylindrical electrodes: cathode, 3 GEM foils and anode, acting also as the readout circuit. The IT of KLOE-2 is constituted by four layers of cylindrical triple-GEM 700 mm long, each of them equipped with a two-dimensional readout. The radius of the layers is from 13 cm to 23 cm, being limited by the beam pipe and the DC inner wall. The minimum is chosen to preserve quantum interference. Including the carbon fibers support, the detector has a material budget of $\sim 1.5\% X_0$. According to simulations, the Inner Tracker will improve by a factor of 3 spatial resolution on the $K_s \to \pi\pi$ vertex (presently ~ 6 mm).

In order to validate the idea of the cylindrical GEM, a full scale prototype (300 mm diameter and 352 mm active length) was built and studied at the CERN-PS T9 area [31], [32] with a 10 GeV pion beam. The detector, filled with Ar:CO_2 70:30 gas mixture at 1 bar pressure, was operated at a gain of $2 \cdot 10^4$. The readout was provided by axial strips, 650 μm pitch, equipped with a FEE dedicated chip: GASTONE [33]. The detection efficiency was measured as a function of the impact parameter of the tracks. A spatial resolution of ~ 200 μm has been achieved, in agreement with what is expected for a 650 μm pitch readout by digital FEE.

The IT readout is performed with an X-V pattern of strips on a polymide foil substrate. The X strips with 650 μm pitch will provide the $r - \phi$ coordinate while the V strips are realized with pads, connected through internal vias to supply the second coordinate. The Front-End Electronics is based on the GASTONE ASIC, a 64-channels chip featured by a low input equivalent noise and a low power consumption (~ 200 W for 30000 channels), composed by four different stages: a charge preamplifier with 20 mV/fC sensitivity, a shaper, a leading-edge discriminator with a programmable threshold and a monostable stretcher of the digital signal, to synchronize with the KLOE Level1 trigger.

In order to simulate working condition at KLOE, five small (10×10 cm^2) planar triple-GEM chambers were tested in magnetic field [34] at the H4 beam line (CERN-SPS). Four chambers were equipped with orthogonal strips (X-Y readout) and used as external trackers, while for the fifth chamber the X-V readout has been adopted.The magnetic field was provided by GOLIATH dipole and it could be set up to 1.5 T in a $3 \times 3 \times 1$ m^3 volume. They were placed with the magnetic field orthogonal to the chamber electric field. Two effects of the magnetic field on the GEM were observed: i) a systematic displacement of electrons with respect to the track position and ii) a larger spread of the electronic cloud with respect to the no-field case. The electron displacement was measured reversing the X-V chamber with respect to the others: the shift is mirrored and the

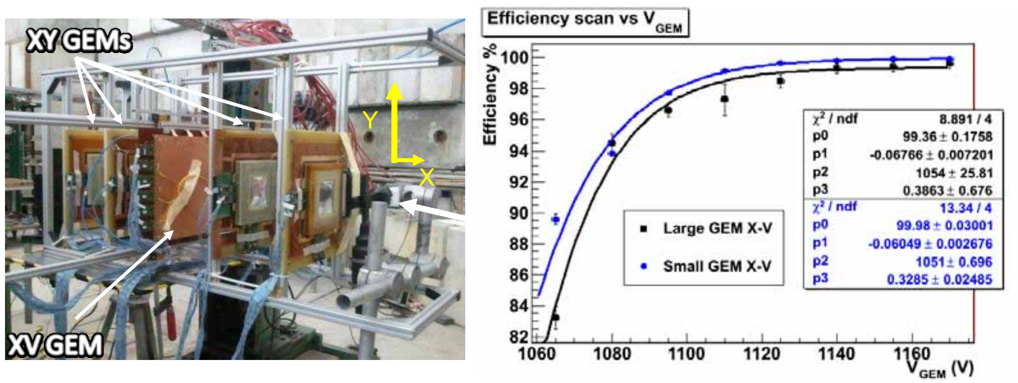

Figure 5: Setup of the Large Area GEM test beam (left) and detection efficiency as a function of the sum of the voltage applied to the GEM foils of a triple-GEM (right). The blue points are obtained by the double-mask manufactured GEMs while the black ones refer to the GEM realized with the new single-mask technique. The fit is obtained by Fermi-Dirac functions.

distance of the hits from the track is 2x the expected displacement. This quantity was measured as a function of the magnetic field, for detector electric fields set at 1.5/2.5/2.5/4 kV/cm.

The detection efficiency as a function of the magnetic field and of the working point of the GEM was measured. The increase of the magnetic field, inducing a spread of the charge on the readout, results in an efficiency drop that can be recovered by higher gain. The outermost layer of the IT requires 1440×700 mm^2 GEM foils obtained splicing three 480×700 mm^2 foils. Large GEM foils led to a change of the manufacturing procedure by the CERN TS-DEM-PMT laboratory, switching from the double-mask (requiring very fine alignement of the two masks) to single-mask etching [35]. A triple-GEM was realized with the new large foils and tested with a ^{137}Cs source (660 keV photons). The measured current was normalized to the one obtained by a 10×10 cm^2 double-mask manufactured triple-GEM. The measurement shows that the gain for the new hole shape is $\sim 20\%$ lower than in the double-mask case, at fixed HV. The large area triple-GEM was then tested at CERN-PS T9 area, using the same external tracking of the previous test-beam. The chamber was equipped with the final X-V readout. The test beam allowed to validate the final DAQ and FEE chain, constituted by the GASTONE64 chip, the interface boards, the General Intermediate Boards and the Software Interface.

The construction procedure of the C–GEM has been worked out with the realization of the prototypes. The main steps are:

1. the gluing of three GEM foils to obtain the surface needed for the cylindrical electrode. A precise Alcoa plane and the vacuum bag technique are used to obtain homogeneous, dead zone-free electrodes;

2. the large foil is then rolled on a very precise aluminum cylindrical mould covered with a 0.4 mm machined Teflon film, for easy and safe extraction of the cylindrical electrode. The mould is then enveloped with the vacuum bag, and vacuum is applied for the glue curing time (about 12 hours);

3. final assembling of the C–GEM layer is made on the Vertical Insertion System (VIS), a tool

Figure 6: Planar gluing of the three anode foils (left). A Cylindrical GEM (center). Insertion of a CGEM into the anode (right).

designed for smooth and safe insertion of the cylindrical electrodes. The system allows a very precise alignement (0.1 mm on 1 m total length) of the electrodes along their vertical axis. Internal electrode is fixed on its mould, while the external one is slowly moved downwards by a computer controlled step-motor, coupled with a reduction gear system. The operation is performed with the help of a web-camera, for monitoring the radial distance between electrodes ($2-3$ mm). The up-down rotation of the assembly tool allows an easy sealing of the detector on both sides.

The construction and extensive test of the first C-GEM layer has been successfully completed. Final readout configuration, validated with the test of small planar prototypes operating in magnetic field, is being carried out at the cosmic ray stand, equipped with the FEE and DAQ system. The construction and assembling of the second layer has been started and the completion of the inner tracker is scheduled for September 2012.

6 The calorimeters for KLOE upgrade

In February 2011, a matrix of crystals, with transverse dimension of $\sim$2.8 R_M, and longitudinal of $11 \div 12$ X_0, has been prepared and fully equipped for the study and characterization of both, the CCALT and the LET calorimeters.

The prototype consists of an inner matrix of 9 LYSO crystals by SICCAS (20x20x150 mm^3), readout by the Hamamatsu APDs S8664 (10x10 mm^2). A cheaper outer matrix, composed by $PbWO_4$ crystals equipped with standard Hamamatsu Bialcali photomultipliers, 1 inch diameter, has been used for leakage recovery.

Each crystal was first wrapped with a 300 μm Tyvek sheet, for light transmission and for improving light collection on the photosensors, that are in optical contact with the rear surface by means of BICRON grease. The cross-talk among crystals is avoided by the wrapping with 1 mm thick black tape.

The data were taken at the Mainz Microtron facility, MAMI, delivering intense photon beams in the energy range of interest for the experiment. The study was done at fifteen different settings of the photon-beam energy, in the range from 30 to 300 MeV.

The calorimeter response for each channel has been calibrated with minimum ionizing particles, m.i.p., orthogonal to the crystal axis. The charge of the 9 LYSO crystals of the inner matrix and the charge of the 8 PbWO of the external matrix were summed up. The overall noise for the LYSO inner matrix was $\sim$ 3.2 counts. It follows that

$$\sigma(\text{noise})_{\text{tot}} = (3.2\ \text{count} * 9.6\ \text{MeV/cm} * 2\ \text{cm})/120\ \text{count} \approx 500\ \text{keV} \tag{3}$$

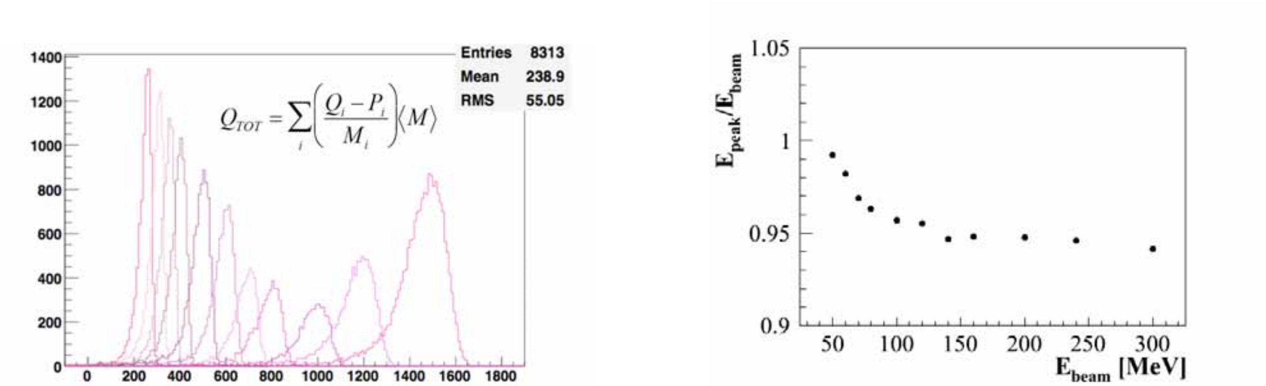

Figure 7: Left - Energy Scan: response for energy from 50 to 300 MeV. Right - Linearity plot: ratio between and photon beam energy, for the inner matrix.

The contribution of each channel is 150 keV as from the pedestal distribution. Thus we observed an excellent scaling with total noise $\sqrt{\mathrm{N_{ch}} * \sigma(\mathrm{noise})_\mathrm{i}^2} = 450\,\mathrm{keV}$. For the external matrix, the overall noise was $\sim$ 2 counts. Thus, we get a total 3.6 counts, i.e. 720 keV of noise. The total response of the detector is defined as:

$$Q_{TOT} = \sum_i (Q_i - P_i) \cdot 1/M_i \tag{4}$$

where Q$_i$ and P$_i$ are the collected charge and the pedestal of the i-th channel and M$_i$ is the minimum ionization peak. The energy deposit in ADC counts, for different photon beam energies is shown in Fig.7. Energy distribution has been fit with a LogGaussian function to determine the

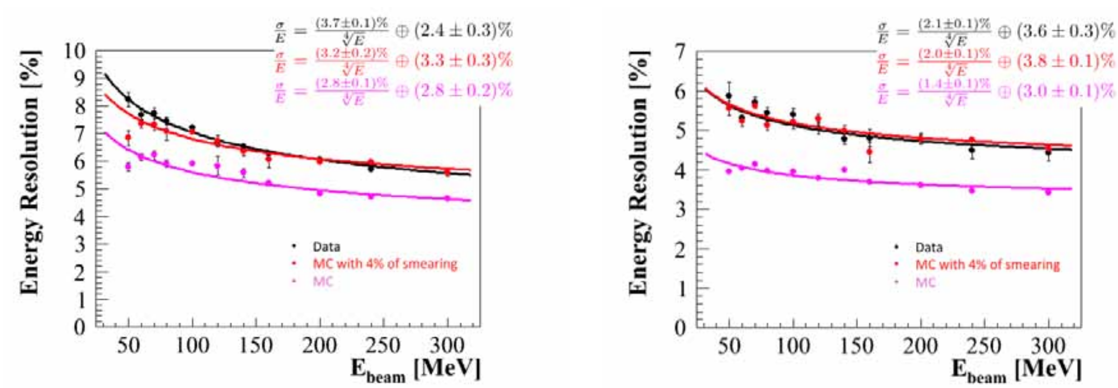

Figure 8: Left - Dependence of the energy resolution on beam momentum, for the inner matrix. Black points: data, red (pink) points: MC with (without) the 4% correction. Right -Dependence of the energy resolution on beam momentum, for all crystals. Black points: data, red (pink) points: MC with (without) the 4% correction.

most probable values, which were used to evaluate the linearity. The linearity is shown in Fig.7 for the different energies. We plotted the ratio between the total response of the calorimeter and the beam energies for the whole (inner) matrix. We set the scale with the lowest energy point (50 MeV) where the shower is fully contained in the matrix. A 2% drop, due to leakage effects, appears up to 70 MeV. Above this point, a linearity better than $\sim 0.5\%$ is observed. The rear leakage begins to be relevant at 300 MeV (a crystal length of 15 cm corresponds to 13 X_0). The energy resolution has been obtained from 50 to 300 MeV. In Fig.8 the energy dependence of the energy resolution for the whole and inner matrix is shown and compared with MC simulations of the crystal response.

The energy resolution has been fit with the equation:

$$\sigma_E/E = a/\sqrt[4]{E[GeV]} \oplus b/E[GeV] \oplus c \tag{5}$$

The noise term, at the 0.06% level, is completely negligible as the photoelectron statistics is. The a term is thus given by the energy dependence of leakage fluctuation. The simulation closely follows data distribution.

Time resolution was studied at the Frascati Beam Test Facility (BTF), obtaining $\sigma_t = 250$ (49) ps at 500 MeV, 291 (120) ps at 100 MeV without (with) correction for the trigger jitter. Both, time and energy resolutions match the experimental requests for the γ–γ tagger (LET) and the photon-veto calorimeter at low polar angle.

7 Papers

1. F. Ambrosino *et al.* (KLOE), *Measurement of $\sigma(e^+e^- \to \pi^+\pi^-)$ from threshold to 0.85 GeV^2 using initial state radiation with the KLOE detector*, Phys. Lett. **B700** (2011) 102

2. F. Ambrosino *et al.* (KLOE), *Observation of the rare $\eta \to e^+e^-e^+e^-$ decay with the KLOE experiment*, Phys. Lett. **B702** (2011) 324

3. F. Ambrosino *et al.* (KLOE), *Precision measurement of the K(S) meson lifetime with the KLOE detector*, Eur. Phys. J. **C71** (2011) 1604

4. A. Balla, G. Bencivenni, S. Cerioni *et al.*, *Status of the cylindrical-GEM project for the KLOE-2 inner tracker*, Nucl. Instrum. & Meth. **A628** (2011) 194

5. D. Babusci, H. Czyz, F. Gonnella *et al.*, *On the possibility to measure the $\pi^0 \to \gamma\gamma$ decay width and the $\gamma\gamma \to \pi^0$ transition form factor with the KLOE-2 experiment* , arXiv:**1109.2461** (2011) [hep-ph]

8 Seminars

1. S. Giovannella, *Hadron Physics with KLOE and KLOE-2* , Seminar at the Jagiellonian University of Krakow, May 10th 2011, Poland

2. E. Czerwinski, *KLOE results in Kaon Physics*, Seminar at the Jagiellonian University of Krakow, June 14th 2011, Poland

3. G. Venanzoni, *KLOE measurement of the $\sigma(e^+e^- \to \pi^+\pi^-(\gamma))$ with Initial State Radiation and its contribution to the muon (g-2). Future prospects with KLOE-2*, Seminar at Brookhaven National Laboratory, July 28th 2011, Upton NY, USA

9 Contributions and Conference Proceedings

1. S. Giovannella *et al.*, (KLOE-2) *Hadron Physics with KLOE and KLOE-2* , Talk at the 8th International Conference on Nuclear Physics at Storage Rings, STORI'11, October 9-14 (2011), Frascati, Italy

2. G. Morello *et al.*, (KLOE-2) *Design and construction of a cylindrical GEM detector as Inner Tracker device at KLOE-2* , Talk at the 8th International Conference on Nuclear Physics at Storage Rings, STORI'11, October 9-14 (2011), Frascati, Italy

3. C. Bloise *et al.*, (KLOE-2) *Kaon physics at KLOE and KLOE-2 prospects.*, Talk at the International Europhysics Conference on High Energy Physics, EPS-HEP, July 21-27 (2011), Grenoble, France

4. G. Venanzoni *et al.*, (KLOE-2) *Measurement of hadronic cross section with ISR and pipi contribution to muon anomaly*, Talk at the International Europhysics Conference on High Energy Physics, EPS-HEP, July 21-27 (2011), Grenoble, France

5. G. Morello *et al.*, (KLOE-2) *Design and construction of a cylindrical GEM detector as Inner Tracker device at KLOE-2* , Talk at the Conference on Technology and Instrumentation in Particle Physics, TIPP 2011, June 9-14 (2011), Chicago, USA

6. D. Domenici *et al.*, (KLOE-2) *Design and Construction of a Cylindrical GEM Detector as Inner Tracker Device at KLOE-2* , Talk at the IEEE Nuclear Science Symposium and Medical Imaging Conference, October 23-29 (2011), Valencia, Spain

7. I. Sarra *et al.*, (KLOE-2) *CCALT: The Crystal Calorimeter with Timing for the KLOE-2 experiment*, Talk at the 13th ICATPP Conference, October 3-7 (2011), Villa Olmo, Como, Italy

8. G. Bencivenni *et al.*, (KLOE-2) *Design and construction of a cylindrical GEM detector as Inner Tracker device at KLOE-2* , Talk at the 2nd International Conference on Micro Pattern Gaseous Detectors 29 August - 1 September 2011, Kobe, Japan

9. S. Miscetti *et al.*, (KLOE-2) *Status and prospects for the KLOE-2 experiment.*, J.Phys.Conf.Ser. **335** (2011) 012070; Proceedings of DISCRETE 2010: Symposium on Prospects in the Physics of Discrete Symmetries

10. E. Czerwinski *et al.*, (KLOE-2) *KLOE results in kaon physics and prospects for KLOE-2*, arXiv: **1112.4898** (2011) [hep-ex]; Proceedings of the Conference From Phi to Psi 2011

11. S. Giovannella *et al.*, (KLOE-2) *Physics with KLOE and KLOE-2 experiments at DAFNE*, AIP Conf.Proc. **1374** (2011) 73; Proceedings of the 12th International Conference on Meson-Nucleon Physics and the Structure of the Nucleon

12. B. Sciascia *et al.*, (KLOE-2) *Test of lepton flavor universality with Ke2 decay at KLOE and KLOE-2*, PoS **HQL2010** (2011) 027; Proceedings of the 10th Nicola Cabibbo International Conference on Heavy quarks and leptons

13. G. Venanzoni *et al.*, (KLOE-2) *A precise new KLOE measurement of* $|F(\pi)|^2$ *with ISR events and determination of* $\pi\pi$ *contribution to* a_μ *from threshold to 0.95* GeV^2, Nucl.Phys.Proc.Suppl. **218** (2011) 207; Proceedings of the 11th International Workshop on Tau Lepton Physics

14. F. Ambrosino *et al.*, (KLOE-2) *Measurement of* $\Gamma(\eta \to \pi^+\pi^-\gamma)/\Gamma(\eta \to \pi^+\pi^-\pi^0)$ *with KLOE experiment*, arXiv: **1107.5733** (2011) [hep-ex]; Contributed paper to the Lepton-Photon 2011 Conference

15. F. Archilli *et al.*, (KLOE-2) γ–γ *physics with the KLOE experiment.*, arXiv: **1107.3782** (2011) [hep-ex] ; Contributed paper to the Lepton-Photon 2011 Conference

16. S. Giovannella *et al.*, (KLOE-2) *U boson searches at KLOE*, J.Phys.Conf.Ser. **335** (2011) 012067 ; Proceedings of DISCRETE 2010: Symposium on Prospects in the Physics of Discrete Symmetries

17. S. Miscetti *et al.*, (KLOE-2) *Hadron physics with KLOE and KLOE-2*, AIP Conf.Proc. **1343** (2011) 290; Proceedings of the 9th Conference on Quark Confinement and the Hadron Spectrum

18. M. Cordelli *et al.*, *CCALT: A crystal calorimeter for the KLOE-2 experiment*, J.Phys.Conf.Ser. **293** (2011) 012010; Proceedings of the 14th International Conference on Calorimetry in High Energy Physics

19. A. Balla *et al.*, *A new cylindrical-GEM inner tracker for the upgrade of the KLOE experiment*, Nucl.Phys.Proc.Suppl. **215** (2011) 76 ; Proceedings of the 12th Topical Seminar on Innovative Particle and Radiation Detectors

20. E. De Lucia *et al.*, (KLOE-2) *Determination of Vus at the KLOE experiment: Present results and future perspectives*, arXiv: **1101.5016** (2011) [hep-ex]; Proceedings of the 6th International Workshop on the CKM Unitarity Triangle

References

1. F. Ambrosino et al. (collaboration for the KLOE), Eur.Phys.J. **C71**, 1604 (2011), `1011.2668`
2. F. Ambrosino et al. (KLOE Collaboration), Phys.Lett. **B700**, 102 (2011), `1006.5313`
3. F. Ambrosino et al. (KLOE-2 collaboration), Phys.Lett. **B702**, 324 (2011), `1105.6067`
4. F. Ambrosino et al. (KLOE), Phys. Lett. **B619**, 61 (2005), `hep-ex/0505012`
5. F. Ambrosino et al. (KLOE), JHEP **12**, 011 (2006), `hep-ex/0610034`
6. G. Amelino-Camelia, F. Archilli, D. Babusci, D. Badoni et al., EPJ **C68**, 619 (2010)
7. A. Di Domenico et al. (KLOE), J. Phys. Conf. Ser. **171**, 012008 (2009)
8. F. Jegerlehner, A. Nyffeler, Phys.Rept. **477**, 1 (2009), `0902.3360`
9. G.W. Bennett et al. (Muon g-2), Phys. Rev. **D73**, 072003 (2006), `hep-ex/0602035`
10. S. Binner, J.H. Kuhn, K. Melnikov, Phys.Lett. **B459**, 279 (1999), `hep-ph/9902399`
11. H. Czyz, A. Grzelinska, J.H. Kuhn, G. Rodrigo, Eur.Phys.J. **C39**, 411 (2005), `hep-ph/0404078`
12. M. Benayoun, P. David, L. DelBuono, P. Leruste, H.B. O'Connell, EPJ **C31**, 525 (2003)
13. C. Picciotto, Phys.Rev. **D45**, 1569 (1992)
14. N. Arkani-Hamed, D.P. Finkbeiner, T.R. Slatyer, N. Weiner, PR **D79**, 015014 (2009)

15. R. Essig, P. Schuster, N. Toro, Phys. Rev. **D80**, 015003 (2009), `0903.3941`

16. B. Batell, M. Pospelov, A. Ritz, Phys. Rev. **D79**, 115008 (2009), `0903.0363`

17. M. Reece, L.T. Wang, JHEP **07**, 051 (2009), `0904.1743`

18. N. Borodatchenkova, D. Choudhury, M. Drees, Phys. Rev. Lett. **96**, 141802 (2006)

19. P.F. Yin, J. Liu, S.h. Zhu, Phys. Lett. **B679**, 362 (2009), `0904.4644`

20. J.D. Bjorken, R. Essig, P. Schuster, N. Toro, Phys. Rev. **D80**, 075018 (2009), `0906.0580`

21. B. Batell, M. Pospelov, A. Ritz (2009), `0906.5614`

22. R. Essig, P. Schuster, N. Toro, B. Wojtsekhowski (2010), `1001.2557`

23. M. Freytsis, G. Ovanesyan, J. Thaler, JHEP **01**, 111 (2010), `0909.2862`

24. M.N. Achasov et al., Phys. Lett. **B504**, 275 (2001)

25. T. Junk, Nucl.Instrum.Meth. **A434**, 435 (1999), `hep-ex/9902006`

26. M. Pospelov, Phys. Rev. **D80**, 095002 (2009), `0811.1030`

27. H. Merkel et al. (A1 Collaboration), Phys.Rev.Lett. **106**, 251802 (2011), `1101.4091`

28. S. Abrahamyan et al. (APEX Collaboration), Phys.Rev.Lett. **107**, 191804 (2011), `1108.2750`

29. M. Adinolfi et al., Nucl. Instrum. Meth. **A488**, 51 (2002)

30. M. Adinolfi et al., Nucl. Instrum. Meth. **A482**, 364 (2002)

31. G. Bencivenni, S. Cerioni, D. Domenici et al., NSS CR 2008. IEEE **1**, 2268 (2008)

32. G. Bencivenni, S. Cerioni, D. Domenici et al., NSS CR 2008. IEEE **6**, 4666 (2007)

33. A. Balla, G. Bencivenni, M. Beretta, S. Cerioni et al., NIM **A604**, 23 (2009)

34. A. Balla, G. Bencivenni, S. Cerioni, P. Ciambrone, E. De Lucia et al., Nucl.Instrum.Meth. **A628**, 194 (2011), `1003.3770`

35. M. Alfonsi, G. Bencivenni, I. Brock, S. Cerioni et al., NIM **A617**, 151 (2010)

LHCb

M. Anelli (Tecn.), F.Archilli (Ass. Ric.), G. Bencivenni, P. Campana,
M. Carletti (Tecn.), G. Capon, P. Ciambrone, P. de Simone, G. Felici,
G. Lanfranchi, F. Murtas, M. Palutan, R. Rosellini (Tecn.), M. Santoni (Tecn.),
A. Sarti (Ass.), B.Sciascia, A. Sciubba (Resp.Ass.), F. Soomro (Bors. PD)

In collaboration with:
"LNF-SSCR"
(M. Arpaia, G. Bisogni, A. Cassará, A. Ceccarelli, E. Iacuessa, U. Martini, A. Saputi);
"LNF-SEA"
(A. Balla, G. Corradi, M. Gatta, D. Tagnani)

1 Introduction

The LHCb experiment has had a remarkable 2011 year, moving from first results to world-beating measurements of B-hadron properties, such as the oscillation frequency of the B_s meson, CP and forward-backward asymmetries, as well as limits on rare decays. Even though the physics harvest is now in full flow, the collaboration is already planning for the eventual upgrade of the experiment, which is scheduled to be ready for data-taking in 2019. The instantaneous luminosity delivered to LHCb has steadily increased throughout the year, reaching 4×10^{32} cm^{-2}s^{-1} by the end of the run, already twice the original design luminosity for the experiment. The goal for this year was 1 fb^{-1} of integrated luminosity, which (thanks to the excellent performance of the LHC) was comfortably passed with a few weeks to spare; it represents more than 30 times as much data as last year. The expectation is to at least double that sample again in 2012, but for the longer term the collaboration plans to upgrade the experiment so that it can operate at higher luminosity and accumulate an order of magnitude more data. This will allow even higher precision in the search for new physics in the flavour sector. In this pattern of events, the LHCb LNF group had a key role in many aspects, starting from Pierluigi Campana that the 1^{st} June 2011 iniziated his three years mandate as spokeperson of LHCb collaboration.

From the beginning the main focus of the LNF group activities has been on the muon detector. On this side the work naturally continued with contribution to detector maintenance (spare chambers assembly and reparation), with muon piquet shifts, with the development of a software to the online monitor of the muon chamber efficiency, (sec.2), with a six month assignement as Operation Coordinator of the Muon System (P. de Simone), and finally with the finalization of the validation and calibration of the offline muon identification algorithm (sec.3) employed in many data analyses.

After the publication [1] of the study of J/ψ production in pp collisions (with measurement of the contribution from b-decays), the effort on data analysis concentrated in the measurement of the branching fraction of the very rare decays $B_s^0 \to \mu^+\mu^-$ and $B^0 \to \mu^+\mu^-$; in this the LNF team partecipated in all of the aspects of the analysis (sec.4), giving a strong contribution (G. Lanfranchi as a convener of the analysis group, too) to the publication of many results along the 2011 year. In March the result obtained with 2010 data [2, 3] has been published; an update (from the first 300 pb^{-1} of 2011 data taking) has been presented at 2011 summer conferences [4, 5]; a measurement with 370 pb^{-1} has been published at the end of 2011 [6, 7], while the whole group worked in paralel to finalize the analysis of the whole 1 fb^{-1} data sample [8], for which the result will be presented at the 2012 winter conferences.

Finally, for what concern the far future the key to the upgrade will be to read out the full experiment at 40 MHz, the design bunch-crossing rate of the LHC, and to perform the trigger software in a powerful computer farm. For this to succeed, collisions will indeed have to be provided by the LHC at 40 MHz at the time of the upgrade, rather than at the current rate of 20 MHz. The LNF group will garantee the full operation of the Muon System at 40 MHz, the production of the needed muon chambers, and the possible production of new chambers for the inner part of the system (the highest rate region). The rise in occupancy foreseen in the innermost part of the LHCb tracking stations from a higher LHC luminosity, suggests alternative tracking solutions should be explored for the LHCb upgrade. A new tracking option will require a more granular and faster detector, capable of withstanding degradation from the higher radiation rates and must also satisfy the requirement of covering the large area of the innermost region while retaining good spatial resolution with a low material budget. As part of the R&D collaboration effort in this respect, during 2011 a a prototype of tracking detector constructed with thick ($\sim$1 mm) plastic scintillating fibres has been built and tested at LNF [9].

2 Monitoring of the muon chamber efficiency

The LHCb muon sistem, which has the purpose of muon triggering and the offline muon identification, is composed of five stations (M1-M5) of rectangular shape, placed perpendicular to the beam axis. The full system comprises 1380 chambers of MWPC type, except in the highest rate region of M1, where triple-GEM's are used.

The procedure to monitor the muon chamber efficiency developed by the Frascati group and described in the 2009 report is now part of the official package to monitor the quality of the collected collision data, the left panel of figure 1 shows the corresponding data quality page.

Recently the procedure has been completed with the monitor of the first station M1, and with a new selection that removes from the probe μ tracks sample, the bias

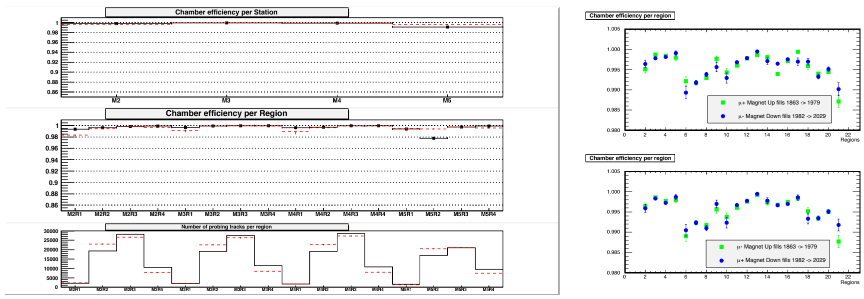

Figure 1: Left: the first plot is the muon chamber efficiency per station (M2-M5), the second plot is the efficiency per region (each station is divided into 4 regions), and the third plot is number of probe muon tracks with $p > 15$ GeV/c selected per region, and used to measure the efficiency. The dotted red lines are the reference histograms. Right: muon chamber efficiency per charge measured using $J/\psi \to \mu^+\mu^-$ from b hadrons inclusive decays, selected on about 200 pb^{-1} magnet up and magnet down data samples.

introduced by the μ tracks that contribute to the trigger decision. In addition, plots to monitor the efficiency per muon charge have been added, the right panel of figure 1 shows the muon chamber efficiencies per charge and magnet polarity.

3 Offline muon identification

Using the first 300 pb^{-1} acquired in 2011 we studied of the performance of the muon identification algorithm, the muonID [10]. The higher statistics available with respect to the previous study [11] allows to a deeper understanding of different effects (like the systematics arising from the method used to measure the efficiency) formerly hidden behind the statistical fluctuation of the measurements.

To measure the efficiency of the muonID we use an abundant source of muons provided by the $J/\psi \to \mu^+\mu^-$ inclusive decays from b hadrons, which has a very clean signature, while we exclude the prompt J/ψ , to avoid the combinatorial background due to the tracks coming from the primary vertex. The cross section for $J/\psi \to \mu^+\mu^-$ from b decays has been measured by the LHCb experiment with the 2010 data at $\sqrt{s} = 7$ TeV: $\sigma(J/\psi$ from b, $p_T < 14\,\mathrm{GeV}/c$, $2 < y < 4.5) = 1.14 \pm 0.01 \pm 0.16\mu$b. Taking into account trigger and reconstruction efficiencies ($\sim$5% on average, the actual value depending on variable trigger conditions), $\sim$10 events of $J/\psi \to \mu^+\mu^-$ from b per nb^{-1} are available.

The tag-and-probe method is applied on the $J/\psi \to \mu^+\mu^-$ sample, where one of the muon is requested to be identified by the muonID (μ_{tag}) while the second muon is selected without using any information from the muon system (μ_{probe}). This second muon is used to estimate the efficiency of the muonID, and the perfomance of Muon DLL hypothesis test.

The muonID efficiency can be factorized into two steps. The first contribution is the geometrical acceptance, α_μ, i.e. the request that the $\mu_{\rm probe}$ points to the muon detector. The second contribution is related to the efficiency of finding hits in the muon stations within same defined FIeld Of Interest (FoI), ϵ_μ.

The values of the MuonID acceptance, α_μ, and the efficiency given acceptance, ϵ_μ, are extracted from the above samples of unbiased $\mu_{\rm probe}$, properly selecting the events around the J/ψ mass peak. Since the average acceptance or efficiency measured in a given mass window includes contributions from both muons from J/ψ and spurious tracks, a background subtraction procedure has to be applied. We measure α_μ as

$$\alpha_\mu = \frac{S(MuFlag=1)}{S(MuFlag=1)+S(MuFlag=0)},$$

where S(MuFlag=1) and S(MuFlag=0) are the number of $\mu_{\rm probe}$ from Jpsi (signal events) found in the events mass distribution satisfying or not satisfying the proper muon condition, respectively. The signal is obtained by subtracting from the number of events in the signal mass region the background events in the same region extrapolated from a linear fit to the mass sidebands. The use of a different method to evaluate α_μ and/or of a different approach to subtract the background, translate into four possible estimates. Differences between the latters allow to asses a systematic error due to the chosen method. The same considerations hold for the determination of ϵ_μ.

Figure 2 shows the muon acceptance α_μ (left panel) and efficiency ϵ_μ (right panel) measured using the $J/\psi \to \mu^+\mu^-$ inclusive decay from b decays for the first 325 pb^{-1} collected in 2011, as a function of the $\mu_{\rm probe}$ momentum. For both α_μ and ϵ_μ all of the four methods give consistent errors, at the per mill level. Important issues, such as the trigger unbias and the selection strategies, can give systematic shifts (of up to $\sim$1%) in the above efficiency determinations. In both cases, the underlying effect seems related to a modification of the p_T (or p) spectrum, which can only be overcome by performing the analysis along two axes, p vs p_T (or p vs η). This is actually the next step of this analysis, and it will be addressed on the whole 1 fb^{-1} 2011 data set.

4 Search for the rare decays $B_s^0 \to \mu^+\mu^-$ and $B^0 \to \mu^+\mu^-$

The main goal of the LHCb experiment is to perform precision tests of the Standard Model (SM) in the flavour sector, namely the decays of the b−hadrons, with enough sensitivity to disentangle possible new physics effects. One of the most promising results in the initial phase of the LHCb physics program is certainly the search for the very rare dimuon decays of the B^0 and B_s^0 mesons. Within the SM these decays, which are in addition helicity suppressed, can only happen through loop diagrams (see fig.3). They can have very different branching fractions ($\mathcal{B}$) in new physics models, especially in those with an extended Higgs sector; in particular, in supersymmetric models large enhancements are possible. The SM predictions have

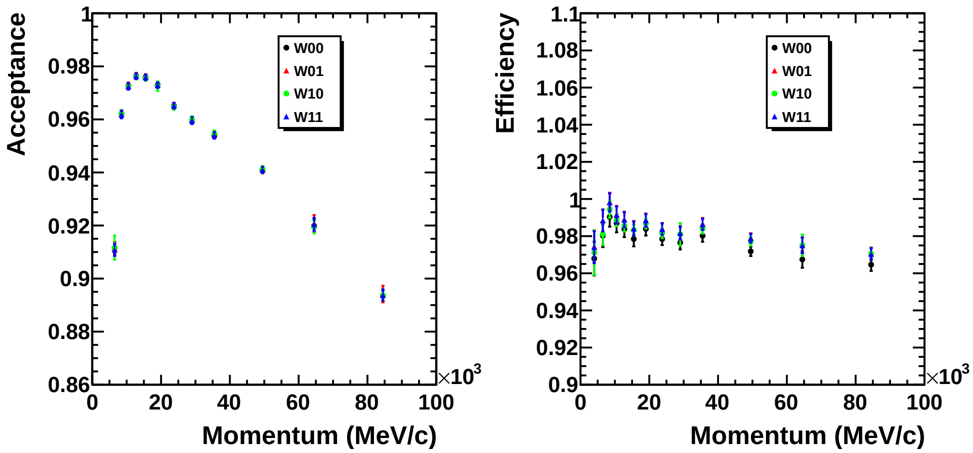

Figure 2: Comparison of α_μ (left) and ϵ_μ (right) as a function of $\mu_{\rm probe}$ momentum evaluated on *JpsiFromB* 2011 data, using two different methods and two different background subtraction strategies.

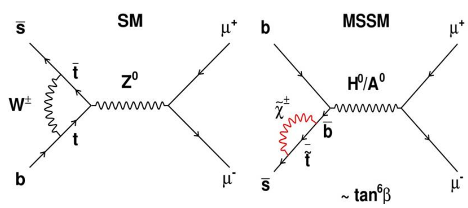

Figure 3: *Dominant Feynman diagram contribution to the branching ratio within the SM (left) and within the MSSM with R-parity conservation (right).*

a relative precision of less than 10%:

$$\mathcal{B}(B^0_s \to \mu^+\mu^-)_{\rm SM} = (3.2 \pm 0.2) \times 10^{-9} \tag{1}$$

$$\mathcal{B}(B^0 \to \mu^+\mu^-)_{\rm SM} = (1.0 \pm 0.1) \times 10^{-10}. \tag{2}$$

Published upper limits from the D0, CDF, and CMS collaborations set already stringent limits to possible deviations from the SM predictions. The best published limits to date come from the LHCb collaboration (using 0.37 fb^{-1} of the 2011 data set) $\mathcal{B}(B^0_s \to \mu^+\mu^-) < 1.4 \times 10^{-8}$ and $\mathcal{B}(B^0 \to \mu^+\mu^-) < 3.2 \times 10^{-9}$ at 95% CL: they are about a factor 4 and 30 respectively above the SM predictions. The CDF collaboration has also reported an excess of $B^0_s \to \mu^+\mu^-$ candidates compatible with $\mathcal{B}(B^0_s \to \mu^+\mu^-) = 1.8^{+1.1}_{-0.9} \times 10^{-8}$. In the following we will give a summary of the LHCb measurement and the perspectives for the 1 fb^{-1} update.

The LHCb experiment is well suited for such searches due to its excellent invariant mass resolution, vertex resolution, muon identification and trigger acceptance. Moreover, among the LHC experiments, LHCb has a unique trigger capability of providing large samples of hadronic $B_q^0 \to h^+h^-$ decays. These are used as control samples in order to reduce the dependence of the results on the simulation [6].

Assuming the branching fractions predicted by the SM, and using the $b\bar{b}$ cross-section measured by LHCb in the pseudorapidity interval 2<6 and integrated over all transverse momenta of $\sigma_{b\bar{b}} = (75 \pm 14)\mu b$, approximately 3.9 $B_s^0 \to \mu^+\mu^-$ and 0.4 $B^0 \to \mu^+\mu^-$ events are are expected to be triggered, reconstructed and selected in the analysed sample embedded in a large background

The first step of the analysis is a very efficient selection which removes the biggest amount of background while keeping most of the signal within the LHCb acceptance. The number of observed events is compared to the number of expected signal and background events in bins of two independent variables, the invariant mass and the output of a multi-variate discriminant. The discriminant is a Boosted Decision Tree (BDT) constructed using the TMVA package. It supersedes the Geometrical Likelihood used in the previous analysis [2] as it has been found more performant in discriminating between signal and background events in simulated samples. No data were used in the choice of the multivariate discriminant in order not to bias the result. The combination of variables entering the BDT discriminant is optimized using simulated events. The probability for a signal or background event to have a given value of the BDT output is obtained from data using $B_q^0 \to h^+h^{'-}$ candidates (where $h^{'-}$ can be a pion or a kaon) as signal and sideband $B_{(s)}^0 \to \mu^+\mu^-$ candidates as background.

The invariant mass line shape of the signals is described by a Crystal Ball function with parameters extracted from data control samples. The central values of the masses are obtained from $B^0 \to K^+\pi^-$ and $B_s^0 \to K^+K^-$ samples. The B_s^0 and B^0 mass resolutions are estimated by interpolating those obtained with di-muon resonances (J/ψ, $\psi(2S)$ and $\Upsilon(1S, 2S, 3S)$) and cross-checked with a fit to the invariant mass distributions of both inclusive $B_s^0 \to h^+h^{'-}$ decays and exclusive $B^0 \to K^+\pi^-$ decays. The central values of the masses and the mass resolution are used to define the signal regions.

The number of expected signal events, for a given branching fraction hypothesis, is obtained by normalizing to channels of known branching fractions: $B^+ \to J/\psi(\mu^+\mu^-)K^+$, $B_s^0 \to J/\psi(\mu^+\mu^-)\phi(K^+K^-)$ and $B^0 \to K^+\pi^-$. These channels are selected in a way as similar as possible to the signals in order to minimize the systematic uncertainty related to the different phase space accessible to each final state. Using these normalization channels the branching ratios can be calculated as:

$$\begin{aligned} \mathcal{B}_{sig} &= \mathcal{B}_{norm} \times \frac{\epsilon_{\rm norm}^{\rm REC}\epsilon_{\rm norm}^{\rm SEL|REC}\epsilon_{\rm norm}^{\rm TRIG|SEL}}{\epsilon_{\rm sig}^{\rm REC}\epsilon_{\rm sig}^{\rm SEL|REC}\epsilon_{\rm sig}^{\rm TRIG|SEL}} \times \frac{f_{\rm norm}}{f_{B_q}} \times \frac{N_{\rm B^0_{(s)}\to\mu^+\mu^-}}{N_{\rm norm}} \qquad (3) \\ &= \alpha^{\rm norm}_{\rm B^0_{(s)}\to\mu^+\mu^-} \times N_{\rm B^0_{(s)}\to\mu^+\mu^-}. \qquad (4) \end{aligned}$$

This normalization ensures that the knowledge of the absolute luminosity and total cross-section is not needed. In Eq.4, f_{B_q} and $f_{\rm norm}$ denote the probabilities that a b-quark fragments into a B_q^0 and into the b-hadron relevant for the chosen normalization channel with branching fraction $\mathcal{B}_{norm}$. LHCb has measured $f_s/f_d = 0.267^{+0.021}_{-0.020}$. The reconstruction efficiency (ϵ^{REC}) includes the acceptance and particle identification, while $\epsilon^{\mathrm{SEL|REC}}$ denotes the selection efficiency on reconstucted events. The trigger efficiency on selected events is denoted by $\epsilon^{\mathrm{TRIG|SEL}}$. Finally, $\alpha^{\mathrm{norm}}_{\mathrm{B}^0_{(s)}\to\mu^+\mu^-}$ is the normalization factor (or single event sensitivity) and $N_{\mathrm{B}^0_{(s)}\to\mu^+\mu^-}$ the number of observed signal events. For each normalization channel N_{norm} is obtained from a fit to the invariant mass distribution.

The BDT output and invariant mass distributions for combinatorial background events in the signal regions are obtained using fits of the mass distribution of events in the mass sidebands in bins of the BDT output.

The definition of the BDT variable is such that background events cluster around zero, and signal events will be uniformly distributed between zero and one. Therefore the *sensitive region* (i.e. the region from which most of the sensitivity to the $B_s^0 \to \mu^+\mu^-$ and $B^0 \to \mu^+\mu^-$ branching fractions comes from) is defined by the 2-dimensional region BDT > 0.5 and $M_B - 60\mathrm{MeV/c^2} < M(\mu^+\mu^-) < M_B + 60\mathrm{MeV/c^2}$.

The two-dimensional space formed by the invariant mass and the BDT output is binned. For each bin we count the number of candidates observed in the data, and compute the expected number of signal events and the expected number of background events. The binning is unchanged with respect to the 2010 analysis. The compatibility of the observed distribution of events in all bins with the distribution expected for a given branching fraction hypothesis is computed using the CLs method, which allows a given hypothesis to be excluded at a given confidence level.

At the end, a weighted average of the three normalization channels, assuming the tracking and trigger uncertainties to be correlated between the two J/ψ normalization channels and the uncertainty on f_d/f_s to be correlated between the $B^+ \to J/\psi(\mu^+\mu^-)K^+$ and $B^0 \to K^+\pi^-$, gives

$$\alpha^{\mathrm{norm}}_{\mathrm{B^0_s}\to\mu^+\mu^-} = (8.38 \pm 0.74) \times 10^{-10}, \quad (5)$$

$$\alpha^{\mathrm{norm}}_{\mathrm{B^0}\to\mu^+\mu^-} = (2.20 \pm 0.11) \times 10^{-10}. \quad (6)$$

These normalization factors are used to determine the limits. The two dimensional ($M(\mu^+\mu^-)$, BDT) distribution of selected dimuon events can be seen in fig. 4.

The compatibility of the distribution of events inside the search window in the (mass,BDT) plane with a given branching fraction hypothesis is evaluated using the CL$_s$ method. This method provides three estimators: CL$_{s+b}$, a measure of the compatibility of the observed distribution with the signal and background hypotheses, CL$_b$, a measure of the compatibility with the background-only hypothesis and CL$_s$, a measure of the compatibility of the observed distribution with the signal and background hypotheses normalized to the background-only hypothesis. The expected CL$_s$ values are shown in Fig. 5 for $B_s^0 \to \mu^+\mu^-$ and $B^0 \to \mu^+\mu^-$ as dashed black lines under the hypothesis that background and SM events are observed. The

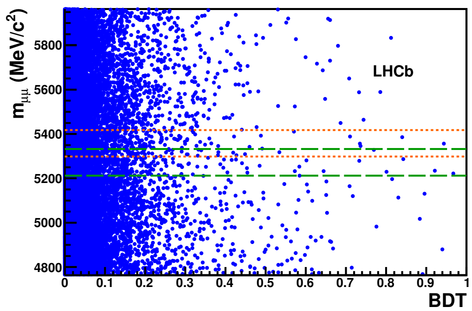

Figure 4: *Observed distribution of selected dimuon events in the plane GL vs dimuon invariant mass.The green long-dashed (orange short-dashed) lines indicates the* $B^0 \pm 60\mathrm{MeV/c}^2 (B_s \pm 60\mathrm{MeV/c}^2)$ *search windows.*

shaded areas cover the region of $\pm 1\sigma$ of compatible observations. The observed values of CL_s as a function of the assumed branching ratio is shown as dotted blue lines on both plots.

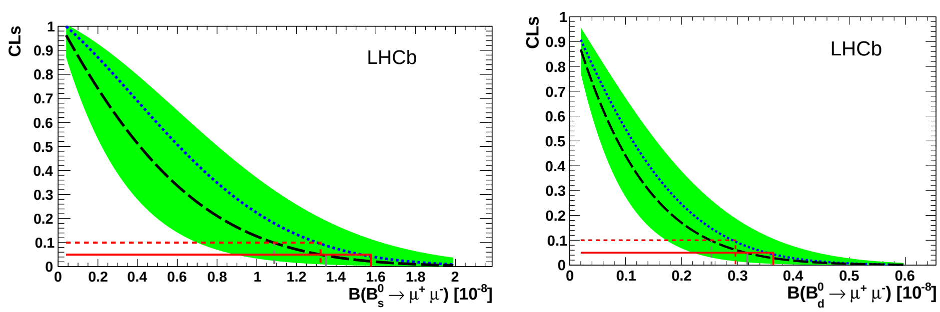

Figure 5: *CL_s as a function of the assumed $\mathcal{B}$. Expected (observed) values are shown by dashed black (dotted blue) lines. The expected CL_s values have been computed assuming a signal yield corresponding to the SM $\mathcal{B}$. The green (grey) shaded areas cover the region of $\pm 1\sigma$ of compatible observations. The measured upper limits at 90% and 95% CL are also shown. Left: $\mathcal{B}(B_s \to \mu^+\mu^-)$, right $\mathcal{B}(B^0 \to \mu^+\mu^-)$.*

The expected limits and the measured limits at 95% CL are:$\mathcal{B}(B_s^0 \to \mu^+\mu^-) < 14 \times 10^{-9}$ and $\mathcal{B}(B^0 \to \mu^+\mu^-) < 3.2 \times 10^{-9}$ For the $\mathcal{B}(B_s \to \mu^+\mu^-)$ decay, the expected limits are computed allowing the presence of $\mathcal{B}(B_s \to \mu^+\mu^-)$ events according to the SM branching fraction. For the $\mathcal{B}(B^0 \to \mu^+\mu^-)$ decay the expected limit is computed in the background-only hypothesis and also allowing the presence of $\mathcal{B}(B^0 \to \mu^+\mu^-)$ events with the SM rate: the two results are identical. In the determination of the limits, the cross-feed of $\mathcal{B}(B_s^0 \to \mu^+\mu^-)$ ($\mathcal{B}(B^0 \to \mu^+\mu^-)$)

events in the B^0 (B_s^0) mass window has been taken into account assuming the SM rates. The observed CL_b values at 95% CL are: $\mathcal{B}(B_s^0 \to \mu^+\mu^-) < 16 \times 10^{-9}$ and $\mathcal{B}(B^0 \to \mu^+\mu^-) < 3.6 \times 10^{-9}$ The comparison of the observed distribution of events with the expected background distribution results in a p-value ($1-\mathrm{CL}_b$) of 5% for the $\mathcal{B}(B_s^0 \to \mu^+\mu^-)$ and 32% for the $\mathcal{B}(B^0 \to \mu^+\mu^-)$ For the $\mathcal{B}(B_s^0 \to \mu^+\mu^-)$ decay, the probability that the observed events are compatible with the sum of expected background events and signal events according to the SM rate is measured by $1-\mathrm{CL}_{s+b}$ and it is 33%. The result obtained in 2011 with 0.37 fb^{-1} has been combined with the published result based on $\sim$37 pb^{-1}. The expected limits for 95 % CL for the combined results are: $\mathcal{B}(B_s^0 \to \mu^+\mu^-) < 13 \times 10^{-9}$ and $\mathcal{B}(B^0 \to \mu^+\mu^-) < 3.0 \times 10^{-9}$. The observed limits for 95 % CL for the combined results are: $\mathcal{B}(B_s^0 \to \mu^+\mu^-) < 14 \times 10^{-9}$ and $\mathcal{B}(B^0 \to \mu^+\mu^-) < 3.2 \times 10^{-9}$.

5 List of Conference Talks by LNF Authors in Year 2011

1. Rare decays results and prospects with LHCb, M. Palutan LHCb-TALK-2011-047.- Geneva : CERN, 2011 - 38.
   Presented at : 13th International Conference on B-Physics at Hadron Machines, Amsterdam, Netherlands, 4 - 8 Apr 2011

2. Rare decay results and prospects with LHCb, M. Palutan, PoS BEAUTY 2011 042,2011.

3. Ricerca di effetti di nuova fisica nel decadimento $B_{(s)}^0 \to \mu^+\mu^-$ a LHCb, M. Palutan, IFAE 2011, Perugia, 28 Aprile 2011.

4. Search for New Physics in $B_{(s)}^0 \to \mu^+\mu^-$ Decays at LHCb, F. Archilli, LHCb-TALK-2011-216.- Geneva : CERN, 2011 - 20. Presented at : Brookhaven Forum 2011: A first Glimpse of the Tera Scale, Upton, Ny, United States Of America, 19 - 21 Oct 2011

5. Exclusive rare B decays: $B_s^0 \to \mu^+\mu^-$ and $B^0 \to \mu^+\mu^-$, G. Lanfranchi LHCb-TALK-2011-189.- Geneva : CERN, 2011 - 54. Presented at : Flavour and the Fourth Family, Durham, Royaume Uni, 14 - 16 Sep 2011

6. Search for the rare decays $B_s^0 \to \mu^+\mu^-$ and $B^0 \to \mu^+\mu^-$ with LHCb, G. Lanfranchi LHCb-TALK-2011-030.- Geneva : CERN, 2011 - 49. Presented at : Les Rencontres de Physique de la Valle d'Aoste, La Thuile, Italy, 27 Feb - 5 Mar 2011

7. Operation and Performance of the LHCb Experiment, P. de Simone on behalf of the LHCb Collaboration LHCb-TALK-2011-002.- Geneva : CERN, 2011 - 25. Presented at : Cracow Epiphany Conference on the First Year of the LHC, Cracow, Poland, 10 - 12 Jan 2011

6 Publications and internal notes

References

1. R. Aaij *et al.* The LHCb Collaboration Measurement of $J\psi$ production in pp collisions at $\sqrt{s} = 7$ TeV arXiv:1103.0423; Eur. Phys. J. C **71** 1645 (2011).

2. C. Adrover *et al.*, Search for the rare decays $B^0_{(s)} \to \mu^+\mu^-$ with the LHCb experiment, CERN-LHCb-ANA-2011-007.

3. R. Aaij *et al.* The LHCb Collaboration Searches for the rare decays $B^0_s \to \mu^+\mu^-$ and $B^0 \to \mu^+\mu^-$, arXiv:1103.2465; Phys. Lett. B **699** 330-340 (2011)

4. *et al.* The LHCb Collaboration, Search for the rare decays $B^0_s \to \mu^+\mu^-$ with 300 pb^{-1} at LHCb,
   LHCb-CONF-2011-037, Conference report prepared for the 2011 Europhysics Conference on High-Energy Physics (EPS-HEP 2011), Grenoble, France 21-27 July 2011

5. Search for the rare decay $B^0_s \to \mu^+\mu^-$ at the LHC with the CMS and LHCb experiments. Combination of LHC results of the search for $B^0_s \to \mu^+\mu^-$ decays. CMS-PAS-BPH-11-019; LHCb-CONF-2011-047; Geneva CERN (2011)

6. C. Adrover *et al.* Search for the rare decays $B^0_s \to \mu^+\mu^-$ with 370 pb^{-1} at LHCb, LHCb-ANA-2011-078

7. R. Aaij *et al.* The LHCb Collaboration Searches for the rare decays $B^0_s \to \mu^+\mu^-$ and $B^0 \to \mu^+\mu^-$, arXiv:1112.1600v3 [hep-ex]; Phys. Lett. B **708** 55-67 (2012)

8. C. Adrover *et al.*, Search for the rare decays $B^0_s \to \mu^+\mu^-$ and $B^0 \to \mu^+\mu^-$ with 1.1 fb^1 at LHCb, LHCb-ANA-2011-102; CERN-LHCb-ANA-2011-102.- Geneva : CERN, 2011

9. B.D. Leverington, M. Anelli, P. Campana, R. Rosellini, A 1 mm Scintillating Fibre Tracker Readout by a Multi-anode Photomultiplier, arXiv:1106.5649v2 [physics.ins-det] (2011).

10. K. Akiba *et al.*, Results on Muon identification efficiency with 2011 data at LHCb. LHCb-INT-2011-045; CERN-LHCb-INT-2011-045

11. K. Akiba *et al.*, Muon Identification performance at LHCb with the 2010 data LHCb-INT-2011-048; CERN-LHCb-INT-2011-048

NA62

A. Antonelli (Resp.), M. Moulson,
M. Raggi (Art. 23), T. Spadaro,

In collaboration with
E. Capitolo, R. Lenci, B. Ponzio, V. Russo,
M. Santoni, S.Valeri, T. Vassilieva;
the Servizio di Progettazione Apparati Sperimentali (SPAS):
C. Capoccia, A. Cecchetti;
the Servizio di Sviluppo e Costruzione Rivelatori (SSCR):
G. Bisogni, A. Franceschi
the Divisione Acceleratori, Servizio di Vuoto:
R. Di Raddo, V. Lollo
and the Servizio di Elettronica:
G. Corradi, C. Paglia, D. Tagnani

1 The NA62 Experiment

The branching ratio (BR) for the decay $K^+ \to \pi^+\nu\bar{\nu}$ can be related to the value of the CKM matrix element V_{td} with minimal theoretical uncertainty, providing a sensitive probe of the flavor sector of the Standard Model. The measured value of the BR is $1.73^{+1.15}_{-1.05} \times 10^{-10}$ on the basis of seven detected events [1]. NA62, an experiment at the CERN SPS, was originally proposed as P326 with the goal of detecting $\sim$100 $K^+ \to \pi^+\nu\bar{\nu}$ decays with a S/B ratio of 10:1 [2]. The experimental layout is illustrated in Fig. 1.

The experiment will make use of a 75 GeV unseparated positive secondary beam. The total beam rate is 800 MHz, providing $\sim$50 MHz of K^+'s. The decay volume begins 102 m downstream of the production target. 5 MHz of kaon decays are observed in the 65-m long fiducial vacuum decay region. Ring-shaped large-angle photon vetoes are placed at 12 stations along the decay region and provide full coverage for decay photons with 8.5 mrad $< \theta <$ 50 mrad. The last 35 m of the decay region hosts a dipole spectrometer with four straw-tracker stations operated in vacuum. The NA48 liquid krypton calorimeter [3] is used to veto high-energy photons at small angle. Additional detectors further downstream extend the coverage of the photon veto system (e.g. for particles traveling in the beam pipe).

The experiment must be able to reject background from, e.g., $K^+ \to \pi^+\pi^0$ decays at the level of 10^{12}. Kinematic cuts on the K^+ and π^+ tracks provide a factor of 10^4 and ensure 40 GeV of electromagnetic energy in the photon vetoes; this energy must then be detected with an inefficiency

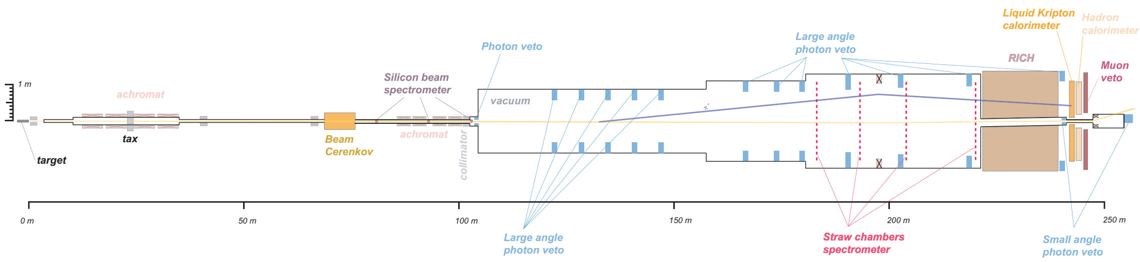

Figure 1: *The NA62 experimental layout.*

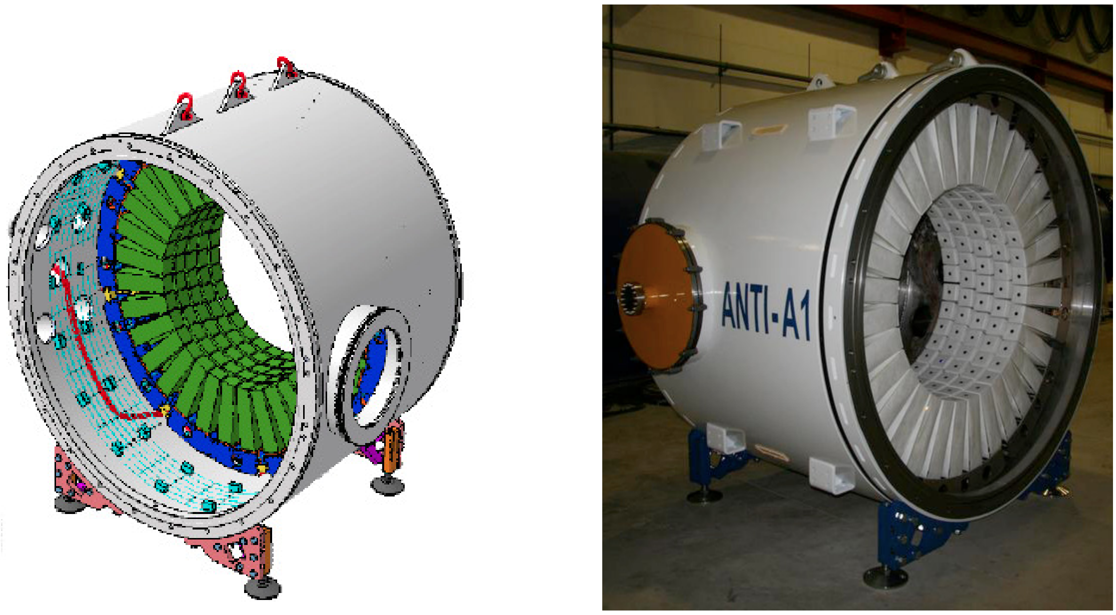

Figure 2: *Left: Design study for the upstream LAV stations. Right: Photograph of the prototype ANTI-A1.*

of $\leq 10^{-8}$. For the large-angle photon vetoes, the maximum tolerable detection inefficiency for photons with energies as low as 200 MeV is 10^{-4}. In addition, the large-angle vetoes (LAVs) must have good energy and time resolution and must be compatible with operation in vacuum.

The principal involvement of the LNF NA62 group is in the design and construction of the LAV system. In 2011, the main responsibilities of the LNF NA62 group were the following:

- continued development of tools and procedures for assembly of the ANTI station;
- production of final drawings for the downstream LAV stations 9,10,11;
- assembly of 4 LAV stations;
- vacuum testing and outgassing measurements for finished LAV stations;
- prototype production and testing of the front-end electronics for the LAV system;
- coordination of the NA62 Photon Veto working group.

2 Large-Angle Photon Vetoes

The LAV design is based on the reuse of the lead-glass blocks from the central part of the OPAL electromagnetic calorimeter barrel [4]. The blocks are made of SF57 lead glass and have an asymmetric, truncated square-pyramid shape. The front and rear faces of the blocks measure about 10×10 cm^2 and 11×11 cm^2, respectively; the blocks are 37 cm long. The modules are read out at the back side by Hamamatsu R2238 76-mm PMTs, coupled via 4-cm cylindrical light guides of SF57. The LAV system consists of 12 stations. The diameter of the stations increases with distance from the target, as does the number of blocks in each, from 160 to 256, for a total of about 2500 blocks. Each station consists of four or five rings of blocks, with the blocks staggered in azimuth in successive rings. The total depth of a five-layer station is 27 radiation lengths. This structure guarantees high efficiency, hermeticity, and uniformity of response. The final design for the first five stations is illustrated in Fig. 2, left.

2.1 LAV construction

The first LAV station, ANTI-A1, was constructed in 2009 and served as a prototype; three more of the upstream LAV stations, ANTI-A2, A3, and A4, were built at LNF during 2010. In 2011 with the construction of A5, the series of stations of smallest diameter was completed. The prototype A1 station was refurbished to include modifications to the design made after the analysis of the 2009 A1 test beam data. The construction of the A6 and A7 stations, of intermediate diameter, together with a new set of appropriate handling and construction tools, was also completed. Details on the assembly procedure can be found in [6]. So far during the construction of the LAV detectors, more than 1400 lead-glass blocks ($\sim 57\%$ of the total) have been tested. Only 0.7% of these were discarded due to insufficient photomultiplier gain.

Much progress has also been made on the mechanical designs for the larger stations. The executive drawings for the vacuum vessels of the large-diameter vessels (A9-A11) have been finalized and the construction contract has been assigned. The construction of the A8 vessel was started at the Fantini SpA facility in Anagni (FR) at the end of 2011.

2.2 LAV front-end electronics

Monte Carlo simulations have shown that photons from $K^+ \to \pi^+\pi^0$ decay with a wide range of energies, from a few tens of MeV to several GeV, reach the veto stations. To allow photons from $\pi^+\pi^0$ events to be rejected with a maximum inefficiency of 10^{-4}, the detectors must simultaneously furnish time and energy measurements. The time resolution is dominated by the intrinsic contribution from the detectors. For the energy measurement, the biggest challenge in the design of the readout electronics is the need to accept signals over an extended dynamic range, from a few millivolts to tens of volts, while providing charge measurements with a precision of better than 10%.

Since 2010, the LNF group has been responsible for the design and construction of the front-end electronics for the large-angle veto system. The basic idea is to exploit the time-over-threshold technique to measure the signal charge over a broad interval. A custom 9U board designed by the LNF Servizio di Elettronica converts the analog signals from the PMTs into an LVDS logic signal of the same width. The width will be measured by a TDC and its value used to reconstruct the charge. The energy can thus be measured via TDC time measurements only. Five prototype 9U front-end electronics boards were produced, assembled, and tested during 2011.

The LAV front-end board is implemented on a 9U VME standard layout with the J1 power connector only at the top of the backplane side. No VME bus line is connected to the board; only customs ±12V power lines are used. The $\pm 12V$ supply voltage is reduced to $\pm 7.5V$ by custom designed very-low-noise switching voltage regulators and then distributed all along the board. At the bottom, the 32 analog inputs are connected to the board using two DB37 connectors (see Fig. 3). Each single input produces two different outputs due to the presence of two programmable thresholds on each channel. The resulting 64 LVDS digital outputs are connected to the TDC using two SCSI2 connectors placed on the front panel of the board. The analog sums of 4 and 16 channels are provided on 8 + 2 LEMO00 connectors for monitoring of the analog signal. The communication and the threshold settings are managed via two RJ-45 connectors using the CANOPEN protocol. To simplify maintenance and reduce costs, the board has a modular structure. The 9U motherboard manages input, output, and power distribution, while the other functions are implemented on 4 different mezzanines:

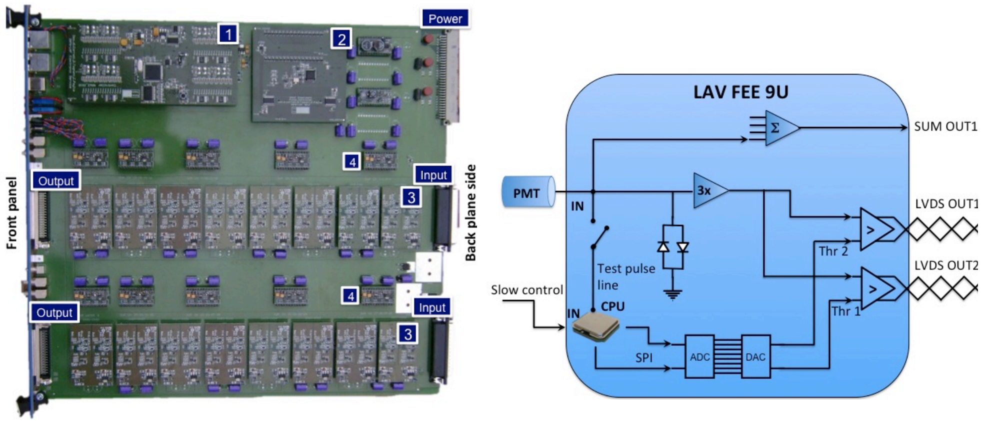

Figure 3: *The LAV front-end board (left) and its block diagram (right).*

1. Board controller mezzanine
2. Test pulse generator mezzanine
3. Time over threshold (ToT) mezzanine
4. Sum-of-4 mezzanine

A detailed description of each mezzanine can be found in [5]. Prototypes of all of the mezzanines were produced and tested in early 2011 at LNF. All electric and functional tests were successful. The production of the five 9U motherboards was started in fall 2011. The assembly of the five prototype 9U boards was made and a test completed. The measured value of time resolution and threshold linearity were within expectation. After minor modifications to the design, the production of 30 boards, to be used in the NA62 2012 technical run will start at the beginning of 2012.

3 LAV front end simulation

Much progress has also been made on the simulation of the system. The representation of the geometry of the LAV detectors in the NA62 Monte Carlo has been updated and completed. In order to better understand the performance of the detector and its electronics, a detailed Monte Carlo simulation has been developed in Frascati for the LAV digitization procedure. In the simulation, the number of photons on the PMT photocathode, their energies, and their arrival times are obtained from the official NA62 GEANT4 Monte Carlo. The behavior of the R2238 PMT is then simulated including the photocathode quantum efficiency as a function of the wavelength, the multiplication process in the 12 dynodes, the output RC circuit, and the cables. The simulated PMT signal is then processed by the simulation of the front end, which, taking into account thresholds and hysteresis, produces the value of the simulated leading and trailing times for pulses, allowing the calculation of the time over threshold (ToT). To validate the simulation, the curve of time over threshold vs charge has been compared with test beam data obtained in the ANTI-A2 test beam in 2010. The result is shown in Fig. 4, left. Very good agreement with the data is obtained over a large range of charge, from a few pC to $\sim$100 pC. Using this detailed simulation, a first study of the photon detection efficiency has been performed (Fig. 4, right).

The MC simulation will be validated by detailed comparison with test-beam data. Moreover, to assess the detector performance, methods will be implemented that are able to run both on data and MC, in particular exploiting the closed kinematics of $K^+ \to \pi^+\pi^0$ decays. A detailed study of the expected LAV performance as a function of detector and run conditions (electronic noise, muon beam halo, dead and noisy channels, miscalibration of FEE thresholds) will be performed.

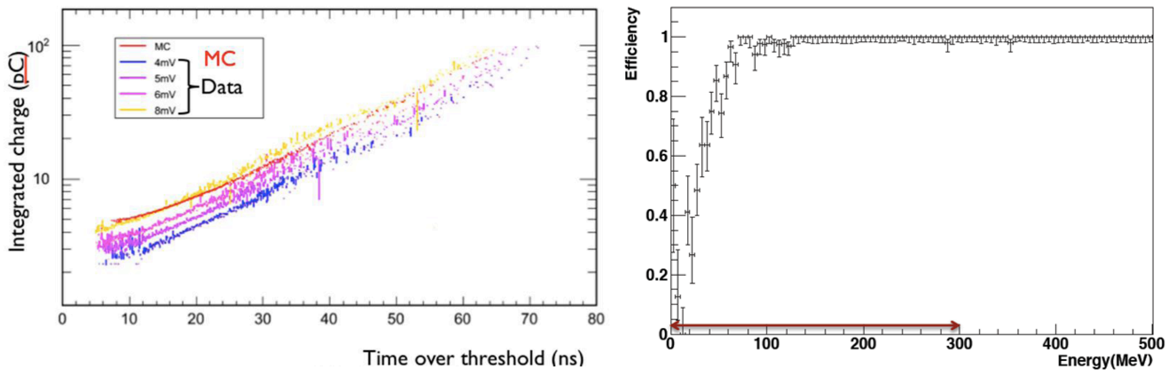

Figure 4: *Data-Monte Carlo comparison of time over threshold vs charge curve.*

4 Conference talk by NA62 LNF memebers

M. Raggi: Topical Workshop on Electronics for Particle Physics.
Vienna, Austria, 26^{th} to 30^{th} September 2011.
Poster: "The Readout Electronics of the NA62 Large Angle Photon Veto System".

M. Moulson: IEEE NSS/MIC
Valencia, Spain, 25-Oct-11
Poster: "The large-angle photon veto system for the NA62 experiment at CERN".

References

1. E949 Collaboration, A. Artamonov *et al.*, Phys. Rev. Lett. **101**, 191802 (2008).
2. F. Hahn *et al*, NA62 Technical Design Document, NA62-10-07 (2010).
3. NA48 Collaboration, V. Fanti *et al.*, Nucl. Instrum. Meth. A **574**, 433 (2007).
4. OPAL Collaboration, K. Ahmet *et al.*, Nucl. Instrum. Meth. A **305**, 275 (1991).
5. A. Antonelli *et al.*, JINST **7**, C01097 (2012)
6. F. Ambrosino *et al.*, arXiv:1111.4075 [physics.ins-det].

THE *SuperB* ACCELERATOR PROJECT

M.E. Biagini (resp.), R. Boni, M. Boscolo, A. Clozza, T. Demma, A. Drago, M. Esposito, S. Guiducci, S. Liuzzo, G. Mazzitelli, M. Preger, P. Raimondi, C. Sanelli, M. Serio, A. Stella, S. Tomassini, M. Zobov

1 Introduction

SuperB [1] is an asymmetric (6.7 GeV HER, 4.2 GeV LER) e^+e^- collider at the center of mass B pairs production energy (10.58 GeV), to be built in Italy, with a design peak luminosity of 10^{36} cm^2 s^{-1}. A collider like *SuperB* will open a unique window on this physics because it allows a high statistics study of the current hints of new aggregations of quarks and gluons. Besides the physics one can study in running at the Υ(4S) resonance, the following alternative energies are of interest: Υ(3S) (at least 0.3 ab^{-1}) and a high luminosity scan between 4-5 GeV (5 MeV steps of 0.2 fb^{-1} each would require a total of 40 fb^{-1}). While this is not huge statistics, this scan is only feasible with *SuperB*. The only possible competitor, BES-III, is not planning to scan above 4 GeV, since their data sample would, in any case, be lower than that of the B Factories alone. Finally, the search for exotic particles among the decay products of the "bottomonia" can probe regions of the parameters space of non-minimal supersymmetric models that cannot be otherwise explored directly, for instance at LHC.

The superiority of *SuperB* with respect to the planned upgrade of KEKB lies both in the ten times higher statistics, which broadens the range of cross sections the experiment is sensitive to, but also in the flexibility to change center of mass energy, and the possibility to collide with a polarized electron beam. Moreover the *SuperB* design will also allow for running at the τ/charm threshold with an expected luminosity of 10^{35} cm^2 s^{-1}.

The *SuperB* project has been approved by the Italian Government as part of the National Research Plan. The design is based on a large Piwinski angle and Crab Waist scheme already successfully tested at the DAΦNE $\Phi-$Factory in Frascati, Italy. The project combines the challenges of high luminosity colliders and state-of-the-art synchrotron light sources, with two beams with extremely low emittances and small beam sizes at the Interaction Point. As unique features, the electron beam will be longitudinally polarized at the IP and the rings will be able to ramp down to collide at the tau/charm energy threshold with one tenth the luminosity. The relatively low beam currents (about 2 A) will allow for low running (power) costs compared to similar machines. The insertion of beam lines for synchrotron radiation users is the latest feature included in the design. The lattice has been recently modified to accommodate insertion devices for X-rays production.

The construction site for *SuperB* has been selected in the campus of the Tor Vergata Rome II University, just 5 km away from the Frascati Laboratories. Fig. 1 is a sketch of the rings in the new site. In October 2011 for the construction and operation of the facility the "Nicola Cabibbo Laboratory" has been founded, as a consortium between INFN and the University of Rome II at Tor Vergata. Memorandum Of understanding (MOU) are in progress with France, SLAC and BINP (Russia).

Four general *SuperB* meetings have been organized in 2011: in March at LNF, in June at Elba (Italy), in September at Queen College (London, UK) and in December at LNF. A complete description of the work done is available from the meetings slides at:

http://agenda.infn.it/categoryDisplay.py?categId=109.

In the following section the work performed at LNF on the design of the accelerator will be briefly described. This activity at LNF has been funded by the INFN NTA commission, and has received by INFN a special funding in 2010-2011.

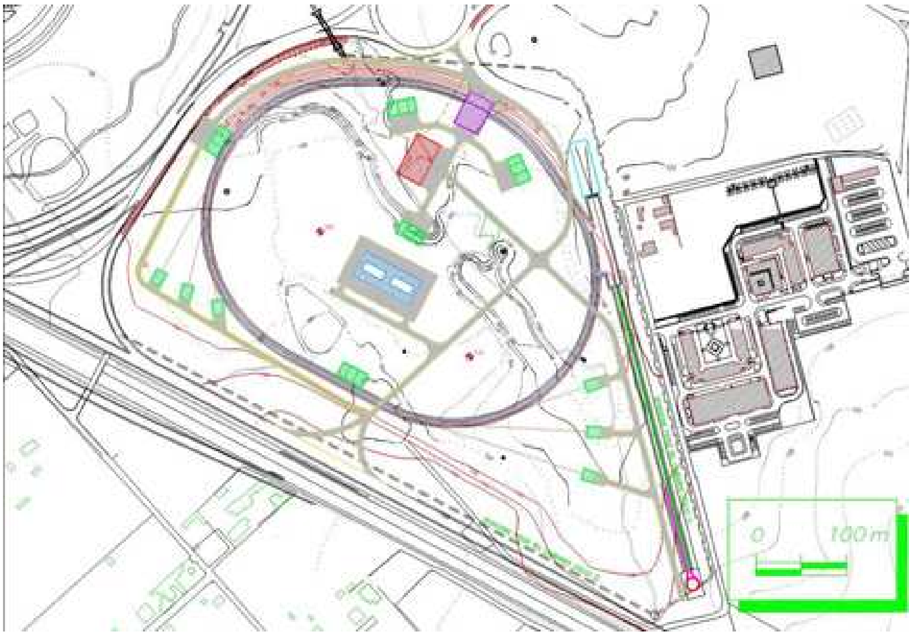

Figure 1: *Layout of SuperB accelerator at Tor Vergata.*

2 Design strategy

SuperB consists of two rings of different energy (positrons in HER, 6.7 GeV, electrons in LER, 4.2 GeV) colliding in one IR at a large (60 mrad total) horizontal angle. Spin rotator sections in the LER will provide helicity of a polarized electron beam. With respect to the past years design an important change is to have polarized electrons in the LER instead of the HER. This was chosen for easier insertion of Spin Rotator (SR) sections in LER lattice. Also the beam energies have been changed in order to avoid spin resonances, with a consequent small reduction of the center-of-mass boost.

The two rings lay in the horizontal plane, each has two arcs and two long straight sections. The Final Focus (FF) in one straight is combined with the two Arcs in two half-rings (one inner, one outer) and a straight section on the opposite side. The straight section comes naturally to close the ring and readily accommodate the RF system and other necessities (e.g. injection). In this utility region crossing without collisions for the two rings will be provided.

SuperB design is based on very low H-V emittances, low emittance coupling and very small beam sizes at the IP. Moreover the crab-waist sextupoles demand for particular care in designing the chromaticity correction in the FF. The accelerator lattice optics has been modified in 2011 to be able to install Insertion Devices in some of the stright sections, for future use as a Synchrotron Light Source. A separate chromaticity correction scheme has been developed for the two rings Arc-cells and for the FF. In the Arcs a scheme where all sextupoles are paired with a (-I) transfer matrix provides optimum correction and very small chromatic W functions and second order dispersion function in both planes. In the FF a special scheme has been designed with separate YCCS and XCCS sections (H-V chromaticity correction sextupoles) in phase with the IP, where the β functions reach a maximum, which works very well in terms of dynamic aperture and off momentum behavior of β functions and tunes. It has to be noted that a perfect correction is preferable for the crab-waist sextupoles, located at both ends of the FF, to avoid reduction of the dynamic aperture. A coupling correction scheme with the detector solenoid ON has been also designed.

3 Year 2010 activity

3.1 Beam dynamics

During 2011 a lot of work has been done on the most relevant beam dynamics issues, such as e-cloud instability, intra-beam scattering (IBS), Touschek backgrounds, etc. Touschek effect is the main source of lifetime reduction, even if the limiting effect for lifetime are the luminosity backgrounds. Touschek lifetime is computed with a tracking code which takes into account the lattice design and nonlinear elements. Special care is needed to control Touschek particle losses and reduce possible showers in the detectors. A set of collimators that fulfils this requirement has been found, with 3 primary H collimators in the FF, intercepting most of the particles that would be lost in the IR. A secondary collimator at s=-21 m will stop the remaining Touschek scattered particles generated so close to the IR that primary collimators cannot be effective. With the insertion of collimators the computed lifetime is 6.6 min in LER and 33.2 min in HER. The rings lifetime in collision is however dominated by the luminosity beam lifetime, a few minutes for each ring.

A Low Emittance Tuning (LET) procedure has been developed to correct magnet misalignments and BPM errors to achieve minimum coupling, β beating and vertical emittance. Tables of error tolerances have been produced for both the LER and HER elements. The β beating due to magnet misalignments after correction is between 3-5% in both planes for a rms misalignment error of 300 microns, the emittance coupling factor is always less than 0.1% (design is 0.25%). A comparison of performances with the LOCO tool, used for tuning in most SR rings, has been performed at the DIAMOND facility at RAL, showing that LET can indeed achieve comparable results in much less time.

IBS of particles inside a bunch can lead to an unwanted increase of the emittances and bunch length. Calculations based on a high energy approximation of the Bjorken-Mtingwa formalism show that IBS should be manageable in both *SuperB* rings. However some interesting aspects such as the impact of IBS during the damping process and its effect on beam distribution have been investigated using a newly developed multi-particle tracking code, based on the Zenkevich-Bolshakov algorithm. Benchmarking with conventional IBS theories gave good results, and a new semi-analytical model fits simulation results very well, being thus able to predict IBS effect at various bunch currents.

The effect of electron cloud instability in the positron ring has been also estimated. Build up and instability simulations show that e-cloud is a serious issue for the HER. An antechamber absorbing 99% of the synchrotron radiation and a maximum SEY of the surface below 1.2 could ensure stable operation because it would prevent e-cloud formation and its detrimental effect on the positron beam. A test of e-cloud clearing electrodes has been carried out successfully at the DAΦNE ring to check their effectiveness in suppressing the instability.

The installation of SR beam lines (50-100m long for large demagnification) in the HER has been proposed. Several experiments can be carried out, such as X-ray diffraction, SAXS, imaging with phase contrast, all requiring photon energy between 4 and 15 keV. Low divergence (1 mrad to 1 microrad) and very small spot size (1 micron) are also required. For this purpose the lattice has been modified to have at least 6 straight sections where Insertion Devices (ID) can be installed. Particular care has been devoted to maintain the small horizontal emittance and at the same time obtain betatron functions suitable to the ID needs. Work is in progress to evaluate ID parameters, such as undulator gaps, to avoid narrow gap IDs and impedance issues with high current operation.

3.2 IP quadrupoles

The *SuperB* collision scheme requires a short focus final doublet to reduce the vertical β function down to β_y^*=0.2 mm at the IP. The final doublet will be composed by a set of permanent samarium cobalt magnets (PM) and superconducting (SC) quadrupoles. In the present design the HER (LER values in parentheses) PM quadrupoles provide an integrated gradient of 23.1 T (11.2 T) over a magnetic length of 11 cm (7cm). The front pole face will be placed at 38 cm (30 cm) from the IP. The remaining vertical focusing strength will be provided by two (one) SC quadrupoles having an integrated gradient of 39.2 T (28.7 T) over a total magnetic length of 45 cm (30 cm). A cold bore design for the SC quadrupoles is not viable since the synchrotron radiation coming from the upstream dipoles will deposit about 200W on the beam pipe section inside the SC. The requested horizontal beam stay clear fixes both the warm bore diameter to 24 mm and the maximum thickness allowed for the cryostat and the SC cold mass to 22 mm. This limited amount of available space together with the requested field purity and gradient strength poses very demanding constraints on the SC magnets design. An advanced design of the quadrupole has been developed, based on the double helical coil concept. A prototype has being constructed and results of test of a model of the superconducting quadrupole based on NbTi technology are very encouraging. The design is a collaboration among LNF, INFN-Pisa and INFN-Genova.

3.3 Feedbacks

R&D on the longitudinal and transverse bunch by bunch feedbacks is continuing. The DAΦNE feedback systems have been upgraded last year also to test bunch-by-bunch feedback architectures proposed for *SuperB*. Both e^+ and e^- longitudinal feedback systems have been completely replaced with new hardware for increased reliability and better diagnostics. In the effort to reduce residual dipole beam motion, determined by the front-end and quantization noise floor, vertical feedback systems now feature a 12-bit ADC, in place of the old 8 bit design. For the "luminosity" IP feedback, which is an essential component of the luminosity tuning for the high performances requested at *SuperB*, at present two approaches are being considered. One is an extension of the fast luminosity feedback already operating at PEP-II B-Factory. It uses fast dither coils to induce a fairly high dither rate for the x position, the y position and the y angle at the IP. The luminosity signal is read out with three independent lock-in amplifiers. An overall correction is computed, based on the lock-in signal strengths, and beam corrections for x and y position and y angle at the IP are simultaneously applied to the beam. The other approach is based on the FONT5 intra-train feedback system developed for the ATF facility at KEK, aiming at stabilizing the beam orbit by correcting both the position and angle jitter in the vertical plane on a bunch-to-bunch timescale, providing micron level stability at the entrance to FF system. Studies of both systems will be carried out next year, probably both will be adopted.

3.4 Control System

SuperB is pushing us to study and implement new ideas in controls, to be up to date in integrating commercial web technologies and to overcome the primary issue coming from previous architectures: the limits due to the usage of specific hardware and software. The Frascati and Tor Vergata control groups have a long experience in design, development and implementation of innovative Control System. This experience and know-how is available today for a new challenging project. The idea is to design a new controls system based on the present software trends, dominated by web technologies and services, where large databases and the most robust available data bus, Ethernet, are used to match very high throughput. The large community of developers and users involved guarantees a good support and may give hints on the longevity of the product. The new CS, must be designed in such a way to accommodate any kind of devices to reduce the hardware dependence and the development time by exploiting the availability of many devices with embedded programmable CPU. Furthermore, the CS has to be able to control and, where needed, to acquire data with performance limited only by the hardware capability. These requirements suggest inverting the typical CS device-client data flow from polling (the client polls) to pushing (the device push) information. A Control Library (CL) completely manages data and commands flow, the control processes and the devices configuration. The devices programmer is only asked to develop the driver for the specific controlled hardware. The plans have been to develop the core software of the Control Library and to explore its critical issues, if any, by the end of 2011. Some preliminary test started on the DAΦNE and SPARC accelerators at LNF, where is available a natural gym to understand any possible problem and rapidly solve it in a real operative contest. These preliminary tests have confirmed that the performance of a non-relational database resident on RAM is practically limited only by Ethernet bandwith. The systems load is very low, while redundancy and scalability allows being confident on the behaviour for a larger accelerator complex such as the *SuperB*.

3.5 Injection system

The injection complex has been updated to better exploit the necessity of high efficient e^+ production and top-up injection of polarized e^- beam into the rings. The very low beam lifetime requires continuous injection at high repetition rate in order to keep the luminosity almost constant at the peak value. The present design features only one damping ring (DR) for e^+, lower energy e^+ production and polarized gun for the e^-. A sketch is shown in Fig. 2. The main difference with

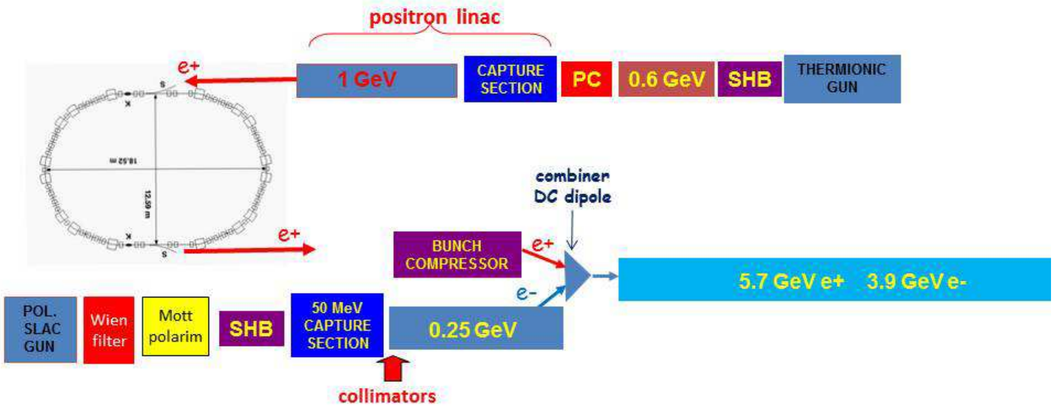

Figure 2: *Sketch of the SuperB injection system.*

respect to the previous scheme is the fact that only the positron beam is stored in the DR while the electron beam is directly accelerated and injected. In this way the positrons can be stored in the damping ring for the time between two injection pulses (before it was half this time) achieving the same emittance damping factor at twice the repetition frequency. Therefore it is possible with a 100 Hz linac to inject at 50 Hz in each ring using a single bunch per pulse to make the current per bunch very uniform along the ring. The e^+ conversion will be performed at low energy (0.6 GeV) thanks to a newly designed high efficiency system, consisting of an adiabatic capture system after the conversion target, followed by a L-band section to inject at 1 GeV into the DR, allowing for an increase of the capture yield to about 30 %. In the electron mode 12 out of 40 RF stations of the 6 GeV linac are switched off to accelerate the beam at 4.2 GeV. The positron converter is followed by a 1 GeV L-band linac that allows a large positron capture and transport efficiency. L-band, room temperature linacs are unusual in the field of particle accelerators: one is in operation at the University of Osaka, another one is foreseen for injection into the SuperKEKB collider. Both are based upon the use of 30-40 MW Klystrons and SW two meter length copper sections, with average gradient of 12 to 13 MV/m. R&D on these cavities is being carried out at LAL, Orsay. An S-band Linac at 100 Hz will be used for main rings injection at 50 Hz. Two electron guns will be used: a "high current" for e^+ production and a "low emittance" polarized gun for e^- injection. This scheme reduces transfer lines and kickers for DR injection/extraction. The possibility to use C-band Linacs to reduce the Linac length is also under study.

3.6 Site studies

The chosen *SuperB* site is very convenient for its vicinity to the Frascati Labs (just 5 km away). Ground vibration measurements have been performed on site and have shown its very good ground stability, even with the highway only 100 m away. For the Final Focus vibrations a budget has been established, including ground motion data, motion sensitivity of machine components and beam feedback system requirements. The small beam sizes at the IP pose stringent vibration requirements. Beam position at the IP is very sensitive to individual motion of IR components. However, the present IR design with shared elements in a common cryostat will cause coherent motion of these elements, greatly reducing the vibration sensitivity of the IR. The vertical displacement of IP and FF quadrupole should be kept below 300 nm rms while the rotation should be less than 2 micro-rad rms. The arc quadrupoles should be kept to less than 500 nm rms. The measured values during last vibration campaign at the IP, FF and Arcs are respectively 20-40 nm, 20-30 nm and 20-30 nm. A fast luminosity feedback system should have a bandwidth of at least 100 Hz, achieving at least 10x vibration reduction at low frequencies. With these requirements in the present lattice the vibration budget can be met even during the noisiest part of the day, with a vibration-induced luminosity loss of less than 1%.

4 Year 2012 activity

The organization chart for the Accelerator structure, including several groups for the different sub-systems, is being decided and will be in charge of the construction of the facility. The first half of 2012 will be devoted to a revision of the accelerator costs by the leaders of the accelerator sub-systems. This will allow to have a full endorsement by the Machine Review Committee in the Fall. In parallel we will proceed as much as possible with the technical drawings of the machine components and site and layout issues.

In the following is a list of the publications the Accelerator Division *SuperB* group has issued in the framework of the *SuperB* collaboration.

5 Publications in 2011

1. M.E. Biagini, R. Boni, M. Boscolo, T. Demma, A. Drago, M. Esposito, S. Guiducci, S.M. Liuzzo, M.A. Preger, P. Raimondi, S. Tomassini, M. Zobov (INFN-LNF), P. Fabbricatore,

S. Farinon, R. Musenich (INFN-Genova), E. Paoloni (INFN-Pisa), W. Wittmer, A. Novokhatski, K.J. Bertsche, A. Chao, Y. Nosochkov, J.T. Seeman, M.K. Sullivan, U. Wienands (SLAC), M.A. Baylac, O. Bourrion, N. Monseu, C. Vescovi (CNRS-LPSC), S. Bettoni (CERN), A.V. Bogomyagkov, E.B. Levichev, S.A. Nikitin, PI.N. Okunev, P.A. Piminov, D.N. Shatilov, S.V. Sinyatkin, P. Vobly (BINP), B. Bolzon, L. Brunetti, A. Jeremie (CNRS-LAPP), A. Chanc (CEA), F. Poirier, C. Rimbault, A. Variola (CNRS-LAL), " *SuperB*: Next-Generation $e^{+}e^{-}$ B-Factory Collider", Proceedings of 2011 Particle Accelerator Conference, New York, NY, USA, 28 Mar - 1 Apr 2011, 2384-2386, SLAC-PUB-14286, Mar 2011.

2. S. Tomassini (INFN-LNF), K Bertsche, W. Wittmer (SLAC) , B. Bolzon, L. Brunetti, A. Jeremie (CNRS-LAPP), "Vibration Budget for *SuperB*", Proceedings of 2011 Particle Accelerator Conference, New York, NY, USA, 28 Mar-1 Apr 2011, SLAC-PUB-14423, Mar 2011.

3. M.E. Biagini, "The *SuperB* project: accelerator status and R&D", Proceedings of 2nd International Particle Accelerator Conference IPAC 2011, San Sebastian, Spain, 4-9 Sep 2011.

4. T. Demma, M.E. Biagini, M. Boscolo (INFN-LNF), A.W. Chao, K.L.F. Bane, M.T.F. Pivi (SLAC), "Multiparticle simulation of intrabeam scattering for *SuperB*", Proceedings of 2nd International Particle Accelerator Conference IPAC 2011, San Sebastian, Spain, 4-9 Sep 2011.

5. A. Drago (INFN-LNF), D. Teytelman (Dimtel Co.), "DAΦNE bunch-by-bunch feedback upgrade as *SuperB* design test", Proceedings of 2nd International Particle Accelerator Conference IPAC 2011, San Sebastian, Spain, 4-9 Sep 2011.

6. S. Guiducci, M.E. Biagini, R. Boni, M.A. Preger, P. Raimondi (INFN-LNF), A. Chanc (CEA), J. Brossard, O. Dadoun, P. Lepercq, C. Rimbault, A. Variola (CNRS-LAL), John Seeman (SLAC), "Updated design of the italian *SuperB* factory injection system", Proceedings of 2nd International Particle Accelerator Conference IPAC 2011, San Sebastian, Spain, 4-9 Sep 2011.

7. S. M. Liuzzo, M.E. Biagini, P. Raimondi (INFN-LNF), R. Bartolini (Diamond), "Tests for Low Vertical Emittance at Diamond using LET Algorithm", Proceedings of 2nd International Particle Accelerator Conference IPAC 2011, San Sebastian, Spain, 4-9 Sep 2011.

8. G. Mazzitelli, C. Bisegni, P. Ciuffetti, G. Di Pirro, A. Stecchi (INFN-LNF), S. Calabr, L. G. Foggetta (CNRS-LAL), L. Catani, F. Zani (INFN-Roma II), "High performance WEB applications for particle accelerator Control Systems", Proceedings of 2nd International Particle Accelerator Conference IPAC 2011, San Sebastian, Spain, 4-9 Sep 2011.

9. E. Paoloni, F. Bosi, N. Carmignani, F. Pilo (INFN-Pisa), M. E. Biagini, P. Raimondi (INFN-LNF), S. Bettoni (CERN), P. Fabbricatore, S. Farinon, R. Musenich (INFN-Genova), M. Sullivan (SLAC), "Advances in the design of the *SuperB* final doublet", Proceedings of 2nd International Particle Accelerator Conference IPAC 2011, San Sebastian, Spain, 4-9 Sep 2011.

10. S. Tomassini, M.E. Biagini, P. Raimondi, C. Sanelli (Frascati) , B. Bolzon (CERN) , G. Deleglise, A. Jeremie, (Annecy, LAPP), J. Seeman (SLAC), "Site studies for the *SuperB* collider and synchrotron radiation facility project", Proceedings of 2nd International Particle Accelerator Conference IPAC 2011, San Sebastian, Spain, 4-9 Sep 2011.

11. M. Zobov, (INFN-LNF), Y. Zhang (IHEP), "Coherent beam-beam resonances in *SuperB* with asymmetric rings", Proceedings of 2nd International Particle Accelerator Conference IPAC 2011, San Sebastian, Spain, 4-9 Sep 2011.

6 References

1 "*SuperB* Progress Report - Accelerator", arXiv:1009.7178v3 [physics.acc-ph] Dec. 2010.

Pmu2e

S. Miscetti (Resp.)

Not received

UA9

S.B. Dabagov (Resp.), F. Murtas, D. Hampai (Art. 23), G. Claps (Bors.), A. Babaev (Osp.)

Participant Institutions:
Italy: INFN Laboratori Nazionali di Frascati
Russia: RAS P.N. Lebedev Physical Institute, Moscow
National Research Nuclear University "MEPhI", Moscow
Tomsk Laboratory of Computational Physics, Tomsk
Tomsk Polytechnic University, Tomsk

The main UA9 scope is to study experimentally (at CERN facilities) and theoretically, the fundamental properties of channeling interactions for relativistic particles (protons and ions) in crystals that aim in the crystal-assisted collimation of the SPS beams. After the set of successful experiments on the beam collimation by various schemes of crystal bent systems the project is suggested to be continued in order to study the crystal technique feasibility for the LHC beams collimation.

1 Introduction

The UA9 LNF team activity can be separated into 4 sections as follows:

- crystal collimation activity at UA9 (SPS beams, bent crystal technique);
- crystal characterization for experiments at CERN;
- channeling studies for ultrarelativistic particles;
- channeling studies for relatively low energy particles.

These studies aim in preparation, installation and managing GEM & Medipix detectors to be used in UA9 experiments at CERN as well as in computer simulations of proton & ion beams deflection by bent crystal potentials taking into account all the processes of beam scattering in a crystal. Within the project we are dealing with the reorganization of testing facility at X-Lab Frascati for crystal testing that includes the analysis of various technique for crystal characterization like either diffraction technique or stress analysis. Moreover, the studies within the project pushed us in the developing both dechanneling and radiation theories for light & heavy positive as well as negative relativistic particles based on the solution of Fokker-Planck equations for straight and bent crystals. And finally we have extended our interests to the fundamental studies on particle-crystal interactions resulting in the research on the features of coherent/incoherent scattering of light and heavy particles in crystals under channeling conditions as well as on the physics of X-ray parametric (PXR) and diffraction radiations (DR).

For the mentioned period we have already developed new theoretical approaches to study the particles diffusion/scattering processes based on Fokker-Planck equations and multiple scattering simulations. Developing radiation theory of relativistic particles channeled in various crystals and crystalline structures the detailed theoretical analysis of the channeling and channeling radiation processes for both planar and axial cases have been performed. Special computer codes to study hadron/lepton scattering in various crystals (by composition as well as geometry) have been written.

2 Activity in 2010-2011

2.1 Experiments on GEM & MEDIPIX Monitoring for PXR Studies

The main goal of the UA9 experiment for the period of 2010-2011 was to study crystal channeling for heavy particle beams as a technique for beam collimation as well as parametric X-ray radiation emitted by the projectiles in bent crystals for experiment diagnostics. All studies were performed for relativistic protons, and lead ions of different fragmentations with the energy of $120 \div 400$ GeV/c and 80 GeV/nucleon, respectively. Measurements on crystal-assisted experiments were done at the H8 site. Additional to the main subject of the project, i.e. crystal-assisted beam collimation, according to theoretical calculations PXR is emitted when a projectile crosses the crystal in well-defined direction with respect to the main crystallographic planes. One of the features of PXR becoming of our interests is its emission direction, which is rather distant from the direction of projectile traveling, namely, quasi-orthogonal to it. This peculiarity makes it very useful for diagnostics purposes. So, we have proposed to measure PXR for the beam monitoring at channeling. The first run of measurements was done by means of a Medipix detector.

Medipix is a new semiconductor hybrid detector developed within the CERN collaboration. It consists of a thin layer of silicon semiconductor bump-bonded to a CMOS chip having the same area. The active area of 1.98 cm^2 is divided into a matrix of 256×256 square pixels. Each pixel has a side of 55 μm. For our experiments it was used like a simple counter: each particle interaction in a pixel of the active semiconductor area produces a digital count in the corresponding microscopic electronics bump-bonded underneath.

The detector was mounted very close (1 cm) to the crystal along a direction orthogonal to the particle beam. Results of this measurements revealed no significant signal with respect to the scattered radiation in the experimental site. A more refined measurements have been conducted using an X-ray spectrometer, which was appropriately shielded against the surrounding scattered radiation.

2.2 PXR Measurements

The experiment layout is designed for quasi mosaic (QM) and strip (ST) crystals, respectively. The beam entered the crystal in the collimation geometry such that it is parallel to the deflecting planes, which are the (111) and (110) crystallographic planes for both QM and ST crystals, respectively. A high precision goniometer was used to align the crystal planes with respect to the beam axis with an accuracy of 2 μrad. The accuracy of the preliminary crystal alignment using a laser beam was about 0.1 mrad. Five pairs of microstrip silicon detectors S1$\div$S5, two upstream and three downstream of the crystal, were used to measure incoming and outgoing angles of particles with an angular resolution in each arm of about 3 μrad (Fig. 1). The planes responsible for the radiation (PXR) form the angles about $\theta_B = 35.26^o$ and 45^o with respect to the deflecting planes, and, hence, relative the beam.

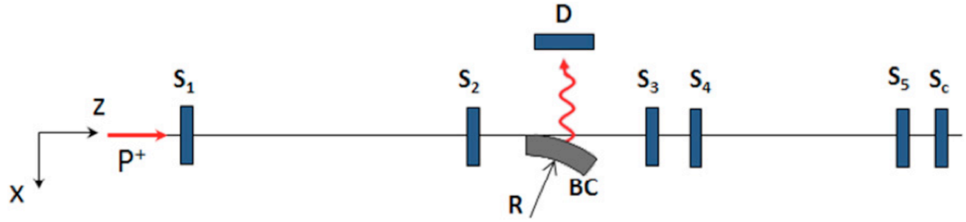

Figure 1: The scheme of experiment layout for PXR measurements.

As X-ray detector we have used a silicon drift detector (SDD), with the 30 mm^2 sensitive area, the energy resolution of less than 130 eV at 5.9 keV (Mn K_α-line), the rate counting of 100 kHz, a polymeric window and the detection efficiency of 60÷70% at the energy 5÷20 keV. The detector was placed close to the PXR maximum direction, $\theta_D = 2\theta_B$, and the detection angles θ_D were 70.25^o and 90^o, respectively. In Fig. 2 the PXR data for relativistic ions in a shift of 10 hours is shown.

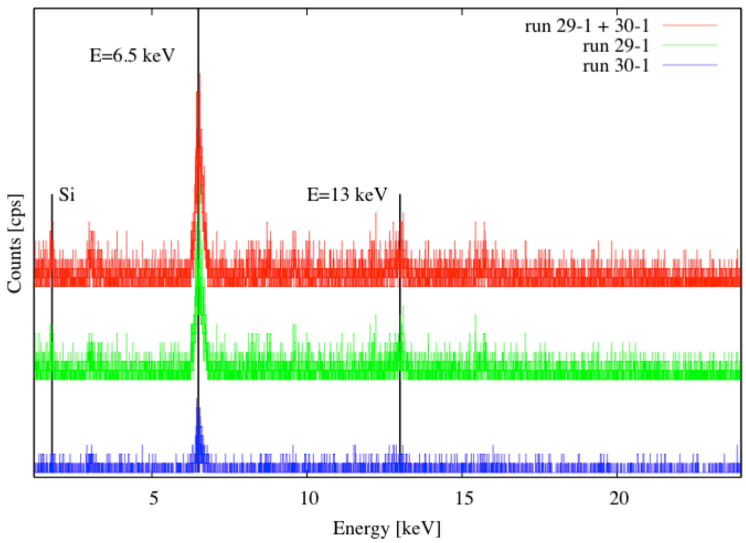

Figure 2: The spectrum of PXR registered by SDD of X Lab Frascati. Due to the large fragmentation of ion beam the final resolution of various PXR peaks, expected, are rather small.

2.3 GEM Monitor Detectors for Beam Collimation Studies

Within the main frame of the ion beam collimation studies in the UA9 project, an experimental set-up has been arranged at two H8 sites. In the first one, there was a crystal positioned along the beam path and mounted on the goniometer controlled remotely. The second H8 site located about 40 m far from the first was equipped with the GEM detectors. The goal was not only to monitor the channeled beam but also to test this kind of a gas detector.

A new kind of GEM detectors constructed by the LNF group are made of an anode, a cathode and three successive GEM foils interposed between them (shown in Fig. 3). Each of these elements has an area of 10×10 cm and is closed in a sealed chamber so that a gas mixture can flow inside. Gas mixture used for this tests is $ArCO_2$ (70/30). The gaps between them are 1, 2, 1 and 3 or 40 mm if gaps are considered starting from the anode. The last gap (called a drift region) is a sensitive volume of the detector and defines different detector geometry for various radiation observation directions. When the drift region is of a 3 mm wide, the detector works as a head-on chamber, and registered radiation is detected while it crosses a cathode surface. When the drift region is of a 40 mm wide, on the contrary, the detector works as a side-on chamber and the radiation is detected when it propagates parallel to the cathode. The anode is divided in pads and, according to the requirements, that allows the anode different dimensions and geometrical configuration.

The opposite side of the anode maintains a set of 8 connectors for the front-end electronics (FEE). The FEE boards used for this development are based on the Carioca-GEM chip; each board houses 16 ASD. A FPGA mother board is plugged just on the top of the eight boards: mainly it has the function to set threshold levels and read digital data derived from the underlying electronics. The other important element to set-up a GEM detector is its power supply: it provides the correct high voltage to all detector electrodes (anode, cathode and all GEM electrodes) in order to have required drift and multiplication electric fields in the gap regions and GEM holes, respectively. Typically, the gain reached by the GEM detector goes from several hundreds to more than 10^4. Unlike the old ones, a new power can also provide a measurement of the currents collected on the electrodes.

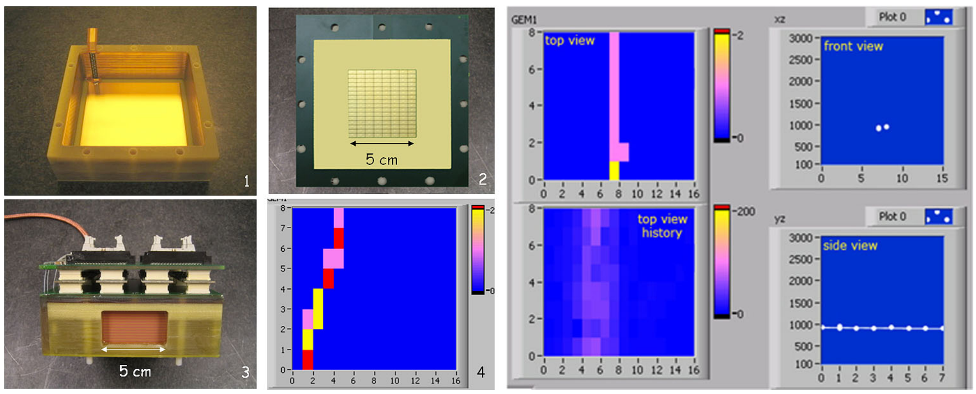

Figure 3: The GEM TPC assembling and a 2D view of a cosmic ray trace (left); a 3D view of the BTF electron trace (right).

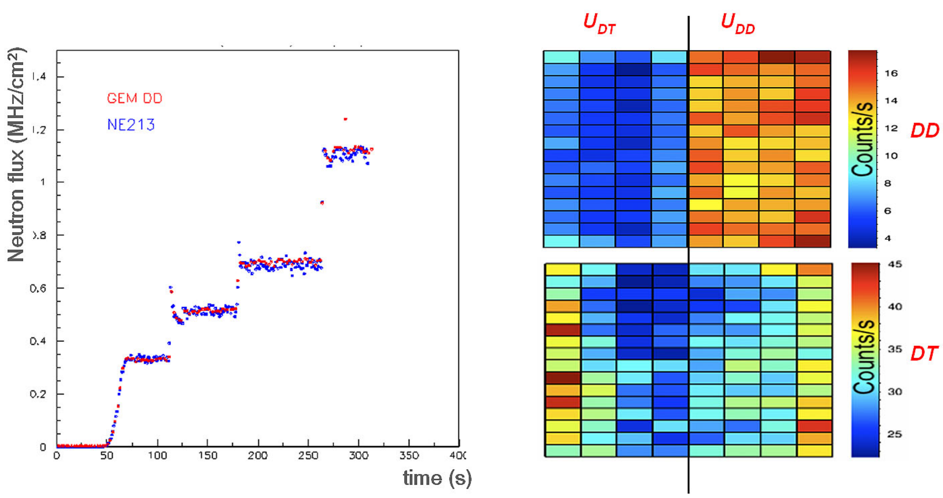

Figure 4: The beam trace released by 80 GeV/c Pb passing through TPC (left); the history of beam traces of the same ions taken during a long period of acquisition (right).

The first measurement conducted at the second H8 site was made for a proton beam of 400 GeV. The monitor detectors used were a Medipix and a side-on GEM detectors placed one behind other along the beam trajectory. The detector anode was divided into a matrix of 16×8 pads, in which each pad is characterized by the dimension of 12×6 mm. The detector works in a scaler mode so that, for each pad, it can provide a digital count for each interacting particle. This apparatus allows a simultaneous measurement of both beam and its halo by means of two detectors in order to check the correct functionality of the GEM detector for this kind of a beam.

Fig. 4 reports the screen shoots from both Medipix and GEM detector monitor displays. Also the control electronics have shown an excellent resistance to high energy proton beam. In the same figure a screen shoot of the currents measured by the GEM power supply is presented. As seen, a current peak was observed when the beam spill was undergoing the detector.

For a second run, particle beams were composed of lead ions of 80 GeV/nucleon. For that case, both Medipix and head-on GEM detectors were replaced by two side-on GEM detectors. One of the side-on detectors had a pad of 3×6 mm distributed in a matrix of 16×8 and acquired data working in a TDC mode. This kind of detector looks as a "small TPC", which measures drift time intervals necessary for electrons to reach the anode pads. Moreover, this acquisition electronics allows us to measure also a time length of the electric current pulse that reaches a pad, a bit of information linked to the charge released by ions interacting in the gas mixture. The other side-on detector has a pad of 0.5×0.5 mm distributed along two rows of 64 separated by a 5 cm gap. It works in a scaler mode like the head-on detector. A first measure was made with TPC. Fig. 5 shows drift time distributions registered during the passage of a lead ions beam though the chamber as well as corresponding signal time duration. This acquisition mode allows the time intervals of 20 ns to be also measured. And then, if electron drift velocity is known, it is possible to obtain higher resolution of a beam profile along the drift direction.

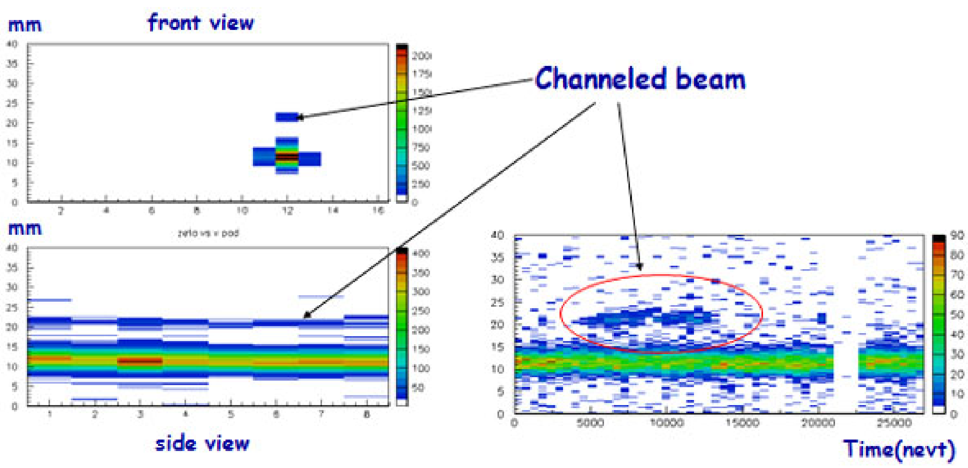

Figure 5: The installation of GEM monitor on one face of the crystal tank (left); main beam as well as channeled beam seen by GEM TPC (right).

3 Theoretical Studies on Proton/Ion Beams Deflection by Bent Crystals

Penetration of relativistic protons into bent crystals at small angles with respect to the bent crystallographic planes has been evaluated within continuous potential approximation. Namely, the numerical solution of the equation of motion for both channeled and quasi-channeled relativistic protons is performed. Proton trajectories under the conditions of channeling as well as volume reflection were simulated. The angular distributions of outgoing beam protons are calculated with the parameters of recent CERN experiments. The rather good agreement with experimental data is achieved.

Theoretical work within the UA9 project aims at developing a new computer code to simulate the deflection of relativistic protons as well as ions/nuclei by means of a bent crystal. In our work the simulation results have been obtained following mainly the previously developed by other authors model, but with some distinctions. In particular, in our approach there is no necessity for integrating the proton motion equations. We have tested this code to describe the experimental results, in which the motion of 400 GeV/c protons through a Si crystal bent along (220) planes has been investigated. The angular distributions of protons in the outgoing beam are calculated. The angular divergence for initial proton beam is also taken into account (Fig. 6).

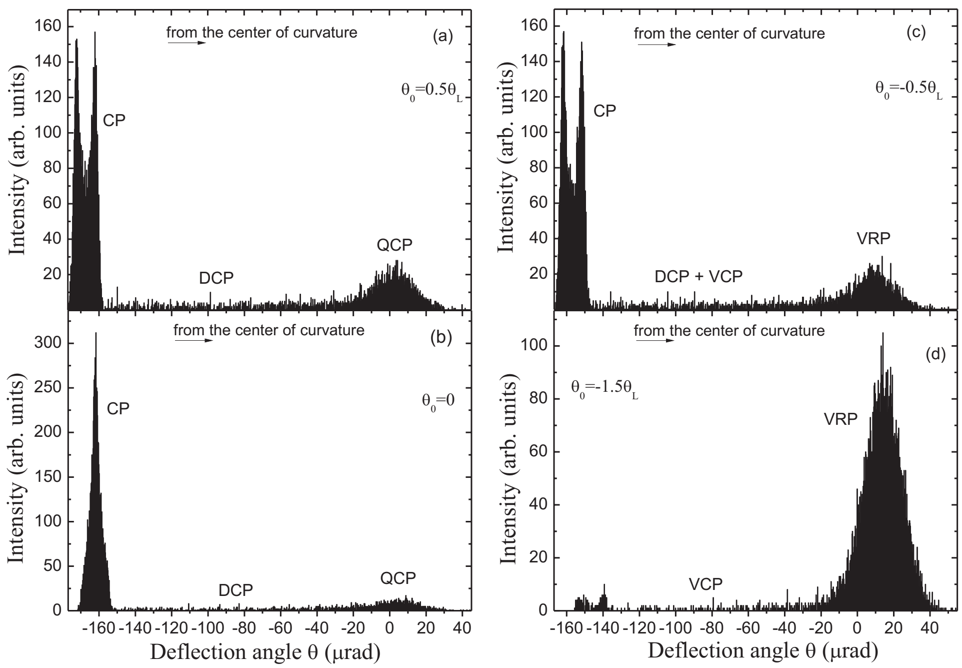

Figure 6: Angular distributions of $E_{\text{kin}} = 400$ GeV protons passed through a Si crystal bent along (220) planes with the curvature radius $R = 1852$ cm (the bend angle $\alpha_R = 162$ μrad) at various angles θ_0 as a function of the deflection angle θ: a) $\theta_0 = 0.5\theta_L$; b) $\theta_0 = 0$; c) $\theta_0 = -0.5\theta_L$; d) $\theta_0 = -1.5\theta_L$. The fractions in outgoing proton beam are defined as follows: CP — channeled protons; QCP — quasichanneled non-reflected protons; DCP — dechanneled protons; VRP — quasichanneled reflected protons; VCP — captured protons.

While the proton moves into the crystal, its radial energy might be transferred from the particle to the crystal and vice versa. As a result, two effects are taking place: dechanneling when energy is transferred from crystal to projectile, and volume capture when energy is transferred from projectile to crystal. Moreover, some accompanying effects might take a place. Dechanneling as well as volume capture lead to the transitions of protons from the channeling regime to the quasi-channeling one, and vice versa. The influence of these effects on a proton beam is observed in experiments.

Moreover, we have studied the probability of inelastic nuclear interactions for relativistic channeled and quasi-channeled protons in a bent crystal. Multiple passage of projectiles through experimental setup was in details considered. Simulation results were compared with known experimental ones (120 GeV/c), paying attention to the features observed (Fig. 7).

The main interest of theoretical work is to study the influence of multiple scattering on both channeling and quasichanneling of relativistic projectiles in a bent crystal. For this purpose the multiple scattering has been included in our model. The final goal was to obtain the angular

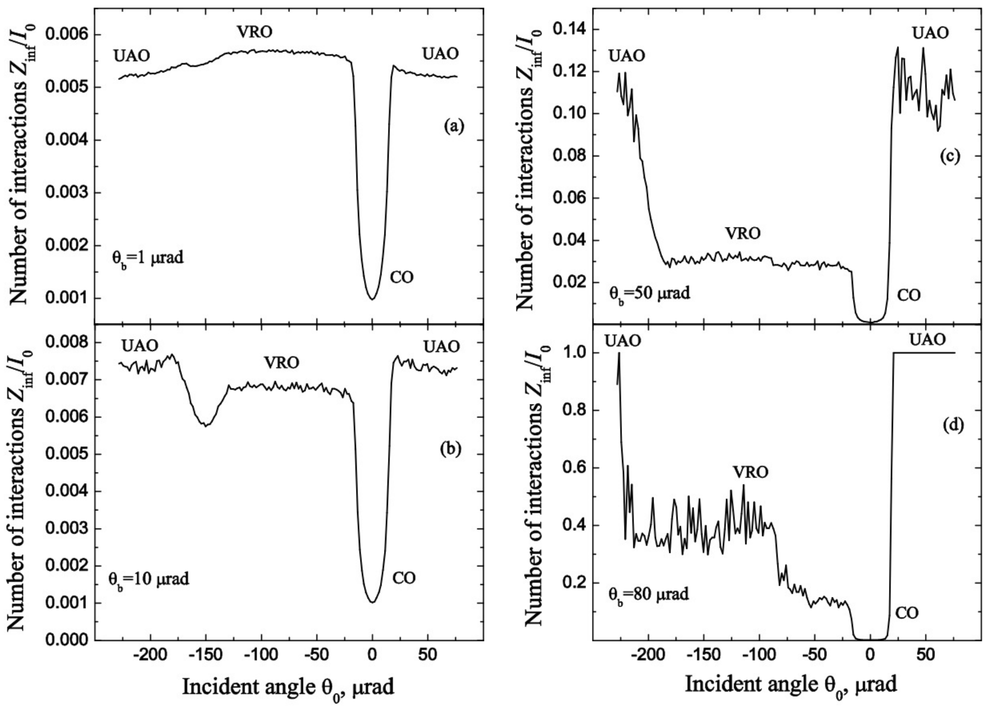

Figure 7: The INI (Inelastic Nuclear Interactions) number for the saturation state $Z_{\rm inf}$ (full number of nuclear reactions at saturation) with respect to the initial number of protons I_0 in dependence on the incident angle θ_0 at different cutting angles θ_b: a) $\theta_b = 1\,\mu$rad, b) $\theta_b = 10\,\mu$rad, c) $\theta_b = 50\,\mu$rad, d) $\theta_b = 80\,\mu$rad. The case of 120 GeV protons passing through Si crystal bend along (220) planes over the angle $\alpha_R = 150\,\mu$rad with the radius $R = 1333$ cm is considered. The designations in the figure are: UAO – unaligned orientation, when the deflection of protons is determined mainly by multiple scattering; VRO – volume reflection orientation, when the deflection of protons is determined mainly by the volume reflection; CO – channeling orientation, when the deflection of protons is determined mainly by the channeling.

distributions of projectiles in the outgoing beam. Simulation results have demonstrated two specific features of projectiles motion in a bent crystal that related to multiple scattering, namely, beams dechanneling and volume capture. The contribution of these effects to total intensity of the outgoing beam was evaluated as small one at the conditions of experiments at considered crystal thickness. It was shown that multiple scattering leads to significant broadening of quasichanneled projectiles distribution mainly due to the scattering on crystal nuclei. Simultaneously, multiple scattering for channeled projectiles is suppressed. We have shown that, if two kinds of positively charged projectiles have the same ratio p/Z, they pass through the bent crystal quite similar under the same other conditions. Indeed, the angular distributions of 33 TeV Pb nuclei are almost the same as for the case 400 GeV protons channeled in Si crystal bent along (220) planes. Nevertheless, one can point out the process, which can be sufficient for the case of heavy nuclei and positive high-charged ions. While an ion moves through the solid, its charge state can be changed due to the ionization or the electron capture from medium. Hence, both the effective potential energy and the screening radius a_{TF} change. Namely, this effect leads to the increase (at the ionization) or to the decrease (at the electron capture) of the planar potential barriers, which define the ion trajectory. This effect is negligible for light projectile as a proton, but might be significant for highly-charged projectile. This effect might be considered as additional mechanism of dechanneling and volume capture in a bent crystal. It should be underlined that the change of the projectile charge state is significant for nonrelativistic and moderate kinetic energies. Moreover, for the case of ultrarelativistic 33 TeV Pb nuclei the data point out the negligible role of the electron capture processes. The code developed to obtain the angular distributions has provided the results, which are in good agreement with experimental data. Taking into account its simplicity the code will be useful to simulate both channeling and quasichanneling of relativistic projectiles in bent crystals of several mm thickness, as well as other accompanying features of projectiles scattering in various crystals. Moreover, new computer scheme proposed is undoubtedly of strong interest in developing a powerful simulation code for heavy relativistic ion channeling. In particular, these simulations are necessary to prepare future experiments planned within the projects on crystal collimation.

4 Conferences, Seminars

1. F. Murtas, "Applications in beam diagnostics with triple GEM detectors", 11th Pisa Meeting On Advanced Detectors: Frontier Detectors For Frontier Physics, La Biodola, Isola d'Elba, Italy (*oral*).
2. S.B. Dabagov, "Channeling Physics in Crystals and Capillaries: Following Frascati's Projects", 1st Intern. seminar "Novel Radiation Sources and Applications: LI2FE in Moscow", July 7-8, 2011, Moscow, Russia (*oral*).
3. S.B. Dabagov, "Channeling of Radiations: from Crystal to Capillary Guides", Intern. Conference "Electron, Positron, Neutron and X-ray Scattering under External Influences", October 18-22, 2011, Yerevan, Armenia (*plenary*).
4. F. Murtas, "GEM Detectors for UA9 experiments", 4th Intern. Conference "Charged & Neutral Particles Channeling Phenomena - Channeling 2010", October 3-8, 2010, Ferrara, Italy (*oral*).
5. "Channeling 2010" - 4th Intern. Conference "Charged & Neutral Particles Channeling Phenomena", October 3-8, 2010, Ferrara, Italy
   Chairmen: S.B. Dabagov, L. Palumbo, and V. Guidi

References

1. R. Villari et al., "Development of the DT GEM: A Gas Electron Multiplier Detector for Neutron Diagnostics in Controlled Thermonuclear Fusion", IEEE Trans. Nucl. Sci. **56** (2009) 3.
2. S.B. Dabagov, L. Palumbo, and V. Guidi, Eds., "Channeling 2010, Proc. of the 4th International Conference "Charged and Neutral Particles Channeling Phenomena" (Ferrara, October 3-8, 2010), Nuovo Cimento **C 34 (4)** (2011) 560 pp.
3. A. Babaev, and S.B. Dabagov, "Deflection of 120 GeV protons by bent Si crystal: computer experiment", Russian Physics Journal **54 (11/2)** (2011) 81.
4. W Scandale et al., "The UA9 experimental layout", Journal of Instrumentation, **6** (2011) T10002.

5. B. Azadegan, S.B. Dabagov, and W. Wagner, “Computer simulation of the radiation of electrons axially channeled in a thin Ge single crystal”, Nucl. Instr. Meth. **B 269** (2011) 2098.

6. W. Scandale et al., “Comparative results on collimation of the SPS beam of protons and Pb ions with bent crystals” , Physics Letters **B 703** (2011) 547.

7. W. Scandale et al., “Observation of parametric X-rays produced by 400 GeV/c protons in bent crystals”, Physics Letters **B 701** (2011) 180.

8. H. Backe et al., “Future aspects of X-ray emission from crystal undulators at channeling of positrons”, Il Nuovo Cimento **C 34 (4)** (2011) 175.

9. B. Azadegan, S.B. Dabagov, and W. Wagner, “Simulation of axial channeling radiation on a thin Ge single crystal”, Il Nuovo Cimento **C 34 (4)** (2011) 149.

10. A. Babaev, and S.B Dabagov, “Angular distributions of bent-crystal deflected protons”, Il Nuovo Cimento **C 34 (4)** (2011) 417.

BENE - DTZ

F. Terranova (Resp.)

Not received

CUORE

M. A. Franceschi (Resp.)

Not received

ICARUS

P. Picchi (Resp.)

Not received

NEMO

Orlando Ciaffoni (Tecn.), Marco Cordelli, Agnese Martini
Luciano Trasatti (Resp.), Roberto Habel (Ass.)

March 5, 2012

The NEMO collaboration, in the framework of the KM3Net initiative, aims at building a 1 km3 Cerenkov neutrino detector in the Mediterranean Sea. During the year 2011 the collaboration has continued the construction of NEMO Phase II, an 8 floor tower to be deployed at the final site, 100 km SE of Capo Passero, in the summer of 2012, taking advantage of the electrooptical cable already deployed from the site to the counting room in Portopalo. In 2011 the LNF group has completed the construction of four PORFIDO probes, that are going to be installed in the NEMO Phase II apparatus. The probes have been delivered to the LNS group responsible for the assembly of the Optical Modules. In the mean time the collaboration has developed the design of the PPM, (PreProduction Module), to be deployed in 2012, containing the DOM (Digital Optical Module), a 17" glass sphere containing 31 small PMTs. The LNF group, as a consequence, has developed PORFIDOM, a version of PORFIDO that can be fitted in the new DOM. In 2012 the LNF group will concentrate on the integration in PORFIDO of high resolution temperature and salinity sensors.

Publications

Marco Cordelli, Agnese Martini, Roberto Habel, Luciano Trasatti. PORFIDO: Oceanographic data for neutrino telescopes. Published in Nucl. Instrum. Meth. A626-627 (2011) S109-S110.

The OPERA experiment

V. Chiarella, B. Dulach, G. Felici, A. Franceschi, F. Grianti (Ass.),
A. Gambarara (Tecn.), N. Intaglietta (Tecn.), A. Mengucci (Tecn.), T. Napolitano,
L. Pellegrino, N. Mauri (Ass.Ric.), A. Paoloni (Resp.), C. Sanelli,
M. Spinetti, F. Terranova, T. Tonto (Tecn.), M. Ventura (Tecn.), L. Votano

in collaboration with

LNF-SEA (Div. Ric.): A. Balla, G. Corradi, U. Denni, A. Frani,
M. Gatta, G. Paoluzzi, G. Papalino
LNF-SPAS (Div. Ric.): A. Cecchetti, S. Cerioni, D. Orecchini
LNF-SPCM (Div. Tec.): G. Catitti, A. Ceccarelli, A. Tiburzi
LNF-SIE (Div. Tec.): C. Fusco, F. Iungo

1 The experiment

OPERA [1] has been designed to provide a very straightforward evidence for $\nu_\mu \rightarrow \nu_\tau$ oscillations in the parameter region indicated by Super-Kamiokande as the explanation of the zenith dependence of the atmospheric neutrino deficit. It is a long baseline experiment located at the Gran Sasso Laboratory (LNGS) and exploiting the CNGS neutrino beam from the CERN SPS. The detector [2] is based on a massive lead/nuclear emulsion target. The target is made up of emulsion sheets interleaved with 1 mm lead plates and packed into removable "bricks" (56 plates per brick). Each brick is equipped with a detachable emulsion doublet ("Changeable Sheet", CS), which is scanned before the full development of the brick emulsions. The bricks are located in a vertical support structure making up a "wall". These bricks were produced in situ by a "brick assembly machine" (BAM) located near the OPERA experimental Hall; they are inserted into the wall support structure by a dedicated robot (BMS). Nuclear emulsions are used as high resolution tracking devices for the direct observation of the decay of the τ leptons produced in ν_τ charged current interactions. Electronic detectors positioned after each wall locate the events in the emulsions. They are made up of extruded plastic scintillator strips read out by wavelength-shifting fibers coupled with photodetectors at both ends. Magnetized iron spectrometers measure charge and momentum of muons. Each spectrometer consists of a dipolar magnet made of two iron walls interleaved with pairs of precision trackers. The particle trajectories are measured by these trackers, consisting of vertical drift tube planes. Resistive Plate Chambers (RPC) with inclined strips, called XPC, are combined with the precision trackers to provide unambiguous track reconstruction in space. Moreover, planes of RPC are inserted between the magnet iron plates. They allow for a coarse tracking inside the magnet to identify muons and ease track matching between the precision trackers. They also provide a measurement of the tail of the hadronic energy leaking from the target and of the range of muons which stop in the iron. A block of 31 walls+scintillator planes, followed by one magnetic spectrometer constitutes a "super-module". OPERA is made up of two supermodules (SM) located in the Hall C of LNGS (see Fig. 1). Since 2008 all bricks have been inserted: the OPERA target is made of 150036 bricks corresponding to a target mass of 1.25 kton.
OPERA is able to observe the ν_τ signal with an impressively low background level. The direct and unambiguous observation of $\nu_\mu \rightarrow \nu_\tau$ appearance will constitute a milestone in the study

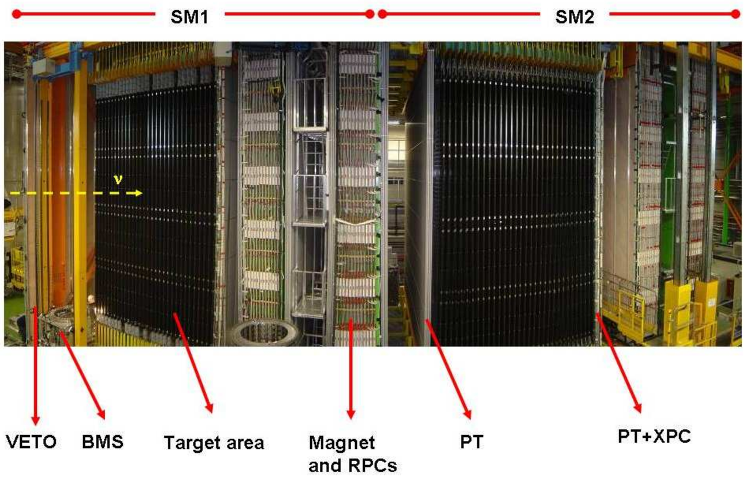

Figure 1: A fish-eye view of the OPERA experiment. The upper red horizontal lines indicate the position of the two identical supermodules (SM1 and SM2). The "target area" is made up of planes of walls filled with lead-emulsion bricks interleaved with planes of plastic scintillators (TT): the black covers visible in the photograph are the end-caps of the TT. Arrows show also the position of the VETO planes, the drift tubes (PT) followed by the XPC, the magnets and the RPC installed among the magnet slabs. The Brick Manipulator System (BMS) is also visible. The direction of incoming neutrinos from CERN is indicated by the yellow arrow.

of neutrino oscillations. Moreover, OPERA has some sensitivity to the sub-dominant $\nu_\mu \rightarrow \nu_e$ oscillations in the region indicated by the atmospheric neutrino experiments. It has been shown [3] that the CNGS beam optimized for ν_τ appearance, will improve significantly (about a factor of three) the current limit of CHOOZ. Further results, concerning sterile neutrinos and non-standard interactions have been considered in [4, 5].
Opera is an international collaboration (Belgium, Croatia, France, Germany, Israel, Italy, Japan, Russia, Switzerland, Tunis and Turkey) and the INFN groups involved are Bari, Bologna, LNF, LNGS (Gran Sasso), Naples, Padova, Rome and Salerno. The Technical Coordinator (M. Spinetti) and the Coordinator for detector operation and maintenance (A. Paoloni) are LNF researchers.

2 Overview of the OPERA activities in 2011

The 2011 run has been extremely successful in terms of duration and accumulated statistics. It has been the longest since the CNGS startup. The CNGS facility accumulated 4.84×10^{19} proton-on-target, corresponding to about 4762 events in the bricks, with an overall duty-cycle for the accelerator complex of 79%. The run started on March 18 and finished on November 16: the OPERA subdetectors were, thus, active and in nominal conditions for about 8 months.

The collaboration completed the analysis of 2008 and 2009 data sample, corresponding to 5.3×10^{19} proton-on-target, with only one tau candidate [6]. The observation of a single candidate is consistent with the expectation of (1.65 ± 0.41) events. The estimated number of background

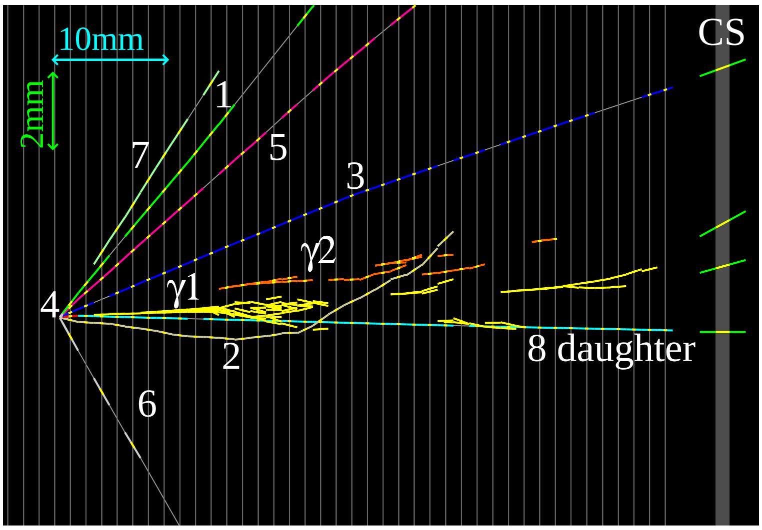

Figure 2: The first OPERA tau candidate (see [6] for details).

events is (0.16 ± 0.03), corresponding to a significance of 95%. The tau candidate, shown in Fig.2 was interpreted as a 1 prong hadronic decay.

With respect to the analysis reported in the OPERA proposal [1], the increased charm background, consequence of the new measured charm cross sections [7], has been compensated by a higher muon identification efficiency, obtained following the neutrino vertex tracks in the consecutive bricks. The study of highly ionizing tracks left by protons and nuclear fragments, associated to hadronic re-interactions, permitted a reduction of about 20% in the background of hadronic tau decays.

The analysis of the large event sample collected in 2010 and 2011 CNGS runs, corresponding to 8.88×10^{19} proton-on-target, is in progress. In order to reduce the scanning load for the event location in the emulsion bricks, events with muons having a reconstructed momentum greater than 15 GeV are not analyzed.

Based on the electronics detectors data acquired on CNGS beam from 2009 to 2011, the collaboration reported the observation of super-luminal neutrinos, arriving at LNGS with an anticipation of about 60 ns with respect to the light speed, with a 6 σ significance. This observation was later explained as due to a combination of two opposite effects: the bad connection of the optical fiber bringing the external GPS signal to the OPERA master-clock and the frequency of the OPERA oscillator, used to produce the events time-stamp, being higher than the nominal 20 MHz by about 123 ns every second.

3 Activities in Frascati

The Frascati group has been responsible for the design and construction of the dipolar magnets and the general support structure for the subdetectors. It shares responsibility with INFN Padova and LNGS for the construction and running of the bakelite RPC planes. Frascati and Naples also designed and prototyped the wall support structures housing the lead/emulsion bricks and LNF was responsible for their production and installation. The Frascati group is also involved, with the University of Hamburg, in the trigger of the drift tubes, performed by the Resistive Plate Chambers. Moreover, the group contributes to software development and to analyses. On the emulsion side, LNF was highly involved in the construction and operation of the Brick Assembly Machine (BAM) and, since 2008, contributes to the emulsion scanning with two dedicated microscopes located in Frascati. Finally, since 2007 LNF follows the brick handling of OPERA, i.e. the operation chain that goes from the extraction of the brick after an interaction has occurred up to the emulsion development.

3.1 OPERA General layout

The OPERA general support structure is a project by LNF-SPAS and external firms and it has been mounted in parallel with the electronic subdetectors and the brick walls between 2003 and 2006 [8]. The project was completed in 2006 and, during 2007 and 2008, only auxiliary installations were added. The structure has been designed by LNF-SPAS; construction and mounting has been carried out by external firms under the supervision of LNF. LNF-SPAS has also been involved in the realignment and revision of the structure after the April 2009 earthquake and it takes care of the maintenance during the run of the BMS.

3.2 Magnets

The OPERA magnets and their infrastructures have been commissioned in spring 2006 and were fully operative since the first CNGS run [9].

During the 2010 physics runs the magnets were operated continuously for about 240 days and the performances were well in specs. During the run, the downtime of the magnets amounted to 32 h, mainly because of freon leaks in the chiller used for the closed-cycle cooling system of OPERA [8]. During the repair of the chiller, the backup cooling system based on the water circuits of LNGS was employed.

3.3 Resistive Plate Chambers

After major contributions in the construction of the RPC system, the LNF group is still highly involved in its running during the CNGS data taking. One of the duties of the group is the monitoring of the performances as a function of time (aging, efficiency fluctuations etc.). In OPERA, Resistive Plate Chamber with bakelite electrodes are arranged into layers, 22 in each spectrometer, inserted into 2 cm gaps inside the magnetized iron. Two additional layers are placed in each Super-Module between the Target Tracker and the spectrometer. The XPC layers and 7 out of 22 RPC layers in each spectrometer are instrumented with dedicated Timing Boards (TBs) for triggering the drift tubes. A complete description of the OPERA RPC system can be found on [2, 10, 11].

The detectors are operated in streamer mode at 5.7 kV with the gas mixture $Ar/C_2H_2F_4/i-C_4H_{10}/SF_6 = 75.4/20.0/4.0/0.6$ [12]. An automatic correction is applied for the pressure, according to [13]; the temperature is quite stable, between 15 and 18^{o}C, depending on the detectors position. Signals from the vertical strips, measuring the bending coordinate, are discriminated at

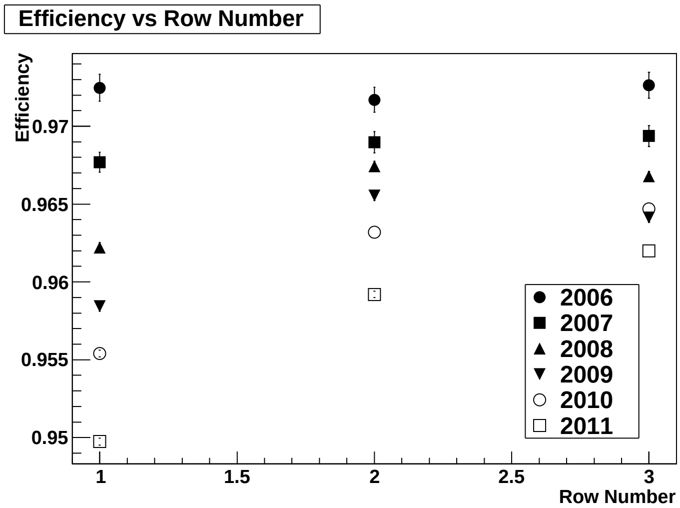

Figure 3: Average RPC efficiency along the gas flow for the different data taking years.

40 mV, while the threshold for the horizontal strips is 26 mV, in order to correct for the different impedance matching with the read-out twisted flat cables.

The full RPC system ran smoothly during the 2011 run, with almost no dead-time and with performances similar to those observed in previous years [8], matching the required specifications, with efficiency greater than 90% and time resolutions better than 5 ns.

The main aging effect observed on OPERA RPCs is the progressive drying of the electrodes. Since the gas mixing is in common between the bakelite RPCs (instrumenting the spectrometers) and the glass ones (instrumenting the VETO system), both detectors are indeed flushed with a dry mixture. The chambers in the spectrometers are disposed in rows of three chambers, with the gas flowing from column 1 to column 3. In figure 3 it is shown the average efficiency measured on cosmic rays as a function of the RPC position along the gas flow. During the years of operation, efficiency have slightly decreased, especially at the entrance of the gas, as expected.

In figure 4 the time resolutions measured on rock muons (produced by external neutrino interactions) during the last three years of data taking are also reported.

3.4 Brick Assembly Machine

After the production of the bulk of the target in 2007-2008, the Brick Assembly Machine (BAM) has been reactivated in 2009 for a short time to build additional 3000 bricks. In fact, such production was originally scheduled in 2008, as well, but it was delayed by an accident occurred at the firm producing the lead for OPERA (JL Goslar, Germany). In February 2009 the BAM was finally put in standby mode. The whole facility was dismounted in winter 2010 by the LNF-SPAS and the LNGS Technical Division; the anthropomorphic robots were reset and sold back to external firms in 2011; two of them have also been re-employed by INFN for the CUORE experiment and used by INFN workshops (Naples) to automatize soldering procedures.

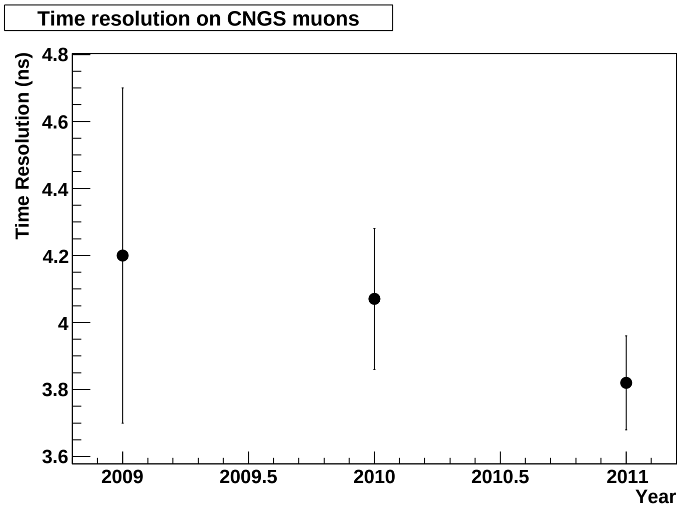

Figure 4: RPC time resolutions measured in the last three years of data taking on rock muons.

3.5 The LNF scanning station

The OPERA brick is based on the Emulsion Cloud Chamber technique, fulfilling the requirements of high granularity and micro-metric resolution necessary to distinguish the τ decay vertex from the primary ν_τ interaction. The brick (see Sec.1) acts as a standalone detector, that can be selectively removed from the target, developed and analyzed after the interaction took place.

Each emulsion film is made of two active layers 44 μm thick poured on a 210 μm plastic base. The nuclear emulsions consist of AgBr crystals suspended in a gelatin binder. The passage of charged particles creates perturbations at atomic scale (latent image), amplified by a chemical-physical process called development: the resulting silver grains of about 0.6 μm diameter are visible with an optical microscope. About 30 grains every 100 μm are left by a minimum ionizing particle. The excellent emulsion space ($\sim 1\,\mu$m) and angular ($\sim$ 2 mrad) resolutions are ideal for detection of short-lived particles. The three-dimensional tracks of charged particles crossing the brick are reconstructed from the optical tomography of each field of view obtained adjusting the focal plane of the objective lens through the emulsion thickness. A detailed description of the automatic microscopes developed for OPERA can be found in Ref. [14]. The brick dimensions and length are optimized to contain the primary as well the decay vertex and to provide particle identification and kinematic reconstruction. The use of passive material, combined with high accuracy tracking devices, allows for momentum measurement of charged particles via multiple Coulomb scattering (MCS) and for electromagnetic shower identification [15].

The bricks selected by the electronic detectors as containing a neutrino interaction vertex are extracted from the OPERA target and equally shared between Japan and Europe for the scanning. For the events assigned to the European side the CS doublets are analyzed at the LNGS scanning station. The CS doublet acts as a confirmation of the trigger provided by the Target Tracker: the brick is developed only if the prediction is confirmed, otherwise the CS is replaced and the brick is put back in the target.

In case of positive CS result, the brick is assigned to one of the European scanning laboratories dedicated to the neutrino vertex localization in Switzerland (Bern) and Italy. LNF is part of a network of italian scanning laboratories including Bari, Bologna, LNGS, Napoli, Padova and Roma1. The scanning load at the LNGS scanning station is shared among the European members of the OPERA Collaboration. Since 2008 the LNF group contributes to the CS doublets scanning performing shifts at the LNGS station, in addition to the work load at the home scanning laboratory.

The LNF emulsion scanning station is located in Building 29. It is hosted in a climatised environment to ensure good conditions for emulsion storage. The station is equipped with a motorized optical microscope instrumented with a system for the emulsion plates loading on the microscope stage (Plate Changer), in order to scan in full automatic mode (Fig. 5, left). The installation of the Plate Changer electronics and of its hardware interfaces to the microscope has been completed early last year and the system is now routinely used for the data taking.

The whole chain for brick scanning at LNF is fully operational since 2008. It consists of three phases: the brick scanning, the event reconstruction and the data publication on the central database.

The brick scanning procedure for vertex localization is carried on in different steps. When the brick is shipped from LNGS to the scanning laboratory, the information of the tracks found in the CS doublet are downloaded at LNF from the central database. The tracks are extrapolated into the brick and searched for with a prediction scan. Once the so-called connection between the CS and the brick is validated, the tracks are followed with a prediction scan from film to film (ScanBack). When tracks converge and stop, the stopping point gives a first indication of the neutrino interaction vertex. A general scan is performed around the stopping point to reveal all the particles that are involved in the interaction (TotalScan). The TotalScan is a wide area scan (1 cm^2) for 15 consecutive emulsion films, in which all the tracks are searched for, contrary to the ScanBack. The volume is large enough to reconstruct all primary and possible decay daughter particle tracks.

After the scanning phase, once the vertex is located, the reconstruction process links the tracks of the different films in 3-D tracks, evaluates the momentum of charged particles and analyze the event kinematics. With the information of all particle trajectories, a dedicated decay search procedure is applied, to search for interesting decay topologies.

At the end of the brick analysis, the scanning laboratory publishes a feedback of the vertex localization and of the decay search results, as well as the complete set of emulsions scanning data in the central OPERA database, where they are made available to the whole Collaboration for global analysis.

Bricks from Physics Runs 2008, 2009 and 2010 were assigned to the Frascati laboratory. The scanning and analysis flow is smoothly running on-time with the brick assignation. The LNF scanning laboratory shows good performances with a 75% location efficiency, in agreement with the expectations.

Besides the above-mentioned location activity, LNF lab has focused on a particular task (scanforth) which is shared with Bern and Salerno laboratories: vertex tracks are followed downstream

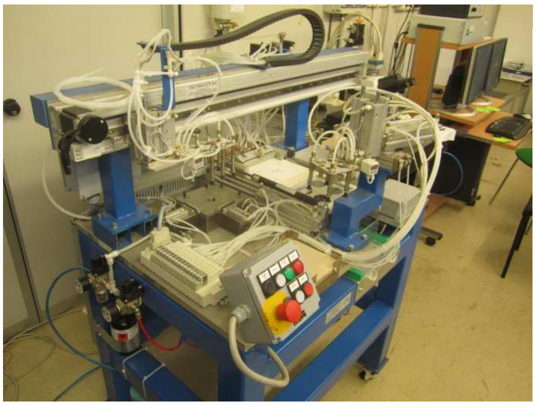

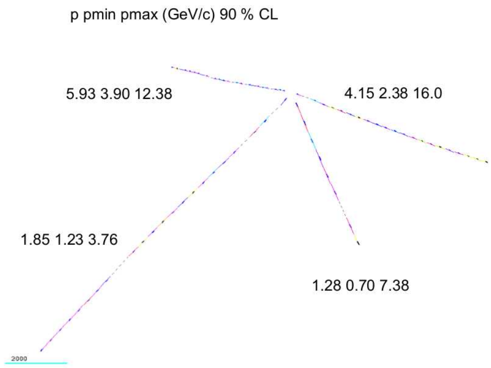

Figure 5: Left: the automatic plate changer. Right: display of one charged current neutrino interaction seen in the plane orthogonal to the incoming neutrino. Momenta are determined with a multiple scattering analysis of tracks analyzed in the full brick volume. The horizontal line corresponds to 2 mm.

with the automatic plate changer and the momentum is estimated using the dispersion of the angles of the track induced by multiple Coulomb scattering in the 1 mm thick lead plates. This information is extracted for a selection of "minimum bias" muon neutrino charged current events with the goal of studying the kinematic properties of the interaction, in particular: the balancing of the transverse momentum of the hadronic system and the muon in the plane transverse to the incoming neutrino direction (p_T^{miss}) and their relative angle ($\Delta\phi_{\mu-h}$).

In Fig. 5 (right) we show an example of a ν_μ^{CC} with four reconstructed charged tracks followed inside a full brick as seen in the transverse plane. Reconstructed momenta are indicated. Low energy muons allow also to test the match between momentum reconstruction with emulsions and with the magnetic spectrometer. When a track is found to stop, a general scan, similar to that necessary to determine the neutrino vertex topology is applied to reconstruct eventual visible hadronic interactions.

The importance of this sample resides in the fact that kinematic cuts applied to the τ analysis, have to be validated by doing a detailed data-Monte Carlo comparison. Once a good agreement is achieved/verified more sophisticated analyses (based for example on multivariate techniques) could be reliably applied to enhance even further the S/B ratio. Secondly this is a good benchmark to improve the simulation of the data taking in the emulsions. A by-product of this work is the possibility to constrain the probability that an hadron undergoing an early interaction could survive all cuts and mimic a τ decay. Despite the lower statistics with respect to studies based on pion test beams this sample has the advantage of corresponding to the peculiar characteristics of the neutrino sample in terms of background, angular and momentum spectrum of tracks.

The recent result of T2K hinting at a large value for the θ_{13} mixing angle has revived the interest of addressing $\nu_\mu \to \nu_e$ mixing with OPERA which, differently from T2K, is operating far away from the oscillation maximum.LNF has joined the effort of developing a systematic and reproducible search for ν_e interactions. In July 2011 a remarkable ν_e candidate was identified with our microscopes during this campaign which is based on tagging shower-like topologies in the CS

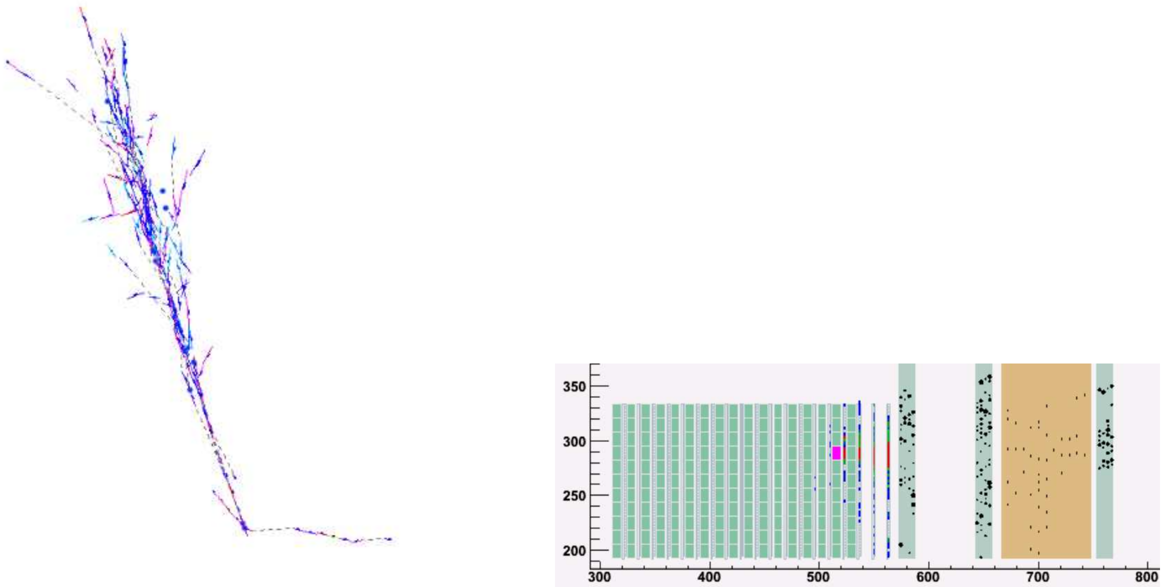

Figure 6: Left: a ν_e interaction in an OPERA brick found at the LNF scanning station in the frontal view. The estimated electron energy from emulsion information is 13 GeV. Right: the same event seen in the OPERA electronic detectors (units in cm). The extracted brick is displayed in magenta.

sheets. An event display is shown in Fig. 6.

In view of the summer conferences, since February 2012, the LNF scanning station has resumed the vertex location activities on a signal enriched sample of NC-like interactions registered by the detector in 2011 with the aim of exploring as much as possible the occurrence of new τ candidates.

3.6 Cosmic rays analysis with OPERA detector

The OPERA detector is used to measure the atmospheric muon charge ratio $R_\mu = N_{\mu^+}/N_{\mu^-}$ in the highest energy region. The atmospheric muon charge ratio at sea level was extensively studied in the past since it is an highly informative observable for cosmic rays and particle physics. It allows to study both high energy hadronic interactions in kinematic regions not yet explored at accelerators and the nature of the primary cosmic rays.

Atmospheric muons are mainly generated by the decay of charged mesons (typically π and K mesons) which are produced in the hadronic cosmic ray interactions some tens of km above the sea level. The phenomenological description of the evolution of R_μ as a function of the muon energy is a quite complex process as it involves several ingredients at the same time. Since atmospheric neutrinos share the same production mechanisms with muons a careful study of the muon charge ratio may provide new information on the high energy part of the atmospheric neutrino spectrum.

The behavior of the surface muon charge ratio is linked to the mechanism of multiple production of pions and kaons in the atmosphere, to the primary cosmic ray composition (in particular to ratio of protons to heavier primaries) and spectrum (the spectral index γ), and to the contribution of prompt muons at very high energy.

Underground experiments naturally select very energetic muons. The OPERA experiment is located in the underground Gran Sasso Laboratory, at an average depth of 3800 meters of water equivalent (m.w.e.). OPERA is the first large magnetized detector that can measure the muon charge ratio at the LNGS depth with a good acceptance for cosmic ray muons coming from above. The detector observes underground muons with a minimum surface energy of 1 TeV and their energy spectrum has a mean value of about 2 TeV. The average $\langle \mathcal{E}_\mu \cos\theta^* \rangle \simeq 2$ TeV is well above the kaon critical energy. This is the higher accessible energy range for current experiments. In this energy range the muon charge ratio is expected to rise due to the increasing kaon contribution.

Moreover R_μ is expected to depend on the underground muon multiplicity. Given the size of the OPERA detector and the average separation between multi-muons, it is possible to measure separately the muon charge ratio for single and for multiple muon events. This allows to select different energy regions of the primary cosmic ray spectrum and to test the R_μ dependence on the primary chemical composition.

We updated the cosmic ray muon analysis including data of 2008, 2009 and 2010 CNGS Physics Runs, for a total of 1454057 muon events, corresponding to about 407 days of livetime, i.e. a threefold statistics with respect to Ref. [17]. In Fig. 7 R_μ is shown as a function of the "vertical surface energy" $\mathcal{E}_\mu \cos\theta$, for which we optimized the analysis on the surface muon energy estimation. The Gran Sasso mountain profile allowed the determination of the charge ratio up to 7 TeV in $\mathcal{E}_\mu \cos\theta$. Data were compared to expectations and fitted to a simplified model to obtain the relevant parameters characterizing the particle production in atmosphere.

The muon charge ratio was computed for single and for multiple muons separately. Multiple muon bundles originate on average from heavier and more energetic primaries. For primaries heavier than protons the positive charge excess is reduced and so is the muon charge ratio. In this way we can test the dilution of R_μ due to the neutron enhancement in the primary nuclei. A smaller R_μ value is also expected due to kinematic considerations. The selection of high multiplicity events artificially bias the x_F distribution of muon parents towards smaller values, where the charge ratio is smaller. For single muons the R_μ value integrated over the underground muon spectrum is

$$R_\mu^{unf}(n_\mu = 1) = 1.403 \pm 0.008\,(\text{stat.})^{+0.017}_{-0.015}\,(\text{syst.})$$

to be compared to $R_\mu^{unf}(n_\mu > 1) = 1.18 \pm 0.03$ for muon bundles. This difference of about $\sim$7.2σ supports the hypothesis of the decrease of the muon charge ratio with increasing primary mass. This is the first indication of such an effect which provides a further handle for the correct understanding and modelling of the secondary production in the atmosphere. With a large statistics, fitting the muon charge ratio as a function of the underground muon multiplicity could disentangle the chemical composition and the hadronic interactions effects discussed above.

The behaviour of the muon charge ratio above 2 TeV is under investigation. Complemented with a thorough discussion of systematics, the final analysis will appear in a forthcoming publication.

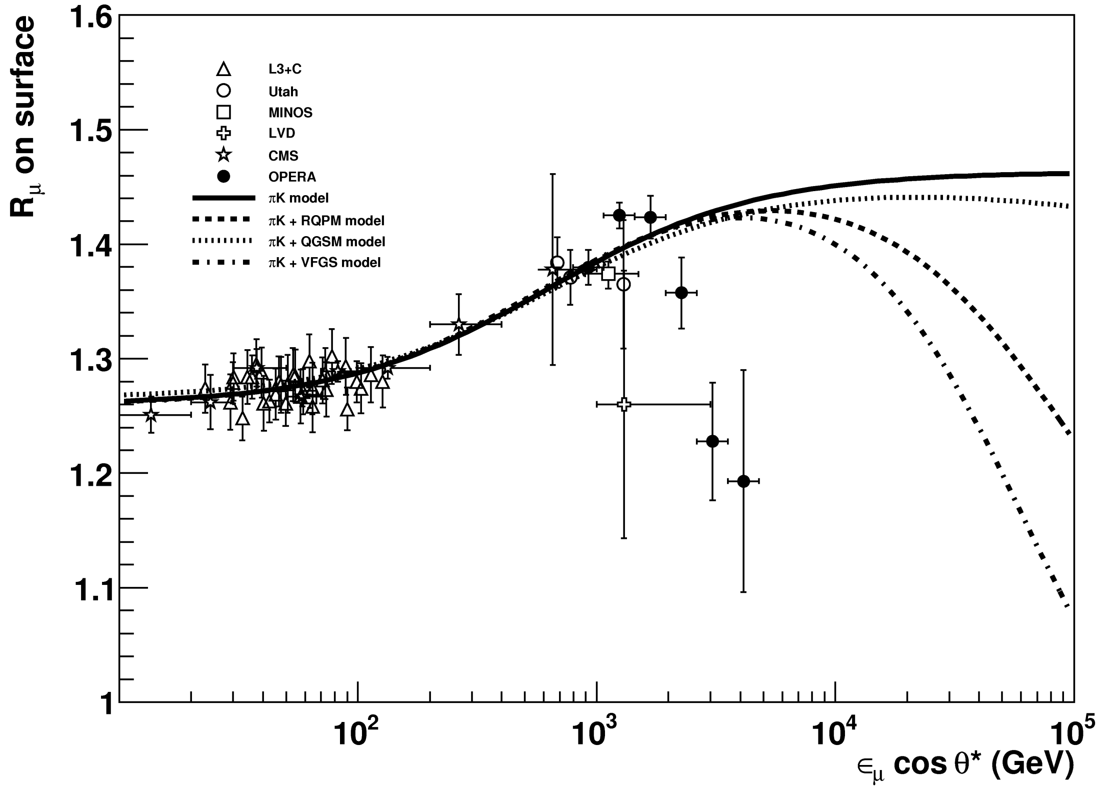

Figure 7: R_μ values measured by OPERA in bins of $\mathcal{E}_\mu \cos\theta^*$ (black points). Also plotted are the data in the low energy region from MINOS-ND and L3+C and in the high energy region from Utah, MINOS and LVD experiments. The result of the fit of OPERA and L3+C data is shown by the continuous line. The dashed, dotted and dash-dot lines are, respectively, the fit results with the inclusion of the RQPM, QGSM and VFGS models for prompt muon production in the atmosphere.

3.7 Brick handling

During nominal CNGS operation, about 20 neutrino interactions per day occur in the OPERA target and several candidate bricks are tagged as containing the corresponding primary vertex. These predictions are validated scanning preliminarily a pair of detachable emulsions ("changeable sheets", CS [16]). If confirmed, the corresponding brick is extracted, aligned using an X-ray machine and sent to the facilities located on surface for cosmic ray exposure (high precision alignment) and development. All the operations of CS and brick handling require dedicated tools and personnel running synchronously with the CNGS data taking. LNF is responsible of the coordination of these tasks and provides most of the tools for brick handling. In particular, during the 2010 run, the whole Brick Handling (BH) chain has been re-optimized and synchronized with the operation of the BMS. In particular, the shift duties have been redefined to speed up the procedure and provide support to the BMS operators, as well. Since 2010, OPERA is able to run simultaneously the BMS and BH chain employing at most 4 operators (8h/shift). Moreover, it has been demonstrated that the extraction of the candidate bricks at nominal CNGS performance can be achieved running BMS+BH in 1 shift/day mode for the whole year and supplementing the running of the BMS with an additional 8h shift (2 shift mode) from September to November. In 2011, an upgrade of the emulsion development facilities has started, with the installation of an automatic temperature regulation of the tanks. The upgrade will continue in 2012.

4 List of Conference Talks by LNF Authors in Year 2011

1. A. Longhin “Measurement of the neutrino velocity”, Frontiers in diagnostic technologies, Frascati, Italy, 28 - 30 November 2011.

References

1. M. Guler *et al.*, OPERA proposal, CERN/SPSC 2000-028, SPSC/P318, LNGS P25/2000.
2. R. Acquafredda *et al.*, JINST **4**, P04018 (2009).
3. M. Komatsu, P. Migliozzi, F. Terranova, J. Phys. **G29**, 443 (2003); P. Migliozzi, F. Terranova, Phys. Lett. **B563**, 73 (2003).
4. A. Donini, M. Maltoni, D. Meloni, P. Migliozzi and F. Terranova, JHEP **0712**, 013 (2007).
5. M. Blennow, D. Meloni, T. Ohlsson, F. Terranova and M. Westerberg, Eur. Phys. J. **C56**, 529 (2008).
6. N. Agafonova *et al.* [OPERA Collaboration], Phys. Lett. **B691**, 138 (2010).
7. CHORUS Collaboration, A. Kayis-Topaksu et al., CERN-PH-EP-2011-109, arXiv:1107.0613 [hep-ex], submitted to New J. Phys.
8. See “LNF 2009 Annual Report”, D. Babusci ed., LNF-10/15 (IR), p.97, “LNF 2008 Annual Report”, D. Babusci ed., LNF-09/04 (IR), p.99, “LNF 2007 Annual Report”, M. Antonelli ed., LNF-08/20 (IR), p.103; “LNF 2006 Annual Report”, M. Antonelli ed., LNF-07/10 (IR), p.87; “LNF 2005 Annual report”, E. Nardi ed., LNF-06/10 (IR), p.78; “LNF 2004 Annual Report”, E. Nardi ed., LNF-05/5 (IR), p.70; “LNF 2003 Annual Report”, S. Dell’Agnello ed., LNF-04/08 (IR), p.64.
9. A. Cazes *et al.*, JINST **2**, T03001 (2007).
10. S. Dusini *et al.*, Nucl. Instrum. Meth., **A602**, 631 (2009).
11. A. Paoloni *et al.*, Nucl. Instrum. Meth., **A602**, 635 (2009).
12. A. Mengucci, A. Paoloni, M. Spinetti, L. Votano, Nucl. Instrum. Meth., **A583**, 264 (2007); A. Paoloni *et al.*, LNF Technical Note **LNF-08/14(NT)** (2008).
13. M. Abbrescia *et al.*, Nucl. Instrum. Meth., **A359**, 603 (1995).

14. N. Armenise *et al.*, Nucl. Instrum. Meth. A **551**, 261 (2005).

15. L. Arrabito *et al.*, JINST **2**, P05004 (2007).

16. A. Anokhina *et al.* [OPERA Collaboration], JINST **3**, P07005 (2008).

17. N. Agafonova et al., Eur. Phys. J. C (2010) 67: 25-37.

ALICE

N. Bianchi, G.P. Capitani (Ass.), L. Cunqueiro (Ass.), A. Casanova Diaz (Ass.),
P. Di Nezza (Resp. Loc.), A. Fantoni, P. Gianotti, S.Liuti (Ass.), A. Moregula (Ass.), V. Muccifora,
A. Orlandi (Tecn.), W. Quian (Ass.), A.R. Reolon, F. Ronchetti (Ass.), A. Viticchié (Tecn.)

1 Introduction

ALICE is an experiment at CERN which involves about 1100 physicists from more than 100 Institutions from several Countries. Italy participates with 12 groups and about 200 physicists. The Frascati group is deeply involved in the electromagnetic calorimeter project (EMCal), both on the hardware and software side, and in the physics of the jets. The latter choice comes from the fact that the EMCal enables ALICE, like no other experiment before, to explore the physics of jet quenching, i.e. the interaction of energetic partons with the QCD hot and dense medium, over the large kinematic range provided by the LHC. The EMCal provides both fast triggers (level 0 and 1) for photons, electrons, and jets and a High Level Trigger (HLT) as well. The EMCal also measures the neutral energy component of jets, enabling full jet reconstruction in all collision systems, from proton-proton to Pb-Pb, passing through the p-Pb collisions scheduled for the 2012. The combination of the EMCal, the excellent ALICE charged tracking capabilities, and the modest ALICE magnetic field strength, is a preferred configuration for jet reconstruction in the high background environment of heavy ion collisions, allowing detailed optimization of background rejection while preserving the crucial jet quenching signals at low transverse momenta. During the 2011 run both p-p and Pb-Pb were collected with high efficiency bringing the statistics on tape, for heavy ion, to more than a factor 10 than the one collected in 2010. Part of the data collected in 2010 have been already published, like the first paper on jets where the Frascati group was co-first author. The data from 2011 are currently under analysis opening the frontiers to rare events and very high transverse momentum jets. An EMCal extension, called DCal, has been approved, funded and is under construction. The Frascati group is contributing with tools and expertize acquired for the EMCal.

2 EMCal

At the beginning of 2011 the EMCal was completely installed. Modules have been assembled in Frascati using two production lines composed by two stacking fixture and four kits of pressor sensors used to apply and measure the internal load of the modules, as already done in previous years. Four bundles of 36 polished, aluminized and glued wavelength shifting fibers, produced at LNF, have been inserted in each module longitudinally through the Pb/Scint stack providing light collection (Shashlik). The calorimeter is composed by 10 super-modules (7 American and 3 European), which represent the basic structural unit of the detector. 4 super-modules have been installed in ALICE in 2010, while the other 6 super-modules have been installed during the winter shutdown in January 2011, completing the full detector made by 2880 modules in total. In Fig. 1 a picture of the full EMCal detector after the installation is shown.

In 2011 the DOE approved an EMCal extension of two reduced width (1/3) super-modules, composed by 24 strips, each of them made by 4 modules, in order to maximize the calorimeter angular coverage, using the small space between the EMCal active modules and the support structure. These modules have been assembled in USA and the corresponding mini-strips have been assembled and tested in France with the help of the Frascati group, at the end of 2011. The installation of the two reduced super-modules has been completed in the winter shutdown 2011-2012. The Frascati group provided also all the fibers for those modules, for a total of about 30000

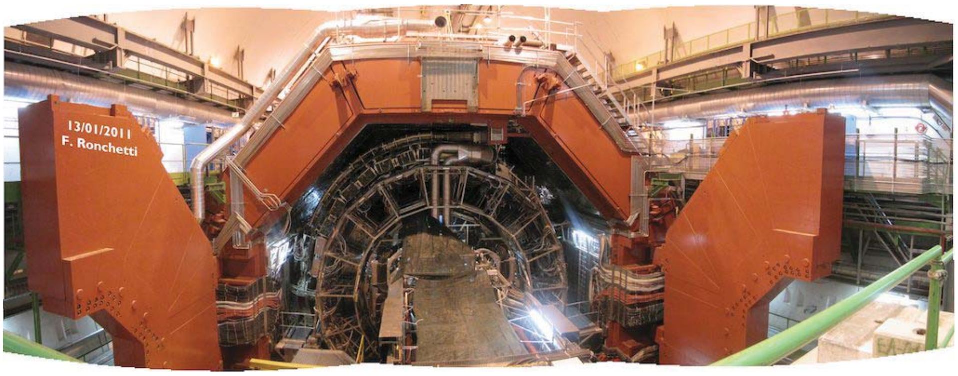

Figure 1: *Picture of the full EMCal (up-right inside the magnet) after the full installation.*

fibers, grouped in 830 bundles, with 36 fibers each, cut, ice-polished and aluminized, using a thin film deposition made by the sputtering chamber built in the LNF at the beginning of the EMCal modules production.

3 DCal

Even though EMCal was the last ALICE detector to be proposed, approved, assembled, and also installed, the first upgrade approved by the ALICE collaboration is an extension of the EMCal, denominated DCal (Di-jet Calorimeter). The DCal expands the physics capabilities of the EMCal by enabling back-to-back correlation measurements, which are difficult with the EMCal alone, and are essential to obtain a complete picture of the physics addressed by the EMCal. Together, the DCal and the EMCal form a two-arm electromagnetic calorimeter. The EMCal subtends 110° and the DCal subtends 60° in the azimuthal angle ϕ, with both detectors covering $|\eta| <0.7$, thereby providing good acceptance for di-jets up to transverse momenta $p_T \sim$ 150-200 GeV/c. From a technical perspective, the DCal can be considered an extension of the EMCal. Its super-modules are built exactly as they are in the EMCal, out of strip-modules, but with reduced length in η: in fact, each DCal super-module contains 16 strip-modules instead of the 24 present in the EMCal. The new calorimeter will be situated adjacent to the PHOS in a way that DCal+PHOS can be considered as one integrated detector system for the study of jets; consequently, all simulations done include PHOS as well as DCal super-modules. On the left panel of Fig. 2 is shown a schematic view of the 6 DCal super-modules with the PHOS super-modules in between and on the right panel the beam view of the EMCal and the DCal is illustrated.

The DCal Collaboration is formed by the EMCal Collaboration extended to the Tsukuba (Japan) and Wuhan (China) groups. The Frascati group has the responsibility of coordinating the construction and the assembly in the European-Asiatic zone.

The two full assembly stations used in Frascati for the EMCal have been sent to Wuhan, where about 200 modules have been already assembled in 2011 to prepare one DCal super-module, always under the Frascati supervision and coordination. In 2011, the Frascati group provided all WLS fibers for 1.5 DCal super-module, including cutting, ice-polishing and aluminization. A total of about 45000 fibers, grouped in 1200 bundles, with 36 fibers each have been produced at LNF, part of those in collaboration with the Wuhan group. As for the EMCal, each fiber bundle is made by two sub-bundles to match the different path lengths between central and peripheral fibers in the four towers of the single module. All DCal super-modules will be installed in the ALICE

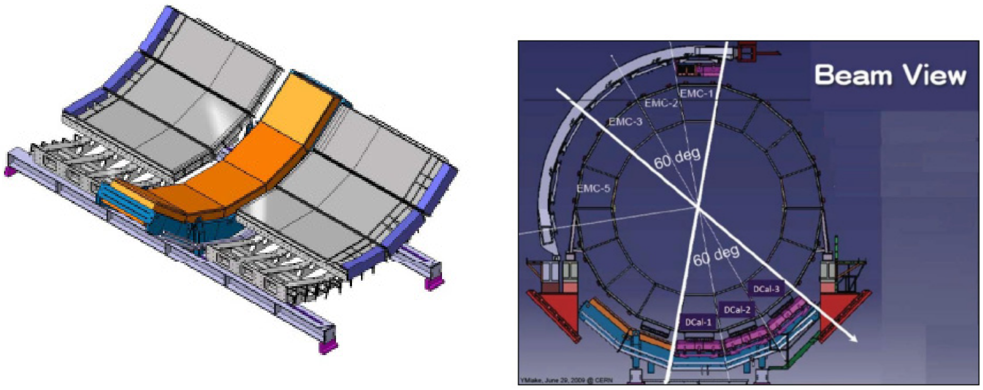

Figure 2: *Left panel: 6 DCal super-modules (in gray) with the PHOS super-modules (in orange) in between. Right panel: beam view of the EMCal and the DCal.*

spectrometer during next long shutdown in 2013.

4 EMCal commissioning

The full installation of the EMCal detector has been completed by inserting the additional six calorimeter super-modules into the ALICE solenoid, augmenting the overall ϕ azimuthal coverage of the EMCAL from $40°$ to $100°$. The installation work lasted less than two weeks and has been carried on slightly ahead of schedule during the 2010-11 LHC winter shutdown. The readout of the additional EMCal super-modules was fully tested for reliability and firmware performance of the Redout Control Units (RCU). A new RCU firmware was released for the direct handling of the Front End Cards (FEC) sparsification in order to lower the detector dead time from 630μs down to 260μs had in p-p collisions. The newly installed super-modules have already been setup with a different readout controller so to replace the GTL bus based readout of the RCUs with point to point links, called SRU (Scalable Readout Unit). In this setup each FEC communicates directly with the SRU controller via a dedicated link based on the Ethernet standards using a custom Data and Trigger Control (DTC) protocol. The SRU implementation was realized by installing a half-size board on each FEC. The new and the old readout will coexist until the full commissioning of the SRU will be over in 2012. The parallel management of the FECs will be able to bring the EMCal readout rates up to 30 kHz for the p-p collisions. The full ten super-modules of the EMCal detector have been successfully operated in 2011 during the p-p and Pb-Pb data taking both for triggering and data taking.

5 EMCal L0/L1 trigger

Full exploitation of the LHC luminosity delivered to ALICE requires fast triggers at Level-0 and Level-1. They must be both efficient for the signals of interest and have sufficient rejection of background in order to meet the ALICE recording bandwidth requirements, including a high flexibility in order to accommodate the variation in interaction rates and complexity of backgrounds. Specifically, the EMCal measures high-p_T photons, electrons, and jets, and for this reason optimized triggers have been developed for p-p and Pb-Pb collision systems both at the L1 and the HLT trigger levels. The overall trigger strategy is to provide the minimum necessary rejection at L0/L1 with as many events as possible transferred to the High Level Trigger (HLT) where the full event information from all ALICE subsystems is available and an event analysis, with a precision approaching that of the offline analysis, is carried out. In addition, it is mandatory to have optimal decisions about event rejection.

The Frascati group participated into the EMCal L0/L1 trigger commissioning and optimization for photons and electrons. This is provided by the functionality of the Front End Electronics (FEE) that generates fast analog 2x2 tower sums, which are then summed in the FPGA of the Trigger Region Unit (TRU) into 4x4 regions for high-energy shower trigger decisions at L1. Since the ALICE interaction trigger will potentially be biased, the EMCal provides also trigger inputs at L0 using a low threshold in order to record all events with activity, without bias, from other trigger detectors.

The measured clusters are correlated with the centrality measurements; the single shower triggers, with a fixed threshold, induce clearly a centrality bias. For this reason, it is highly preferable to trigger on L1 single shower trigger where the information from the centrality may be used to adjust the threshold and apply a centrality variable threshold setting. This strategy ensures a more uniform statistics in peripheral centrality bins where the trigger is really needed. The hardware EMCal jet trigger is provided by the L1 electronics and requires additional considerations. A tower/cell trigger for jets (which is effectively a hard π^0 trigger) generates significant trigger bias. Consequently, unbiased recording of rare, high-E_T jets by the EMCal, requires a specialized jet trigger designed to integrate the energy over a large phase space area (called jet-patch), in order to measure a significant fraction of the jet energy as input to the L1 trigger decision.

An event is considered to have been triggered if a given patch has been fired. The rejection factor is the ratio of the number of events triggered with respect to the total number of events considered. For this purpose a sample of 2.5M PbPb minimum bias data have been analyzed with patches sizes of 24x24, 32x32, and 40x40 for different thresholds in order to evaluate how much do we need to reject events to fit in the 10Hz rate (the allotted bandwidth for the EMCal).

First of all, a study of the L1 rejection factor vs. centrality has been calculated for four different thresholds: 10-40 GeV, and two patch sizes of 24x24 and 40x40 towers, Fig. 3. Once the rejection starts, the rate drops almost exponentially for all thresholds. In addition, for the lowest threshold (10 GeV) almost no rejection is achieved up to high centrality values. On the other hand, it can be seen that the highest threshold of 40 GeV keeps about 1/7-1/10 of events.

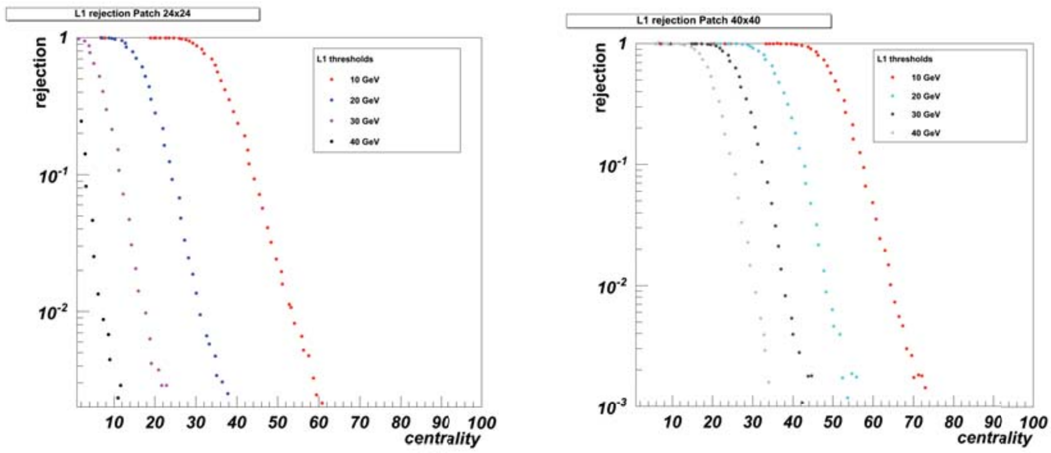

Figure 3: *L1 rejection factor for different thresholds and patch size of 24x24 (left), 40x40 (right).*

The conclusion is that the biggest the patch, the harder is to reject events, the higher the thresholds has to be set. Correspondingly, the study of the L1 thresholds for a rejection factor of

50 and three different patch sizes shows the non-linear dependence of the threshold vs. centrality for each patch size. Such study allows selecting a threshold as a function of centrality, depending of the needed rejection factor. The EMCal L1 trigger has been validated during the p-p data taking in October 2011 and fully activated for real rejection in the November heavy-ion running of LHC.

6 High Level Trigger

ALICE has an overall data rate up to 25 GByte/s, so an on-line data processing must be applied in order to reduce such data high volume. The experiment applies a multi-level hardware scheme via the so-called Central Trigger Processor where fast detectors are used to feed the L0/L1 hardware trigger chain. At the end of the hardware trigger chain a more refined filtering stage is introduced: the High-Level Trigger (HLT), which is able to reduce the data stream to the permanent storage down to 1.25 GB/s. The HLT layer is designed to perform complex event selection functions via fast reconstruction algorithms in order to provide trigger decisions, Regions-of-Interest, and compressed data to the DAQ in order to reduce the data rate to permanent storage. In addition to event selection and triggering tasks, HLT produces online detector performance monitoring histograms (QA) and calibration information. The EMCal Front End Electronics (FEE) provides information to the HLT chain, as the full copy of the EMCal FEE raw data, the list of the trigger clusters that have satisfied the trigger condition from the STU, and the time-integrated trigger data from all 2x2 channels.

The HLT online software run within the publisher-subscriber data transport framework. In this context, dedicated processing components have been developed by the Frascati group in order to perform the EMCal specific reconstruction, monitoring and triggering.

The EMCal HLT online analysis chain can use different clusterization algorithms according to the LHC collision modes. In case of p-p collisions the event multiplicity is low enough to allow a clusterization algorithm oriented to the inclusion of all the possible nearby cells which fire above threshold. Since there is no underlying event, this approach guarantees clusters with a high accuracy in the energy measurement which are still composed by a reasonable number of cells. On the other hand, in a Pb-Pb event, the multiplicity can be high enough to practically fire all cells in the calorimeter, so a sharper cut must be included in the clusterization algorithm. The EMCal HLT chain clusterizers look for the highest energy cell to start the clusterization process, then in turn, add to the cluster all edge cells above threshold. The cells timing and energy contents are checked for proper ordering and gradient respectively.

The reconstructed cluster information can than be used to produce a single shower trigger which has several advantages over the hardware triggers. In fact, the L0 shower trigger is a space sum of 2x2 towers. Each TRU module scans 1/3 of an EMCal super-module with a 4x4 sliding window. A trigger is generated when a 2x2 into the 4x4 patch is found over the threshold set for the 4x4 as a whole, and a trigger bit is set for each 2x2 which fired within the 4x4. In addition, the 4x4 sliding window is confined inside the 1/3-wide slice of a super-module in case only the L0 trigger is active (typically the case for p-p). On the other hand, the HLT cluster trigger uses a full fledged cluster reconstruction which spans a whole sector in azimuth (since the clusterizer algorithm can cross the $\eta = 0$ boundary between two super modules) and uses up to date OCDB information for the bad channel maps and calibrations. Such an approach can sharpen the trigger turn on curve (quantitative studies are on-going) with respect to the hardware trigger responses introducing additional rejection power and trimming the quota of unusable events sent to the offline reconstruction. Another important feature of the HLT is the improvement of the electron trigger which enhances the sample of the collected electrons helping the decision when a low enough L0 threshold is used. The efficiency and the gain has been evaluated by a simulation, as shown in figure 4.

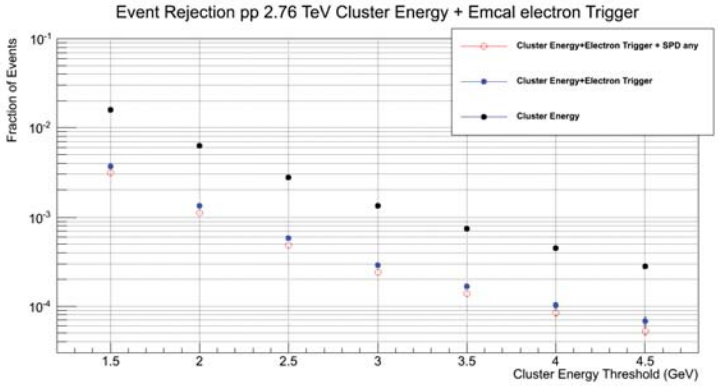

Figure 4: *Improvement of the event selection for $E_e > 1$ GeV/c from AliRoot simulation with Minimum Bias p-p @ 2.76 TeV (EMCAL full geometry).*

Last but not least, the EMCal HLT jet trigger component can provide an unbiased jet sample by refining the L1 trigger decisions using the TPC track information. The component uses an anti-k_T FASTJET jet finder which has been included in the standard AliRoot trunk.

7 Offline analysis

7.1 Photons and π^0 discrimination in the EMCal

In strong interactions, when a photon and a parton are produced in opposite directions, the detection of the photon is very important because it gives a measurement of the energy of the opposite parton that originated the jet. Detection of these photons is highly contaminated by the decay into two photons of the neutral meson π^0, whose production is predicted to be higher in both p-p and Pb-Pb collisions. To discriminate whether the produced signal is due to the π^0 photon decay or other source of direct photons, we have developed the method of the "Shower Shape Analysis" (SSA), which is based on the probability of forming one or two separated clusters, depending on the opening angle of the two-photon decay. The approach consists in defining parameters characterizing the shape of the electromagnetic cascade, among which is the "shower shape". The latter is defined by the intersection of the cone that contains the frontal plane of the calorimeter and can be expressed in terms of the covariant matrix

$$\begin{pmatrix} s_{xx} & s_{zx} \\ s_{xz} & s_{zz} \end{pmatrix}, where\ s_{xx} = \left\langle (x-\bar{x})^2 \right\rangle = \frac{\sum w_i x_i^2}{\sum w_i} - \left(\frac{\sum w_i x_i}{\sum w_i}\right)^2. \tag{1}$$

The sum is done over all the cluster towers and the w$_i$ values represent the logarithmic weight of the deposited energy in the tower i defined as:

$$w_i = max\left[0, p + log\left(\frac{e_i}{E}\right)\right], \tag{2}$$

where e_i is the energy deposited in the tower i and p is a parameter whose value is determined empirically as 4.5. Similar definitions are for s_{zz}, s_{xz} and s_{zx}. The eigenvalues λ_0 and λ_1 of the matrix 1 are dimensionless parameters that define the main axes of the electromagnetic cascade. The cascades produced by different particles can be identified by comparing the distribution of the above parameters for each particle. By studying the behavior of these parameters it was found that the most discriminative parameter to differentiate between these particles is the square of the largest eigenvalue of the covariant matrix 1.

At low energies, the separation of the two-photon decay of π^0 can still be large enough to form individual clusters. In this case, the reconstruction of the π^0 is performed by the standard invariant mass method. For this reason, during the analysis of the π^0, the values of λ_0^2 are taken only in those cases where the two photons generate a single cluster in the detector. For energies below 16 GeV, the λ_0^2 distributions are well separated by a visible differentiation of photons respect to π^0 and a value of λ_0^2 (λ_{0-opt}^2) can be determined such as only photons have $\lambda_0^2 < \lambda_{0-opt}^2$ while $\pi^0 s$ have larger values of λ_0^2. As the energy increases, to separate photons and π^0 with merged clusters, the λ_{0-opt}^2 value must be tuned in order to obtain the largest number of correctly identified particles for each energy. Besides, the effectiveness of the method can be quantified by determining the identification and misidentification probabilities. Figure 5 (left) shows the probability of correctly identifying photons, P(γ, γ), as the fraction of photons with $\lambda_0^2 < \lambda_{0-opt}^2(\gamma)$ of the total photons. The values stay above 90% over the whole energy range. On the contrary, P(γ, π^0) has values close to zero. Figure 5 (right) shows the probability P(π^0, π^0) of correctly identifying π^0, as the fraction of π^0 with $\lambda_0^2 > \lambda_{0-opt}^2(\pi^0)$ of the total π^0. This reaches a maximum of 95% with values above 80% between 10 [1] and 25 GeV. For energies above 25 GeV, it decreases as the cluster size generated by these features is similar to the cluster formed by a single photon. Here, another method, called "isolation cut", has higher efficiency and can be better applied.

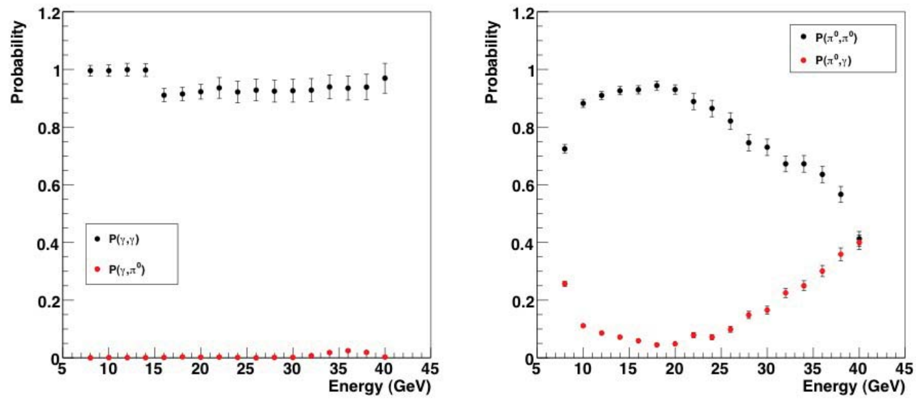

Figure 5: Identification and misidentification probability for photons (left) and π^0 (right).

7.2 Jet Reconstruction in ALICE: background fluctuations and jet energy uncertainty

In heavy ion collisions, jets are one of the main probes to access the hot medium since the interaction of the scattered partons with the medium induces changes to the internal jet structures and may alter the jet size. The modification of these properties of the reconstructed jets are the observables for the jet quenching.

The LNF group is deeply involved in the jet physics being responsible for the jet reconstruction algorithms implementation, the background fluctuation analysis and for the effects induced by the interplay between jet finding and limited acceptance.

First Alice paper on jet reconstruction is based on data collected in the first Pb-Pb run of the LHC in 2010 using charged particles from inner tracking detectors only. However, the techniques developed and described in the first paper for charged particles are general, and will be applied

[1] Below 10 GeV the identification method is different, as discussed previously.

$f(pt)$ folded with	relative yield for $pt = 60 - 68\,\mathrm{GeV}/c$		
δpt	RC	tracks	jets
$pt_{min} = 0.15\,\mathrm{GeV}/c$	9.8 ± 1.7	11.4 ± 1.1	10.9 ± 3.4
$pt_{min} = 2\,\mathrm{GeV}/c$	1.30 ± 0.02	1.31 ± 0.02	1.65 ± 0.25
Gauss			
$\sigma = 11\,\mathrm{GeV}/c$	1.82 ± 0.04		
$\sigma = 5\,\mathrm{GeV}/c$	1.05 ± 0.01		

Table 1: Yield modification for power law spectrum. Relative yield in the bin $pt = 60 - 68\,\mathrm{GeV}/c$ for a power law spectrum ($f(pt) = 0.7/(0.7 + pt^5)$ and $pt > 4\,\mathrm{GeV}/c$), folded with the different δpt distributions for 0-10% centrality and with a Gaussian, where the width is similar to the standard deviation of the δpt distributions.

directly in the analysis based on 2011 data which include neutral particles from calorimetry, in particular from EMCal. The LNF group has participated as main author in the first detailed study of event background fluctuations for jet reconstruction using charged particles in Pb-Pb collisions at the LHC. Jet reconstruction in the complex environment of a heavy-ion collision requires a quantitative understanding of background-induced fluctuations of the measured jet signal and the effects of the underlying heavy-ion event on the jet finding process itself. Here, region-to-region background fluctuations are the main source of jet energy or momentum uncertainty and can have a large impact on jet structure observables, such as the fraction of energy inside the jet core or the shape of the jet, and will distort the measured jet energy balance even in the absence of medium effects. To measure region-to-region background fluctuations, three probes are embedded into the Pb-Pb events measured by ALICE: (i) rigid area random cones, (ii) single high-pt tracks at various pt, and (iii) p-p jet events generated using PYTHIA followed by a detailed simulation of the full detector response. Jet candidates are reconstructed from the event using the anti-kt algorithm with R = 0.4 and matched to the embedded probe, by either finding the single track in it, or by requiring that the pt of the embedded tracks within the reconstructed jet sum up to at least 50% of the original probe jet transverse momentum. The difference between the reconstructed, background subtracted jet and the embedded probe is then given by $\Delta pt = pt^{jet,rec} - A^{jet,rec} * \rho - pt^{probe}$. The response may depend on the jet finder, its settings, and the properties of the embedded probe, such as pt^{probe}, area, and fragmentation pattern. In particular the insensitivity to the latter is essential for a robust and unbiased reconstruction of jets in heavy-ion collisions, where the fragmentation pattern is potentially modified relative to that in pp collisions, and is indeed the observable of interest. The standard deviation of the fluctuations in the 10% most central events is $\sigma = 10.98 \pm 0.01$ GeV/c within a rigid cone of $R = 0.4$ and for a low pt cut-off of 0.15 GeV/c. It has been shown that the non-statistical sources of fluctuations are driven in part by the anisotropy of the particles emitted from the collision (elliptic and triangular flow). The variation of multiplicity in different orientations with respect to the event plane, induces shifts in the background-subtracted jet pt even for central PbPb-collisions. The anti-kt jet finder response for charged particle jet reconstruction has a modest dependence on the method used to characterize the fluctuations. For embedded, simulated pp-jets the standard deviation increases to 11.34 ± 0.02 GeV/c. In addition, certain rare fragmentation patterns in p-p are likely to be split in the heavy-ion environment leading to minor effects in the background response, as it is apparent in Fig.6.

The observed differences between the two types of embedded probes (namely single tracks and p-p jets) do not indicate a strong sensitivity of the reconstructed anti-kt jet spectrum on fragmentation. The case of a strong broadening of the jet due to medium effects has not been considered here. The use of reconstructed charged particles down to $pt_{min} = 0.15$ GeV/c allows a

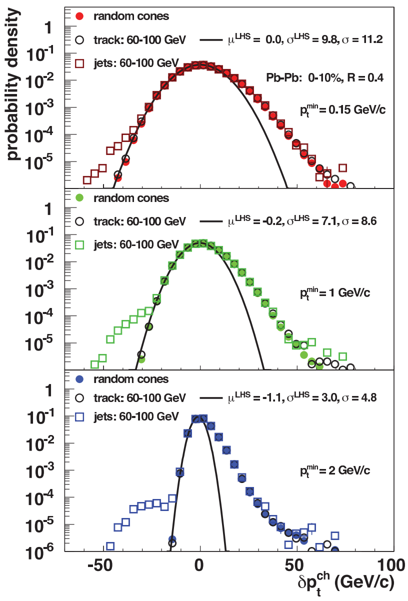

Figure 6: δpt distribution of charged particles for jet reconstruction with the three methods in the 10% most central Pb-Pb events for pt_{min} = 0.15, 1, and 2 GeV/c.

comparison of the impact of background fluctuations with a minimal bias on hard fragmentation in jet finding to the case with increased bias ($pt_{min} > 1$ GeV/c). The observed reduction of the standard deviation to $\sigma = 4.82 \pm 0.01$ GeV/c for the unbiased sampling and $pt_{min} = 2$ GeV/c is driven by the smaller number fluctuations and the reduced influence of soft region-to-region fluctuations. The asymmetric shape of the delta pt distribution with a tail towards positive fluctuations has a large impact on the jet measurement, compared to purely Gaussian fluctuations, though the role of signal jets contributing to the tail has to be considered. Using different assumptions on the shape of the true jet spectrum it is found that for $pt_{min} = 0.15$, GeV/c fluctuations can have a large influence on the charged jet yield for transverse momenta up to 100 ± 15 GeV/c, as reported in Table.1.

8 Conferences and Papers by LNF Authors in Year 2011

8.1 Publications

1. The ALICE Collaboration, Suppression of Charged Particle Production at Large Transverse Momentum in Central Pb-Pb Collisions at $\sqrt{s_{NN}} = 2.76$ TeV, Phys.Lett.B **696** (2011) 30

2. The ALICE Collaboration, Centrality dependence of the charged-particle multiplicity density at mid-rapidity in Pb-Pb collisions at $\sqrt{s_{NN}} = 2.76$ TeV, Phys.Rev.Lett. **106**, 032301 (2011)

3. The ALICE Collaboration, Two-pion Bose-Einstein correlations in central PbPb collisions at $\sqrt{s_{NN}} = 2.76$ TeV, Phys.Lett.B **696** (2011) 328

4. The ALICE Collaboration, Strange particle production in proton-proton collisions at $\sqrt{s} =$ 0.9 TeV with ALICE at the LHC, Eur.Phys.J. C 71 (3), **1594** (2011)

5. The ALICE Collaboration, Rapidity and transverse momentum dependence of inclusive J/ψ production in pp collisions at $\sqrt{s} = 7$ TeV, Phys.Lett.B **704** (2011) 442
6. The ALICE Collaboration, Higher harmonic anisotropic flow measurements of charged particles in Pb-Pb collisions at 2.76 TeV, Phys.Rev.Lett. **107**, 032301 (2011)
7. The ALICE Collaboration, Production of pions, kaons and protons in pp collisions at $\sqrt{s} =$ 900 GeV with ALICE at the LHC, Eur.Phys.J. C **71** (6) 1655, 2011
8. The ALICE Collaboration, Femtoscopy of pp collisions at sqrts=0.9 and 7 TeV at the LHC with two-pion Bose-Einstein correlations, Phys.Rev.D **84**, 112004 (2011)

8.2 Conferences and Talks

1. N.Bianchi, Partonic energy loss in cold and hot nuclear matter, WONP-NURT, Havana, February 2011
2. N.Bianchi, Hadron Multiplicities in SIDIS off Nucleons and Nuclei, EDS Blois Workshop, Qui Nhon (Vietnam), December 2011
3. L.Cunqueiro, Jet Physics with ALICE, Alice Italia Meeting, Frascati, March 2011
4. L.Cunqueiro, Jet Physics in ALICE, IFAE2011, Perugia, April 2011
5. L.Cunqueiro, Jets in ALICE, DIS2011, Newport News (USA), April 2011
6. L.Cunqueiro, Jet Reconstruction at LHC (invited talk), LHC11, Trento, October 2011
7. L.Cunqueiro, Jet Physics with ALICE, invited seminar in Theory Group, Santiago de Compostela, December 2011
8. P.Di Nezza, The ALICE experiment at the LHC, Winter Institute Meeting, Frascati, March 2011
9. P.Di Nezza, ALICE in the early Universe Wonderland (invited talk), Suzaku Conference, Palo Alto, SLAC, July 2011
10. A.Fantoni, The ALICE experiment and its electromagnetic calorimeter EMCAL (invited talk), BCVSPIN Advanced Study Institute in Particle Physics and Cosmology, Hue', Vietnam , July 2011
11. F.Ronchetti, The ALICE HLT project, WONP-NURT, Havana, February 2011

8.3 Conferences Organization

1. N.Bianchi International Advisory Committee of WONP-NURT, Havana, 7-11 February 2011

8.4 Proceeding and Notes

1. A.Casanova Diaz, L.Cunqueiro Mendez et al., Photons and π^0 discrimination in the electromagnetic calorimeter (EMCal) of the ALICE experiment, LNF Note 11/13(P)
2. A. Fantoni, The ALICE electromagnetic calorimeter, Journal of Physics, Conference Series 293 (2011) 012043
3. A. Fantoni, The ALICE electromagnetic calorimeter EMCAL: its status and its physics capabilities, Proceedings of Science Kruger2010 (2011) 009

Activity Report 2011 - JLAB12

M. Aghasyan (Ass.), S. Anefalos Pereira (Art. 23), E. De Sanctis, D. Hasch, L. Hovsepyan (Post-doc), V. Lucherini, M. Mirazita, J. de Oliveira Echeimberg (Post-doc), A. Orlandi (Tech.), S. Pisano (Ass.), E. Polli, P. Rossi (Resp. Naz.), A. Viticchié (Tech.)

1 Introduction

The Frascati JLAB12 group participates into the physics program carried on by the CLAS collaboration in the Hall B of the Jefferson Laboratory (JLab) with the 6 GeV Continuous Electron Beam Accelerator Facility (CEBAF). The CEBAF accelerator will run with the 6 GeV beam till May 2012, when it will be shut down for an upgrade of the facility that will bring the maximum electron energy to 12 GeV by the middle of 2013. All the detectors will also be upgraded and the Hall B will be equipped with the new CLAS12 specrometer.

The physics program of the group is focused on the precision study of the three-dimensional structure of the nucleon and its internal dynamics. This is achieved through the determination of new parton distribution functions, the so-called TMDs, which include information not only on the longitudinal but also on the transverse distributions of partons in a fast moving hadron. TMDs can be studied through the measurement of azimuthal asymmetries in Semi-Inclusive Deep Inelastic Scattering (SIDIS) processes, in which one (or more) hadron is detected in coincidence with the scattered electron.

In the period covered by this report, the group has continued to work to the analysis of already available experimental data with 6 GeV and in the preparation of the physics program with the 12 GeV beam.

2 Transverse Momentum Dependent parton distribution functions (TMDs)

The exploration of the internal structure of the hadrons has undergone enormous progress in the last decades. The Transverse Momentum Dependent (TMD) parton distribution and fragmentation functions [1, 2] are one of the framework to obtain information towards a genuine multi-dimensional picture of the nucleon structure. They are the three-dimensional generalization of the collinear Parton Distribution Functions (PDFs) introduced in the 60s to explain the Deep Inelastic Scattering (DIS) experiments. A major role in the TMD study is played by by Semi-Inclusive Deep-Inelastic Scattering (SIDIS) processes, where in addition to the scattered lepton, also a hadron is detected in the final state. This hadron is generated in the fragmentation of the scattered quark, the so-called Current Fragmentation Region (CFR).

There are eight leading-twist quark TMD distributions. Three of them survive after integration over the transverse momenta: the unpolarized and helicity distributions already introduced in the DIS experiments and the transversity distribution, which is related to transverse polarization of quarks. The other five distributions describe the correlations between the transverse momentum of quarks, their spin and/or the spin of the nucleon and provide a way to access the orbital angular momentum of the partons. Similar spin-orbit correlations arise in the hadronization process of the struck quark into the final hadron, described by TMD fragmentation functions. Besides the unpolarized one, the other relevant TMD fragmentation function is the Collins function [3], representing a correlation between the transverse polarization of the fragmenting quark and the transverse momentum of the produced hadron.

The connection between TMDs and the physics observables was put on a firm theoretical basis with the appropriate factorization proof [4, 5]. The cross section for hadron production in

SIDIS processes can be written [2] as a Fourier expansion in the azimuthal angle ϕ of the hadron

$$\sigma \propto \sigma_{UU} + \lambda\sigma_{LU}\sin(\phi) + S_{\parallel}\sigma_{UL}\sin(\phi) + \lambda S_{\parallel}\sigma_{LL} + ... \quad (1)$$

where λ and $S_{\parallel}$ are the electron helicity and longitudinal nucleon target spin and the labels indicate unpolarized (U) or longitudinally polarized (L) beam or target, the first index referring to the beam and the second to the target. The dots represent other contributions, including transverse polarization (T) terms. The different Fourier components of the cross section, each containing a well defined convolution of distribution and fragmentation functions, can be isolated by measuring beam and/or target spin asymmetries.

TMDs studies are one of the primary goal of experiments at JLab with the 12 GeV electron beam, but their investigation has already started with the 6 GeV beam using unpolarized and polarized targets.

3 The 6 GeV program

Several measurements connected with the TMD studies have been progressed by the Frascati group during the 2011.

3.1 *Neutral pion Beam Spin Asymmetry*

The CLAS measurement of the single Beam Spin Asymmetry (BSA) $A_{LU}^{\sin\phi}$ in the π^0 SIDIS electroproduction has been completed in 2011 and published (see Ref. 3 in the publication list). This BSA contains several contributions [6, 7], in which either the distribution or fragmentation function are higher twist. Calculations based on spin-orbit correlations in the distribution functions (including the Boer-Mulders [8] or $g_{\perp}$ [9, 10] functions) give non-zero BSA [11]. In contrast, calculations based on the Collins mechanism [12, 13, 14, 15] predict negligible BSA.

The measurement used a 5.77 GeV electron beam with average polarization $P_B = 79.4 \pm 2.4\%$ and an unpolarized liquid hydrogen target. Neutral pions where detected by looking at the invariant mass of the two decay photons. The BSA has been measured as a function of the Bjorken-x variable and of the pion transverse momentum, as shown in Fig. 1. It is positive and close to the CLAS π^+ data [16], except for the highest x values, suggesting that the Collins contribution cannot be the dominant one. This result underscores the potential of the BSA in studying spin-orbit correlations.

3.2 Λ *semi-inclusive electroproduction*

Hadrons in semi-inclusive reactions can be produced also in the fragmentation of the target remnant quarks (Target Fragmentation Region, TFR), rather than from the struck quark. The formal description of this kind of processes has been recently produced [18] and it is based on the TMD Fracture Function formalism [19, 20]. These new functions represent the joint probability to produce a given hadron when a quark of the nucleon target is struck in a hard process.

The fracture functions can be accessed by looking at backward SIDIS electroproduction of hadrons, as for example Λ. The $ep \to e'\Lambda X$ process has two advantages: (i) TFR can be clearly separated, and (ii) thanks to the $\Lambda \to p\pi^-$ weak decay, the recoil polarization can also be measured. The latter aspect provides a way to study the proton sea quark polarization, being the Λ spin mainly due to the contribution of its strange quark.

Recoil polarization measurement in the Λ SIDIS electroproduction is underway in CLAS using a 5.5 polarized electron beam onto an unpolarized liquid hydrogen target. Preliminary results, presented at the DIS2011 conference, are shown in Fig. 2, where the longitudinal polarization

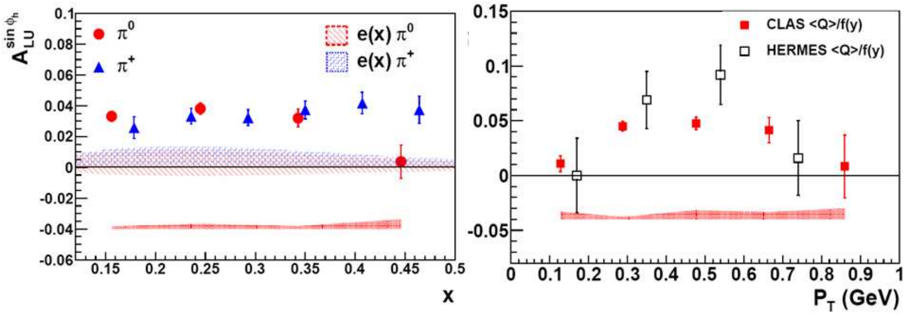

Figure 1: *Neutral pion BSA as a function of the Bjorken-x (left, red circles, compared with CLAS π^+ data blue triangles) and of the transverse momentum (right, red squares, compared with the HERMES results* [17]*, empty squares).*

trasfer from the electron beam to the Λ is shown as a function of the Feynman-x variable. We see that in the CFR ($x_F > 0$) the polarization transfer is compatible with zero, even if with large error bars, while in the TFR it is of the order of 30%. This analysis is in the final stage of the estimation of the systematic uncertainties.

3.3 *Two pion semi-inclusive electroproduction*

When two hadrons are semi-inclusively produced in the CFR, the cross section takes a simpler form than in the single pion case [21]. The Fourier components of eq. (1) are in fact given by a simple product of a TMD distribution function and a TMD DiHadron Fragmentation Function (DiFF). Thus, extraction of TMD information from this process is easier.

The study of two pion SIDIS electroproduction with CLAS data is underway with 6 GeV polarized electron beam and unpolarized as well as longitudinally polarized hydrogen target. The observables to be measured are single (beam) and double (beam and target) spin asymmetries. Currently, the analysis is in the preliminary stage of defining the proper kinematic cuts and of tuning the Monte Carlo event generator and detector simulation for the study of the acceptance.

4 The 12 GeV program

4.1 *Proposals for new measurements*

Two new proposals have been submitted in 2011 by the Frascati group to the Program Advisory Committee (PAC) of JLab.

The first one focuses on measurements of the transverse single and double spin asymmetries in inclusive hadron electroproduction from protons polarized transversely to the beam direction. The measured asymmetries provide access to three leading twist TMD parton distributions: transversity, Sivers function and the so-called pretzelosity function. For full flavor tagging, final state pions as well as kaons have to be detected. The proposal was approved, conditionally to the operation of the transversely polarized HD-Ice target in an electron beam with the neccessary beam current. Test of the HD-Ice target with the electron beam are planned for the first half of 2012.

The second proposal aims to study higher twist distribution functions describing quark gluon correlations and chiral-odd-dihadron fragmentation functions. This can be achieved by measuring azimuthal asymmetries in semi-inclusive di-hadron electroproduction in various flavor combinations

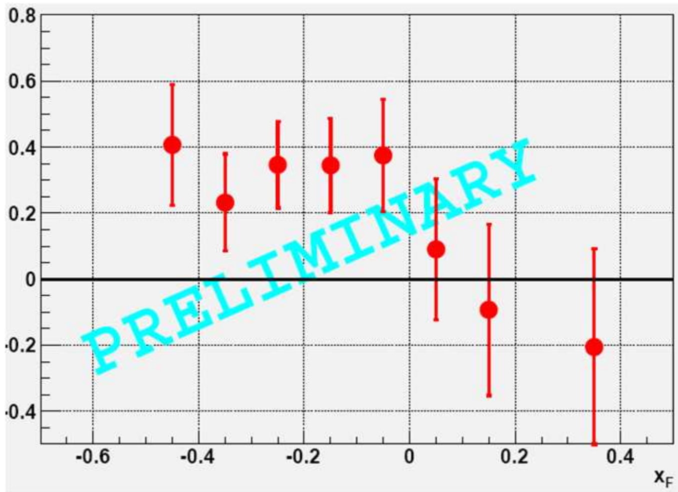

Figure 2: Λ *longitudinal polarization transfer as a function of* x_F *in SIDIS electroproduction measured at CLAS.*

of pions and kaons. The proposal was evaluated as feasible by the PAC, nevertheless it was deferred because of concerns about its priority compared to already approved SIDIS experiments aiming at the study of leading twist distribution functions.

4.2 *A RICH detector for CLAS12*

Some of the most interesting recent experimental results on the TMDs are connected with the comparison between pions and kaons. The PAC of JLab already approved proposals aimed to study kaons in SIDIS reactions with CLAS12, however this program needs improvements in the CLAS12 particle identification. For this reason, the group has proposed the construction of a RICH detector, to be installed in CLAS12, that will allow good kaon identification for momenta up to 8 GeV/c. Schematically, the detector is composed by few cm of aerogel radiator, a 1 meter gap and an array of photodetectors. In order to reduce the large photodetector surface, mirrors will be used to focus the Cherenkov photons emitted at large angles in a smaller area, thus implying multiple passage of the photons through the radiator. The project presents some critical points, some of which have been already addressed in 2011 with laboratory tests of the components. In addition, a test of a preliminary prototype has been performed in summer 2011 using the hadron beam of the T9 line at CERN.

The prototype was composed by an aerogel radiator of different thickenesses and eight multi-anode photomultipliers Hamamatsu H8500, 5×5 cm^2 devices with a matrix of 6 mm 8×8 pixels. The good capabilities of those PMTs as single photon detector have been verified both with a low intensity laser beam and during the hadron beam test. The left plot of fig. 3 shows a single photon spectrum measured during the CERN tests. We see a clear Cherenkov peak, well separated from the pedestal. Rough estimate of the single photon detection efficiency has been measured with the laser tests to be at least 80%. The Cherenkov rings produced by the high energy pions have been clearly measured, as shown in the right plot of fig. 3.

These results are very promising and have been used to validate the GEANT4 simulation of the final detector. A new prototype, with dimensions and geometry closer to those of the final detector, is under construction and will be tested in summer 2012 both with the electron beam of

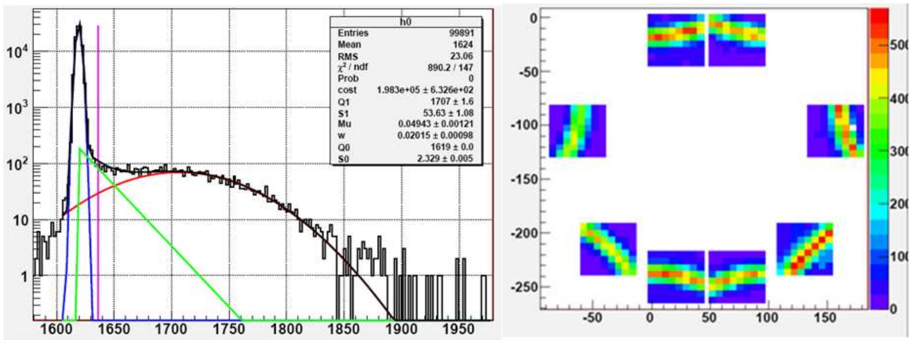

Figure 3: *(left) Single photon spectrum for one H8500 channel measured at CERN (pink vertical line represent the pedestal cut, for the fit see* [22]*); (right) Example of Cherenkov rings for pions with 10 GeV/c momentum, measured with 8 H8500.*

the Beam Test Facility in Frascati and with the CERN-T9 hadron beam.

5 List of Conference Talks by JLAB12 members in 2011

1. P. Rossi, *Kaon Physics Opportunities with a RICH detector in CLAS12*, Seminar at UTFSM, Valparaiso (Chile) - February 23, 2011.
2. M. Mirazita, *Lambda polarization in electroproduction at CLAS*, XIX International Workshop on Deep-Inelastic Scattering and Related Subjects, April 11-15, 2011, Newport News, USA.
3. S. Pisano, *Results and achievements at CLAS*, XIX International Workshop on Deep-Inelastic Scattering and Related Subjects, April 11-15, 2011, Newport News, USA.
4. S. Anefalos Pereira, *Strangeness Production in CLAS*, XIX International Workshop on Deep-Inelastic Scattering and Related Subjects, April 11-15, 2011, Newport News, USA.
5. P. Rossi, *The Jefferson Lab Program at 12 GeV*, IFAE2011 Incontri di Fisica delle Alte Energie, April 27-29, 2011, Perugia, Italy.
6. M. Aghasyan, *Studies of 3D structure of the nucleon with CLAS at JLab*, PacSPIN 2011, June 20-24 2011, Cairns, QLD, Australia.
7. D. Hasch, *The 3D structure of the nucleon at an EIC*, lecture at the Enrico Fermi school, Course CLXXX - "Three-dimensional Partonic Structure of the Nucleon", June 28 - July 08, 2011, Varenna, Italy.
8. M. Aghasyan, *JLab results: TMD measurements*, Third International Workshop on Transverse Polarisation Phenomena in Hard Processes (Transversity 2011), August 28 - September 3, 2011, Veli Losinij, Croatia
9. D. Hasch, *DVCS and Hard exclusive Meson production - an experimental review*, Third International Workshop on Transverse Polarisation Phenomena in Hard Processes (Transversity 2011), August 28 - September 3, 2011, Veli Losinij, Croatia.
10. S. Pisano, *First look at the dihadron production with the 6 GeV CLAS data*, DiHdron Fragmentation Function miniworkshop, September 5-7, 2011, Pavia, Italy.

11. S. Anefalos Pereira, *Semi-inclusive ρ^+ and ρ^0 asymmetries using eg1-dvcs*, DiHdron Fragmentation Function miniworkshop, September 5-7, 2011, Pavia, Italy.

12. D. Hasch, *GPDs - an overview*, Partons in Nucleons and Nuclei (PINAN11), September 26 - 30, 2011, Marrakech, Marocco.

13. P. Rossi, *TMD Measurements - Future*, Partons in Nucleons and Nuclei (PINAN11), September 26 - 30, 2011, Marrakech, Marocco.

14. S. Pisano, *Studio della produzione di due adroni con CLAS12 al Jefferson Lab*, Congresso della Societa' italiana di Fisica, September 26-30, L'Aquila, Italy.

15. P. Rossi, *Studies of the 3D structure of the nucleon with p and k production in hard processes*, Seminar at Duke University, October 20, 2011.

16. S. Pisano, *DiHadron analysis at CLAS*, EINN2011, October 31 - November 4 2011, Paphos, Cyprus

17. M. Mirazita, *Considerations on multi-dimensional maximum likelihood fits*, Monte Carlo workshop 2011, November 7-8 2011, Frascati, Italy.

18. S. Anefalos Pereira, *Monte Carlo generators for two-hadron analyses, what are the special needs?*, Monte Carlo workshop 2011, November 7-8 2011, Frascati, Italy.

19. M. Mirazita, *Overview of recent results from CLAS*, Workshop on Meson Production at Intermediate and High Energies, November 10-11, 2011, Messina, Italy.

20. D. Hasch, *WP3: TMDnet – mapping out the transverse structure of the nucleon*, Final report at the HP2 Collaboration Committee Meeting, Dec 02/03, 2011, Frascati, Italy.

6 Publications

1. Near-threshold photoproduction of mesons from deuterium
   CLAS Collaboration, W. Chen *et al.*, Phys. Lett. **B 696**, 338 (2011).

2. Coherent photoproduction of + from 3He
   CLAS Collaboration, R. Nasseripour *et al.*, Phys. Rev. C **83**, 034001 (2011).

3. Beam Spin Asymmetries in Semi-Inclusive π^0 production
   CLAS Collaboration, M. Aghasyan *et al.*, Phys. Lett. **B 704** 397 (2011).

4. Electromagnetic decay of the $\Sigma^0(1385)$ to $\Lambda\gamma$
   CLAS Collaboration, D. Keller *et al.*, Phys. Rev. **D 83**, 072004 (2011).

5. Upper limits for the photoproduction cross section for the $\Phi^{--}(1860)$ pentaquark state off the deuteron
   CLAS Collaboration, H. Egiyan *et al.*, Phys. Rev. **C 85** (2012) 015205.

6. Measurement of the nuclear multiplicity ratio for K0s hadronization at CLAS
   CLAS Collaboration, A. Daniel *et al.*, Phys. Lett. **B 706** (2011) 26-31.

7. The CLAS12 large area RICH detector
   M. Contalbrigo, E. Cisbani and P. Rossi, Nucl. Instrum. Meth. **A639** (2011) 302.

8. Transverse Momentum Dependent Parton Distribution/Fragmentation Functions at an Electron-Ion Collider
   M. Anselmino *et al.*, Eur. Phys. J. **A 47** (2011) 35.

9. Shrunken particles pass freely through nuclear matter
   CLAS Collaboration, L. El Fassi *et al.*, Phys. Lett. **B**, submitted.

10. Measurement of the neutron F2 structure function via spectator tagging
    CLAS Collaboration, N. Baillie *et al.*, Phys. Rev. Lett., submitted.

11. Branching Ratio of the Electromagnetic Decay of the $\Sigma^+(1385)$
    CLAS Collaboration, D. Keller *et al.*, Phys. Rev. **D**, submitted.

12. Measurement of the generalized form factors near threshold via $\gamma^* p \to n\pi^+$ at high Q^2
    CLAS Collaboration, K. Park *et al.*, Phys. Rev. **C**, submitted; arXiv:1201.0903.

References

1. P.J. Mulders and R.D. Tangerman, Nucl. Phys. **B461**, 197 (1996).
2. A. Bacchetta et al., JHEP **02**, 093 (2007).
3. J.C. Collins, Nucl. Phys. **B396**, 161 (1993).
4. J.C. Collins and D.E. Soper, Nucl. Phys. **B193**, 381 (1981).
5. X. Ji, J. Ma and F. Yuan, Phys. Rev. **D71**, 034005 (2005).
6. A. Afanasev and C.E. Carlson, hep-ph/0308163.
7. F. Yuan, Phys. Lett. **B589**, 28 (2004).
8. R. L. Jaffe, X.-D. Ji, Nucl. Phys. **B 375**, 527 (1992).
9. A. Metz, M. Schlegel, Eur. Phys. J. **A 22**, 489 (2004).
10. L. P. Gamberg, G. R. Goldstein, M. Schlegel, Phys. Rev. **D 77**, 094016 (2008); L. Gamber, private communication.
11. F. Yuan, Phys. Lett. **B 589**, 28 (2004).
12. P. Schweitzer, Phys. Rev. D 67 (2003) 114010.
13. A. V. Efremov, K. Goeke, P. Schweitzer, Phys. Rev. D 73 (2006) 094025.
14. P. Schweitzer, private communication (2011).
15. A. V. Belitsky, D. Mueller, Nucl. Phys. **B 503**, 279 (1997).
16. H. Avakian, L. Elouadrhiri, "High Energy Spin Physics Proc.", Editors A.V. Efremov and O.V. Teryaev (2003) 239.
17. A. Airapetian, et al., Phys. Lett. **B 648**, 164 (2007).
18. M. Anselmino, V. Barone and A. Kotzinian, Phys. Lett. **B699**, 108 (2011).
19. L. Trentadue and G. Veneziano, Phys. Lett. **B323**, 201 (1994).

20. F.A. Ceccopieri, L. Trentadue, Phys. Lett. **B636**, 310 (2006).

21. A. Bacchetta and M. Radici, Phys. Rev. **D69**, 074026 (2004).

22. R. Perrino *et al.*, Nucl. Intrum. Math. **A 457** (2001) 571.

KAONNIS

M. Bazzi (Assoc.), C. Berucci (Assoc.), M. Bragadireanu (Bors. UE), A. Clozza,
C. Curceanu Petrascu (Resp. Naz.), A. D'Uffizi (Ass. Ric.),
C. Guaraldo (Art. 2222), M. Iliescu (Ass.), P. Levi Sandri, F. Lucibello (Tecn.),
S. Okada (Art. 23), D. Pietreanu (Ass. Ric.), K. Piscicchia (Bors.),
M. Poli Lener (Art. 23), A. Rizzo (Bors.), A. Romero Vidal (Art. 23), E. Sbardella (Bors.),
A. Scordo (Ass. Ric.), D. Sirghi (Art. 23), F. Sirghi (Bors. UE),
O. Vazquez Doce (Art. 23)

1 The KAONNIS scientific program

KAONNIS represents an integrated activity in the field of the low-energy kaon-nucleon/nuclei interaction studies. Under KAONNIS the following activities are performed:

- the study of kaonic atoms by the SIDDHARTA and SIDDHARTA-2 experiments
- the study of kaon-nuclei interaction at low energies in the framework of AMADEUS.

We present in what follows these scientific lines, together with the 2011 activities and the plans for 2012. The KAONNIS scientific program and its realization are partially financed within the FP7 HadronPhysics2 and HadronPhysics3 EU programs.

2 The SIDDHARTA experiment

The objective of the SIDDHARTA (Silicon Drift Detector for Hadronic Atom Research by Timing Application) experiment and of its successor, SIDDHARTA-2, is to perform high precision measurements of X-ray transitions in exotic (kaonic) atoms at DAΦNE.

The precise determination of the shift and width of the 1s level with respect to the purely electromagnetic calculated values, in kaonic hydrogen and kaonic deuterium, generated by the presence of the strong interaction, through the measurement of the X-ray transitions to this level, will allow the first precise experimental determination of the isospin dependent antikaon-nucleon scattering lengths, fundamental quantities in understanding low-energy QCD in strangeness sector.

An accurate determination of these scattering lengths will place strong constraints on the low-energy K^-N dynamics, which, in turn, constraints the SU(3) description of chiral symmetry breaking in systems containing the strange quark. The implications go from particle and nuclear physics to astrophysics.

SIDDHARTA performed the most precise measurement of kaonic hydrogen and the first exploratory one of kaonic deuterium. Moreover, the kaonic helium 4 and 3 transitions to the 2p level were measured, for the first time in gas (He4) and for the first time ever (He3). Presently, a major upgrade of SIDDHARTA, namely SIDDHARTA-2, is under way, with the aim to measure kaonic deuterium and other types of kaonic atoms in the near future.

2.1 The SIDDHARTA setup

SIDDHARTA represented a new phase in the study of kaonic atoms at DAΦNE. The previous DEAR experiment's precision was limited by a signal/background ratio of about 1/70 for the kaonic hydrogen measurement. To significantly improve this ratio, a breakthrough was necessary.

An accurate study of the background sources present at DAΦNE was redone. The background includes two main sources:

- synchronous background: coming together with the kaons – related to K^- interactions in the setup materials and also to the ϕ-decay processes; it can be defined as hadronic background;
- asynchronous background: final products of electromagnetic showers in the machine pipe and in the setup materials originating from particles lost from primary circulating beams either due to the interaction of particles in the same bunch (Touschek effect) or due to the interaction with the residual gas.

Accurate studies performed by DEAR showed that the main background source in DAΦNE is of the second type, which shows the way to reduce it. A fast trigger correlated to a kaon entering into the target would cut the main part of the asynchronous background. X rays were detected by DEAR using CCDs (Charge-Coupled Devices), which are excellent X-ray detectors, with very good energy resolution (about 140 eV FWHM at 6 keV), but having the drawback of being non-triggerable devices (since the read-out time per device is at the level of 10 s). A new device, which preserves all good features of CCDs (energy resolution, stability and linearity), but additionally is triggerable - i.e. fast (at the level of 1μs), was implemented. The new detector was a large area Silicon Drift Detector (SDD), specially designed for spectroscopic application. The development of the new 1 cm^2 SDD device, together with its readout electronics and very stable power supplies, was partially performed under the Joint Research Activity JRA10 of the I3 project "Study of strongly interacting matter (HadronPhysics)" within FP6 of the EU.

The trigger in SIDDHARTA was given by a system of scintillators which recognized a kaon entering the target making use of the back-to-back production mechanism of the charged kaons at DAΦNE from ϕ decay: of the type:

$$\phi \to K^+K^-. \tag{1}$$

The SIDDHARTA setup contained 144 SDD chips, 1 cm^2 each, placed around a cylindrical target, containing high density cryogenic gaseous hydrogen (deuterium or helium). The target was made of kapton, 75μm thick, reinforced with aluminium grid.

The SIDDHARTA setup was installed on DAΦNE in late summer 2008, see Figure 1 - and the period till the end of 2008 was used to debug and optimize the setup performances (degrader optimization included). The kaonic atoms (hydrogen, deuterium, helium4 and 3) measurements were done in 2009 and data analysis during 2010 and 2011.

2.2 SIDDHARTA activities in 2011

SIDDHARTA was in data taking until 9 November 2009. In 2011 the group activity was dedicated to finalize the kaonic helium 3 and haonic hydrogen data analyses, and publish them, and to the refinement of the proposal for the upgrade of the setup, SIDDHARTA-2, to perform in the future the kaonic deuterium and other precision kaonic atoms measurements.

2.2.1 Kaonic hydrogen results

The kaonic hydrogen measurement was performed in the period 15 March - 31 July 2009 and during October 2009, for a total of about 400 pb^{-1} of integrated luminosity.

The data analyses was completed in 2011 and a paper published in Phys. Lett. B704 (2011) 113-117, see Fig. 2 for the kaonic hydrogen spectrum. The results for shift and width:

$$\epsilon = -283 \pm 36(stat.) \pm 6(syst.)\ eV \tag{2}$$

$$\Gamma = 541 \pm 89(stat.) \pm 22(syst.)\ eV. \tag{3}$$

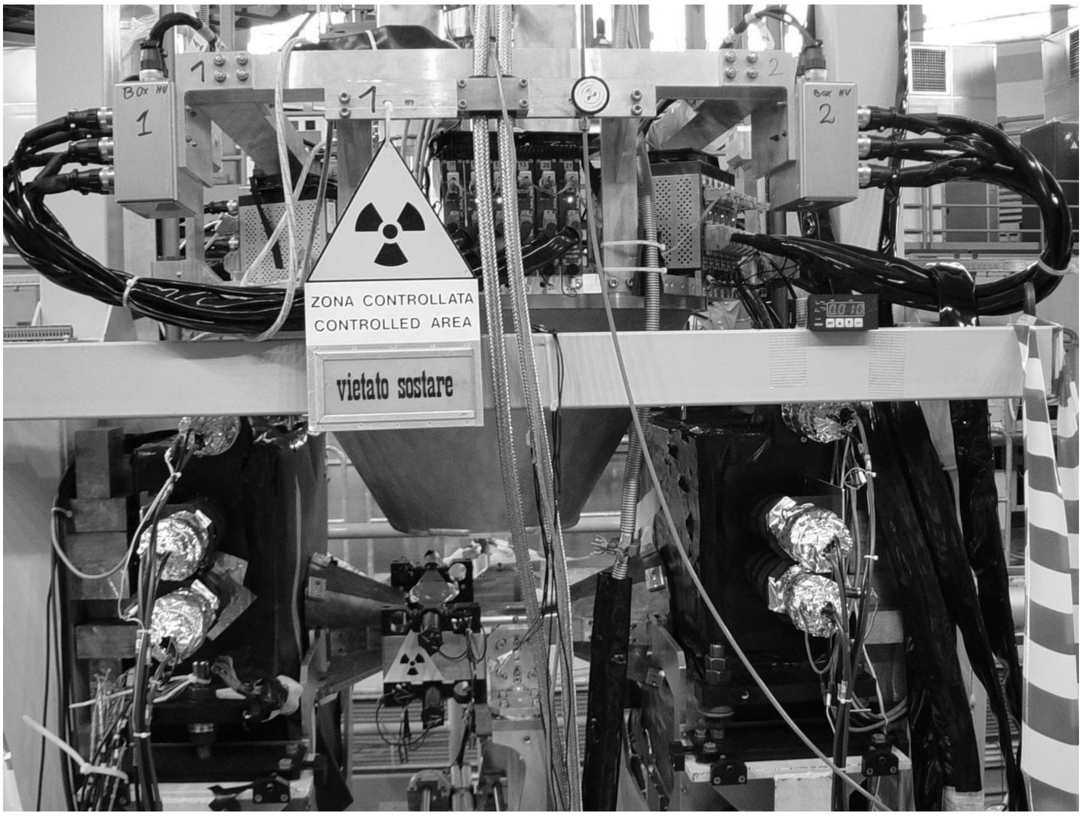

Figure 1: The SIDDHARTA setup installed at DAΦNE

are the most precise ones ever measured.

2.2.2 *Kaonic helium 3 results*

In the last days of data taking, early November 2009, we measured for the first time ever the kaonic Helium3 L-transitions. The total integrated luminosity for this measurement was about 10 pb^{-1}. The data analysis produced the spectrum shown in Fig. 3. The result for the shift was:

$$\Delta E_{2p} = -2 \pm 2(stat.) \pm 4(syst.)\ eV \tag{4}$$

A paper was published in Phys. Lett. B697 (2011) 199.

2.2.3 *SIDDHARTA-2*

In 2010 the proposal for the SIDDHARTA upgrade was put forward. The upgrade concerns mainly the cryogenic system, the target, the shielding and the trigger system, and is going to improve on the signal and signal/background ratio such as to allow the kaonic deuterium and other exotic atoms measurements in the near future. In 2011 various tests on prototypes were performed, together with Monte Carlo simulations to optimize the setup.

More details can be found in the various presentations to the LNF International Scientific Committee on the LNF-INFN web-site.

2.3 Activities in 2012

The LNF group main activities in SIDDHARTA and SIDDHARTA-2 for 2012 are the following ones:

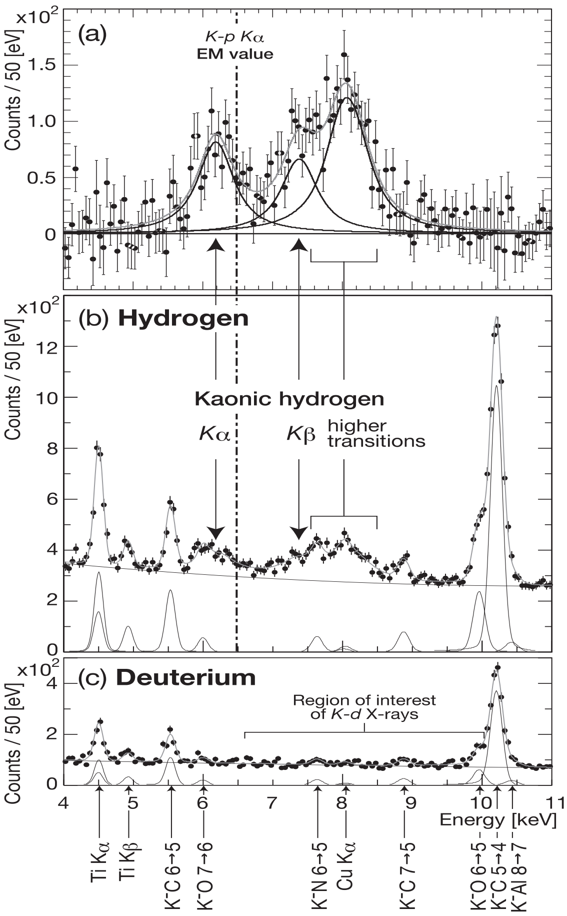

Figure 2: A global simultaneous fit result of the X-ray energy spectra of hydrogen and deuterium data. (a) Residuals of the measured kaonic-hydrogen X-ray spectrum after subtraction of the fitted background, clearly displaying the kaonic-hydrogen K -series transitions. The fit components of the $K^{-}p$ transitions are also shown, where the sum of the function is drawn for the higher transitions (greater than K_β). (b), (c) Measured energy spectra with the fit lines. Fit components of the background X-ray lines and a continuous background are also shown. The dot-dashed vertical line indicates the EM value of the kaonic-hydrogen K_α energy. (Note that the fluorescence K_α line consists of $K_{\alpha 1}$ and $K_{\alpha 2}$ lines, both of which are shown.)

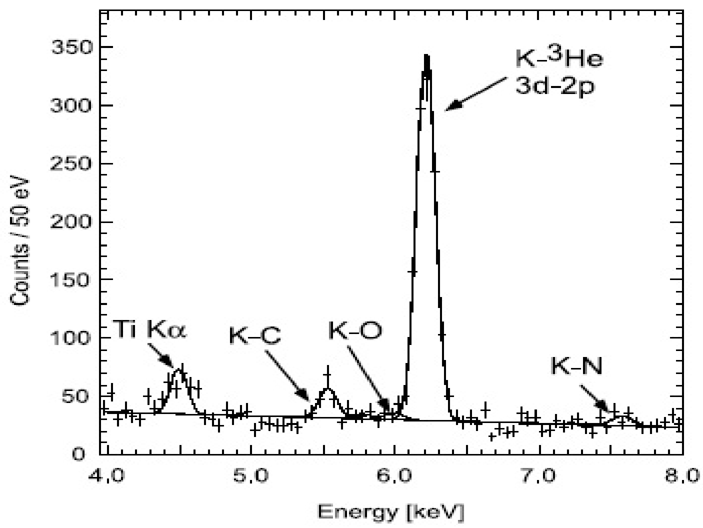

Figure 3: The Kaonic Helium3 spectrum where the 6.2 keV line of kaonic helium transitions is clearly visible.

- analysis of widths of kaonic helium transitions to 2p level and publications;
- analysis of the yields for kaonic hydrogen and helium and publication of results;
- finalize analyses of kaonic deuterium data and publish them;
- Monte Carlo simulations for the SIDDHARTA-2 setup and physics;
- construction of the SIDDHARTA-2 setup: target, veto counters, new trigger, new cryogenic systems;
- definition of the strategy for SIDDHARTA-2 measurements (including interaction region definition and construction).

The SIDDHARTA scientific program is important part of the Network LEANNIS (WP9) in the framework of the EU FP7 HadronPhysics2 and HadronPhysics3 programs.

3 The AMADEUS proposal

The AMADEUS experiment plans to perform a complete study of the interaction of low-energy charged kaons with nuclei, by using various cryogenic gaseous targets, as: deuterium, helium 3 and helium 4. In particular, AMADEUS plans to study, in formation and decay, the so-called "deeply bound kaonic nuclei", if existent (the scientific case is strongly debated presently). The AMADEUS collaboration plans to implement inside the KLOE drift chamber a dedicated setup, containing a beam pipe, a target and a trigger system and, maybe, an inner additional tracker. The scientific case of AMADEUS, as well as R&D performed on various items were presented in various LNF Scientific Committees and can be found on the respective dedicated web pages.

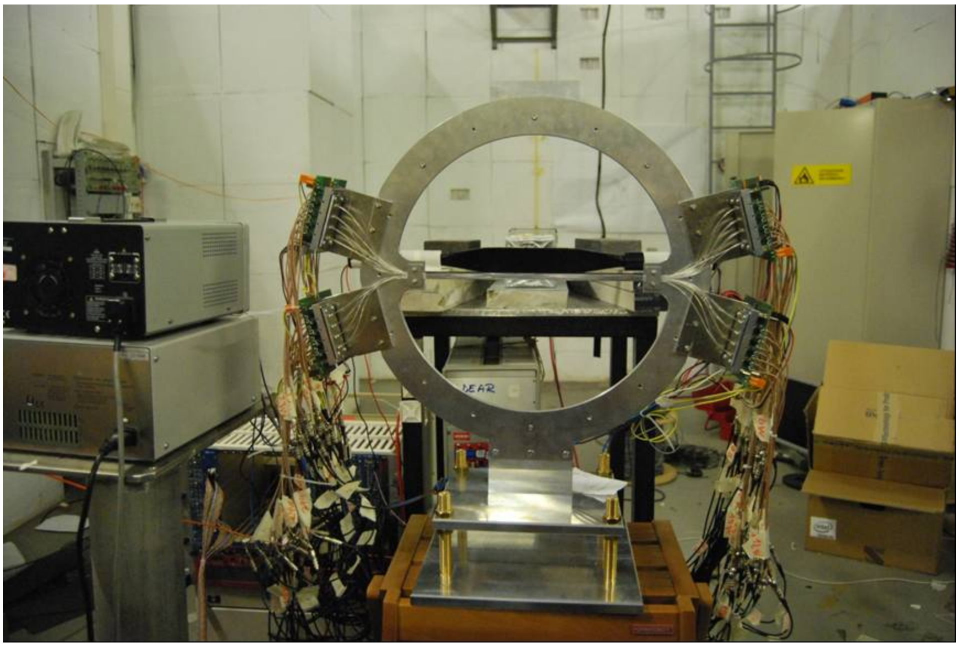

Figure 4: The AMADEUS trigger ptototype, based on scintillating fibers read at both ends by SiPM

3.1 AMADEUS activities in 2011

The main activities of AMADEUS in 2011 concerned:

- R&D for the trigger system: a prototype based on scintillating fibers read by Silicon Photo-Multipliers (see Fig. 4) was tested in the laboratory and PSI pion beam:
- R&D for the inner tracker - a small TPC-GEM prototype, Fig. 5, was built and tested:
- Monte Carlo simulations:
- KLOE data analyses for the data 2002-2005 to search for processes generated by stopped kaons in the Drift Chamber volume (which contains helium) - see the LNF Scientific Committee presentations.

3.2 AMADEUS activities in 2012

The main activities of AMADEUS in 2012 will be

- continuation of the R&D for the trigger system: tests of the prototype and readout electronics at BTF-LNF and PSI:
- continuation of the R&D for the inner tracker: tests of the prototype at BTF-LNF and PSI
- Monte Carlo simulations:
- finalization of the KLOE 2002-2005 data analyses for the search of processes due to K^-interaction in the Drift Chamber volume and publication

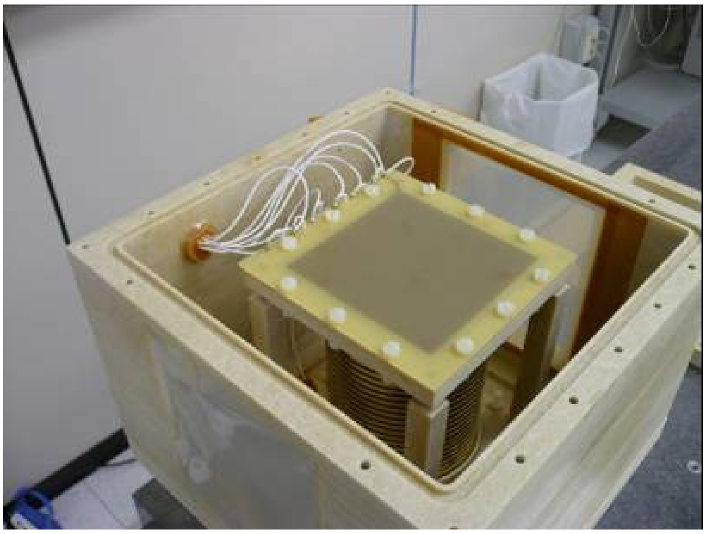

Figure 5: The TPC-GEM prototype

- definition of the experiment strategy

To be mentioned that the AMADEUS activities are supported in the framework of the EU FP7 HadronPhysics2 and HadronPhysics3, as WP24 (GEM), WP28 (SiPM) and WP9 (Network on kaon-nuclei interaction studies at low energies) programs.

Acknowledgements
The support from HadronPhysics2 and HadronPhysics3 FP7 projects is acknowledged.

4 List of Conference Talks by LNF Authors in Year 2011

1. A. Scordo, "Development of a trigger system with scintillating fibers and SiPM readout for the AMADEUS experiment", The 23^{rd} Indian Summer School of Physics and 6^{th} HADES Summer School, 3-8 October 2011, Rez.Prague, Czech Republic.
2. A. Scordo, "Investigating low energy QCD with kaonic atoms: the SIDDHARTA experiment at DAΦNE" (poster), the 50^{th} International Winter Meeting on Nuclear Physics in Memoriam of Ileana Iori, 22-27/01/2012, Bormio (MI), Italy.

3. A. Scordo, “Kaonic helium (3 and 4) precision X-ray transitions measurements by SIDDHARTA at DAΦNE”, The XLIX International Winter Meeting on Nuclear Physics, 23-19/01/2011, Bormio (MI), Italy.

4. A. Rizzo, “Kaonic Atoms measurements at the AΦNE accelerator: the SIDDHARTA experiment”, the III^{rd} International Conference on Hadron Physics - Troia’11 - 22 26 August 2011, Canakkale, Turkey.

5. A. Rizzo, “Kaonic atoms measurements by the SIDDHARTA experiment at the DAΦNE collider”, Physics@FAIR, 23^{rd} Indian-Summer School of Physics and 6^{th} HADES Summer School, October 3-7 2011, Rez. Prague, Czech Republic.

6. S. Okada, “A new measurement of kaonic hydrogen X-rays”, HADRON2011, 13-17 June 2011, Munchen, Germany.

7. S. Okada, “SIDDHARTA results and future plans”, ECT* – Strange Hadron Matter, 26-30 September 2011, ECT*, Trento, Italy.

8. A. DUffizi, “Esperimento AMADEUS Sistema Elettronico di acquisizione” , Societá Italiana di Fisica XCVII Congresso Nazionale, 26-30 September 2011, L ‘Aquila, Italy.

9. M. Bazzi, “Experimental test for a trigger prototype for the AMADEUS experiment”, Silicon Multiplier Workshop, 6-7 October 2011, GSI, Germany.

10. K. Piscicchia, “Kaon-nuclei interactions studies at low energies (the AMADEUS project)”, STORI’11, 8th Int. Conf. On Nuclear Physics at Storage Rings, 9-14 October 2011, Laboratori Nazionali di Frascati, Frascati (RM), Italy.

11. K. Piscicchia,“Kaon-nuclei interactions studies at low energies (the AMADEUS project)”, Societa’ Italiana di Fisica, XCVII Congresso Nazionale, 26-30 Settembre 2011, L’Aquila, Italy.

12. K. Piscicchia, “Studio dell’interazione a bassa energia kaoni-nuclei (l’esperimento AMADEUS)”, IFAE 2011, Incontri di Fisica delle Alte Energie, 27-29 Aprile 2011, University of Perugia, Perugia, Italy.

13. D. Sirghi, “Kaonic Helium 3 and 4 measurements by the SIDDHARTA experiment at DAΦNE”, 8th International Conference on Nuclear Physics at Storage Rings - STORI’11 , 9-14 October 2011, Laboratori Nazionali di Frascati, Frascati, Rome, Italy.

14. C. Curceanu, “Low energy kaon-nucleon/nuclei interactions studies at DAΦNE(SIDDHARTA and AMADEUS)”, colloquium, 9 June 2011, Univ. Bonn, Germany.

15. C. Curceanu, “Low energy kaon-nucleon/nuclei interactions studies at DAΦNE(SIDDHARTA and AMADEUS)”, colloquium, 27 June 2011, Rez, Prague, Czech Republic.

16. C. Curceanu, “The wonderland of kaonic atoms: the SIDDHARTA experiment at DAΦNE”, colloquium, 28 November 2011, TUM, Munchen, Germany.

17. C. Curceanu, “ Low energy kaon-nucleon/nuclei interactions studies at DAΦNE (SIDDHARTA and AMADEUS)”, IFAE 2011, Incontri di Fisica delle Alte Energie, 27-29 Aprile 2011, University of Perugia, Perugia, Italy.

18. C. Berucci, “Kaonic deuterium studies by SIDDHARTA-2 at DAΦNE”, Societá Italiana di Fisica, XCVII Congresso Nazionale, 26-30 Settembre 2011, L‘Aquila, Italy.

19. C. Curceanu, “Experimental tests of the trigger prototype for the AMADEUS experiment based on SciFi read by SiPM ”, NDIP2011, 4-8 July 2011, Lyon, France.

20. O. Vazquez Doce, “KLOE data analysis and AMADEUS ”, LEANNIS Meeting, , 30 June - 1 July 2011, Heidelberg, Germany.

21. O. Vazquez Doce, “Studies of the antikaon-nucleon interaction at DAΦNE”, International Conference on Exotic Atoms and Related Topics - EXA2011, 5-9 September 2011, Vienna, Austria.

22. O. Vazquez Doce, “SiPM + Scintillating fibers for AMADEUS experiment”, I3HP-FP7 Silicon Multiplier Workshop, October 2011, GSI Darmstadt.

23. M. Iliescu, “Kaonic atoms study with SIDDHARTA” , International workshop on e^+e^-collisions ”From Φ to Ψ ” Budker Institute of Nuclear Physics, Novosibirsk, September 19 - 22, 2011, Novosibirsk, Russia.

5 Publications

References

1. M. Bazzi *et al.*, “A new measurement of kaonic hydrogen X-rays”, Phys. Lett. **B 704** 113-117 (2011).

2. M. Bazzi *et al.*, “First measurement of kaonic helium 3 X-rays”, Phys. Lett. **B 697** 199-202 (2011).

3. M. Bazzi *et al.*, “Performance of silicon-dift detectors in kaonic atom X-ray measurements”, Nucl. Instr. Meth. in Physics Reserach Section **A 628** 264-267 (2011).

4. C. Curceanu *et al.*, “Low-energy Kaon-Nucleon/Nuclei Interactions Studies at DAΦNE (SIDDHARTA and AMADEUS)”, Few-Body Systems, **50** 447-449 (2011).

5. T. Hiraiwa *et al.*, “The search for deeply bound kaonic nuclear states at J-PARC”, International Journal of Modern Physics **A 26** 561-563 (2011).

6. D.L. Sirghi *et al.*, “Kaonic Helium measurements in the SIDDHARTA experiment”, Int. Journal of Modern Physics **A 26** 601-603 (2011).

7. A. Romero Vidal *et al.*, “X-Ray spectroscopy of kaonic atoms at DAΦNE”, Int. Journal of Modern Physics **A 26** 432-437 (2011).

8. B.K. Wuenschek *et al.*, “Status and plans of experiment E17 at J-PARC”, Int. Journal of Modern Physics **A 26** 604-606 (2011).

9. J. Zmeskal, “Recents results and furure plans for AMADEUS”, Int. Journal of Modern Physics **A 26** 414-419 (2011).

10. M. Bazzi *et al.*, “Kaon-nuclen/nuclei intercation studies by kaonic atoms measurements: the SIDDHARTA experiment at DAΦNE”, 9^{th} International Conference on Beauty, Charm and Hyperons in Hadronic Intercations, Nucl. Phys.B Proceedings Supplements **210-211** 189-192 (2011).

11. C. Curceanu *et al.*, “Low-energy kaon-nucleon/nuclei interaction studies at DAΦNE”, Incontri di Fisica delle Alte Energie - IFAE, Il Nuovo Cimento **C 34** 23-27 (2011).

12. M. Cargnelli *et al.*, “Studies of antikaon interactions with nucleons at DAΦNE”, International Conference on the structure of baryons (BARYONS’10), AIP Conference Proceedings **1388** 212 (2011).

13. O. Vazquez Doce *et al.*, “Studies of antikaon interactions with nucleons at DAΦNE”, International Conference on the structure of baryons (BARYONS’10), AIP Conference Proceedings **1388** 572-575 (2011).

14. S. Enomoto *et al.*, “Spectroscopic study of Λ via the in-flight (Kn) reaction on deuteron”, International Conference on the structure of baryons (BARYONS’10), AIP Conference Proceedings **1388** 599-601 (2011).

15. T. Hashimoto *et al.*, “Performance evaluation of Silicon Drift Detectors for a precision X-ray spectroscopy of kaaonic helium-3”, International Nuclear Physics Conference 2010 (INPC2010), Journal of Physics: Conference Series **312** (2011).

16. K. Piscicchia *et al.*, “Kaon-nuclei interaction studies at low energies (the AMADEUS experiment)”, Incontri di Fisica delle Alte Energie - IFAE, Il Nuovo Cimento **C 6** 21-22 (2011).

17. S. Okada *et al.*, “Experimental studies of kaonic atoms at DAΦNE”, International Conference on the structure of baryons (BARYONS’10), AIP Conference Proceedings **1388** 576-579 (2011).

18. M. Sato *et al.*, “Precision spectroscopy of kaonic helium3 X-rays at J-PARC”, 12^{th} International Conference on Meson-Nucleon physics and the structure of the nucleon (MENU 2010), AIP Conference Proceedings **1374** 216 (2011).

19. M. Sato *et al.*, “Precision spectroscopy of kaonic helium3 X-rays at J-PARC”, International Nuclear Physics Conference 2010 (INPC2010) Journal of Physics: Conference Series **312** 022020 (2011).

20. H. Shi *et al.*, “Kaonic helium X-ray measurement in the SIDDHARTA experiment”, International Nuclear Physics Conference 2010 (INPC2010) Journal of Physics: Conference Series **312** 022021 (2011).

21. A. Scordo *et al.*, “Kaonic helium (3 and 4) precision X-ray transitions measurements by SIDDHARTA at DAΦNE”, PoS BORMIO2011 058 (2011).

22. C. Curceanu, J. Zmeskal, “Mini-Proceedings of ECT* Workshop “Strangeness in Nuclei” , Apr. 2011, 41 pp arXiv:1104.1926 [nucl-ex].

MAMBO

D. Babusci, C. Berucci, P. Levi Sandri (Resp.), A. Saputi (Tecn.)

1 Introduction

MAMBO groups together three complementary INFN activities in Germany: the experimental activity with the MAMI-C microtron in Mainz, approved until 2011, the development of MRPC counters and the preliminary measurements towards a full proposal to measure the electric dipole moments (EDM) of proton and deuteron, and the new BGO-OD experiment at Bonn-ELSA. LNF are involved in the last two activities.

2 BGO-OD experiment

The BGO-OD esperiment is performed in collaboration between INFN sections of Roma2, LNF, Messina, Pavia, ISS-Roma1 and Torino, the University of Bonn, Physikalisches Institut, ELSA department, the University of Bonn, Helmholtz Institut für Strahlen- und Kernphysik, the University of Edinburgh, the National Science Center Kharkov Institute of Physics and Technology, the University of Moscow, Russia, the Petersburg Nuclear Physics Institute (PNPI), Gatchina and the University of Basel. More that 70 physicists participate to this experimental program foreseen to last until 2017.

The INFN contribution consist in the *Rugby Ball* calorimeter and associated detectors previously used at GRAAL, the target system, the cylindrical tracking chambers and the MRPC detector.

3 2011 activity

At the end of 2010 and during the first months of 2011, the mounting of the BGO-OD experiment started on the S-Beamline at Bonn-ELSA. On June the 6-th at 6:30 a.m., the power supply of the tagger spectrometer magnet for the experiments CBELSA/TAPS and BGO-OD got a short circuit and was irreversibly destroyed. This short circuit caused a local fire in the supply and a power failure in the local area around the university institutes. Fortunately nobody was injured.

Due to poisonous particles in the air, the access to the area was prohibited for 10 days. This incident caused a 3 months delay in the installation of the detector. The installation could be resumed only in late September, after a careful cleaning af all the experimental area. The BGO-OD apparatus suffered some damage in the TOF wall detector. No major damages were detected in the rest of the apparatus.

During the rest of the year the installation of the *Rugby Ball* calorimeter with its new electronics was completed and eventually the target system was reistalled and successfully tested.

4 2012 activity

During 2012 the commissioning of the beam and of the detector will start. The missing detector components, scintillator barrel, cylindrical chambers, MRPC chambers, all under INFN responsibility, will be installed. The first data taking period is foreseen in the second half of the year.

$\overline{\text{P}}$ANDA - $\overline{\text{p}}$ Annihilation at Darmstadt

N. Bianchi, A. M. Bragadireanu (Ass.), B. Dulach (Ass.), P. Gianotti (Resp. Naz.), M. Giardoni, C. Guaraldo (Ass.), M. A. Iliescu (Ass.), V. Lucherini, D. Orecchini (Tec.). E. Pace, L. Passamonti (Tec.), D. Pierluigi (Tec.), A. Russo (Tec.), D. L. Sirghi Diana (Ass.)

1 Introduction

$\overline{\text{P}}$ANDA is one of the biggest experiments of hadron and nuclear physics that will be carried out at the new Facility for Antiproton and Ion Research (FAIR) at Darmstadt, Germany. It is dedicated to the study of the annihilations of antiprotons on nucleons and nuclei up to a maximum center-of-mass energy in $\overline{\text{p}}$p of 5.5 GeV.

The $\overline{\text{P}}$ANDA collaboration consists of 420 physicists from 17 countries spread all over the world. The Italian groups involved are: Torino, University, Politecnico and INFN, Trieste, University and INFN, Genova INFN, Pavia, University and INFN, Ferrara, University and INFN, Legnaro INFN laboratory and Frascati INFN laboratory. The LNF group is involved in the design and construction of the central straw tube tracker of the $\overline{\text{P}}$ANDA detector.

2 $\overline{\text{P}}$ANDA experiment

A new facility for hadronic physics is under construction in Germany. It consists of a major upgrade of the presently running GSI accelerator complex of Darmstadt [1]. An intense, high momentum

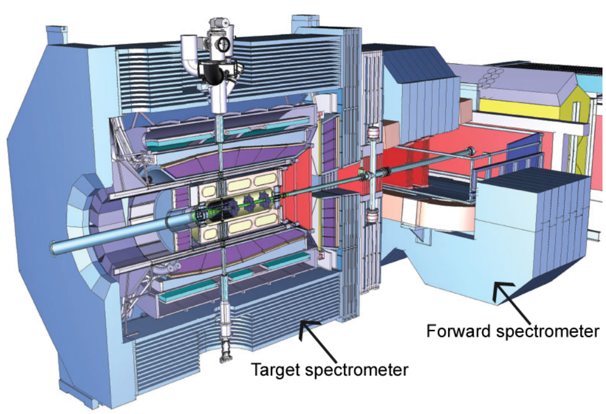

Figure 1: *A schematic view of the $\overline{\text{P}}$ANDA apparatus consisting of two distinct detectors: the target spectrometer (left) and the forward spectrometer (right).*

resolution antiproton beam, with momenta between 1.5 and 15 GeV/c, will be available at the High Energy Storage Ring (HESR), and the experimental activity will be carried out using a general purpose detector $\overline{\text{P}}$ANDA that will be build surrounding an internal target station installed in one of the two straight sections of the storage ring. Figure 1 shows a schematic drawing of the $\overline{\text{P}}$ANDA apparatus. It is designed as a large acceptance multi-purpose detector consisting of two distinct parts: a solenoidal spectrometer, surrounding the interaction target region, and a forward spectrometer to cover the solid angle between 5 and 22 degrees. It will allow the detection and the identification of either the neutral and the charge particles emitted following $\bar{p}$ annihilation.

3 The $\overline{\text{P}}$ANDA Central Tracker

For tracking charge particles in the target spectrometer, $\overline{\text{P}}$ANDA will use different detectors: a silicon Micro Vertex Detector (MVD) a Straw Tube Tracker (STT) and a set of forward GEM chambers [3]. The requirements for the overall system are:

- almost full solid angle coverage;
- momentum resolution $\delta p/p \sim 1.5\%$;
- low material budget $X/X_0 \sim$ few %;
- good spatial resolution $\sigma_{r,\phi} = 150$, μm, $\sigma_z =$ few mm.

The STT detector has been recently preferred by the collaboration with respect to a TPC chamber. Then, the Technical Design Report (TDR) of the detector has been completed and will be evaluated by the FAIR technical committees.

The LNF $\overline{\text{P}}$ANDA group is one of the proponents of the STT and is involved in its realization.

3.1 Layout of the straw tube detector

The $\overline{\text{P}}$ANDA STT will consist of two identical chambers separated by the beam-target cross-pipe that is cutting the x, y plane in two halves (see fig. 2). Each chamber is made of aluminized mylar straw tubes, diameter 10 mm, length 1500 mm, thickness 30 μm, arranged in planar double layers.

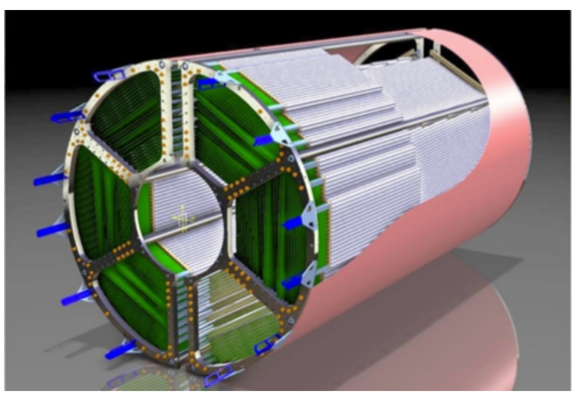

Figure 2: *CAD drawing of the $\overline{\text{P}}$ANDA Straw Tube Tracker*

Inside a double layer the tubes are glued together and operated with an Ar+CO_2 (90+10) gas mixture with an over-pressure of 1 bar. This solution has been chosen to avoid strong support structures and to keep the detector design modular and simple. To measure also particle z coordinate, some layers will be mounted with a skew angle $\pm 3^o$ with respect to the beam axis.

Figure 3 shows the layout for the STT. There are 4 internal double-layers parallel to the beam axis, then 4 double-layers mounted with opposite skew angles, and finally 2 other layers parallel to the beam axis. To fill up the cylindrical volume, the remaining region houses smaller tube layers.

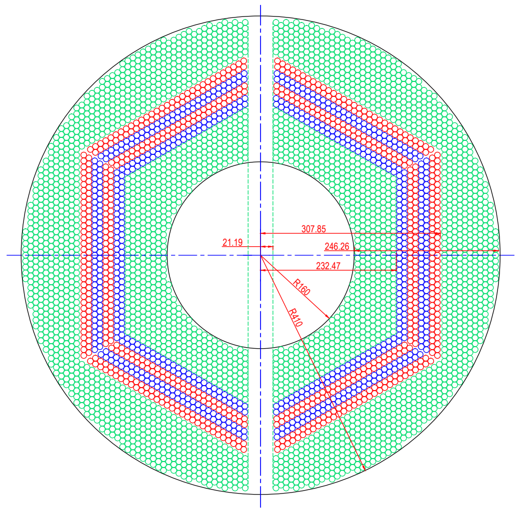

Figure 3: *The layout of the STT. In green the axial tubes, in red and blue colour the skewed layers (see text for more details).*

4 Activity of the LNF $\overline{\mathrm{P}}$ANDA group

The STT mechanical structure has to support also the beam-target cross-pipe and the MVD. This frame, has to be extremely light and has to allow the movement of the whole block of detectors during the installation procedure or the maintenace operations (see fig. 4). The activity of the

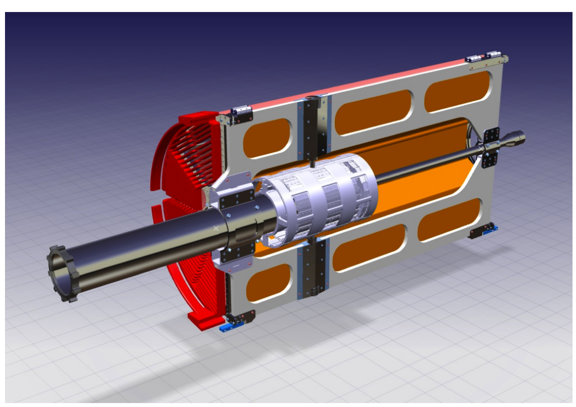

Figure 4: *Layout of one half of the STT mounted on the Central Frame that hold also the target-beam cross-pipe and the MVD.*

LNF $\overline{\mathrm{P}}$ANDA group during 2011 has been devoted to the following tasks:

- test of straw tubes prototypes in oder to determine the detector performances;
- development, together with the Torino INFN group, of the mechanical arrangement of STT

Figure 5: *The Central Frame prototype (see text for more details)*

and MVD detectors;

- the TDR preparation.

Concerning the first item, LNF $\overline{\text{P}}$ANDA group has collected data with radioactive sources, cosmic rays, and performed a test beam at the BTF in April 2011. The results of this activity have been included in the detector TDR.

5 List of Conference Talks presented by LNF group members in Year 2011

1. P. Gianotti, "Results and perspectives in Hadron Spectroscopy", invited talk at the Nordic Conference on Nuclear Physics 2011 14 JUN. 2011, Stockholm, Sweeden.

2. P. Gianotti, "Tracking with Straw Tubes in the PANDA Experiment", talks at the 13th ICATPP Conference on Astroparticle, Particle, Space Physics and Detectors for Physics Applications, 3-7 OCT. 2011, Como, Italy

6 Publications

1. P. Gianotti,"Highlights of meson spectroscopy: An experimental overview", J. Phys. Conf. Ser. **312** (2011) 032001.

References

1. http://www.fair-center.com/.

2. http://www-panda.gsi.de/.

3. S. Costanza *et al.*, Nucl. Instr. Meth. **A617**, 148-150, 2010.

VIP

S. Bartalucci, M. Bazzi (Assoc.), A. Clozza, C. Curceanu Petrascu (Resp. Naz.),
C. Guaraldo, M. Iliescu (Assoc.), F. Lucibello (Tecn.),
S. Okada (Art. 23), D. Pietreanu (Bors. UE), A. Romero Vidal (Art. 23),
A. Scordo (Ass. Ric), D. Sirghi (Art. 23), F. Sirghi (Bors. UE), O. Vazquez Doce (Art. 23)

1 The VIP scientific case and the experimental method

The Pauli Exclusion Principle (PEP), which plays a fundamental role in our understanding of many physical and chemical phenomena, from the periodic table of elements, to the electric conductivity in metals and to the degeneracy pressure which makes white dwarfs and neutron stars stable, is a consequence of the spin-statistics connection. Although the principle has been spectacularly confirmed by the huge number and accuracy of its predictions, its foundation lies deep in the structure of quantum field theory and has defied all attempts to produce a simple proof. Given its basic standing in quantum theory, it seems appropriate to carry out precise tests of the PEP validity and, indeed, mainly in the last 15-20 years, several experiments have been performed to search for possible small violations. The indistinguishability and the symmetrization (or antisymmetrization) of the wave-function should be checked independently for each particle, and accurate tests were and are being done.

The VIP (VIolation of the Pauli Exclusion Principle) experiment, an international Collaboration among 6 Institutions of 4 countries, has the goal to improve the limit on the probability of the violation of the PEP for electrons, (P $<$ 1.7 x 10^{-26} established by E. Ramberg e G. A. Snow: *Experimental limit on a small violation of the Pauli principle*, Phys. Lett. **B 238** (1990) 438) by three-four orders of magnitude (P $<10^{-29\div-30}$), exploring a region where new theories might allow for a possible PEP violation.

The experimental method consists in the introduction of electrons into a copper strip, by circulating a current, and in the search for X-rays resulting from the forbidden radiative transition that occurs if one of the new electrons is captured by a copper atom and cascades down to the 1s state already filled by two electrons with opposite spins. The energy of this transition would differ from the normal K_α transition by about 300 eV (7.729 keV instead of 8.040 keV) providing an unambiguous signal of the PEP violation. The measurement alternates periods without current in the copper strip, in order to evaluate the X-ray background in conditions where no PEP violating transitions are expected to occur, with periods in which current flows in the conductor, thus providing "fresh" electrons, which might violate PEP. The rather straightforward analysis consists in the evaluation of the statistical significance of the normalized subtraction of the two spectra in the region of interest.

The experiment is being performed at the LNGS underground Laboratories, where the X-ray background, generated by cosmic rays and natural radioactivity, is reduced.

2 The VIP experimental setup

The VIP setup was realized in 2005, starting from the DEAR setup, reutilizing the CCD (Charge Coupled Devices) X-ray detectors, and consists of a copper cylinder, 4.5 cm in radius, 50 μm thick, 8.8 cm high, surrounded by 16 equally spaced CCDs of type 55.

The CCDs are at a distance of 2.3 cm from the copper cylinder, grouped in units of two chips vertically positioned. The setup is enclosed in a vacuum chamber, and the CCDs are cooled to about 165 K by the use of a cryogenic system. A schematic drawing of the VIP setup is shown in Fig. 1.

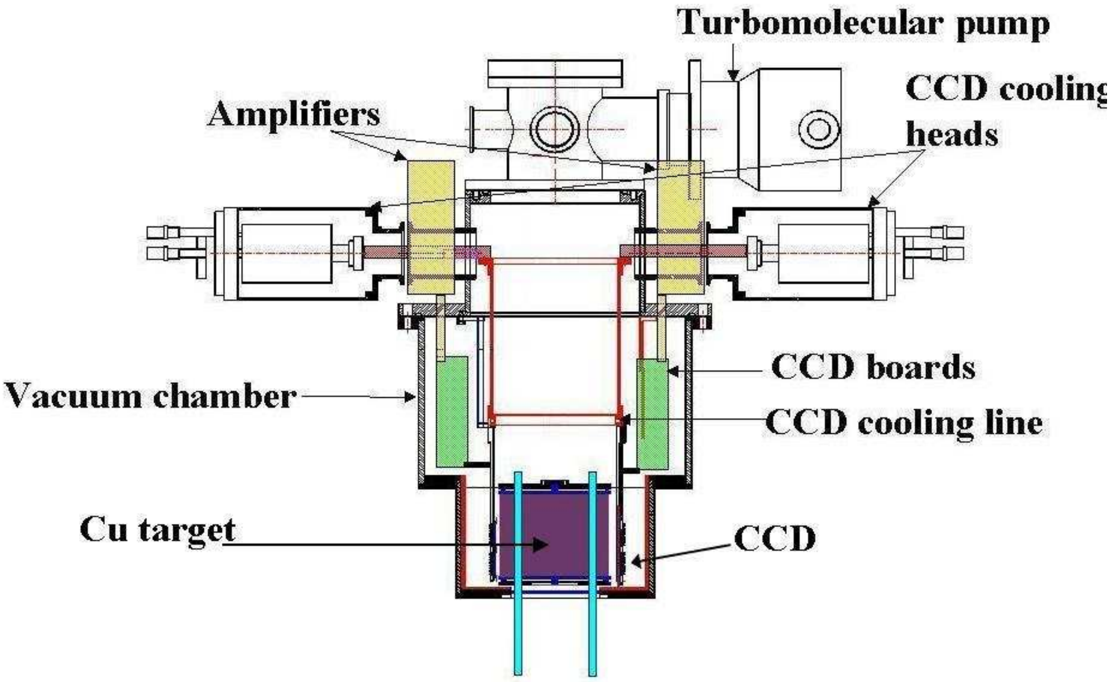

Figure 1: *The VIP setup. All elements af the setup are identified in the figure.*

The DAQ alternates periods in which a 40 A current is circulated inside the copper target with periods without current, referred as background.

VIP was installed at the LNGS Laboratory in Spring 2006 and was taking data in this configuration until Summer 2010 (presently, see below, we are working on an improved version of the setup). The setup was surrounded by layers od copper and lead (as seen in the picture) to shield the setup against the residual background present inside the LNGS laboratory, see Fig. 2.

3 Activities in 2011

3.1 VIP analyses results

Until summer 2010 the VIP experiment was in data taking, alternating periods of "signal" (I=40 A) with periods without signal (I=0 A). Data analyses were performed (energy calibration, sum of spectra, subtraction of background) and the probability of violation of PEP for electrons obtained (upper limit):

$$\frac{\beta^2}{2} < 4 \times 10^{-29} \tag{1}$$

3.2 Discussion of the results

We are attempting an interpretation of our results in the framework of quon-theory, which turned out to be a consistent theory of *small* violations of PEP. The basic idea of quon theory is that (anti)commutators, are replaced by weighted sums

$$\frac{1-q}{2}\left[a_i, a_j^+\right]_+ + \frac{1+q}{2}\left[a_i, a_j^+\right]_- = a_i a_j^+ - q a_j^+ a_i = \delta_{i,j} \tag{2}$$

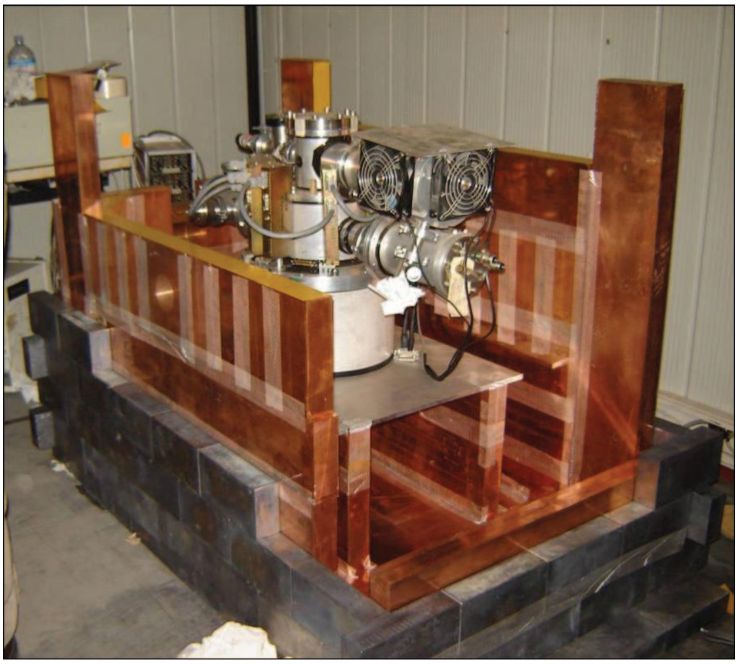

Figure 2: The VIP setup at the LNGS laboratory during installation.

where $q = -1$ ($q = 1$) gives back the usual fermion (boson) commutators. The statistical mixture in equation (2) also shows that the PEP violation probability is just $(1 + q)/2$ and thus our best experimental bound on q is

$$\frac{1+q}{2} < 4 \times 10^{-29} \tag{3}$$

A consistent interpretation of the VIP results can thus be based on quon theory; however here we note that is not easy to devise tests of PEP, because of many conceptual difficulties, presented in our published papers (see list at the end).

Even if at the moment these are just speculations we do strongly feel that the test is meaningful and we are now planning an improved version.

3.3 The VIP upgrade

The VIP setup used CCD detectors, which are excellent X-ray detectors, but very slow. We plan to switch to a new type of detectors for precision X-rays measurements, the triggerable Silicon Drift Detectors (SSD) which have a fast readout time ($\simeq 1\mu$s) and large collection area (100 mm^2). These detectors were successfully used in the SIDDHARTA experiment at LNF-INFN (see report on KAONNIS) for measurements of the kaonic atoms transitions at the DAΦNE accelerator of LNF-INFN; using a proper trigger system a background rejection factor of the order of 10^{-4} was achieved in SIDDARTHA.

We plan to built a new setup, much more compact, with higher current circulating and with a veto system against background coming from outside.

In 2011 we performed intensive Monte Carlo simulations and a series of tests at LNF and at LNGS with a test setup which showed that is possible to gain about two orders of magnitude in the probability of PEP violation. A schematic layout of the new setup is shown in fig. 3.

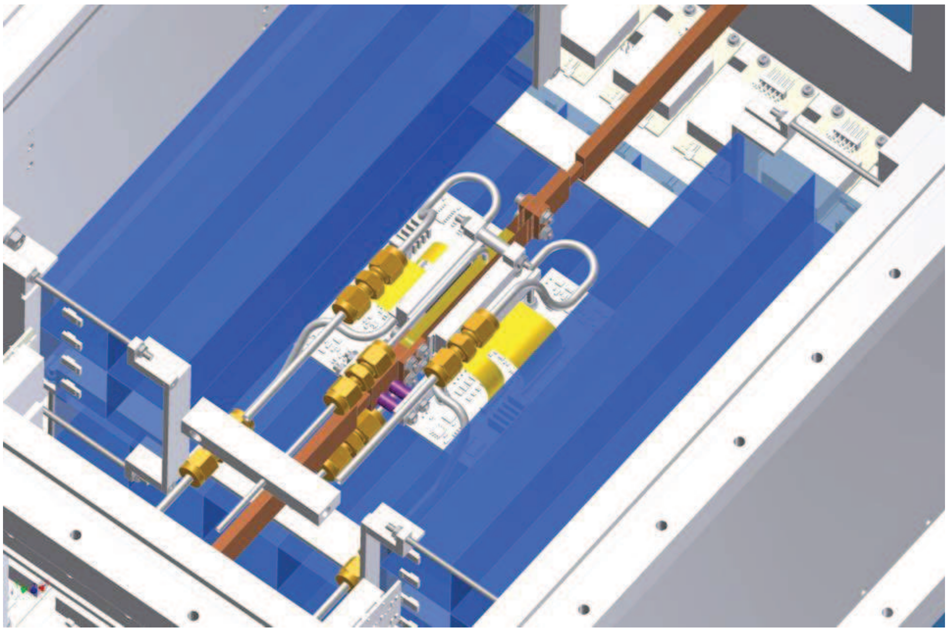

Figure 3: The VIP setup experiment using SDD detectors and an external veto-system.

4 Activities in 2012

In 2012 we plan to proceed with the construction of the VIP upgraded setup and to install at LNGS. We are, as well, considering to extend the scientific program towards a feasibility study of limits on parameters of the collapse model (as a solution of the measurement problem, put initially forward by Ghirardi, Rimini and Weber) by measurements of X rays spontaneously emitted in the continuous spontaneous localization (CSL) model.

Acknowledgements

The VIP Collaboration wishes to thank all the LNGS laboratory staff for the precious help and assistance during all phases of preparation, installation and data taking. The support from the HadronPhysics FP6, HadronPhysics2 and HadronPhysics3 FP7, from EU COST 1006 Action and MIUR PRIN2008 2008LX2X28-004 projects is acknowledged.

5 List of Conference Talks by LNF Authors in Year 2011

1. A. Rizzo, "Spontaneous X-Ray emission by free electrons in the collapse models: A closer look", Speakable in quantum mechanics: atomic, nuclear and subnuclear physics tests, ECT*, 29 August-2 September 2011, Trento, Italy.

2. C. Curceanu, "From the Pauli Exclusion principle violation tests (VIP experiment) to collapse models experimebtal investigation plans", Speakable in Quantum mechanics: atomic, nuclear and subnuclear physics tests, ECT*, 29 August-2 September 2011, Trento, Italy.

3. A. Clozza, "Future plans for upgrade of the VIP experiment for the study of the violation of the Pauli Exclusion Principle for electrons", Speakable in Quantum mechanics: atomic, nuclear and subnuclear physics tests, ECT*, 29 August-2 September 2011, Trento, Italy.

4. C. Curceanu, “Experimental tests of quantum mechanics: Pauli Exclusion Principle and spontaneous collapse models”, seminar at Univ. Milano, 31 May 2011, Italy.

5. C. Curceanu, “Experimental tests of quantum mechanics: Pauli Exclusion Principle and spontaneous collapse models”, Accademia Nazionale dei Lincei Entanglemnet, Quantum Information and the Quantum - to Classical Transition Roma, May 5-7, 2011, Italy.

6. C. Curceanu, “Experimental tests of quantum mechanics from the Pauli Exclusion Principle to spontaneous collapse models”, Sesto meeting on Quantum mechanics, 26 July 2 August 2011, Sesto, Italy.

7. C. Curceanu, “Experimental tests of quantum mechanics: the Pauli Exclusion Principle and spontaneous collapse models”, FPP6 - Foundation of Probability and Physics Conference, 13-16 June 2011, Vaxjo, Sweden.

8. C. Curceanu, “A glimpse into the Pandora Box of Quantum Mechanics: from the Pauli Exclusion Principle violation tests to collapse Models”, colloquium, LMU Munchen, 29 November 2011, Germany.

9. C. Curceanu, “Experimental tests of quantum mechanics: from the Pauli Exclusion Principle violation tests to collapse models”, FFP12, 21-23 November 2011, Udine, Italy.

10. C. Curceanu, “Experimental tests of quantum mechanics: from the Pauli Exclusion Principle violation tests to collapse models”, Emergent Quantum Mechanics Conference, 11-13 November 2011, Vienna, Austria.

6 Publications

References

1. C. Curceanu *et al.*, “Experimental tests of quantum mechanics Puali Exclusion Principle Violation (The VIP experiment) and future perspectives, Int. Journal of Quantum Information **9** (Supplementary Issue 1) 145-154 (2011).

2. C. Curceanu, J. Marton, E. Milotti, “Mini-proceedings ECT*: Speakable in quantum mechanics: atomic, nuclear and subnuclear physics tets”, arXiv:11121273.

3. C. Curceanu, J. Marton, E. Milotti, “Quantum mechanics in the 21^{th} century”, CERN Courier, October 2011.

4. C. Curceanu *et al.*, “The VIP Experiment”, Foundations of Physics **41** 282-287 (2011).

5. C. Curceanu *et al.*, “Experimental tests of quantum mechanics: Pauli Exclusion Principle Violation (the VIP experiment) and future prespectives”, 2^{nd} International Workshop on the Physics of fundamental Symmetries and Interactions -PSI2010, Phys. Procedia **17** 40-48 (2011).

6. J. Marton *et al.*, “Thesting the Pauli Exclusion Principle for electrons”, DISCRETE 2010: Symposium on Prospects in the Physics of Discrete Symmetries, Journal of Physics: Conference Series **335** 012060 (2011).

7. J. Marton *et al.*, “A high sensitivity test of the Pauli Exclusion Principle for electrons”, International Conference on Advances in Quantum Theory, AIP Confererence Proceedings, **1327** 423-428 (2011).

8. C. Curceanu Petrascu *et al.*, "Experimental tests of quantum mechanics and Pauli exclusion principle violation (the VIP experiment)", 5^{th} Internationmal Workshop DICE2010: Space-Time-Matter-Current Issues in Quantum Mechanics and Beyond, Journal of Physics: Conference Series **306** 012036 (2011).

FA51: Fisica Astroparticellare

C. S. Fong (Bors.), E. Nardi (Resp.)

Description of the 2011 activity

i. The general idea of *effective theory* for studying particle physics processes in the early Universe has been put on firm grounds in ref. [1]. A relevant situation in which the rigorous application of the correct early Universe effective theory can change the numerical results by orders of magnitude, is the case of soft leptogenesis when it occurs at temperatures $T > 10^7$ GeV. We have shown that in this regime, the main source of the B-L asymmetry is the CP asymmetry of a new anomalous R-charge that couples to generalized anomalous electroweak processes. Baryogenesis thus occurs mainly through R-genesis, and with an efficiency that can be up to two orders of magnitude larger than in usual estimates. Contrary to common belief, we have shown that a sizeable baryon asymmetry is generated also when thermal corrections to the CP asymmetries in sneutrino decays are neglected which, in soft leptogenesis, implies vanishing lepton-flavour CP asymmetries. We have also worked out the general Boltzmann equations for leptogenesis valid for all temperature regimes.

ii. A comprehensive account of the theory of *soft leptogenesis* has been presented in ref. [2]. We have explained the motivations for soft leptogenesis and reviewed all its basic ingredients: the different CP-violating contributions, the crucial role played by thermal corrections in canonical soft leptogenesis, and the enhancement of the efficiency from lepton flavour effects. We have also discussed the high temperature regime $T > 10^7$ GeV in which the cosmic baryon asymmetry originates from an initial asymmetry of an anomalous R-charge, and soft leptogenesis reembodies in R-genesis.

iii. In refs. [3,4] We have analyzed the most natural formulations of the minimal lepton flavour violation (LFV) hypothesis compatible with a type-I seesaw structure with three heavy singlet neutrinos N, and satisfying the requirement of being predictive, in the sense that all LFV effects can be expressed in terms of low energy observables. We have found a new interesting realization which predicts sizeable enhancements of $\mu \to e$ transitions with respect to LFV processes involving the τ lepton, which thus represents the experimentally most promising scenario.

iv. In ref. [5] we have discussed an attempt to explain the fermion mass hierarchy starting from the assumption that the Yukawa couplings correspond to vacuum expectation values of a spontaneously broken flavour symmetry. By studying the corresponding symmetry invariant scalar potential, we have found that a strong hierarchy for the Yukawa couplings, and a quark mixing matrix that approaches a diagonal form are indeed solutions of the minimum equations, that can be obtained in a natural way from non hierarchical $\mathcal{O}(1)$ parameters.

v. The general theory of leptogenesis, with special attention to its most striking phenomenological consequences, and including all the most recent refinements, constituted the main research topic of the group during the past few years and also during 2011. The expertise of the group in this field has gained an undisputed worldwide recognition, that is witnessed by the frequent invitations for review talks at major conferences [6,7]. Nevertheless, the group is also active in other lines of research, among which quite notably is the construction of theoretical models for neutrino masses in GUT theories [8] as well as in scenarios with extra dimensions [9].

References

1. **"Early Universe effective theories: The Soft Leptogenesis and R-Genesis Cases,"**
   C. S. Fong, M. C. Gonzalez-Garcia and E. Nardi,
   JCAP **1102**, 032 (2011).
2. **"Leptogenesis from Soft Supersymmetry Breaking (Soft Leptogenesis),"**
   C. S. Fong, M. C. Gonzalez-Garcia and E. Nardi,
   Int. J. Mod. Phys. A **26**, 3491 (2011).
3. **"Minimal flavour violation extensions of the seesaw,"**
   R. Alonso, G. Isidori, L. Merlo, L. A. Munoz and E. Nardi,
   JHEP **1106**, 037 (2011).
4. **"Lepton flavor violation in minimal flavor violation extensions of the seesaw,"**
   E. Nardi,
   arXiv:1112.4418 [hep-ph]. (In Press: Nucl Phys. **B** Proc. Suppl.).
5. **"Naturally large Yukawa hierarchies,"**
   E. Nardi,
   Phys. Rev. D **84**, 036008 (2011).
6. **"Leptogenesis and neutrino masses,"**
   E. Nardi,
   Nucl. Phys. Proc. Suppl. **217**, 27 (2011).
7. **"Selected Issues in Leptogenesis,"**
   E. Nardi,
   To be published in Nucl Phys. **B** (Proc. Suppl.).
8. **"Neutrino masses in $SU(5) \times U(1)_F$ with adjoint flavons,"**
   E. Nardi, D. Restrepo and M. Velasquez,
   arXiv:1108.0722 [hep-ph]. To appear in Eur. Phys. J. **C**.
9. **"Majorana Neutrinos from Inverse Seesaw in Warped Extra Dimension,"**
   C. S. Fong, R. N. Mohapatra and I. Sung,
   Phys. Lett. B **704**, 171 (2011).

Talks at Conferences

1. *"Naturally Large Yukawa Hierarchies".*
   Enrico Nardi,
   Invited talk at: *"Plank 11 - From the Planck Scale to the ElectroWeak Scale"*,
   30 May- 3 June, 2011; *"Instituto Superior Técnico (IST)"* Lisboa, Portugal.
   [https://indico.cern.ch/contributionDisplay.py?sessionId=31&contribId=65&confId=112851].
2. *"Lepton flavor violation in minimal flavor violation extensions of the seesaw,"*
   E. Nardi,
   Invited talk at the *"Workshop on e^+e^- Collisions from Φ to Ψ"*,
   September 19-22, 2011, Novosibirsk, Russia.
3. *"Selected Issues in Leptogenesis,"*
   E. Nardi,
   Invited talk at the *"15th Lomonosov Conference on Elementary Particle Physics"*,
   August 18-24, 2011, Moscow State University, Moscow (Russia).

LF21: PHENOMENOLOGY OF ELEMENTARY PARTICLE INTERACTIONS AT COLLIDERS

G. Corcella, V. Del Duca, G. Isidori (Resp.), J. Jones Perez (Post-doc), G. Pancheri (Ass. senior)

1 Summary of the project

The research topics investigated within this project can be divided into two main areas:

- Flavour physics, precision tests and physics beyond the Standard Model (G. Isidori, J. Jones Perez);
- Theoretical and phenomenological aspects of QCD and collider phyiscs (G. Corcella, V. Del Duca, G. Pancheri).

Some of the most significant projects completed in 2011 in these two research areas are listed below.

I. *Flavour physics, precision tests, and physics beyond the Standard Model*

Formulation of a supersymmetric extension of the Standard model based on the $U(2)^3$ flavor symmetry and analysis of its phenomenological implications in B physics. [1, 2)]

Analysis of the implications of the hints of a Higgs boson , with mass around 125 GeV, both in the Standard Model and in this minimal supersymmetric extension. [6, 7)]

Analysis of the first LHC data in constraining the structure of the minimal supersymmetric extension of the Standard Model. [8, 9, 10)]

II. *Theoretical and phenomenological aspects of QCD and collider phyiscs*

Derivation of a general formula to describe the infrared structure of generic scattering amplitudes, within gauge theories, in the high-energy limit. [12, 13, 15)]

Analysis of various scattering amplitudes in the maximally supersymmetric $N = 4$ Yang-Mills Theory. [16, 17, 14)]

Theoretical predictions for the total and the inelastic cross-sections at the LHC at $\sqrt{s} = 7$ TeV and beyond. [18)]

2 Main contributions to Conference Proccedings published in 2011

1. G. Isidori, PoS HQL **2010** (2011) 067.
2. G. Pancheri and Y. N. Srivastava, PoS QCD **-TNT-II** (2011) 033.
3. G. Pancheri, R. M. Godbole, A. Grau and Y. N. Srivastava, Nucl. Phys. Proc. Suppl. **219-220** (2011) 239.
4. Y. Srivastava, A. Grau, G. Pancheri and O. Shekhovtsova, AIP Conf. Proc. **1350** (2011) 211.

3 Full list of publications of the year 2011

References

1. R. Barbieri, G. Isidori, J. Jones-Perez, P. Lodone and D. M. Straub, Eur. Phys. J. C **71** (2011) 1725 [arXiv:1105.2296 [hep-ph]].

2. R. Barbieri, P. Campli, G. Isidori, F. Sala and D. M. Straub, Eur. Phys. J. C **71** (2011) 1812 [arXiv:1108.5125 [hep-ph]].

3. G. Isidori, J. F. Kamenik, Z. Ligeti and G. Perez, arXiv:1111.4987 [hep-ph], to appear in Phys. Lett. B.

4. G. Isidori and J. F. Kamenik, Phys. Lett. B **700** (2011) 145 [arXiv:1103.0016 [hep-ph]].

5. R. Alonso, G. Isidori, L. Merlo, L. A. Munoz and E. Nardi, JHEP **1106** (2011) 037 [arXiv:1103.5461 [hep-ph]].

6. O. Buchmueller, R. Cavanaugh, A. De Roeck, M. J. Dolan, J. R. Ellis, H. Flacher, S. Heinemeyer and G. Isidori *et al.*, arXiv:1112.3564 [hep-ph], submitted for publication to Eur. Phys. J. C.

7. J. Elias-Miro, J. R. Espinosa, G. F. Giudice, G. Isidori, A. Riotto and A. Strumia, Phys. Lett. B **709** (2012) 222 [arXiv:1112.3022 [hep-ph]].

8. O. Buchmueller, R. Cavanaugh, A. De Roeck, M. J. Dolan, J. R. Ellis, H. Flacher, S. Heinemeyer and G. Isidori *et al.*, arXiv:1110.3568 [hep-ph], to appear in Eur. Phys. J. C.

9. O. Buchmueller, R. Cavanaugh, D. Colling, A. De Roeck, M. J. Dolan, J. R. Ellis, H. Flacher, S. Heinemeyer and G. Isidori *et al.*, Eur. Phys. J. C **71** (2011) 1722 [arXiv:1106.2529 [hep-ph]].

10. O. Buchmueller, R. Cavanaugh, D. Colling, A. de Roeck, M. J. Dolan, J. R. Ellis, H. Flacher, S. Heinemeyer and G. Isidori *et al.*, Eur. Phys. J. C **71** (2011) 1634 [arXiv:1102.4585 [hep-ph]].

11. L. Calibbi, R. N. Hodgkinson, J. Jones-Perez, A. Masiero and O. Vives, arXiv:1111.0176 [hep-ph], to appear in Eur. Phys. J. C.

12. V. Del Duca, C. Duhr, E. Gardi, L. Magnea and C. D. White, arXiv:1201.2841 [hep-ph].

13. V. Del Duca, C. Duhr, E. Gardi, L. Magnea and C. D. White, JHEP **1112** (2011) 021 [arXiv:1109.3581 [hep-ph]].

14. V. Del Duca, C. Duhr, E. Gardi, L. Magnea and C. D. White, arXiv:1108.5947 [hep-ph].

15. V. Del Duca, L. J. Dixon, J. M. Drummond, C. Duhr, J. M. Henn and V. A. Smirnov, Phys. Rev. D **84** (2011) 045017 [arXiv:1105.2011 [hep-th]].

16. V. Del Duca, C. Duhr and V. A. Smirnov, JHEP **1107** (2011) 064 [arXiv:1105.1333 [hep-th]].

17. V. Del Duca, C. Duhr, V. A. Smirnov, C. Duhr and V. A. Smirnov, Phys. Lett. B **703** (2011) 363 [arXiv:1104.2781 [hep-th]].

18. A. Achilli, R. M. Godbole, A. Grau, G. Pancheri, O. Shekhovtsova and Y. N. Srivastava, Phys. Rev. D **84** (2011) 094009 [arXiv:1102.1949 [hep-ph]].

19. R. M. Godbole, A. Grau, K. A. Mohan, G. Pancheri and Y. N. Srivastava, Nuovo Cim. **034C** (2011) 129.

20. S. Biondini, O. Panella, G. Pancheri, Y. N. Srivstava and L. Fano, arXiv:1201.3764 [hep-ph].

21. M. Cirelli, G. Corcella, A. Hektor, G. Hutsi, M. Kadastik, P. Panci, M. Raidal and F. Sala *et al.*, JCAP **1103** (2011) 051 [arXiv:1012.4515 [hep-ph]].

LF61: Low-dimensional strongly correlated electron systems, spin-Hall effect and nanoscale science and technology

S. Bellucci (Resp. Naz.), M. Benfatto, M. Cini (Ass.), L. Coderoni (Bors.), K. Hatada (Borsista PD), K. Hayakawa (Borsista PD), F. Micciulla (Ass. Ric.), C. Natoli (Ass.), P. Onorato (Borsista PD), F. Palumbo (Ass.), N. Pugno (Ass.), I. Sacco (Bors.), G. Stefanucci (Ass.)

External collaborating Institutions:

IHEP-Protvino, Russia
Univ. Pavia, Italy
Belorus State Univ. Minsk,
Department of Physics, Yerevan State University, Armenia
Department of Physics, Univ. Roma Tor Vergata, Italy
Institute of Solid State Physics, University of Latvia, Kengaraga Str. 8, 1063 Riga, Latvia
Instituto de Ciencia de Materiales de Aragon, CSIC-Universidad de Zaragoza, 50009 Zaragoza, Spain.
ICB, UMR 5209 Universite' de Bourgogne - CNRS, BP 47870, F-21078 Dijon, France
Institut de Physique de Rennes, UMR UR1-CNRS 6251, Campus de Beaulieu, Universite' de Rennes1, 35042 Rennes-cedex, France

Research Activity

We reported on the comparative study of the electromagnetic shielding effectiveness provided by different forms of nanocarbon dispersed in epoxy resin in low concentration widely used for aerospace applications. The data of theoretical simulation on the basis of generalized Maxwell Garnett theory proved that the shielding effectiveness of the investigated composites in microwaves is determined mostly by the conductivity of nanocarbon inclusions.

Our theoretical study in collaboration with Riga, Latvia focused on junctions between the carbon nanotubes (CNTs) and contacting metallic elements of a nanocircuit. Numerical simulations on the conductance and resistance of these contacts have been performed using the multiple scattering theory and the effective media cluster approach. Two models for CNT-metal contacts have been considered in our collaboration: a) first principles “liquid metal” model and b) semi-empirical model of “effective bonds” based on Landauer notions on ballistic conductivity. Within the latter, which is a more adequate description of chirality effects, we have simulated both single-wall (SW) and multi-wall (MW) CNTs with different morphology. Results of calculations on resistance for different CNT-Me contacts look quantitatively realistic (from several to hundreds kOhm, depending on chirality, diameter and thickness of MW CNT). The inter-wall transparency coefficient for MW CNT has been also simulated, as an indicator of possible ‘radial current’ losses.

We carried out Ab Initio Simulations on Electric Properties for Junctions Between Carbon Nanotubes and Metal Electrodes. The cluster approach based on the multiple scattering theory formalism, realistic analytical and coherent potentials, as well as effective medium approximation (EMA-CPA), was used by us with Riga collaborators, for modeling of nanosized systems. This allowed us to calculate the dispersion law E(k), electronic density of states, conductivity, etc. The multiple scattering problems were stated for radial (e.g., quantum dots) and axial (e.g., nanowires, nanotubes) symmetry approaches. The reason for our interest in such systems, is due to their potential applications on carbon nanotubes (CNTs) of varying morphology, including their contacts with other conducting elements of a nanocircuit, which can be applied for interconnects in a high-speed electronics. The main problems solving for the resistance in CNT junctions with metal particles appear due to the influence of chirality effects in interconnects of single-wall (SW) and multi-wall (MW) CNTs with the fitting metals (Me = Ni, Cu, Ag, Pd, Pt, Au) for a predefined CNT geometry. Using the model of 'effective bonds' as developed in this study within the formalism of Landauer theory, we can predict the resistivity properties for both SW and MW CNT-Me interconnects.

In our study on the atomic and electronic structure of both perfect and nanostructured Ni(111) surfaces, we performed first principles simulations on both atomically smooth and nanostructured Ni(111) slabs. The latter contains periodically distributed nickel nanoclusters atop a thin metal film gradually growing from adatoms and serving as a promising catalyst. Applying the generalized gradient approximation within the formalism of the density functional theory we compared the atomic and electronic structures of Ni bulk, as well as both perfect and nanostructured (111) surfaces obtained using two different ab initio approaches: (i) the linear combination of atomic orbitals and (ii) the projector augmented plane waves. The most essential inter-atomic forces between the Ni adatoms upon the substrate have been found to be formed via: (i) attractive pair-wise interactions, (ii) repulsive triple-wise interactions within a triangle and (iii) attractive triple-wise interactions within a line between the nearest adatoms. The attractive interactions surmount the repulsive forces, hence resulting in the formation of stable clusters from Ni adatoms. The magnetic moment and the effective charge (within both Mulliken and Bader approaches) of the outer atoms in Ni nanoparticles increase as compared to those for the smooth Ni(111) surface. The calculated electronic charge redistribution in the Ni nanoclusters features them as possible adsorption centers with increasing catalytic activity, e.g., for further synthesis of carbon nanotubes.

Also, we have performed ab initio DFT calculations on the gradually growing 2D periodic models of capped single-wall carbon nanotubes (SW CNTs) upon their perpendicular junctions with the Ni(111) substrate, in order to understand the peculiarities of the initial stage of their growth on either smooth or nanostructured catalytic particles. Appearance of the adsorbed carbon atoms upon the substrate follows from the dissociation of CVD hydrocarbon molecules, e.g., CH4: (CH4)ads II (CH)ads+3Hads and (CH)ads II Cads+Hads. (Since the effective growth of CNTs upon Ni nanoparticles occur inside the nanopores of amorphous alumina, we have also simulated analogous surface reactions upon the -Al2O3(010) slabs). Association of the adsorbed carbon atoms upon the catalyst surface precedes further swelling of the (Cn)ads islands after appearance of pentagonal defects within a honeycomb sheet which are more probable upon the catalyst surface containing either defects or nanoclusters (as in the case of the nanostructured substrate). The gradual growth of the capped CNTs is considerably more effective upon the nanostructured Ni(111) substrate compared to a smooth nickel substrate (cf. values of CNT adhesion energy per boundary C atom for chiralities of either armchair-type, 4.04 vs. 2.51 eV, or zigzag-type, 4.61 vs. 2.14 eV, respectively). The electronic charge transfer from the Ni catalyst towards the CNTs has been calculated for both chiralities (> 1 e per C atom), i.e., quite strong chemical bonds are formed within the CNT/Ni(111) interconnects.

We discussed also the electron transport for a spin polarized current through a ballistic quantum nanojunction formed by two quantum dots (QDs) and a semiconducting quantum wire. We explored the possibilities of designing spintronic logic gates at the nano-scale level derivedfrom this device. Just one electron with a given spin polarization fills each QD and the stationary binary digit consists of the spin-up and spin-down of a single electron. Thus the spin polarizations of those electrons were treated as the two inputs of the gates. The AND, XOR, XNOR, and NOR gate response in the system is investigated beginning with the calculation of the low bias conductance-energy characteristic in the ballistic regime. Our study suggested that, for an appropriate choice of the working Fermi energy and of the distance between the QDs, a high output current (in the logical sense) appears for certain combinations of the inputs while it vanishes for others. It clearly demonstrated the logic gate behavior and this aspect may be utilized in designing a spintronic logic operator.

In collaboration with Armenia, we suggested to use the action-angle variables for the study of properties of (quasi)particles in quantum rings. For this purpose we presented the action-angle variables for three two-dimensional singular oscillator systems. The first one is the usual (Euclidean) singular oscillator, which plays the role of the confinement potential for the quantum ring. We also propose two singular spherical oscillator models for the role of the confinement system for the spherical ring. The first one is based on the standard Higgs oscillator potential. We show that, in spite of the presence of a hidden symmetry, it is not convenient for the study of the system's behaviour in a magnetic field. The second model is based on the so-called CP1 oscillator potential and respects the inclusion of a constant magnetic field.

We also reviewed, with our Armenian collaborators, the parallels between spinning particle models described by the Lagrangians depending on the extrinsic curvatures of the worldline, and the DNA molecules. As an example of the possible transfer of the constructions of spinning particle systems to the polymer physics we suggested to reinterpret the DNA effective energy model by Feoli, Nesterenko and Scarpetta as a linear density of the energy of the DNA molecule. We performed the geometric coupling of this model to the external field and gave the Hamiltonian formulation of this system.

We studied theoretically the memory effects due to different kinds of initial conditions in the transport properties of one-dimensional systems described by the Tomonaga-Luttinger model. We showed that in presence of electron–electron interactions the sudden switching of a weak link between two initially uncontacted reservoirs induces a qualitative change in the transient current with respect to the contacted case. In particular the different switching process produces a change in the powerlaw temporal relaxation of the current towards the steady-state as well as a significant suppression of the transient oscillations. Even more dramatic is the response to a sudden interaction quench, which remarkably leads to a current–voltage characteristic differing from the one displayed if the system was initially interacting.

We presented a comprehensive analysis of the relaxation dynamics of a Luttinger liquid subject to a sequence of sudden interaction quenches. The critical exponent governing the decay of the steady-state propagator was expressed as an explicit functional of the switching protocol. At long distances depends only on the initial state while at short distances it is also history dependent. Continuous protocols of arbitrary complexity can be realized with infinitely long sequences. For quenches of finite duration we proved that there exists no protocol to bring the initial non-interacting system in the ground state of the Luttinger liquid, albeit thermalization occurs at short distances. The adiabatic theorem was then investigated with ramp switchings of increasing duration and several analytic results for both the propagator and the excitation energy were derived.

The absence of sharp structures in the Auger line shapes of partially filled bands has severely limited the use of electron spectroscopy in magnetic crystals and other correlated materials. By a novel interplay of experimental and theoretical techniques we achieve a combined understanding of the photoelectron, Auger, and Auger-photoelectron coincidence spectra (APECS) of the antiferromagnetic CoO. A recently discovered dichroic effect in angle resolved (DEAR) APECS reveals a complex pattern in the Auger line shape, which is here explained in detail, labeling the final states by their total spin. Since the dichroic effect exists in the antiferromagnetic state but vanishes at the N?el temperature, the DEAR-APECS technique detects the phase transition from its local effects, thus providing a unique tool to observe and understand magnetic correlations where the usual methods are not applicable.

Auger-photoelectron coincidence spectroscopy was used for investigating the electronic properties of a CoO thin film above and below the magnetic transition temperature (TN). By using the dichroic effect in angle-resolved measurements, we identified and assigned well-defined high-spin and low-spin structures in spite of the otherwise featureless Auger singles spectra, typically found for open-band systems. The disappearance of the dichroism for temperatures just above TN indicates a collapse of the surface short-range magnetic order, presumably due to a strongly reduced exchange field in the surface compared to that in the bulk.

Nanoscopic rings pierced by external magnetic fields and asymmetrically connected to wires behave in sharp contrast with classical expectations. By studying the real-time evolution of tight-binding models in different geometries, we showed that the creation of a magnetic dipole by a bias-induced current is a process that can be reversed: connected rings excited by an internal ac flux produce ballistic currents in the external wires. In particular we pointed out that by employing suitable flux protocols, single-parameter nonadiabatic pumping can be achieved, and an arbitrary amount of charge can be transferred from one side to the other. We also proposed a setup that could serve a memory device, in which both the operations of writing and erasing can be efficiently performed.

In circuits containing closed loops the operator for the current is determined by charge conservation up to an arbitrary divergenceless vortex current. We proposed a formula to calculate the magnetically active circulating current Iring flowing along a quantum ring connected to biased leads. By gedanken experiments we argued that Iring can be obtained from the response of the grancanonical energy of the ring to a concatenated magnetic flux. The results agree with those of the conventional approach in the case of isolated rings. However, for connected rings Iring cannot be obtained as a linear combination of bond currents.

We studied time-dependent electron transport through an Anderson model. The electronic interactions on the impurity site are included via the self-energy approximations at Hartree-Fock (HF), second Born (2B), GW, and T-matrix levels as well as within a time-dependent density functional (TDDFT) scheme based on the adiabatic Bethe-ansatz local density approximation (ABALDA) for the exchange-correlation potential. The Anderson model was driven out of equilibrium by applying a bias to the leads, and its nonequilibrium dynamics was determined by real-time propagation. The time-dependent currents and densities were compared to benchmark results obtained with the time-dependent density matrix renormalization group (tDMRG) method. Many-body perturbation theory beyond HF gives results in close agreement with tDMRG, especially within the 2B approximation. We found that the TDDFT approach with the ABALDA approximation produces accurate results for the densities on the impurity site, but overestimates the currents. This problem is found to have its origin in an overestimation of the lead densities, which indicates that the exchange-correlation potential must attain nonzero values in the leads.

We demonstrated that the zero-temperature conductance of the Anderson model can be calculated within the Landauer formalism combined with static density-functional theory. The proposed approximate functional is based on finite-temperature density-functional theory and yields the exact Kohn-Sham potential at the particle-hole symmetric point. Furthermore, in the limit of zero temperature it correctly exhibits a derivative discontinuity which is shown to be essential to reproduce the conductance plateau. On the other hand, at the Kondo temperature the exact Kohn-Sham conductance overestimates the real one by an order of magnitude. To understand the failure of density-functional theory, we resorted to its time-dependent version and concluded that the suppression of the Kondo resonance must be attributed to dynamical exchange-correlation corrections.

The cornerstone of time-dependent (TD) density functional theory (DFT), the Runge–Gross theorem, proves a one-to-one correspondence between TD potentials and TD densities of continuum Hamiltonians. In all practical implementations, however, the basis set is discrete and the system is effectively described by a lattice Hamiltonian. We pointed out the difficulties of generalizing the Runge–Gross proof to the discrete case and thereby endorse the recently proposed TD bond-current functional theory (BCFT) as a viable alternative. TDBCFT is based on a one-to-one correspondence between TD Peierl's phases and TD bond-currents of lattice systems. We applied the TDBCFT formalism to electronic transport through a simple interacting device weakly coupled to two biased non-interacting leads. We employed Kohn–Sham Peierl's phases which are discontinuous functions of the density, a crucial property to describe Coulomb blockade. As shown by explicit time propagations, the discontinuity may prevent the biased system from ever reaching a steady state.

We investigated the effects of the electron-electron interaction between a molecular junction and the metallic leads in time-dependent quantum transport. We employed the recently developed embedded Kadanoff-Baym method [Phys. Rev. B 80, 115107 (2009)] and showed that the molecule-lead interaction changes substantially the transient and steady-state transport properties. We first showed that the mean-field Hartree-Fock (HF) approximation does not capture the polarization effects responsible for the renormalization of the molecular levels neither in nor out of equilibrium. Furthermore, due to the time-local nature of the HF self-energy there exists a region in parameter space for which the system does not relax after the switch-on of a bias voltage. These and other artifacts of the HF approximation disappear when including correlations at the second-Born or GW levels. Both these approximations contain polarization diagrams which correctly account for the screening of the charged molecule. We found that by changing the molecule-lead interaction the ratio between the screening and relaxation time changes, an effect which must be properly taken into account in any realistic time-dependent simulation. Another important finding was that while in equilibrium the molecule-lead interaction is responsible for a reduction of the HOMO-LUMO gap and for a substantial redistribution of the spectral weight between the main spectral peaks and the induced satellite spectrum, in the biased system it can have the opposite effect, i.e., it sharpens the spectral peaks and opens the HOMO-LUMO gap.

We proved a generalized Wick theorem to calculate the Green's function of bosonic and fermionic systems in an arbitrary initial state. It was shown that the decomposition of the non-interacting n-particle Green's function is equivalent to solving a boundary problem for the Martin-Schwinger hierarchy; for non-correlated initial states a one-line proof of the standard Wick theorem is presented. Our result leads to new self-energy diagrams and an elegant relation with those of the imaginary-time formalism was derived.

Scissors modes were predicted in the framework of the Two-Rotor Model. This model has an intrinsic harmonic spectrum, so that the level above the Scissors Mode, the first overtone, has excitation energy twice that of the Scissors Mode. Since the latter is of the order of 3 MeV in the rare earth region, the energy of the overtone is below threshold for nucleon emission, and its width should remain small enough for the overtone to be observable.

Multiple scattering is a method of solving the Schrodinger equation not only for bound states but also for scattering states. As such can be effectively used to calculate many electron spectroscopies, including all those cases in which the excited electron is not observed but is virtual (as in absorption and resonant scattering). A package to calculate these various spectroscopies has been submitted and published on Computer Physics Communications.

Likewise we developed a general method to apply multiple scattering theory to describe ground state properties of correlated systems in the framework of the so-called multi-channel multiple scattering theory, an extension of the independent particle model already applied to excited states to calculate spectroscopic response functions in correlated systems (P. Kruger and C.R. Natoli, Phys Rev B 70: 245120 2004). The paper has been submitted to Journal of Physics - Condensed matter.

Finally, in collaboration with with Prof. J. Bartolom? of the University of Zaragoza we have calculated the Fe K-edge absoprtion spectrum of iron Phtalocyanin deposited on a substrate in order to establish the stacking geometry of the various molecules. The simulations favor a geometry similar to what found by Chen et al (PRL 101, 197208 (2008)) in cobalt phthalocyanine.

List of Conference Talks

S. Bellucci, Electron emission from vertically aligned few-layer graphene and carbon nanotubes: a comparative study. Presented at the AIM Conference, XX Convegno Italiano di Scienza e Tecnologia delle Macromolecole Terni 4 - 8 Settembre 2011.

N. Pugno, Nanomechanics of graphene nanoscrolls, Presented at Nanoscience & Nanotechnology 2011, Laboratori Nazionali di Frascati 19-23 September 2011.

M. Cini, Magnetic properties of quantum rings, Presented at Nanoscience & Nanotechnology 2011, Laboratori Nazionali di Frascati 19-23 September 2011.

S. Bellucci, Towards a description of strongly correlated quantum transport using TDDFT, Presented at Nanoscience & Nanotechnology 2011, Laboratori Nazionali di Frascati 19-23 September 2011.

E. Perfetto, Electron correlations in the time-dependent transport at the nanoscale, Presented at Nanoscience & Nanotechnology 2011, Laboratori Nazionali di Frascati 19-23 September 2011.

Publications by LNF Authors in the Year 2011

S. Bellucci and P. Onorato, Transport Properties in Carbon Nanotubes, in Physical Properties of Ceramic and Carbon Nanoscale Structures, Lecture Notes in Nanoscale Science and Technology Volume 11: Physical Properties of Ceramic and Carbon Nanoscale Structures:The INFN Lectures - Vol II, Bellucci, S. ed., 2011, p. 45-110.

Fermionic condensate in a conical space with a circular boundary and magnetic flux.
S. Bellucci, E.R.Bezerra de Mello, A.A. Saharian, Phys. Rev. D 83, 085017 (2011) [15 pages], e-Print: arXiv:1101.4130 [hep-th]

“Theoretical simulations on the inter-shell interactions in double-wall CNTs of different morphology”, S. Piskunov, V. Kashcheyevs, Y. Zhukovskii, S. Bellucci, Computational and Theoretical Chemistry, 2011;

Crystal-Assisted Beam Extraction and Collimation at the U-7 Circular Accelerator. A.G. Afonin et al. IHEP-PREPRINT-2010-12, Published in Instrum.Exp.Tech.54:1-7,2011. e-Print: arXiv:1102.2711 [physics.acc-ph]

External field influence on semiflexible macromolecules: geometric coupling. Stefano Bellucci, Yevgeny Mamasakhlisov, Armen Nersessian, Mod. Phys. Lett. B 22 (2011) 1809-1819, e-Print: arXiv:1011.0644 [cond-mat.soft]

Thermodynamic Geometry: Evolution, Correlation and Phase Transition. S. Bellucci, B.N. Tiwari, e-Print: arXiv:1010.5148 [cond-mat.stat-mech]

Quantum ring models and action-angle variables. Stefano Bellucci, Armen Nersessian, Armen Saghatelian, Vahagn Yeghikyan, Journal of Computational and Theoretical Nanoscience, Volume 8, Number 4, April 2011, pp. 769-775(7) e-Print: arXiv:1008.3865 [cond-mat.mtrl-sci]

Yuri N. Shunin, Yuri F. Zhukovskii, Viktor I. Gopejenko, Natalia Burlutskaya, BELLUCCI S. (2011). Ab Initio Simulations on Electric Properties for Junctions Between Carbon Nanotubes and Metal Electrodes. NANOSCIENCE AND NANOTECHNOLOGY LETTERS, vol. 3; p. 816-825, ISSN: 1941-4900.

Quantum nanojunctions as spintronic logic operators: Gate response in a two input ballistic interferometer. S. Bellucci and P. Onorato. J. Appl. Phys. 109, 123715 (2011); http://dx.doi.org/10.1063/1.3598127 (6 pages).

Differential Geometry in DNA Molecules. Bellucci, Stefano; Mamasakhlisov, Yevgeny; Nersessian, Armen. Nanoscience and Nanotechnology Letters, Volume 3, Number 6, November 2011 , pp. 922-926(5).

Zhukovskii YF, Piskunov S, Kotomin EA, BELLUCCI S. (2011). Simulations on the mechanism of CNT bundle growth upon smooth and nanostructured Ni as well as theta-Al(2)O(3) catalysts RID C-7063-2011 RID D-3126-2011 RID C-9235-2011. CENTRAL EUROPEAN JOURNAL OF PHYSICS, vol. 9; p. 530-541, ISSN: 1895-1082, doi: 10.2478/s11534-010-0079-8.

BELLUCCI S., Alexander Malesevic, Federico Micciulla, Immacolata Sacco, Raymond Kemps, Annick Vanhulsel, and Chris Van Haesendonck (2011). Comparative Field Emission from Vertically Aligned Few-Layer Graphene and Carbon Nanotubes. NANOSCIENCE AND NANOTECHNOLOGY LETTERS, vol. 3; p. 907-912, ISSN: 1941-4900.

Shunin YN, Zhukovskii YF, Burlutskaya N, BELLUCCI S. (2011). Resistance simulations for junctions of SW and MW carbon nanotubes with various metal substrates RID C-7063-2011 RID C-

9235-2011. CENTRAL EUROPEAN JOURNAL OF PHYSICS, vol. 9; p. 519-529, ISSN: 1895-1082, doi: 10.2478/s11534-010-0086-9

Yu.N. Shunin, Yu.F. Zhukovskii, N. Burlutskaya, BELLUCCI S. (2011). Theoretical Simulations on Electric Properties of CNT-Me and GNR-Me Interconnects Using Effective Media Approach. In: Proceedings of the 2nd European Future Technologies Conference and Exhibition 2011 (FET 11), vol. 7, p. 343-345

On the thermalization of a Luttinger liquid after a sequence of sudden interaction quenches. E. Perfetto, G. Stefanucci. EPL Volume 95 Issue 1 Year 2011, p. 10006.

Magnetically induced pumping and memory storage in quantum rings. M. Cini, E. Perfetto. PHYSICAL REVIEW B, Volume 84 Issue 24 Year 2011

Insight on Hole-Hole Interaction and Magnetic Order from Dichroic Auger-Photoelectron Coincidence Spectra. M. Cini, E. Perfetto et al., PHYSICAL REVIEW LETTERS, Volume 107 Issue 21 Year 2011

Origin of the pre-peak features in the oxygen K-edge x-ray absorption spectra of LaFeO(3) and LaMnO(3) studied by Ga substitution of the transition metal ion. Lafuerza, S., Subias, G., Garcia, J., Di Matteo, S. Blasco, J., Cuartero, V., Natoli C., JOURNAL OF PHYSICS-CONDENSED MATTER, Volume 23 Issue 32 Year 2011

MsSpec-1.0: A multiple scattering package for electron spectroscopies in material science. Sebilleau, Didier; Natoli, Calogero; Gavaza, George M.; Zhao, Haifeng; Da Pieve, Fabiana; Hatada, Keisuke, COMPUTER PHYSICS COMMUNICATIONS Volume 182 Issue 12 Year 2011

Scissors modes: The first overtone, Hatada K, Hayakawa K, Palumbo F, Phys. Rev. C 84 (2011) 011302(R)

Atomic and electronic structure of both perfect and nanostructured Ni(111) surfaces: First-principles calculations. Sergei Piskunov, Guntars Zvejnieks, Yuri F. Zhukovskii, Stefano Bellucci, Thin Solid Films, Volume 519, Issue 11, 31 March 2011, Pages 3745–3751

"Atomic carbon adsorption on flat and nano-structured Ni catalyst with further CNT growth: predictions from first principles calculations", Y. Zhukovskii, S. Piskunov, E. Kotomin, S. Bellucci, Physica E, 2011.

"CNT-metal interconnects: Electronic structure calculations and resistivity simulations", Y. Shunin, Y. Zhukovskii, N. Burlutskaya, S. Bellucci, Journal of Nano-electronic and Optoelectronic, 2011;

A.-M. Uimonen, E. Khosravi, A. Stan, G. Stefanucci, S. Kurth, R. van Leeuwen, and E. K. U. Gross Comparative study of many-body perturbation theory and time-dependent density functional theory in the out-of-equilibrium Anderson model. Phys. Rev. B 84, 115103 (2011) [10 pages].

Towards a Description of the Kondo Effect Using Time-Dependent Density-Functional Theory. G. Stefanucci and S. Kurth. Phys. Rev. Lett. 107, 216401 (2011)

Time-dependent bond-current functional theory for lattice Hamiltonians: Fundamental theorem and

application to electron transport, S. Kurth, G. Stefanucci. Chemical Physics Volume 391, Issue 1, 24 November 2011, Pages 164–172

Circulating Currents and Magnetic Moments in Quantum Rings. Cini, Michele; Perfetto, Enrico; Stefanucci, Gianluca. Nanoscience and Nanotechnology Letters, Volume 3, Number 6, November 2011 , pp. 902-906(5).

Initial Correlation Effects in Time-Dependent Transport with One-Dimensional Interacting Leads Perfetto, E.; Stefanucci, G.; Cini, M., Nanoscience and Nanotechnology Letters, Volume 3, Number 6, November 2011 , pp. 877-881(5).

Evidence for the collapse of short-range magnetic order in CoO at the Neel temperature. R. Gotter, F. Offi, A. Ruocco, F. Da Pieve, R. Bartynski, M. Cini and G. Stefani, 2011 EPL 94 37008.

Low-dimensional nanostructures and a semiclassical approach for teaching Feynman's sum-over-paths quantum theory. P. Onorato. 2011 Eur. J. Phys. 32, 259.

The theory of multiple peeling. Nicola M. Pugno. International Journal of Fracture Volume 171, Number 2, 185-193, DOI: 10.1007/s10704-011-9638-2.

MI-11 Strong Interactions and Lattice Field Theory

M.P. Lombardo (resp.) and K. Miura (INFN fellow)

1 Research

Our activity focusses of the analysis of strong interactions along two main , interrelated avenues : the study of the phase diagram of QCD in the temperature– density plane, and the analysis of QCD with a large number of fermions, when the theory becomes distinctly different from ordinary QCD and can be used to model mechanisms of electroweak symmetry breaking inspired by Technicolor. During 2011 we have investigated the phase transition of QCD at high temperature and analsyized its universality class [1], studied the pattern of suppression of bottomonium around the LHC working condition (our results compare well with the CMS analysis) [2–3], and made progress on the strong coupling expansion at non zero density [4–7]. We have initiated and published one first letter on thermodynamics with a large number of flavors [8–9], which allows an independent estimate of the "Technicolor–like" region, and has interesting implications on the analysis of the strong interactive Quark Gluon Plasma, a long standing interest of ours[10]. Our first principle results compare well with the approximate ones coming from analytic studies, thus validating them. Further, we have continued our investigation of the conformal window of QCD, measuring the anomalous dimension of the theory – a crucial ingredient for phenomenological applications [11] as well uncovering and discussing interesting new phenomena in the lattice strong coupling limit [12]. Projects which have started during 2011 and have not yet produced publication include an alternative method of attack to the computation of the spectral functions at high temperature, again aiming at a comparison with LHC heavy ion results, and a novel study of glueball spectrum in different thermodynamic conditions - the latter especially relevant in the so far elusive scalar sector. Our research is supported by CINECA (200 Khours on IBM Power6 and IBM BG/P) (MpL PI), by MIUR via PRIN (MpL responsabile della ricerca) and by EU under I3HP2, WP22.

Service & teaching

We have organized two sessions of the LNF Institute devoted to frontier aspects of strong interactions. MpL has been a member of the IAC for Extreme QCD 2011 and 2012, and of the reading committee and of the thesis commeettee for Dr. Albert Deuzeman, University of Groningen. and a Guest Professor at the Physics Department, Humbold University, Berlin, during the Summer Semester 2011.

2 List of Conference Talks by LNF Authors in Year 2011

1. *Thermodynamics of many flavor QCD* at Lattice 2011, Lake Tahoe, July 2011 (KM);
2. *QCD with many flavors* at Extreme QCD 2011, August 2011, San Carlos, Mexico (MpL);
3. *Bottomonium in the Quark Gluon Plasma*, invited at QWG 2011, 8-th International Workshop on Heavy Quarkonium, GSI, Darmstadt, October 2011 (MpL) ;

4. Panelist at the round tables on *Lattice Simulations with 2+1+1 flavors',* and *Quarkonium in media*, QWG 2011 (MpL) ;

5. *Equation of state, and chiral condensate renormalization* invited at Chiral dynamics with Wilson fermions', ECT*, Trento, October 2011 (MpL).

3 Publications

1. F. Burger, E. -M. Ilgenfritz, M. Kirchner, M. P. Lombardo, M. Muller-Preussker, O. Philipsen, C. Urbach and L. Zeidlewicz, *The thermal QCD transition with two flavours of twisted mass fermions* submitted to Phys. Rev. D;

2. G. Aarts, C. Allton, S. Kim, M. P. Lombardo, M. B. Oktay, S. M. Ryan, D. K. Sinclair and J. I. Skullerud, *What happens to the Upsilon and η_b in the quark-gluon plasma?* JHEP **1111** (2011) 103

3. G. Aarts, S. Kim, M. P. Lombardo, M. B. Oktay, S. M. Ryan, D. K. Sinclair and J. - I. Skullerud, *Bottomonium above deconfinement in lattice nonrelativistic QCD,* Phys. Rev. Lett. **106** (2011) 061602

4. A. Ohnishi, K. Miura, T. Z. Nakano, N. Kawamoto, H. Ueda, M. Ruggieri and K. Sumiyoshi, *QCD critical point in the sclQCD and during black hole formation,* arXiv:1201.6206 [nucl-th].

5. P. de Forcrand, M. Fromm, J. Langelage, K. Miura, O. Philipsen and W. Unger, *Towards corrections to the strong coupling limit of staggered lattice QCD,* PoS(Lattice2011);

6. K. Miura, T. Z. Nakano, A. Ohnishi and N. Kawamoto, *Strong-coupling lattice study for QCD phase diagram including both chiral and deconfinement dynamics,* PoS(Lattice2011);

7. T. Z. Nakano, K. Miura and A. Ohnishi, *Chiral and deconfinement transitions in strong coupling lattice QCD with finite coupling and Polyakov loop effects,* Phys. Rev. D **83** (2011) 016014;

8. K. Miura, M. P. Lombardo and E. Pallante, *Thermodynamic Study for Conformal Phase in Large Nf Gauge Theory,* PoS(Lattice2011);

9. K. Miura, M. P. Lombardo and E. Pallante, *Chiral phase transition at finite temperature and conformal dynamics in large Nf QCD,*, Physics Letters B, in press;

10. M. D'Elia, F. Di Renzo and M. P. Lombardo, *Strongly interacting quark-gluon plasma and the critical behaviour of QCD at imaginary mu,* Indian J. Phys. **85** (2011) 51.

11. A. Deuzeman, M. P. Lombardo and E. Pallante, *On the spectrum of QCD-like theories and the conformal window,* PoS(Lattice 2011) ;

12. A. Deuzeman, M. P. Lombardo, T. N. da Silva and E. Pallante, *Bulk transitions of twelve flavor QCD and $U_A(1)$ symmetry,* PoS(Lattice2011).

MI12: Gauge and String Theories

S. Bellucci (Resp.), S. Ferrara (Ass.), E. Latini (Dott.), S. Krivonos (Osp.), A. Marrani (Bors. PD), V. Ohanyan (Osp.), A. Shcherbakov (Bors. PD), A. Saharian (Osp.), A. Sutulin (Osp.), B.N. Tiwari (Bors. PD), V. Yeghikyan (Bors. PD), A. Yeranyan (art. 23)

Research Activity

We studied a class of fluctuating higher dimensional black hole configurations obtained in string theory/M-theory compactifications. We explored the intrinsic Riemannian geometric nature of Gaussian fluctuations arising from the Hessian of the coarse graining entropy, defined over an ensemble of brane microstates. It has been shown that the state-space geometry spanned by the set of invariant parameters is non-degenerate, regular and has a negative scalar curvature for the rotating Myers-Perry black holes, Kaluza-Klein black holes, supersymmetric AdS_5 black holes, D_1-D_5 configurations and the associated BMPV black holes. Interestingly, these solutions demonstrate that the principal components of the state-space metric tensor admit a positive definite form, while the off diagonal components do not. Furthermore, the ratio of diagonal components weakens relatively faster than the off diagonal components, and thus they swiftly come into an equilibrium statistical configuration. Novel aspects of the scaling property suggest that the brane-brane statistical pair correlation functions divulge an asymmetric nature, in comparison with the others. This approach indicates that all above configurations are effectively attractive and stable, on an arbitrary hyper-surface of the state-space manifolds. It is nevertheless noticed that there exists an intriguing relationship between non-ideal inter-brane statistical interactions and phase transitions. The ramifications thus described are consistent with the existing picture of the microscopic CFTs. We conclude with an extended discussion of the implications of this work for the physics of black holes in string theory.

We studied the state-space geometry of various extremal and nonextremal black holes in string theory. From the notion of the intrinsic geometry, we offer a new perspective of black hole vacuum fluctuations. For a given black hole entropy, we explicated the intrinsic state-space geometric meaning of the statistical fluctuations, local and global stability conditions and long range statistical correlations. We provided a set of physical motivations pertaining to the extremal and nonextremal black holes, i.e. the meaning of the chemical geometry and physics of correlation. We illustrated the state-space configurations for general charge extremal black holes. In sequel, we extended our analysis for various possible charge and anticharge nonextremal black holes. From the perspective of statistical fluctuation theory, we offered general remarks, future directions and open issues towards the intrinsic geometric understanding of the vacuum fluctuations and black holes in string theory.

We examined the statistical nature of the charged anticharged non-extremal black holes in string theory. From the perspective of the intrinsic Riemannian Geometry, the first principle of the statistical mechanics shows that the stability properties of general nonextremal nonlarge charged black brane solutions are divulged from the positivity of the corresponding principle minors of the space-state metric tensor. Under the addition of the Kaluza-Klein monopoles, a novel aspect of the Gaussian fluctuations demonstrates that the canonical fluctuations can be ascertained without any approximation. We offered the state-space geometric implication for the most general non-extremal black brane configurations in string theory.

We reconsidered the sub-leading quantum perturbative corrections to N = 2 cubic special K?hler geometries. Imposing the invariance under axion-shifts, all such corrections (but the imaginary constant one) can be introduced or removed through suitable, lower unitriangular symplectic transformations and dubbed Peccei-Quinn (PQ) transformations. Since PQ transformations do not belong to the d = 4 U-duality group G4, in symmetric cases they generally have a non-trivial action on the unique quartic invariant polynomial I4 of the charge representation R of G4. This leads to interesting phenomena in relation to theory of extremal black hole attractors; namely, the possibility to make transitions between different charge orbits of R, with corresponding change of the supersymmetry properties of the supported attractor solutions. Furthermore, a suitable action of PQ transformations can also set I4 to zero, or vice versa it can generate a non-vanishing I4: this corresponds to transitions between "large" and "small" charge orbits, which we classify in some detail within the "special coordinates" symplectic frame. Finally, after a brief account of the action of PQ transformations on the recently established correspondence between Cayley's hyperdeterminant and elliptic curves, we derived an equivalent, alternative expression of I4, with relevant application to black hole entropy.

We constructed a new N=4 supersymmetric mechanics describing the motion of a particle over a CP(n) manifold in U(n) background gauge fields. Also, we provided a Lagrangian formulation of N = 4 supersymmetric mechanics describing the motion of an isospin carrying particle on conformal to hyper-K?hler spaces in a non-Abelian background gauge field. In two examples we discussed in details, this background field was identified with the field of BPST instantons in the flat and Taub-NUT spaces. Moreover, we constructed a new N = 2 supersymmetric extension of a massive particle moving near the horizon of the extreme Kerr black hole. Our supercharges and Hamiltonian contain the proper number of fermions (two for each bosonic variables). The key ingredient of our construction is a proper choice of the bosonic variables which all have a clear geometric meaning.

We coupled N=4 chiral supermultiplet with an auxiliary N=4 fermionic supermutiplet containing on-shell four physical fermions and four auxiliary bosons. The latter ones play the role of isospin variables. We chose the very specific coupling which results in a component action containing only time derivatives of fermionic components presented in the auxiliary supermultiplet, which therefore may be dualized into auxiliary ones. The resulting component action describes the interaction of the chiral supermultiplet with a magnetic field constant on the pseudo-sphere SU(1,1)/U(1). Then we specified the prepotential of our theory to get, in the bosonic sector, the action for the particle moving over the pseudo-sphere -- Lobachevsky space. We provided also the Hamiltonian formulation of this system and show that the full symmetry group of our system is SU(1,1) x U(1). The currents forming the su(1,1) algebra are modified, as compared to the bosonic case, by the fermionic and isospin terms, while the additional u(1) current contains only isospin variables. One of the most important features of our construction is the presence in the Hamiltonian and supercharges of all currents of the isospin group SU(2). Despite the fact that two of the su(2) currents enter the Hamiltonian only through the Casimir operator of the SU(2) group, they cannot be dropped out, even after fixing the total isospin of the system, because these currents themselves enter into the supercharges.

We also presented the Hamiltonian and supercharges describing the motion of a particle over the sphere in the background of constant magnetic field. In this case the additional isospin currents form the su(1,1) algebra.

We classified the stability region, marginal stability walls (MS) and split attractor flows for two-center extremal black holes in four-dimensional N=2 supergravity minimally coupled to n vector multiplets. It was found that two-center (continuous) charge orbits, classified by four duality invariants, either support a stability region ending on an MS wall or on an anti-marginal stability (AMS) wall, but not both. Therefore, the scalar manifold never contains both walls. Moreover, the BPS mass of the black hole composite (in its stability region) never vanishes in the scalar manifold. For these reasons, the "bound state transformation walls" phenomenon does not necessarily occur in these theories. The entropy of the flow trees also satisfies an inequality which forbids "entropy enigma" decays in these models. The non-BPS case, due to the existence of a "fake" superpotential satisfying a triangle inequality, can be treated as well, and it can be shown to exhibit a split attractor flow dynamics which, at least in the n=1 case, is analogous to the BPS one.

We classified 2-center extremal black hole charge configurations through duality-invariant homogeneous polynomials, which are the generalization of the unique invariant quartic polynomial for single-center black holes based on homogeneous symmetric cubic special K? hler geometries. A crucial role is played by a horizontal SL(p,math) symmetry group, which classifies invariants for p-center black holes. For p = 2, a (spin 2) quintet of quartic invariants emerge. We provided the minimal set of independent invariants for the rank-3 N = 2, d = 4 stu model, and for its lower-rank descendants, namely, the rank-2 st2 and rank-1 t3 models; these models, respectively, exhibit seven, six, and five independent invariants. We also derived the polynomial relations among these and other duality invariants. In particular, the symplectic product of two charge vectors is not independent from the quartic quintet in the t3 model, but rather it satisfies a degree-16 relation, corresponding to a quartic equation for the square of the symplectic product itself.

We identified a particularly simple class of supergravity models describing superconformal coupling of matter to supergravity. In these models, which we call the canonical superconformal supergravity models, the kinetic terms in the Jordan frame are canonical, and the scalar potential is the same as in the global theory. The pure supergravity part of the total action has a local Poincar? supersymmetry, whereas the chiral and vector multiplets coupled to supergravity have a larger local superconformal symmetry. The scale-free globally supersymmetric theories, such as the NMSSM with a scale-invariant superpotential, can be naturally embedded into this class of theories. After the supergravity embedding, the Jordan frame scalar potential of such theories remains scale free; it is quartic, it contains no mass terms, no nonrenormalizable terms, no cosmological constant. The local superconformal symmetry can be broken by additional terms, which, in the small field limit, are suppressed by the gravitational coupling. This can be achieved by introducing the nonminimal scalar-curvature coupling, and by taking into account interactions with a hidden sector. In this approach, the smallness of the mass parameters in the NMSSM may be traced back to the original superconformal invariance. This allows one to address the mu problem and the cosmological domain wall problem in this model, and to implement chaotic inflation in the NMSSM. We discussed the gravitino problem in the NMSSM inflation, as well as the possibility to obtain a broad class of new versions of chaotic inflation in supergravity.

We determined the two-centered generic charge orbits of magical N = 2 and maximal N = 8 supergravity theories in four dimensions. These orbits are classified by seven U-duality invariant polynomials, which group together into four invariants under the horizontal symmetry group. These latter are expected to disentangle different physical properties of the two-centered black-hole system.

Freudenthal duality, introduced in Borsten et al. (2009) and defined as an anti-involution on the dyonic charge vector in d=4 space–time dimensions for those dualities admitting a quartic invariant, was proved to be a symmetry not only of the classical Bekenstein–Hawking entropy but also of the critical points of the black hole potential. Furthermore, Freudenthal duality was extended to any generalized special geometry, thus encompassing all N>2 supergravities, as well as N=2 generic special geometry, not necessarily having a coset space structure.

List of Conference Talks

S. Ferrara, Black Holes in Supergravity, Invited Presentation at the Round Table Italy-JINR, Black Holes in Mathematics and Physics, December 15-18, 2011

S. Bellucci, Near-horizon particle dynamics in extremal Kerr black hole, Invited Presentation at the Round Table Italy-JINR, Black Holes in Mathematics and Physics, December 15-18, 2011

S. Ferrara, Invited talk at the conference "From dual models to strings and branes", Torino, Italy (28-29/10/2011)

S. Ferrara, Invited talk at Pontificial Academy of Science "Subnuclear Physics: past, present and future", Vatican City (30/10-02/11, 2011)

S. Ferrara, Invited lecture at "Black Objects in Supergravity School, BOSS 2011", Frascati, Italy (9-13/05/2011)

Publications by LNF Authors in the Year 2011

State-space manifold and rotating black holes. Stefano Bellucci and Bhupendra Nath Tiwari.
Journal of High Energy Physics Volume 2011, Number 1, 118, DOI: 10.1007/JHEP01(2011)118

Topics in cubic special geometry. Stefano Bellucci, Alessio Marrani, and Raju Roychowdhury.
J. Math. Phys. 52, 082302 (2011); http://dx.doi.org/10.1063/1.3622851 (29 pages).

N=4, d=1 supersymmetric hyper-K?hler sigma models with isospin variables. Stefano Bellucci, Sergey Krivonos and Anton Sutulin. Journal of High Energy Physics Volume 2011, Number 2, 38, DOI: 10.1007/JHEP02(2011)038.

Strong Interactions, (De)coherence and Quarkonia. Stefano Bellucci, Vinod Chandra and Bhupendra Nath Tiwari. J. Phys.: Conf. Ser. 335 (2011) 012062 doi:10.1088/1742-6596/335/1/012062.

N=2 supersymmetric particle near extreme Kerr throat. Stefano Bellucci and Sergey Krivonos. Journal of High Energy Physics Volume 2011, Number 10, 14, DOI: 10.1007/JHEP10(2011)014.

Five-dimensional N=4 supersymmetric mechanics. Stefano Bellucci, Sergey Krivonos, Anton Sutulin. Proceedings of 19th International Colloquium On Integrable Systems And Quantum Symmetries (ISQS-19), 17-19 Jun 2010, Prague, Czech Republic, e-Print: arXiv:1012.2253 [hep-th]

Split attractor flow in N=2 minimally coupled supergravity, Sergio Ferrara, Alessio Marrani, Emanuele Orazi, Nuclear Physics B Volume 846, Issue 3, 21 May 2011, Pages 512–541

4D localization in Randall-Sundrum 2 supergravity and in Vasiliev theories, S. Ferrara, M. Porrati,

Physics Letters B, Volume 704, Issue 3, 13 October 2011, Pages 249–254

Attractors and first order formalism in five dimensions revisited, S. Bellucci, S. Ferrara, A. Shcherbakov, A. Yeranyan,Phys. Rev. D 83, 065003 (2011)

BLACK STRINGS, BLACK RINGS AND STATE-SPACE MANIFOLD, Bellucci, Stefano; Tiwari, Bhupendra Nath, International Journal of Modern Physics A, Volume 26, Issue 32, pp. 5403-5464 (2011).

CP(n) supersymmetric mechanics in U(n) background gauge fields. Stefano Bellucci, Sergey Krivonos, Anton Sutulin, Phys. Rev. D84 (2011) 065033, e-Print: arXiv:1106.2435 [hep-th]

N=4, d=1 Supersymmetric Hyper-Kaehler Sigma Models and Non-Abelian Monopole Background. Stefano Bellucci, Sergey Krivonos, Anton Sutulin, Published in JHEP 1102 (2011) 038.

Extended SUSY quantum mechanics: transition amplitudes and path integrals, Bastianelli, Fiorenzo et al., JOURNAL OF HIGH ENERGY PHYSICS, 2011, 1106-023

ON THE THERMODYNAMIC GEOMETRY OF HOT QCD, Bellucci, Stefano et al., Int.J.Mod.Phys.A26:43-70,2011

Freudenthal duality and generalized special geometry, Ferrara, Sergio et al., Physics Letters B Volume 701, Issue 5, 27 July 2011, Pages 640–645

GEOMETRIC IIA SUPERGRAVITY THEORIES IN THE STRING FRAME, Nicoletti, Riccardo; Orazi, Emanuele, International Journal of Modern Physics A, Volume 26, Issue 26, pp. 4585-4602 (2011).

ON ATTRACTOR FLOW AND SMALL BLACK HOLES, Sanjay Siwach, Bhupendra Nath Tiwari, Mod.Phys.Lett.A26:967-974,2011

ON REAL INTRINSIC WALL CROSSINGS, Stefano Bellucci, Bhupendra Nath Tiwari, INT J MOD PHYS A 26 (2011) 5171-5209

On the black-hole/qubit correspondence, L. Borsten, M.J. Duff, A. Marrani, W. Rubens, Eur.Phys.J.Plus 126:37,2011

Four curious supergravities. M.J. Duff, S. Ferrara, Phys.Rev.D83:046007,2011.

Generalized mirror symmetry and trace anomalies. M.J. Duff, S. Ferrara, Class.Quant.Grav.28:065005,2011.

Quaternionic Kahler Detour Complexes and N=2 Supersymmetric Black Holes, D. Cherney, E. Latini and A. Waldron, Communications in Mathematical Physics, Volume 302, Number 3, 843-873

Small black hole constituents and horizontal symmetry, Ceresole, Anna et al., J HIGH ENERGY PHYS , Volume 2011, Number 6, 78

Superconformal symmetry, NMSSM, and inflation Ferrara, Sergio et al. Phys. Rev. D 83, 025008 (2011)

THERMODYNAMIC GEOMETRIC STABILITY OF QUARKONIA STATES, Bellucci, Stefano et al., Int.J.Mod.Phys.A26:2665-2724,2011

Two-center black holes duality-invariants for stu model and its lower-rank descendants, Ferrara, Sergio et al., J. Math. Phys. 52, 062302 (2011)

Creation of matter in the universe and groups of type E7, Sergio Ferrara and Renata Kallosh, Journal of High Energy Physics Volume 2011, Number 12, 96.

Black Holes and First Order Flows in Supergravity, L. Andrianopoli, R. D'Auria, S. Ferrara and M. Trigiante, Supersymmetry in Mathematics and Physics, Lecture Notes in Mathematics, 2011, Volume 2027/2011, 17-43, DOI: 10.1007/978-3-642-21744-9_2

Two-centered magical charge orbits, Andrianopoli, Laura et al., Phys. Rev. D 83, 025008 (2011)

PG21: TOTAL and INELASTIC CROSS-SECTIONS at COLLIDERS

G. Pancheri (Senior Associate)

1 Total and inelastic pp cross-sections at LHC [1]

During the year 2011, the TOTEM, ATLAS and CMS collaborations have published their measurements of the total and inelastic cross-section at LHC. These measurements have been the object of our investigations in 2011. Following our studies of hadronic physics, on which we have been working for many years, our research has focused on understanding the phenomenological implications of the large distance behaviour of QCD through the study of hadronic cross-sections. This work was done in collaboration with Y.Srivastava and Andrea Achilli from Universiy of Perugia, A. Grau and O. Shekhovtsova from Spain and Rohini Godbole from India.

We have focused on the two following problems:

- calculation of the total cross-section at LHC in light of current measurements by TOTEM
- comparison of models with ATLAS and CMS data for the inelastic cross-sections for pp at LHC at current $\sqrt{s} = 7\ TeV$
- understanding of the structure, *the dip*, in the elastic differential cross-section measured by TOTEM at LHC

Work on the last problem is in progress and its resuts will be published in the year 2012. The first problems have been studied in details and results presented in the poster session of 2012 Lepton-Photon Conference in Bombay, and given as invited talks in number of Workshops and conferences (see list). In [1] we have examined the question of our predictions for the total cross-section as described by our model with mini-jets and soft gluon resummation, on which we have reported in previous years. Fig. 1 from [1] shows our recent major results : i) our band of predictions for σ_{total} (green band), which had appeared in Physics Letters B in 2008, includes the value measured by TOTEM, a value considered surprisingly high by various authors, ii) the inelastic cross-section in the central region (dotted line) is well described by our model and its extension to the diffractive region is well understood (blue lower band in the figure).

2 Other activities: historical research and Workshop organization

In 2011, I was the lead organizer of a Workshops on Linear Collider Physics in ECT* in Trento, 12-16 september 2011. This workshop was part of a series of workshops focused on Linear Collider Physics, which was started in Frascati 5 years ago. Proceedings for this Works are under publication as part of Frascati Physics Seriers. I am member of the Organizing Committee for the yearly Bruno Touschek Memorial Lectures (BTML). This year BTML were held in Frascati, on December 1, 2011, together with celebration of 50 year anniversary of AdA, the first e+e- colliding beam.

A major scholarly activity in 2011 has been research on the life of Bruno Touschek and his contribution both to the birth of electron positron colliders as well as to the development of theoretical physics in Rome and Frascati during 1950 and 1960. Together with Luisa Bonolis, I have published an article in EPJ for History [2], for which I was also awarded, together with Luisa

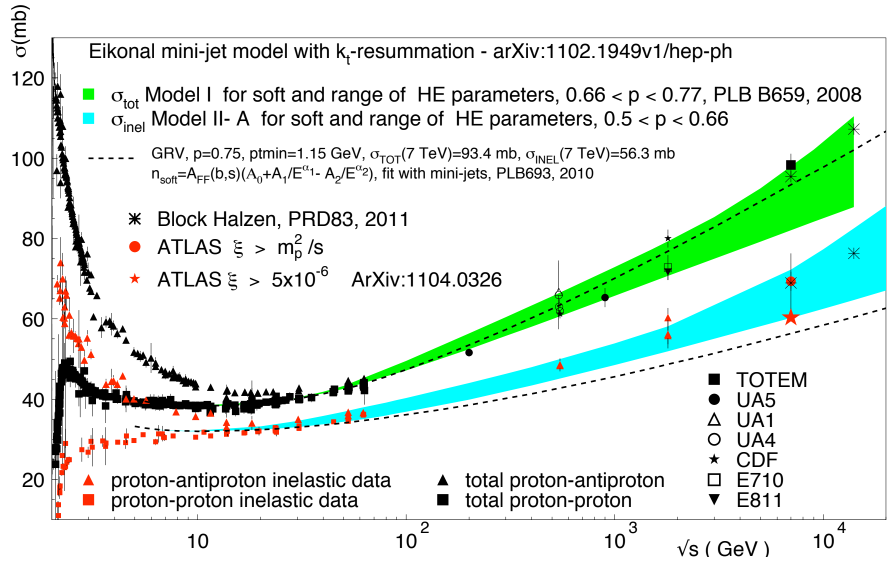

Figure 1: *Comparison of data for total and inelastic cross-sections for pp, and $\bar{p}p$ with our description, based on eikonal minijet model with soft gluon k_t-resummation* [1].

Bonolis, a prize from Societa' Italiana di FIsica (SIF). This article was presented at the annual meeting of SIF and at the BTML2011.

In addition, I have participated to outreach activities, such as giving a talk on "Donne nella Scienza" at the Istituto di Studi Germanici di Villa Sciarra, in Roma.

3 Contributions to Conference Proceedings in 2011 and other invited talks

1. G. Pancheri, R.M. Godbole, A. Grau, Y.N. Srivastava, *A model for probing large distance behaviour in high energy collisions*, Nucl. Phys. Proc. Suppl. **219-220** (2011) 239-246.

2. G. Pancheri and Y.N. Srivastava,*Probing long distance QCD effects at LHC through the total cross-section*, PoS QCD-TNT-II:033,2011.

3. R.M. Godbole, A. Grau, K.A. Mohan, G. Pancheri, Y.N. Srivastava, *LC10 Hadronic backgrounds from two photon processes at e+e-* Nuovo Cim.**034C** (2011)129-138.

4. Y.N. Srivastava, A. Grau, G. Pancheri, O.Shekhovtsova, *Modeling pion and nucleon total cross-sections*, AIP Conf. Proc. **1350** (2011) 211.

5. Poster presentation on *Modeling large distance QCD via kt-resummation in total and inelastic cross-sections at LHC*, 2012 Lepton-Photon Conference, Bombay India.

6. 29 August 2011, invited talk on *Total and Inelastic cross-sections at LHC or modeling large distance QCD via kt-resummation in total cross-sections*, Bombay IIT, India

7. 29 September 2011, invited talk on *Bruno Touschek e AdA: fisico teorico e padre delle collisioni fra elettroni e positroni* at L'Aquila, Riunione Annuale SIF

8. December 1st 2011, invited talk on *Bruno Touschek and Wideroe: the birth of e+e- idea*, at Frascati, BTML2011

9. 20 October 2011, invited talk on *Le Donne nella Scienza: passato, presente e futuro*, at Villa Sciarra, Roma

References

1. A. Achilli , R. M. Godbole, A. Grau , G. Pancheri, O. Shekhovtsova, Y. N. Srivastava, *Total and inelastic cross-sections at LHC at sqrts = 7 TeV and beyond*, Phys. Rev. **D84** (2011) 094009.

2. L. Bonolis and G. Pancheri, *Bruno Touschek: Particle physicist and father of the* e^+e^- *collider*, Eur. Phys. J.**H36** (2011)1-61.

PI-11

F. Palumbo (Resp.)

Not received

BEATS

A.L. Bacci, M. Bellaveglia, A. Clozza, G. Di Pirro, M. Ferrario, A. Gallo, T. Levato, E. Pace,
A.R. Rossi, C. Vaccarezza (Resp.)
Laboratori Nazionali di Frascati
P. Oliva
Sezione INFN Cagliari
M. Gambaccini
Sezione INFN Ferrara
V. Petrillo, L. Serafini
Sezione INFN Milano
U. Bottigli, P. Delogu, D. Giulietti
Sezione INFN Pisa

1 Introduction

The Thomson scattering X-ray sources show relevant features for several applications due to the capability of producing intense, quasi-monochromatic, tunable X-ray beams, after collimation, still with a reasonably small size apparatus. Applications to medical physics are straightforward, in particular in mammography where dose control in screening programs is the main relevant issue. The fluence rate is low if compared to those typically achievable by synchrotron sources,but still compatible with the requirements of radiography, moreover the facilities based on TS can be in perspective much more compact and less expensive than synchrotrons, well in excess of one order of magnitude in both items. Hence TS sources represent an appealing alternative to conventional X-ray tubes.
The PLASMONX Thomson source combines a high brightness electron beam (SPARC [5]) and a high intensity laser beam (FLAME project [4]) see Fig:1; the source will be able to provide a high flux (up to $10^{10}\gamma/s$) of quasi-monochromatic photons and the mean energy can be varied from 20 keV to hundreds keV by changing the electrons energy.
The BEATS experiment is an imaging application of the Thomson radiation used on a standard mammographic phantom devoted to improve the contrast between normal and cancerous tissues while lowering the absorbed dose. Theoretical and experimental studies on the mammographic imaging suggest that the ideal X-ray source for mammography should produce a low tunable energy spectrum, with a narrow energy band, in the 17-20 keV energy range [1, 2], and that the transfer of the radiological potential of monochromatic sources to a clinical diagnosis is advisable together with the reduction in size and cost compared with the synchrotron facility. In the 2011 the X-ray detection apparatus has been set up for the Thomson source characterization at LNF ; in spring 2012 it will be installed in the SPARC bunker and the first collision experiment is foreseen in fall 2012.

2 The Thomson scattering process

The Thomson scattering(TS) is the electromagnetic process in which each electron absorbs one (linear Thomson scattering) or more (non linear Thomson scattering) photons from (typically) a laser pulse, emitting one photon. If the electrons are ultra relativistic the scattered radiation looks frequency upshifted and it is emitted forward with respect to the motion of particles, in a small cone of aperture roughly given by the inverse of their Lorentz relativistic factor. The physics of TS is quite complex in the non linear regime which holds when the density of the incoming photons is large enough, i.e. when the laser pulse strength $a_0 = 8.5 \times 10^10(I\lambda^2)^{1/2}$ reaches unity, being I and λ the pulse intensity and the wavelength, respectively. At intensities above the so-called relativistic

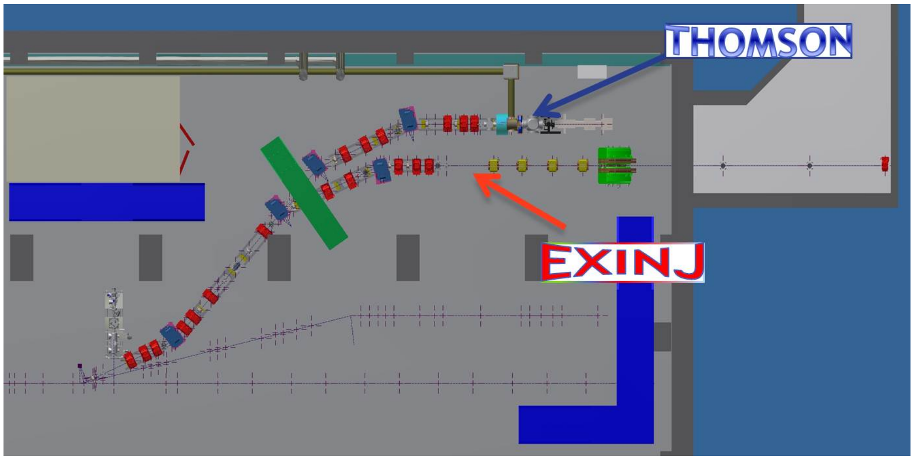

Figure 1: *CAD drawing of the PlasmonX electron beam transfer lines layout.*

intensity $I\lambda^2 = 10^{18} mm^2 W/cm^2$ the extremely intense electric field makes the electrons quivering speed approaching the light speed, making the magnetic field relevant for dynamics thus generating a complex particle motion.The computation in the far-field of the scattered photons distribution Ng of pulsation ω can be performed in the classical regime provided that the energy of the electrons is far below tens of GeV, as it is our case . A detailed description of the analytical computation of the scattered radiation distribution valid in the case of a planar, flat-top pulse can be found in [6]; the analytic results show that the spectral distribution of the photons emitted by a single particle is almost completely correlated with the scattering angle and it is composed by a sum of harmonics

$$\frac{d^2 N_\gamma}{d\omega\Omega} \cong \sum_{n-1}^{\infty} V(n,\theta,\phi)\delta(\omega - n\omega_f) \tag{1}$$

of the fundamental pulsation:

$$\omega_F \cong \omega_L \cdot 4\gamma^2/(1+\gamma^2\tilde{\theta}^2 + a_0^2/2) \tag{2}$$

being γ the Lorentz relativistic factor, ω_L the laser pulsation, $V(\theta,\phi)$ a structure function with complex dependance on particle energy, incidence and scattering angles (θ_e, ϕ_e), see [**?**] What is relevant is that in the linear regime ($a_0 \ll 1$), that is our case, only one harmonic is produced while with a weak non linearity ($a_0 \approx 1$) only a few harmonics are generated.

3 The electron beam

The electron beam generation system must be able to produce and transport electron bunches characterized by an energy $E_{beam} \approx 30MeV$, (corresponding to $\gamma = 60$), reaching the focal spot with a transverse size comparable with the laser focal spot size ($\sigma_x, y \approx 810\mu m$) and minimizing the hourglass effect [7], in order to allow the optimization of the geometrical overlapping with the laser pulse on the whole interaction duration. These considerations imply severe constraints on the longitudinal energy spread and on the transverse emittance of the electron beam at the interaction point: the SPARC-LAB Thomson source is meant to produce high brightness electron beam able to accomplish to the experiment requirements, the electron beam transfer lines provide the beam transport from the phoinjector up to the interaction point preserving the 6D-phase space characteristics and providing the required final strong focusing for the interaction with the laser pulse. In Fig. 2 the transverse beam rms size evolution is reported for the reference working point setup starting from the photoinjector down to the IP as obtained from the simulations performed with the Tstep code tracking 15 kparticles, for a beam energy of 30 meV, and a quite high value for the starting normalized emittance $\epsilon_{nx,y} \approx 2.7\mu m$.

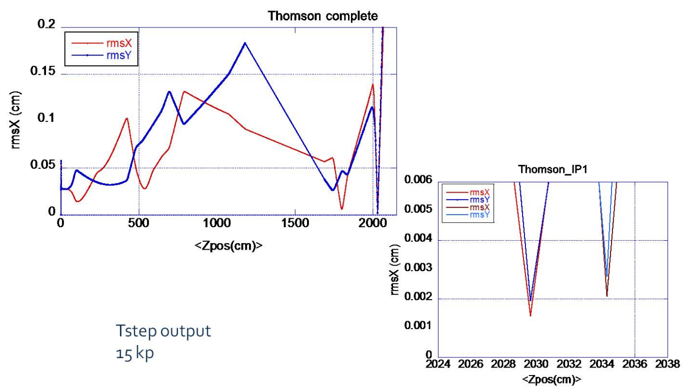

Figure 2: *Rms beams sizes evolution along the transfer line (left), and detail of longitudinal "tunability" of the beam waist at the interaction point.*

4 The source simulation

The properties of the photons emitted by the whole electron bunch can be simulated by summing up the intensity contributions of each electron (i.e .in the incoherent regime). To do that we have employed the Thomson scattering simulation tool $(TS)^2$ code developed by P. Tomassini *et al* [3]. The code works as follows: the secular trajectory of each particle of the bunch is first computed by neglecting transverse ponderomotive effects (this approximation is fully consistent with the laser pulse and electron bunch parameters considered in this paper, see Tomassini et al. [6]. Since the analytical outcome sketched in Eq. 1 and 2 are valid only for the case of planar long flat-top laser pulse, the code decomposes the pulse in a sequence of single cycles of the laser pulse, each cycle having its own phase shift and intensity. While the particle is moving along its secular path, it interacts with different cycles of the pulse and the coherent summation of the radiation emitted in each cycle gives rise to the radiation emitted during the entire interaction.

5 The TS laser pulse parameter optimization

The laser used in this experiment is the FLAME laser at LNF: a Ti-sapphire laser able to deliver pulses with energy up to 6J, whose duration can vary from a few ps down to 20 fs, with a repetition rate of 10Hz [16]. In our case to fit the electron bunch length the laser pulse willbe only partially compressed to attain few ps duration. A well optimized laser is meant to generate the highest X-ray flux while keeping the relative energy spread of the radiation below 20% FWHM for the fundamental harmonic. An additional requirement is that high order harmonics should be as low as possible in order to prevent their enhancement after filtration.
Free parameters are:

- pulse focusing size w_0 (waist size),

- pulse duration T,
- acceptance angle θ_M of the scattered radiation.

Two, competitive phenomena play the major role: at very small focusing size the diffraction makes the laser pulse to spread transversally in a longitudinal size $2Z_R = 2\pi w_0^2/\lambda$ smaller than the electron bunch length σ_L, making the queue of the bunch to interact with a poorly intense laser pulse; on the opposite side, a too large focusing size reduces the pulse intensity and thus the scattered radiation yield. Further the pulse duration T is linked to the non linear phenomena that appear at high pulse intensity while the diffraction effect imposes an upper limit to T.
The requirements for the maximum energy spread and high order harmonics maximum intensity impose strong constrain on the maximum collecting (or acceptance) angle θ_M, Since the energy of a scattered photon is almost completely correlated with the scattering angle, see 2, in a linear or weakly non linear regime it comes out that by collecting the radiation within a cone of half aperture $\theta_M = 1/\gamma$ an overall energy spread exceeding 50% is obtained. As result of the optimization process described in detail in [8] a laser pulse of waist size $w_0 = 15\mu m$, duration $T = 6ps$, intensity $I = 2.3 \times 10^{17} W/cm^2$ and amplitude $a_0 = 0.33$ has been chosen to collide with the electron bunch. The backscattered radiation will be collected within a cone of aperture $\theta_M = 8mrad$, yielding a flux of $1.5 \times 10^8 photons/shot$ with an energy spread of 20% FWHM. In Fig. 3 the spectral-angular (integrated in the azimuthal angle ϕ) distribution of the collected radiation is shown.The fundamental at energy about 20 keV and the second harmonics are clearly visible while the third harmonic is much less intense. Note the dependence of the energy on the scattering angle.

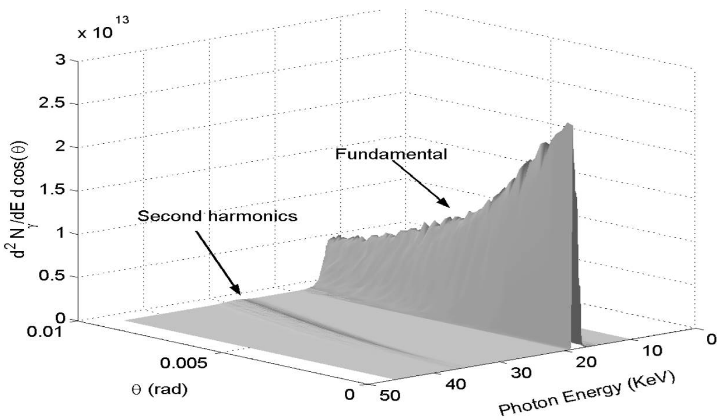

Figure 3: *Spectral-angular(integrated in the azimuthal angle ϕ) distribution of the collected radiation for the optimized parameters $w_0 = 15\mu m$ and duration $T = 6ps$ $\theta_M = 8mrad$*

6 X-ray imaging simulation

The X-ray spectrum produced by the simulation code $(TS)^2$ is used to generate images of a breast equivalent phantom, in order to evaluate image quality. A set of Monte Carlo simulations have been performed to explore the image quality of a mammographic phantom upon the parameter variation [8]; the code described in [9] has been used to generate the images: in the spectral distribution of the Thomson source , Fig. **??** a central area with the mean energy $E_{mean} = 20.6keV$ and standard deviation of 1.7 keV has been selected, the fluence is supposed to be uniform over the phantom. The object to be imaged is a phantom made of 50% adipose and 50% glandular tissue. For elemental composition and density of adipose and glandular tissue values from ICRU Report 44 [10] are used. The thickness of the phantom is 5 cm.Tumor-like masses of thickness 1, 2, 5 and 10 mm are simulated. Tumor-like masses are supposed to have the same chemical composition of glandular tissue and a higher density (1.044g/cm3) [11]. The considered detector is a digital flat panel detector based on amorphous selenium (a-Se). The absorber is a direct converting a-Se of 0.25 mm of thickness, with a density of $4.28 g/cm^3$. These parameters are typical for mammographica-Se flat detectors. Other detector layers and structures are supposed to be negligible in the detection process [11]. Noise is considered to follow Poisson statistics. The pixel pitch is $100\mu m$. The image quality is evaluated in terms of dose efficiency or quality factor Q [11], defined as the ratio of the squared signal-to-noise ratio (SNR) to the mean glandular dose (MGD) [**?**, **?**]. Hence:

$$Q = \frac{SNR^2}{MGD} \tag{3}$$

The dose efficiency Q is expressed in arbitrary units in order to compare the imaging performances of different spectral distributions and the influence of detector resolution and blurring and the effect of any visual system are neglected [11]. In Fig. 4 the dose efficiency calculated for the TS source is reported as a function of detail thickness. For comparison Q values are also reported for monochromatic sources at optimal energy and for the X-ray tube.

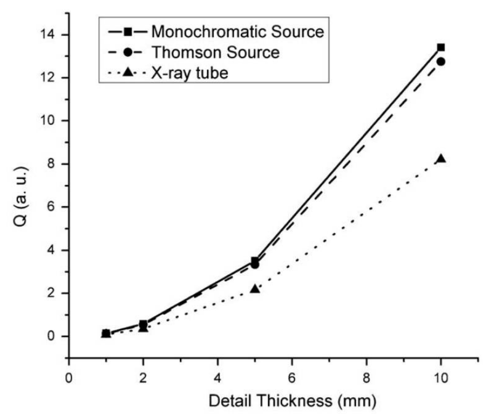

Figure 4: *Dose efficiency of Thomson scattering source, as a function of detail thickness. For comparison Q is also reported for the optimal monochromatic energy and for the X-ray tube for digital mammography.*

It can be seen that Q values forTS source are $5 \div 6\%$ smaller than maximum Q values obtained by monochromatic beams. On the other hand X-ray tube shows dose efficiencies that are about 40% smaller than optimal values. The percent reduction of Q values (with respect to peak Q values for the same detail) for the TS source and for the X-ray tube depends on the discrepancy between the mean energy of the beams and the optimal energy to image the detail. The mean energy of the TS source (20.6 keV) is very close to the optimal energies to image the details (between 20.3 and 20.7keV) while the mean energy of the X-ray tube is only 17.7 keV. The different performances of the TS source and the X-ray tube are also due to the different energy spreads of the two beams: the TS source presents an energy spread of 1.7 keV, while the spectrum of the polychromatic beam differs significantly from zero in the range $10 \div 30 keV$.

7 The Experimental apparatus

In 2011 the BEATS apparatus has been set up and installed, a picture of the X-ray beamline is shown in Fig. 5.

(a) (b)

Figure 5: *X-ray beamline, (a) detail of the apparatus for collimation, monitoring and characterization; (b) a view of the complete x-ray beamline*

The first stage of the X-ray beamline is for x-rays monitoring and characterization, in particular this system consists of:

- first wide collimation and lead shutter for beam stopping;
- a rotating collimator holder that allows to reduce the angular divergence of the beam, equipped with six different collimator corresponding to angular acceptance varying from about 9 mrad to 1 mrad;
- a free-air ionization chamber, used as a x-ray beam monitoring;
- two additional filter/collimator holders with six available position each, for beam filtration or further collimation;
- a removable device based on a silicon PIN diode for X-ray flux measurement.

In Fig. 5 is also shown the table that will provide the support for imaging detectors and sample. An additional table will be placed downstream the beam to permit the study of imaging techniques such as free-propagation phase contrast that require longer propagation distances.

7.1 X-ray beam monitor

The monitoring of the production of x-ray pulses, in order to verify the correct operation and the pulse-to-pulse intensity repeatability, is provided by a ionization chamber that collects the charge produced in air by radiation, without affecting the beam. This device was designed and assembled by Ferrara research unit and has been tested for stability and linearity at Larix Laboratories of Ferrara University, at University of Pisa and at the ELETTRA synchrotron facility (SYRMEP beamline) both with polychromatic and monochromatic beams and continuous and pulsed irradiation. A picture of the chamber and of the electrometer used for acquisition is shown in Fig.6. The minimum number of photons per pulse that produce a readable signal is about 10^6 photons with an average energy of 20 keV.

Figure 6: *Xray fluence measurement system in detail.*

7.2 PIN diode system for flux measurement

The current produced in a PIN diode by an x-ray beam is proportional to the rate of energy released in the photodiode active area by the radiation. The rate of energy released in a silicon slab depends on the incident photon energies and the flux. Owen et al. [**?**] demonstrate that it is possible to measure the flux of a monochromatic x-ray beam impinging on the diode, multiplying the photon induced current by a coefficient calculated from the energy absorbed in the silicon layer. For our measurements a PIN diode HAMAMATSU mod. S3584-09 operating in photo-voltaic mode (*i.e.* without applying a reverse polarization) is used. The sensitive area of this detector is 28 x 28 mm^2. The diode is mounted in a metallic box with an entrance window made of an aluminum-coated polymide film to avoid photocurrent production by visible light. The x-ray absorption of the entrance window is negligible in the energy range of interest. A picture of the system is shown in Fig. 7

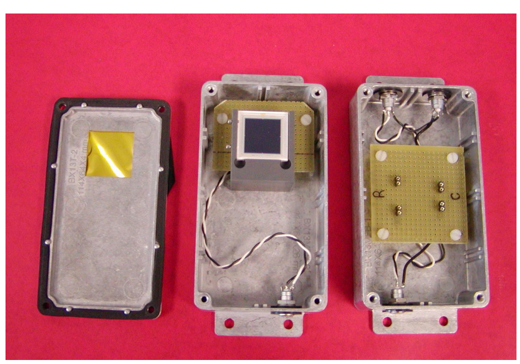

Figure 7: *Silicon PIN diode system for x-ray flux measurement.*

The photocurrent produced is measured by an electro-meter Keithley mod. 6517B (Keithley Instruments Inc., Ohio, US).

Table 1: Diode calibration coefficients K, measured at synchrotron facility and evaluated from theoretical model.

E (keV)	K (ph/C)	K_T (ph/C)	Ratio
16	$2.99 \pm 0.09 \times 10^{15}$	3.04×10^{15}	1.02
18	$3.43 \pm 0.10 \times 10^{15}$	3.56×10^{15}	1.04
20	$4.14 \pm 0.12 \times 10^{15}$	4.18×10^{15}	1.01
22	$4.79 \pm 0.14 \times 10^{15}$	4.91×10^{15}	1.03
24	$5.50 \pm 0.16 \times 10^{15}$	5.73×10^{15}	1.04

If Q is the charge created by the interaction of a flux φ of x-rays with an energy $h\nu$ (¡ 35 keV) on a silicon diode, the photocurrent produced is $I = \varphi Q$, and the $photoconversionratio$ K can be expressed as:

$$K = \frac{\varphi}{I} = \frac{\epsilon}{e[1 - \exp(-\mu_{pe} t])]}, \tag{4}$$

where ϵ is the average energy to create an electron-hole pair, e is the electron charge and μ_{pe} is the photoelectric linear attenuation coefficient of silicon. This photoconversion factor K can be evaluated theoretically or measured, for this reason the system was previously tested at the ELETTRA synchrotron facility (Trieste, Italy) with monochromatic x-rays in the energy range between 16 and 24 keV. Diode response has been calibrated comparing its signal to the air-dose signal provided by two suitable free-air ionization chambers. The coefficients K to convert the current produced in the diode to the flux are shown in Table 1 in comparison with the ones predicted by the theoretical model K_T, showing good agreement.

The minimum number of photons per pulse that produce a readable signal is about 10^3-10^4 photons with an average energy of 20 keV. PIN diode have proved to work properly at high x-ray fluxes (up to 10^{12} ph/s) but in continuous irradiation condition. High instantaneous fluxes of a pulsed source, in the case of BEATS experiment $< 10^{20}$ ph/s, could produce in the diode a charge density extremely high, leading to recombination and partial collection of charge, so to an underestimation of the real number of interacting photons. Sources with an instantaneous x-ray flux as high as needed in order to perform test on our devices are not available, and a preliminary test on a pulsed laser (800 nm) showed the possibility to be in such a regime of partial collection. For this reason is ongoing the measure of diode response coupled to a slow scintillator (CsI) in order to increase the time of charge production in the diode and decrease the istantaneous charge density.

7.3 System for energy distribution evaluation

The use of traditional spectroscopic techniques based on single photon detection, either with photomultiplier coupled to scintillator or solid state device, is very difficult because of the extremely high instantaneous flux produced by the source. In fact with this kind of detectors it is not feasible to operate with sub-picosecond data acquisition time. In order to evaluate the energy distribution of the x-rays produced a technique based on the analysis of the diode photocurrent produced by beam filtered with suitable k-edge materials has been implemented [13]. Using filters of Mo, Nb Zr and Al with thicknesses properly selected it is possible to obtain a measure of the energy distribution in an energy range from 16 to 22 keV. The technique was also tested measuring the energy distribution of an x-ray beam having a spectrum similar to the BEATS expected one by using a tungsten anode x-ray tube properly filtered and powered. In Table 2 is shown a comparison of the normalized energy distribution measured with a traditional HPGe detector φ(E) and the one measured with k-edge technique φ_{k-edge}(E). It is possible to notice that the two energy distribution

Table 2: Energy distribution of the x-ray tube measured φ(E) and obtained from PIN diode current φ_{PD}(E) (normalized data).

E (keV)	φ(E) (norm.)	φ_{k-edge}(E) (norm.)
<18	0.204	0.191
18-19	0.169	0.158
19-20	0.202	0.198
>20	0.425	0.451

are in good agreement (maximum discrepancy about 7%).

References

1. M. Gambaccini *et al*, Nucl. Instr. and Meth. in Phys. Res. A 365 (1995) 248-254.
2. P. Oliva *et al*, Med. Phys. 36 11, 5149-61, 2009
3. P. Tomassini *et al*, IEEE Trans. on Plasma Science Volume: 36 Iss. 4
4. L.A.Gizzi *et al* Eur. Phys. J. ST 175 3-10, 2009.
5. M. Ferrario *et al* ICFA Beam Dyn. Newslett. 46 49-58, 2008
6. P. Tomassini, A.Giulietti, D.Giulietti, L.A.Gizzi, Appl. Phys. B 80 (2005) 419
7. R.J.Loewen, SLAC-Report-632,June,2003
8. P. Oliva *et al*, Nucl. Instr. and Meth. in Phys. Res. A 615 (2010) 93-99
9. P. Oliva *et al*, Nucl. Instr. and Meth. in Phys. Res. A 608 S106 (2009)
10. ICRU, Tissue substitutes in radiation dosimetry and measurement, Report 44 of the International Commission on Radiation Units and Measurements, Bethesda, MD 1989.
11. J.P. Bernhardt, T. Mertelmeier, M. Hohisel, Med. Phys. 33 (11)(2006)4337.
12. R.L. Owen *et al*, Journal of synchrotron radiation 16 (2009) 143-51.
13. P. Cardarelli *et al*, submitted to J App Physics

GEMINI:
GEM Instruments for Nuclear Interactions

A. Balla, G. Cappuccio, G. Corradi (Tecn.), G. Claps, D. Dabagov, D. Hampai, F. Murtas (Resp.), L.Quintieri, D. Tagnani (Tecn.)

1 Introduction

The main tasks of this R&D is the development of different detectors basted on GEM technologies essentially for beam diagnostics. The use of GEM foils for detector construction started in Frascati on 2002 with the R&D for LHCb muon chambers M1R1. Ever since, several triple GEM chambers have been built for different applications. The results obtained in several beam tests show high performances: high rate capability ($> 50MHz/cm^2$), good time resolution ($\sim 4ns$), good space resolution $O(200\mu m)$, and good aging resistance after $2C/cm^2$ of integrated charge. The GEMINI R&D is devoted to the developments on detectors for neutrons and hadrons and the construction of readout electronics and power supply. The scientific activity of GEMINI for the 2010-2011 can be resumed in these five main items:

- Developments on a Compact TPC for high intensity beam;
- Characterization and installation at FTU (ENEA) of a fast neutron flux monitor;
- Characterization and installation at ToreSupra (Cadarache CEA) of a X ray monitor;
- Triple GEM monitors for fast neutrons tested at ISIS RAL;
- Design and construction of a new HV Power Supply for triple GEM detectors
- Design and construction of a new Readout Electronics FPGA based ;

2 Construction and test of a Compact TPC for beam monitoring

A compact Time Projection Chamber (TPC) has been designed, built and tested, for beam monitoring. The main idea in developing this detector is to place a standard triple GEM detector parallel to the beam and to use it as a time projection chamber, by enlarging the drift gap. In this way the material crossed by the particle is particularly small (only two kapton windows) and the beam position measurement could be more precise, $O(50\mu m)$, in the coordinate along the drift, by measuring the time of arrival of the electron clusters. Moreover, a very compact detector can be realized, using standard $10 \times 10cm^2$ GEM foils and a drift gap of 4 cm. The 128 readout channels can be organized in two configuration :

- a matrix of 8×16 pads $3x6mm^2$ each
- two array of 64 pads $0.5x0.5mm^2$ each ;

obtain a good resolution O(1 mm) or better also in the other two coordinates.

The TPC, working without a magnetic field, has been operated with a gas mixture $ArCO_2$ (70/30) or $ArCO_2CF_4$ (45/15/40) at a Gain 10^4. The high rate capability of GEM technology allows the use of this monitor not only for single tracks events but also for multiparticle beam. The electron drift velocity measured at $2KV/cm$ in the CF based gas mixture was $5.3\mu m/ns$. One similar device has been used also for the monitoring of proton and ion beam in UA9 exsperiment for the monitoring of channeled beam. Thanks to a small material budget crossed by the

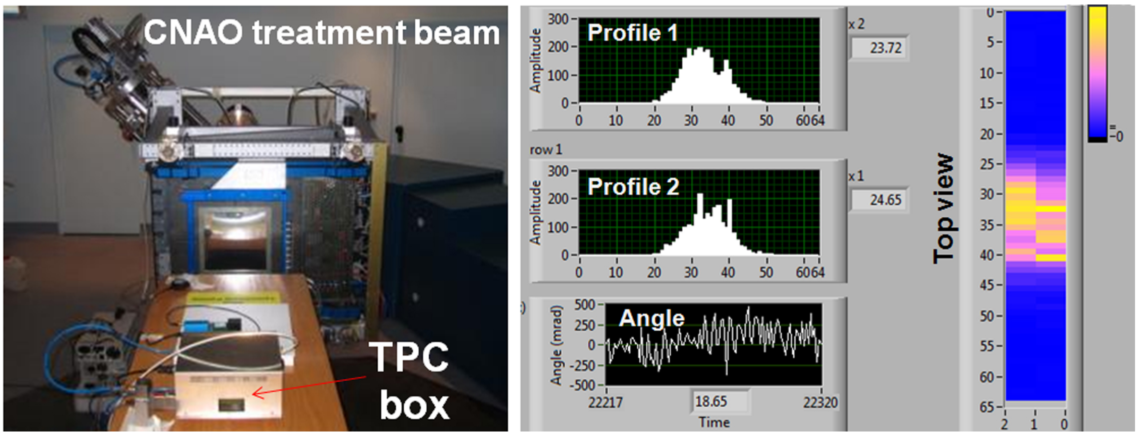

Figure 1: *On the left the GEM TPC placed on the treatment table at CNAO; on the right the beam profile and beam angle measurement vs time.*

particle ($0.2\%X_0$) and the 3D reconstruction of the particles track, its use for ion beam monitor in hadrotherapy. We test this detector in June 2010 at CNAO in Pavia on a high intensity 400 MeV proton beam. The beam profile can be seen in Fig. 1. The intensity of the beam can be reconstruct with the current measurements made through the nanoammeter of our new HVGEM module descrbed below. This results have been shown by F.Murtas at IEEE NSS Conference in Valencia in October 2011 talk.

3 Characterization and installation at FTU (ENEA) of a fast neutron flux monitor

In 2010, a prototype $10 \times 10cm^2$ made of a triple GEM with a cathode of aluminum and polyethylene, has been placed in front of one port of Frascati Tokamak Upgrade. The neutron produced by the burning plasma, impinging on polyethylene, is converted in proton that releases its final energy inside the gas, producing electrons. The 128 readout pads, organized in a matrix 16×8, allow to create an intensity map of the fast neutrons. This detector was characterized in 2009 showing a good linearity up to $12MHz/cm^2$ (the maximum flux for Frascati Neutron Generator). The detector efficiency is not high (4×10^{-4}), but enough for this type of measurements. The active area of this monitor has been divided into two parts with the polyethylene converter optimized for the two energies (2.4 and 14 MeV from DD and DT nuclear interaction respectively)

Thanks to the strength signal released by the proton inside the gas, the low gain settings of the chamber allow to have a good rejection to photons produced by the radio activation of material around the detector.

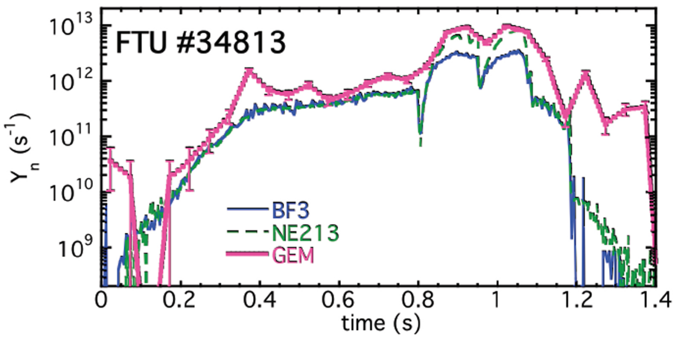

Figure 2: *GEM signal compared to the neutron monitor signal in FTU deuterium discharge*

Fig.2 shows the comparison between the GEM and neutron monitors signals in plasma discharge: note that the GEM and NE213 are pretty close in the high neutron emission phase (in which the BF3 detector saturate). The tests on FTU have demonstrated that the detector can operate as a neutron diagnostic monitor in a tokamak environment. Future activity should focus on the design of a new GEM detector prototype and in particular on the optimization of the neutron converter, the use of new read-out electronics board and reducing as much as possible the distance of the GEM from the plasma for fast neutron flux maximization. The detailed results has been described on EFDA Final Report WP10-DIA-04-01-02

4 Characterization and installation at ToreSupra of a X-ray monitor;

In 2011 a triple GEM has been used as an X-ray tomography system and was installed at the tokamak Tore Supra in Cadarache (CEA) for the burning plasma diagnostic. The ultimate aim is to use this information produced by this system in real time for visualization but also potential feedback, with a particular emphasis on the optimization of the reconstruction technique.

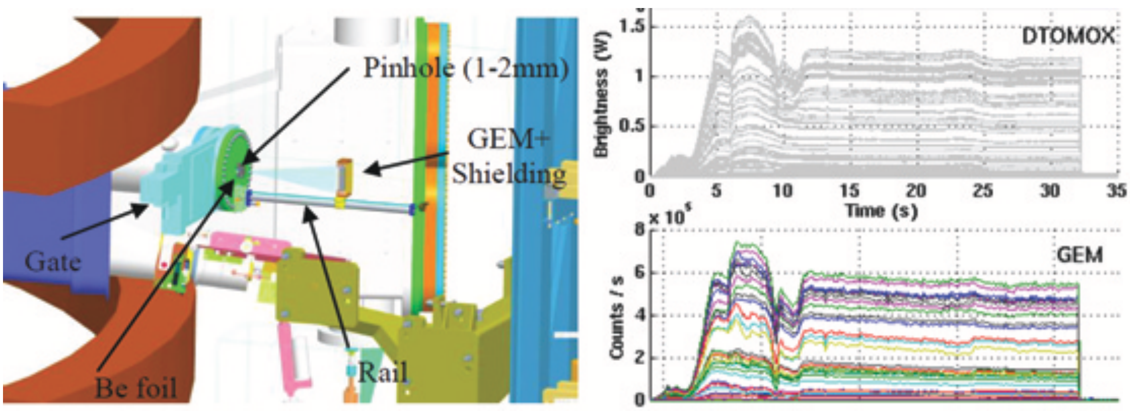

Figure 3: *Installation of GEM in Tore Supra (left). Comparison between DTOMOX and GEM time traces (right)*

Various GEM acquisitions were then performed during the 2011 experimental campaign at Tore Supra. In total more than 150 shots were acquired, some of them lasting several minutes. The acquisition system and the high voltage power supply were remarkably stable during several hours of continuous functioning. As an example of such acquisition, a comparison of the time traces of each GEM pixels with the time traces of DTOMOX is shown on Fig. **??** with a good agreement between the two diagnostics.

5 Triple GEM monitors for fast neutrons tested at ISIS RAL

Fast neutron beams available at large scale facilities are becoming strategic for industrial applications, especially in relation to the assessment of radiation hardness of silicon-based nano-sized electronic chips. A stringent request for neutron beam lines dedicated to chip irradiation is the possibility to monitor and characterize the neutron beam above 1 MeV (the more concerning energy region of the spectrum) with a spatial resolution in the millimeter range or below.

A triple Gas Electron Multiplier (GEM) detector was developed as a fast neutron beam monitor for the ISIS spallation neutron source in UK. The test on beam was performed at the VESUVIO beam line, by placing the detector on the primary flight path (see Fig. 4). The spatial distribution of the neutrons was measured in real time in the energy region between 2 and 800 MeV achieving a spatial resolution of a few millimeter thanks to the patterned readout of the detector.

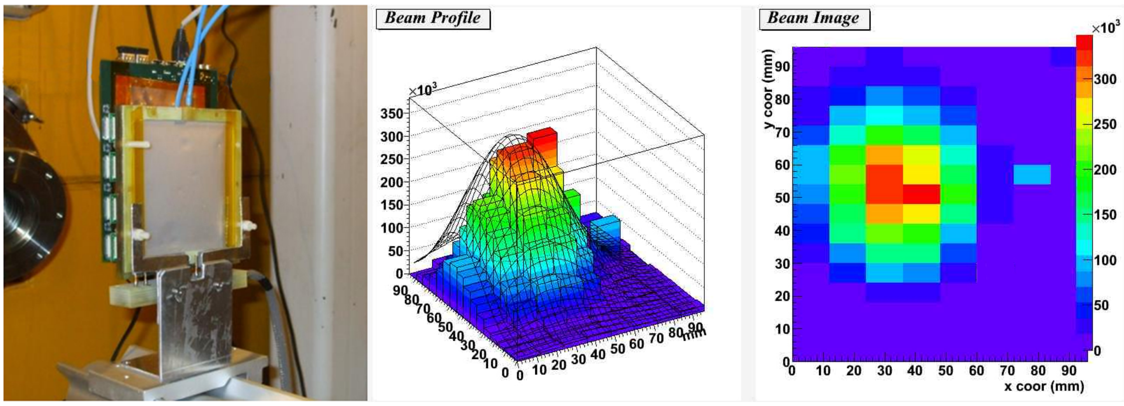

Figure 4: *On the left the teh experimental setup; on the right the online beam spot monitor*

Figure 4 shows the intensity profiles along the x and y directions (the plane perpendicular to the neutron beam axis), over an integrated proton beam current of $355.4\mu Ah$ (with an average proton current of $177.7\mu Ah$).

Also a time scan of the beam was performed: the start signal for time of flight recording (the ISIS clock) was delayed over $3\mu s$ in steps of $\Delta t = 100ns$ and the count rate was measured within a time window $\Delta t = 100ns$. The rate distribution over the whole set Δt chosen is shown in Figure 5. In this time scan it is well visible the double bunch structure of the neutrons originating by the protons hitting the spallation target. Because of the time structure of the proton beams, the arrival time onto the detector cannot be directly associated to the neutron energy. These initial tests show the high potential of the device as a fast-real time neutron beam monitor featuring a few millimeter spatial resolution. The detector has also a good photon rejection as shown in Fig 5. The performance of the device can be further extended towards spectroscopic capabilities, by characterizing its response function over a wider energy region by properly optimizing the cathode and polyethylene thicknesses. Monte Carlo simulations and new tests on beam are then envisaged to achieve this goal in the next future.

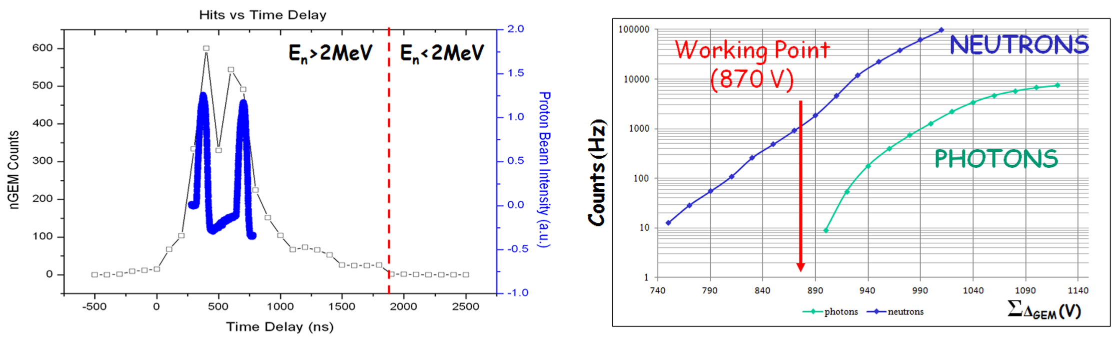

Figure 5: *On the left the comparison between the neutron flux and the two proton bunches ; on the right the detector efficiency vs the HV settings.*

6 Development in electronics

6.1 Design and construction of a new version of HVGEM for triple GEM power supplying.

The HVGEM is a seven stage power supply specifically designed for this type of detector; it can be used also for thick GEM or Micromegas. Two type of stage power supply have been designed in a modular way: - 1400 Volt and $90\mu amp$ - 750 Volt and $180\mu amp$. A new version has been designed in 2009, following the NIM standard (two units modue): each single HV stage can be plugged on the NIM mother board, making the HVGEM more flexible and adaptable to different detectors. The module can be controlled through CANbus and USB port. A version controlled by ethernet is foreseen for 2013.

6.2 New Front End Electronics.

Up to now our GEM detectors have been readout with electronics based on Carioca GEM chip designed and realized for LHCb muon Chambers in 2007. The boards with two 8 channel chips are modular and easy to plug on the backplane of our detectors. In collaboration with Milano Bicocca University a new chip specifically thought for GEM detectors is under construction. It will be able to measure the total charge released in the active area with a good dinamics : from $20fC$ up to $1pC$ with a maximum rate of 2 MHz per channel. The total width of the LVDS signal will be propotional to the charge with a resolution better than 20%. After the tests of this 8 channel chip, a new design with 32 channels is foreseen for 2012.

6.3 Design and construction of a Motherboard FPGA based.

In order to have a more flexible and portable system, a new mother board has been designed by with an FPGA, that will be able to analyze the LVDS signals coming from the FEE board. Two type of data acquisition can be implemented: 128 scalers and/or 128 multihit TDC channel with a resolution of 2 ns, sufficient to record the time drift of electrons along the 4 cm drift. The first three boards has been succesfully testes during 2010 in different sperimental setup. (see fig 6).

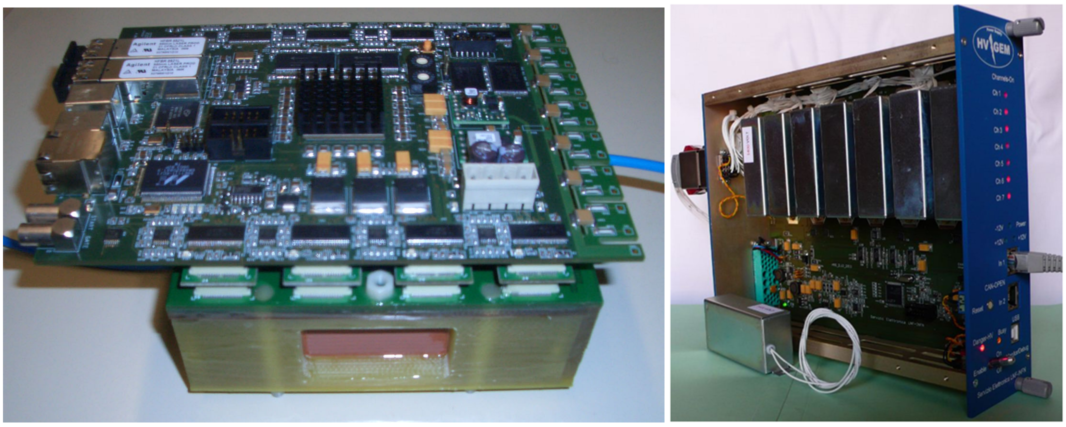

Figure 6: *The mother board FPGA based coupled with the FEE and the GEM detector (left) and the HVGEM NIM module (right).*

7 Future

Other research groups inside INFN, ENEA, CEA and CERN are interested in use of these triple GEM detectors described above and the electronics made in Frascati. Recently also two monitors for X rays have been made for burning plasma diagnostic and will be installed in Frascati Tokamak and Tore Supra at Cadarache.

Any other information can been found on the web site

`http : //www.lnf.infn.it/esperimenti/imagem/`

8 List of Conference Talks and Poster by LNF Authors in Year 2011

1. G. Croci et al.
   A New GEM Based Neutron Diagnostic Concept for High Power Deuterium Beams
   Poster, 2011 IEEE NSS and MIC, 23-29 October 2011, Valencia Spain
2. G. Corradi et al.
   High Voltage Power Supply for Triple GEM Detectors
   Poster, 2011 IEEE NSS and MIC, 23-29 October 2011, Valencia Spain
3. F. Murtas et al.
   Compact TPC GEM for High Intensity Beam Diagnostics
   Talk, 2011 IEEE NSS and MIC, 23-29 October 2011, Valencia Spain
4. F. Murtas et al.
   A Compact TPC GEM for Low and High Intensity Beam Diagnostics
   Poster, Industry meets Accademia: Beam Monitoring Instrumentation and Quality Assurance, GSI, November 10-11, 2011
5. G.Croci et al.
   nGEM fast neutron detectors for beam diagnostics
   Poster, ICFDT2 Conference Frascati December 2011

9 List of Publication in Year 2010-11

1. R.Villari, M.Angelone, B.Esposito, A.Ferrari, D.Marocco, F.Murtas, M.Pillon,
   Design of a GEM-based detector for the measurement of fast neutrons
   NIM A, Volume 617, Issues 13, 1121 May 2010, Pages 155-157
2. F. Murtas, et al.
   Applications in beam diagnostics with triple GEM detectors
   NIM A, Volume 617, Issues 13, 1121 May 2010, Pages 237-241

2011 ACTIVITY REPORT OF THE HCPAF GROUP

S. Bini(art.2222), P. Chimenti(art.15), V. Chimenti(ass.), R. Di Raddo(CTER),
V. Lollo (CTER), M. Migliorati (ass), A. Mostacci (ass). B.Spataro (D.T.) (Resp.)

1 Aim of the experiment

As known the HCPAF Group activity is presently dedicated to set up an X-band, accelerating structure, using different materials and methods. In particular a three cells X-band standing wave structure has been realized entirely in molybdenum using high temperature brazing procedure. Here it will be reported the setup procedure of the second structure completely in molybdenum realized at LNF-INFN and technological problems met on this activity.

2 Technological activity

The activity of testing high-gradient RF sections at 11.424 GHz for the next generation electron-positron linear collider is in progress in order to determine reasons of breakdown mechanisms which limit the high gradient performance. Since the breakdown phenomena is an open problem, a dedicated research and development on this field has been launched within the linear-collider community. An useful trend in terms of DC breakdown study is underway at CERN in order to test candidate materials and surface preparation [1)- 2)], even though it does not represent the real RF behavior. In the framework of the collaboration with SLAC, KEK, INFN-LNF in order to determine the maximum gradient possibilities for normal-conducting RF powered particle beam accelerator an intense technological activity is therefore dedicated to set up X-band, accelerating structures operating at 11.424 GHz, using different materials and methods [3) 4) 5) 6) 7)]. Basically, the main fields under investigation are presently the following: high temperature brazing (800-1000)°C, low temperature (soft) brazing (250-300)°C, electroplating, molybdenum sputtering on copper. In particular a three cells X-band standing wave structure at 11.424GHz has been realized entirely in molybdenum using a high temperature brazing procedure. Then, this section has been tested at high power at SLAC [8)], too. It is shown that the breakdown rate of the brazed Mo structure is higher than that of copper structure for same RF parameters. A structure internal inspection to understand the device behavior is therefore necessary. Here we discuss the possible reasons that affect the molybdenum brazed section performance and related technological problems when constructing it.

3 Brazed section internal inspection

After being removed from high gradient test area, the structure was sectioned along the axis at SLAC klystron lab to allow for internal inspection [9)]. The structure was first split into 2 pieces using EDM (Electrical Discharge Machining). One of the half pieces was split again. On the initial sectioning, one of the molybdenum extension tubes failed adjacent to the SST flange braze, as shown in figure 1. Note that the arrow shown in the image was observed by the machinist, not added during the cutting.

When one of the sections was cut again [also by EDM both flanges on one of the pieces (a 1/4 section of the whole) detached as shown in figure 2.

It appears that in the case where the joint failed in the braze area (see figure 3), the molybdenum cylinder wall was thick enough to withstand the differential expansion forces but that the

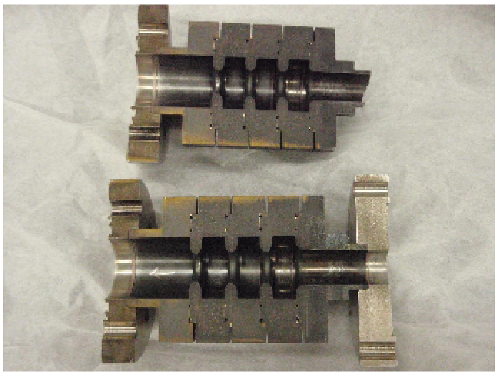

Figure 1: Moly structure was split up into 2 pieces using EDM

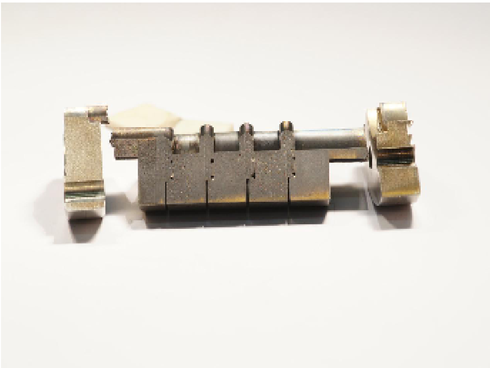

Figure 2: When one of the sections was cut again (also by EDM) both flanges on one of the pieces (a 1/4 section of the whole) detached as shown

braze joint was not.

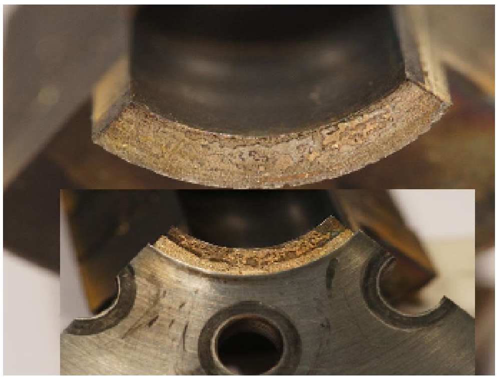

Figure 3: Highlight of joint failed in the right side of figure 2

In the case of the other end, the thinner molybdenum wall was insufficient to withstand the forces applied (see figure 4).

Figure 4: Highlight of molybdenum extension tubes failed adjacent to the SST flange in the left side of figurefigure4.

On closer inspection we found that the joint was not completely filled with alloy which would result in uneven loading and increased/concentrated stress. We think that this increased stress between SST and molybdenum may have contributed to both failures. We speculate that during braze cycle, a large radial gap between SST flange and molybdenum appeared due to larger thermal expansion of the SST flange. This gap may have cause the non-uniform filling of the joint by the alloy. A possible solution that may reduce stresses caused by difference of thermal expansions could make use of an additional flexible part (in this case a cylinder) between molybdenum structure and SST flange. This thin-wall cylinder could be made out of stainless steel, CuNi, or copper and it should be properly designed to accommodate stressed created during the brazing.

The joint between this flexible cylinder and molybdenum could be made with a grove that locks outside diameter of the cylinder as shown on figure 5a. This joint has to be properly designed to have adequate clearance when the parts at heated during the brazing. The design should also take into account thermally induced forces between the locking grove and the cylinder. The joint can be strengthened by locking not only outside diameter of the flexible cylinder, but also its inside

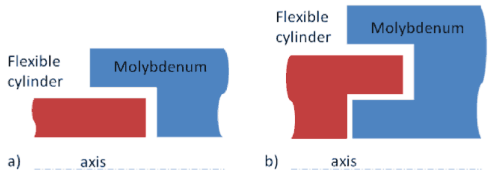

Figure 5: Possible joint designs between molybdenum and a flexible cylinder: a) locking outside diameter of the flexible cylinder; b) locking both inside and outside diameters of the flexible cylinder.

diameter as shown on figure 5b. This, for example could be done for the flexible cylinder with large diameter.

We think that the joins between structure cells could be improved by removing a void created by two contact surfaces on the iris side of the cell. This void is clearly visible on figure 6. The void could contribute to gas contamination and gas load during structure brazing and operation. For example, if inner contact surface has a vacuum leak and larger-diameter contact surface is vacuum tight, than this may adversely effect structure operation but would be hard to detect using conventional vacuum leak detection. By removing second-larger-diameter contacting surface we can improve contact between surfaces and avoid the uneven-alloy-filling of the joint seen on zoomed part of figure 6.

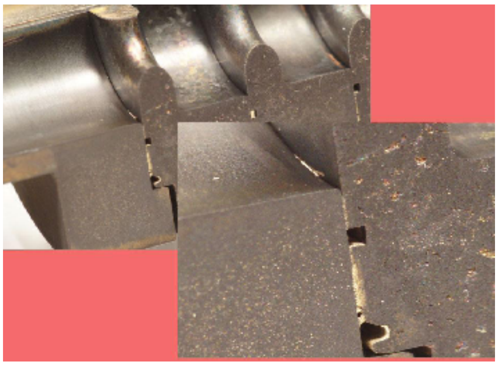

Figure 6: The image highlights a body/iris joint typical of moly structure.

We suggest a joint consisting of a single set of mating faces 1-3 mm wide between the body and iris. We may also use nested cells by creating a cylindrical step of about 1.5mm depth to lock the cells. The single mating surface will ensure contact at the cell-iris joint, would allow the cells to be made from much less material, and may significantly reduce the potential for contamination and virtual leaks. A multi-step braze sequence can be used to facilitate braze fillet control. In the noted design the first step would be a diffusion bond or an alloy assisted diffusion bond, if the body material and desired temperatures and pressures prevent direct bonding. Alloy assisted bonding uses temperature and pressure to create a bond between both sides of a filler (a thin washer in this case) and the base materials. If proper surface finishes, materials, temperatures, and pressures are used the resulting bond should be leak tight with a well filled joint. The joint can then be brazed traditionally with a lower temperature alloy to provide additional strength. We think that for a case of copper-diffusion-bond and secondary braze the molybdenum can retain considerable hardness and strength. For example typical TZM (titanium zirconium molybdenum) molybdenum stress relieving schedule would run to 980 ℃ and a full re-crystallization schedule may run above 1180 ℃ for over an hour.

4 Bulk Molybdenum, three cells structure

The realization of second molybdenum brazed three-cell structure designed at LNF has been attempted. More details on the mechanical drawings and assembly will be given on a request. Following the steps of the previous realization, the procedure began doing the machining of the structure components, three cells plus connections to the end CF flanges using a proper lathe and tools. Final machining of roughly 300 nm was obtained starting by a sintered Mo bar (figure 7). Brazing procedure followed for the other molybdenum radio frequency structure has been applied. A film of electrodeposited copper has been applied to the joints surface in order to facilitate the operation.

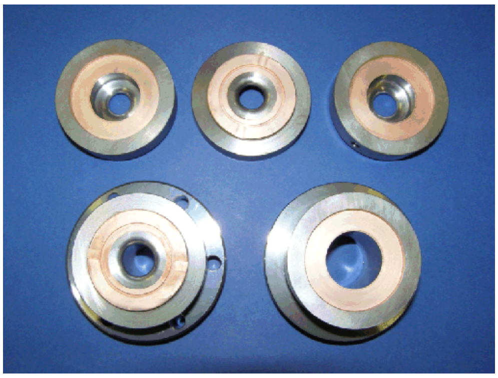

Figure 7: Components of moly structure, three cells plus connections to the end CF flanges.

This time during high temperature brazing sequence several problems were occurred. The following procedure was applied for each connection made between the pieces: brazed joints were removed from the vacuum oven, checked for vacuum leaks, and only if vacuum test gave positive results, the brazing procedure carried on. Firstly, the external cells were brazed by using PalCusil 10 alloy (copper-based alloys are normally acceptable in the creation of relatively low resistance joints) with stainless steel flanges: the vacuum check gave positive results. After that the sequence continued with the brazing of the tuners; three cells, two tuners each one, two tuners each one, means a total of six tuners. The braze of these pieces was performed in two steps. Step 1: the first three tuners were joined using Palcusil 10. Step 2: Once done, the other three tuners were brazed with Palcusil 5 in order to avoid problems with the previous joint done. After that the entire structure was assembled and the final braze was attempted. To avoid problems related to previous brazed parts, Cusil was adopted because the brazing temperature is less than Palcusil. Cusil was used to achieve the final structure, putting a thin layer of electrolytic copper placed at the joining surfaces. After that, during vacuum check, a leak in the part of conjunction between the molybdenum and stainless steel was found. We tried to redo the braze to see if leak disappeared but without results. We tried to redo the brazing procedure alternating Cusil with Palcusil alloy but no improvements took place. We also tried to make a new geometry of the joints surface to facilitate the brazing process, but again without results. In the figure 8 the assembled molybdenum structure is shown. Unfortunately the vacuum leak between the molybdenum and stainless steel right flange is again present. The thermal treatments on the structure changed significantly the dimensions, especially in the conjunction area between molybdenum and stainless steel; in order to keep the initial dimensions the structure has been machined again and a new brazing process was attempted in order to close the vacuum leak at stainless steel flanges, but again without results.

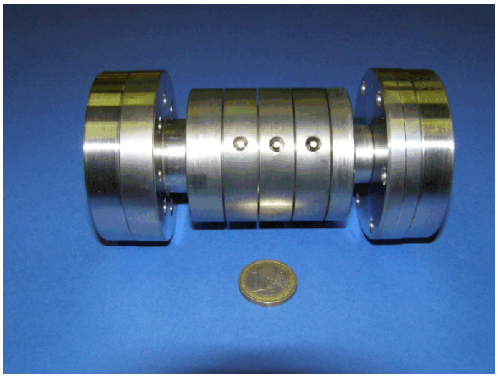

Figure 8: The assembled molybdenum structure.

5 Conclusion

The realization of second molybdenum X-band accelerating structure using brazing procedure has been described. The first structure realized at LNF following the same procedure worked at RF higher power [8]. This time several problems were occurred. Thermal treatments on the structure changed significantly its dimension, especially in the conjunction area between molybdenum and stainless steel; the deformations unfortunately are stochastic and no repeatable, and this could be due to the nature of the material (sintered metal). If so, the future of the bulk Mo structures is linked to the possibility to find on the market the proper Molybdenum. Obviously other ways (with low stress on Mo) can be tested for the connections. For example:1) Tin brazing procedure or 2) Electron beam welding.

References

1. J.T. Ramsvik, et al., Investigations of DC Breakdown Fields, EPAC06, Edinburgh, UK June 26-30, 2006
2. A. Descoeudres et al., DC Breakdown Experiments for CLIC, Proceedings of EPAC08, Genoa
3. S. Bini, P. Chimenti, V. Chimenti, R. Di Raddo, V. Lollo, B. Spataro, F. Tazzioli: Electroforming Procedures Applied to the Construction of 11.4 GHz Linear Accelerating Structures: Status Report on SALAF Activity", RF-07/003, 29/05/2007.
4. S. Bini, P. Chimenti, V. Chimenti, R. Di Raddo, V. Lollo, B. Spataro, F. Tazzioli, 2008 Status report on SALAF technical activity on X-band linear accelerating structures project at Frascati Laboratories, SPARC-RF-08/001,July 31, 2008.
5. S. Bini, P. Chimenti, V. Chimenti, R. Di Raddo, V.A.Dolgashev,V. Lollo, B. Spataro, Status report on SALAF technical activity during the first half of 2009, SPARC-RF-09/002 April 30, 2009.
6. S. Bini, P. Chimenti, V. Chimenti, R. Di Raddo, V.A.Dolgashev,V. Lollo, B. Spataro, SALAF Group technological activity , SPARC-RF-09/003 June 30, 2009.

7. S. Bini, P. Chimenti, V. Chimenti, R. Di Raddo, V.A. Dolgashev,Y. Higashi,V. Lollo, B. Spataro Activities on the sputtered metals thin films for accelerating cavity applications, RF-10/001 12/01/10,

8. D. Alesini, M. Calvetti, V. Chimenti, L. Palumbo, B. Spataro, V.A. Dolgashev, S. Tantawi: High Power Test Results on X-Band Copper and Molybdenum Structures, Low Power RF Measurements of Copper Electroformed Structures and Technological Activity, RF-09/004, 01/09/2009

9. A. Haase, Comments and observation on 1C-SW-A5.65-T4.6-Mo-Frascati-1, SLAC internal note, 28 August, 2009.

iFCX

S.B. Dabagov (Resp. Naz.), D. Hampai, G. Cappuccio, A. Esposito, A. Gorghinian,
L. Allocca (Ass.), L. Marchitto (Ass.), S. Alfuso (Ass.),
R.M. Montereali (Osp.), F. Bonfigli (Osp.), E. Pace (Osp.), A. De Sio (Osp.)

Participant Institutions:

Italy: INFN Laboratori Nazionali di Frascati
CNR ENEA, Frascati
CNR Istituto Motori, Napoli

Russia: P.N. Lebedev Physical Institute, Moscow
National Research Nuclear University "MEPhI", Moscow

The iFCX (Fast Contrast X-Ray Imaging) project aims in X-ray high resolution imaging studies based on the use of polycapillary optical elements. The main scope is to design a prototype unit for new imaging technique to investigate low contrast and fast developing processes in X-ray range of 5÷30 keV.

1 Introduction

The principal expected result of the project is in design and development of an experimental chamber dedicated to high resolution X-imaging. At the present the setup is realized and the preliminary tests have been yet started. At the moment, the best results can be highlighted in two principal points:

- very high resolution through the combination of polycapillary optics and LiF detectors on geological samples;
- projection imaging / axial tomography / 3D rendering through polycapillary optics on organic samples.

2 Activity in 2010-2011

2.1 High Resolution X-ray Imaging based on Polycapillary-LiF Systems

During 2010-2011 we explore the possibility to use a low divergent X-ray beam from a polycapillary lens system combined with a micro X-ray tube for contact X-ray imaging experiments on novel high-spatial-resolution LiF-based detectors. In this way, we have proposed and successfully developed laboratory table-top X-ray microscopy systems to easily perform X-ray imaging in very simple configurations, like the contact one. The radiation source used is a 50 W Cu X-ray tube with a source spot size of about 50 μm (Oxford Apogee 5000). A half-lens was used to obtain a quasi parallel beam. Its length is about 60 mm, the inlet and outlet dimensions are 3 and 4 mm, respectively, while each single channel has an average diameter of about 5 μm. A residual divergence of about 1.4 mrad and a total transmission of about 60% for Cu X-ray characteristic lines were measured. The samples studied were exposed in a special vacuum chamber placing them in direct contact with LiF plates. The X-ray micro-radiographies stored in the LiF detectors, consisting of crystals (5x5x0.5) mm^3 polished on both surfaces, were read by a CLSM, Nikon Eclipse C1-80i, in fluorescence mode equipped with a CW Coherent Argon laser (INNOVA90) at ENEA C.R. Frascati.

Figure 1 (a) shows the image of a sample directly obtained by the optical microscope under white-light illumination in transmission mode. Figure 1 (b) shows the X-ray radiography of a sample stored in a LiF crystal detector and read by the CLSM in fluorescence mode. Brighter areas in the LiF micro-radiography correspond to lower X-ray absorbing parts, while darker ones represent the higher X-ray absorbing regions of the investigated geological sample. Several features and internal structures can be identified, like: absorbing circular dot (1), straight inclusions (2), very high absorbing area (3) and more transparent straight inclusions (4). Due to the optical transparency of the investigated samples, some of them are recognizable in the corresponding optical images. The brighter straight inclusions (4), transparent to X-ray, in the optical image in fact correspond to absorbing areas. On the contrary, more transparent areas in the visible image appear more absorbing to X-rays. These latter features can be identified by comparing the two images as tiny inclusions of a Fe-rich silicate (biotite: K(Fe, Mg) (AlSi3 O10) (OH)2) which is dispersed in the more absorbing areas. Figure 1 (c) and (d) show the intensity profiles, with the corresponding FWHM, of the brighter inclusions (4) along horizontal L and vertical L′ black traverse of Figure 1 (b). Inspection of these profiles suggests that the high spatial resolution and the dynamic range of LiF detectors allow to distinguish details few microns wide.

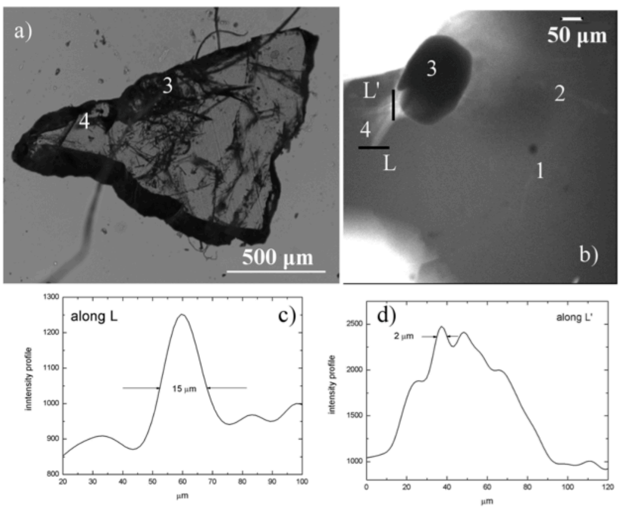

Figure 1: (a) Optical image under white-light illumination in transmission mode of a doubly polished (010) section of cordierite (sample 1). (b) Radiography stored in a LiF crystal and read by a CLSM in fluorescence mode; (c) and (d) show the intensity profiles, with the corresponding FWHM, of brighter inclusions along lines L and L′ of (b).

2.2 X-ray Imaging for Organic-Based Fast Developing Processes

The investigation of fuel sprays to measure spatial densities and droplet dimensions is typically done by non-intrusive optical techniques using coherent visible light through optically accessible windows. This is challenging because the sprays are very dense finely atomized droplets (less than 20÷30 μm in diameter) and the incident light experiences attenuating multi-scattering phenomena. For this reason studies are limited at low injection pressures, for wide dispersed sprays and on the jets boundary. In this way, the most worldwide used systems to study these phenomena are based on optical techniques for direct imaging of the sprays and their evolution in the engine. However, these diagnostic techniques are limited by the density of the investigated volume: the large number of droplets surrounding or comprising the dense spray core prevents obtaining quantitative data from near-nozzle and central spray regions. Recently, X-ray techniques have been used for investigating highly dense sprays. They offer various advantages such as weak interaction with the fuel structure as well as, lack of multiple-scattering inside the jets. Specially dedicated optical systems, such as polycapillary optics and laboratory X-ray sources, can provide rather high flux beams. Polycapillary optical elements allow shaping low divergence X-ray beams (with energy of

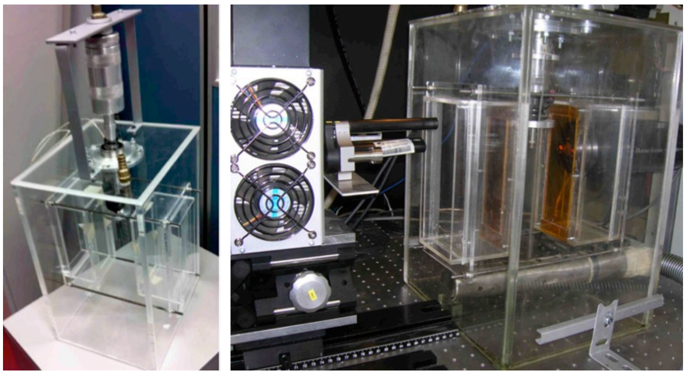

Figure 2: A new facility for fast processes studies: the injector prototype is on the left; the setup - on the right.

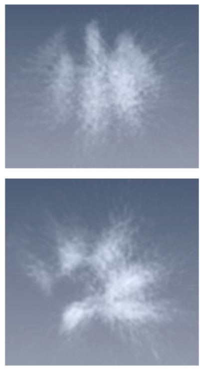

Figure 3: Tomography images of a 6-injection spray: side and top views.

up to 30 keV) that can be applied for high contrast imaging. For preliminary investigations on fuel sprays from a Gasoline Direct Injection (GDI) six-hole nozzle by polycapillary X-ray technique, a Cu K_α X-ray source has been used (50 kV, 1 mA, spot 45x45 μm^2) in combination with a half polycapillary lens (focal distance 91 mm, transmission 60%, residual divergence 1.4 mrad). The detector is a Photonic Science CCD (area 14.4x10.7 mm^2, resolution 10.4x10.4 μm^2).

A rotating system allows the injector body rotation along its axis by means of a stepping motor and enabling to irradiate the spray under different angles with respect to the source-detector alignment. Off-line tomography reconstruction has been performed at the angular steps of 1 deg.

Figure 4: Laboratory μCT of the ant sample: the sample surface reconstruction (left); the tomography of the internal parts of a sample.

Moreover, a 3D image reconstruction experiment was carried out using an ant. The exposure time of the CCD was 250 ms, necessary to not saturate the CCD. An ant as a sample to be studied is positioned on a XYZ micro-positioner and rotated by 0.50 deg per image, for a total of 720 projection images: the rotation velocity is 0.5 deg/s, then the entire scan time is 720 s. As a pre-processing, each image is treated with the image provided program of the CCD (Image-Pro Express) in order to remove the background noises. The reconstruction work, i.e. convert projection images into slice images, has been done with the OCTOPUS program (trial version) and the rendering work was carried out with the AMIRA program (trial version). The figure shows the 3D rendering of an ant from the reconstructed slice images.

3 Conferences, Seminars

1. S.B. Dabagov, "Channeling Physics in Crystals and Capillaries: Following Frascati's Projects", 1st Intern. seminar "Novel Radiation Sources and Applications: LI2FE in Moscow", July 7-8, 2011, Moscow, Russia (*oral*).
2. S.B. Dabagov, "Frascati's BTF/SPARC Facilities and Radiation Related Projects", 3rd Intern. conf. on Quantum Electrodynamics and Statistical Physics, August 29 - September 2, 2011, Kharkov, Ukraine (*plenary*).
3. S.B. Dabagov, "XLab LNF INFN: Studies on X-ray Optics & Applications", 21st Intern. Congress on X-ray Optics and Microanalysis, September 5-8, 2011, Campinas, Brazil (*oral*).
4. S.B. Dabagov, "XLab Frascati: X-ray Optics & Imaging Applications", 4th Intern. workshop "Imaging Techniques with Synchrotron Radiation", September 24-27, 2011, Bordeaux, France (*invited*).
5. D. Hampai, S.B. Dabagov, F. Bonfigli, R.M. Montereali, L. Allocca, L. Marchitto, S. Alfuso, G. Della Ventura, F. Bellatreccia and M. Magi, "High Resolution X-ray Imaging based on Polycapillary Optics", 4th Intern. workshop "Imaging Techniques with Synchrotron Radiation", September 24-27, 2011, Bordeaux, France (*oral*).
6. S.B. Dabagov, "Channeling of Radiations: from Crystal to Capillary Guides", Intern. conf. "Electron, Positron, Neutron and X-ray Scattering under External Influences", October 18-22, 2011, Yerevan, Armenia (*plenary*).
7. D. Hampai, F. Bonfigli, S.B. Dabagov, R.M. Montereali, G. Della Ventura, F. Bellatreccia and M. Magi, "LiF-Polycapillary Systems for Advanced X-Ray Imaging", 2nd International Conference on Frontiers in Diagnostics Technologies (ICFDT2), INFN - Laboratori Nazionali di Frascati, November 28-30, 2011 (*poster*).
8. L. Gabellieri, A. Romano, V.Piergotti, B. Tilia, D. Mazon, P. Malard, F. Murtas, S. B. Dabagov, and D.Hampai, "Polycapillary optics for SXR diagnostics for magnetic fusion plasmas", EFDA Workshop on Diagnostics, Garching, March 30-31, 2010 (*oral*).
9. S.B. Dabagov, "Novel Channeling Based Sources for Advanced X-ray Analysis", EXRS 2010 European Conference on X-ray Spectrometry, June 2025, 2010, Figueira da Foz, Coimbra, Portugal (*plenary*).
10. D. Hampai, S.B. Dabagov, G. Cappuccio, and V. Guglielmotti, "Spectroscopy Studies at X-Lab LNF", EXRS 2010 European Conference on X-ray Spectrometry, June 2025, 2010, Figueira da Foz, Coimbra, Portugal (*oral*).
11. F. Bonfigli, D. Hampai, R.M. Montereali, M.A. Vincenti, and S.B. Dabagov, "Combination of LiF detectors with polycapillary optics for X-ray high resolution imaging", EXRS 2010 European Conference on X-ray Spectrometry, June 2025, 2010, Figueira da Foz, Coimbra, Portugal (*poster*).
12. D. Hampai, S. B. Dabagov, G. Cappuccio, and V. Guglielmotti, "X-Lab - a X-ray facility at LNF", Channeling 2010, Ferrara, October 3-8, 2010 (*oral*).
13. V. Guglielmotti, S. Orlanducci, V. Sessa, F. Toschi, M. L. Terranova, D. Hampai, M. Rossi, S. B. Dabagov, A. T. Dideikin, A. Ya. Vul, A. Mascioletti, and P. De Stefanis, "Carbon Nanotube Based Cold Cathodes and Channeling Phenomena for a New Generation of X-Ray Systems", Channeling 2010, Ferrara, October 3 - 8, 2010 (*oral*).

14. D. Pacella, S. B. Dabagov, F. Murtas, L. Gabellieri, A. Romano, D. Hampai and D. Mazon, "Polycapillary Optics for Soft X-ray Diagnostics in Magnetic Fusion Plasmas", Channeling 2010, Ferrara, October 3 - 8, 2010 (*oral*).

References

1. S.B. Dabagov, "On X-Ray and Neutron Channeling in Carbon Nanotubes", Nanoscience and Nanotechnology Letters **3** (2011) 24-27.

2. D. Hampai, F. Bonfigli, S. B. Dabagov, R. M. Montereali, G. Della Ventura, F. Bellatreccia, and M. Magi, "High Resolution X-ray Imaging based on PolyCapillary Optics - LiF Combination", Europhysics Letters **96** (2011) 60010.

3. D. Hampai, L. Marchitto, S. B. Dabagov, L. Allocca, G. Cappuccio and S. Alfuso, "Laboratory μ-CT", Nature (2012) (submitted).

4. S.B. Dabagov, L. Palumbo, and V. Guidi, Eds., Channeling 2010, Proc. of the 4th International Conference "Charged and Neutral Particles Channeling Phenomena" (Ferrara, October 3-8, 2010), Nuovo Cimento **C 34 (4)** (2011) 560 pp.

5. S.B. Dabagov, and L. Palumbo, Eds., Charged and Neutral Particles Channeling Phenomena - Channeling 2008, Proc. of the 51st Workshop of the INFN Eloisatron Project, World Scientific, (2010) 823 pp.

6. L. Allocca, S.B. Dabagov, and L. Marchitto, "X-ray refraction 3D-simulation software: ?rst approach", Il Nuovo Cimento **C 34 (4)** (2011) 553-559.

7. V. Guglielmotti, S. Orlanducci, V. Sessa, F. Toschi, M.L. Terranova, D. Hampai, M. Rossi, A. Mascioletti, P. De Stefanis, and S.B. Dabagov, "Carbon nanotube based cold cathodes for a new generation of X-ray systems", Il Nuovo Cimento **C 34 (4)** (2011) 529-535.

8. D. Pacella, S. Dabagov, F. Murtas, A. Romano, D. Hampai, L. Gabellieri, and D. Mazon, "Polycapillary optics for soft X-ray imaging and tomography", Il Nuovo Cimento **C 34 (4)** (2011) 513-520.

MoonLIGHT-ILN

G. Bellettini (Ass.), S. Berardi (Bors.), G. Bianco (Ass.), A. Boni (Dott.), C. Cantone (AR),
E. Ciocci (Bors.), S. Dell'Agnello, G.O. Delle Monache, M. Garattini (Dott.), C. Graziosi (Bors.),
N. Intaglietta (Tecn.), C. Lops (Dott.), M. Maiello (PhD), R. March (Ass.),
M. Martini (Bors.), G. Patrizi (Bors.), R. Tauraso (Ass.), M. Tibuzzi (Bors.), R. Vittori (Ass.)

1 Introduction

Lunar Laser Ranging (LLR) experiment, performed since 1969 with retro-reflector arrays deployed by Apollo 11, 14 and 15, is the only Apollo experiment, designed by a team led by C. O. Alley, D. Currie, P. Bender and Faller et al [4], still taking data today. In the past 40 years, laser ranging to these arrays has provided most of the definitive tests of the many parameters describing General Relativity [5, 7]. In addition, the analysis of the LLR data, has greatly enhanced our understanding of the interior structure of the Moon [6, 7, 8, 9]. Initially, the Apollo arrays contributed a negligible portion of the LLR error budget. Nowadays, the ranging accuracy of ground stations has improved by more than two orders of magnitude: the new APOLLO station at Apache Point, USA, is capable of mm-level range measurements [1]; MRLO, at the ASI Space Geodesy Center in Matera, Italy, has re-started LR operations. Now, because of lunar librations, the Apollo arrays dominate the LLR error budget, which is a few cm. The University of Maryland, Principal Investigator for the Apollo arrays, and INFN-LNF are proposing an innovative CCR array design that will reduce the error contribution of LLR payloads by more than two orders of magnitude, down to tens of microns. This is the goal of the MoonLIGHT-ILN (Moon Laser Instrumentation for General relativity High-Accuracy Tests for the ILN)[2], a technological experiment of INFN and of the SCF, the CCR space test facility at LNF.

2 Science Objectives of MoonLIGHT-ILN

Lunar Laser Ranging (LLR) has for decades provided the very best tests of a wide variety of gravitational phenomena, probing the validity of Einstein's theory of General Relativity. The lunar orbit is obviously influenced by the gravity fields of the Earth and Sun, but also is sensitive to the presence of many other solar system bodies. This makes the dynamics of the lunar orbit complex, but the system is relatively pure in that non-gravitational influences (solar radiation pressure, solar wind, drag) are negligible. This makes the Earth-Moon distance a useful tool for testing the nature of gravity, constraining potential deviations from general relativity[3]. LLR currently provides the best constraints on tab.1.

The equivalence principle states that any mass, independent of composition, will react (accelerate) in precisely the same way when placed in a gravitational field. This is the same as saying that the inertial mass and gravitational mass of any object are precisely the same. The equivalence principle is fundamental to GR, allowing gravity to be treated as an aspect of the geometry of spacetime. In general, scalar additions to general relativity – motivated by string theories or quantum gravity – produce a violation of the equivalence principle and also lead to secular changes in the fundamental constants. Scalar fields are also frequently invoked to account for the apparent acceleration of the expansion of the universe. Thus tests of the equivalence principle are a vital part of understanding the interface between gravity and quantum mechanics, and in probing our cosmological fate.

The equivalence principle comes in two flavors. The WEP relates to the composition of an object, in effect probing electromagnetic, strong nuclear, and weak nuclear energy contributions. The SEP extends to include gravity itself. The Earth-Moon system allows a test of the SEP in a way that laboratory tests cannot, in that the contribution of gravitational self-energy to the total

Phenomenon	Current limit	1 mm ranging	100 μm ranging	Measur. timescale
Weak EP (Δa/a)	10^{-13}	$\sim 10^{-14}$	$\sim 10^{-14}$	2yr
Strong EP (Nordvedt param.)	4×10^{-4}	$\sim 10^{-5}$	$\sim 10^{-6}$	2yr
$\dot{G}/G$	10^{-12} per year	$\sim 10^{-13}/yr$	$\sim 10^{-14}/yr$	4yr
Geodetic Precession	$\sim 5 \times 10^{-3}$	5×10^{-4}	$\sim 5 \times 10^{-5}$	6-10 yr
$1/r^2$ deviations	$10^{-10}\times$ gravity	$\sim 10^{-11}$	$\sim 10^{-12}$	6-10yr

Table 1: *The expected improvements on the GR measurements with MoonLIGHT are shown in table, together with their measurement time scale.*

mass-energy budget is 5×10^{-10} for the earth, but only 10×10^{-27} for typical laboratory masses. LLR allows us to ask the questions: "Do the Earth and Moon fall at the same rate toward the sun? Does the gravitational self-energy of the Earth fall toward the Sun at the same rate as the less gravity-burdened Moon? Does gravity pull on gravity in the same way it pulls on ordinary matter?". The Earth-Moon system is currently the best laboratory for answering these questions. If the SEP were to utterly fail – that is, gravitational self-energy failed to gravitate – the Moon's orbit would be shifted by 13 meters. Current LLR constrains this shift to be less than 5 mm, constituting a 4×10^{-4} constraint on violation of the SEP.

LLR can also constrain new theoretical paradigms. An example is an idea to account for the apparent acceleration of the universe by allowing gravitons to leak off of our 4-dimensional spacetime "brane" into another bulk dimension, thus weakening gravity over cosmological scales. Though small, such a process would have an impact on the lunar orbit, causing it to precess by effectively invalidating the $1/r^2$ force law of gravity. LLR needs to see a factor of 15 improvement to reach this level of sensitivity to new physics.

Furthermore much of our knowledge of the interior of the Moon is the product of LLR [8, 9, 10, 11], often in collaboration with other modalities of observation. These physical attributes of the lunar interior include Love number of the crust, the existence of a liquid core, the Q of the Moon, the physical and free librations of the Moon and other aspects of lunar science.

3 2nd Generation of Lunar Laser Ranging

The general concept of the second generation of LLR is to consider a number (notionally eight) large single Cube Corner Retroreflectors (CCRs). Each of these will have a return that, with a single photoelectron detection system such as current APOLLO system located at the Apache Point Observatory, can be used to determine the range to the limit determined by the librational effects of the current arrays and the laser pulse length. By using single CCRs, the return is unaffected by the libration. That is, there is no increased spread of the FWHM due to the CCR and the librational effects. We plan to use eight such single reflectors spread over tens of meters. The return from each of the CCRs will be registered separately and can be identified by comparison with the nominal lunar orbit and earth rotational parameters. This is shown schematically in Fig.1.

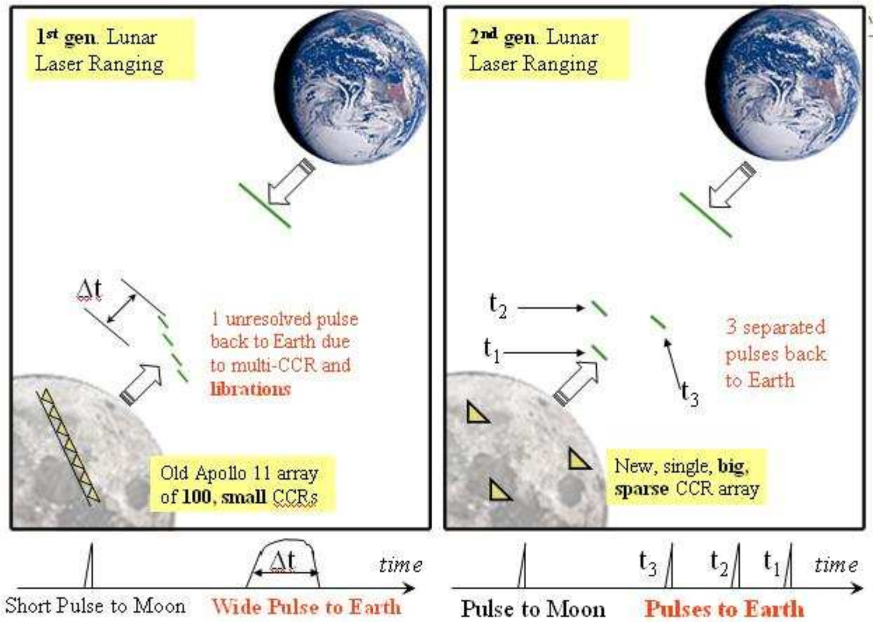

Figure 1: *Concept of the 2nd generation of Lunar Laser Ranging*

4 The New Maryland/Frascati Payload

We currently envision the use of 100 mm CCRs composed of T19 SupraSil I. This is the same material used in LLRA 20^{th} and both LAGEOS satellites. This will be mounted in an aluminum holder that is thermally shielded from the Moon surface, in order to maintain a relatively constant temperature through the lunar day and night. It is also isolated from the CCR, by two coassial "gold cans", so the CCR receives relatively little thermal input due to the high temperature of the lunar day and the low temperature of the lunar night. The mounting of the CCR inside the housing is shown in Fig.2. KEL-F could be used for this mounting (its used in LAGEOS) due to its good insulating, low out-gassing and non-hygroscopic properties.

5 Technical challenges of the MoonLIGHT CCR

The primary technical objectives of the LLRRA-21 are to provide adequate laser return to Earth ground stations and to stable over long term, decades, with respect to the center of mass of the Moon. The major technical/engineering challenges that follow from the technical objective are then:

- Fabricate a large CCR with adequate homogeneity and that meet the required tolerances, mentioned in the previous section.
- Thermal control to reduce thermal gradients inside the CCR to acceptable levels. Thermal gradients produce index of refraction gradients, which cause beam spread and low return.
- Emplacement goal of long-term stability of $10\mu m$ with respect to the Center of Mass of the Moon.

Figure 2: Views of current design of the MoonLIGHT/LLRRA21 CCR: (a) fully assembled; (b) exploded view with its internal mounting elements and outer aluminum housing.

The large diameter of the CCR introduces a great challenge in its fabrication, the availability of such material of the required homogeneity, the fabrication and polishing procedures and the measurement methods. The angle between the three back reflecting faces, which govern the shape of the pattern, have a more challenging tolerance of ± 0.2 arcsec; this is more restrictive by a factor of 2.5 than the current state of the art for SLR CCR fabrication. The material choice is primarily driven by three requirements:

- extremely uniform index of refraction (very good homogeneity)
- resistance to darkening by cosmic radiation
- low solar radiation absorption

To satisfy these requirements, this CCR has been fabricated with SupraSil 1. For the next generation of CCRs, LLRRA-21, we plan to use SupraSil 311 which has even better homogeneity.

The optical performance of the CCR is determined by its Far Field Diffraction Pattern (FFDP), which represents the intensity of the laser beam reflected back to the ground by the CCR. Figure 3 is a simulation of the FFDP of the LLRRA-21 (performed with the software CodeV) according to its dimensions and angle specifications; at the correct velocity aberration the intensity (calculated in optical cross section) should have a value which guarantees that enough photons come back to the ground station. Optical cross section is an intrinsic characteristic of CCRs or LRAs, and its defined as follows:

$$\sigma_{CCR} = I_{CCR/MIRR}\,(\theta_x, \theta y)\, 4\pi \left(\frac{A_{CCR}}{\lambda}\right)^2 \tag{1}$$

Where $I_{CCR/MIRR}$ is the intensity of the FFDP of the CCR, at a certain point of the (θx, θy) plane, referred to a perfect mirror of the same aperture as the CCR, λ is the laser wavelength. One of the most critical challenges of this new model is the issue of the thermal gradient. Since the index of refraction of the fused silica depends upon temperature, a thermal gradient inside the CCR will cause the index of refraction to vary within the CCR and thus modifying the FFDP. In Figure 5, is represented the average intensity over the velocity aberration for the LLRRA-21 at

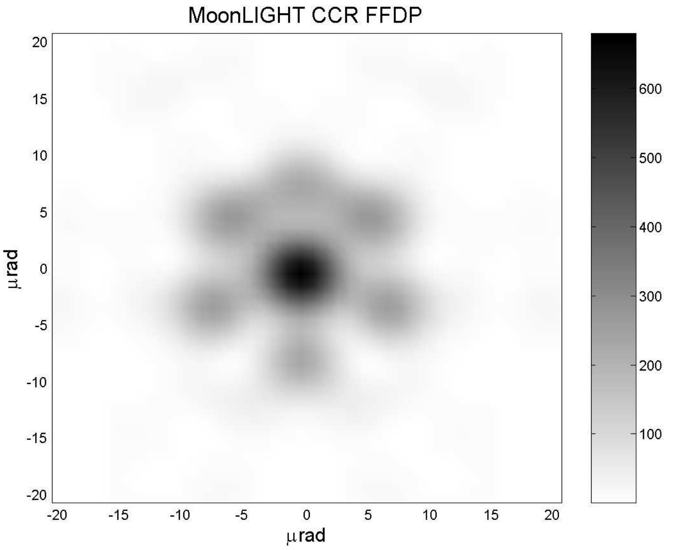

Figure 3: *FFDP of LLRRA-21 under its design specification of offset angles (0.0” 0.0” 0.0”). Grid is in angular dimensions (μrad)*

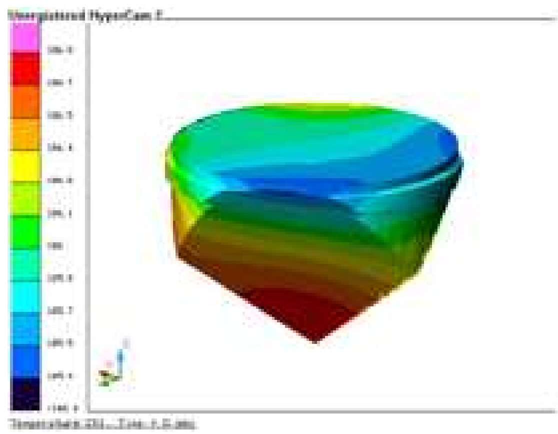

Figure 4: *Typical distribution of temperature inside the CCR for a given set of conditions.*

Standard Temperature and Pressure (STP). At the velocity aberration for the Moon, $\sim 4\mu rad$, we will test thermal perturbations and, if needed, develop an optimized design to control the drop of FFDP intensity to an acceptable level. For this reason we need to understand in detail how the external factors heat the CCR and in what magnitude, either on the Moon or on a satellite. This is accomplished using dedicated programs developed in parallel at LNF and UMD. To perform

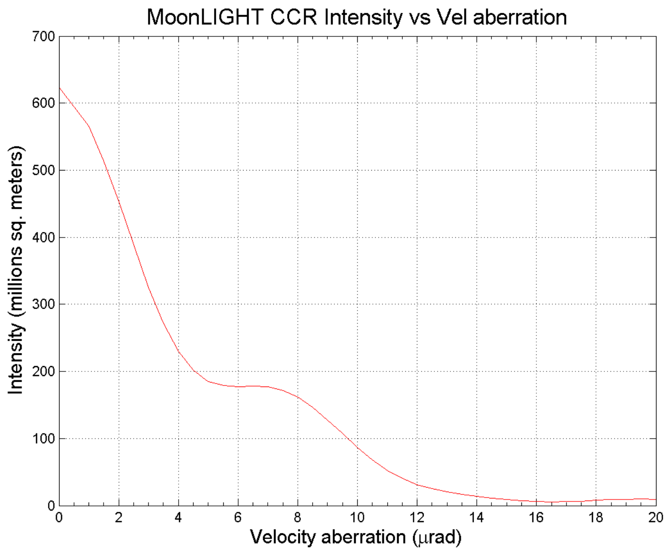

Figure 5: *Average intensity over velocity aberration of an unperturbed MoonLIGHT CCR*

these simulations we use Thermal Desktop, a software package of C&R Technologies of Boulder CO. Then using IDL and CodeV we translate these thermal gradients into the effects on the FFDP of the CCR. There are three primary sources of heat that causes thermal gradients; here we briefly describe their effect:

- *Absorption of solar radiation within the CCR*: during a lunar day, the solar radiation enters the CCR and portions of this energy are absorbed by the fused silica. Since the different wavelengths in the solar radiation are absorbed with different intensity, according to fused silica absorptivity characteristic, the heat is deposited in different parts of the CCR.

- *Heat flux flowing through the mechanical mounting tabs*: if the CCR is at a temperature that is different than the housing temperature there will be a flux of heat passing into (or out of) the CCR through the holding tabs. Conductivity of the mounting rings should be reduced.

- *Radiation exchange between the CCR and the surrounding pocket*: in the case of the Apollo LRAs, the back surfaces of the CCRs view the aluminum that makes up the housing, machined with a relative high emissivity/absorptivity. If the temperatures of the CCR and the aluminum are different there is a radiation exchange of thermal energy, which in turn causes a flux in the CCR as the heat exits out of the front face to cold space. In the Apollo array this is not been a serious issue, but the bigger dimensions of the LLRRA-21 complicate things, and we need to reduce this effect. Thus we enclose the CCR into two thermal shields, with a very low emissivity (2%), that should prevent this radiative heat flow.

Thermal simulations performed on the current configuration show that currently the variation of the ΔT between the front face and the tip of the CCR is within 1K. We are still proceeding to optimize this further, both with optical design procedures and with thermal stabilization of the overall housing.

As mentioned earlier, to achieve the desired accuracy in the LLR, a long term stability is needed with respect the center of mass of the Moon; to attain this we must understand and simulate the temperature distribution in the regolith (and its motion), the effects of a thermal blanket that will be spread about the CCR and the effects of heat conduction in the INVAR supporting rod. A locking depth is chosen such that the thermal motion effects are small ($\sim 1m$). The placement of the thermal blanket further reduces the thermal effects and also reduces the effects of conduction in the supporting rod. This simulation cycles through the lunation and annual cycles.

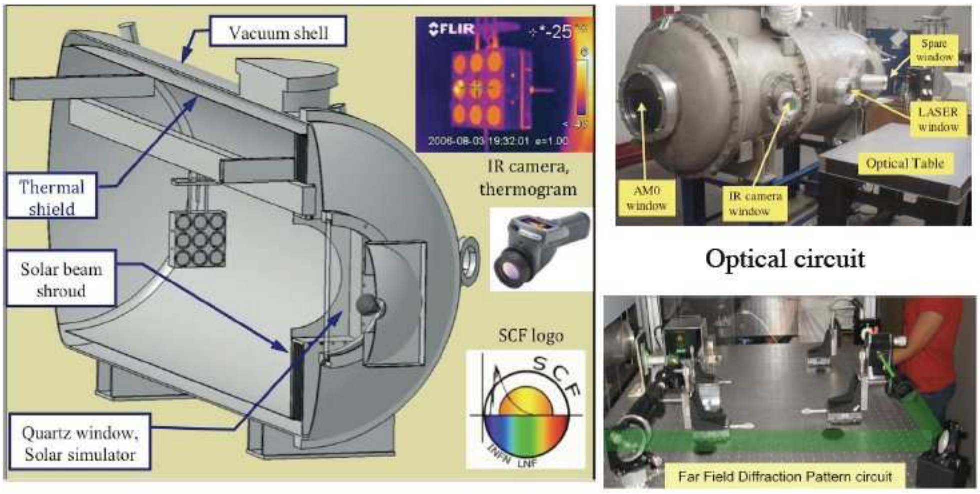

Figure 6: *SCF sketch (left side), SCF cryostat and optical table (right side)*

6 Thermal and Optical Tests in Frascati

SCF, fig.: 6, (Satellite/lunar laser ranging Characterization Facility), at LNF/INFN in Frascati, Italy, is a cryostat where we are able to reproduce the space environment: cold (77 K with Liquid Nitrogen), vacuum, and the Sun spectra. The SCF includes a Sun simulator (www.ts-space.co.uk), that provides a 40 cm diameter beam with close spectral match to the AM0 standard of 1 Sun in space ($1366.1 W/m^2$), with an uniformity better than $\pm 5 W/m^2$ over an area of 35 cm diameter. Next to the cryostat we have an optical table, where we can reproduce the laser path from Earth to the Moon, and back, studying the Far Field Diffraction Pattern (FFDP) coming back from the CCR to the laser station, useful to understand how good is the optical behavior of the CCR. The SCF-Test (Dell'Agnello et al. 2011) is a new test procedure to characterize and model the detailed thermal behavior (fig.: 7 and 8) and the optical performance of laser retroreflectors in space for industrial and scientific application, never before been performed. We perform an SCFTest on the MoonLIGHT CCR to evaluate the thermal and optical performance in space environment. About thermal measurements we use both an infrared (IR) camera and temperature probes, which give a real time measurements of all the components of the CCR and its housing. In particular we look at the temperature difference from the front face to the tip, studying how the FFDP changes during the different thermal phases. This is the best representative of the thermal distortion of the return beam to the Earth. Various configurations and designs of the CCR and the housing have been and are being tested in the SCF Facility, with the solar simulator, the temperature data

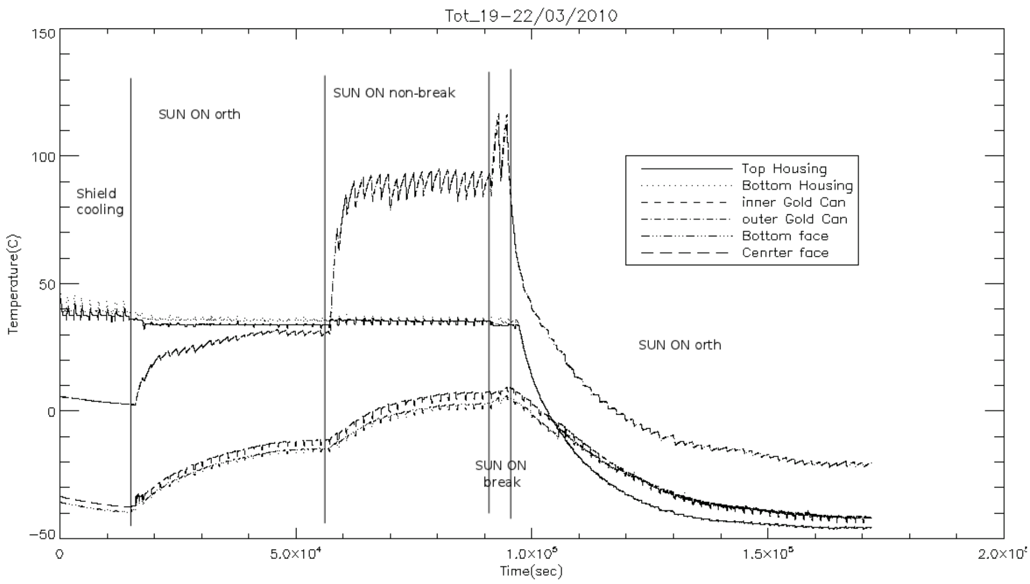

Figure 7: MoonLIGHT/LLRRA-21 flight CCR temperature variations of various housing parts and of CCR (19-22/March/2010).

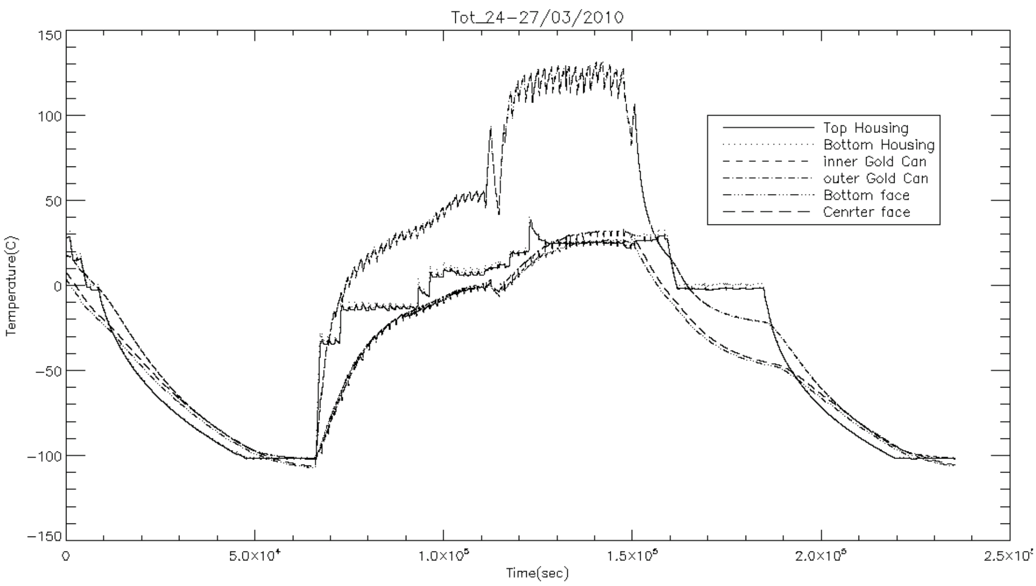

Figure 8: MoonLIGHT/LLRRA-21 flight CCR temperature variations of various housing parts and of CCR (24-27/March/2010).

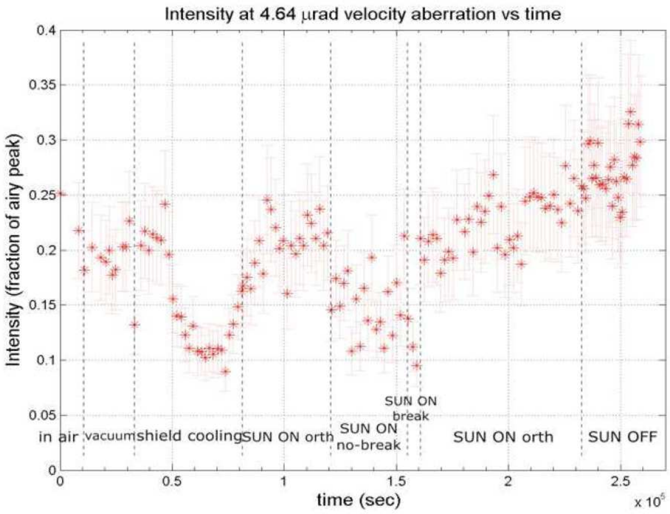

Figure 9: MoonLIGHT/LLRRA-21 flight CCR FFDP intensity variation at Moon velocity aberrations (2V/c) during tests (time subdivision refers to the fig.: 7).

recording, the infrared camera and the measurement of the Far Field Diffraction Pattern (FFDP). In fig.: 9 and 10 is shown the MoonLIGHT/LLRRA-21 flight CCR FFDP intensity variation at Moon velocity aberrations (2V/c) during key points of the SCF-Test: (1) in air, (2) in vacuum, (3) during chambers shields cooling, (4) Sun on orthogonal to the CCRs face with the housing temperature controlled at $T = 310K$, (5) Sun on at 30° of inclination (no break-through), (6) Sun on at $-30°$ of inclination (break-through), (7) Sun on orthogonal with the housing temperature left floating. From this graph we can deduce that the intensity decreases during no orthogonal lighting of the CCR, in particular when the Sun enters in the housing cavity during the break-thru phase. This effect is due to a strong increase of the Tip-Face thermal gradient during this two phase of the test. When the housing temperature is left floating, the intensity slightly increases because the "Tip-Fac" gradient is reducing.

7 Conclusion

The Phase A study was concluded in December 2008 with the final review and the full MAGIA Proposal was submitted to ASI. The MAGIA collaboration is now awaiting the decision of the new ASI management and the new National Space Plan ASI supports ILN. In the meantime, the work of the INFN-LNF group on the development of the MoonLIGHT-P prototype continued in the framework of the ILN and with an RD experiment approved by INFN for the period 2010-2012, called MoonLIGHT-ILN within the ILN.

8 Acknowledgements

We would like to acknowledge University of Maryland via the NASA LSSO (Lunar Science Sortie Opportunities) program (Contract NNX07AV62G) to investigate Lunar Science for the NASA Manned Lunar Surface Science and the LUNAR consortium (http://lunar.colorado.edu), headquartered at the University of Colorado, which is funded by the NASA Lunar Science Institute

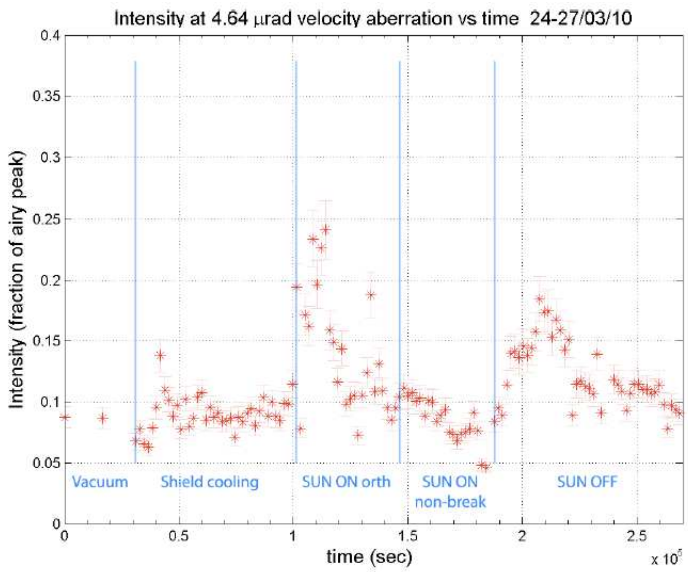

Figure 10: MoonLIGHT/LLRRA-21 flight CCR FFDP intensity variation at Moon velocity aberrations (2V/c) during tests (time subdivision refers to the fig.: 8).

(via Cooperative Agreement NNA09DB30A) to investigate concepts for astrophysical observatories on the Moon. A special thank to Prof. Douglas Currie for his great support and the helpful discussions. Special thanks to the Italian Space Agency (ASI) for the support during the 2007 Lunar Study, the MAGIA Phase A study. In particular we thank S. Espinasse, formerly at ASI, now at ESA, for encouraging the applications of our work for the ILN and ESAs first lunar lander.

References

1. Murphy T., Battat J., et al., *"The Apache Point Observatory Lunar Laser-Ranging Operation (APOLLO): two years of Millimeter-Precision Measurements of the Earth-Moon Range"*, PASP 121, 29 (2009).

2. D.G.Currie, S. Dell'Agnello, *"A Lunar Laser Ranging Retroreflector Array for the 21st Century"*, AMOS 2009.

3. J.G.Williams, S.G.Turyshev, D.H.Boggs, *"Progress in Lunar Laser Ranging Test of Relativistic Gravity"*, Phys.Rev.Lett.93:261101,2004.

4. Bender P. L., et al, *"The Lunar Laser Ranging Experiment"*, Science, Volume 182, Issue 4109, pp. 229-238, 1973.

5. Williams J. G., Turyshev S. G., Boggs D. H., Ratcliff J. T., *"Lunar Laser Ranging Science: Gravitational Physics and Lunar Interior and Geodesy"*, 35th COSPAR Scientific Assembly, July 18-24, 2004.

6. Williams J. G., Boggs D. H., Ratcliff J. T., *"A larger lunar core?"*, 40th Lunar and Planetary Science Conference, March 23-27, 2009.

7. Williams J. G., Turyshev S. G., Boggs D. H., *"Lunar Laser Ranging Test of the Equivalence Principle with the Earth and Moon"*, International Journal of Modern Physics D, Volume 18, 1129-1175, 2009.

8. Rambaux N., Williams J. G., Boggs D. H., *"A Dynamically Active Moon-Lunar Free Librations and Excitation Mechanisms"*, 39th Lunar and Planetary Science Conference, March 10-14, 2008.

9. Williams J. G., Boggs D. H., Ratcliff J. T., *"Lunar Tides, Fluid Core and Core/Mantle Boundary"*, 39th Lunar and Planetary Science Conference, March 10-14, 2008.

10. Nordtvedt K., *"Lunar Laser Ranging: a comprehensive probe of post-Newtonian gravity"*, Gravitation: from the Hubble length to the Planck length, edited by Ciufolini I., Coccia E., Gorini V., Peron R., Vittorio N., ISBN 07503 0948, published by Institute of Physics Publishing, the Institute of Physics, London, 2005, p.97.

11. Murphy T. W., Adelberger E. G., Strasburg J. D., Stubbs C. W., Nordtvedt K., *"Testing Gravity via Next Generation Lunar Laser-Ranging"*, Nuclear Physics B Proceedings Supplements, Volume 134, 155-162.

12. Nordtvedt K., *"Testing the Equivalence Principle with laser ranging to the Moon"*, Adv. in Space Research, Volume 32, Issue 7, 1311-1320.

13. Dvali G., Gruzinov A., Zaldarriaga M., *"The Accelerated Universe and the Moon"*, Physical Review D, Vol. 68, Issue 2, id. 024012.

14. Currie D. G., et al., *"A Lunar Laser Ranging Retro-Reflector Array for NASA's Manned Landings, the International Lunar Network, and the Proposed ASI Lunar Mission MAGIA"*, 16th International Workshop on Laser Ranging Instrumentation, October 13-17, 2008.

15. Prete F., *"Contact structural analysis of the MoonLIGHT Laser Retro-reflector Assembly with ANSYS"*, Bachelor thesis (unpublished), Dipartimento di Meccanica e Aeronautica, University of Rome "La Sapienza".

16. Minghiglioni A., *"Modal analysis of the MoonLIGHT Laser Retro-reflector Assembly with ANSYS"*, Bachelor thesis (unpublished), Dipartimento di Meccanica e Aeronautica, University of Rome "La Sapienza".

17. `http://ilrs.nasa.gov/docs/retroreflectorspecification070416.pdf`

18. Pearlman M. R., Degnan J. J., Bosworth J. M., *"The International Laser Ranging Service"*, Adv. in Space Research, Vol. 30, No. 2, 135-143, 2002.

19. Urschl C., Beutler G., Gutner W., Hugentobler U., Schaer S., *"Contribution of SLR tracking data to GNSS orbit determination"*, Adv. in Space Research, 39(10), 1515-1523, 2007.

20. Urschl C., Beutler G., Gutner W., Hugentobler U., Ploner M., *"Orbit determination for GIOVE-A using SLR tracking data"*, ILRS Workshop, 2006.

21. `http://ilrs.nasa.gov/docs/ILRSRetroreflectorStandards200812.pdf`

22. Neubert R., Neubert J., Munder J., Grunwaldt L., *"Proposed Single Open Reflector for the GALILEO Mission"*, International Technical Laser Workshop on SLR Tracking of GNSS Constellations, 2009.

MUEXC

M. Cestelli Guidi (Art. 23), G. Della Ventura (Ass.), D. Di Gioacchino (Resp. Naz.),
L. Gambicorti (Ass.), A. Marcelli, A. Mottana (Ass.), E. Pace (Ass.), P. Postorino (Ass.),
A. Puri (Ass.), N. Saini (Ass.), F. Tabacchioni (Tech.), R. Sorchetti (Tech.)

1 *MUEXC* project

MUEXC is an experimental program based on the PRESS-MAG-O apparatus designed to make possible experiments under extreme conditions of pressure, magnetic field in a wide temperature range on materials for technological applications of the interest of the Institute. The project is based on a large collaboration between INFN personnel of the LNF, of the INFN section at the University of Florence, the 'High-pressure Raman group' and the 'Spectroscopy group' of the Department of Physics of the Sapienza University and the Department of Geological Science of the Roma Tre University and Department of Physics of the University of Camerino.

In 2011 the main *R&D* activities of the *MUEXC* collaboration can be summarized as follows: **a)** *Operation on PRESS-MAG-O insert*: we proceeded in the commissioning of the PRESS-MAG-O insert and to this purpose we setup a cryostat at liquid helium immersion that has allowed to test its components. Moreover, we realized the wiring of the insert and the low temperature characterization of the excitation coil has been also performed using a power supply designed by the Department of Electronics and Automation (SEA) of the LNF. We also completed tests at liquid helium temperature of the micro-SQUID gradiometer inside the high-pressure DAC cell;

b) *Amorphous carbon patterns on CVD diamond*: in collaboration with the INFN unit of Florence we continued tests for the R&D of a small device to control in situ the temperature of the sample inside the diamond anvil cell. During the year we completed the first characterization of a set of carbon resistive lines made via laser annealing. We also did the first exposures with the Focused Ion Beam of the University of Roma Tre to manufacture similar devices dedicated to temperature measurements or micro-heaters obtained by FIB patterning on CVD diamond plates;

c) *Maintenance of the cryostat*: almost at the end of the commissioning, unfortunately, during the transport by the staff in charge of the internal handling in the LNF, on 17/11/2010 the crate containing the cryostat and the magnet inside have been damaged falling down. During the year we had to take care of the insurance file, the evaluation of the damage to the systems, and the procedures to fix the damages occurred.

2 Operation on the PRESS-MAG-O insert

A challenging issue of any magnetic measurement inside a DAC cell is the extremely small sample volume (10^{-5} - 10^{-7} cm^{-3}) with the extremely low filling factors of the detection coils. To improve the magnetic sample response respect to the background, an original high sensitive micro-gradiometer coupled to the SQUID (Fig. 1) has been designed and manufactured (SUPRACON, Jena). The geometrical configuration developed has been optimized to match the DAC in order to be as near as possible to the gasket between the two anvils with the sample loaded just between the two pick-up coils. The micro-gradiometer sensor made by two Nb-Ti thin coils in a Cu matrix (0.05 mm of diameter) has been manufactured by a photolithography technique on a mono-crystal silicon wafer. Each coil of the gradiometer has 8 turns with an external diameter of 2 mm and an internal one of 1.6 mm. The Nb-Ti wires to the pickup coil are twisted and embedded in a bundle of five Cu wires (0.1 mm of diameter) soldered to the PCB SQUID holder, in order to allow the good thermal contact with the He bath. In the middle of the bundle a loop guarantees the thermal contact with the cold finger. The Cu wires have no electrical contact with the pickup circuit. The pickup coils and the Cu wires are glued to the Si chip patterned as a fork (Fig.1 left) to fit between the two anvils.

Figure 1: *The micro-gradiometers (left), the SQUID system (center) and the Nb3Sn shield (right)*
.

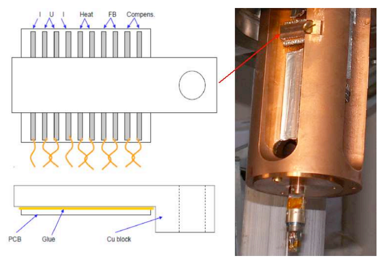

Figure 2: *The micro-gradiometers (left), Layout of the heat sink of the SQUID system (left) and the mounting on the insert (right).*
.

The chip with a thickness of 0.35 mm is coated by a SiN film $\sim \mu$m thick (necessary to produce a lithographic etching). The Stycast 2850 FT glue with some special additives was used to glue components . The current sensor SQUID (Model CE1blue) is mounted on the PCB holder inside the set of the superconducting shields. The SQUID has an equivalent input noise level better than 1.5 pA/sqrt (Hz). It has also integrated feedback coils on the chip. On the PCB holder there are contact pads to solder wires to the SQUID and to a compensation transformer. This is used to compensate the parasitic signal in the pickup circuit, due to a non-perfect gradiometer balance. The transformer has one turn of Cu wire covered by Pb-Sn solders and two turns of an Nb-Ti wire connected in series with the pickup coils. The SQUID leads and the compensation transformer are made by twisted pairs of Cu wires. To have a good heat sink, wires are soldered to the PCB and to the plate and fixed with a thin glue layer to the insert, ensuring the stability of the low temperature of the SQUID system. In Figure 2 we show a layout of the heat sink and its mounting on the insert. The SQUID system (Fig. 1 center) has a Nb3Sn shield (Fig. 1 right) to reduce to $\leq$100 Gauss the background magnetic field ($\geq$1 T), when the superconducting magnet is at its maximum value (8 T). This complex shield is made by three layers and its performance has been measured with a superconducting solenoid. In the test, a current sensor SQUID was mounted inside the shield and its flux-voltage characteristics were monitored while the magnetic field was increased at the rate of $\sim$0.5 T/min. No change in the SQUID characteristics was detected up to 850 mT. The gradiometer works inside the DAC, near the anvils, and it is driven to the proper position by a slider through a break manufactured on the sample holder. Several measurements have been performed to test the SQUID gradiometer operation with the system at 4.2 K and a superconducting sample (a YBCO sample of dimension $\sim 0.16 mm^3$) loaded in the DAC cell mounted on the insert as in a real case. To remove unwanted noises caused by interferences of RF signals, we shielded all cables with Al foils and standard ferrite RF filters. Using the exciting coil of the insert we generated an AC field at the frequency of 22.7 Hz in the mGauss amplitude range. The persistent current in the gradiometer coils induces in the SQUID a flux whose amplitude depends by the exciting field. Tests showed that the SQUID works within the specifications.

3 Pattern of amorphous carbon on diamond

The heather set-up we are developing in cooperation with the INFN unit of Florence and the Diamond Material GmbH, is an anvil integrated heating system based on resistive lines directly patterned on diamond plates and in the future on diamond anvils. At present, to characterize the properties of these micro-devices we patterned lines on diamond slabs as showed in Fig. 3. A full morphological and structural characterization of the resistive lines (for more details see Fig. 4) is under way using the Focused Ion Beam (FIB) of the LIME laboratory of the University of Roma Tre. Preliminary results regarding the morphology of these resistive lines were obtained using a laser source. The characterizations performed indicated that micro-devices compatible with the geometry of the diamond anvils can be realized in the near future. To identify the characteristic of the material patterned on the diamond slabs (Fig. 3D), micro-Raman measurements lines have been performed.

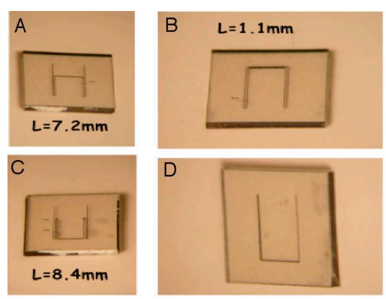

Figure 3: *Simple layouts of resistive patterns realized on thin CVD diamond plates*

.

The area probed by the system was $\sim$1 μm^2 with an estimated thickness $\leq$20 μm. We investigated different areas of one of the patterns showed in Fig. 3D while in Fig. 4 we report two magnified images showing magnified details of these amorphous carbon based patterns. Raman spectra associated to these patterns clearly points out the presence of both a carbon glass phase and a nano-crystalline diamond phase.

In particular, it has been verified the heating properties of one resistive pattern using a four contacts technique, through a Cu sample-holder inserted in a liquid helium cryostat. Either experimental tests at room temperature and at low temperature point out that these techniques can be used to design a micro-heater device. In Fig. 5 are showed the results obtained from a resistive pattern, exhibiting stable temperature plateau at increasing power. In principle, the same device could be also used as a thermometer. Indeed, we measured with the same pattern a resistance vs. temperature behavior similar to that of a 51 Ω Speer CGR (Fig. 6). Further work is in progress to manufacture a reliable thermal device based on similar patterns. At the same time, instead of the laser annealing process, we are attempting to manufacture more accurate patterns using a FIB source. The latter approach appears more suitable to produce more accurate and repetitive patterns.

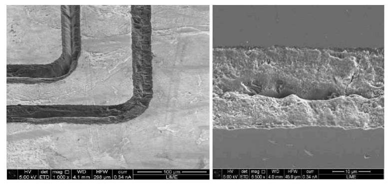

Figure 4: *FIB/SEM images of laser patterned lines on diamond. Corners of resistive lines (left); a smaller detail at higher magnification (right).*

.

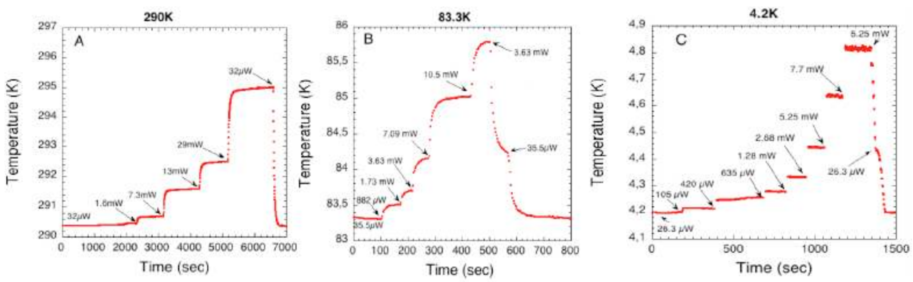

Figure 5: *Temperature dependence of an amorphous carbon line measured in a thermal bath at* $290K$ *(A),* $83.3K$ *(B) and* $4.2K$ *(C) vs. time increasing the applied power*

.

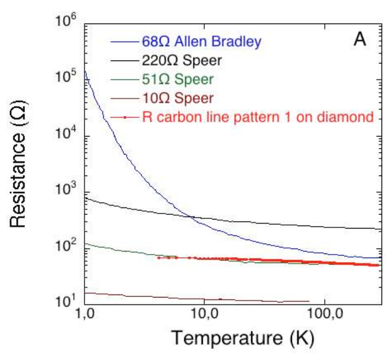

Figure 6: *Comparison of the R-T curve of an amorphous carbon pattern and commercial thermometers*

.

4 Maintenance PRESS-MAG-O cryostat

Following the fall of the crate containing the cryostat and the magnet, the LNF had to open a file to fix damages occurred to the PRESS-MAG-O cryostat still open at present. The orders to fix mechanical damages occurred to the cryostat vessel are under way while safety tests of the superconducting magnet have been completed by AMI Inc (TN, USA) who manufactured the device. We expect to reassembly the system in the first months of 2012.

5 Experimental activity

In addition to the commissioning of the PRESS-MAG-O instruments and the R&D of thermal devices, we continued researches on highly correlated materials. Here we show data of the 1111 $NdFeAsO_{0.86}F_{0.14}$ iron pnictide superconductor and of the 11 $FeSe_{0.88}$, $FeSe_{0.5}Te_{0.5}$, $FeSe_{0.25}Te_{0.75}$, $FeTe_{0.8}S_{0.2}$ iron chalcogenide superconductors.

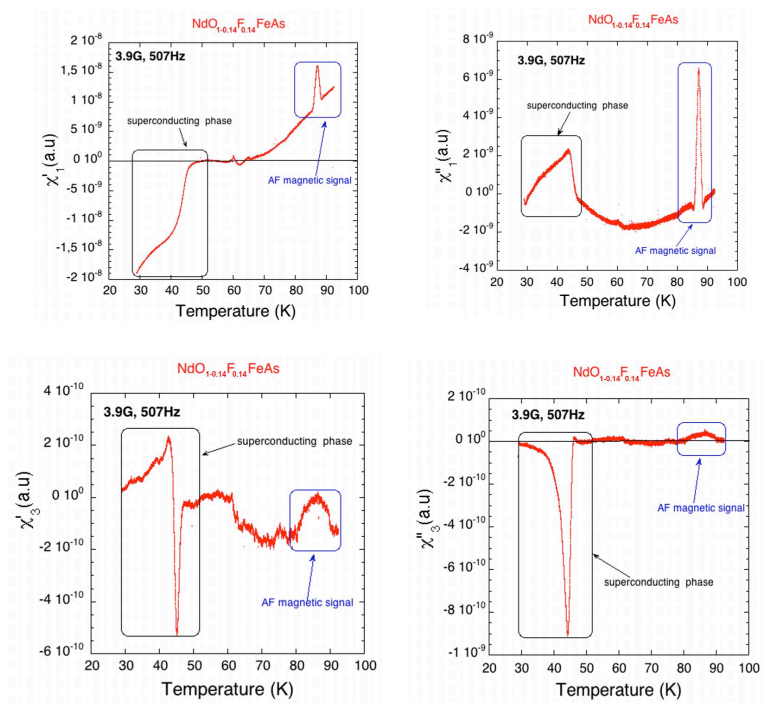

Figure 7: *AC multi-harmonic susceptibility experiments of* $NdFeAsO_{0.86}F_{0.14}$*: (top): real (* χ'_1*) and imaginary part (*$\chi"_1$*) of the first harmonic. (bottom): real* χ'_3*) and imaginary part (*$\chi"_3$*) of the third harmonic*

.

A comparison of the properties of these systems, using multi-harmonic magnetic susceptibility data under high magnetic fields ($\leq$5T) at low temperature ($\geq$4.2K) points out: a) the coexistence of a superconducting (T_c= 47K) and a magnetic phase (T_m= 90K) in the 1111 $NdFeAsO_{0.86}F_{0.14}$, iron pnictide system; b) a good bulk 3D pinning characteristics with a crossover to a 2D behavior for a H_{dc} field of 1T occurs in the superconducting phase of the 1111 iron pnictides with a characteristic layered crystal structure with alternate superconducting iron-pnictogen active layers and rare earth-oxide spacer layers; c) a superconducting phase (T_c= 10K) coexisting with a magnetic (T_m= 125K) phase also in the 11 $FeSe_{1-x}Te_x$ iron chalcogenide; d) a good bulk 3D pinning characteristics at low magnetic fields also for the superconducting phase in the 11 iron-chalcogenides. The comparison between the 1111 $NdFeAsO_{0.86}F_{0.14}$ iron pnictide superconductor and the 11 iron chalcogenide superconductors, where only iron-chalcogen active planes are present, also points out that despite its higher thermal activation, the 1111 iron superconductor has a stronger pinning force probably associated to important role played by the (NdO) spacer layer.

Research Doctorate and thesis: During 2011 our PhD Dr. Alessandro Puri completed his research program in the framework of the MUEXC project he joined in 2009. Currently we have two undergraduate students of the Camerino university working on their research thesis. One is involved in the characterization of the carbon patterns on diamond and to the development of a thermal sensor while the second is involved in a study of the superconducting flux dynamic in the $SmFeAsO_{0.85}F_{0.15}$, one important system of the new Fe-HTSC superconductor of the pnictide family.

6 Acknowledgements

We thank the technical staff of the DAΦNE-Light laboratory for their continuous and invaluable technical support. Thanks are also due to E. Woerner for the realization of the resistive lines on diamond; S. Mangialardo for the Raman characterization of the carbon patterns; A. Notargiacomo for the studied with the Focused Ion Beam (FIB) and Y. Kamili for his contribution during the test runs of the resistive lines.

References

1. D. Di Gioacchino, A. Marcelli, M. Cestelli Guidi, A. Puri, P. Postorino, E. Pace, A. De Sio and L. Gambicorti, PRESS-MAG-O: a unique instrument to probe materials and phenomena under extreme conditions at Frascati, High Pressure Research 31 (2011) 9197

2. D. Di Gioacchino A. Marcelli, A. Puri, A. Iadecola, N.L. Saini, A. Bianconi Influence of the extra layer on the transport properties of $NdFeAsO_{0.86}F_{0.14}$ and $FeSe_{0.88}$ superconductors from magneto dynamic analysis J. Supercond. Nov. Magn. (2011) in press

3. D. Di Gioacchino, A. Marcelli, M. Cestelli Guidi, A. Puri, P. Postorino, E. Pace, A. De Sio, L. Gambicorti PRESS-MAG-O: new advances in the instrument commissioning Internal note LNF- 11/ 19 (NT) (2011)

4. Dr. Alessandro Puri PhD Materials Science Universita Sapienza Rome, *Experiments on strongly correlated materials under extreme conditions*, 2011/12

NESCOFI@BTF
NEutron Spectrometry in COmplex FIelds @ Beam Test Facility

R. Bedogni (Resp., Art. 23), D. Bortot (Ass.), B. Buonomo, M. Chiti (Tech.)
M. De Giorgi (Tech.), A. Esposito, A. Gentile (Tech.), J. M. Gomez-Ros (Ass.),
G. Mazzitelli, M.V. Introini (Ass.), A. Pola (Ass.), L. Quintieri (Art. 23)

In collaboration with:
Politecnico di Milano and INFN-Milan
CIEMAT-Madrid, Spain

1 Introduction and motivation

NESCOFI@BTF started in 2011 with the aim of developing innovative neutron sensitive instruments for the spectrometric and dosimetric characterization of neutron fields, intentionally produced or present as parasitic effects, in particle accelerators used in industry, research and medical fields. Neutron spectra in these fields range from thermal (1E-8 MeV) to tens or hundreds MeV, thus spanning over more than 10 decades in energy. As shown in Fig.1, only the multisphere spectrometer [1] (or Bonner Sphere spectrometer) is able to simultaneously determine all energy components over such a large energy interval. The main disadvantage of this spectrometer is the

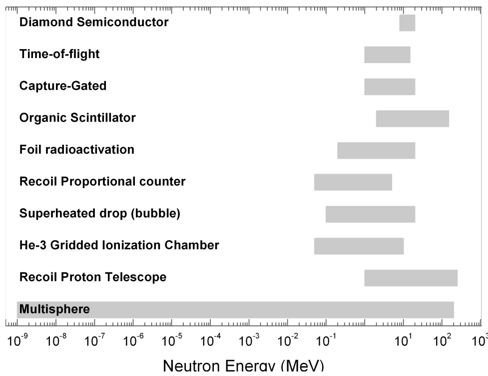

Figure 1: Energy interval covered by different available neutron spectrometry techniques.

need to sequentially expose a considerable number (usually more than 10) of detector+moderator configurations, thus leading to time-consuming irradiation sessions. The idea behind NESCOFI is to provide real-time spectrometers able to simultaneously provide all energy components in a single irradiation. These could be employed for:

1. Monitoring the neutron fields in terms of energy-integrated neutron flux and spectral neutron flux in energy intervals of interest.

2. Active real-time control of possible deviations from nominal field properties and of possible modifications induced by materials introduced in the radiation field (samples, waste elements, materials to be tested).

The final users of the NESCOFI products will be a variety of facilities interested to monitor not only the intensity of a neutron beam, but also and simultaneously its energy and/or direction distribution (chip-irradiation, material science neutron beam-lines, reference neutron fields, research and cancer therapy facilities).
The basic idea behind the project is to exploit the moderation of neutrons in hydrogenated materials, as extensively done in Bonner Sphere spectrometers [2], [3], [4], [5], but new designs and computational methods have been introduced. Particularly, instead of estimating the neutron energy distribution by exposing different detector+moderator configurations, this project aims at a single moderator embedding several "direct reading" thermal neutron detectors at different positions. The energy or angle distribution of the neutron field will be obtained using unfolding algorithms relying on the device response matrix and on the reading of the different detectors. This "unfolding" problem has a number of analogies with the spectrum reconstruction with Bonner Sphere spectrometers, for which a special code called FRUIT [6], [7] (FRascati Unfolding Interactive Tools) was developed at LNF.

The NESCOFI project planned to be completed in three years (2011-2013), organized as follows:

2011: (1) optimization (via Monte Carlo simulation) of the spectrometer geometry and development of a prototype working with passive detectors

(2) establishment of a reference neutron field for testing purposes, namely the photo-neutron beam from the n@BTF facility at the LNF.

2012: Development of suitable direct reading (or active) thermal neutron detectors to be embedded in the final spectrometers

2013: Establishment and calibration of the final spectrometers

2 Achievements of the first year (2011)

2.1 Establishing a reference neutron field for testing purposes: the n@BTF photo-neutron beam at the LNF [8]

A photo-neutron beam based on the BTF facility (See Fig. 2) was obtained in the framework of the n@BTF project [9]. The photo-neutron source is obtained by a 510 MeV electron pulsed beam impinging on an optimized tungsten target located in a polyethylenelead shielding assembly. The resulting neutron field is released into the 100 m^2 BTF irradiation room. In addition to an extensive simulation campaign based on the Monte Carlo codes FLUKA and MCNPX, the neutron spectrum was experimentally determined using a Bonner sphere spectrometer equipped with Dysprosium activation foils [10] and the FRUIT unfolding code. The spectrum [8], [11], normalized to one electron impinging the target, is shown in Fig. 3 in equi-lethargy representation.

The simulations well agree with the experimental data. In terms of total neutron fluence, the yield is $(8.2 \pm 0.2)10^{-7}\ cm^{-2}$ per incident electron at the reference position (90^o direction, 120 cm from the target). Operatively, the fast neutron flux may be as high as $10^4\ cm^{-2}s^{-1}$.

To ensure an accurate monitoring of the neutron beam for the NESCOFI testing needs, in terms of either the neutron flux or its directional distribution, a pair of long counters have been set up at different angles from the neutron-emitting target. The central detectors are BF_3 counters type Centronic 50EB60.

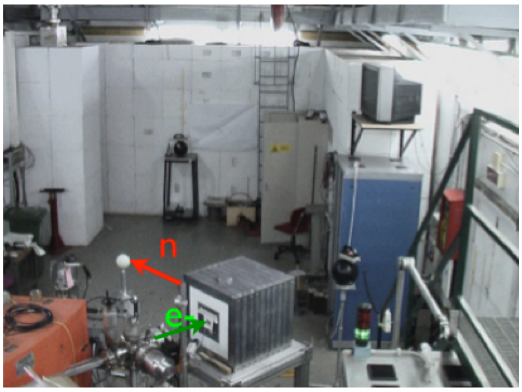

Figure 2: The n@BTF facility.

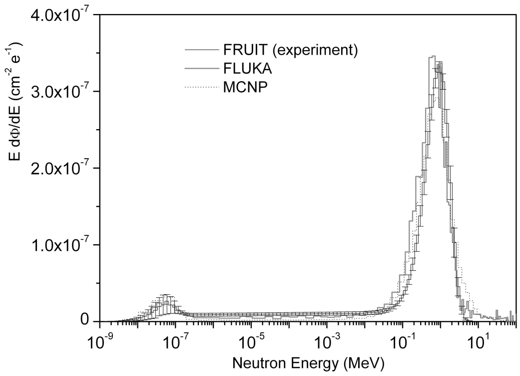

Figure 3: The neutron spectrum at the n@BTF facility.

2.2 Study and optimization of the spectrometer geometry [12)]

A simulation campaign was done to identify the appropriate moderator dimension and internal distribution of the thermal neutron detectors. The resulting design (See Fig. 4), called SP^2 (SPherical SPectrometer), has spherical shape and includes 31 thermal neutron detectors. At this stage, Dysprosium neutron activation foils were selected as suitable thermal neutron detectors because of their very reduced dimensions (1 cm diameter x 0.1 mm thickness) and the good knowledge of the Dy capture cross section.

The SP^2 has diameter 25 cm and the 31 detectors are symmetrically positioned along the three perpendicular axis. The assembly also includes a 1 cm lead shell having inner diameter 3.5 cm. This acts as (n,xn) degrader and allows extending the energy interval of the response up to hundreds of MeV neutrons. The Monte Carlo transport code MCNPX was used to design the spectrometer in terms of sphere diameter, number and position of the detectors, position and thickness of the lead shell. In addition, it was used to derive the response matrix of the final configuration.

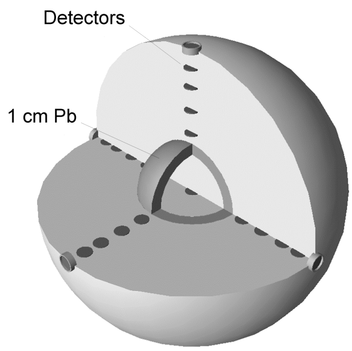

Figure 4: Sketch of the SP^2 geometry.

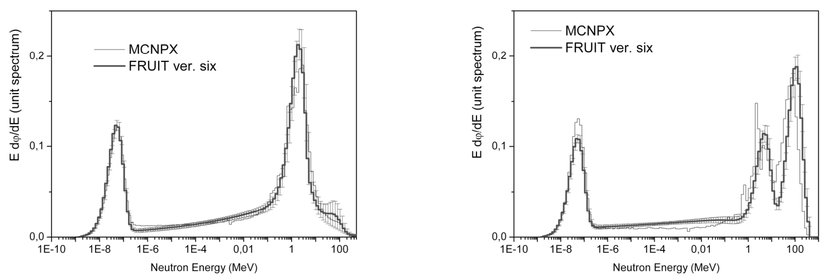

Figure 5: Testing the SP^2 design in an electron accelerator scenario.(on the left). Testing the SP^2 design in a proton accelerator scenario.(on the right).

The spectrometric capabilities were verified by simulating the exposure of SP^2 in neutron fields representing different irradiation conditions (test spectra). The simulated SP^2 readings were then unfolded with the FRUIT unfolding code and the unfolded spectra were compared with the known test spectra. Two test neutron spectra were simulated supposing a 3 GeV electron beam (left side Figure 5) and a 1 GeV proton beam (right side Figure 5) impinging a high-Z target. The simulated spectrometer readings have been processed in blind condition, i.e. without pre-information on the neutron field. The unfolded spectra well agree with the test spectra, thus allowing to approve the production of a prototypal spectrometer.

2.3 Developing and testing a prototypal SP^2 equipped with Dysprosium activation foils

The SP^2 prototype equipped with Dy activation foils, was assembled (Fig. 6) and tested in quasi monochromatic reference fields in the $E < 20$ MeV range (PTB Braunschweig, Germany) and in the $50 < E < 180$ MeV (TSL Uppsala, Sweden). The analysis of the data from the low-energy testing experiment, performed at PTB, are actually in progress. However, the preliminary profiles obtained at 1.2 MeV and 14.8 MeV demonstrate that the SP^2 response matrix is accurate within

Figure 6: The SP^2 prototype equipped with Dy activation foils.

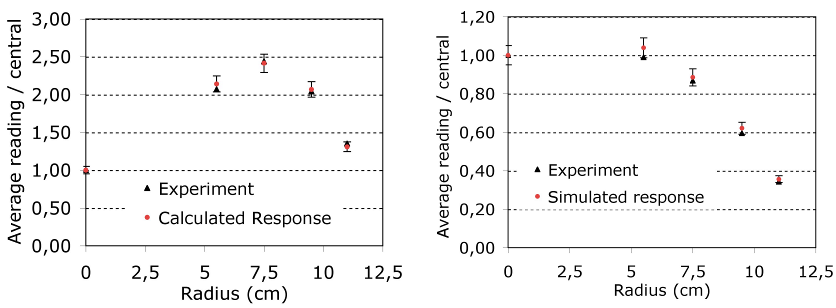

Figure 7: Irradiation with 1.2 MeV monochromatic neutrons (on the left). Irradiation with 14.8 MeV monochromatic neutrons (on the right).

an overall accuracy of few %. This is shown in Fig. 7, where the simulated response of the detectors in given positions is compared with the experimental response. In these figures, the average reading of the detectors placed at the same radius in the sphere is compared with the expected reading, i.e. obtained by applying the simulated SP^2 response matrix to the known reference neutron spectrum.

Similar agreement was obtained in the high-energy irradiations at TSL Uppsala, Sweden (See Fig. 8).

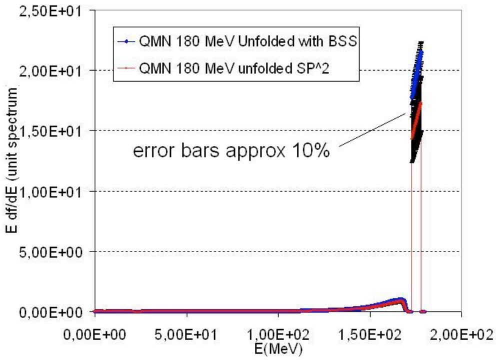

Figure 8: Irradiation with 180 MeV quasi-monochromatic neutrons. The SP2 has been used to unfold the spectrum. The resulting spectrum is compatible (within 10% on the single energy bin) with the reference spectrum, obtained with a Bonner Sphere spectrometer.

3 Publications 2011

- J. M. Gomez-Ros, R. Bedogni, M. Moraleda, A. Esposito, A. Pola, M.V. Introini, G. Mazzitelli, L. Quintieri, B. Buonomo. Designing an extended energy range single-sphere multi-detector neutron spectrometer. Nucl. Instr. Meth. A (2012), doi: 10.1016/j.nima.2012.02.033.

- L. Quintieri, R. Bedogni, B. Buonomo, A. Esposito, M. De Giorgi, G. Mazzitelli, P. Valente, J. M. Gomez-Ros. Photoneutron source by high-energy electrons on high-Z target: comparison between Monte Carlo codes and experimental data. Trans. Fus. Sci. Tech. 61 (2012) 314-321.

- R. Bedogni, K. Amgarou, C. Domingo, S. Russo, G.A.P. Cirrone, M. Pelliccioni, A. Esposito, A. Pola, M.V. Introini. Experimental characterization of the neutron spectra generated by a 62 AMeV carbon beam on a PMMA phantom by means of extended range Bonner sphere spectrometers. NIM A, submitted manuscript.

- R. Bedogni, J. M. Gomez-Ros, A. Esposito, A. Romero, M. Angelone. Calibration and workplace testing of a single-sphere multi-detector neutron spectrometer. NIM A, submitted manuscript

- R. Bedogni, C. Domingo, M. J. Garcia Fuste, M. de-San-Pedro, A. Esposito, A. Gentile, L. Tana, F. d'Errico, R. Ciolini, A. Di Fulvio. Calibration of neutron sensitive devices in the neutron field produced in the treatment room of a medical LINAC. Radiat. Meas., submitted manuscript.

- R. Bedogni, L. Quintieri, B. Buonomo, A. Esposito, G. Mazzitelli, L. Foggetta, J.M. Gomez-Ros, Nucl. Instr. Meth. A 659 (2011) 373-377.

- K. Amgarou, R. Bedogni, C. Domingo, A. Esposito, A. Gentile, G. Carinci, S. Russo. Measurement of the neutron fields produced by a 62 MeV proton beam on a PMMA phantom using extended range Bonner sphere spectrometers. Nucl. Instr. Meth. A 654 (2011) 399-405.

References

1. Alevra, A. V. and Thomas, D. J. Neutron spectrometry in mixed fields: multisphere spectrometers. Radiat. Prot. Dosim. 107(1-3), 37-72 (2003).

2. Bedogni, R., Esposito, A., Gentile, A., Angelone, M., Gualdrini, G., 2008. Determination and validation of a response matrix for a passive Bonner Sphere Spectrometer based on gold foils. Radiat. Meas. 43, 1104 -1107.

3. Bedogni, R., Esposito, A., 2009. Measurements of neutron spectrum in the high-energy DAFNE accelerator complex with an extended range Bonner sphere spectrometer. Nuclear Technology 168 (615-619).

4. Bedogni, R., Esposito, A., Andreani, C., Senesi, R., De Pascale, M. P., Picozza, P., Pietropaolo, A., Gorini, G., Frost, C.D., Ansell, S., 2009. Characterization of the neutron field at the ISIS-VESUVIO facility by means of a Bonner sphere spectrometer. Nuclear Instruments and Methods in Physics Research A 612, 143-148.

5. Esposito, A., Bedogni, R., Lembo, L., Morelli, M., 2008 Determination of neutron spectra around a 18 MV medical LINAC with a passive Bonner spere spectrometer based on gold foils and TLD pairs. Radiat. Meas. 43, 1038 -1043.

6. Bedogni, R., Domingo, C., Esposito, A., Fernandez, F., 2007. FRUIT: an operational tool for multisphere neutron spectrometry in workplaces. Nucl. Instr. Meth. A 580, 1301-1309.

7. Bedogni, R., Pelliccioni, M., Esposito, A., 2010. A parametric model to describe neutron spectra around high-energy electron accelerators and its application in neutron spectrometry with Bonner Spheres. Nucl. Instr. Meth. A 615, 78-82.

8. R. Bedogni, L. Quintieri, B. Buonomo, A. Esposito, G. Mazzitelli, L. Foggetta, J.M. Gomez-Ros, Nucl. Instr. Meth. A 659 (2011) 373-377.

9. B. Buonomo, et al. A wide range electrons, photons, neutrons beam facility, EPAC-2008, June 2008 23-27, Genova, Italy

10. Bedogni, R., Ferrari, P., Gualdrini, G., Esposito, A. Design and experimental validation of a Bonner Sphere Spectrometer based on Dysprosium activation foils. Radiat. Meas. 45, 1201-1204 (2010).

11. L. Quintieri, R. Bedogni, B. Buonomo, A. Esposito, M. De Giorgi, G. Mazzitelli, P. Valente, J. M. Gomez-Ros. Photoneutron source by high-energy electrons on high-Z target: comparison between Monte Carlo codes and experimental data. Trans. Fus. Sci. Tech. 61 (2012) 314-321.

12. J. M. Gomez-Ros, R. Bedogni, M. Moraleda, A. Esposito, A. Pola, M.V. Introini, G. Mazzitelli, L. Quintieri, B. Buonomo. Designing an extended energy range single-sphere multi-detector neutron spectrometer. Nucl. Instr. Meth. A (2012), doi: 10.1016/j.nima.2012.02.033.

OPTICAL DIFFRACTION RADIATION INTERFEROMETRY

E. Chiadroni (Resp.), L. Cacciotti (Tecn.), M. Castellano (Dir. Ric.), G. Gatti (Ric.) R. Sorchetti (Tecn.)

Participant Institutions:
Italy: INFN LNF, Roma 2-Tor Vergata; University of Roma Tor Vergata.
Germany: DESY (Hamburg)

1 Introduction

The successful development of both FEL in the X-ray range and linear colliders requires the characterization of high charge density, high energy electron beams, for which standard, intercepting diagnostics might not be suitable. Diffraction radiation (DR) diagnostic is based on the observation of the DR angular distribution emitted by an electron beam passing through an aperture in a metallic foil. DR is produced by the interaction of the electromagnetic field of an electron beam with the screen surface. Since the beam goes through the aperture, DR-based diagnostics is suitable for measuring the properties of such beams in a non-intercepting, non-perturbing way.

2 ODRI experiment

The aim of the experiment, set up at FLASH (DESY), is studying the angular distribution of incoherent optical DR (ODR) which gives information on both transverse beam size and angular divergence, to allow a single shot emittance measurement provided the beam has its waist on the DR screen. Some limitations of ODR diagnostic [1] can be overcome by mounting a shielding mask normally to the beam and in front of the DR screen. Since the two slits have different apertures (1 mm the mask and 0.5 mm the DR screen), the amplitudes of the two sources are different both in intensity and in angular distribution, resulting in an advantageous interference effect. We call it ODRI, i.e. Optical Diffraction Radiation Interference, produced by the interference between forward ODR emitted on the shielding mask and backward ODR from the DR target [2]. The main benefits are given by the reduction of synchrotron radiation background, the increase of the sensitivity of the angular distribution on the beam size, and the possibility to distinguish effects caused by beam size and offset [3] within the slit.

3 Achievements in 2011

The beam time first scheduled for Autumn 2010, was delayed to January 2011 due to the upgrade in energy.

The activity in 2011 was focused on the commissioning of the new optical system in situ and during beam time, allowing an easier optical alignment procedure and a significant reduction in the number of temporary accesses during operation.

The round beam configuration was studied at higher beam energy, i.e. 1.2 GeV, for two different transverse sizes (50 μm and 100 μm).

A detailed study of the vertical polarization of ODRI angular distribution has been performed at different wavelengths in the visible range in order to retrieve from a fitting procedure the vertical beam size of the round shape electron beam. A standard quadrupole scan has been also performed at the ODRI station, by imaging the Optical Transition Radiation (OTR) to eventually cross-check the vertical beam size and angular divergence evaluated from the fit. An additional information has been retrieved from the quadrupole scan. Indeed, since the dimension of the rectangle around the

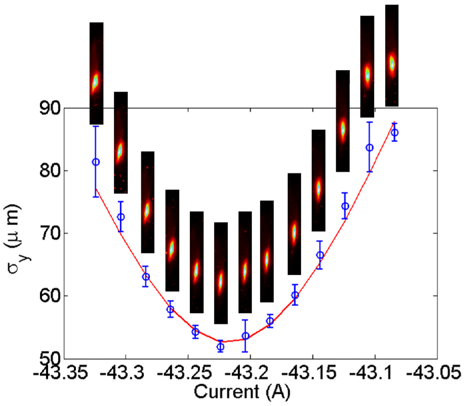

Figure 1: *Quadrupole scan imaging the OTR. The rectangles correspond to the slit dimensions, highlighting the possibility of performing a totally non intercepting quadrupole scan by means of ODRI angular distribution measurement.*

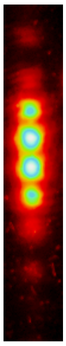

Figure 2: *Image of the vertical component of the ODRI angular distribution (800 nm, 1.2 GeV, 80 nC integrated charge).*

beam image is equivalent to the slit dimension, a totally non-intercepting emittance measurement could have been done by letting the beam go through the slit and measuring the ODRI angular distribution.

However, measurements were strongly disturbed by a new dose detection system, for radio-protection purposes, which caused the beam to stop from time to time and forced the operation at 1Hz for setting the beam transport.

For this reason, the time foreseen for the optimization of the beam transport in the by-pass was not enough preventing the possibility of performing systematic studies of ODRI angular distribution.

Nevertheless a large amount of high quality data has been collected [4)]. As an example, Fig. 2 shows one image of the angular distribution of the ODRI vertical polarization at 800 nm and with 80 nC integrated charge. Furthermore, we succeded to detect and measure even the horizontal polarization of ODRI. To our knowledge this is the first time one measures the ODRI horizontal angular distribution.

Finally measurements of ODR imaging were performed at different wavelengths, with and without polarizer. This method might provide an additional method for beam energy evaluation.

4 Outlook for 2012 Activity

Next beam time for the ODRI experiment is scheduled in February 2012. We plan

- to measure the ODRI angular distribution from beams with different aspect ratio, i.e. flat beam typical for colliders, which means different angular divergences. This measurement would allow to prove experimentally that the beam angular divergence in the plane normal to the slit can be distinguished and its contribution identified;

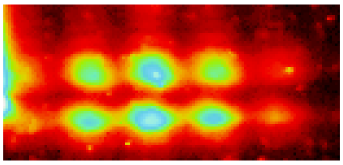

Figure 3: *Image of the horizontal component of the ODRI angular distribution (800 nm, 1.2 GeV, 80 nC integrated charge).*

- to perform a totally non intercepting quadrupole scan, therefore measure the normalize transverse emittance by means of ODRI angular distribution.

Afterwards, in Summer 2012, the bypass line will be dismounted to allow the upgrade to FLASH2. The ODRI diagnostics station has been requested to be mounted at FLASH2 on the main line after the variable gap undulator, where optimized electron beam transport is foreseen.

In addition to the operation of ODRI as standard diagnostics, further experiments are foreseen to study the contribution and the effects of coherent emission due to microbunching within the electron beam.

5 Publications

- M. Castellano, E. Chiadroni, A. Cianchi, "Phase Control Effects in Optical Diffraction Radiation from a Slit", Nucl. Instr. and Methods in Physics Research A **614**, 163 - 168 (2010).
- A. Cianchi *et al.*, "Nonintercepting electron beam size monitor using optical diffraction radiation interference", Phys. Rev. Special Topics - Accel. and Beams **14**, Issue 10, 102803 (2011).
- E. Chiadroni, M. Castellano, A. Cianchi, K. Honkavaara, G. Kube, "Effects of transverse electron beam size on transition radiation angular distribution", Nucl. Instr. and Methods in Physics Research A **673**, 56 - 63 (2012).

6 Acknowledgment

Authors wish to thank colleagues collaborating from participant institutions: L. Catani, A. Cianchi (INFN Roma 2-Tor Vergata) and K. Honkavaara, G. Kube (DESY).

References

1. E. Chiadroni *et al.*, Nucl. Instr. and Meth. in Phys. Res. B **266**, 37893796 (2008).
2. E. Chiadroni, M. Castellano, A. Cianchi, K. Honkavaara, G. Kube, TUOA02, in: Proc. of DIPAC 2009, Basel, Switzerland.
3. A. Cianchi *et al.*, "Nonintercepting electron beam size monitor using optical diffraction radiation interference", Phys. Rev. Special Topics - Accel. and Beams **14**, Issue 10, 102803 (2011).
4. A. Cianchi *et al.*, Proc. of the RREPS Conference, London, UK (2011).

SPACEWEATHER

M.A.Franceschi, G.Mazzenga (Tecn.), T. Napolitano, M.Ricci (Resp.), B.Spataro

Participant Institutions:

ITALY: INFN Bologna, LNF, Napoli, Perugia and Roma 2-Tor Vergata; ASI (Italian Space Agency);
RUSSIA: MePhi, IBMP, Roscosmos
CHINA:CNSA (Chinese Space Agency), CEA (Chinese Earthquake Administration)

1 Introduction

The SPACEWEATHER experimental program (previously named ALTCRISS/SI-RAD) is devoted to the exploration - through dedicated space missions - of three main research fields:

1. Interaction between terrestrial geophysical events and Earth radiation belts.
2. Physics of the space environment in Earth orbits.
3. Biomedical effects of space radiation on human body.

These tasks will be achieved by:

1. The study of the correlation between seismic events and perturbation of the Van Allen belts.
2. Monitoring of the radioactive environment and of the nuclear abundances inside and outside the ISS (International Space Station).
3. Measurements of passive shielding to reduce the dose on astronauts.
4. Study of the "light flashes" phenomenon observed by astronauts in space.

This program is a continuation and an extension of the activities carried out for the experiments SIEYE1 and SIEYE2 on board the Russian Space Station MIR in the years 1995-2002 and for the experiment SIEYE3/ALTEINO on board the International Space Station (ISS), still running [1) 2) 3)].

2 The Experimental Program

In 2011, the SPACEWEATHER experiment received the approval for the development and the realization of a series of detectors (mini-magnetic spectrometer, electric field detector, magnetic field detector, low frequency e.m. wave detector), under the acronym CSES (Chinese Seismo-Electromagnetic Satellite), to study the fast variations of the fluxes of protons and electrons trapped in the radiation belts due to pertrbations caused by seismic events. In the Sections of Roma Tor Vergata and in the LNF an executive project to set up the sensors for the measurement of the electric field and of the first level data acquisition system has been carried out. Laboratory tests are in progress. The Section of Perugia is developing the design of the magnetic spectrometer and is carrying out laboratory tests as well. The mechanics of the experiment is being designed in Bologna. Roma Tor Vergata is also in charge of the general system of data acquisition, storage and telemetry of the italian portion of the experiment. Agreements between the Space Agencies ASI and CSNA have started during this year and are in progress. In Fig.1, a sketch of the CSES Satellite and the Payload instruments is shown.

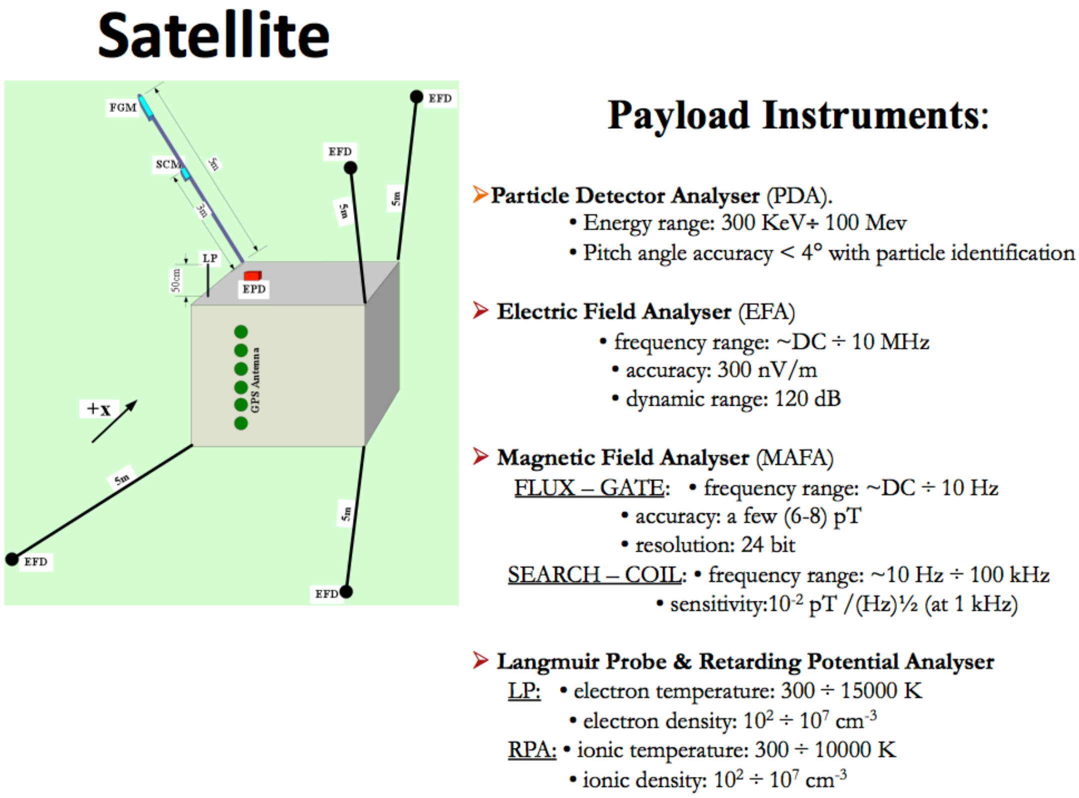

Figure 1: Sketch of the CSES Satellite with the Payload Instruments.

The task of the SI-RAD-ALTCRISS experiment (approved by ESA and ASI in Phase A) was to develop a detector to be placed on the external part of the ISS. The detector will be used to monitor cosmic rays and radiation environment in Low Earth Orbit. Long term (Solar modulation) and short term (coronal mass ejections, orbit dependence) effects on the particle flux will be monitored as well as the dose absorbed by the astronauts. In addition, data will be compared with measurements taken inside the ISS with ALTEA [4)], ALTEINO and LAZIO/SIRAD [5)] detectors to validate radiation transport and dose estimation codes. At the same time, the investigation, with a more sophisticated instrument, of the "Light Flashes" phenomenon [6)], will be conducted to improve and refine the results obtained with the previous SIEYE experiments.

The preparation of the next SI-RAD extended mission is advancing towards the completion and test of the full flight instrument consisting of a 16-plane tower of double-sided silicon detectors (8x8 cm^2 area) equipped with trigger and anticoincidence counters, as shown in Fig.2. The total weight is about 15 kg and the total power consumption should not exceed 30 W. The hardware set-up is accomplished through three steps by the construction of a laboratory prototype model, an engineering model and the final flight, space qualified model.

The activity has been mainly focused on the development of the following systems of the engineering model:

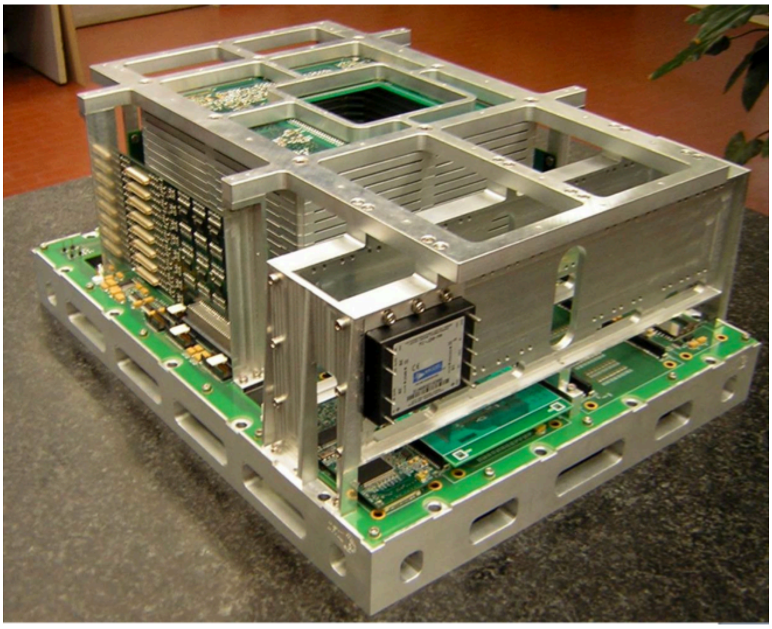

Figure 2: The SI-RAD detector.

- Trigger system.
- Development of Silicon Photomultiplier (SI-PM) technology for space applications and test of different SI-PM configurations.
- Completion and test of a highly integrated silicon board (16 cm x 16 cm).
- Production and test of a low-power, low-mass Digital Processing Unit (DPU).

For the year 2012, the planned activity includes the completion of the engineering unit and the set-up of the flight configuration equipped with autotrigger capabilities for heavy nuclei and a trigger for crossing protons and nuclei. The interface with the ISS Space Station will be realized with an intermediate CPU to manage the telecommands from ground and the download of the data. Beam tests at the LNF-BTF, GSI/Darmstadt and other facilities are also planned together with the continuation of the R&D on the SI-PM technology.

3 Activity of the LNF group

The LNF group has taken the responsibility of the design, construction and test of the mechanical structures and interfaces of the three models of the SI-RAD detector also contributing to the integration of the mechanical support for the DAQ. This activity is carried out with the support and the participation of the LNF Service for Design and Mechanical Costructions (SPCM). The activity in 2011 has been mainly devoted to the completion of the mechanical support of the engineering model and to the interfaces of the front-end and DAQ with the detector, ready to be tested on beams. These systems are being developed for the final space-qualified flight configuration in the year 2012. The LNF group participates as well in the beam test activities at the above mentioned facilities having the responsibility of the beam trigger counters and of the general arrangement and set-up. Finally, the LNF is actively participating in the definition studies and first executive designs of CSES prototypes of the sensors for the measurement of the electric field and for the DAQ of the experiment.

4 Selection of recent publications

1. V. Zaconte *et al.*, "The radiation environment in the ISS-USLab measured by ALTEA", Adv. Sp. Res. **46**, 797 (2010).
2. V. Zaconte *et al.*, "High Energy Radiation fluences in the ISS-USLab: ion discrimination and particle abundances", Rad. Meas. **45**, 168 (2010).
3. C. La Tessa *et al.*,"Estimate Of The Space Station Shielding Thickness At A USLab Site Using ALTEA Measurements And Fragmentation Cross Sections", Nucl. Instr. Meth. Phys. Res. **B267**, 3383 (2009)
4. M. Casolino *et al.*," Investigation of radiation environment and Light Flash phenomenon on board manned space stations with silicon detector telescopes", Nuovo Cim. **31C**, 77 (2008).
5. M. Casolino *et al.*,"The ALTCRISS project on board the International Space Station", Adv. Space Res. **40**, 1746 (2007).

References

1. V.Bidoli *et al.*,"In-flight performances of SilEye-2 Experiment and cosmic ray abundances inside space station MIR"; Journal of Physics G: Nuclear and Particle Physics **27**, 2051(2001).
2. M.Casolino *et al.*,"The Sileye/3-Alteino experiment on board the International Space Station"; Nucl.Phys. **113B**, 88 (2002).
3. V.Bidoli *et al.*, "Dual origin of light flashes in space", Nature **422**, 680 (2003).
4. L.Narici *et al.*,"ALTEA: Anomalous long term effects in astronauts. A probe on the influence of cosmic radiation and microgravity on the central nervous system during long flights", Adv. Space Res. **31**, 141 (2003).
5. F.Altamura *et al.*,"Preliminary results from the LAZIO-Sirad experiment on board the International Space Station", Proc. XXIX ICRC, Pune (2005), SH35 p.101.
6. G. Horneck, "Radiobiological experiments in space: a review", Nucl. Tracks Radiat. Meas., **20**, 185 (1992).

TERASPARC: THE TERAHERTZ RADIATION SOURCE AT SPARC

P. Calvani (Resp., Ass.), M. Bellaveglia, M. Boscolo, M. Castellano, M. Cestelli Guidi (Art. 23), E. Chiadroni, G. Di Pirro, M. Ferrario, G. Gatti, A. Nucara (Ass.)
L. Palumbo (Ass.), R. Sorchetti (Tecn.), C. Vaccarezza

Participant Institutions:
INFN LNF, Roma 1-La Sapienza, Roma 2-Tor Vergata, LNS, Torino; Univ. of Roma Tor Vergata; SBAI Dept. Univ. of Roma La Sapienza.

1 Introduction

The motivation for developing a linac-based THz source at SPARC stays in the ever growing interest of filling the so-called THz gap with high peak power radiation. From simulations, the peak power expected at SPARC is in the order of 10^8 W. This result has been confirmed by measurements presented in [1]. The corresponding energy per pulse is of the order of tens of μJ, that is well above standard table top THz sources.

Applications of this kind of source concern mainly time domain THz spectroscopy and frequency domain measurements on novel materials [2]. Beyond these applications, coherent THz radiation is also used as longitudinal electron beam diagnostics to reconstruct the beam charge distribution [3].

In addition, taking advantage from electron beam manipulation techniques, high power, narrow-band THz radiation can be also generated at SPARC [4, 5]. This provides a unique chance to realize, with the SPARC THz source, THz-pump/THz-probe spectroscopy, a technique practically unexplored up to now.

2 The THz source at SPARC

The TERASPARC project, which aims at the development and characterization of THz radiation at SPARC [6], is the result of a collaboration between LNF, INFN-Roma1, LNS, INFN-Torino, INFN-Roma2 and University of Roma Tor Vergata.

The source is Coherent Transition Radiation (CTR) from an aluminum coated silicon screen. The screen is placed in the vacuum pipe at the end of the by-pass, at 45^o with respect to the electron beam direction (Fig. 1). TR is extracted at 90^o with respect to the beam axis through a z-cut quartz window and then collected by a 90^o off-axis paraboloid mirror. The parallel beam is then reflected down to a flat mirror at 45^o which reflects radiation horizontally. Figure 2 shows the two schemes foreseen: one for interferometer measurements and one for integrated CTR measurements with the possibility of selecting custom band pass filters in the THz range [7].

CTR is emitted by both an ultra-short high-brightness electron beam and a longitudinally modulated one [1]. The technique used at SPARC to manipulate such electron beam relies on low energy RF compression, i.e. the velocity bunching [8] and on the use of properly shaped trains of UV laser pulses hitting the photo-cathode, i.e. laser comb beam [9].

3 Achievements in 2011

The activity in 2011 was focused on the commissioning of the Martin-Puplett interferometer [10] for frequency domain measurements in order to characterize the coherent THz radiation emitted by both single sub-ps electron beams and comb ones in the spectral range between 100 GHz and 5 THz.

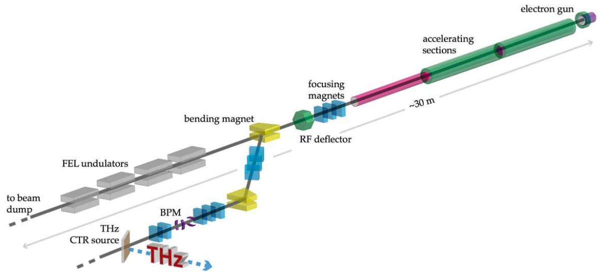

Figure 1: *Layout of the SPARC accelerator, with the THz source placed at the end of the by-pass line.*

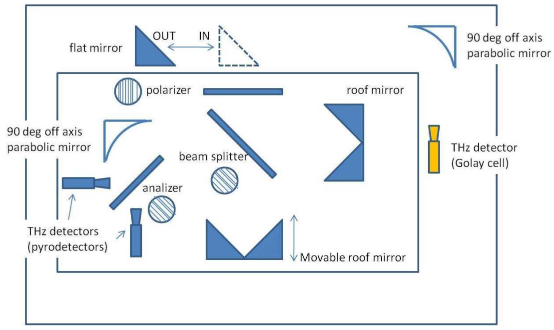

Figure 2: *Drawing of the experimental layout for detection of THz radiation (top view).*

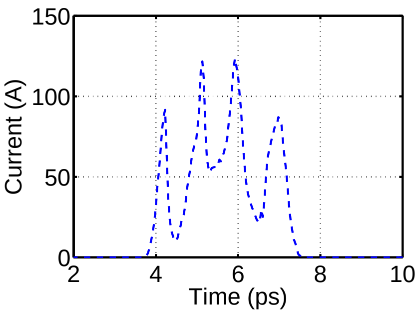

Figure 3: *Current profile of the 4-pulses comb beam as measured at the beginning of the dogleg.*

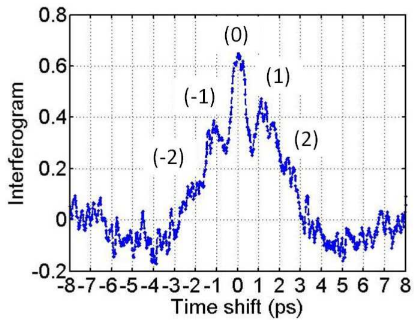

Figure 4: *Multipeaked interferogram, typical of a comb beam, measured by means of the Martin-Puplett interferometer.*

The main advantages with respect to a well-known Michelson interferometer derive from the beam splitter properties. The beam splitter is a wire grid whose reflectivity coefficients depend on wires diameter and spacing. Furthermore, it splits polarizations, thus measuring the intensity of both polarizations, the difference interferogram can be normalized to the sum. Correlated fluctuations due to electron beam instabilities are then canceled.

Autocorrelation measurements of the SPARC THz source have been performed with different electron beam configurations, i.e. single bunch and laser comb (2 and 4 bunches in the train), in order to exploit different regimes of coherent THz emission, i.e. broad band and narrow band, respectively. Figures 3-6 report one of the interesting results we obtained so far at SPARC. A four-pulses electron beam, with pulse separation of the order of ps and total beam charge of 200 pC has been produced and optimized by combining both velocity bunching and laser comb techniques, to generate quasi-narrow band THz radiation.

Both curves of Fig. 6 are obtained by taking into account the single particle TR spectrum in far field approximation and for a finite target size. The experimental system transfer function is also considered. A well defined narrow band peak centered around 0.8 THz is visible, as expected from the interferogram peaks distance.

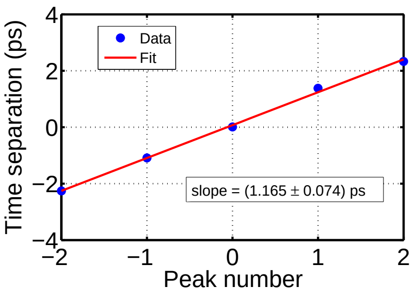

Figure 5: *Bunch separation in the train.*

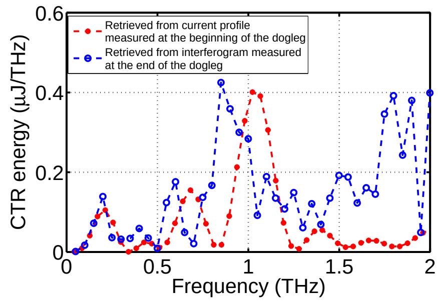

Figure 6: *CTR energy per pulse from the measured interferogram (blue curve) and as expected (red curve) from the 4-pulses comb beam measured at the beginning of the dogleg.*

4 Outlook for 2012 Activity

The activity in 2012 will be dedicated to the installation and commissioning of an optical delay line for pump-probe THz measurements. In particular, we will measure (in collaboration with Roma III and CNR) the lifetime of excited states in quantum wells (QW) finalized to the realization of a new kind of Quantum Cascade Laser built by Si-Ge instead of GaAlAs.

An additional THz station will be installed at the end of the third linac section in Spring 2012. Both CTR and Coherent Diffraction Radiation (CDR) can be produced, the lattest however being dependent on the SPARC upgrade in energy after the installation of the two C-band structures.

The THz station on the main line will allow also to investigate the coherent optical transition radiation (COTR) spectrum expected from the modulation on the electron beam induced by intense IR laser pulses.

In Summer 2012, the installation of the magnetic chicane on the by-pass line, right before the first THz station, will allow to explore the hybrid electron beam compression, i.e. moderate compression at low energy by means of velocity bunching and final compression at high energy with the magnetic compressor.

Both THz stations will be used to characterize high-speed bolometer detectors in collaboration with the INFN section of Torino and Catania, and THz CCD sensors.

Finally, the two THz stations will provide a valid and permanent tool for the reconstruction of the electron beam longitudinal profile along the accelerator.

5 List of Conference Talks by LNF Authors in Year 2010

- E. Chiadroni, Characterization of the THz source at SPARC, Invited seminar at Karlsruhe Institut of Technology - ANKA (2010), Karlsruhe, Germany.
- E. Chiadroni, Characterization of the THz source at SPARC, International Particle Accelerators Conference IPAC'10, Kyoto, Japan.
- E. Chiadroni, The THz Radiation Source at the SPARC Facility, 6th Workshop on Infrared Spectroscopy and Microscopy with Accelerator-Based Sources, Trieste (2011).
- E. Chiadroni, The THz radiation source at SPARC, Invited talk at RREPS Conference, London (UK), 2011.

6 Publications

- E. Chiadroni *et al.*, "Characterization of the THz radiation source at SPARC", in: Proc. of IPAC'10 Conference, Kyoto, Japan (2010).
- E. Chiadroni *et al.*, "Production of high power terahertz radiation through the SPARC Free-Electron Laser", in: Proc. of the 35th International Conference on Infrared Millimeter and Terahertz Waves (IRMMW-THz), Rome (2010).
- E. Chiadroni *et al.*, "The THz Radiation Source at the SPARC Facility", in: Proc. of the 6th Workshop on Infrared Spectroscopy and Microscopy with Accelerator-Based Sources, Trieste (2011).
- E. Chiadroni *et al.*, "The THz radiation source at SPARC", in: Proc. of RREPS Conference, London (UK), 2011.

7 Acknowledgment

Authors wish to thank colleagues collaborating from participant institutions:

- INFN Roma 1-La Sapienza: O. Limaj, S. Lupi
- University of Rome La Sapienza, SBAI: L. Palumbo, A. Mostacci
- INFN Roma 2-Tor Vergata: L. Catani, A. Cianchi, B. Marchetti, S. Tazzari
- INFN LNS: A. Rovelli
- INFN Torino: R. Gerbaldo, G. Ghigo, L. Gozzellino, E. Mezzetti, B. Minetti

References

1. E. Chiadroni *et al.*, Proc. of IPAC 2010, TUOARA03, Kyoto (2010).
2. M.S. Sherwin *et al.*, Opportunities in THz Science, Report of a DOE-NSF-NIH Workshop (2004).
3. E. Chiadroni, "Bunch Length Characterization at the TTF VUV-FEL", TESLA-FEL 2006-09 (2006).
4. A. Mostacci *et al.*, Proc. of IPAC 2011, THYB01, San Sebastian (2011).
5. E. Chiadroni *et al.*, Proc. of the RREPS Conference, London (UK) (2011).
6. D. Alesini *et al.*, Nucl. Instrum. and Meth. in Phys. Res. A 507, 345 (2003).
7. N. I. Landy, 1-4244-1449-0/07/$25.00 c 2007 IEEE (2007); P. Carelli *et al.*, unpublished (arXiv:0907.3620v2).
8. M. Ferrario *et al.*, Physical Review Letters **104**, 054801 (2010).
9. M. Ferrario *et al.*, Nucl. Instrum. and Meth. in Phys. Res. A (2010), doi:10.1016/j.nima.2010.02.018.
10. D. H. Martin and E. Puplett, Infrared Physics, vol. 10, pp. 105-109 (1970).

TPS

V. Patera (Resp.)

Not received

BY-NanoERA

(Institutional Development of Applied Nanoelectromagnetics: Belarus in ERA Widening)

S.Bellucci (Resp. INFN), R. Baldini (Tecn.), L. Coderoni (Bors.), G. Giannini (Ass. Ric.), F. Micciulla (Ass. Ric.), I. Sacco (Bors.)

External collaborating Institutions:

Institute of Nuclear Problems of Belarusian State University,
Institut fuer Festkoerperphysik, Technische Universitaet Berlin,
Central Laboratory of Physico-Chemical Mechanics, Bulgarian Academy of Sciences, Sofia,
Institute of Electronic Structure and Laser (IESL), Heraklion, Crete,
Belarusian Institute of System Analysis and Information Support of Scientific Technical Sphere,
Science & Technology Park “Metolit” at Belarusian National Technical University.

We participate as a partner (the INFN unit) to the Coordination and support actions of the FP7-INCO-2010-6. BY-NanoERA has a duration of 36 months and started its activities on 1st January 2011. The consortium binds together four Universities, two Research Organizations and an industry (Science & Technology Park).

Project objectives:

The main objectives of the project BY-NanoERA are to prove necessity and promising capability of nanoelectromagnetics in the core objective of FP7 Theme 4 'Nanosciences,Nanotechnologies, Materials and new Production Technologies – NMP' and to develop a concept of nanoelectromagnetics as a perspective direction in NMP. We also wish to establish network with research centers in Member States or Associated Countries in the field of applied nanoelectromagnetics aimed with the progress in solving concrete scientific problems and submission of joint research projects, as well as to organize a set of workshops and seminars on nanoelectromagnetics.

Publications by LNF Authors in the Year 2011

P. Kuzhir, V. Ksenevich, A. Paddubskaya, T. Veselova, D. Bychanok, A. Pliyushch, A. Nemilentsau, M. Shuba, S. Maksimenko, L. Coderoni, F. Micciulla, I. Sacco, G. Rinaldi, BELLUCCI S. (2011). CNT Based Epoxy Resin Composites for Conductive Applications. NANOSCIENCE AND NANOTECHNOLOGY LETTERS, vol. 3; p. 889-894, ISSN: 1941-4900

List of Conference Talks by LNF Authors in the Year 2011

S. Bellucci, “Spectral features of carbon based epoxy nanocomposites at Terahertz frequencies”. Presented at Nanoscience & Nanotechnology 2011, Laboratori Nazionali di Frascati 19-23 September 2011.

F. Micciulla, Epoxy-Nano-Carbon Shielding Coating for Super-High-Frequency range, INTERNATIONAL SEMICONDUCTOR CONFERENCE - 34à Edition, October 17 – 19, Sinaia, ROMANIA

S. Bellucci, Spectral features of carbon based epoxy nanocomposites at Terahertz frequencies. XX Convegno Italiano di Scienza e Tecnologia delle Macromolecole Terni 4 - 8 Settembre 2011.

DENSE

Development and Electromagnetic Characterization of Nano Structured Carbon Based Polymer CompositEs

S. Bellucci (Resp. INFN), R. Baldini (Tecn.), L. Coderoni (Bors.), G. Giannini (Ass. Ric.), F. Micciulla (Ass. Ric.), I. Sacco (Bors.)

External collaborating Institutions: Univ. Roma La Sapienza, Università degli Studi di SALERNO, Università degli Studi di PALERMO.

We participate as a partner (the INFN unit) to the PROGRAMMA DI RICERCA SCIENTIFICA DI RILEVANTE INTERESSE NAZIONALE (PRIN) of the Italian MINISTERO DELL'ISTRUZIONE DELL'UNIVERSITà E DELLA RICERCA DIREZIONE GENERALE DELLA RICERCA. DENSE has a duration of 36 months and started its activities on 1st January 2010. The consortium binds together three Universities (with four different Departments) and one Research Organization.

Project objectives:

The main objectives of the project DENSE are the realization and characterization of new multifunctional polymeric nanocomposites employing as nanofillers graphene and multiphase systems clay/Carbon Nanotubes (CNTs). Such nanocomposites, based on thermosetting (epoxy) resin are intended for industrial applications, such as aeronautics, automotive, electronics, where remarkable thermal and mechanical properties and, at the same time, tailored and controlled electromagnetic (EM) performances are required. The design and realization of such nanocomposites will be performed from the tailoring of the electromagnetic performances.

In fact, although several interesting results had been obtained in the realization of new and improved nanocomposites, the researchers are still far from obtaining a precise control of the desired nanostructure and thus optimize the materials performances. To reach such a goal it is required to act on both the choice of the most appropriate nanofillers and the fabrication techniques. The present research proposal pursues both aspects, by deepening the knowledge of the basic chemical and physical mechanisms and enhancing the technological competences required for the production of nanocomposites based on graphene and multiphase clay/CNTs. These nanocomposites are potentially very interesting for different industrial applications but, up to now, have not been intensively and accurately investigated.

An extensive structural and morphological analysis will be carried out on nanofillers and nanocomposites in order to provide detailed information on nanostructures. These data will be correlated with the information obtained from an accurate characterization at both micro and macro scale concerning EM properties (at low and high frequency), thermal and mechanical characteristics in order to improve the physical and numerical models adopted in materials analysis and design.

A further effort is aimed at the global optimization of the base materials properties (nanofillers and polymer) and parameters of the production process able to lead to the desired EM performances of the nanocomposites. Robust optimization techniques will be employed to overcome the drawbacks of the currently adopted approaches consisting in the choice of the best solution for each step of the production process parameters (local optimization) which generally may not lead to the global optimum. The main objectives are pursued by a multidisciplinary research team composed by five Research Units which develop complementary and integrated research lines.

Relevant results achieved:

L`attività condotta dall` INFN-LNF ha riguardato la caratterizzazione meccanica ed elettrica di materiali nanocompositi, i quali sono stati realizzati utilizzando come matrice una resina epossidica (EPIKOTE 828) caricata con diversi tipi di fillers quali: nanotubi di carbonio, carbon black (nero fumo) e grafite.

Il lavoro ha riguardato lo studio delle proprietà meccaniche ed elettriche, condotto su materiali epossidici nanostrutturati. Sono stati studiati gli effetti che la concentrazione e il grado di dispersione dei nanotubi di carbonio (Cnts) producono sullo sforzo a trazione e sulla conducibilità elettrica dei nanocompositi. Al fine di realizzare questi materiali, è stata utilizzata come matrice una resina epossidica (EPIKOTE 828), che si presenta come un liquido a viscosità medio-bassa a temperatura ambiente ed à induribile mediante reazione di curing con poliammine. L'indurente, denominato A1 (peso specifico 1.02g/cm3 e viscosità 0.21Pa s a 25à C), à stato ottenuto partendo da una comune TEPA (tetraetilenpentammina) fatta reagire con formaldeide (CH2O). Tale resina à stata caricata con diverse percentuali di nanofillers conduttivi, quali Cnts sintetizzati ai LNF dalla nostra Unità (gruppo NEXT di nanotecnologie) con il metodo della scarica ad arco. Per verificare l'efficienza del rivestimento, sono stati presi, come fillers di riferimento, grafite e carbon black, sui quali sono state eseguite sia prove meccaniche che elettriche.

Da un punto di vista meccanico, l'analisi ha mostrato che:

- Le proprietà meccaniche della matrice non vengono migliorate dai fillers, in quanto si tratta di fibre corte (o materiale amorfo).

- A parità di concentrazioni, i compositi caricati con i Cnts risultano essere sostanzialmente migliori rispetto a quelli caricati sia con carbon blak che con grafite.

Da un punto di vista elettrico, l'analisi ha mostrato che:

- La conducibilità elettrica aumenta all'aumentare della concentrazione dei Cnts. Cià probabilmente avviene perchà essi si distribuiscono in maniera tale da creare un percorso preferenziale per il passaggio della corrente all'interno della matrice stessa.

- A parità di concentrazioni poi, i compositi caricati con i Cnts hanno conducibilità elettrica maggiore di quelli caricati con carbon black e grafite.

In un secondo momento, poichè i Cnts hanno mostrato valori di conducibilità elettrica maggiori rispetto agli altri fillers, abbiamo ritenuto opportuno confrontarli con Swnts e Mwnts commerciali, ottenuti con la tecnica CVD (Chemical Vapor Deposition). Sui nanocompositi ottenuti con tali fillers sono state eseguite misure elettriche in corrente continua e misure di permittività nel campo delle microonde.

Per quanto riguarda le misure elettriche in corrente continua, a basse percentuali di carica i risultati ottenuti sembrano indicare che il metodo di sintesi con la tecnica a scarica ad arco fornisca risultati migliori rispetto alla crescita dei nanotubi tramite la tecnica CVD. A tal proposito i campioni sono stati sottoposti a micrografie T.E.M. e S.E.M., le cui immagini mostrano come i Cnts-INFN (scarica ad arco) presentino minori difetti rispetto a quelli commerciali (CVD). A percentuali di carica maggiori, invece, si puà notare che mentre i valori di resistività della matrice con Cnts-Infn e della matrice con Mwnts sono confrontabili tra loro, il valore della resistività della matrice caricata con Swnts à all'incirca di 3 ordini di grandezza inferiore. Crescendo dunque il contenuto di nanotubi si attiva il meccanismo di percolazione, in cui si forma un network interconnesso (si à dunque superato la soglia di percolazione).

Infine, per quanto riguarda le misure nel campo delle microonde, si à riscontrato che i Mwnts commerciali sono più efficaci dei Swnts per la realizzazione di materiali compositi conduttivi in corrente continua. Allo stesso tempo, utilizzando gli stessi compositi resina/Cnts nella banda Ka (26-37 GHz), i risultati hanno dimostrato che nel range 26-27 GHz, entrambe le cariche hanno quasi la stessa efficienza, anche se i Swnts mostrano risultati leggermente migliori.

Publications by LNF Authors in the Year 2011

BELLUCCI S., L. Coderoni, F. Micciulla, G. Rinaldi, and I. Sacco (2011). Mechanical and Electrical Characterization of Polymer Nanocomposites with Carbon Nanotubes. NANOSCIENCE AND NANOTECHNOLOGY LETTERS, vol. 3; p. 826-834, ISSN: 1941-4900

The Electrical Properties of Epoxy Resin Composites Filled with Cnts and Carbon Black.
Bellucci, S.; Coderoni, L.; Micciulla, F.; Rinaldi, G.; Sacco, I., Journal of Nanoscience and Nanotechnology, Volume 11, Number 10, October 2011 , pp. 9110-9117(8)

P. Kuzhir, V. Ksenevich, A. Paddubskaya, T. Veselova, D. Bychanok, A. Pliyushch, A. Nemilentsau, M. Shuba, S. Maksimenko, L. Coderoni, F. Micciulla, I. Sacco, G. Rinaldi, BELLUCCI S. (2011). CNT Based Epoxy Resin Composites for Conductive Applications. NANOSCIENCE AND NANOTECHNOLOGY LETTERS, vol. 3; p. 889-894, ISSN: 1941-4900

BELLUCCI S., L. Coderoni, F. Micciulla, I. Sacco (2011). Development of Micro and Nano Electro--Mechanical Technologies for Space Transportation Systems. NANOSCIENCE AND NANOTECHNOLOGY LETTERS, vol. 3; p. 876-876, ISSN: 1941-4900

BELLUCCI S., S. Bini, F. Micciulla, A. Dinescu, and M. Danila (2011). Synthesis of Titanium Nitride Film by RF Sputtering. NANOSCIENCE AND NANOTECHNOLOGY LETTERS, vol. 3; p. 856-864, ISSN: 1941-4900

Dabrowska A, Huczko A, Soszynski M, Bendjemil B, Micciulla F, Sacco I, Coderoni L, BELLUCCI S. (2011). Ultra-fast efficient synthesis of one-dimensional nanostructures. PHYSICA STATUS SOLIDI B-BASIC RESEARCH, vol. 248; p. 2704-2707, ISSN: 0370-1972, doi: 10.1002/pssb.201100054

List of Conference Talks by LNF Authors in the Year 2011

“Nanotechnology”, S. Bellucci, PRIN DENSE Meeting Univ. Roma Sapienza, 22 Feb. 2011;

R. D’Elia, “Carbon nanotubes into ablative Thermal Protection Systems (TPS)”, Presented at Nanoscience & Nanotechnology 2011, Laboratori Nazionali di Frascati 19-23 September 2011.

DAΦNE

The DAΦNE Team
D. Alesini, M.E. Biagini, S. Bini (Osp.), C. Biscari, R. Boni, M. Boscolo, B. Buonomo, A. Clozza, G. Delle Monache, T. Demma (Art. 23), E. Di Pasquale (Art. 23), G. Di Pirro, A. Drago, L. Foggetta (Osp.), A. Gallo, A Ghigo, S. Guiducci, C. Ligi, S. Liuzzo (Dott.), F. Marcellini, G. Mazzitelli, C. Milardi, L. Pellegrino, M. Preger, L. Quintieri (Art. 23), P. Raimondi (Art. 23, Resp.), R. Ricci, U. Rotundo, C. Sanelli, M. Serio, F. Sgamma B. Spataro, A. Stecchi, A. Stella, S. Tomassini, C. Vaccarezza, M. Zobov

The DAΦNE Technical Staff
G. Baldini, P. Baldini, A. Battisti, A. Beatrici, M. Belli, B. Bolli, L. Cacciotti, G. Ceccarelli, R. Ceccarelli, A. Cecchinelli, S. Ceravolo, P. Chimenti (Art. 15), P. Ciuffetti, R. Clementi, O. Coiro, S. De Biase, M. De Giorgi, R. Di Raddo, G. Ermini, M. R. Ferrazza, G. Fontana, U. Frasacco, C. Fusco, F. Galletti, E. Gaspari, M. Giabbai, O. Giacinti, E. Grossi, F. Iungo, V. Lollo, M. Marchetti, S. Martelli, C. Marini, M. Martinelli, A. Mazzenga, C. Mencarelli, M. Monteduro, M. Paris, E. Passarelli, V. Pavan, S. Pella, D. Pellegrini, G. Piermarini, S. Quaglia, M. Rondinelli, L. A. Rossi (Art. 15), M. Sardone, M. Scampati, G. Sensolini, R. Sorchetti, A. Sorgi, M. Sperati, A. Sprecacenere, S. Strabioli (Art. 15), R. Tonus, T. Tranquilli, M. Troiani, V. Valtriani, R. Zarlenga, A. Zolla

DAΦNE is an electron-positron Φ *meson factory* operating at Frascati since 1997. Factories are storage ring colliders designed to work at the energies of the meson resonances, where the production cross section peaks, to deliver a high rate of events to high resolution experiments.

The factory luminosity (the number of events per unit time produced by the reaction under investigation divided by its cross section weighted by the acceptance of the detector) is very high, about two orders of magnitudes larger than that obtained at the same energy in colliders of the previous generation. One of the key-points to get a substantial luminosity increase is the use of separated vacuum chambers for the two beams merging only in the interaction regions (IRs). When sharing the same ring the two N-bunch trains cross in $2N$ points and the maximum luminosity is limited by the electromagnetic beam-beam interaction. The unwanted effects of this interaction can be reduced with a very strong focussing (called "low-β") at the interaction point (IP), obtained by means of quadrupole doublets or triplets. However these magnetic structures take up much space and excite chromatic aberrations which must be corrected elsewhere in the ring.

This limitation does not hold for the double ring option, consisting in two separate rings crossing at two low-β points. The number of bunches that can be stored in such a collider is limited only by the geometry of the IR's.

DAΦNE is an accelerator complex consisting of a double-ring collider, a linear accelerator (LINAC), an intermediate damping ring to make injection easier and faster and 180 m of transfer lines connecting these machines. The beam accelerated by the Linac can also be switched into a laboratory called "Beam Test Facility (BTF)", for dedicated experiments and calibration of detectors. Three synchrotron radiation lines, two from bending dipoles and the other from the wiggler are routinely operated by the DAΦNE-LIGHT group in a parasitic mode, providing photons from the infrared to soft x-rays.

1 Injection System

In a low energy electron-positron collider, such as DAΦNE, the lifetime of the stored current is mainly limited by the Touschek effect, namely the particle loss due to the scattering of the particles inside the bunches. In the present typical operating conditions the Touschek lifetime is below 1000 s. It is therefore necessary to have a powerful injection system, capable of refilling the beam without dumping the already stored one. In addition, flexibility of operation requires that any bunch pattern can be stored among the 120 available buckets. The injection system of DAΦNE is therefore designed to deliver a large rate of particles in a single bunch at the working energy of the collider. It consists of a linear accelerator with a total accelerating voltage of 800 MV. In the positron mode, electrons are accelerated to ≈ 250 MeV before hitting a tungsten target (called positron converter) where positrons are generated by bremsstrahlung and pair production with an efficiency of $\approx 1\%$. The positrons exit from the target with an energy of few MeV and are then accelerated by the second section of the LINAC to their final energy of ≈ 0.51 GeV. The positrons are then driven along a transfer line and injected into a small storage ring, called Accumulator, at frequency of 50 Hz. Up to 15 positron pulses are stacked into a single bucket of the Accumulator, then injection stops and the bunch damps down to its equilibrium beam size and energy spread, which are much smaller than the LINAC ones. Damping takes ≈ 0.1 s and then the beam is extracted from the Accumulator and injected into the positron main ring at an overall repetition rate of 2 Hz. A powerful and flexible timing system allows the storage of any desired bunch pattern in the collider. In the electron mode, a magnetic chicane deviates the particle trajectory around the positron converter and electrons are directly accelerated to 0.51 GeV and injected into the Accumulator in the opposite direction with respect to positron operation. They are then extracted like in the positron case and injected into the electron main ring through the second transfer line.

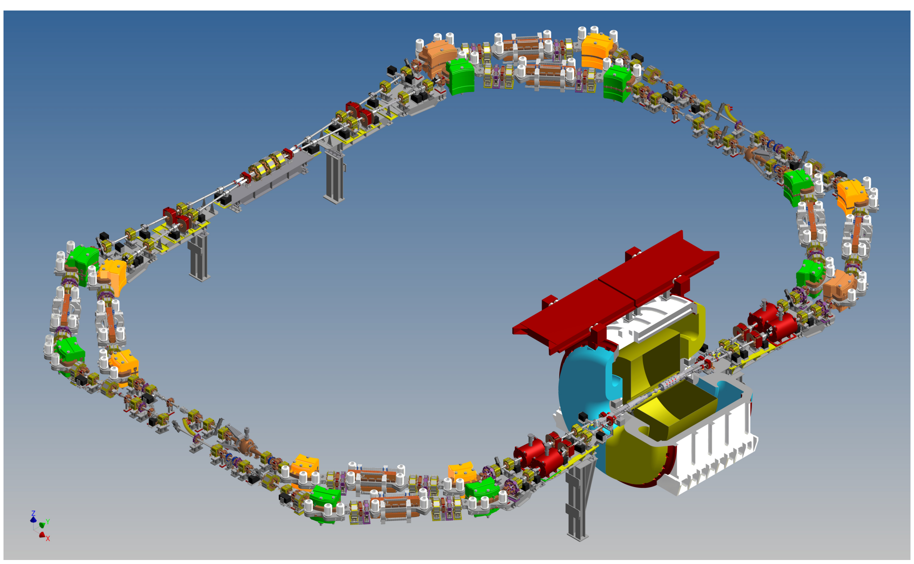

Figure 1: *The DAΦNE Main Rings in the present crab-waist scheme for the KLOE-2 run.*

The Accumulator ring has been introduced in the accelerator complex to increase the injection efficiency, especially for the positrons that are produced by the LINAC at 50 Hz rate in 10 ns pulses with a charge of $\approx$ 0.5 nC. Since the design charge of the main ring at the maximum luminosity is ≈ 1.5 μC and the longitudinal acceptance of the main rings is only 2 ns, the number of 50 Hz pulses necessary to fill the ring is of the order of 10^4. In order to avoid saturation it is therefore necessary that at each injection pulse a fraction smaller than 10^{-4} of the already stored beam is lost, and this is not easy to achieve. The Accumulator instead works with a lower frequency RF cavity and therefore with a larger longitudinal acceptance. In this way the full charge coming from the LINAC can be stored in a single RF bucket. In a complete injection cycle, that has a duration of 500 ms, up to 15 LINAC pulses can be stored in a single Accumulator RF bucket, and after being damped to the ring equilibrium emittances and energy spread, the whole stacked charge can be stored into a single RF bucket of the main ring. In this way the nominal single bunch charge can be stored with only one pulse from the Accumulator, reducing to 120 the number of injection pulses (at 2 Hz) into each main ring. As an additional benefit, the transverse beam size and energy spread of the beam coming from the Accumulator are at least one order of magnitude smaller than those of the LINAC beam, and this strongly reduces the aperture requirements of the main ring and, as a consequence, the overall cost of the collider.

2 Main Rings

In the DAΦNE collider the two beam trajectories cross at the interaction point (IP) with an horizontal angle that has been recently increased from ≈ 25 mrad to ≈ 50 mrad. A positron bunch leaving the IP after crossing an electron one will reach the following electron bunch at a distance of half the longitudinal separation between bunches from the IP.

Due to the horizontal angle between the trajectories of the two beams, the distance in the horizontal direction between the two bunches is equal to the horizontal angle times half the longitudinal distance between the bunches in each beam. The beam-beam interaction can be harmful to the beam stability even if the distance in the horizontal direction between bunches of opposite charge is of the order of few bunch widths at points where the β function is high and this sets a lower limit on the bunch longitudinal separation and therefore on the number of bunches which can be stored in the collider. However, the so called *crab waist collision scheme* (CW) recently implemented in the machine alleviates this problem, as it will be exhaustively explained in the following of this report.

By design the minimum bunch separation at DAΦNE has been set to ≈ 80 cm, and the maximum number of bunches that can be stored in each ring is 120. This number determines the frequency of the radiofrequency cavity which restore at each turn the energy lost in synchrotron radiation, which must be 120 times the ring revolution frequency. The luminosity of the collider can therefore be up to 120 times larger than that obtainable in a single ring with the same size and optical functions. Crossing at an angle could in principle be a limitation to the maximum single bunch luminosity. In order to make the beam-beam interaction less sensitive to this parameter and similar to the case of single ring colliders where the bunches cross head-on, the shape of the bunches at the IP is made very flat (typical ranges of r.m.s. sizes are $15 \div 30$ mm in the longitudinal direction, $0.2 \div 1.5$ mm in the horizontal and $2.5 \div 10$ μm in the vertical one). The double ring scheme with many bunches has also some relevant challenges: the total current in the ring reaches extremely high values (5 A in the DAΦNE design, $\approx$ 1.4 A in the DAΦNE operation so far) and the high power emitted as synchrotron radiation needs to be absorbed by a complicated structure of vacuum chambers and pumping systems in order to reach the very low residual gas pressure levels necessary to avoid beam loss. In addition, the number of possible oscillation modes of the beam increases with the number of bunches, calling for sophisticated bunch-to-bunch feedback systems.

The double annular structure of the DAΦNE collider as it is now after the recent modifications to implement the crab waist scheme (described in the following sections) with KLOE is shown schematically in Fig. 1. Both rings lay in the same horizontal plane and each one consists of a

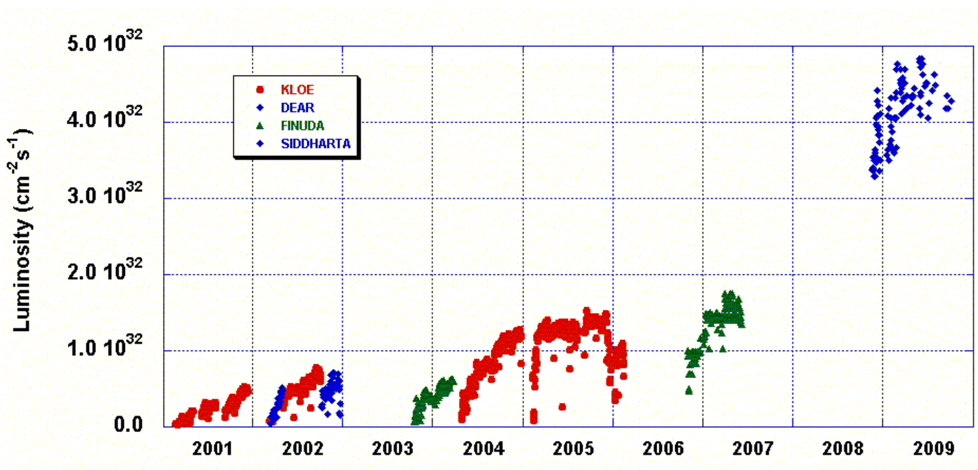

Figure 2: *Peak luminosity at DAΦNE.*

long external arc and a short internal one. Starting from the IP the two beams share the same vacuum chamber while traveling in a common permanent magnet defocusing quadrupole (QD) which, due to the beam off-axis trajectory increases the deflection of the two beam trajectories to $\approx$ 75 mrad. Shortly after the QD, the common vacuum chamber splits in two separated ones connected to the vacuum chambers of the long and short arcs. Two individual permanent magnet quadrupoles (QFs) are placed just after the chamber separation. Together with the previous QD they constitute the low-β doublets focusing the beams in the IP. The long and short arcs consist of two "almost achromatic" sections (deflecting the beam by $\approx$ 85.4 degrees in the short arc and $\approx$ 94.6 degrees in the long one) similar to those frequently used in synchrotron radiation sources, with a long straight section in between. Each section includes two dipoles, three quadrupoles, two sextupoles and a wiggler. This structure is used for the first time in an electron-positron collider and it has been designed to let DAΦNE deal with high current beams.

The amount of synchrotron radiation power emitted in the wigglers is the same as in the bending magnets and the wigglers can be used to change the transverse size of the beams. The increase of emitted power doubles the damping rates for betatron and synchrotron oscillations, thus making the beam dynamics more stable, while the possibility of changing the beam sizes makes the beam-beam interaction parameters more flexible.

The straight section in the long arc houses the kickers used to store into the rings the bunches coming from the injection system, while in the short straight arc there are the radiofrequency cavity and the equipment for the feedback systems which are used to damp longitudinal and transverse instabilities. The vacuum chambers of the arcs have been designed to stand the nominal level of radiation power emitted by the beams (up to 50 KW per ring). They consist of 10 m long aluminum structures built in a single piece: its cross section exhibits a central region around the beam and two external ones, called the antechambers, connected to the central one by means of a narrow slot. In this way the synchrotron radiation hits the vacuum chamber walls far from the beam and the desorbed gas particles can be easily pumped away. The chambers contain water cooled copper absorbers placed where the radiation flux is maximum: each absorber has a sputter ion pump below and a titanium sublimation pump above. The Main Rings have undergone many readjustments during the years to optimize the collider performances while operating for different detectors.

In principle the rings could host two experiments in parallel, but only one at a time has been operated so far. Three detectors, KLOE, DEAR and FINUDA, have taken data until 2007 and logged a total integrated luminosity of ≈ 4.4 fb^{-1} with a peak luminosity of $\approx 1.6 \cdot 10^{32}$ cm^{-2} s^{-1} and a maximum daily integrated luminosity of ≈ 10 pb^{-1}.

KLOE has been in place on the first IP from 1999 to 2006, while DEAR and FINUDA have alternatively run on the second one. The detectors of KLOE and FINUDA are surrounded by large superconducting solenoid magnets for the momentum analysis of the decay particles and their magnetic fields represent a strong perturbation on the beam dynamics. This perturbation tends to induce an effect called "beam coupling", consisting in the transfer of the betatron oscillations from the horizontal plane to the vertical one. If the coupling is not properly corrected, it would give a significant increase of the vertical beam size and a corresponding reduction of luminosity. For this reason two superconducting anti-solenoid magnets are placed on both sides of the detector with half its field integral and opposite sign, in this way the overall field integral in the IR vanishes.

The rotation of the beam transverse plane is compensated by rotating the quadrupoles in the low-β section. In the case of KLOE the low-β at the IP was originally designed with two quadrupole triplets built with permanent magnets, to provide high field quality and to left room to the detector. The structure of the FINUDA IR is quite similar to the KLOE one. Since its superconducting solenoid magnet has half the length (but twice the field) of the KLOE one, the low-β focusing at the IP was obtained by means of two permanent magnet quadrupole doublets inside the detector and completed with two other conventional doublets outside.

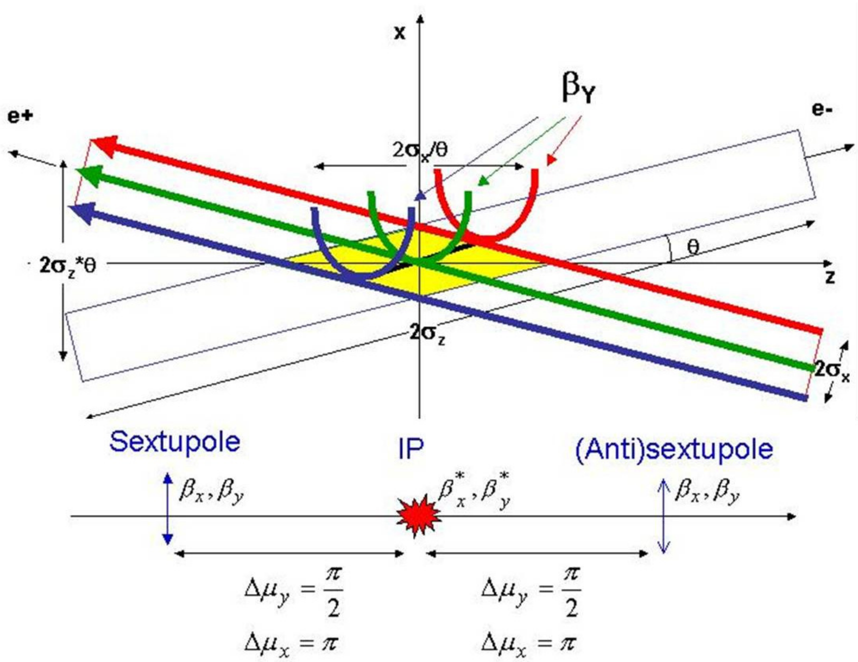

Figure 3: *Crab waist scheme*

The DEAR experiment, which was installed on the IR opposite to KLOE, took data during the years 2002-2003. It does not need magnetic field and therefore only conventional quadrupoles were used for the low-β. FINUDA rolled-in at DEAR's place in the second half of 2003 and took data until spring 2004. It was then removed from IP2 in order to run the KLOE experiment with only one low-β section at IP1, and rolled-in back in 2006 for a second data taking run ended in June 2007. After that the detector has been rolled-out again, and presently there are no detectors installed in IR2. The two chambers are vertically separated so that the two beams do not suffer from parasitic interactions in the whole IR2. A summary of the peak luminosity during these runs is shown in Fig. 2.

3 The large Piwinski angle and crab waist collision scheme at DAΦNE

In standard high luminosity colliders the key requirements to increase the luminosity are: very small vertical beta function β_y at the IP, high beam intensity I, the small vertical emittance ϵ_y and large horizontal beam size σ_x and horizontal emittance ϵ_x required to minimize beam-beam effects. The minimum value of β_y is set by the bunch length to avoid the detrimental effect on the luminosity caused by the hour-glass effect. It is very difficult to shorten the bunch in a high current ring without exciting instabilities. Moreover, high current implies high beam power losses, beam instabilities and a remarkable enhancement of the wall-plug power. In the CW scheme of beam-beam collisions a substantial luminosity increase can be achieved without bunch length reduction and with moderate beam currents. For collisions under a crossing angle θ the luminosity L and the horizontal ξ_x and vertical ξ_y tune shifts scale as:

$$L \propto \frac{N\xi_y}{\beta_y} \propto \frac{1}{\sqrt{\beta_y}} \tag{1}$$

$$\xi_y \propto \frac{N\sqrt{\beta_y}}{\sigma_z \theta}; \tag{2}$$

$$\xi_x \propto \frac{N}{(\sigma_z \theta)^2} \tag{3}$$

The Piwinski angle ϕ is a collision parameter defined as:

$$\phi = \frac{\sigma_z}{\sigma_x} \tan\left(\frac{\theta}{2}\right) \approx \frac{\sigma_z}{\sigma_x}\frac{\theta}{2} \tag{4}$$

with N being the number of particles per bunch. Here we consider the case of flat beams, small horizontal crossing angle $\theta << 1$ and large Piwinski angle $\phi >> 1$. In the large Piwinski angle and Crab Waist scheme described here, the Piwinski angle is increased by decreasing the horizontal beam size and increasing the crossing angle. In such a case, if it were possible to increase N proportionally to $\sigma_z\theta$, the vertical tune shift ξ_y would remain constant, while the luminosity would grow proportionally to $\sigma_z\theta$. Moreover, the horizontal tune shift ξ_x would drop like $1/\sigma_z\theta$. However, the most important effect is that the overlap area of the colliding bunches is reduced, as it is proportional to σ_x/θ (see Fig. 3). Then, the vertical beta function β_y can be made comparable to the overlap area size (i.e. much smaller than the bunch length):

$$\beta_y \approx \sigma_x/\theta << \sigma_z \tag{5}$$

We get several advantages in this case:

- Small spot size at the IP, i.e. higher luminosity L.
- Reduction of the vertical tune shift ξ_y with synchrotron oscillation amplitude.
- Suppression of synchrobetatron resonances.

Table 1: DAΦNE Beam parameters for KLOE (2006) and SIDDHARTA (2008-2009)

PARAMETERS	KLOE Run	SIDDHARTA Run
L [cm^{-2}s^{-1}]	$1.5 \cdot 10^{32}$	$4.5 \cdot 10^{32}$
N_{part}/bunch	$2.65 \cdot 10^{10}$	$2.65 \cdot 10^{10}$
I_{bunch} [mA]	13	13
ϵ_x [10^{-9} m $\cdot$ rad]	340	260
ϵ_y [10^{-9} m $\cdot$ rad]	1.5	1
σ_x [μm]	760	200
σ_y [μm]	5.4	3.5
σ_z [mm]	25	17
β_x^* [m]	1.7	0.25
β_y^* [mm]	17	9
θ [mrad]	2×12.5	2×25

There are also additional advantages in such a collision scheme: there is no need to decrease the bunch length to increase the luminosity as proposed in standard upgrade plans for B- and Φ-factories. This will certainly help solving the problems of HOM heating, coherent synchrotron radiation of short bunches, excessive power consumption etc. Moreover, parasitic collisions (PC) become negligible since with higher crossing angle and smaller horizontal beam size the beam separation at the PC is large in terms of σ_x.

However, large Piwinski angle itself introduces new beam-beam resonances which may strongly limit the maximum achievable tune shifts. At this point the crab waist transformation enters the game boosting the luminosity, mainly because of the suppression of betatron (and synchro-betatron) resonances arising (in collisions without CW) through the vertical motion modulation by the horizontal oscillations. The CW vertical beta function rotation is provided by sextupole magnets placed on both sides of the IP in phase with the IP in the horizontal plane and at $\pi/2$ in the vertical one (see Fig. 3).

For comparison, the parameters used during the last DAΦNE run with the KLOE detector (2005-2006) are shown in Table 1. As discussed above, in order to realize the CW scheme in DAΦNE, the Piwinski angle ϕ should be increased and the beam collision area reduced: this is achieved by increasing the crossing angle θ by a factor 2 and reducing the horizontal beam size σ_x. In this scheme the horizontal emittance ϵ_x is reduced by a factor 1.5, and the horizontal beta function β_x lowered from 1.5 to 0.2 m. Since the beam collision length decreases proportionally to σ_x/θ, the vertical beta function β_y can be also reduced by a factor 3, from 1.8 cm to 0.6 cm. All other parameters are similar to those already achieved at DAΦNE.

4 Hardware upgrades for the Crab Waist test at DAΦNE with the SIDDHARTA run

DAΦNE has been upgraded to allow the CW collision scheme test with the SIDDHARTA run during the summer shutdown of 2007.

The major upgrades on the machine are summarized as:

- new IR1 geometry for the CW test;
- new IR2 geometry with two completely separated vacuum chambers with half moon profile;
- new shielded bellows;

- the four e^+ e^- transverse feedbacks have been upgraded;
- solenoid windings in the two long IRs sections of the e^+ ring;
- new calorimeter for luminosity measurement and tuning;
- new longitudinal position of the two IRs horizontal collimators;
- new injection kickers.

The need of a new IR geometry is essentially due to have a very small β_y (9 mm) and a large crossing angle (25 mrad per beam). Splitter magnets installed in the original design have been removed thanks to the large crossing angle in the CW scheme. Defocusing and focusing quadrupoles (QD, QF) on both sides of the IP have been placed to obtain the required low-β structure. Further trajectory separation is provided by two small dipole correctors upstream and downstream the quadrupole doublets, while other three quadrupoles are used to match the betatron functions in the arcs.

The low-β section quadrupoles near the IP are of permanent magnet (PM) type. The QDs are located near the IP where the beams share a common vacuum chamber, while the QFs are positioned where the chambers are splitted and each one acts on a single beam. Therefore a total of two QDs and four QFs is required to get the two doublets around IP1. Four corrector dipoles provide a deflection of 9.5 mrad to match the inlet and outlet arc chamber flanges.

CW sextupoles are placed at ~ 9.3 m far from the IP1. Bending dipoles facing the IRs have been rotated and their field adjusted according to requirements. They have been powered with independent supplies to match these requirements.

For the SIDDHARTA experiment a new aluminium alloy (AL6082T6) chamber with two thin windows (0.3 mm 0.02 thickness) in the top and bottom sides has been designed and built.

Electromagnetic simulations have shown the presence of trapped modes which add resonant contributions to the beam coupling impedance in the Y-chamber junctions, the regions where the two separate ring pipes merge in the common vacuum chamber near the IP. In the worst possible scenario, that occurs when a beam spectrum line at a frequency equal to a multiple to the bunch repetition rate is in full coupling, the joule loss does not exceed 200 W. To keep this effect under control the Y-chambers have been equipped with cooling pipes.

This additional cooling circuit allows to remove the beam induced HOM heating and, if necessary, to reduce it by detuning the mode frequencies with respect to the dangerous beam spectrum lines.

A new design of the central IR2 beam pipe has been implemented, the two vacuum chambers are completely separated and their cross section has an half moon profile.

The main Bhabha monitor consists of a 4-modules sandwich calorimeter, made of lead and scintillator. Four modules of calorimeters surround the final permanent quadrupole magnets, located at a distance of 32.5 cm on both sides of the IR. They cover an acceptance of $18 \div 27$ degrees in polar angle, and are segmented in azimuthal angle in five sectors, 30 degrees wide.

Two gamma monitor detectors are located 170 cm away from the IR, collecting the photons radiated by electron or positron beam. The detectors are now made of four PbW04 crystals (squared section of 30×30 mm^2 and 110 mm high) assembled together along z, in order to have a 30 mm face towards the photon beam, and a total depth of 120 mm corresponding to about 13 X_0. Thanks to the high rate, those detectors are mainly used as a fast feedback for the optimization of machine luminosity versus background, since the relative contribution of background is changing with the machine conditions. A total systematic uncertainty on the luminosity measurement of 11% can be estimated.

Table 2: DAΦNE luminosity performances with the CW scheme and low-β parameters compared to the KLOE and FUNUDA runs. SIDDHARTA data taking does not profit of the fast injection rate system, that would increase $L_{\int logged}$.

	SIDDHARTA March 08 ÷ Nov 09	KLOE May 04 ÷ Nov 05	FINUDA Nov 06 ÷ Jun 07
L_{peak} [cm^{-2}s^{-1}]	4.5	1.5	1.6
$L^{MAX}_{\int day}$ [pb^{-1}]	15.24	9.8	9.4
$L^{MAX}_{\int hour}$ [pb^{-1}]	1.033	0.44	0.5
$I^{-\ MAX}_{coll}$ [A]	1.4	1.4	1.5
$I^{+\ MAX}_{coll}$ [A]	1	1.2	1.1
$n_{bunches}$	105	111	106
$L_{\int logged}$ [fb^{-1}]	2.9	2.0	0.966
β^*_x [m]	0.25	1.5	2.0
β^*_y [m]	0.009	0.018	0.019
ϵ_x [10^{-6} m·rad]	0.25	0.34	0.34
ξ_y	0.0443	0.025	0.029

5 Luminosity achievements during the SIDDHARTA run

The commissioning of the upgraded machine started in November 2007. At the end of the year the ring vacuum was almost recovered, the beams were stored in the upgraded rings, all the sub-systems went quickly to regime operation.

The first collisions in the CW scheme have been obtained in February 2008, with the first experimental confirmation of the potentiality of the new configuration in terms of specific luminosity growth and reduction of the beam-beam detrimental effects. DAΦNE luminosity as a function of the colliding bunches compared to past runs is reported in Fig. 4. Blue and red dots refer

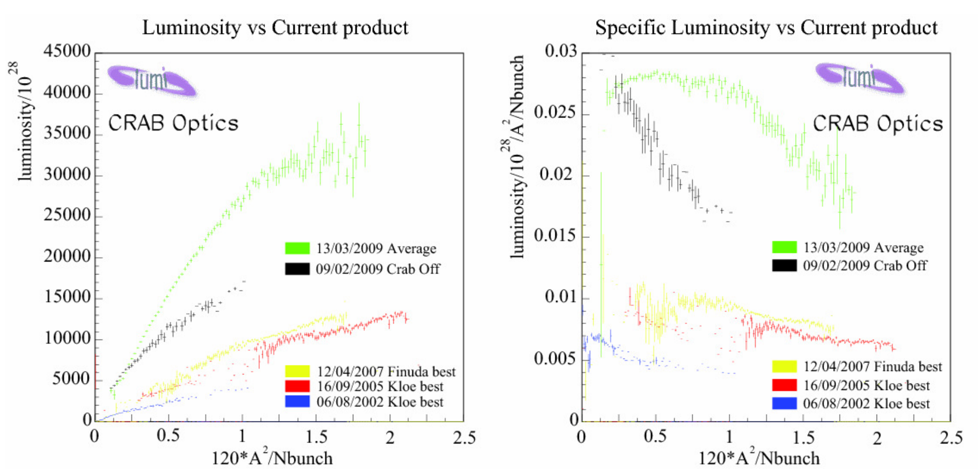

Figure 4: *Comparison of the upgraded DAΦNE perfomance (green) with respect to the results during previous KLOE (blue, red) and FINUDA runs (yellow).*

to the two KLOE runs, with the initial triplet low-β IR quadrupoles and with the new IR doublet, respectively. Yellow dots refer to the FINUDA run; in green is the luminosity with the CW scheme. The gain provided by the new IR gets higher with the products of the currents and the difference with respect to collisions with the crab sextupoles off can reach 50%. During 2009 the peak luminosity has been progressively improved by tuning the collider and increasing the beam currents; the maximum value achieved is $\approx 4.5 \cdot 10^{32}$ cm^{-2}s^{-1} measured in several runs with good luminosity to background ratio. The present peak luminosity is close to the nominal one predicted by numerical simulations. The highest single bunch luminosity achieved is $\approx 5 \cdot 10^{30}$ cm^{-2}s^{-1} measured with 20 bunches in collisions instead of the usual 105.

The single bunch specific luminosity, defined as the single bunch luminosity divided by the product of the single bunch currents, at low currents exceed by 4 times the best value measured during the past DAΦNE runs (present values are red and blue dots in Fig. 5). It gradually decreases with colliding beam currents, as can be seen in Fig. 5. This reduction can be only partially explained by the growing beam size blow up due to the beam-beam interaction. Another factor comes from the fact that in the large Piwinski angle regime the luminosity decreases with the bunch length, which in turn is affected by the ring coupling impedance. The impact of the Crab-Waist sextupoles can be recognized comparing runs taken with CW sextupoles on and off (Fig. 5). At low current the luminosity is the same in the two cases and higher than the one measured with the original collision scheme. As the product of the stored currents exceed 0.3 A, the luminosity with CW sextupoles off becomes lower and a corresponding transverse beam size blow up and beam lifetime reduction are observed as a consequence of the uncompensated beam-beam resonances. The convolved vertical beam size at the IP in collision has been measured by means of a beam-beam scan technique. The measured Σy of 5.6 μm is compatible with the value obtained by using the coupling value ($k = 0.7\%$) as measured at the Synchrotron Light Monitor (SLM), being the single vertical beam size at the IP1 of the order of 4 μm.

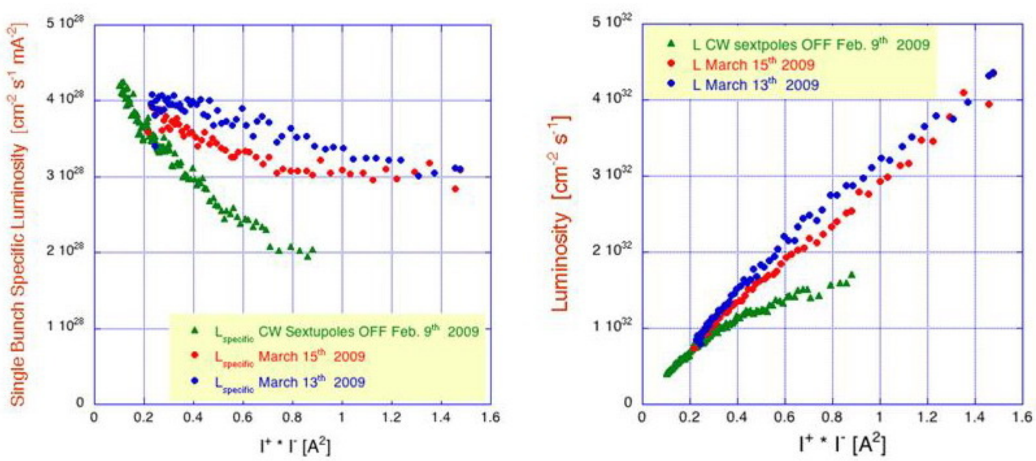

Figure 5: *Single bunch specific luminosity (left) and luminosity (right) versus the product of the colliding currents for two of the best run and for the crab waist sextupoles off.*

Fig. 6 reports another proof of the crab sextupoles effectiveness, where the positrons transverse beam profile measured at the synchrotron light monitor with crab sextupoles OFF (left plot) and with crab sextupoles ON (right plot) is shown. The measurement refers to collision in a strong-weak regime (1 A electrons beam current against 0.1 A of positrons beam current): it is evident that the transverse beam size is smaller and its shape remains Gaussian during collision with the sextupoles ON.

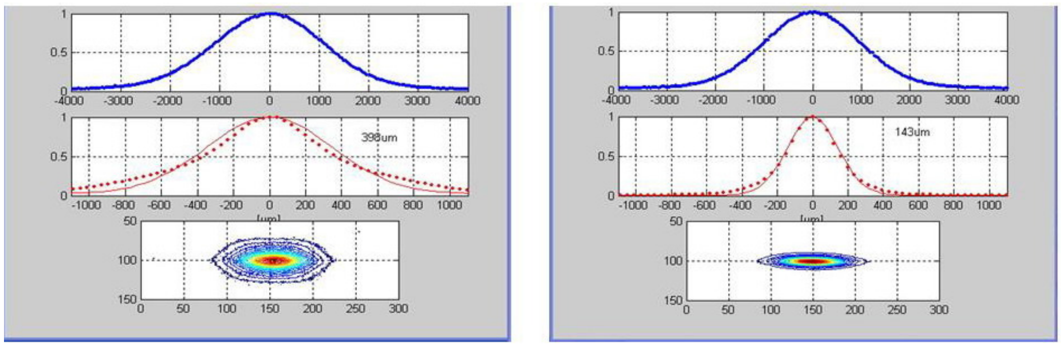

Figure 6: *Transverse positron beam profile as measured at SLM with crab sextupoles off (left) and crab sextupoles on (right) for beams in collisions (103 bunches).*

The crab waist sextupoles proved to be of great importance for the collider luminosity increase, since much lower luminosity is achieved with crab sextupoles off, with a larger blow up and a sharp lifetime reduction is observed for single bunch currents greater than 8-10 mA. This is in agreement with beam-beam simulations taking into account the DAΦNE nonlinear lattice. The results achieved at DAΦNE have pushed several accelerator teams to study and consider the implementation of this scheme on their machines. Besides, the physics and the accelerator communities are discussing a new project of a Super B-factory with luminosity as high as 10^{36} cm^{-2}s^{-1}, i.e. by about two orders of magnitude higher with respect to that achieved at the existing B-factories at SLAC and KEK.

6 Hardware modifications for the KLOE-2 run

During 2009 the new interaction region design for KLOE has been completed and several components of the new hardware have been acquired. In beginning 2010 the KLOE detector has been rolled in on IR1.

The new IR magnetic layout, sketched in Fig. 7, has been designed in order to maximize the beam stay clear letting the beam trajectory pass as much as possible through the center of the magnetic elements. The field integral introduced by the solenoidal detector is almost cancelled by means of two anti-solenoids, installed symmetrically with respect to the IP in each ring, which provide compensation also for off-energy particles. Due to the larger crossing angle, the vertical displacement of the beam in the IR is about an order of magnitude larger than in the last KLOE run. To keep the beam vertical trajectory within reasonable values, two permanent magnet dipoles (PMD) have been added just after the first permanent magnet horizontally focusing quadrupole, inside the detector magnetic field, in each one of the four IR branches (see Fig. 7). The PMDs are based on a modular design in view of a possible KLOE-2 run at a lower solenoidal field. Since the two beams are vertically deflected in opposite directions by the KLOE solenoid, they provide a horizontal magnetic field directed towards the center of the ring in the positron ring and towards the outside in the electron one. Four new skew quadrupoles have been added on the IR, just outside the KLOE magnet, to provide fine tuning for the coupling compensation.

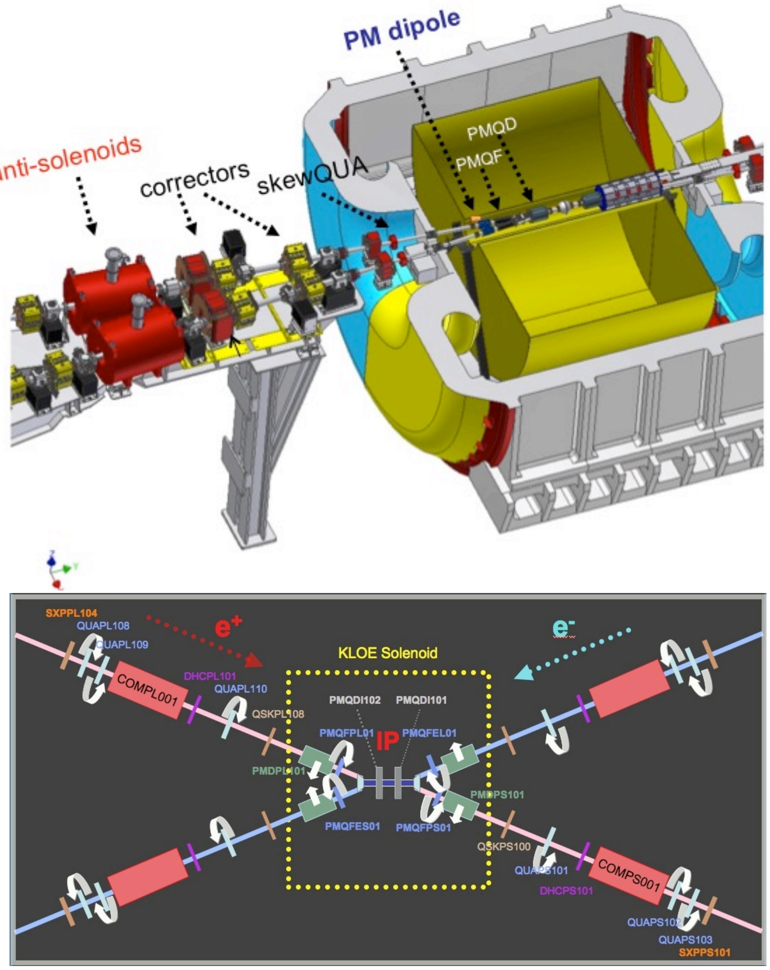

Figure 7: *(Top) The KLOE-2 detector and the new DAΦNE Interaction Region 1. (Bottom) Schematic drawing of the DAΦNE Interaction Region 1 magnetic layout.*

The shimmed plates added on the wiggler poles in 2004 have been removed and the poles displaced alternately in the horizontal direction by ±8 mm with respect to the wiggler axis in order to keep the beam trajectory as much as possible centered with respect to the pole axes. Due to the reduction of the gap and of the overall length of the magnetic circuit, this new configuration allows to reach, at a current of 450 A, a magnetic field still higher than that achieved at 550 A in the previous configuration with shimmed plates inserted. A further improvement has been obtained by powering in series all the 7 poles of the wigglers, while before each couple of terminal poles was powered independently. This has been obtained by short-circuiting one out of the five windings in the terminal poles coils and correcting the field integral in each wiggler below 1 Gm by tuning the end pole clamps aperture. In this way eight power supplies are no more necessary and the cycling procedure at startup is much more reliable. All the DAΦNE wigglers have been removed, modified and measured.

New stripline electrodes have been designed and inserted in the wiggler and dipole vacuum chambers of the positron ring. These electrodes, powered by DC voltages, counteract the parasitic electron cloud formation, which helps in increasing the positron beam current threshold.

The exhausted LINAC gun cathode has been replaced with a new one.

The modifications on the machine for the KLOE-2 run have been completed at the beginning of May. At the end of June the KLOE magnet has been partially warmed-up to allow the installation of the anti-solenoids cryogenic transfer lines. Since then, and up to mid November, several problems at the cryogenic plant and its ancillary systems occurred, preventing the KLOE solenoid energization. In September a magnetic setup without the KLOE magnet, but using the anti-solenoids, has been found to allow the DAΦNE beam conditioning. Up to about 1 A of positrons has been stored in the main ring with this optics, while the electron current was limited to ≈ 0.1 A due to ion trapping. On November 16th, the KLOE magnet was cooled and energized and beam conditioning in the nominal configuration was started with currents around 0.8 A stored at the same time in both rings, with half circumference filled in each one to avoid beam-beam interactions.

The first phase of the main ring commissioning has been done with the KLOE detector off. The lack of focusing from the solenoid has a strong impact on the ring optics, which had to be deeply modified. In November all the six DAΦNE bunch-by-bunch feedback systems have been upgraded to new software and hardware versions. The two (electron and positron) longitudinal feedbacks have been completely replaced with new ones, with the goal to have more compact systems with updated hardware components and new software programs compatible with the currently used operating system. These efforts are motivated also by reaching lower noise in detecting and better performance in damping the beam longitudinal oscillations. The vertical feedback systems have been equipped with 12-bit AD and DA converters in place of the 8-bit old units to reduce the quantization noise impact in the system gain. The positron ring horizontal feedback power has been doubled (1 kW now) providing about 40% increase in the kick strength. Furthermore, the horizontal feedback kicker has been replaced with a device with a double length stripline and reduced plate separation, providing larger shunt impedance at the low frequency typical of the positron horizontal unstable modes. The kicker has been also moved in a position with a higher horizontal β value.

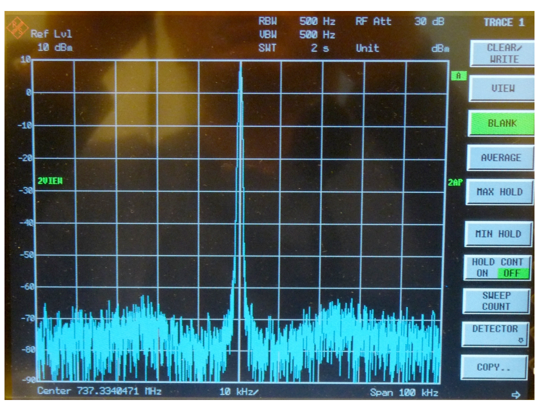

Figure 8: *Beam spectrum snapshot.*

7 DAΦNE commissioning for the KLOE-2 run

DAΦNE upgrade for the KLOE-2 run completed last July 2010. KLOE cool-down started on the second half of April 2010, however several problems involving the cryo-plant prevented to energize

the detector till October 25^{th}.
From November 2010 until June 2011 there have been several faults involving:

- injection septum of the positron ring;
- linac gun cathode and D modulator of the injection system;
- cooling system of the KLOE magnet power supply;
- vertical orbit oscillation in both rings.

These faults slowed down the commissioning and caused two major unscheduled shut-down periods. On January 11^{th} the 34 degrees injection septum of the positron ring got permanently damaged due to a water leakage together with a fault in the alarm system. Since no spare part was available it has been impossible to store the positron beam for three months. However, the accident had a positive drawback: the new septum coil has been optimized by reducing the coil gap and changing the geometrical dimension of the conductor, thus achieving a 50% reduction in the wall plug power with respect to the original device.
The cooling system of the KLOE magnet power supply experienced a faulty behaviour (from February 20^{th} to March 30^{th}), which has been linked, eventually, to the internal oxidation of the cooling circuit, that has been fixed in two weeks.

The Linac had several problems concerning the D modulator system, essential for positron production and the gun cathode, which required several replacements till to run out of spare parts by mid-May. This circumstance forced the last, and more relevant, unscheduled shut-down four months long.

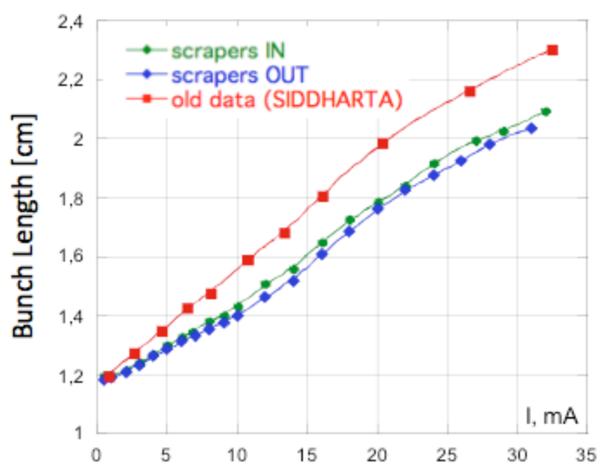

Figure 9: *Bunch length measurements in the electron ring.*

Suspending the DAΦNE activity gave a useful opportunity to start an extensive program of maintenance and consolidation involving almost all the collider subsystems.
It is the case of the test and replacement activities involving several Linac components such as: radio frequency loads in the gun area, modulators with their high power units, buncher phase shifter, diagnostic tools and cathode test station.
Concerning magnetic elements: all the four 34 degrees septa have been replaced and four correctors in the IR replaced with devices having better field quality.

About mechanics and layout many vibration measurements have been done in the Interaction Region area to sort out the source of the vertical oscillation observed, on both beams. Measurement analysis indicated how to consolidate the Interaction Region supports halving the vertical oscillation.

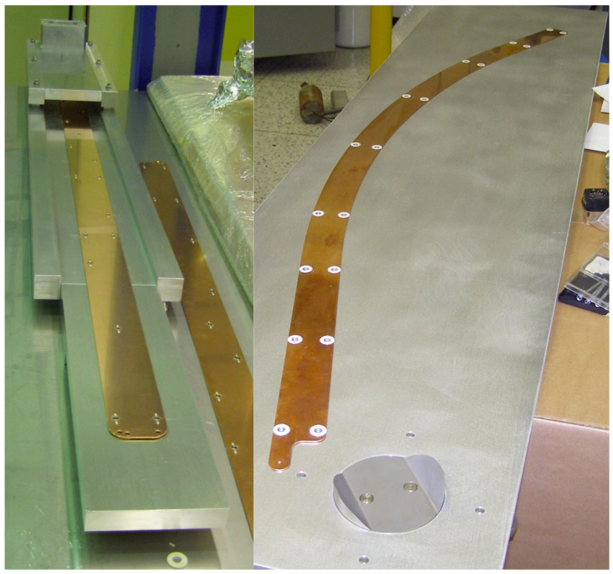

Figure 10: *Pictures of the electrodes inserted in the chambers of the dipole (on the right) and in the wiggler (left picture).*

Alignment has been revised in several sections of the main rings relying on beam measurement analysis.
The cryogenic plant has been maintained with a standard cleaning procedure.
Concerning controls: the fluid plant low-level interface has been upgraded and front-end controls for several class of elements have been ported to new more performing processors.
A lot has been done to reduce and optimize the demand for electric power. In fact the electric power necessary to run DAΦNE is $\approx 3.34\ MW$ now, which is $\approx 2.56\ MW$ lower than during the last KLOE run with a consequent reduction of $\approx 2.0\ Meuros$ on the electric bill due for a 200 days long run.

Although the collider uptime has been very limited, especially for the positron ring, some relevant work has been done to test the upgraded systems and to tune the Main Rings optics.

As for all circular colliders, the DAΦNE beam longitudinal dynamics is very much affected by the Low Level Radio-Frequency (LLRF) control. In particular, the dynamics of the beam barycentre motion (the coupled bunch zero-mode) is very sensitive to the large RF cavity detuning required to compensate the reactive beam loading, which is particularly huge at DAΦNE where the operating conditions are characterized by relatively low accelerating gradients ($\approx$ 200 kV) e large stored currents (up to 2 A). For this reason a fully analog RF feedback loop has been added to the LLRF system and commissioned on both e^+ and e^- rings, resulting in a drastic limitation of the synchrotron zero-mode coherent frequency shift that have affected the operation of the collider in the past. The measured beam spectrum around the RF 2^{nd} harmonics is shown in Fig. 8, where the sidebands of the longitudinal barycentre motion appear much lower and broader compared to what we observed in the past before the feedback implementation. The efficiency of the RF system

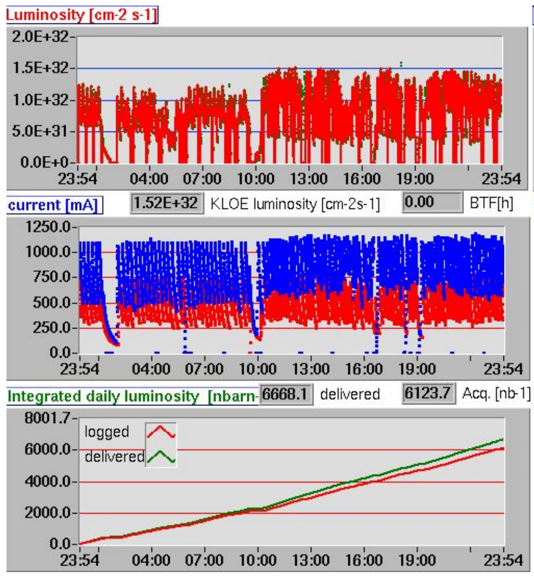

Figure 11: *(Top) Luminosity, (Middle) beam currents, (Low) Integrated luminosity for the best day, Dec.* 17^{th} *2011.*

has been also increased since no extra cavity detuning is necessary with direct RF feedback in operation. The RF systems of both rings are now operating reliably in the new configuration. In the mid-term future there is a plan to implement the new architecture in a digital platform to add flexibility and adaptivity to the LLRF controls.

The ring impedance has been estimated relying on bunch length measurements as a function of bunch current. Numerical fits based on potential well as well as microwave regime converge to a ring coupling impedance of 0.3Ω; it was 0.4Ω during the previous run (see Fig. 9).

One of the main limitations in the maximum stored current of the positron ring has been identified in previous runs, in a horizontal instability due to the electron cloud effect. To mitigate such instability, metallic -copper- electrodes have been inserted in all dipoles and wigglers chambers of the machine and have been connected to external dc voltage generators in order to absorb the photo-electrons. With a dc voltage of about 200 V applied to each electrode we expect a reduction of such density by two orders of magnitude that will contribute to reduce substantially the source of the instability. The pictures of the electrodes inserted in the dipole and wiggler chambers are shown in Fig. 10.
The dipole electrodes have a length of 1.4 or 1.6 m depending on the considered arc (short or long), while the wiggler ones are 1.4 m long. They have 50 mm width, 1.5 mm thickness and their distance from the chamber is about 0.5 mm. This distance is guaranteed by special ceramic supports made in SHAPAL and distributed along the electrodes. This ceramic material is also thermo-conducting in order to partially dissipate the power released from the beam to the electrode through the vacuum chamber. Moreover, the supports have been designed to minimize their beam coupling impedance as well as to sustain the strip. First experimental measurements on the electrodes effectiveness in mitigating the electron cloud effects in the positron beam are very encouraging.

The new configuration of the wiggler magnets, based on shifted poles has proved to be effective in reducing the non-linear terms in the magnetic field (B) . The field quality has been tested by measuring the beam tune shift induced by a horizontal closed orbit bump at the wiggler place. This bump, including the two dipoles adjacent to the wiggler, slightly changes the ring energy: this

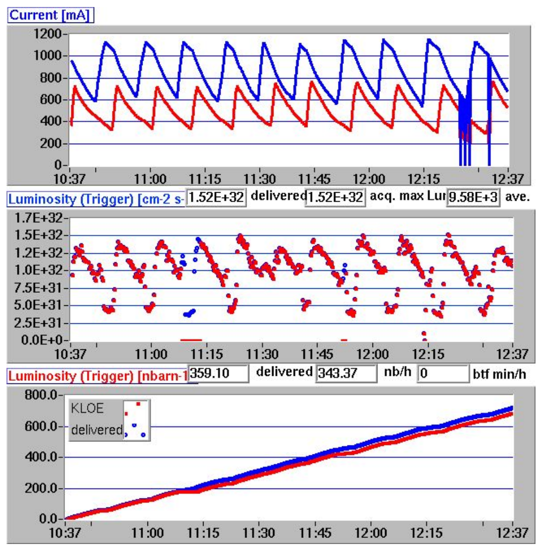

Figure 12: *Best two hours for KLOE-2 run.*

effect has been carefully compensated tuning the frequency of the RF cavity. The orbit position at the wiggler centre has been obtained by averaging the readout from two beam position monitors (BPM) placed at the magnet end side. For large values of the bump the BPMs non-linearity have been taken into account and properly corrected. The measured horizontal and vertical tune shifts exhibit a clear linear behaviour.

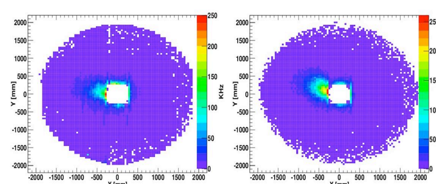

Figure 13: *Transverse profile of the backward EmC rates. Left and right plots are data and MC, respectively.*

The lattice for the KLOE-2 run with the crab-waist scheme has been optimized and matched to the real beams, relying on optics measurements (beta functions, dispersion, chromaticity, coupling, betatron tunes). The lowest value of the betatron coupling that has been measured is as small as 0.14% with a $\sigma_y = 75\mu m$ at the syncrotron light monitor. The vertical beam-beam luminosity scan showed that vertical orbit oscillation does not affect beam size at the IP, $\sigma_y = 3\mu m$ has been measured at IP. The new configuration of the wiggler magnets, based on shifted poles has proved to be effective in reducing the non-linear terms in the magnetic field. Luminosity is still not at nominal value due to different reasons, however beam-beam is not a limiting factor, and crab-waist sextupoles work well, as expected.

The luminosity has been optimized by storing 100 bunches in collision at low current. The single bunch specific luminosity at low currents is of the order of about $\approx 4.5 \cdot 28$ cm^{-2} s^{-1}, the same as the one measured during the crab-waist test without the detector solenoid. The DAΦNE performances at the end of December 2011 reproduced the best ones obtained during the previous

KLOE run. In fact, up to now the maximum peak luminosity is $1.52 \cdot 10^{32}$ cm^{-2} s^{-1}, obtained on December 17^{th} 2011, with $I^- = 0.93$ A and $I^+ = 0.719$ A stored in 100 bunches. This value can be compared to the same luminosity $1.53 \cdot 10^{32}$ cm^{-2} s^{-1} with $I^- = 1.4$ A and $I^+ = 1.2$ A with 111 bunches, achieved during the KLOE run in 2005. The same day (December 17^{th}) has been also the best day in terms of daily integrated luminosity (see Fig. 11).

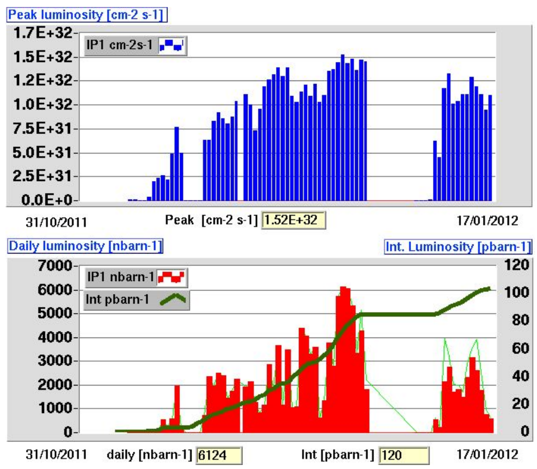

Figure 14: *Summary of current and luminosity during year 2011.*

The plot with the highest luminosity per hour is shown in Fig. 12. The best hourly integrated luminosity is 0.359 pb^{-1}, which might provide 8.62 pb^{-1} per day.

However, an efficient data taking requires not only high luminosity but also background rates induced in the detector as low as possible.

The two collimators mostly effective are the one upstream the IR and the one just after the old IP2, as predicted also by numerical simulations. The beam stay clear at these two collimators has been reduced to intercept Touschek scattered particles that would be lost at the IR. They proved to be very much effective in reducing background showers. However, after careful orbit optimization and collimator tuning, an additional lead shielding 1 cm thick has been added around the inner layer (QCAL) of the KLOE-2 detector to prevent background contamination in the physics events without reducing the detector acceptance. A full Monte Carlo (MC) simulation that allows a direct comparison between the expected and measured background rates at the KLOE electromagnetic calorimeter (EmC) has been developed in the new KLOE-2 configuration. The data/MC background rates are in agreement within a factor of two in the different regions of the KLOE EmC and the main features of the shapes are well reproduced (see Fig. 13). A good agreement for the Touschek lifetime is found between measured and calculated lifetime with scrapers inserted at the experimental set. On the contrary, the comparison without scrapers shows a disagreement of about a factor 1.9, which might be explained by a misalignment of the on-energy beam orbit that induced beam scraping in the IP2 section. This allows us to expect some margins of optimization, especially by correcting orbit and dynamic aperture.

The summary of current and luminosity during year 2011 is shown in Fig. 14. In order to push the collider performances in terms of luminosity, multibunches and high current operation must be consolidated and improved by tuning the working points in the two rings, the coupling at the IP for the two beams, the non-linear beam dynamics and, last but not least, beam-beam interaction. Background has been improved especially at high current and mainly for the positron ring. Dedicated studies may help to optimize the collimator configuration and to understand the possibility to introduce additional shieldings between the beam pipe and the detector.

8 Publications

1. A. Drago, P. Raimondi, M. Zobov (INFN-LNF), D. Shatilov (BINP), "Synchrotron Oscillation Damping by Beam-beam Collisions in DAΦNE ", Physical Review Special Topics - Accelerators and Beams, 14, 092803 (2011).

2. A. Drago (INFN-LNF) and D. Teytelman (Dimtel, San Jose), "DAΦNE Bunch-by-bunch Feedback Upgrade as SuperB Design Test", Proc. of IPAC2011, San Sebastian, Spain (2011).

3. C. Milardi *et al.*, "DAΦNE Tune-up for the KLOE-2 Experiment", Proc. of IPAC2011, San Sebastian, Spain (2011).

4. S. Bettoni (PSI, Villigen) A. Drago, S. Guiducci, C. Milardi, M.A. Preger, P. Raimondi (INFN-LNF), "Beam Based Measurements with the Modified Wigglers in DAΦNE ", Proc. of IPAC2011, San Sebastian, Spain (2011).

5. M. Boscolo, P. Raimondi (INFN-LNF), E. Paoloni (University of Pisa and INFN-Pisa) A. Perez (INFN-Pisa), "Touschek Effect at DAΦNE for the New KLOE Run in the Crab-Waist Scheme", Proc. of IPAC2011, San Sebastian, Spain (2011).

THE DAΦNE BEAM TEST FACILITY (BTF)

BTF staff: B. Buonomo, L. Foggetta (T.D.), G. Mazzitelli (Resp.), L. Quintieri (art. 23), P. Valente (Osp.)

BTF secretariat: M. R. Ferrazza

DAΦNE operation staff: G. Baldini, A. Battisti, A. Beatrici, M. Belli, B. Bolli, G. Ceccarelli, R. Ceccarelli, A. Cecchinelli, O. Coiro, S. De Biase, M. De Giorgi, G. Ermini, G. Fontana, C. Fusco, O. Giacinti, E. Grossi, F. Iungo, C. Marini, M. Martinelli, C. Mencarelli, E. Passarelli, V. Pavan, D. Pellegrini, G. Piermarini, S. Quaglia, M. Sardone, G. Sensolini, A. Sorgi, M. Sperati, A. Sprecacenere, R. Tonus, T. Tranquilli, M. Troiani, R. Zarlenga

BTF technical staff: V. Ciuffetti, P. Lollo, R. U. Frasacco, A. Mazzenga, F. Galletti

LNF-DR – Reparto Automatismi e Controlli: U. Denni, M. A. Frani, G. Papalino

BTF Committee: P. Di Nezza, F. Gatti (INFN Genova), C. Matteuzzi (INFN Milano, Chair), G. Mazzitelli (*ex officio*), A. Passeri (INFN Roma Tre), P. Valente (INFN Roma)

1 Summary

During the 2011 the DAFNE Beam Test Facility (BTF) has continued its activity mainly devoted to testing and calibration of HEP detectors. At the same time, the beam characteristics have been optimized in order to host some particular experiments, as the crystal channeling ones. The availability of few hundreds MeV positron beam indeed qualifies the BTF as one of the few suitable facility for such kind of measurements.

Unfortunately during the last two years the DAFNE accelerator complex suffered of a number of faults, limiting the time allocated to the beam-test facility, both in dedicated and parasitic mode. Part of the experimental program however took place before the end of the year and the most part of the TARI supported users tests beam and experiments have been just shifted in time and successfully took place before the end of the HadronPhysics2 project, concluding their scientific program.

Table 1: *Assigned and cancelled beam-days in 2011*

	assigned days 2011	cancelled days 2011
All users	250	145
TARI program	115	42

The 2011 activities[1] of the facility can be divided in tree class:

1. Test & calibration of apparatus:
    - TPS drift chamber
    - SIDDHARTA/AMADEUS
    - SuperB drift chamber

[1]available at the link http://www.lnf.infn.it/acceleratori/btf/php/schedule.php?year=2011&acc=1.

- RAPID
- FIRST
- SuperB LYSO calorimeter
- BES-III luminosity monitor
- TO_ASIC
- JLAB12-Genova

2. Channeling an electromagnetic interaction study:
   - VEER
   - RAINPC
   - C-SPEED
   - AMY
   - RICCE
3. Test, optimization and detectors R&D of the neutron BTF line:
   - BTF_NRCA
   - NESCOFI@BTF

Detailed information about the experiments propose are reported on the BTF web page ate the link: `http://www.lnf.infn.it/acceleratori/public/BTF_user/`.

In 2011 the BTF become also part of the European project AIDA, addressing infrastructures required for detector development for future particle physics experiments. In line with the European strategy for particle physics, AIDA targets user communities preparing experiments at a number of key potential future accelerators: SLHC (luminosity-upgraded LHC), future Linear Colliders (ILC and CLIC), future accelerator-driven neutrino facilities or future B-physics facilities (e.g. Super-B).

One of the milestones of the AIDA project is the design, contraction, and implementation in the facility of a remotely controlled table where allocate, align and remotely adjust the experiments under test. A collaboration with the LNF-DR - Reparto Automatismi e Controlli allowed to equip the BTF with a new table with the characteristics listed in Tab. 2 (and shown in Fig. 1):

disposable area	600×600 mm^2
minimum height	915 mm
maximum height	1250 mm
horizontal excursion	1000 mm
maximum load	200 kg
accuracy	≤ 1 mm^2

Table 2: *Main parameters of the remote controlled table.*

Operation with users done during last year test beam was extremely satisfactory for all typical users configurations and requirements.

During this years the BTF have allocated an average of 250 days per year, rejecting about 20% of request due to limited availability of time or technical incompatibility with the beam-line characteristics. The requested beam-time during the last seven years of operation – illustrated in

Figure 1: *New remotely controlled table for detectors precise movement.*

Figure 2: *Beam time assigned in years 2004-2011; parallels tests counts twice.*

Fig. **??** – clearly shows the effect of the long running of complex experiments, such as the AGILE satellite payload, or the limited beam availability due to DAFNE machine complex upgrades. In 2009 the large requests were probably connected to the non-availability of the CERN test lines, and in 2013 the CERN beam line are also foreseen to be shut down.

At the same time, the scientific productivity of the facility looks to be in agreement with the main European facilities: in fact a simple search of publications with the key BTF+INFN shows an average of 18 publication per year that can be referred to data collected at the BTF. This number should be considered a lower limit because many users do not cite the facility where the data are collected, as shown in Fig.. 3.

Figure 3:

It is also possible to perform a (rough) cost estimation of the facility in order to understand the quality of the infrastructure, and its perspective: up to now the investment per year is shadowed manly by DAFNE collider operation, where one of the major cost is due to the LINAC system. The cooling and power supply system, as well as the plug cost is not optimized for a standalone operation of the BTF, implying a probable 20-30% saving respect to first two item of Tab. 3 .

shadowed by DAFNE operations			
Infrastructure LINAC+PS+cool.	Mains	Personnel	Consumables and Supplies
400	375	200	50

Table 3: *Estimation of the BTF cost in keuro/year based on the today, not optimized DAFNE complex services. Today cost, shadowed by DAFNE costs, is about 50 Keuro/year*

Five researchers are currently part of the BTF scientific staff, corresponding to 2 full-time equivalent, plus a secretariat support (0.2 FTE), that is essential in order to guarantee the administration of access to LNF, etc. Its is interesting to note that if a cost per year of one million of euro is assumed, the number of publications/Meuro produced is in agreement with that of the scientific productivity of the major European infrastructure (20publication/Meuro of investment).

In the meantime the BTF staff is also studying the possibility to use extracted beam in the Cabibbo lab area, where the Super-B Linac will deliver a 6 GeV electron beam, and hadrons and neutrons can be produced with interesting efficiency for beam-testing and applications in material and natural science.

2 List of Conference Talks by LNF Authors in Year nnnn

Include a list of conference talks by LNF authors.

1. ICENES 2011:15th International Conference on Emerging Nuclear Energy Systems, May 15-19, 2011 Hyatt Hotel at Fisherman's Wharf, San Francisco, California. Session: Modelling and Simulations: "Photo-neutron Source by High Energy Electron on High Z Targets: Comparison Between Monte Carlo Codes and Experimental Data.

2. UCANS-II:-Second Meeting of the Union for Compact Accelerator- Driven Neutron Sources Indiana University, Bloomington July 5-8, 2011. "A photo-neutron source at the Dafne Beam Test facility of the INFN National Laboratories in Frascati: design and first experimental results".

3 Publications

R. Bedogni *et al.*, Experimental and numerical characterization of the neutron field produced in the n@BTF Frascati photo-neutron source, Nucl. Instrum. Meth. **A659**, 373 (2011).

P.W. Cattaneo *et al.*, First results about on-ground calibration of the silicon tracker for the AGILE satellite Nucl. Instrum. Meth. **A630**, 251 (2011).

DAΦNE-Light Laboratory and Activity

A. Balerna (Resp.), P. Calvani (Ass.), M. Cestelli Guidi (Art. 23), R. Cimino, M. Commisso (Ass. Ric.), A. De Sio (Osp.), L. Gambicorti (Osp.), A. Grilli (Tecn.), R. Flammini (Ass.),D. R. Grosso (Bors.), R. Larciprete (Ass.), C. Mirri (Osp.), A. Nucara (Ass.), E. Pace (Ass.),M. Pietropaoli (Tecn.), A. Raco (Tecn.), V. Sciarra (Tecn.), V. Tullio (Tecn.), G. Viviani (Tecn.).

1 Summary

The scientific activity on the DAΦNE-Light synchrotron radiation beamlines, in 2011, was performed with synchrotron radiation and conventional sources, due to the not continuous DAΦNE operation. The experimental teams that got access to the DAΦNE-Light laboratory were from Italian Universities and research Institutions, and from EU countries within the FP7-E.LI.S.A. program and the INFN-FAI framework. During this year it was possible to give access to the EU users, in order to satisfy the approved experiments within the end (August 2011) of the EU FP7-I3 initiative E.LI.S.A. (European LIght Source Activities) for research cooperation involving the world largest network of synchrotron and FEL facilities in Europe. The experimental activities, performed in 2011, were also dedicated to the upgrade of the IR beamline with new instrumentations and the realization of a clean-room laboratory for biological sample preparation, the upgrade of the UV beamline and also the construction of the two new XUV beamlines that will hopefully be commissioned in 2012.

2 Activity

2.1 SINBAD - IR beamline

The experimental activity on the SINBAD IR beamline mainly concerns the study of biological samples at micrometric spatial resolution, owing to the imaging capabilities of the IR microscope coupled to the synchrotron source. This activity has been carried out by many experimental teams, within the framework of the FP7 E.LI.S.A. project and the INFN-FAI collaborations. A clean-room laboratory to support the sample preparation and conservation has been realized in 2011 and dedicated instrumentation have been purchased for this purpose. In particular, we have setup a cryo-microtome to allow thin tissue preparation (down to 1 micron sections), a -85°C freezer for cryo-conservation, and other instruments (thermal bath, centrifuge, inverted microscope, laminar flow hood). The clean-room was installed in 2011 and is now available for users to support the experiments. The imaging capabilities of the beamline have been improved by the construction of a system to image live biological cells. This system development, which was co-funded by the V Commission of INFN, consists of an Attenuated Total Reflection (ATR) microscope objective modified to allow cell growth and immersion in their culture medium. The system is completed by a dedicated IR spectrometer Vertex70v with unprecedented performance for vacuum microspectroscopy, and a dedicated optical coupling with the synchrotron beamline. All the system is placed on an optical table to be isolated from vibrations. The complete setup has been installed at the end of 2011 and is now fully operational for users to perform the first live cell experiments. The ATR objective is now available and its performances will be tested in the following months. Experimental groups from Italian and European Universities and Research Institutions carried out their research activity at the SINBAD beamline. The main results were obtained in the field of FTIR imaging and its applications in life science, radiobiology, earth science and solid state physics. The DAΦNE storage ring restarted its activity in January 2011 and beam-time was given to the experimental proposals with a delivered total amount of 588 beam-time hours. Some experimental results are reported:

1. *Detection of collagens in brain tumors based on FTIR imaging and chemometrics.*

   Cyril PETIBOIS - University of Bordeaux 2, CNRS UMR 5248 CBMN

   Fourier transform infrared (FTIR) imaging has been used as a molecular histopathology tool on brain tissue sections after intracranial implantation and development of glioma tumors (Fig. 1). Healthy brain tissue (contralateral lobe) as well as solid and diffuse tumor tissues were compared for their collagen contents. IR spectra were extracted from IR images for determining the secondary structure of protein contents and compared to pure product spectra of collagens (types I, III, IV, V, and VI). Multivariate statistical analyses of variance and correspondence factorial analysis were performed to differentiate healthy and tumor brain tissues as well as their classification according to their secondary structure profiles. Secondary structure profiles revealed that no collagen was present in healthy tissues; they are also significantly different from solid and diffuse tumors ($p < 0.05$). Solid and diffuse tumors could be discriminated with respect to the secondary structure profile of fibrillar and non-fibrillar collagens, respectively. This study has shown that secondary structure parameters of main collagen types found in tissues can be used for characterizing tumors and healthy tissues. It was noteworthy that diffuse and solid forms of glioma tumors could be discriminated by FTIR imaging on the basis of molecular parameters and also characterized with respect to the secondary structure profile of main collagen types found in mammalian tissues. This study thus opens the way to reliable molecular histology using FTIR imaging. We can thus propose to develop FTIR imaging for histopathology examination of tumors on the basis of collagen contents.

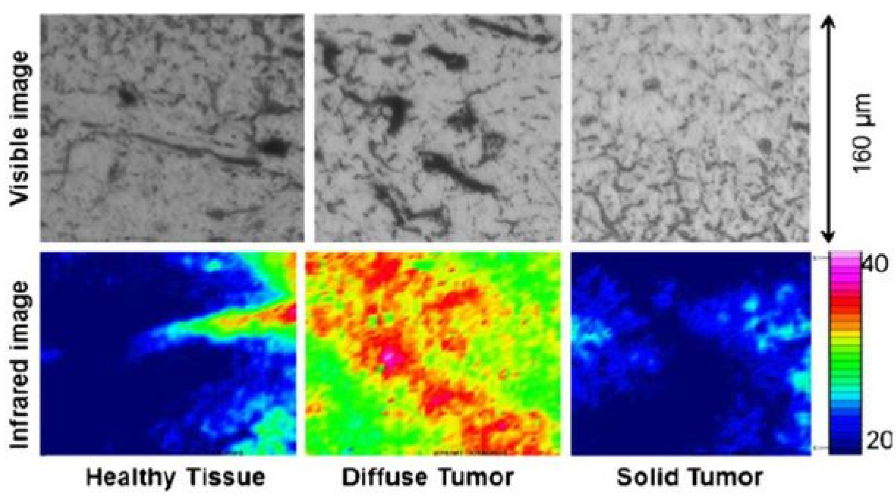

Figure 1: FTIR images of brain tissue sections. Top: Visible images of tissue sections (thickness 20μm). Bottom: Spectral images of tissue sections at 1720 -1600 cm^{-1} (Amide I band).

2. *Synchrotron FT-IR to unravel peculiar behaviors of Spin Crossover solids under pressure and/or arising from extended weak interactions (IRSCOUP).*

   Olivier ROUBEAU- ICMA, CSIC and Universidad de Zaragoza

   The spin-crossover (SCO) phenomenon represents a widely studied field of research, in which the reversible high to low spin (LS) change of transition-metal ions (Fig. 2), especially Fe(II) ions in an octahedral environment can be induced by temperature, irradiation and applied pressure. Applied pressure has also been shown to induce variations in the thermally-induced SCO and to produce crystallographic phase transitions with variable impact on the SCO properties. In some instances, and even in well-studied compounds, there remain though unexplained or disagreeing behaviors and results. FT-IR spectroscopy is one of the tools used to follow the thermally and optically-induced spin-state changes in SCO solids, mostly through vibrations influenced by the spin-state (typically M-ligand vibrations, or vibration of the coordinated ligands such as thiocyanates). On the other hand, intra- and intermolecular (lattice) vibrations are known to play a prominent role on the SCO phenomenon, particularly with respect with the occurrence of cooperative SCO, at the origin of the potential interest of these materials.

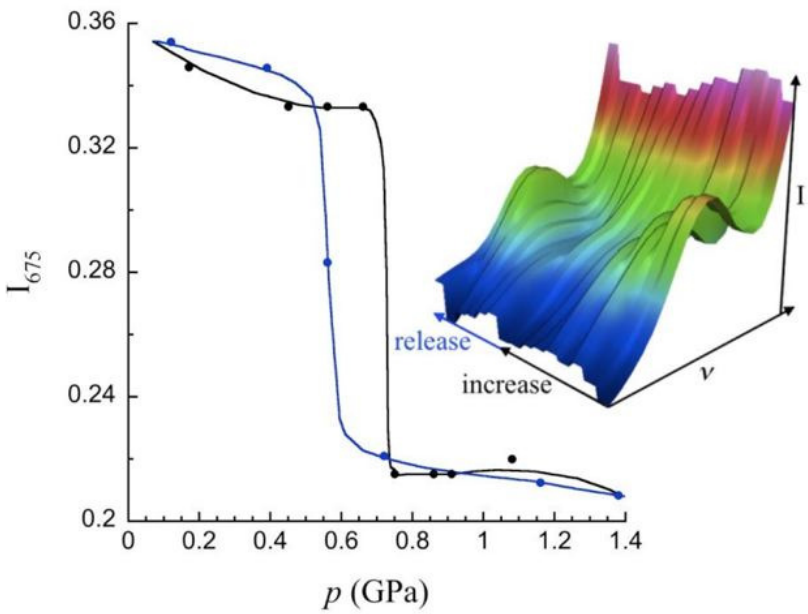

Figure 2: Pressure-induced transition to low spin state can be followed through the R3 ring band at about 1410 cm^{-1}. The transition occurs at about 0.7 GPa increasing the pressure and 0.6 GPa releasing it.

3. *In vivo skin leptin modulation after 14 MeV neutron irradiation: a molecular and FTIR spectroscopy study.*

   Roberto AMENDOLA - ENEA, UT BIORAD-RAB, Roma

   This work discusses the possibility of identifying, by high resolution FT-IR imaging spectroscopy, suitable radiation responsive genes to be used as new molecular markers of radiation response in mice skin treated by mono-energetic 14 MeV neutron irradiation. The irradiation was performed at the ENEA Neutron Generator Facilities (FNG), specifically dedicated to biological samples. FNG is a linear electrostatic accelerator that produces up to 1.0x1011 n/s 14 MeV neutrons via the D-T nuclear reaction. The functional genomic approach has been performed on four animals for each experimental point: un-irradiated; 0,2 Gy and 1 Gy, 6 hours and 24 hours delayed time after exposure. Co-regulation of a sub-class of keratin and keratin-associated protein genes which are physically clustered in the mouse genome and functionally related to skin and hair follicle proliferation and differentiation has been observed. Most of these genes are transiently up-regulated at 6 hours from the lower dose delivered, leptin protein is constantly found up-regulated upon irradiation with both doses. Leptin is a key protein that regulates lipid accumulation in tissues and its absence provokes obesity. The tissue analysis has been performed with FT-IR imaging spectroscopy monitoring the skin lipid accumulation and the distribution (Fig. 3). The overall picture describes a differential modulation of key genes in the epidermis homeostasis that points out the activation of a self-renewal process at low dose of irradiation.

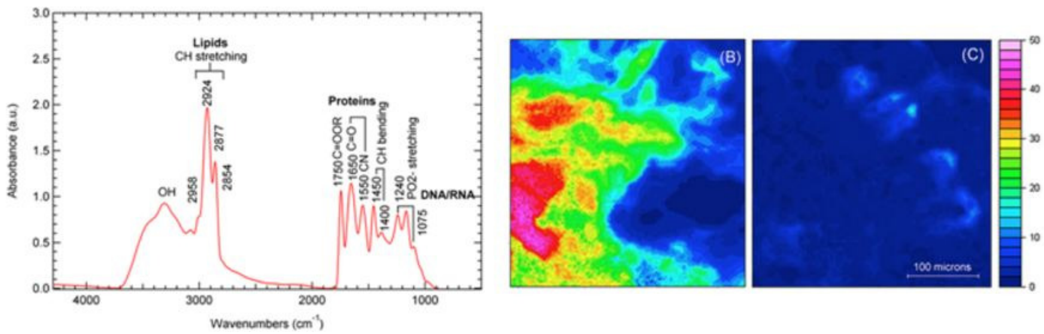

Figure 3: (A) FTIR absorbance spectrum of a control skin sample. Contribution from distinct chemical absorption (lipids, proteins and carbohydrates - DNA/RNA region) are distinguished at specific spectral positions; (B,C) FTIR imaging maps of the C=O lipid stretching mode centered at 1750 cm^{-1} in a control skin sample (B) and a 1Gy-24h irradiated one (C). The color scale shows significant differences in the lipid content and distribution, attributed to the up-regulation of leptin after neutron irradiation.).

2.2 DXR1 - Soft X-ray Beamline

The DAΦNE soft X-ray beamline, DXR-1, is mainly dedicated to soft X-ray absorption spectroscopy. The X-ray source of this beamline is one of the 6-poles equivalent planar wiggler devices installed on the DAΦNE electron ring (0.51 GeV) for the vertical beam compaction. The 6 wiggler poles and the high storage ring current (higher then 1 Ampere) give a useful X-ray flux for measurements well beyond ten times the critical energy. The useful soft X-ray energy range is 900 eV - 3000eV where the lower limit is given by the Beryl crystals used in the double-crystal monochromator and the higher limit is given by the wiggler working conditions. During 2011 some tests were performed on a new system to control, set and include in the experimental files the values of the pressures of the ionization chambers and small changes in the acquisition program were performed. After the long DAΦNE shut down a beamline realignment was necessary and performed at the end of 2011 when beam condition was more stable. The experimental results published in 2011 are here summarized:

1. *First approach to studies of sulfur electron DOS in prostate cancer cell lines and tissues studied by XANES.*

   Wojciech M. KWIATEK - Institute of Nuclear Physics PAN, Krakow, Poland

   Urological cancers comprise approximately one-third of all cancers diagnosed in men worldwide and out of these, prostate cancer is the most common one (WHO World Cancer Report, 2008). Several risk factors such as age, hormone levels, environmental conditions and family history are suspected to play a role in the onset of this disease of otherwise obscure aetiology.

It is therefore the medical need that drives multidisciplinary research in this field, carried out by means of various experimental and theoretical techniques. Out of many relevant factors, it is believed that sulphur can take an important part in cancer transformations. The prostate cancer cell lines and tissues have been investigated , along with selected organic and inorganic compounds used as references, by the X-ray absorption fine structure spectroscopy near the sulphur edge energy region. Particularly, the comparison of the experimental results collected during XANES measurements and theoretical calculations of electron density of states with use of the FEFF8 code and LAPW (linearised augmented plane-wave) method has been performed and in this work the first results of our studies are presented. The achieved results demonstrate that the FEFF8 code is a useful tool also in the case of simple organic samples and it can simulate the experimental XANES spectra quite well(Fig. 4). Joint use of theoretical and experimental results can provide new and useful information about the mechanism of carcinogenesis. However, the cancer tissue and cells are far more complex systems than single amino acids and relevant theoretical models are high in our further research priority list. This kind of approach is unique in providing otherwise unattainable microscopic characterization of biological samples, and until now for sulfur-containing materials was made only by Pickering in 1998.

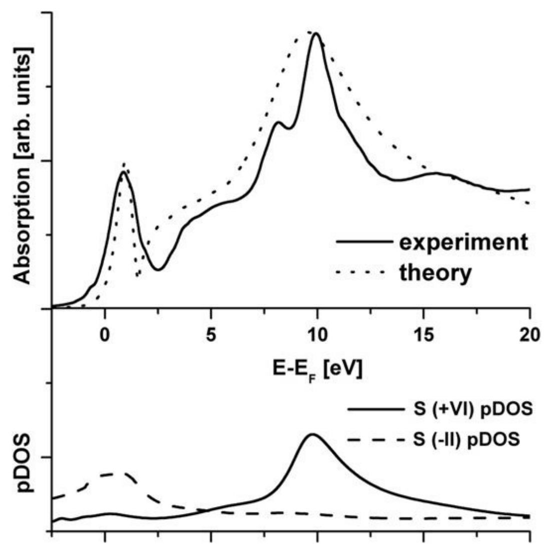

Figure 4: Comparison of experimental and calculated spectra (upper part) for the $Na_2S_2O_3$ reference compound. The bottom part of the figure presents the calculated projected p-type density of states for the core sulfur atom in the same reference compounds. The contributions of the core sulfur atom on the +VI oxidation state (solid line) and the core sulfur atom on the +II oxidation state (dashed line) in sulfur p-type density of states are also shown. The calculations were made using FEFF 8.4.).

2.3 DXR2 -UV branch Line

The synchrotron radiation (SR) photon beam from a wiggler installed on the DAFNE storage ring is split by a grazing incidence Au-coated mirror (θ_i = 40 mrad, cut-off energy about 800 eV), in order to provide the X-ray and UV beamlines. The reflected UV radiation travels through the UV beamline and ends in a 38 mm diameter sapphire window. The commissioning of the experimental apparatus installed at the exit window of the branch-line was expected during 2010, but unfortunately the SR was available just at the very beginning of 2011. We used the first two months of the year for a quick commissioning of the optical setup, in order to assess the quality of the optical design and the alignment of the optical elements. We got the first light on February the

Figure 5: First nearly focussed UV synchrotron radiation light.

2nd as shown in Fig. 5. After the assessment tests, we decided to upgrade part of the apparatus, to redesign the optical setup to meet new requirements on scientific applications and to improve the spot size quality, decreasing the stray light observed during the assessment. In the mean time the DXR2 apparatus was used with lamps feeding the branch line to perform some scientific experiments. Concerning the experimental apparatus, the major activities were: 1) variation on the SR optical path; 2) upgrade instrumentation and light sources; 3) joining the UV beamline to the IR beamline SINBAD.

1. The optical design of the branch line was revised in order to improve the expected performance of the whole system. The previous design was based on a focusing optical system producing a 1mm spot at 2 m distance from the last folding mirror at the entrance mirror camera. In order to improve aperture matching and therefore spectral resolution and beam intensity with the monochromators, the design was changed in a collimated beam from the folding mirror. The collimated beam is focused with the proper aperture at the entrance slit of each of the two monochromators and of the optical fiber feeding the white beam channel. The new mirrors were fabricated and put on the optical path, so that a 35 mm collimated beam is now available.

2. Instrumentation has been upgraded with a new VUV monochromator (UVXL200 by Jobin Yvon) operating in the 120-250 nm spectral range. This will be put on the SR beam line after focusing the collimated beam on the entrance slit with the appropriate aperture (F# = 4.3). The previous monochromator (by RMP) will be used coupled to a high power Heraeus Deuterium lamp. This solution will improve the performance of the VUV SR channel and it will offer the opportunity to double the VUV light sources available for experiments, such as UV irradiation, UV ageing, photobiology, etc.

3. An experimental apparatus joining UV and IR radiation was arranged based on a Bruker interferometer performing FTIR spectra. This is the first apparatus in the world, as far as we know, combining UV and IR SR for real time experiments. It will be possible to irradiate samples with UV radiation and producing FTIR spectra providing real time information on the evolving process dynamics. This is appealing for a number of application aimed at measuring how any transforming process occurs in time. SR and Hg/Xe or D2 lamps can be used as UV sources (Fig. 6) and UV radiation is transferred through solarised fiber optics

on the sample inside the IR interferometer. The measured radiation transfer efficiency of the fiber and optical coupling is 70%.

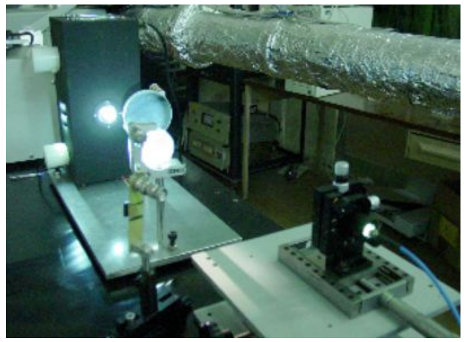

Figure 6: UV radiation transferred through solarised fiber optics

During 2011, two different types of experiment were performed using the Xe-Hg high power lamp: (1) ageing of FOAM materials for space applications; (2) irradiation of nucleic acids with UV irradiation.

1. *Ageing of FOAM.* This is a memory form material that has been developed for space application. Memory form materials are used to recover the original form of the material after being properly modified for the application; so, it can be stretched, pressed, turned and it can recover the original form by applying thermal energy warming it at around 100C. Many applications of interest might benefit from using such a material and it is under study for characterization. UV ageing is one of the main issues, because there is a lot of UV radiation in outer space and this material might undergo degradation after prolonged exposure to UV radiation. Samples of this material were irradiated for several hours (from 1 up to 30 hours) with a 10^{14} phs white beam. The samples were put firstly on the focus and then on the defocused beam to avoid any effect of thermal degradation. After irradiation the samples show brownish regions corresponding to the beam (see Fig. 7). Irradiated materials were characterized by the Differential Scanning Calorimetry (DSC) technique; the DSC curve shows no variation highlighting that no UV ageing effects were occurred. To assess this result the sample was irradiated with IR radiation to have a direct comparison between photo ageing and thermal ageing.

2. *Irradiation of nucleic acids.* Experiments were performed using the new facility combining UV an IR radiation for irradiation and FTIR real time analysis. UV radiation source was the high power Xe-Hg lamp and the Globar was used as IR radiation source. The aim of the experiment was to measure the variation of the molecular structure of the nucleic acids; in particular, the first measurement was on Uracil. The absorbance of the Uracil is only in the 200-300 nm region; so, radiation from the UV source is effective only in that range, where the lamp is not very intense. It was exposed to a total effective photon flux of 10^{13} phs on a spot size of about 2 mm for 120 minutes and a FTIR spectrum was registered every 10 minutes (see Fig. 8) in the wave vector region 500-4000 cm^{-1}. The result shows a clear degradation of the molecules, even if the peaks highlight a variation of the vibration modes, that is of the molecular structure, but not a molecule break. This experiment is the first of a series that will study how UV radiation modifies the nucleic acid molecules and how inorganic material

might protect such molecules, by reducing the radiation damaging. The use of SR will largely improve the results of such experiments, especially for the UV irradiation.

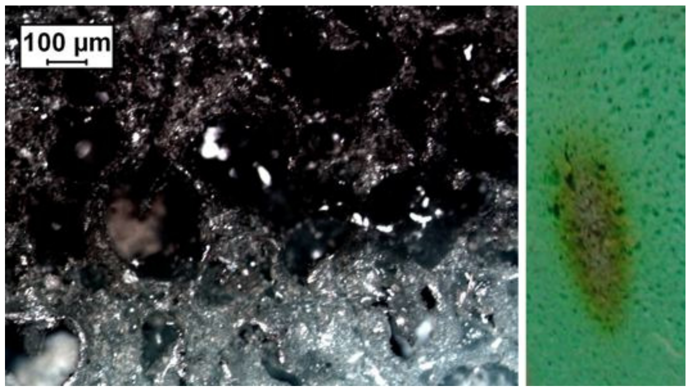

Figure 7: Irradiated FOAM sample after 8 hours at the focus (right) as it appears at a zoomed observation (left)

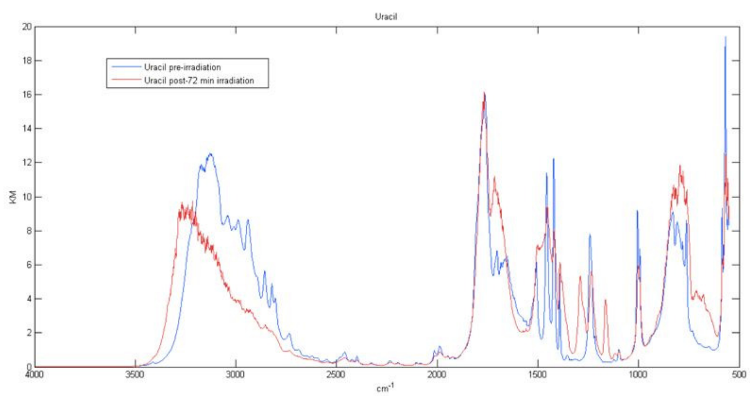

Figure 8: FTIR spectrum of the as-prepared and irradiated Uracil sample.

2.4 New XUV beamlines

In 2011, the new XUV laboratory has continued its construction, based both on the detailed plans approved by the SRL Committee and on available resources. Aim of this laboratory is to host two bending magnet beamlines covering the photon energy range from 30 eV to 1000 eV. One beamline will cover the low energy part of this interval (30-200 eV) and is called LEB (Low Energy Beamline), the other will cover the energy range from 60 eV to 1000 eV and is called HEB (High Energy Beamline). The laboratory as it stands at the end of the year is shown in fig. 9. Both beam lines are in UHV and directly connected to the vacuum of the main DAΦNE electron ring. All the safety protocol and control system are ready and tested and the two beam lines are ready to start commissioning with light as soon as it becomes available. All the optical elements and UHV vacuum chambers needed for the construction of the HEB Beam line have been delivered

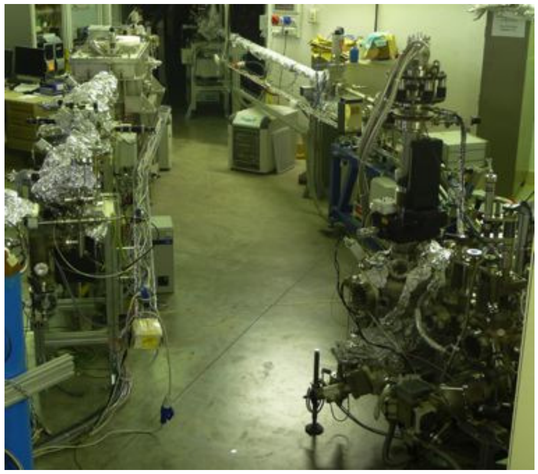

Figure 9: Overwiew of the XUV DAΦNE-L laboratory. On the right side: the LEB beamline and (in front) its experimental chamber. On the left side: the HEB beamline with the recently mounted PGM monochromator.

and mounted. Both beam lines have available and running two *state of the art* end stations (Fig. 10) to perform UHV spectroscopy experiments with SR.

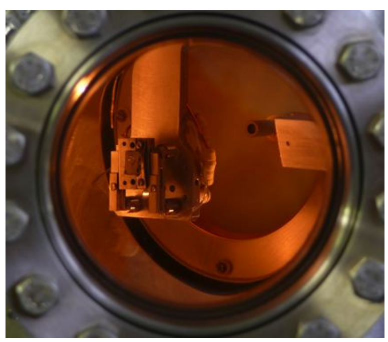

Figure 10: Internal view of the HEB beamline end station.

Both experimental set-ups have been equipped with commercial laboratory sources (X-ray lamp and He-discharge lamps), electron sources and all the needed tools to perform detailed tests on their functionality. For the low energy beam line experimental set-up, the need to test the final performances of the angle resolved analyzer has required to update the existing He lamp, with a mechanical support that can allow *in situ* alignment and with a focusing capillary to irradiate, with VUV photons, our sample mimicking what will happen during SR experiments. Such items are under construction or object of a call for tender. The tests of the experimental chambers are also used to perform experiments on SEY (Secondary Electron Yield) reduction versus electron bombardment, surface conditions and Carbon deposition, which are the objectives of IMCA-NTA Project (see this annual report) and are done in collaboration with R. Larciprete (ISC-CNR) and R. Flammini (IMIP-CNR) associated to the project. In connection to this scientific project it has been decided to equip the laboratory with a *state of the art* micro-Raman station. The call for tender has been launched and final decision and delivery are expected by the first semester of 2012.

3 List of Conference Talks

1. M. Cestelli-Guidi ″ATR-FTIR synchrotron real-time imaging of living cells: a new approach″, WIRMS: 6 International Workshop on Infrared Spectroscopy and Microscopy with Accelerator-Based Sources, Trieste, September 4-8, 2011.

2. M. Cestelli-Guidi, ″FTIR synchrotron real-time imaging of single cells″, 4 ITSR Workshop -Imaging Techniques With Synchrotron Radiation - Bordeaux 24-27 September 2011.

References

1. W.W. Peng, P. Roy, L. Favaro, E. Amzallag, J.B. Brubach, A. Congeduti, M. Cestelli Guidi, A.M. Huntz, J. Barros and R. Ttot. ″Experimental and ab initio study of vibrational modes of stressed alumina films formed by oxidation of aluminum alloys under different atmospheres″, Acta Materialia **59**, 2723 (2011)

2. J. A. Abraham , H. J. Snchez , C. A. Marcelli, M. Grenn, M. Cestelli Guidi, M. Piccinini, ″ A crystallinity study of dental tissues and tartar by infrared spectroscopy″, Anal Bioanal Chem **399**, 1699 (2011)

3. R. Noreen, R. Pineau, C-C. Chien, M. Cestelli-Guidi, Y. Hwu, A. Marcelli, M. Moenner, C. Petibois ″] Functional histology of glioma vasculature by FTIR imaging″, Anal Bioanal Chem **401**, 795 (2011)

4. M. Abbas, M. Ali, S. K. Shah, F. D′Amico, P. Postorino, S. Mangialardo, M. Cestelli Guidi, A. Cricenti, and R. Gunnella, ″. Control of Structural, Electronic and Optical Properties of Eumelanin Films by Electrospray deposition ″, J. Phys. Chem. B **115**,11199 (2011)

5. B.V. Robouch, I.V. Kutcherenko, M. Cestelli-Guidi, A. Kisiel, A. Marcelli, P. Robouch, M. Piccinini, A. Nucara, R. Triboulet, E. Burattini, J. Cebulski, E.M. Sheregii, J. Polit ″Ion distribution preferences in ternary crystals $Zn_xCd_{1-x}Te$, $Zn_{1-x}Hg_xTe$ and $Cd_{1-x}Hg_xTe$ ″, Eur. Phys. J. B **84**, 183 (2011)

6. W. M. Kwiatek, J. Czapla, M. Podgrczyk, A. Kisiel, J. Konior, A. Balerna, ″First approach to studies of sulphur electron DOS in prostate cancer cell lines and tissues studied by XANES.″, Radiation Physics and Chemistry **80**, 1104 (2011)

GILDA - GENERAL PURPOSE ITALIAN BEAMLINE FOR DIFFRACTION AND ABSORPTION - AT ESRF.

A. Balerna, A. Grilli (Tecn.), S. Mobilio (Resp.), A. Raco (Tecn.),
V. Sciarra (Tecn.), V. Tullio (Tecn.)

1 Introduction

GILDA (General Purpose Italian BeamLine for Diffraction and Absorption), is the Italian CRG beamline, built to provide the Italian scientific community with an easy access to the European Synchrotron Radiation Facility to perform experiments with a high energy and brilliance X-ray photon beam. GILDA was proposed, designed, constructed and commissioned by a collaboration between LNF and a large number of University groups; it is operative since autumn 1994. Today GILDA is funded by the Italian public research Institutes: Consiglio Nazionale delle Ricerche (CNR) and Istituto Nazionale di Fisica Nucleare (INFN). Experimental stations for X-ray Absorption Spectroscopy, Anomalous X-ray Scattering and X-ray Diffraction (XRD) are present on the GILDA beamline.
The LNF group is involved in the technical maintenance and update of the beamline, with particular emphasis to the electronic and software controls of all the instrumentation and to the apparatus for X-ray diffraction.

2 Technical activity on the GILDA beamline during 2011

During 2011 the main implementations on the instrumentation were:

1. a new Hp-Ge multi-detector for fluorescence was purchased by the European Molecular Biology Lab of Hamburg and installed on the XAS station; it is composed of 12 detectors with a resolution of 215 eV at 6.4 KeV using a shaping time of 1 ms. Now two multi-detectors are available to GILDA users for a total of 25 detectors.

2. A significant advance in the data acquisition at high energy was achieved by the use of a Si(755) crystal: now it is possible to reach 90 KeV using the first harmonic of the crystal. Previously the same energy was reached by using the third harmonic of a Si(311) crystal, but it was necessary to use filters to remove the first harmonic of that crystal, with a significant loss of intensity.

3. In the diffraction hutch a fast beam shutter was installed and commissioned; moreover thanks to the control of the oven, now possible through the SPEC software, simultaneous time resolved XAS and XRD spectra can be recorded during thermal treatments.

3 Beamtime use during 2011 and scientific outcomes

During 2011 ESRF delivered beam for more than 5000 hours; about 4000 hours were used for user's experiments, the remaining for in-house research, beamline improvements, maintenance and alignment. On GILDA 29 experiments were performed, 20 of Italian users and 9 of European users. All the experiments were approved by the ESRF review panels for the public beamtime and by the Italian GILDA scientific committee for the Italian beamtime.
During 2011, 27 paper were published in International journal with referee, the main topics being

material science, catalysis, nanoparticles and cultural heritage. The following studies are to be mentioned:

1. *X-ray absorption spectroscopy studies of the adducts formed between cytotoxic gold compounds and two major serum proteins*
   Gold metallodrugs form a class of promising antiproliferative agents showing a high propensity to react with proteins. We exploit here X-ray absorption spectroscopy (XAS) methods [both X-ray absorption near-edge spectroscopy (XANES) and extended X-ray absorption fine structure (EXAFS)] to gain insight into the nature of the adducts formed between three representative gold(I, III) metallodrugs (i.e., auranofin, [Au(2,2'-bipyridine)(OH)(2)](PF(6)), Aubipy, and dinuclear [Au(2)(6,6'-dimethyl-2,2'-bipyridine)(2)(mu-O)(2)](PF(6))(2), Auoxo6) and two major plasma proteins, namely, bovine serum albumin (BSA) and human serum apo-transferrin (apoTf). The following metallodrug-protein systems were investigated in depth: auranofin/apoTf, Aubipy/BSA, and Auoxo6/apoTf. XANES spectra revealed that auranofin, upon protein binding, conserves its gold(I) oxidation state. Protein binding most probably takes place through release of the thiosugar ligand and its subsequent replacement by a thiol (or a thioether) from the protein. This hypothesis is independently supported by EXAFS results. In contrast, the reactions of Aubipy with serum albumin and of Auoxo6 with serum apoTf invariantly result in gold(III) to gold(I) reduction. Gold(III) reduction, clearly documented by XANES, is accompanied, in both cases, by release of the bipyridyl ligands; for Auoxo6 cleavage of the gold-gold dioxo bridge is also observed. Gold(III) reduction leads to formation of protein-bound gold(I) species, with deeply modified metal coordination environments, as evidenced by EXAFS. In these adducts, the gold(I) centers are probably anchored to the protein through nitrogen donors. In general, these two XAS methods, i.e., XANES and EXAFS, used here jointly, allowed us to gain independent structural information on metallodrug/protein systems; detailed insight into the gold oxidation state and the local environment of protein-bound metal atoms was achieved in the various cases.

2. *XAS study of lead speciation in a central Italy calcareous soil*
   The Pb absorption processes on a heavy textured calcareous soil, typical of central Italy, were studied in order to probe the structure and chemical nature of Pb in contaminated soils and achieve precise description of Pb ions localization into these contaminated soils. The quantitative analysis of near edge (XANES) as well extended (EXAFS) regions of Pb L_3 edge absorption spectra, in comparison with Pb XAS data of selected reference compounds, allowed the precise determination of local structure and chemical environment of Pb ions in these soil samples. Four components were individuated as the major responsible of Pb retention in calcareous soils: the carbonates, the metal oxide surfaces, the organic matter, and the colloidal inorganic surfaces containing clay components. The structural analysis suggests that, within these experimental conditions, the Pb adsorbed on the soil is generally present as Pb hydroxide with poor crystallization degree. However, the presence of carbonates ($CaCO_3$) induces the co-precipitation of PbCO3-like phases with some degree of crystallinity.

3. *Structure and magnetism in compressed iron/cobalt alloys.*
   Combined Co K-edge XANES-XMCD and XRD measurements were used to shed light on the magnetic and structural phase diagram of the $Fe_{1-x}Co_x$ alloy under HP in the Co-rich region (x $\geq$0.5). At 0.5 $\leq$ 0.75, the alloy shows a pressure-induced structural/magnetic phase transition from bcc-FM to hcp non-FM phase just like pure iron but at higher pressures. The x = 0.9 sample has an fcc structure in the pressure range investigated but presents an FM to non-FM transition at P = 64 GPa, a significantly lower pressure compared with pure Co (predicted $\approx$ 120 GPa), showing that Fe impurities strongly affect the HP Co response.

4. *Atomic scale mechanism for the Ge-induced stabilization of the tetragonal, very high-kappa, phase of ZrO(2).*
   Using x-ray absorption fine structure aided by ab initio structural simulations we demonstrate the atomic scale mechanism responsible for the stabilization of the otherwise unstable very high-kappa tetragonal phase of ZrO(2) by the incorporation of Ge atoms. In tetragonal ZrO(2) the cation has a split first coordination shell formed by eight oxygen atoms. We provide a direct experimental proof that when Ge is incorporated in the oxide, four of the eight O atoms collapse towards Ge giving rise to a local structure strongly reminiscent of that found in quartz-like GeO(2), thus stabilizing the tetragonal phase.

5. *Local structure at interfaces between hydride-forming metals: A case study of Mg-Pd nanoparticles by x-ray spectroscopy*
   The structure at the interface between elements or phases that exhibit different hydrogen (H) binding energies exerts a profound influence on the thermodynamics of H in nanophase materials. In this paper, we study the local structure at the Mg/Pd interface in Mg nanoparticles with partial Pd coating, and we map its evolution in response to annealing and H sorption. This task is accomplished by x-ray photoelectron spectroscopy and x-ray absorption spectroscopy, also including in situ experiments, with the support of crystallographic information from x-ray diffraction. It is shown that the initial Pd surface layer reacts with Mg at relatively low temperatures, leading to irreversible formation of a Mg-rich intermetallic phase Mg_6Pd. Due to the high Mg-H binding energy, this phase reversibly transforms, upon H absorption, into a nanophase mixture of magnesium hydride and a Pd-rich intermetallic with H in solid solution, MgPdH. These reversible structural changes are discussed with reference to recent calculations that highlight their relevance to the thermodynamics of the metal-hydride transition. The picture drawn here might be relevant to other multiphase materials presently investigated in the field of hydrogen-related science and technology.

6. *Modified Naples yellow in Renaissance majolica: study of PbSbZn and PbSbFe ternary pyroantimonates by X-ray absorption spectroscopy*
   X-Ray absorption spectroscopy investigations combined with ab initio structural simulations of ternary forms (PbSbZn and PbSbFe) of the pigment Naples yellow ($Pb_2Sb_2O_7$) allowed to achieve a detailed insight into the incorporation route of Zn and Fe ions inside the pigment lattice. The study of newly synthesised yellow pyroantimonates provided direct evidence that Zn and Fe ions enter the pyrochlore octahedral sites replacing Sb ions. Experimental results were discussed considering, also, the information provided by Raman spectroscopy used in this study as a sensitive probe of the pyrochlore lattice distortions in modified yellow pyroantimonates. Finally, by exploiting the non-invasiveness of the X-ray absorption spectroscopy technique, the same structural arrangement has been unambiguously observed for Zn cations in a modified Naples yellow pigment of a Renaissance ceramic shard.

4 2012 - GILDA Forseen Activity

During 2012 both the user facility operations and technical activities will be strongly influenced by the foreseen long shutdown of the storage ring for the upgrade of the overall facility. The main foreseen activities for 2012 are:

1. the user facility operation will continue but will be limited to about 3/4 of that of previous years.

2. A new holder for the first crystal of the monochromator will be installed and commissioned in order to have the possibility to mount a couple of flat first crystals at the same time;

only one of them will be illuminated at a time by using 1/2 of the horizontal fan of the beam; in this way for a specific second crystal a very wide energy range will be available, by illuminating one of the two first crystals of the couple. Using a first crystals couple made of a Si(111)and a Si(511) and a Si(111) second crystal, the available spectral range will be 4.8 - 48; with the couple Si(311) and Si(755) with a Si(311) as second crystal the spectral range will be 6.0 - 90.0 KeV. This implementation will strongly fasten many experiments, giving the opportunity to span a wide spectral range and to measure multiple K-edges in the same run, as very often requested by experiments.

3. All motors of the beamlines will be changed to step by step motors controlled by SPEC software under the ICEPAP ESRF standard, a very important step to increase the reliability of the beamline; it is particularly important for the motors of the II mirror, whose recent fault forced the beamline to operate for some weeks without mirrors.

4. In order to increase the reliability of the beamline the software for data acquisition and control of the XAFS experiments will be implemented under SPEC; this will be a first step towards the migration of all the acquisition and control electronics towards up to date systems.

5 Publications

1. L. Messori *et al.*,"X-ray absorption spectroscopy studies of the adducts formed between cytotoxic gold compounds and two major serum proteins", J. of Biol. Inorganic Chem. **16**, 491 (2011).

2. T. Comaschi, C. Meneghini, D. Businelli, S. Mobilio, M. Businelli, "XAS study of lead speciation in a central Italy calcareous soil", Env. Science and Poll. Res.**18**, 669 (2011).

3. L. Pasquini *et al.*, "Local structure at interfaces between hydride-forming metals: A case study of Mg-Pd nanoparticles by x-ray spectroscopy", Physical Rev. B**83**, 184111 (2011).

4. R. Torchio *et al.*, "Structure and magnetism in compressed ironcobalt alloys", High Pressure Research **31**, 148 (2011).

5. F. Boscherini *et al.*, "Atomic scale mechanism for the Ge-induced stabilization of the tetragonal, very high-kappa, phase of ZrO(2)", Applied Physics Letters **99**, 121909 (2011).

6. L. Cartechini *et al.*, "Modified Naples yellow in Renaissance majolica: study of PbSbZn and PbSbFe ternary pyroantimonates by X-ray absorption spectroscopy", Journal of Analytical Atomic Spectrometry **26**, 2500 (2011).

NTA - CLIC

D. Alesini, C. Biscari , A. Ghigo (Resp.), F. Marcellini, M. Serio, A. Stella

1 Introduction

The Compact Linear Collider Test Facility (CTF3) project aims to study the feasibility of an electron-positron linear collider, with c.m. energy up to 3 TeV, based on two-beam acceleration scheme. Acceleration gradient of 100 MeV/m, provided by high power 12GHz radio-frequency generated by a powerful electron drive beam, has to be demonstrated.

The INFN Frascati Laboratory (LNF) designed and realized the two rings of the drive beam recombination system in the framework of CTF3-CLIC international collaboration. These rings are now routinely operating to produce the RF power for the two beam acceleration experiments. LNF team is now involved in the synchronization experiment of the drive beam with main beam.

The two beams acceleration scheme, basic feature of the Compact LInear Collider CLIC, asks for precise synchronization between the Main Beam and the RF power produced by the Drive Beam in order to keep the energy of the Main Beam constant. Drive Beam timing and intensity errors lead to phase and amplitude RF variation in the accelerating structures, with consequent different acceleration gradient. Main Beam energy variations cause collider luminosity reduction. In order to keep the luminosity reduction less than 2% the RF phase jitter should be less than 0.1 degree (23fs @ 12GHz).

The Main Beam and Drive Beam synchronization has to be assured by a feed-forward system in which the two beams arrival time are compared and the proper correction is applied to the Drive Beam. A feed forward system, similar to the CLIC one, will be tested in the CLIC Test Facility CTF3 now in operation at CERN. The phase measurement is foreseen at the end of the Drive Beam linac and the correction will be applied in the chicane after the combination rings.

The effectiveness of the system will be measured by another phase monitor placed before the RF power production system and by monitoring the RF power production in the decelerating structures. The basic components of the system are the phase monitors and the correction kickers that are now in the construction phase.

2 Beam Phase Monitor

The front end of the phase forward system is the monitor that detects the bunch longitudinal position and is characterized by a time resolution of the order of 20 fs. The pick-up is composed by four slots, equally distributed on the vacuum chamber, with cut-off frequency above the bunch frequency of 12 GHz: the electromagnetic field at that frequency is evanescent in the slot. The beam signal is coupled out of the beam pipe through waveguides with transitions to 50ohm coaxial lines. Commercial vacuum feedtroughs to SMA standard connectors are placed in the coaxial section.

Double ridged design of the waveguide has been chosen in order to optimize the transition frequency response and reduce the cross section. Two notch filters, realized with bumps in the beam pipe at a distance tuned at the bunch detection frequency, are placed at both the pick up sides, providing a resonant volume for the beam electromagnetic field. The filters provide also the rejection of the RF noise and wake field in the working bandwidth that can induce spurious signals that affect the measurements.

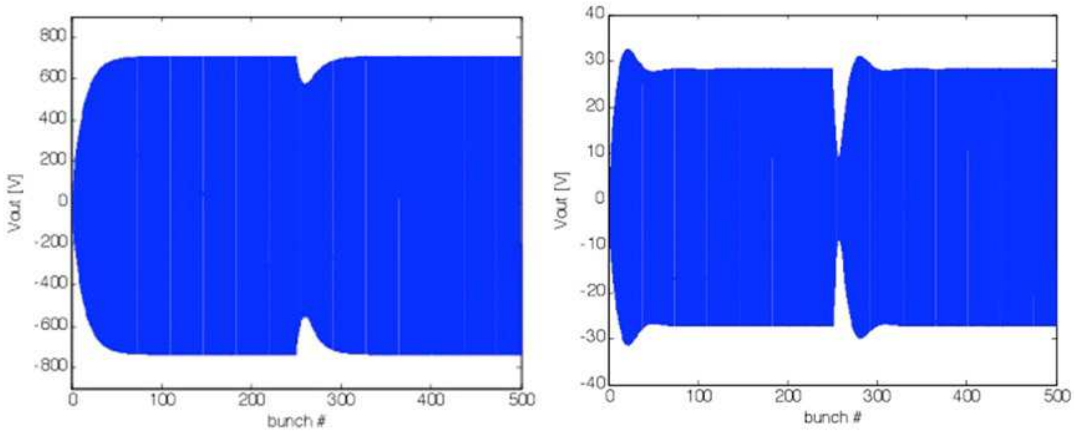

Figure 1: *pickup outputs given by a bunch train at the nominal beam current with a phase jump: tuned version on the left, detuned on the right.*

Time domain simulations have been performed to characterize the pick up response applying a phase jump in a certain bunch of the train and looking at the signal at the monitor exit. Two examples are reported in Fig. 1: the first is the time response signal, in bunch number, of the monitor precisely tuned at the bunch frequency (output voltage larger than 700V at the nominal current). The second is for the same pick-up with the notch filter with slightly different distance that gives the detuned version (signal of 30V). The response time is approximately 50 bunches on 2100 bunches of the train that is a reasonable value for the feedback.

The detuned version is preferrable because the signal level is high enough and better compatible with the SMA standard feedthroughs and the coupling impedance is much lower. Components for two prototypes, one tuned and one detuned, have been fabricated and tested with RF measurements before welding. Fig. 2 shows pictures of the prototype components.

Figure 2: *pickup prototype before welding. From Left to right:waveguide profile, monitor assembly, notch filters, coupling slots to waveguide*

The measurements have given the expected results in terms of frequency response and confirmed the results obtained by simulations. Little discrepancies in the Q value and frequency could be also ascribed to not perfect electrical contact among the assembled parts. Measurements will be repeated soon after the welding.

3 Kicker

The phase correction is provided by changing the electron beam trajectory in a dispersive region by transversally kicking the bunch with fast kicker magnets: the path length variation due to the trajectory closed bump provides the longitudinal position correction.

Figure 3: *kicker mechanical design*

A two strip-line kicker structure Fig. 3 has been chosen to satisfy the following requirements:
-Fast response to the input pulse signal (few ns)
-High kick efficiency
-50 ohm characteristics impedance to match the high voltage pulser avoiding pulse reflection
-Low longitudinal coupling impedance to limit the energy spread degradation

The kickers will be installed in the dog-leg line that connects the Combiner ring to the CLIC experimental area. With this configuration a voltage of 1.4kV applied to each strip, with opposite polarity, provides the requested 1mrad kick angle at the CTF3 beam energy (150 MeV).

4 CLIC Combiner Ring studies

During 2011, in the framework of the collaboration between the LNF Accelerator Division and the CLIC Study Group, the Drive Beam Recombination Complex (DBRC) design has been finalized, and is the subject of a chapter of the CLIC Conceptual Design Report, presently under completion as the result of a wide international collaboration effort.

LNF owns the responsibility of the DBRC design, and coordinates the work of the team which includes CERN and LNF Staff. The DBRC compresses the bunch trains and raises the average current up to 100 A over the pulse, by means of a staged recombination process: a Delay Line (DL) for the first factor of 2, the first Combiner Ring (CR1) for a factor of 3, and the second one (CR2) for the last factor of 4.

The beam from CR2 is then transported through a Long Turnaround (LTA) up to the sequential Turnarounds (TAs), which inject the beam into decelerating sections. The DBRC is designed to preserve the transverse and longitudinal beam emittances, by isochronicity and careful high order chromatic effect corrections. Fig. 4 shows the schematic layout of the whole complex.

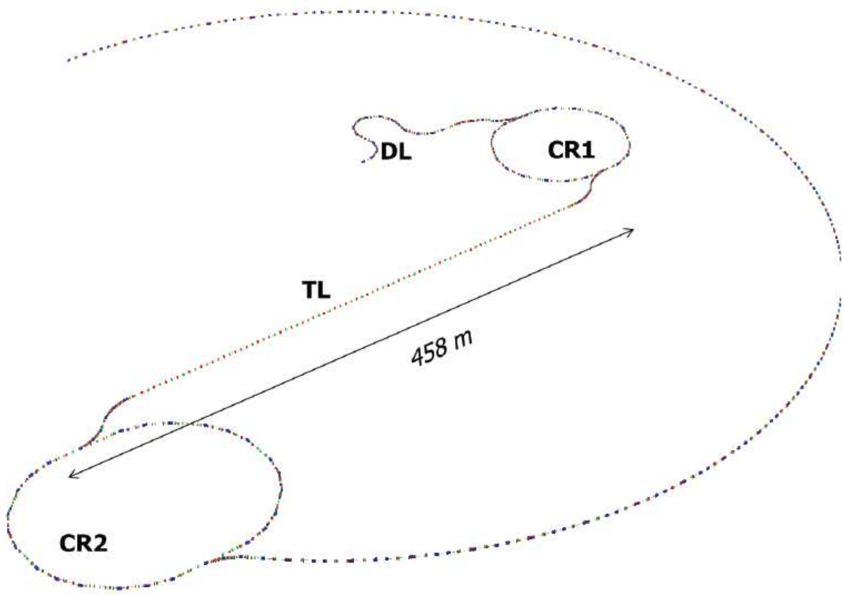

Figure 4: *Schematic layout of CLIC DBRC*

5 Publications

1. CLIC International Collaboration *et al.*: "CLIC Conceptual Design Report", http://project-clic-cdr.web.cern.ch

NTA ILC

D. Alesini, M. E. Biagini, S. Bini, R. Boni, R. Cimino, A. Clozza, A. Gallo, A. Ghigo, S. Guiducci (Resp.), F. Marcellini, P. Raimondi, A. Stecchi

Introduction

The INFN has contributed to the GDE (Global Design Effort) for the International Linear Collider (ILC) since the beginning in 2005 with a qualified participation to the project design and R&D. At present INFN is providing an important contribution to the completion of the Technical Design Report to be realised by the end of 2012. This activity is fully integrated at the international level with INFN responsibilities in the GDE on Main Linac (Milano-LASA) and the responsibility of the Damping Rings (DR) area system at LNF.

The LNF activity is focused on damping rings and consists of studies and simulations and on the realization of prototypes of some critical elements. The possibility of making experimental observations at DAFNE offers a great opportunity to test simulation studies and prototypes.

2 Year 2011 Activities

In the present phase the GDE main objective is the preparation of the Technical Design Report. LNF has chaired the write-up of the DR section of the “Technical Progress Report” [1], published in March, that gives updated specifications on the ILC design and reports on the status of the research and development activities for the TDR.

In a dedicated workshop, BAW2, at SLAC in January the choice of the baseline for the TDR has been finalised [2, 3]. The new baseline foresees operation of the ILC with 1312 bunches per pulse, in comparison with the nominal ILC Reference Design Report (RDR) value of 2625 bunches. This allows reducing the DR circumference by a factor of 2 while maintaining the same 6.2 ns bunch separation and particles per bunch as specified in the RDR. Extensive work has been done on the lattice design of the 3.2 km DR and on beam dynamics studies to evaluate the performance of the shorter ring.

Leading up to the ALCPG11 meeting, held in March 2011 in Eugene, US [4, 5], a lattice evaluation process was initiated in order to select the new baseline lattice [6, 7]. The baseline lattice description and the status of the DR technical systems, in particular the Radiofrequency system, were reported at the DR Technical Baseline Review meeting held at LNF on 7-8 July 2011 [8, 9, 10]. The meeting objectives were to review R&D and baseline design decisions, to consolidate and sign-off documentation, to review requirements for the conventional facilities and costs.

One of the main R&D activity on critical issues for the ILC DR has been the installation in 2010 of electron clearing electrodes in DAFNE in order to reduce by more than one order of magnitude the e-cloud density in the dipole and wiggler vacuum chambers [11]. During 2011 systematic beam tests of their effect have been performed and the effectiveness in mitigating the e-cloud instability has been proven at high beam currents. The results will be the subject of an oral presentation at the International Particle Accelerator Conference IPAC12, New Orleans, US, 20-25 May 2012.

Another activity aimed at developing e-cloud mitigation techniques is the realization of a sputtering system for thin film deposition on vacuum chamber samples in order to reduce the Secondary Emission Yield (SEY). A set-up for coating small aluminium objects using a RF magnetron operating at 13.56 MHz has been realized [12]. The device allows varying the parameters of the coating process, in particular to control the relative pressure of the ionization gas and reactive gas. A few samples coated with TiN have been produced and the SEY value as a function of the electron dose has been measured at the LNF Material Science Laboratory [13] in collaboration with the YMCA experiment.

A Low Emittance Rings Collaboration started from the ILC and CLIC working group on damping rings, with strong involvment of SuperB group, with the scope to bring together scientific communities of synchrotron light sources, storage rings, damping rings and lepton colliders in order to communicate, identify and promote research work on common topics affecting the design of low emittance lepton rings. In this framework LNF has contributed to the organization of an ICFA Beam Dynamics Mini Workshop on Low Emittance Rings (LOWεRING), held at Crete, Greece, October 2011 with large international participation.

3 Plans for Year 2012

LNF will continue to coordinate the Damping Rings (DR) working group within the GDE, with the responsibility of the DR area system for the preparation of the Technical Design Report, due end of 2012. The technical and research activity will be focussed in particular on e-cloud studies. The comparison between simulations and experimental tests at DAFNE will continue in order to improve the comprehension and mitigate the "electron cloud" instability.

4 Publications and talks

1. "International Linear Collider, A Technical Progress Report", ILC Report ILC-REPORT-2011-030, INFN LNF-11/2(NT) 30-03-2011
2. S. Guiducci, "Damping Rings and Upgrade – Low Power Configuration", GDE 2nd Baseline Assessment Workshop, SLAC, January 18-21, 2011
3. S. Guiducci, "Damping Rings at 10 Hz", GDE 2nd Baseline Assessment Workshop, SLAC, January 18-21, 2011
4. S. Guiducci, "Damping Rings Specifications", ALCPG11 Linear Collider Workshop of the Americas, University of Oregon, Eugene, Oregon, USA, 19-23 March 2011
5. S. Guiducci, "DSB3 Lattice Update", ALCPG11 Linear Collider Workshop of the Americas, University of Oregon, Eugene, Oregon, USA, 19-23 March 2011
6. S. Guiducci et al., ``Updates to the International Linear Collider Damping Rings Baseline Design'', p. 32, Proc. of IPAC11, San Sebastian, Spain, (2011)
7. M.T.F. Pivi et al., ``Recommendation for Mitigations of the Electron Cloud Instability in the ILC'', p. 1063, Proc. of IPAC11, San Sebastian, Spain, (2011)
8. S. Guiducci, "DR Parameters ", Damping Ring Baseline Technical Review, INFN-LNF, Frascati, Italy, 7-8 July 2011
9. S. Guiducci, "Summary of Critical Tasks Remaining", Damping Ring Baseline Technical Review, INFN-LNF, Frascati, Italy, 7-8 July 2011
10. A. Gallo, R. Boni, "RF System Specifications for Nominal and 10Hz Operation", Damping Ring Baseline Technical Review, INFN-LNF, Frascati, Italy, 7-8 July 2011
11. D. Alesini, et al., ``Design and Test of the Clearing Electrodes for e^- cloud Mitigation in the e^+ DAΦNE Ring'', p. 1515, Proc. of IPAC10, Kyoto, Japan, (2010)
12. S. Bini, "Synthesis of Nitride Titanium Film by RF Sputtering", ILC-LNF Technical Note, ILC-LNF-004, January 8, 2011
13. R. Cimino, "Development and Characterization of Materials for EC Mitigation @LNF", LCWS11 International Workshop on Future Linear Colliders, Granada, Spain 26-30 September 2011
14. A. Gallo, "Bunch Length Control with 2nd Harmonic Cavity", LCWS11 International Workshop on Future Linear Colliders, Granada, Spain 26-30 September 2011
15. S. Guiducci, "TDR Outline Development and Personnel Assignments", LCWS11 International Workshop on Future Linear Colliders, Granada, Spain 26-30 September 2011

NTA - IMCA (Innovative Materials and Coatings for Accelerator)

A.Balerna, R.Cimino (Resp.), M. Commisso, T. Demma, D. R.Grosso, R. Larciprete (CNR-ISC), S. Guiducci, R. Flammini (CNR-IMIP), C. Milardi, C. Vaccarezza, M. Zobov (INFN-LNF)

March 20, 2012

The IMCA experiment was started in 2010 in order to develop new materials and coatings with stable and low enough SEY(Secondary Electron Yield) to guarantee full operation of present and future accelerator machines. This issue, in fact, is crucial in controlling Electron Cloud formation and in reducing its effects, that are well known to be a potential bottle-neck to the performances obtainable from particles accelerators. Frascati has a long-standing experience in qualifying materials in terms of surface parameters of interest to e-cloud issues. We are routinely measuring SEY, its dependence from electron energy, temperature and scrubbing dose. We are now able to characterize "in situ" the surface chemical composition and eventual modifications occurring during electron or photon irradiation by using XPS with conventional X-ray source and we are ready to exploit for this purpose the synchrotron radiation beamlines in construction at DAΦNE[1]. Our experimental measurements of the relevant parameters can be also confidently compared to simulations, performed by running the EC codes, in order to elucidate the final consequences on machine performances. Such a combined characterization effort is also suggesting ways to produce low SEY materials coatings. This issue is particularly important in view of the possible construction in Italy of a Super-B high luminosity collider [2], where e-cloud issues may be present.

The previous experimental and theoretical results obtained with the Nuvola experiment during the past years, are the scientific base of this project. Indeed during these years in the Surface Laboratory in Frascati, we measured SEY reduction versus the dose (the number of impinging electrons per unit area on sample surfaces). This process is usually called "Scrubbing". We now can correlate the SEY reduction obtained by electron bombardment with the surface

chemical composition by using X-ray photoemission spectroscopy, confirming that the electron bombardment results in the graphitization of the carbon impurities on the copper surface [6]. Such characterizations have suggested also ways to produce low SEY materials, which are still under study. The analysis chamber is now routinely working. This UHV μ-metal chamber, with less than 5 mG residual magnetic field at the sample position, and steadily in a vacuum better than 2×10^{-10} Torr after bake-out, is equipped with an Omicron LEED; an electron gun to measure the SEY of produced samples; a Faraday cup to characterize beam currents and beam profiles; an Omicron electron analyzer and an X-Ray and a UV Lamps to perform photoemission spectra and to obtain chemical information on the studied surface.
In 2011, in collaboration with the major laboratories which are playing an international leading role on the study and characterization of e-cloud effects, we have addressed a series of issues studying different materials. Such activity not only is promoting our Material Science Laboratory in Frascati as one of the most advanced Laboratory in this field, but also provided a quite comprehensive understanding on the physical phenomena governing the SEY and its variations during the various surface modifications.
Here, in brief, we report on some of the running experiments and collaboration.

1. In close collaboration with CERN, we continue studying the energy dependence of the scrubbing of Cu surfaces, representative of LCH dipole chambers. While the lower efficiency in reducing the SEY of the electron with energy lower than 30 eV is well established, we also start to have a clearer understanding on the chemical modification occurring at the surface. SEY reduction can be assigned to the formation of graphitic carbon on the surface and low energy electrons seem not to be able to promote such graphitization as the higher energy electrons do[7, 9].

2. In collaboration with the DAΦNE accelerator division and the DESY vacuum group running PETRA III, we have studied the SEY and the chemical variations of Al samples representative of the two accelerators. PETRA III is a positron ring for very low emittance Synchrotron Radiation and its actual performances seems to be affected by ECE (Electron Cloud Effects). Our study confirms the high SEY value of the Al and that its reduction during scrubbing can vary even due to subtle differences in the experimental conditions. The combined SEY and XPS analysis identify in the extremely high reactivity of Al to oxygen the main cause of variability. Due to this reactivity, C does not undergo the graphitization process, as it does on other surfaces, suggesting Al not suitable for the construction of accelerators with potential ECE[4].

3. In collaboration with RICH, where ECE has been observed on the Stain-

less Steel (SS) walls of the machine arcs, we have studied representative SS samples. We have observed that, also for SS the electron bombardment induces graphitization and a consequent reduction to the measured SEY, down to values anyway larger than those of Cu. Consequences on the machine performances of our set of data are still under analysis.[5]

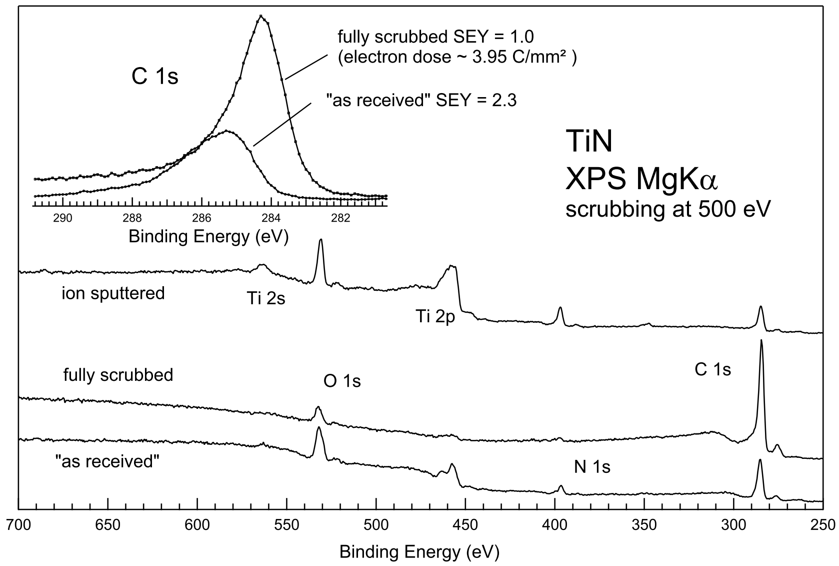

Figure 1: XPS spectra recorded on the "as received", fully scrubbed (at 500 eV electron kinetic energy) and ion sputtered surface; (inset: comparison of the C1s core levels).

4. We have then carefully studied TiN films deposited by means of magneto-sputtering in collaboration with the LNF vacuum group (accelerator division). This coating has been used at PEP to mitigate ECE effects and is a potential candidate to be used at Super-B accelerator. The starting SEY value (2.2) is indeed quite high but can be scrubbed down to about 1 after an electron dose of $10^{-}2$ C/mm^2 (e- energy of 500 eV). Also for this surface, as in the case of Cu surfaces representative of LHC vacuum walls, we measured SEY reduction not only versus dose (the number of impinging electrons per unit area on sample surfaces), but also versus the impinging electron energy with special attention to low energy primary electrons (< 20 eV). In the Fig.1 the XPS spectra recorded on the "as received", fully scrubbed (at 500 eV electron kinetic energy) and ion sputtered surface are shown. In particular, the comparison between the "as

received" and fully scrubbed surfaces demonstrate that the amount of carbon has increased substantially upon electron scrubbing. Moreover, in the inset, the comparison of the sole C1s core levels shows that the scrubbed sample has undergone a "graphitization", because of the binding energy shift recorded. Similar spectra show that the scrubbing at 10 eV primary electron energy, causes, as in the Cu case[7, 9], a less efficient decrease in the SEY and is accompanied by a less effective graphitization, as measured by the C 1s spectrum. [8]

In collaboration with the DAΦNE Light group, it has been decided to equip the laboratory with a state of the art μ-Raman station. The call for tender has been launched, the final decision and delivery are expected in the first semester of 2012. This system will enlarge our capabilities to perform detailed surface analysis both "in situ" and "ex situ", gaining a better understanding of the chemical properties and surface modifications occurring on the different materials under study.

The commissioning of an apparatus able to grow and characterize thin films by dissociation of hydrocarbons by Chemical Vapor Deposition in UHV (Ultra High Vacuum), is still ongoing, and undesired delays are due to the time needed to equip such system with all the necessary safety interlocks required when working with hydrocarbons.

Conference Talks

- R. Cimino: "Surface Studies for SEY reduction by Scrubbing", CERN-GSI Electron Cloud Workshop. CERN 7-3-11
- R. Cimino et al.: "Experimental Efforts To Obtain Low Secondary Electron Yield Materials In Particle Accelerator", PAC 11, New York , NY, U.S.A. March 28 April 1, 2011
- R. Cimino: "Development and Characterization of new Pipe Material and Coatings for e-cloud mitigation @ LNF", XVII SuperB Workshop and Kick Off Meeting May, 29 June, 1; La Biodola, Isola d'Elba.
- R. Cimino: "A surface Study on the origin of SEY reduction on accelerator walls", CERN- e-cloud meetings 28-7-2011.
- D.R. Grosso et al.: "SEY of Al Samples from the Dipole Chamber of PETRA III at DESY", IPAC11, San Sebastian, Spain 4-9 September 2011.
- R. Cimino: "Developement and Characterization of Materials and Coatings for e-cloud mitigation @ LNF", LCWS11 Granada, Spain, 26-30 September 2011

- R. Cimino: "A surface Study on the origin of SEY reduction on accelerator walls". Low Emittance Rings Workshop 2011 (LowERing2011) Heraklion, Crete 03 - 05 October 2011
- R. Cimino: "Status report on Development and Characterization of New Material and Coatings for e-cloud mitigation @ LNF". II SuperB Collaboration Meeting (Frascati) 13-16 December, Frascati (Rome).

References

[1] LNF Annual Report. This and previous issues.

[2] M.E. Biagini, R. Boni, M. Boscolo et. al, proceedings of European Particle Accelerator Conference (EPAC08), and references therein p. 2605.

[3] R. Cimino et al., Phys. Rev. Lett. 93, 14801 (2004).

[4] D.R. Grosso et al SEY of Al Samples from the Dipole Chamber of PETRA III at DESY, proceedings of IPAC11.

[5] D.R. Grosso et al.: "Surface analysis and secondary electron yield of 316N stainless steel samples from RHIC". In preparation.

[6] R. Cimino et al., Experimental efforts at Lnf to reduce secondary electron yield in particle accelerators, proceedings of ECLOUD10, 2010.

[7] R. Cimino et al. : "On the nature of the decrease of the secondary electron yield by electron bombardment and its energy dependence". In preparation.

[8] R. Flammini et al. : "Energy dependence of TiN scrubbing". In preparation.

[9] R. Larciprete et al. : "The chemical origin of SEY at technical surfaces". In preparation.

NTA-PLASMONX

M. Bellaveglia, S. Bellucci, S. Bini, M. Castellano, E. Chiadroni, A. Clozza, L. Coderoni, G. Di Pirro, A. Drago,
M. Esposito, M. Ferrario, D. Fililppetto, A. Gallo, C. Gatti, G. Gatti, P. Gaudio, A. Ghigo,
G. Giannini, T. Levato*, F. Micciulla, M. Migliorati, A. Mostacci, D. Nanni,
E. Pace, L. Palumbo, A. Petrucci, I. Sacco, C. Sanelli, A. Tenore,
F. Terra, S. Tomassini, C. Vaccarezza, C. Vicario
Laboratori Nazionali di Frascati

C. Benedetti, G. Turchetti
Sezione INFN Bologna

A. L. Bacci, F. Broggi, M.M. Cola, A. Flacco, C. Maroli, M. Passoni, V. Petrillo, N. Piovella, R. Pozzoli, M. Romé, A. R. Rossi, L. Serafini
Sezione INFN Milano

D. Batani, R. Benocci
Sezione INFN Milano Bicocca

C.A.Cecchetti, A.Gamucci, D.Giulietti, L.A.Gizzi,
L.Labate, N.Pathak, F. Piastra
Intense Laser Irradiation Laboratory, INO-CNR and Sezione INFN, Pisa

N. Drenska, R. Faccini, P. Valente
Dip. Fisica Univ. La Sapienza, Roma

* also at ILIL, INO-CNR, Pisa, Italy

1 Introduction

In the 2011 the NTA-PLASMONX project has seen the completion of FLAME-laboratory and the successful first experimental champaign in November on self-injection laser plasma electron acceleration at low laser power (10TW). The commissioning activity has been carried on through all the year and also the Self Injection Test Experiment has completed its first phase. The SITE spectrometer activity has seen in this year the development of full MC simulation together with the study of electronic noise remedies and the development of an alternative readout based on optical devices, Also the design and the acquisition process for the high energy version of the spectrometer magnet have been completed. The installation of the electron beam transfer lines for the Thomson Scattering and Plasma Acceleration experiments have been carried on during 2011. The Thomson source interaction final setup will take place on spring 2012 together with the setup of the BEATS2 experiment. The description of this activity is given in the following.

2 FLAME commissioning

During 2011, the FLAME system was fully commissioned with complete hardware installation and extensive performance tests. Special attention was devoted to the performance of the system at full energy. During this year a full training was performed to LNF personnel by the Pisa group to transfer the expertise on any system and subsystem of the Flame Lab, inclusing the laser and the target area. This training, starting from the control of the laser system parameters up to the high power is currently going toward the new experimental phase where the strong collaboration between this two groups on the Laser from one side and the Laser-Plasma interaction from the other will be essential to reach the final goal consisting in GeV level electron acceleration by plasma

wave.
A detailed description of the laser system was already given in the previous report. Here we summarize the system specifications and focus on final performance completed on Dec. 2011. The FLAME Amplitude laser is based upon Ti:Sa, chirped pulse amplification (CPA) system that will deliver 25 fs, 800 nm, up to 220 TW, laser pulses with a 10 Hz repetition rate at a fundamental wavelength of 800 nm. The system features a high, sub-ns contrast ratio ($> 10^{10}$) and has a fully remotely controlled operation mode. The system includes a front-end with pulse contrast enhancement (booster), bandwidth control and regenerative amplifier and yields pulses with 0.7 mJ in 80 nm bandwidth. These pulses are then further amplified by the first amplifier to the 25 mJ level while the second amplifier brings the energy to the 600 mJ level. The third cryogenic amplifier (MP3) is based upon a 50 mm Ti:Sa crystal pumped by 10, frequency doubled Nd:YAG laser pulses for a total of up to 20 J of energy at 532 nm. The extraction energy is as high as 35%, leading to a final energy in the stretched pulses in excess of 7 J. The typical spectrum of the pulse at the exit of MP3 and the stability of the output energy are shown in Fig.1.

As anticipated above, major effort was dedicated during the final phase of the commissioning, to the characterization of the main parameters at full energy.

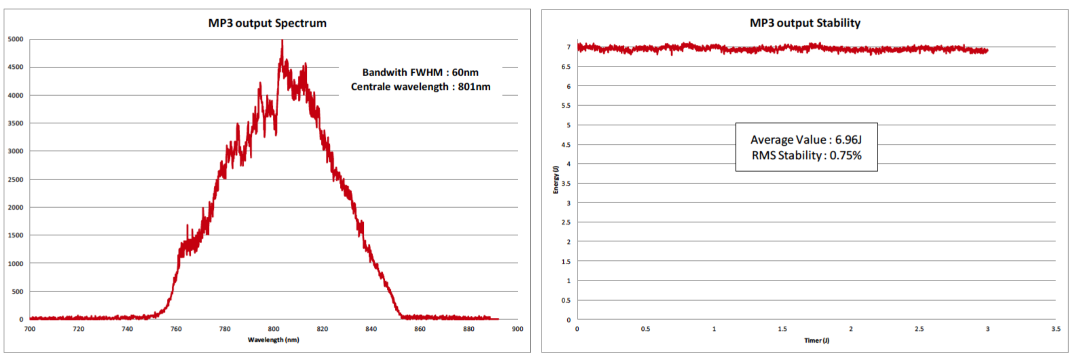

Figure 1: (left)Typical spectrum of the laser pulse at the exit of the power amplifier(MP3) and (right) measurement of the stability of the output energy at close to maximum pumping level.

Pulses at the output of MP3 are then transported in air to the vacuum compressor placed in the underground target area. At the entrance of the compressor the beam pattern, as obtained with the "burn paper" technique, is shown in Fig.2.

The pulse is then compressed to a minimum pulse duration below 30 fs, as shown by the Fig.**??**. Once compressed, the pulse in transported under vacuum to the target chamber via remotely controlled beam steering mirrors. The plot of Fig. 3 shows the cross correlation curve of the FLAME laser system showing the level of ASE just above 10^{-9} of the peak intensity.

This value of the ASE laser contrast is well above the typical value usually found in multi-stage Ti:Sa laser systems in which the typical laser contrast does not exceed 10^7. In the typical experimental conditions of laser wakefield acceleration with self-injection, the laser pulse is focused at peak intensities exceeding 10^{18} W/cm^2 which, with our ASE contrast, gives a precursor laser intensity on target below 10^9 W/cm^2. In the case of interaction with gases with pressures ranging from 1 to 10 bar, this laser intensity is below the plasma formation threshold for laser pulses of sub-nanosecond duration [**?**] which is the typical duration of ASE pulses. Therefore we can reasonably assume that in the cse of interaction with gases, no premature plasma formation occurs and the CPA pulse can be focused directly in the gas. However, according to the cross-correlation curve of Fig. 3 (right) some precursor radiation may be present on the ps time scale before the pulse reaches the peak intensity. This radiation may give rise to premature ionization of the

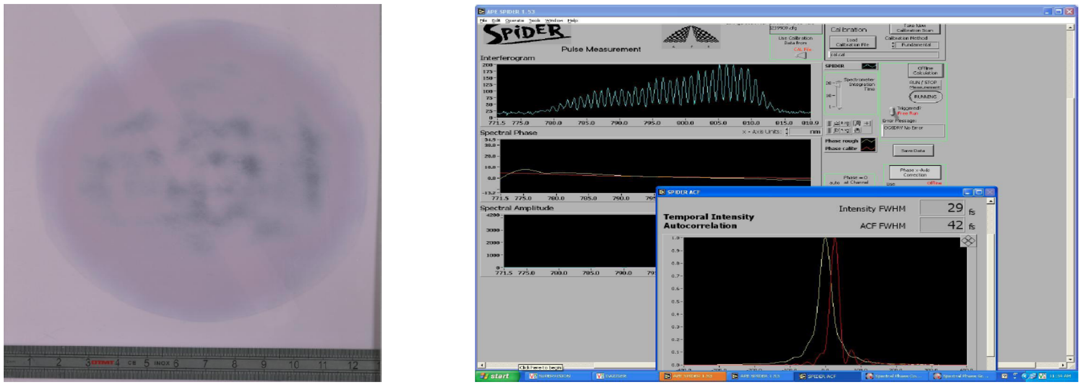

Figure 2: (left)Pattern of the beam intensity at 4.6 J pulse energy, taken at the entrance of the vacuum compressor and (right) pulse duration measurement carried out using the Spider technique

gas. A quantitative analysis of this ionization process will be the subject of investigation of the interferometric measurements which, as discussed below, will rely on femtosecond-scale resolution capability.

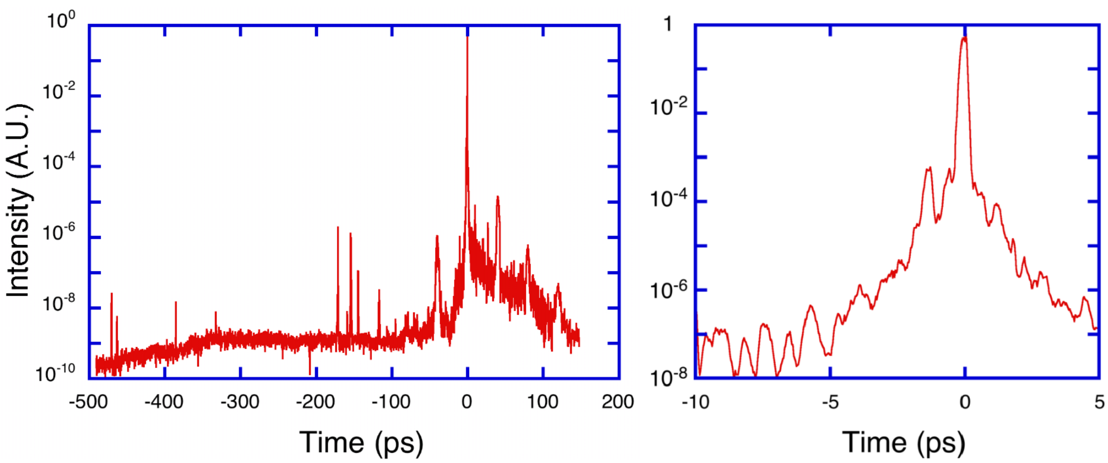

Figure 3: Cross-correlation curve (left) showing the detailed temporal structure of the laser pulse in the 500 ps window before the main pulse. The plot on the left shows that intensity of the amplified spontaneous emission is just above 10^{-9} of the peak intensity. The plot on the right shows the detail of the curve in the ps domain, just before the peak intensity.

Special attention was dedicated to the study of the transverse beam profile, using phase and intensity measurements to evaluate the effective Strehl ratio, i.e. the ratio between the energy in the focal spot and the total energy in the pulse. In fact, the beam quality plays a key role in the control of the quality of the bunches in laser wakefield acceleration. Leading research on self-injection now points at the control of the self-injection process as the key to a high quality and reproducible acceleration. At the same time, the higher power that will be available with systems currently under construction, will enable the parameters of self-injection to move towards higher energy and even more stable and higher bunch quality. Among the different uses of FLAME, the scientific programme of the self-injection experiment (SL-SITE) includes the demonstration of self-injection operations at full laser energy, including optimized phase front corrections. To this purpose, a careful characterisation of FLAME performances, with particular reference to the transverse beam quality was carried out during the commissioning week. The images of Fig. 4 show the measured intensity and the phase of the beam (near field) and the focal spot (far field) calculated using the measured intensity and phase.

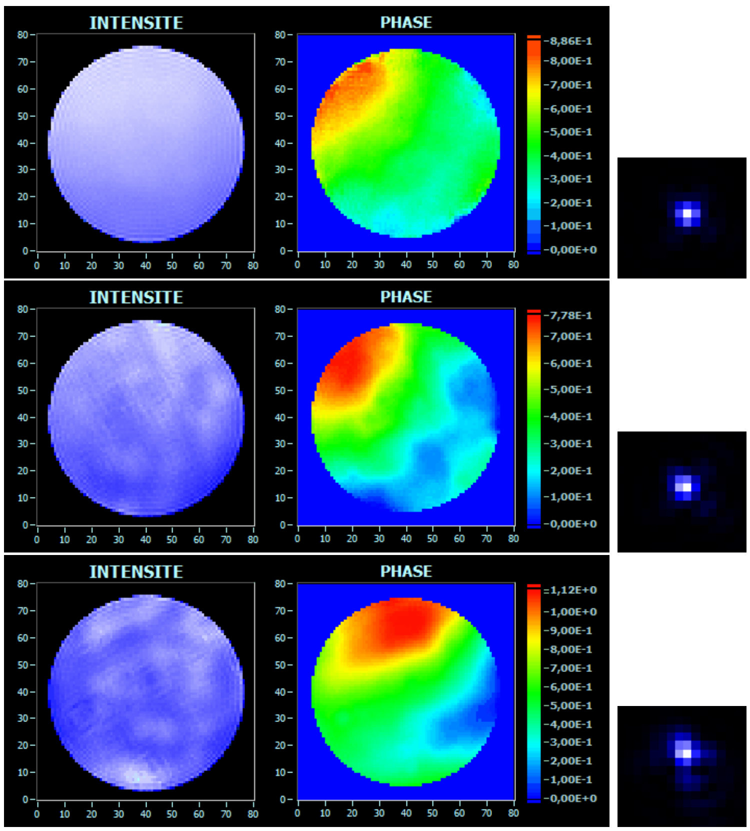

E = 0.9 J SR=0.80

E = 3.3 J SR=0.67

E = 5.6 J SR=0.50

Figure 4: Intensity and phase distribution of the FLAME beam. The Sequence of images shows the the behaviour at increasing laser energy up to the maximum of 7J. The corresponding calculated focal spot intensity is also shown for each frame (right).

According to these results the measured Strehl ratio is greater than 50% up to pulse energies of approximately 6J. For energies between 6 and 7 J, the phase front distortion increases leading to a reduction of the Strehl ratio decreases to a minimum value of 35%. However, our measurements show that the phase front pattern remains very stable from shot to shot at a given pulse energy. This makes the phase front correction with adaptive optics (planned for installation during 2012) a reliable and complete solution to achieve a high quality focal spot.

3 The SITE Spectrometer

During 2011 the activity concerning the electron spectrometer developed along three different lines: development of full MC simulation, study electronic noise remedies, development of an alternative readout based on optical devices, and the design and acquisition of the magnet for the high energy version of the spectrometer itself.

3.1 Full MC

Previous simulations of the expected output of the spectrometer started from a parametrized version of the laser-plasma interactions output and was based on a numerical integration of the equations of motion. We were therefore not sensitive to the low energy tails and to possible scattering on the harware sorrounding the detector (e.g. the magnet)During 2011 a full detector simulation based on GEANT and including both the magnet, the beam-pipe and the supports was setup. Input to this simulation is the output of the PIC simulations so that the effect of low energy or high divergence particles could be estimated. The expected spectrum, compare with the true one is shown in Fig. 5 on the left.

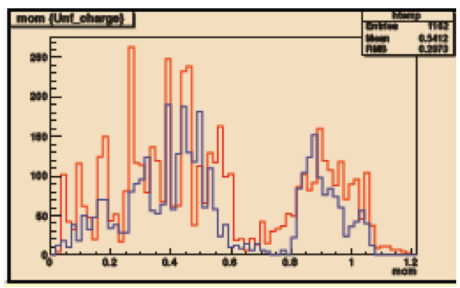

Figure 5: Comparison between the simulated true energy spectrum and the reconstructed one after 50 iterations of the bayesian unfolding.

3.2 Noise fighting

The first electron bunches accelerated with low laser intensity and preliminarly experimental condition in Nov. 2010 showed that the readout electronics suffers from the electromagnetic noise induced by the pulsed high energy field generated in the laser-plasma interaction, making it impossible to discriminate signal from noise. It is worth to stress once again that this was the first attempt of using a not purely optical device in a laser-plasma interaction environment. The most challenging part of the system is indeed the use of photodetectors in a high-noise environment, with both electromagnetic shots and bursts of Xrays directly on multi-pixel photomultipliers.

To reduce the noise the following measures have been taken:

- extend fiber length from 1 to 5 meter, in order to place PMTs and electronics behind the radiation protection wall of the experimental area. The increasing of light attenuation is also an advantage to avoid saturation effects;
- attenuate the signal at the entrance of the Maroc2 chips with customed attenuators realized by the INFN-Roma electronics shop; besides the need to interface the chip with the micro-coaxial cables, the challenging part was to build a device which does not alter the working point of the MAROC chips
- improve the grounding of the whole system
- realize better Faraday cages for screening the PMTs and electronics. The electronics and the PMTs are currently shielded by anodized aluminium, but a μ metal shielding might be required.

This improvements will be tested as soon as the commissioning resumes.

3.3 Optical readout

An alternative and complementary readout system has been set up using 5 digital cameras, each mounted on a metallic support and pointing toward the end of each group of fibers. The cameras are fixed to slide-plates provided with a system of micrometic screws for adjusting the orientation of the support plane (left panel of figure 6). The cameras are operated in a triggered mode. The trigger signal, synchronous with the laser-pulse arrival, is received from a socket located on the back of the housing. The data is then transmitted via ethernet to a dedicated computer.

The data coming from the cameras consist of 8-bit images of the scintillation light exiting the fibres, and has to be converted to a series of numbers representing the light output of each channel. This is done by summing the pixel values of all images of the fibers. The fiber positions in an image are determined by constructing grids on calibration images with a dedicated VI (a LabView program), as shown in the right panel of figure 6. Using these grids a raw spectrum is obtained for each camera image and the output is written to a binary file (figure 7).

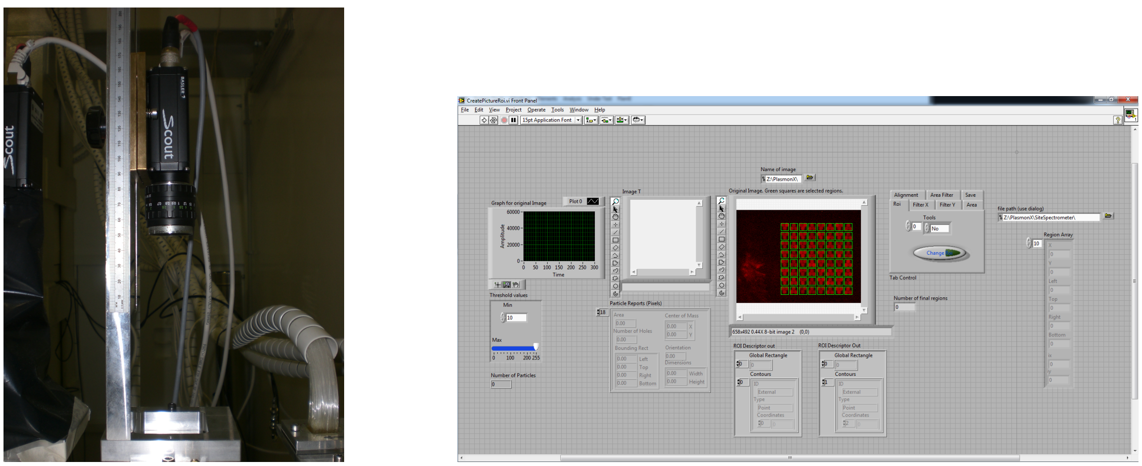

Figure 6: Left:Picture of a camera mounted on the metal support pointing to the fiber matrix. Right: Picture of the LabView Panel of the VI used for identifying the 64 channels from a calibration image obtained with the digital camera.

3.4 Event display and online analysis

Binary files written from photomultiplier readout-electronics and/or from digital-camera DAQ-system are read, eventually in a combined way, and analized online with a dedicated VI. The VI front panel, shown in figure 8, displays raw data (top left), pedestal-subtracted data (bottom left) and unfolded momentum distributions (top right).

3.5 Magnet upgrade

The ultimate goal of the device is to achieve an energy resolution better than 1% at energies as high as 1 GeV and to be sensitive in the multi-GeV regime. To this aim a brand new magnet, with a magnetic length twice as big as the current one and a magnetic field in the plateaux region of more than 1.5T is required. A 3D simulation of the magnetic field and an initial dimensioning of the system has been carried out during 2011, that lead to the issuing of a bid to identify the best

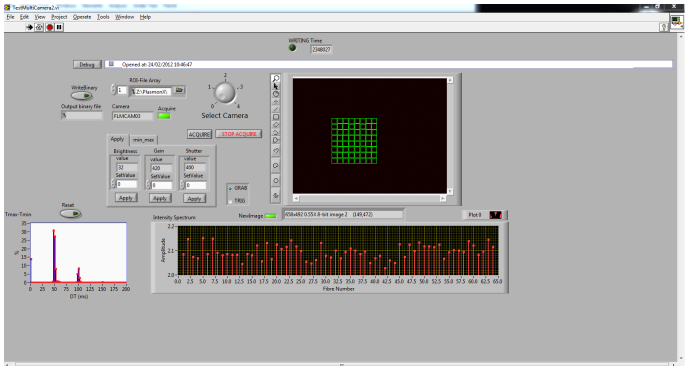

Figure 7: DAQ panel showing the grid used for summing the pixel values of the acquired image and the corresponding raw spectrum.

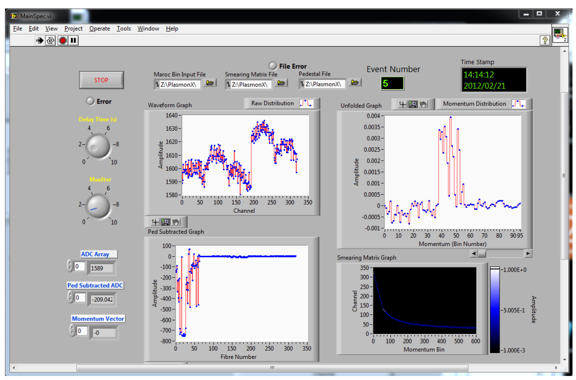

Figure 8: Front panel of the online-monitor VI, showing raw data (top left), pedestal-subtracted data (bottom left) and unfolded momentum distributions (top right).

provider of such a magnet. The expected performances of the spectrometer after the upgrade are shown in Fig. 9 on the right. The bid will close in March 2012.

4 The Thomson Source

The PlasmonX project foresees two kind of experiments such as high gradient plasma acceleration and the production of monochromatic ultra-fast X-ray pulses by Thomson back-scattering(TS). The TS X-ray source [10] will be the first one to be installed and hereby will be described in deeper detail; the key point of the its configuration are the flexibility and the potential compactness with respect to conventional synchrotron sources.
A TS source driven by high-quality electron beams can work in different operating modes, e.g.: the high-flux- moderate-monochromaticity-mode(HFM2) suitable for medical imaging when high-flux sources are needed; the moderate-flux- monochromatic-mode(MFM) suitable to improve the detection/dose performance [11, 12]; short-and-monochromatic-mode (SM) useful for pump-and-probe experiments e.g. in physical-chemistry when tens of femtosecond long monochromatic pulses are needed.

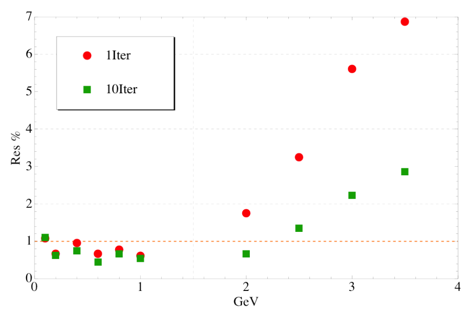

Figure 9: Expected energy resolution with the upgraded magnet.

4.1 Electron beamlines

In 2011 the installation of the PLASMONX beamlines has been almost completed: a twofold transfer line for the electron beam together with a photon beamline that brings the laser pulse from FLAME to the interaction with the SPARC beam. In this configuration the electron beam energy can range from 28 MeV up to 150 MeV, and the electron beam transport is meant to preserve the high brightness coming from the linac and to ensure a very tight focusing and a longitudinal phase space optimization for the whole energy span. The electron beam parameter list for the two interaction points are reported in Table 1. The general layout is showed in Fig. 10, where the PLASMONX electron transfer line departs from a three way vacuum chamber inside the first dipole downstream the RF deflector that is used for the six-dimensional phase space analysis of the SPARC beam. This dipole is also part of the chicane foreseen for the seeding configuration of the SPARC FEL undulator (straight direction downstream the photoinjector) and of the 14 degrees dogleg that brings the electron beam up to the SPARC Therahertz source, see Fig. 11.

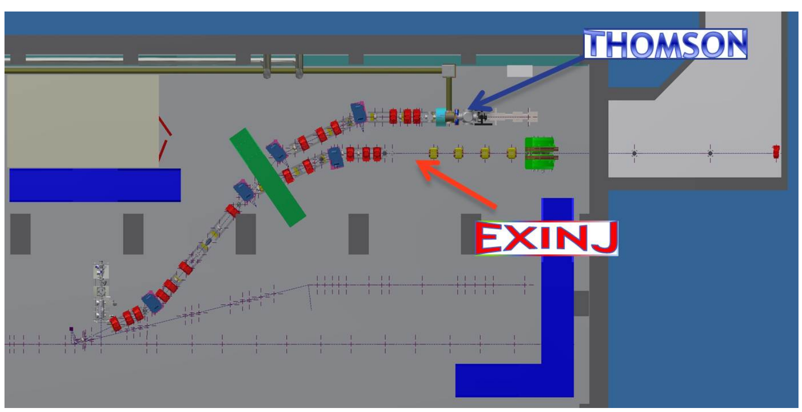

Figure 10: *CAD drawing of the PlasmonX electron beam transfer lines layout.*

The PlasmonX electron beamline consists in a 30 m double dogleg starting, as mentioned, downstream the SPARC photoinjector; they ends in a two branch beam delivery line that provides two separate interaction regions with the possibility to host two different experiments at the same time. The total beam deflection is about six meters from the SPARC photoinjector and undulator axes. A total of six rectangular dipoles and 19 quadrupoles (Fig. 12) are needed to drive the electron beam up to the two IPs, all of them have been installed in autumn 2011 see Fig. 13.

According to the specifications all the magnets have been characterized at the factory mea-

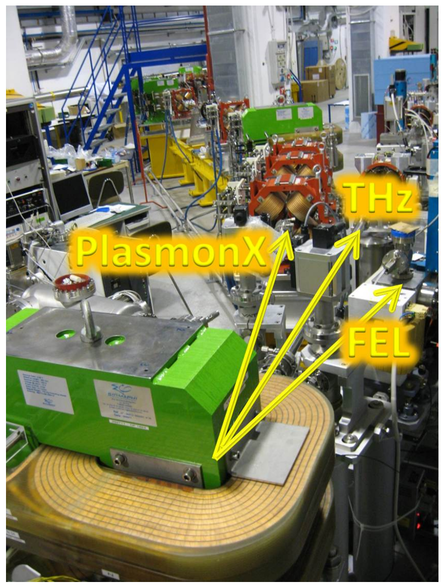

Figure 11: *Three-way branch for the FEL, THZ and PlasmonX beamlines.*

Table 1: Electron beam parameters at the two interaction points.

Parameter	Thomson Scattering Exp.	Plasma Acceleration Exp.
Bunch charge(nC)	$0.2 \div 1.0$	$0.005 \div 0.020$
Energy (MeV)	$28 \div 150$	150
Length (ps)	$15 \div 20$	0.010
$\epsilon_{nx,y}$ (mm-mrad)	$1 \div 5$	$1 \div 0.5$
Energy spread(%)	$0.1 \div 0.2$	0.01
Spot size at interaction point rms (mm)	$5 \div 10$	$5 \div 10$

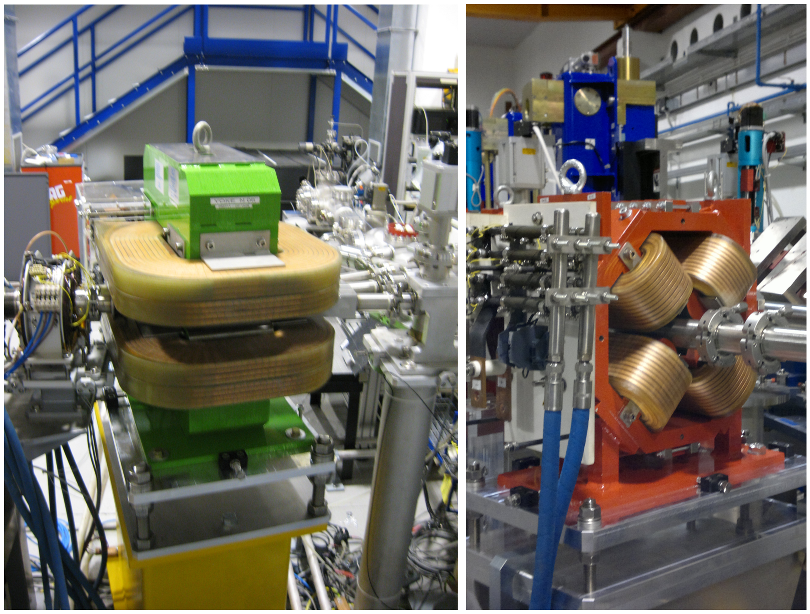

Figure 12: *Dipole (left) and Quadrupole (right) magnets of the PlasmonX electron beamlines.*

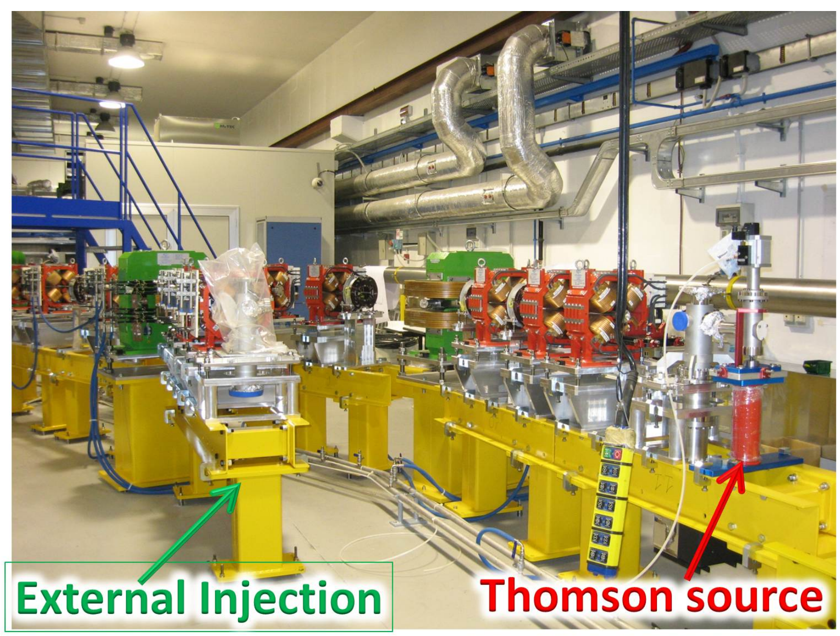

Figure 13: *Final part of the Plasmonx electron beam transfer lines up to the two interaction points.*

suring the magnetic field as a function of the position of a Hall probe inside the magnet poles. As a result at the nominal current all the dipoles show a relative magnetic length deviation of $\sim 0.1\%$ and $\sim 1\%$ from the Tosca 3D code exit value as reported in Fig. 14 while the good field region of $\pm$ 1 cm in both x and y directions shows a maximum deviation of 3×10^{-4}, see Fig. 15.

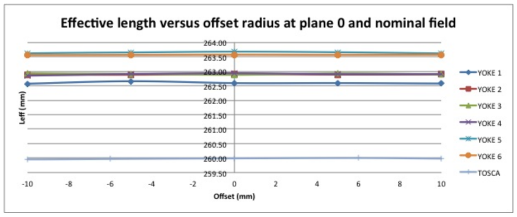

Figure 14: *The effective length of the six dipoles as a result of the magnetic measurements performed with the Hall probe at at the nominal current compared with Tosca code predicted value*

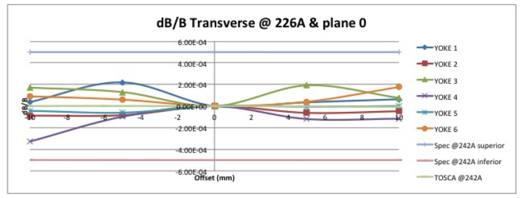

Figure 15: *Measured dipole magnetic field relative deviation vs hall probe position inside the pole expansion.*

The magnetic field quadrupole magnets has been also measured by means of a rotating coil in order to determine the value of the harmonic components up the 20^{th} order and to identify the position of the magnetic axes with the respect of the quadrupole fiducials. In Fig. 16 the relative deviation of the quadrupole gradient is plotted vs the distance from the quadrupole center. After the preliminary alignment performed during the installation of the magnetic elements, a second fine positioning of the magnets will be performed in Spring 2012 to align the magnetic axes on the beam reference trajectory with a resolution of about $50\mu m$.

In place of the foreseen dumping dipole that will be ready at the end of 2012 an existing dipole will be used to dump the electron beam inside the well off in the floor of the hall, this will limit at the beginning the beam energy up to 90 MeV for the 2012 PlasmonX beam experiment. Nine over a total of thirteen Beam Position Monitors are foreseen for the first phase of the Thomson beamline commissioning, together with three high resolution beam imaging setup they will provide the necessary beam diagnostic for the orbit correction and beam phase space measurements. At the beginning the BPM signals will be read by four single pass processors and multiplexed in order to get the whole electron beam orbit readout. By April 2012 the Thomson Interaction vacuum chamber will be delivered, see Fig. 17; the setup consist in two mirror stations that will determine the in & out trajectory of the photon beam, plus an interaction chamber in the middle that hosts the diagnostic for both the electron and photon beams. The parabolic mirror located downstream the interaction point will focus the photon beam at the IP down to a $10\mu m$ spot size, its spatial adjustment is obtained with its x-y movable support that can be also remotely controlled. The real interaction chamber is a tee-vacuum chamber where a double screen movement will be mounted to get the imaging of the electron and photon beam at the IP.

4.2 The laser beam transferline

The laser beam transfer line to the interaction region is composed by a series of high reflectivity mirrors inserted in a vacuum pipe 50 m long. The mirrors, 8 inches diameter, are supported by motorized gimbal mounts in order to assure the alignment up to to the off-axis parabola that focus the laser pulse on the electron beam. The design of the line has been performed with ZEMAX optical code to simulate the effect of the misalignment of the mirrors on the final spot. In 2011 the installation has been almost completed as shown in Fig. 18: the FLAME laser beam is extracted

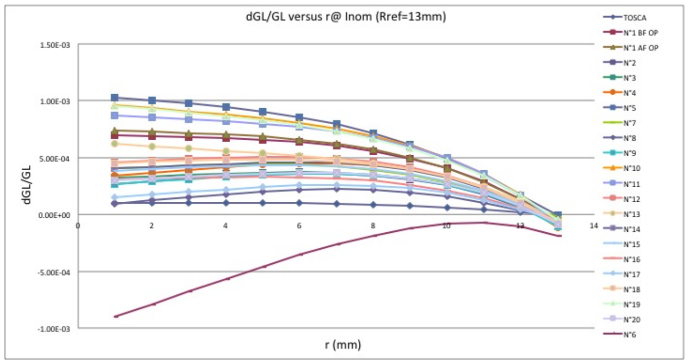

Figure 16: *Relative deviation of the quadrupole gradient plotted vs the distance from the quadrupole center for each of the quadrupole magnet of the transfer lines.*

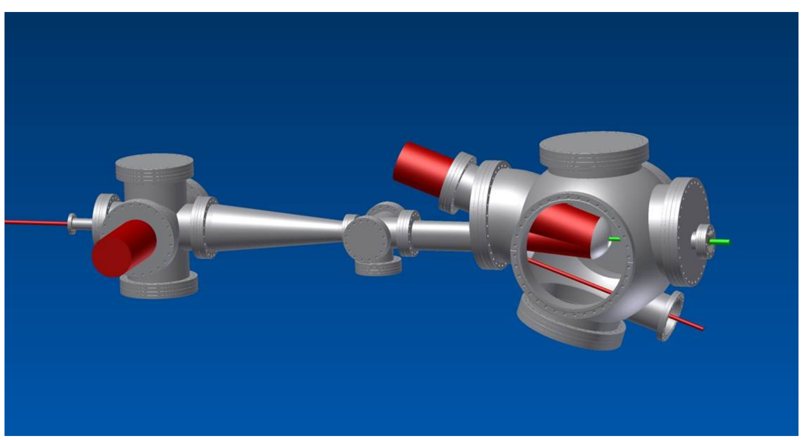

Figure 17: *3-D final drawing of the Thomson scattering interaction chamber*

from the FLAME target area and then guided up to the Thomson IP. A concrete wall has been realized in order to stop any radiation draft from he FLAME area towards the SPARC bunker, and to allow people entering in the SPARC hall during the FLAME laser operation and viceversa, see Fig. 19. The vacuum of the photon beam line is a the level of $10^{-6} Torr$ and suitable for the transport of the compressed laser pulse ($\sim 10 fs$ length) as needed for the plasma acceleration experiment. In Table 2 the laser pulse parameters are reported as foreseen for the Thomson Source application.

Table 2: List of expected laser beam parameters.

Parameter	Value
Wavelength(nm)	800
Compressed pulse energy(J)	5
Pulse duration/bandwidth (ps/nm)	$3 \div 12(80)$
Rep.Rate(Hz)	10
Prepulses contrast	$> 10^6$
Contrast ratio at 1 ns before (ASE)	$> 10^8$
Contrast ratioat 1100 ps before	$> 10^6$
Contrast ratio of replica	$> 10^5$
Beam quality M^2	≤ 1.5
Energy stability	10%
Pointing stability (μm)	< 2
Synchronization with SPARC clock	< 1 ps

4.3 The synchronization system

The Thomson scattering experiment needs an extremely precise synchronization between electron bunch and laser pulse. The relative time of arrival jitter of the two beams is fundamental to obtain a repeatable and efficient interaction. The electrons and photons have to be synchronized with a relative jitter $< 500 fs$. This can be obtained with a standard electrical distribution of the reference signal, already present at SPARC. Anyway an optical distribution is preferable to obtain precise time of arrival measurement resolution (equal or less than 5fs) and to obtain better synchronization between the two beams. This can be achieved by means of an optical cross-correlation between short laser pulses (100200fs). In particular the electrical (or optical) master oscillator in our project will serve two laser oscillator clients: SPARC photo injector for the production of electrons and FLAME laser for the production of the high intensity pulse for the Thomson interaction.

The RF system phase will be also locked to the master oscillator using low noise phase detection; and the phase feedback loops will be implemented too. They can be divided in two general types: slow (bandwidth $< 10Hz$) and fast (10Hz to some MHz bandwidth). The formers are used typically to compensate slow drifts caused by thermal elongation of cables and are implemented by means of high resolution stepper motors. The others are designed to compensate the high frequency noise suffered by the systems that is normally due to mechanical vibrations or electrical noise in the RF circuits or power amplifiers (klystron tubes and driver amplifiers).

4.4 Beam Dynamics

For the commissioning of the Thomson source that is foreseen to start in April 2012 two working points, WP's, have been studied in view also of the first experiment, BEATS2, requirements:

- a)WP1 that foresees a 350pC beam at the energy of 30 MeV, that will be focused at the IP by means of the final quadrupole triplet only.

- b)WP2 that by using a 1.2 Tesla solenoid will reach the tight focusing of the beam with higher charge up to $Q = 350 \div 1nC$.

In the photoinjctor the emittance growth is controlled by the emittance compensation method [9,11], which is one of the main challenges addressed to the SPARC project. The low energy spread values, $\approx 10^{-3}$ will be obtained by a proper setting of the injection phases into the accelerating structures, which compensates the linear correlation of the longitudinal phase-space. In Fig. 20 the transverse beam rms size evolution is plotted for the Thomson scattering setup starting from the photoinjector down to the IP as obtained from the simulations performed with the Tstep code tracking 15 kparticles, for a beam energy of 30 meV (BEATS2 experiment) and a charge $Q \sim 300pC$. With the only triplet focusing a minimum of $\sigma_{x,y} \approx 50\mu m$ is obtained from simulations (WP1 setup). According to simulations the same beam can be focused down to $\sigma_{x,y} \approx 10\mu m$using the normal conducting large solenoid to provide a field on axis of about 0.9T. The delivery is expected by Fall 2012.

Figure 18: *Plasmonx laser transferlines inside the SPARC bunker (left). Motorized mirror vacuum chamber. (right)*

References

1. L. A. Gizzi, F. Anelli, C. Benedetti, C. A. Cecchetti, A. Clozza, G. Di Pirro, N. Drenska, R. Faccini, D. Giulietti, D. Filippetto, S. Fioravanti, A. Gamucci, L. Labate, T. Levato, V. Lollo, P. Londrillo, E. Pace, G. Turchetti, C. Vaccarezza, P. Valente and C. Vicario, Laser-plasma acceleration with self-injection: A test experiment for the sub-PW FLAME laser system at LNF-Frascati, Il Nuovo Cimento C, **32**, 433 (2009)

Figure 19: *Concrete labirinth wall realized in front of the FLAME to SPARC bunker laser beam access, for shielding radiation (left). On the right a detail of the wall connection between the two experimental areas*

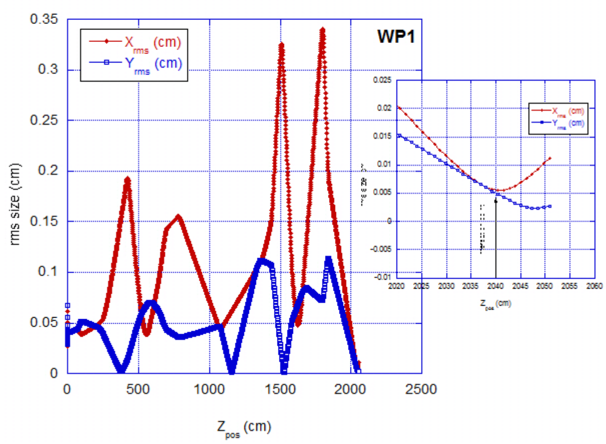

Figure 20: *Evolution of the rms electron beam sizes along the trasnfer line (left) and at the interaction point (right) for the WP1 working point, i.e.* $Q \approx 300pC$ *and with only the final triplet focusing.*

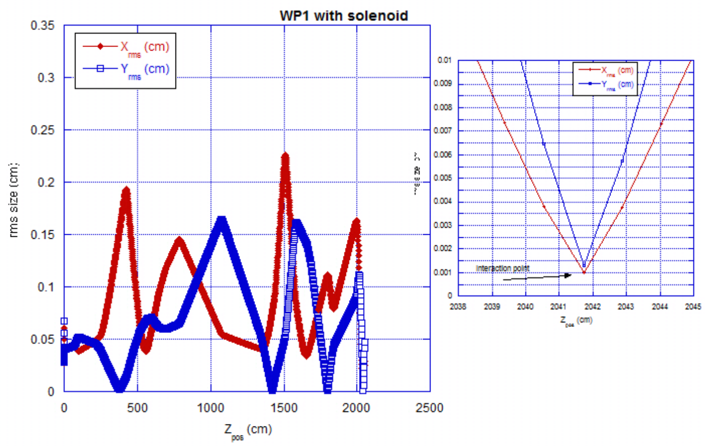

Figure 21: *Evolution of the rms electron beam sizes along the trasnfer line (left) and at the interaction point (right) for the same WP1 with the solenoid magnet focusing.*

2. S. Bellucci S. Bellucci, S. Bini, M. Castellano, A. Clozza, L. Cultrera, G. Di Pirro, A. Drago, M. Esposito, M. Ferrario, D. Filippetto, A. Gallo, G. Gatti, P. Gaudio, A. Ghigo, G. Giannini, A. La Monaca, T. Levato, F. Micciulla, M. Migliorati, D. Nanni, E. Pace, L. Palumbo, A. Petrucci, M. Richetta, C. Sanelli, A. Tenore, F. Terra, S. Tomassini, C. Vaccarezza, C. Vicario, C. Benedetti, G. Turchetti, A. L. Bacci, F. Broggi, M.M. Cola, A. Flacco, C. Maroli, M. Passoni, V. Petrillo, N. Piovella, R. Pozzoli, M. Rom?e, A. R. Rossi, L. Serafini, D. Batani, R. Benocci, C.A.Cecchetti, A.Gamucci, D.Giulietti, L.A.Gizzi, L.Labate, N.Pathak, F. Piastra, N. Drenska, R. Faccini, P. Valente, NTA PlasmonX, on "Annual Activity Report 2009", (2010).

3. L. A. Gizzi, E. Clark, D. Neely, L. Roso, and M. Tolley, High repetition rate laser systems: targets, diagnostics and radiation protection, AIP Conf. Proc. The 2nd International Conference on UltraIntense Laser Interaction Science, Vol. 1209, pp. 134-143, February 2, 2010 doi:10.1063/1.3326308

4. F. Anelli, A. Bacci, D. Batani, M. Bellaveglia, C. Benedetti, R. Benocci, L. Cacciotti, C.A Cecchetti, O. Ciricosta, A. Clozza, L. Cultrera, G.Di Pirro, N. Drenska, R. Faccini, M. Ferrario, D. Filippetto, S.Fioravanti, A. Gallo, A. Gamucci, G. Gatti, A. Ghigo, A. Giulietti, D. Giulietti, L. A. Gizzi, P. Koester, L. Labate, T. Levato, V. Lollo, E. Pace, N. Pathack, A.R. Rossi, L. Serafini, G. Turchetti, C. Vaccarezza, P. Valente, C. Vicario, *Design of the Test Experiment for the Sub-Petawatt Flame Laser System at LNF-Frascati: Electron Acceleration with Self-Injection (SITE)*, Unpublished, October 2009.

5. L. A. Gizzi, C. Benedetti, S. Betti, C. A. Cecchetti, A. Gamucci, A. Giuliettia, D. Giulietti, P. Koester, L. Labate, T. Levato, F. Michienzi, N. Pathak, A. Sgattoni, G. Turchetti and F. Vittori, Laser-Plasma Acceleration: First Experimental Results from the Plasmon-X Project, Proceedings of the 51st Workshop of the CHANNELING 2008 Conference on "Charged and Neutral Particles Channeling Phenomena", World Scientific Publishing, The Science and Culture Series - Physics, pp. 495-501 – Published April 2010, ISBN:978-981-4307-00-0.

6. L.A.Gizzi, T. Levato, L.Labate, C.A.Cecchetti, N.Drenska, R.Faccini, D. Giulietti, S.Martellotti, N.Pathak, F. Piastra, P. Valente, Abstract, Plasma Physics Conference, European Physical Society, 2011

7. M. Galimberti, A. Giulietti, D. Giulietti, L.A. Gizzi, Rev. Sci. Instrum. 76, 053303 (2005)

8. R. Faccini, F. Anelli, A. Bacci, D. Batani,M. bellaveglia, R. Benocci, C. benedetti, L. Cacciotti, C.A. Cecchetti, A. Clozza, L. Cultrera, G. Di Pirro, N. Drenska, M. Ferrario, D. Filippetto, S. Fioravanti, A. Gallo A. Gamucci, G. gatti, A. Ghigo, A. Giulietti, D. Giulietti, L.A.Gizzi, P. Koester, L. Labate, T. Levato, V. Lollo, P. Londrillo, S. Martellotti, E. Pace, N. Patack, A. Rossi, F. Tani, L. Serafini, G. Turchetti, C. Vaccarezza, P. Valente, Multi-GeV electron spectrometer, Nucl. Instrum. Meth. Phys. Res, A 623, 704-708 (2010).

9. M. Ferrario *et al* ICFA Beam Dyn. Newslett. 46 49-58, 2008

10. P. Oliva et al., Nucl. Instrum. Meth. A 615 93-99, (2010)

11. A. Bacci et al, Nucl. Instrum. Meth. A 608 S90-S93, (2009)

12. U. Bottigli, et al., IL NUOVO CIMENTO, **29C**, N.2 , MarzoAprile 2006.

13. W.J. Brown, et al., Phys. Rev. STAB **7** (2004) 060702

14. D. Alesini, et al., Nucl. Instr. and Meth. A **586** (2008) 133.

THE *SuperB* ACCELERATOR PROJECT

M.E. Biagini (resp.), R. Boni, M. Boscolo, A. Clozza, T. Demma, A. Drago, M. Esposito, S. Guiducci, S. Liuzzo, G. Mazzitelli, M. Preger, P. Raimondi, C. Sanelli, M. Serio, A. Stella, S. Tomassini, M. Zobov

1 Introduction

SuperB [1] is an asymmetric (6.7 GeV HER, 4.2 GeV LER) e^+e^- collider at the center of mass B pairs production energy (10.58 GeV), to be built in Italy, with a design peak luminosity of 10^{36} cm^2 s^{-1}. A collider like *SuperB* will open a unique window on this physics because it allows a high statistics study of the current hints of new aggregations of quarks and gluons. Besides the physics one can study in running at the Υ(4S) resonance, the following alternative energies are of interest: Υ(3S) (at least 0.3 ab^{-1}) and a high luminosity scan between 4-5 GeV (5 MeV steps of 0.2 fb^{-1} each would require a total of 40 fb^{-1}). While this is not huge statistics, this scan is only feasible with *SuperB*. The only possible competitor, BES-III, is not planning to scan above 4 GeV, since their data sample would, in any case, be lower than that of the B Factories alone. Finally, the search for exotic particles among the decay products of the "bottomonia" can probe regions of the parameters space of non-minimal supersymmetric models that cannot be otherwise explored directly, for instance at LHC.

The superiority of *SuperB* with respect to the planned upgrade of KEKB lies both in the ten times higher statistics, which broadens the range of cross sections the experiment is sensitive to, but also in the flexibility to change center of mass energy, and the possibility to collide with a polarized electron beam. Moreover the *SuperB* design will also allow for running at the τ/charm threshold with an expected luminosity of 10^{35} cm^2 s^{-1}.

The *SuperB* project has been approved by the Italian Government as part of the National Research Plan. The design is based on a large Piwinski angle and Crab Waist scheme already successfully tested at the DAΦNE $\Phi-$Factory in Frascati, Italy. The project combines the challenges of high luminosity colliders and state-of-the-art synchrotron light sources, with two beams with extremely low emittances and small beam sizes at the Interaction Point. As unique features, the electron beam will be longitudinally polarized at the IP and the rings will be able to ramp down to collide at the tau/charm energy threshold with one tenth the luminosity. The relatively low beam currents (about 2 A) will allow for low running (power) costs compared to similar machines. The insertion of beam lines for synchrotron radiation users is the latest feature included in the design. The lattice has been recently modified to accommodate insertion devices for X-rays production.

The construction site for *SuperB* has been selected in the campus of the Tor Vergata Rome II University, just 5 km away from the Frascati Laboratories. Fig. 1 is a sketch of the rings in the new site. In October 2011 for the construction and operation of the facility the "Nicola Cabibbo Laboratory" has been founded, as a consortium between INFN and the University of Rome II at Tor Vergata. Memorandum Of understanding (MOU) are in progress with France, SLAC and BINP (Russia).

Four general *SuperB* meetings have been organized in 2011: in March at LNF, in June at Elba (Italy), in September at Queen College (London, UK) and in December at LNF. A complete description of the work done is available from the meetings slides at:

http://agenda.infn.it/categoryDisplay.py?categId=109.

In the following section the work performed at LNF on the design of the accelerator will be briefly described. This activity at LNF has been funded by the INFN NTA commission, and has received by INFN a special funding in 2010-2011.

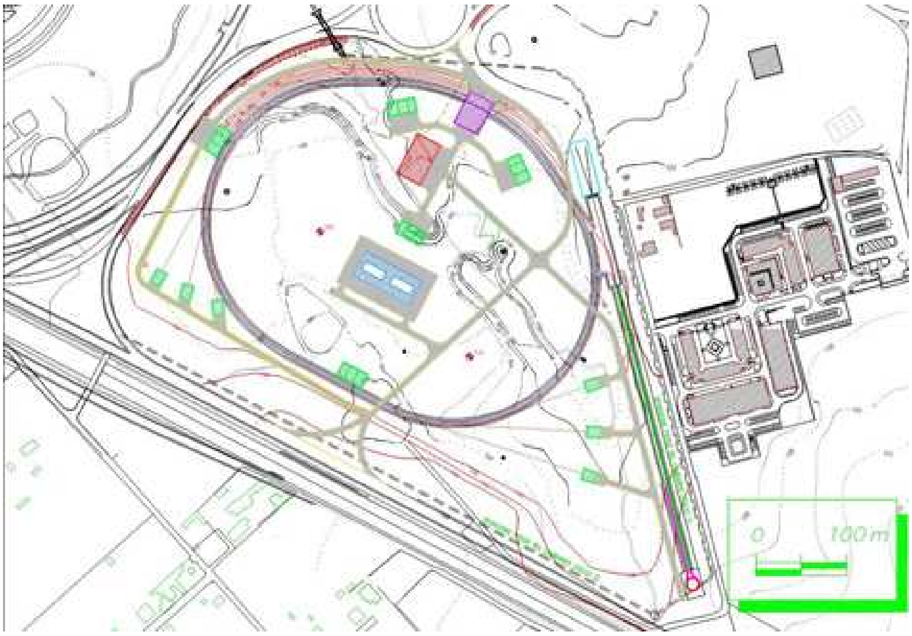

Figure 1: *Layout of SuperB accelerator at Tor Vergata.*

2 Design strategy

SuperB consists of two rings of different energy (positrons in HER, 6.7 GeV, electrons in LER, 4.2 GeV) colliding in one IR at a large (60 mrad total) horizontal angle. Spin rotator sections in the LER will provide helicity of a polarized electron beam. With respect to the past years design an important change is to have polarized electrons in the LER instead of the HER. This was chosen for easier insertion of Spin Rotator (SR) sections in LER lattice. Also the beam energies have been changed in order to avoid spin resonances, with a consequent small reduction of the center-of-mass boost.

The two rings lay in the horizontal plane, each has two arcs and two long straight sections. The Final Focus (FF) in one straight is combined with the two Arcs in two half-rings (one inner, one outer) and a straight section on the opposite side. The straight section comes naturally to close the ring and readily accommodate the RF system and other necessities (e.g. injection). In this utility region crossing without collisions for the two rings will be provided.

SuperB design is based on very low H-V emittances, low emittance coupling and very small beam sizes at the IP. Moreover the crab-waist sextupoles demand for particular care in designing the chromaticity correction in the FF. The accelerator lattice optics has been modified in 2011 to be able to install Insertion Devices in some of the stright sections, for future use as a Synchrotron Light Source. A separate chromaticity correction scheme has been developed for the two rings Arc-cells and for the FF. In the Arcs a scheme where all sextupoles are paired with a (-I) transfer matrix provides optimum correction and very small chromatic W functions and second order dispersion function in both planes. In the FF a special scheme has been designed with separate YCCS and XCCS sections (H-V chromaticity correction sextupoles) in phase with the IP, where the β functions reach a maximum, which works very well in terms of dynamic aperture and off momentum behavior of β functions and tunes. It has to be noted that a perfect correction is preferable for the crab-waist sextupoles, located at both ends of the FF, to avoid reduction of the dynamic aperture. A coupling correction scheme with the detector solenoid ON has been also designed.

3 Year 2010 activity

3.1 Beam dynamics

During 2011 a lot of work has been done on the most relevant beam dynamics issues, such as e-cloud instability, intra-beam scattering (IBS), Touschek backgrounds, etc. Touschek effect is the main source of lifetime reduction, even if the limiting effect for lifetime are the luminosity backgrounds. Touschek lifetime is computed with a tracking code which takes into account the lattice design and nonlinear elements. Special care is needed to control Touschek particle losses and reduce possible showers in the detectors. A set of collimators that fulfils this requirement has been found, with 3 primary H collimators in the FF, intercepting most of the particles that would be lost in the IR. A secondary collimator at s=-21 m will stop the remaining Touschek scattered particles generated so close to the IR that primary collimators cannot be effective. With the insertion of collimators the computed lifetime is 6.6 min in LER and 33.2 min in HER. The rings lifetime in collision is however dominated by the luminosity beam lifetime, a few minutes for each ring.

A Low Emittance Tuning (LET) procedure has been developed to correct magnet misalignments and BPM errors to achieve minimum coupling, β beating and vertical emittance. Tables of error tolerances have been produced for both the LER and HER elements. The β beating due to magnet misalignments after correction is between 3-5% in both planes for a rms misalignment error of 300 microns, the emittance coupling factor is always less than 0.1% (design is 0.25%). A comparison of performances with the LOCO tool, used for tuning in most SR rings, has been performed at the DIAMOND facility at RAL, showing that LET can indeed achieve comparable results in much less time.

IBS of particles inside a bunch can lead to an unwanted increase of the emittances and bunch length. Calculations based on a high energy approximation of the Bjorken-Mtingwa formalism show that IBS should be manageable in both *SuperB* rings. However some interesting aspects such as the impact of IBS during the damping process and its effect on beam distribution have been investigated using a newly developed multi-particle tracking code, based on the Zenkevich-Bolshakov algorithm. Benchmarking with conventional IBS theories gave good results, and a new semi-analytical model fits simulation results very well, being thus able to predict IBS effect at various bunch currents.

The effect of electron cloud instability in the positron ring has been also estimated. Build up and instability simulations show that e-cloud is a serious issue for the HER. An antechamber absorbing 99% of the synchrotron radiation and a maximum SEY of the surface below 1.2 could ensure stable operation because it would prevent e-cloud formation and its detrimental effect on the positron beam. A test of e-cloud clearing electrodes has been carried out successfully at the DAΦNE ring to check their effectiveness in suppressing the instability.

The installation of SR beam lines (50-100m long for large demagnification) in the HER has been proposed. Several experiments can be carried out, such as X-ray diffraction, SAXS, imaging with phase contrast, all requiring photon energy between 4 and 15 keV. Low divergence (1 mrad to 1 microrad) and very small spot size (1 micron) are also required. For this purpose the lattice has been modified to have at least 6 straight sections where Insertion Devices (ID) can be installed. Particular care has been devoted to maintain the small horizontal emittance and at the same time obtain betatron functions suitable to the ID needs. Work is in progress to evaluate ID parameters, such as undulator gaps, to avoid narrow gap IDs and impedance issues with high current operation.

3.2 IP quadrupoles

The *SuperB* collision scheme requires a short focus final doublet to reduce the vertical β function down to β_y^*=0.2 mm at the IP. The final doublet will be composed by a set of permanent samarium cobalt magnets (PM) and superconducting (SC) quadrupoles. In the present design the HER (LER values in parentheses) PM quadrupoles provide an integrated gradient of 23.1 T (11.2 T) over a magnetic length of 11 cm (7cm). The front pole face will be placed at 38 cm (30 cm) from the IP. The remaining vertical focusing strength will be provided by two (one) SC quadrupoles having an integrated gradient of 39.2 T (28.7 T) over a total magnetic length of 45 cm (30 cm). A cold bore design for the SC quadrupoles is not viable since the synchrotron radiation coming from the upstream dipoles will deposit about 200W on the beam pipe section inside the SC. The requested horizontal beam stay clear fixes both the warm bore diameter to 24 mm and the maximum thickness allowed for the cryostat and the SC cold mass to 22 mm. This limited amount of available space together with the requested field purity and gradient strength poses very demanding constraints on the SC magnets design. An advanced design of the quadrupole has been developed, based on the double helical coil concept. A prototype has being constructed and results of test of a model of the superconducting quadrupole based on NbTi technology are very encouraging. The design is a collaboration among LNF, INFN-Pisa and INFN-Genova.

3.3 Feedbacks

R&D on the longitudinal and transverse bunch by bunch feedbacks is continuing. The DAΦNE feedback systems have been upgraded last year also to test bunch-by-bunch feedback architectures proposed for *SuperB*. Both e^+ and e^- longitudinal feedback systems have been completely replaced with new hardware for increased reliability and better diagnostics. In the effort to reduce residual dipole beam motion, determined by the front-end and quantization noise floor, vertical feedback systems now feature a 12-bit ADC, in place of the old 8 bit design. For the "luminosity" IP feedback, which is an essential component of the luminosity tuning for the high performances requested at *SuperB*, at present two approaches are being considered. One is an extension of the fast luminosity feedback already operating at PEP-II B-Factory. It uses fast dither coils to induce a fairly high dither rate for the x position, the y position and the y angle at the IP. The luminosity signal is read out with three independent lock-in amplifiers. An overall correction is computed, based on the lock-in signal strengths, and beam corrections for x and y position and y angle at the IP are simultaneously applied to the beam. The other approach is based on the FONT5 intra-train feedback system developed for the ATF facility at KEK, aiming at stabilizing the beam orbit by correcting both the position and angle jitter in the vertical plane on a bunch-to-bunch timescale, providing micron level stability at the entrance to FF system. Studies of both systems will be carried out next year, probably both will be adopted.

3.4 Control System

SuperB is pushing us to study and implement new ideas in controls, to be up to date in integrating commercial web technologies and to overcome the primary issue coming from previous architectures: the limits due to the usage of specific hardware and software. The Frascati and Tor Vergata control groups have a long experience in design, development and implementation of innovative Control System. This experience and know-how is available today for a new challenging project. The idea is to design a new controls system based on the present software trends, dominated by web technologies and services, where large databases and the most robust available data bus, Ethernet, are used to match very high throughput. The large community of developers and users involved guarantees a good support and may give hints on the longevity of the product. The new CS, must be designed in such a way to accommodate any kind of devices to reduce the hardware dependence and the development time by exploiting the availability of many devices with embedded programmable CPU. Furthermore, the CS has to be able to control and, where needed, to acquire data with performance limited only by the hardware capability. These requirements suggest inverting the typical CS device-client data flow from polling (the client polls) to pushing (the device push) information. A Control Library (CL) completely manages data and commands flow, the control processes and the devices configuration. The devices programmer is only asked to develop the driver for the specific controlled hardware. The plans have been to develop the core software of the Control Library and to explore its critical issues, if any, by the end of 2011. Some preliminary test started on the DAΦNE and SPARC accelerators at LNF, where is available a natural gym to understand any possible problem and rapidly solve it in a real operative contest. These preliminary tests have confirmed that the performance of a non-relational database resident on RAM is practically limited only by Ethernet bandwith. The systems load is very low, while redundancy and scalability allows being confident on the behaviour for a larger accelerator complex such as the *SuperB*.

3.5 Injection system

The injection complex has been updated to better exploit the necessity of high efficient e^+ production and top-up injection of polarized e^- beam into the rings. The very low beam lifetime requires continuous injection at high repetition rate in order to keep the luminosity almost constant at the peak value. The present design features only one damping ring (DR) for e^+, lower energy e^+ production and polarized gun for the e^-. A sketch is shown in Fig. 2. The main difference with

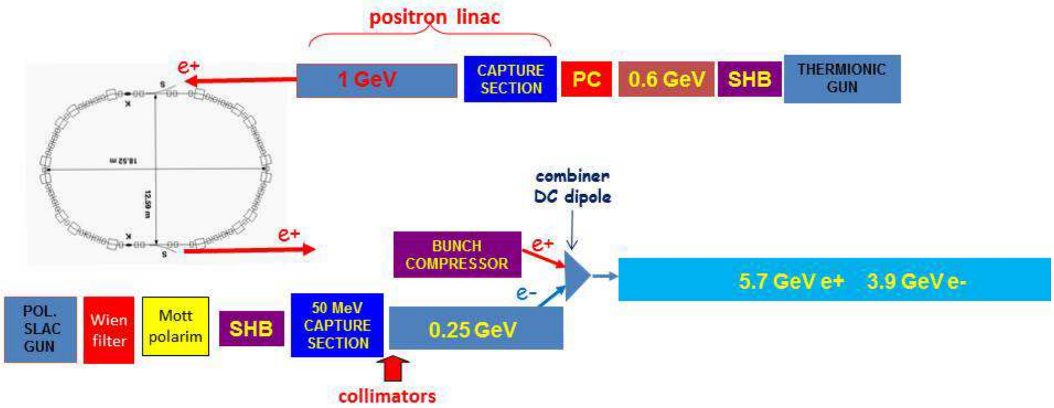

Figure 2: *Sketch of the SuperB injection system.*

respect to the previous scheme is the fact that only the positron beam is stored in the DR while the electron beam is directly accelerated and injected. In this way the positrons can be stored in the damping ring for the time between two injection pulses (before it was half this time) achieving the same emittance damping factor at twice the repetition frequency. Therefore it is possible with a 100 Hz linac to inject at 50 Hz in each ring using a single bunch per pulse to make the current per bunch very uniform along the ring. The e^+ conversion will be performed at low energy (0.6 GeV) thanks to a newly designed high efficiency system, consisting of an adiabatic capture system after the conversion target, followed by a L-band section to inject at 1 GeV into the DR, allowing for an increase of the capture yield to about 30 %. In the electron mode 12 out of 40 RF stations of the 6 GeV linac are switched off to accelerate the beam at 4.2 GeV. The positron converter is followed by a 1 GeV L-band linac that allows a large positron capture and transport efficiency. L-band, room temperature linacs are unusual in the field of particle accelerators: one is in operation at the University of Osaka, another one is foreseen for injection into the SuperKEKB collider. Both are based upon the use of 30-40 MW Klystrons and SW two meter length copper sections, with average gradient of 12 to 13 MV/m. R&D on these cavities is being carried out at LAL, Orsay. An S-band Linac at 100 Hz will be used for main rings injection at 50 Hz. Two electron guns will be used: a "high current" for e^+ production and a "low emittance" polarized gun for e^- injection. This scheme reduces transfer lines and kickers for DR injection/extraction. The possibility to use C-band Linacs to reduce the Linac length is also under study.

3.6 Site studies

The chosen *SuperB* site is very convenient for its vicinity to the Frascati Labs (just 5 km away). Ground vibration measurements have been performed on site and have shown its very good ground stability, even with the highway only 100 m away. For the Final Focus vibrations a budget has been established, including ground motion data, motion sensitivity of machine components and beam feedback system requirements. The small beam sizes at the IP pose stringent vibration requirements. Beam position at the IP is very sensitive to individual motion of IR components. However, the present IR design with shared elements in a common cryostat will cause coherent motion of these elements, greatly reducing the vibration sensitivity of the IR. The vertical displacement of IP and FF quadrupole should be kept below 300 nm rms while the rotation should be less than 2 micro-rad rms. The arc quadrupoles should be kept to less than 500 nm rms. The measured values during last vibration campaign at the IP, FF and Arcs are respectively 20-40 nm, 20-30 nm and 20-30 nm. A fast luminosity feedback system should have a bandwidth of at least 100 Hz, achieving at least 10x vibration reduction at low frequencies. With these requirements in the present lattice the vibration budget can be met even during the noisiest part of the day, with a vibration-induced luminosity loss of less than 1%.

4 Year 2012 activity

The organization chart for the Accelerator structure, including several groups for the different sub-systems, is being decided and will be in charge of the construction of the facility. The first half of 2012 will be devoted to a revision of the accelerator costs by the leaders of the accelerator sub-systems. This will allow to have a full endorsement by the Machine Review Committee in the Fall. In parallel we will proceed as much as possible with the technical drawings of the machine components and site and layout issues.

In the following is a list of the publications the Accelerator Division *SuperB* group has issued in the framework of the *SuperB* collaboration.

5 Publications in 2011

1. M.E. Biagini, R. Boni, M. Boscolo, T. Demma, A. Drago, M. Esposito, S. Guiducci, S.M. Liuzzo, M.A. Preger, P. Raimondi, S. Tomassini, M. Zobov (INFN-LNF), P. Fabbricatore,

S. Farinon, R. Musenich (INFN-Genova), E. Paoloni (INFN-Pisa), W. Wittmer, A. Novokhatski, K.J. Bertsche, A. Chao, Y. Nosochkov, J.T. Seeman, M.K. Sullivan, U. Wienands (SLAC), M.A. Baylac, O. Bourrion, N. Monseu, C. Vescovi (CNRS-LPSC), S. Bettoni (CERN), A.V. Bogomyagkov, E.B. Levichev, S.A. Nikitin, PI.N. Okunev, P.A. Piminov, D.N. Shatilov, S.V. Sinyatkin, P. Vobly (BINP), B. Bolzon, L. Brunetti, A. Jeremie (CNRS-LAPP), A. Chanc (CEA), F. Poirier, C. Rimbault, A. Variola (CNRS-LAL), " *SuperB*: Next-Generation e^+e^- B-Factory Collider", Proceedings of 2011 Particle Accelerator Conference, New York, NY, USA, 28 Mar - 1 Apr 2011, 2384-2386, SLAC-PUB-14286, Mar 2011.

2. S. Tomassini (INFN-LNF), K Bertsche, W. Wittmer (SLAC) , B. Bolzon, L. Brunetti, A. Jeremie (CNRS-LAPP), "Vibration Budget for *SuperB*", Proceedings of 2011 Particle Accelerator Conference, New York, NY, USA, 28 Mar-1 Apr 2011, SLAC-PUB-14423, Mar 2011.

3. M.E. Biagini, "The *SuperB* project: accelerator status and R&D", Proceedings of 2nd International Particle Accelerator Conference IPAC 2011, San Sebastian, Spain, 4-9 Sep 2011.

4. T. Demma, M.E. Biagini, M. Boscolo (INFN-LNF), A.W. Chao, K.L.F. Bane, M.T.F. Pivi (SLAC), "Multiparticle simulation of intrabeam scattering for *SuperB*", Proceedings of 2nd International Particle Accelerator Conference IPAC 2011, San Sebastian, Spain, 4-9 Sep 2011.

5. A. Drago (INFN-LNF), D. Teytelman (Dimtel Co.), "DAΦNE bunch-by-bunch feedback upgrade as *SuperB* design test", Proceedings of 2nd International Particle Accelerator Conference IPAC 2011, San Sebastian, Spain, 4-9 Sep 2011.

6. S. Guiducci, M.E. Biagini, R. Boni, M.A. Preger, P. Raimondi (INFN-LNF), A. Chanc (CEA), J. Brossard, O. Dadoun, P. Lepercq, C. Rimbault, A. Variola (CNRS-LAL), John Seeman (SLAC), "Updated design of the italian *SuperB* factory injection system", Proceedings of 2nd International Particle Accelerator Conference IPAC 2011, San Sebastian, Spain, 4-9 Sep 2011.

7. S. M. Liuzzo, M.E. Biagini, P. Raimondi (INFN-LNF), R. Bartolini (Diamond), "Tests for Low Vertical Emittance at Diamond using LET Algorithm", Proceedings of 2nd International Particle Accelerator Conference IPAC 2011, San Sebastian, Spain, 4-9 Sep 2011.

8. G. Mazzitelli, C. Bisegni, P. Ciuffetti, G. Di Pirro, A. Stecchi (INFN-LNF), S. Calabr, L. G. Foggetta (CNRS-LAL), L. Catani, F. Zani (INFN-Roma II), "High performance WEB applications for particle accelerator Control Systems", Proceedings of 2nd International Particle Accelerator Conference IPAC 2011, San Sebastian, Spain, 4-9 Sep 2011.

9. E. Paoloni, F. Bosi, N. Carmignani, F. Pilo (INFN-Pisa), M. E. Biagini, P. Raimondi (INFN-LNF), S. Bettoni (CERN), P. Fabbricatore, S. Farinon, R. Musenich (INFN-Genova), M. Sullivan (SLAC), "Advances in the design of the *SuperB* final doublet", Proceedings of 2nd International Particle Accelerator Conference IPAC 2011, San Sebastian, Spain, 4-9 Sep 2011.

10. S. Tomassini, M.E. Biagini, P. Raimondi, C. Sanelli (Frascati) , B. Bolzon (CERN) , G. Deleglise, A. Jeremie, (Annecy, LAPP), J. Seeman (SLAC), "Site studies for the *SuperB* collider and synchrotron radiation facility project", Proceedings of 2nd International Particle Accelerator Conference IPAC 2011, San Sebastian, Spain, 4-9 Sep 2011.

11. M. Zobov, (INFN-LNF), Y. Zhang (IHEP), "Coherent beam-beam resonances in *SuperB* with asymmetric rings", Proceedings of 2nd International Particle Accelerator Conference IPAC 2011, San Sebastian, Spain, 4-9 Sep 2011.

6 References

1 "*SuperB* Progress Report - Accelerator", arXiv:1009.7178v3 [physics.acc-ph] Dec. 2010.

SPARC

D. Alesini, F. Anelli (Art. 15), P. Antici (Art. 23), A. Bacci (Art. 23), M. Bellaveglia (Art. 23), R. Boni, M. Boscolo, L. Cacciotti (Tecn.), M. Castellano, E. Chiadroni, P. Chimenti (Art. 15), G. Di Pirro, A. Drago, M. Ferrario (Resp. Naz.), S. Fioravanti (Art. 15), A. Gallo, G. Gatti, A. Ghigo, V. Lollo (Tecn.), M. Migliorati (Ass.), A. Mostacci (Ass.), E. Pace, L. Palumbo (Ass.), L. A. Rossi (Art. 23), A. R. Rossi (Art. 15), M. Serluca (Dott.), R. Sorchetti (Tecn.), B. Spataro, S. Strabioli, (Art. 15), C. Vaccarezza.

1 Introduction

The successful operation in the past year of the SPARC injector in the Velocity Bunching (VB) mode has opened new perspectives to conduct advanced beam dynamics experiments with ultra-short electron pulses. For example a new technique called Laser Comb, able to generate a train of short pulses with high repetition rate has been tested this year in the VB configuration. Up to four electron beam pulses shorter than 300 fs and separated by less than 1 ps have been characterized. In addition two electron beam pulses have been injected in the undulator and a characteristic interference spectrum produced by the FEL interaction in this new configuration has been observed, confirming that both pulses have been correctly matched to the undulator and were both lasing. In this report we summarize the experimental results obtained so far.

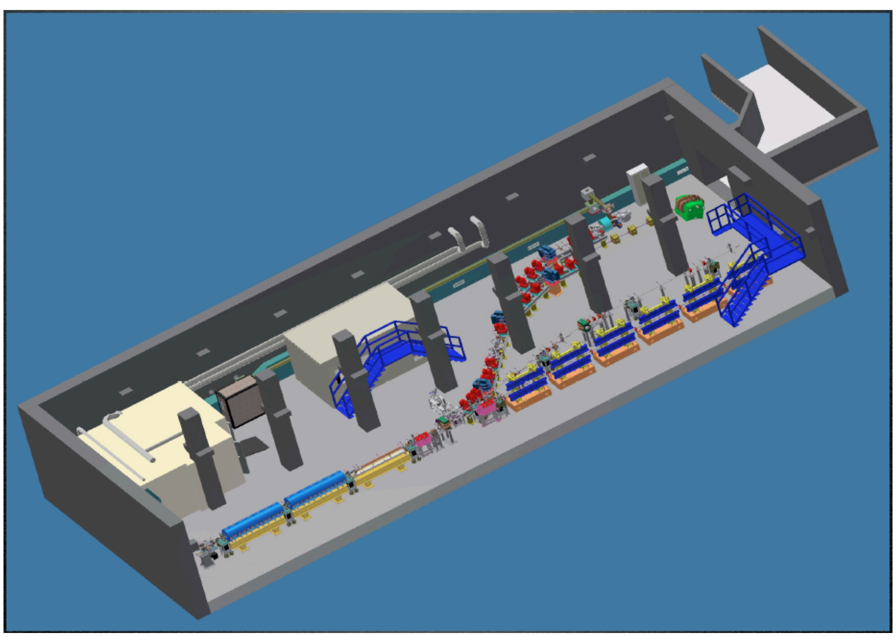

Figure 1: Layout of the SPARC test facility.

SPARC is a test facility for high brightness electron beams dynamics studies [1,2,3], FEL physics experiments in SASE and Seeded modes [4,5] and for THz radiation production [6].

The SPARC photoinjector is a 1.6 cell S-band RF gun, followed by 3 S-band accelerating sections, which boost the beam energy up to 150–200 MeV. Downstream the LINAC there are at present two beam lines: the FEL line composed by six undulators, and a parallel line dedicated to a THz source. Other two beam lines are under installation, one for the future back-scattering Thomson experiments [7] and the other one dedicated to plasma acceleration experiments [8], see Figure 1. All these applications need very high brightness electron beams, that are produced combining the emittance compensation technique [9] for laminar beams at the gun exit with the RF compression technique, the so called velocity bunching (VB) [10], which requires additional solenoid focusing around the first two accelerating structures to keep under control the emittance growth while bunching.

With this machine configuration a new technique called Laser Comb (LC), aiming to produce a train of short electron bunches, has been proposed [11]. In this operating mode the photocathode is illuminated by a comb-like laser pulse to extract a train of electron bunches which are injected into the same RF bucket of the gun. A typical laser comb time profile at the cathode is shown in Figure 2. The SPARC laser system, based on a Ti:Sa oscillator is extensively reported in Ref. [12] and related references, while the upgrade required by the laser comb techniques is reported in Ref.[13]. The technique used here relies on a α-cut beta barium borate (α-BBO) birefringent crystal, where the input pulse is decomposed in two orthogonally polarized pulses with a time separation proportional to the crystal length. A similar scheme is also adopted at Tsinghua University [14]

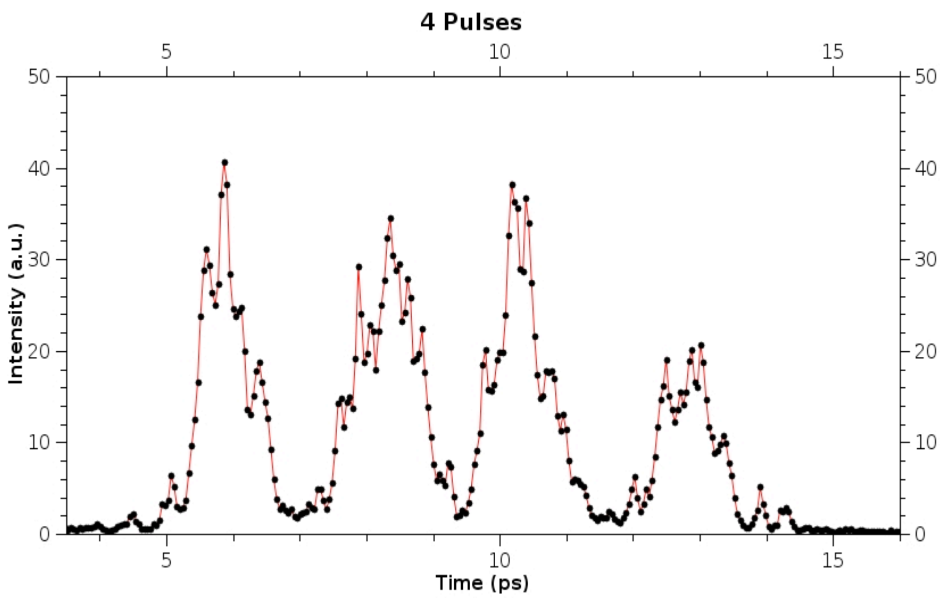

Figure 2: Laser comb time profile at cathode

In the first accelerating structure operating in the VB mode, i.e. injecting the bunch train near the zero crossing of the RF wave, the bunch train is compressed by the longitudinal focusing effect of the RF wave and with a proper choice of injection phase is possible to keep under control both the intra-bunch distance as well as the single bunch length. This method preserves all the extracted charge and it is different from other passive tecniques [15-18], where the train is produced by using a mask that stops a significant fraction of the charge.

Figure 3 shows the simulated compression curve for the case of two bunch train with parameters relevant for the SPARC linac. The compression phase refers to the difference from the injection phase and the ``on crest'' (maximum energy at the linac exit) phase. The compression factor is the ratio between the on crest bunch length and the actual bunch length (which varies with the compression phase). The final energy of the beam depends on the compression phase and ranges from 177 MeV (on crest) to about 100 MeV in over-compression (i.e. for compression phases more negative than the maximum compression one -88). In the figure the longitudinal behavior of the whole bunch and of each sub-bunch are also shown. The black (blue, red) line is the compression factor i.e. the ratio between the length on crest and the length in compression regime. The total bunch length decreases up to a minimum value (-88 deg). Increasing the compression phase, the sub-bunches invert their relative position and they start to become distinguishable and to increase their separation. It is clear that to have good sub-bunch separation, one has to operate in over-compression regime, which implies a careful machine optimization to preserve low emittances.

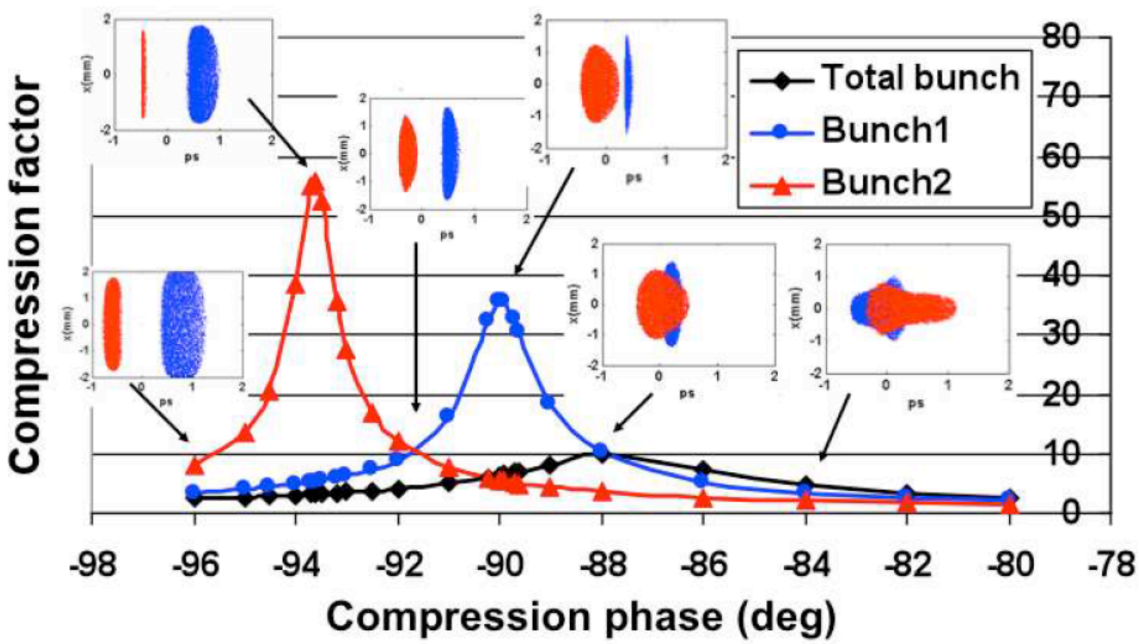

Figure 3 Compression curve for two bunches pulse train at SPARC

The laser-comb scheme can be conveniently considered to drive fast pump and probe FEL experiments [19], resonant exitation of plasma waves in plasma accelerators [15], sources of narrow-band terahertz radiation [6] and other beam dynamics experiments [18].

Up to four electron beam pulses shorter than 300 fs and separated by less than 1 ps have been characterized and a narrowing THz spectrum produced by the bunch train has been measured. In addition two electron beam pulses have been injected in the undulator and a characteristic interference spectrum produced by the FEL interaction in this new configuration has been observed, confirming that both pulses have been correctly matched to the undulator and were both lasing.

When the linac works in VB regime with a relevant compression factor, a very high stability of the machine is very important. The necessary stability has been achieved with VB cooling sistem and RF gun feeding upgrade, with a consequent improvement of the achieved beam emittance, as explained in the next paragraph.

2 The SPARC linac improvements

During previous SPARC runs the RF gun gradient was limited by frequent RF breakdown events in the structure. The incident power was limited to 10MW with a 1.5 μs RF pulse (see

Figure 4, blue points), resulting in a beam energy at the Gun exit of 4.5 MeV. The resulting peak field in the Gun was $E_p \approx 105$ MV/m only, instead of the expected $E_p \approx 120$ MV/m giving 5.6 MeV to the beam, with significant degradation of the beam emittance and peak current.

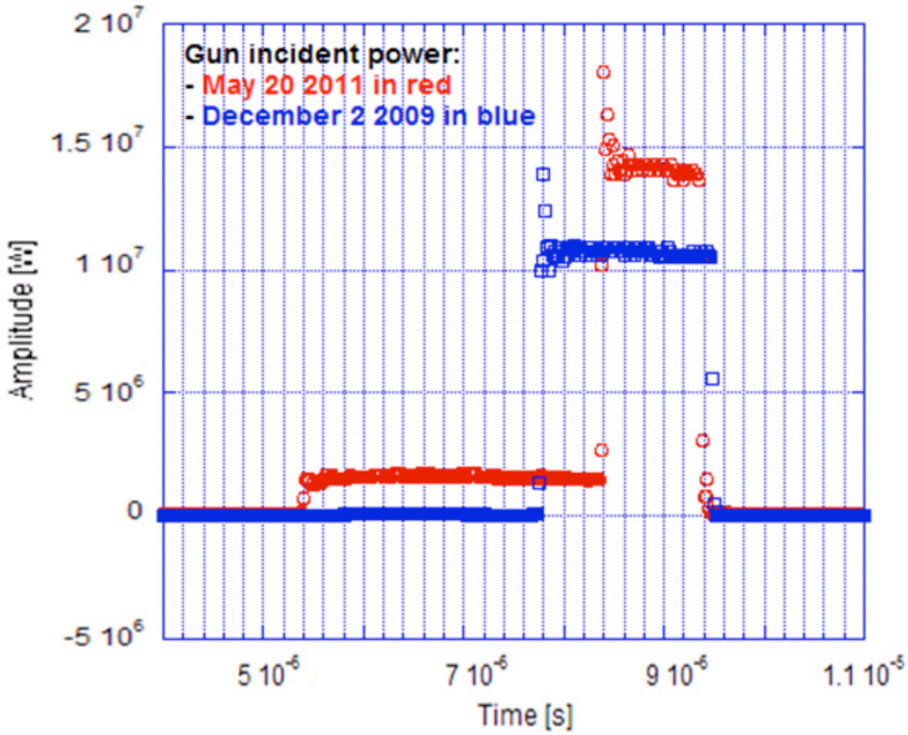

Figure 4: RF Gun pulse profile

This limitation has been successfully overcome by a new shaping of the RF pulse (see Figure 4, red points). In this new configuration the RF incident power is kept at 1 MW during the first three microseconds to allow the klystron phase stabilization loop (PLL) to work correctly [20] and only in the last microsecond the RF power is inreased up to the nominal value. In this way the performance of the klystron PLL in terms of phase noise compression is held down to 55 fs_{rms} inside the gun with a peak power incident to the gun higher than 14.5 MW. Being the gun filling time 0.7 µs, the peak power inside the structure results about 76% of the incident power.

The effect on the beam quality are very promising. The energy of the beam downstream the Gun can now achieve a maximum energy of 6 MeV, corresponding to $E_p \approx 125$ MV/m, with an emittance at the linac exit significantly decreased as discussed in the next paragraph.

Also the vacuum system had some important benefits; the maximum acceptable breakdown rate has decreased from 5÷10 discharge per minute to less than 1 per hour, and now 10^{-10} torr vacuum level inside the Gun are maintained during the machine operation.

The VB process is strongly sensitive also to the RF phase fluctuations by temperature oscillations, resulting in unstable final bunch parameters. Operation in the Comb regime is strongly affected by this phase instability producing an unpredictable distance between the bunches in the train. This distance is a crucial parameter for all the applications and experiments. A major improvement of the VB long term phase stability has been achieved when a dedicated water cooling system (a chiller) for the first TW structure has been installed. The temperature stability is now within 0.2° Celsius (peak-to-peak), which results in a phase variations lower than 0.2 degrees as required for a sufficiently stable VB mode operation.

3 Experimental results with the COMB beam

The measurements reported here have been performed with a train of two and four pulses, with the following procedure: first we characterize the bunches train on the RF crest (0°, maximum energy), then moving the phase of the first TW cavity (φ_{s1}) where VB regime occurs, from the crest value to the phase of maximum compression (-88°). At this phase the bunch train length achieves the minimum value corresponding to a full spatial overlapping of all the partially compressed bunches with a typical energy difference of about 1 MeV. To achieve the foreseen comb structure we have to run in the over-compression regime (typically more than -92) so that the bunch distance can be tuned to the designed value and each pulse is near its minimum length [13].

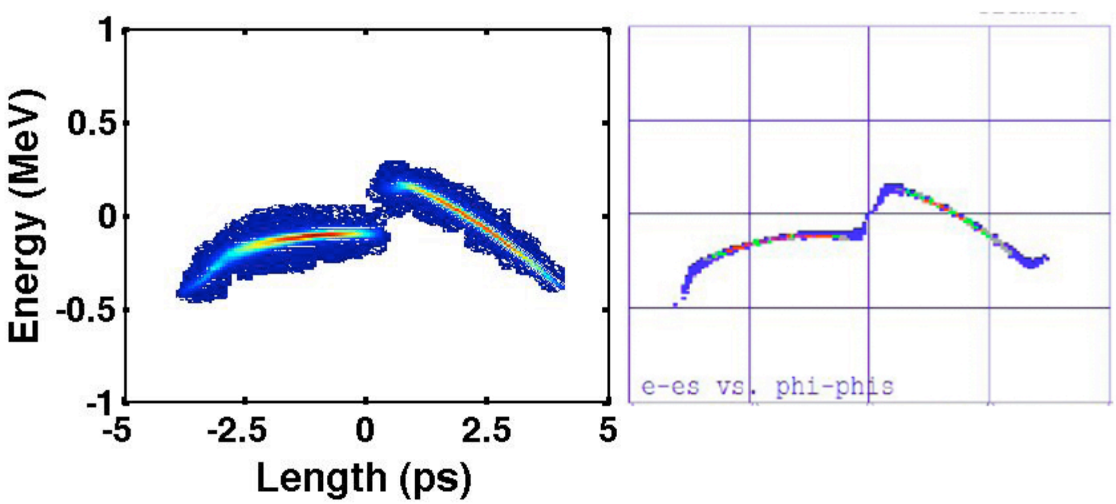

Figure 5: Measured long. phase space on crest (left). The same long. phase space simulated with PARMELA (right)

At the linac exit an RF deflecting cavity allows for bunch length measurements with a resolution of 100 fs [21], if the beam is then bent by a dipole it is possible to reconstruct the beam longitudinal phase space. As a reference case we show in Figure 5 the measured longitudinal phase spaces for two 85 pC bunches (170 pC total charge) running on crest (no compression) in comparison with PARMELA simulations. The agreement is very remarkable also in the details of the phase space distribution. Each pulse results to be 1 ps long with an energy spread less than 0.1%. The emittance measurements have been performed with the standard quad scan technique at the linac exit that do not allow in the present configuration to separate the contribution of each bunch from the total measured emittance. Nevertheless the total rms emittance of this double pulse results to be 0.97 mm (0.52 mm) including 100% (90%) of particles, in fully agreement with simulations. A very remarkable results that couldn't have been possible to achieve without the SPARC linac improvements described earlier.

3.1 Two laser pulses

In Figure 6 are shown the longitudinal phase space and the corresponding current profile for a 170 pC total charge beam in the case of maximum compression. As one can see the two pulses are fully time overlapped and behaves like a single bunch. The total peak current is as high as 350 A, corresponding to a total length of 140 fs with a total rms emittance of 4 μm (3.5 μm) with 100% (90%) of particles. This peculiar beam has a total rms energy spread of 0.8 % at 110 MeV at the linac exit, while the energy spread of the first pulse is 0.25% and the second one is 0.4%. It is actually a two energy levels beam, separated by 1.5 MeV, whose properties as a FEL radiation active medium will be investigated next year.

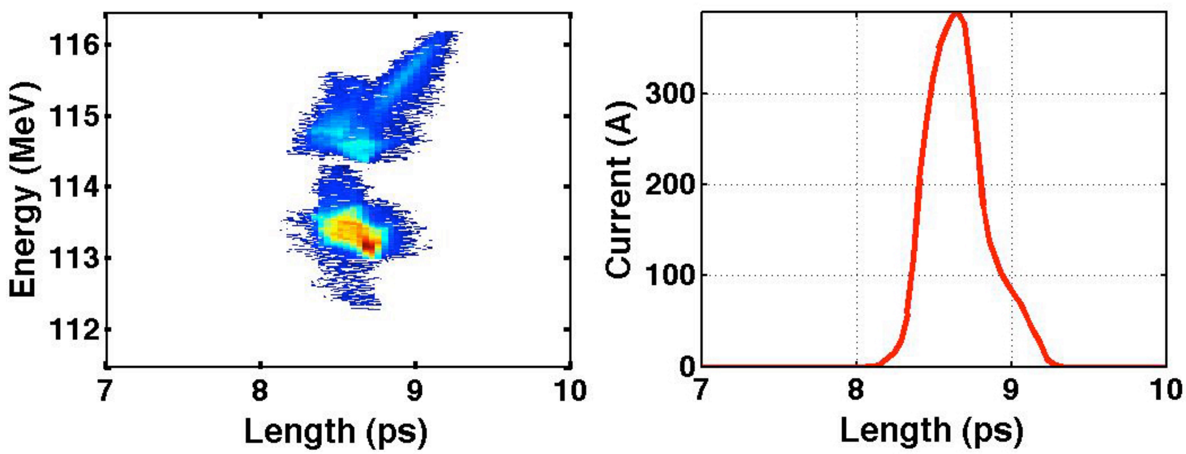

Figure 6: Long. phase space (left) and current profile (right) for a two bunches train (170 pC) at VB phase of maximum compression

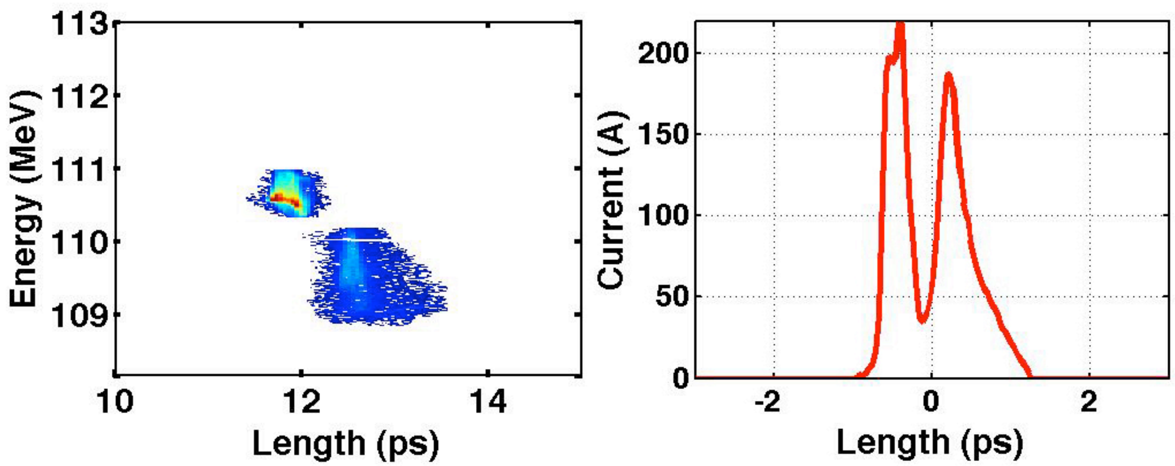

Figure 7: Long. phase space (left) and current profile (right) for a two bunches train (170 pC) at VB phase of over compression

Another interesting case is shown in Figure 7. In this case the VB phase has been set to 95.6 degrees corresponding to the over-compression regime. As expected the two pulses are now well separated by 0.8 ps with a charge unbalance of 10%. The first bunch is 140 fs long and the second one 270 fs long, with a total rms emittance of 6 μm (4.2 μm) with 100% (90%) of particles. It was not the aim of the present experiment to optimize the emittance, so we didn't put enough attention to the fine tuning of the long solenoids, in addition chromatic effects due to the large total energy spread of the train might lead to overestimate the measured emittance. This configuration has a potential interest to generate two FEL radiation pulses for pump and probe experiments.

3.2 FEL experiment with two bunches

A preliminary experiment with two bunches injected in the undulator has been already done. The train of two bunches, in condition of strong compression, similar to the one shown in Figure 7, was matched and transported in the SPARC undulator. The main radiation diagnostic was an in vacuum spectrometer [22], an instrument that allows simultaneous single shot measurements of the vertical beam size and of the spectral distributions [5].

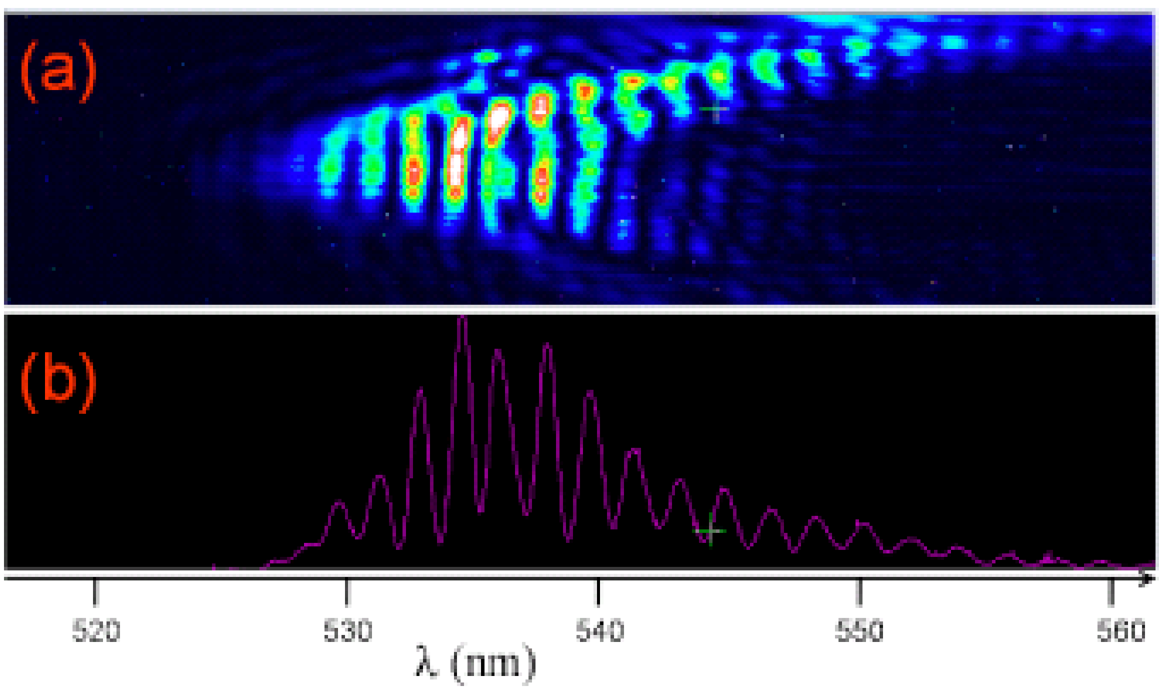

Figure 8: (a) Single shot spectrum measurement in the case of radiation from two bunches starting from noise. The ordinate is the transverse dimension coordinate y. (b) Average value along y of the spectral intensity I. In this case the width of the fringes turns out to be $\Delta\lambda = 1.66$ nm and their visibility $\eta = 0.67$

The typical spectrum observed, and presented in Figure 8, is characterized by the presence of regular fringes due to interference of two light pulses produced by the FEL SASE process, being the distance between the peaks larger than the slippage length. By Fourier transforming a radiation composed by two Gaussian wave packets in the time domain, with same widths and amplitudes respectively $A_{1,2}$, separated by an interval δt, the relation between the fringe dimension $\Delta\lambda$ and δt is given by $\delta t = \lambda^2/\Delta\lambda$. The visibility of the fringes $\eta = I_{max} - I_{min}/(I_{max} + I_{min})$ where I_{max} (I_{min}) is the maximum (minimun) value of the y-average of the spectral amplitude I is moreover connected to the amplitudes of the light pulses by the relation $\eta = 2A_1A_2/(A_1^2 + A_2^2)$. According to our GENESIS [23] simulations, the measured spectrum shown in Fig 8, corresponds to two light pulses quite well balanced, with and estimated difference between the two peaks of about 30%. The distance between the two pulses turns out to be 0.58 ps. As the measurements were performed in non optimal experimental conditions only 40% of the spectra collected shows regular fringes, while 48% presents signature of the amplification of one single bunch and the remaining 12% is strongly affected by noise. The average made on the significative part of 200 measured events leads to a pulse to pulse distance of δt = 0.615±0.155 ps, to be compared with the measured electron bunch separation of δt = 0.843 ps.

This result deserve a more systematic study that will be done during the next FEL SPARC run in 2012. Nevertheless the characteristic interference spectrum produced by the FEL interaction in this new configuration indicates that both pulses have been correctly matched to the undulator and were both lasing.

3.3 Four laser pulses

The four pulses configuration needs to run the VB in a deep over-compression regime, which is well over the maximum compression value. It is necessary to perform a major rotation of the longitudinal phase space to separate the four bunches in the region of balanced current. The total emittance has been measured for a total charge of 200 pC (with a charge distribution among the 4 bunches of 13%, 25%, 40%, 22%) in three configurations: on crest, compression and over-compression, giving respectively, 1.1 μm, 4.0 μm and 4.1 μm at 90% of particles.

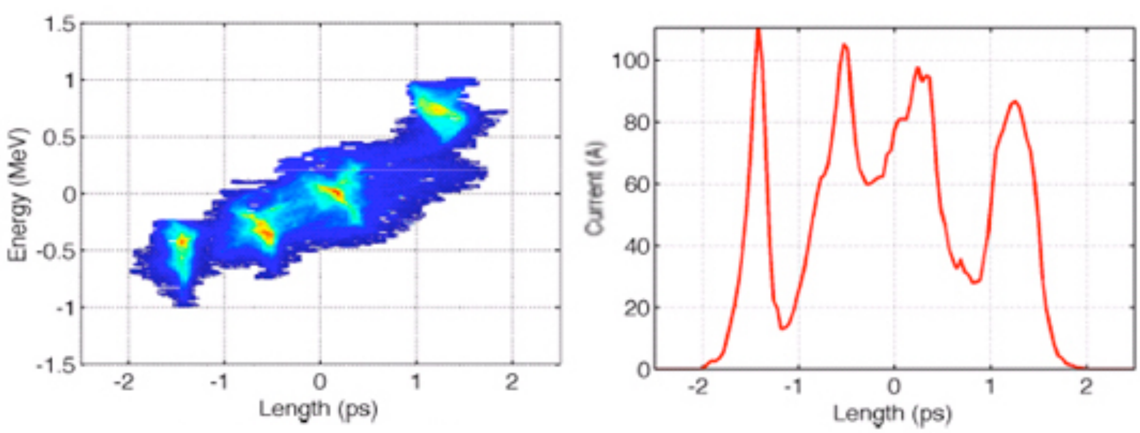

Figure 9: Long. phase space (left) and current profile (right) for a four bunches train (200 pC) at VB phase of deep over compression (107.9 degrees)

Figure 9 shows the longitudinal phase space and the current profile for the over-compression regime with injection phase in the VB 108 degrees off crest. Four spikes spaced by 0.9 ps are clearly visible. The whole bunch train is 3.5 ps long with four bunches of length 140 fs, 200 fs, 280 fs and 230 fs . This time structure has been used in a test experiment to produce narrow band, tunable THz radiation.

3.4 *Narrow band TH radiation*

Narrow band, tunable THz radiation is produced at SPARC combining the VB technique and the comb-like electron beam distribution [6].

A Martin-Puplett interferometer has been installed at the THz station to allow the measurement of the autocorrelation of the radiation pulse (the interferogram), which represents the autocorrelation of the particle distribution. The coherent transition radiation (CTR) spectrum is directly provided by Fourier transforming the autocorrelation function. For a comb beam, the interferogram shows 2N-1 peaks (where N is the number of bunches in the train) whose distance provides the inter-distance of the bunches in the train. Hence the spectrum of the radiation is strongly suppressed outside the comb repetition frequency.

An example of the measured autocorrelation function for a train of N=4 pulses is presented in Figure 10. The peak distance of 0.9 ps corresponds to the bunch-to-bunch separation. The frequency spectrum shows an enhancement of the emission around 0.8 THz.

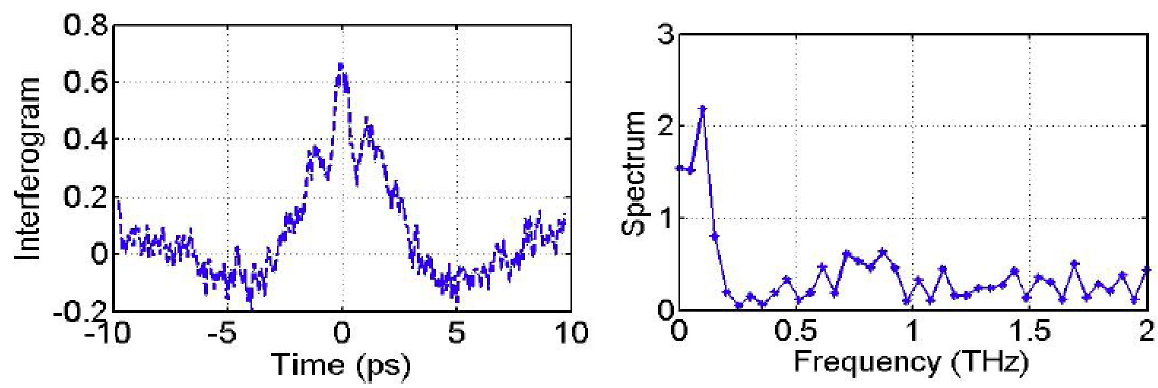

Figure 10: The autocorrelation function measured for the four bunches trainand the corresponding frequency spectrum.

4 The future: SPARC_LAB

The SPARC project was partially funded in 2003 by INFN as a “Progetto Speciale” with the mission to demostrate the capability to produce high brightness electron beams able to drive a Free Electron Laser experiment. All the milestones have been succesfully achieved along the years and the project has now formally reached its natural conclusion as a “Progetto Speciale”. At the end of 2011 INFN has decided to launched a new facility, named SPARC_LAB (Sources for Plasma Accelerators and Radiation Compton with Lasers and Beams), born from the union of the two already existing infrastructures at LNF: SPARC and the TW class laser FLAME developped in the framework of the PLASMONX project, also ending by the end of 2011. With the mission to coordinate and harmonize all the activities making use of the high intensity electrons and photons beams, see Figure 11, SPARC_LAB will become operational in 2012 and will be an interdisciplinary laboratory dedicated to the study of new techniques for particles acceleration (electrons, protons, ions) and the development and application of advanced radiation sources (FEL, THz, Compton-Thomson).

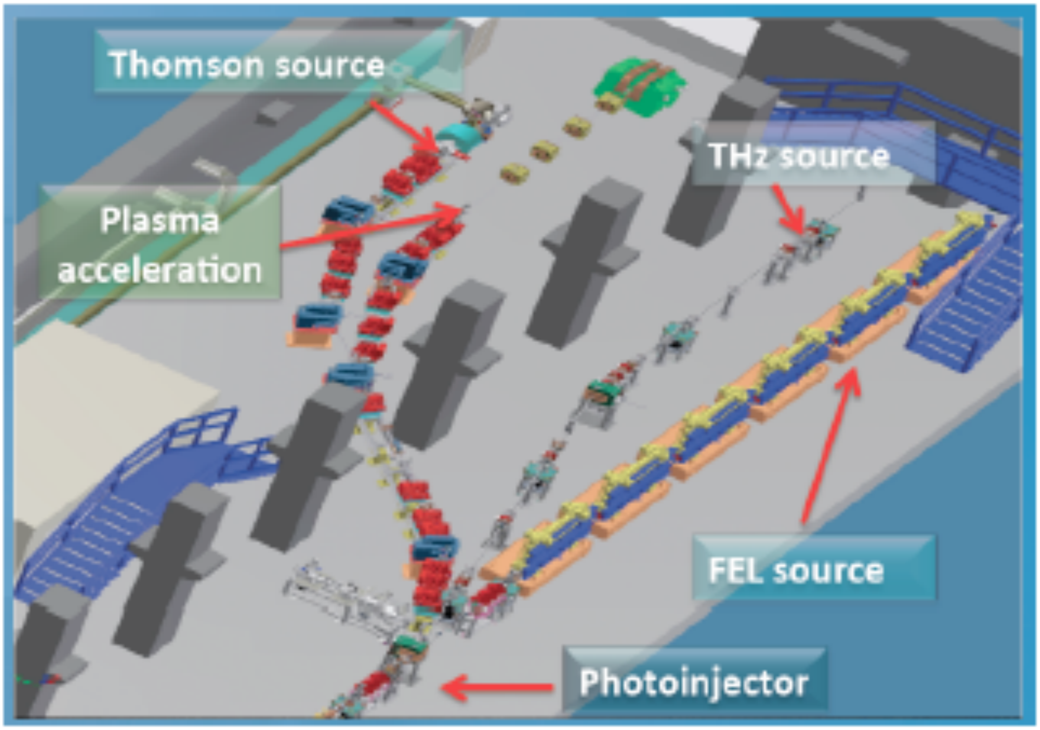

Figure 11: Layout of the SPARC_LAB beam test facility.

5 Pubblications in the year 2011

1) M. Labat et al. *"High-Gain Harmonic-Generation Free-Electron Laser Seeded by Harmonics Generated in Gas* ", Phys. Rev. Lett. 107, 224801 (2011).

2) L. Giannessi et al. *"Self-Amplified Spontaneous Emission Free-Electron Laser with an Energy-Chirped Electron Beam and Undulator Tapering",* Phys. Rev. Lett. 106, 144801 (2011)

3) D. Filippetto et al., *"Phase space analysis of velocity bunched beams",* Phys. Rev. ST Accel. Beams 14, 092804 (2011).

4) C. Maroli, V. Petrillo, and M. Ferrario, *"One-dimensional free-electron laser equations without the slowly varying envelope approximation",* Phys. Rev. ST Accel. Beams 14, 070703 (2011).

5) L. Giannessi et al., "*Self-amplified spontaneous emission for a single pass free-electron laser*", Phys. Rev. ST Accel. Beams 14, 060712 (2011).

6) M. Ferrario et al., "*Laser comb with velocity bunching: Preliminary results at SPARC*", Nuclear Instruments and Methods in Physics Research Section A, Volume 637, Issue 1, Supplement, 1 May 2011,

7) J.B. Rosenzweig et al., "*Teravolt-per-meter beam and plasma fields from low-charge femtosecond electron beams*", Nuclear Instruments and Methods in Physics Research Section A: Accelerators, Spectrometers, Volume 653, Issue 1, 11 October 2011.

8) G. Marcus et al., *"Full Temporal Reconstruction using an Advanced Longitudinal Diagnostic at the SPARC FEL*", Proc. of IPAC, Kyoto, Japan, May 2011.

9) D. Alesini et al., "*Design, Fabrication and High Power RF Test of a C-band Accelerating Structure for Feasibility Study of the SPARC Photo-injector Energy Upgrade*", Proc. of IPAC, Kyoto, Japan, May 2011.

10) A. Mostacci et al., "Advanced Beam Manipulation Techniques at SPARC", Invited talk in Proc. of IPAC, Kyoto, Japan, May 2011.

11) M. Labat et al., "*Seeding Experiments at SPARC*", Invited talk in Proc. of FEL Conference, Shanghai, China, August 2011.

12) D. Filippetto et al., "*Ultrashort Single Spike Pulse Generation at the SPARC Test Facility*", Invited talk in Proc. of FEL Conference, Shanghai, China, August 2011.

13) A. Bacci et al., "*Advanced Beam Dynamics Experiments at SPARC*" Oral presentation, in Proc. of FEL Conference, Shanghai, China, August 2011.

6 Acknowledgments

A. Cianchi, B. Marchetti, R. Pompili, Sezione INFN di Tor Vergata
V. Petrillo, L. Serafini, Sezione INFN di Milano
L. Giannessi, A. Petralia, G. Dattoli, F. Ciocci, M. Del Franco, M. Quattromini, C. Ronsivalle, E. Sabia, I. Spassovsky, V. Surrenti, ENEA C.R. Frascati, IT.
L. Poletto, F. Frassetto, CNR-IFN, IT. J.V. Rau, V. Rossi Albertini ISM-CNR, IT.
G. Marcus, J. Rosenzweig, UCLA, CA, USA.
S. Spampinati, ST, IT and University of Nova Gorica, Nova Gorica,
M. Labat, F. Briquez, M. E. Couprie, SOLEIL, FR.
B. Carré, M. Bougeard, D. Garzella CEA Saclay, DSM/DRECAM, FR.
G. Lambert LOA, FR.

7 References

[1] M. Ferrario et al., PRL 99, 234801 (2007).
[2] A. Cianchi et al., PRST-AB 11, 032801 (2008)
[3] M. Ferrario et al., PRL 104, 054801 (2010).
[4] L. Giannessi et al., PRL 106, 144801 (2011)
[5] L. Giannessi et al., PRST-AB 14, 060712 (2011)
[6] E. Chiadroni, Proc. of IPAC 2010, Kyoto, Japan
[7] A. Bacci et al., NIM A 608.
[8] D. Alesini et al., Proc. of PAC 2005, Knoxville,USA.
[9] B. E. Carlsten, NIM A **285**, 313 (1989).

[10] L.Serafini, M.Ferrario, AIPConf.Proc.581(2001)87.
[11] M. Boscolo, et al., Int. J. Mod. Phys. B 21 (2007).
[12] C. Vicario, et al., Proceedings of PAC 2007.
[13] F. Ferrario, et al., NIM A 637,S43–S46 (2011)
[14] L. Yan *et al.*, NIM A 637, S127-S129 (2010)
[15] P. Muggli, Proc. of PAC 2009.
[16] V. Yakimenko, et al., Proc.of PAC 2009.
[17] J.G. Neumann, et al., J. A. Phys. 105 (2009) 053304.
[18] P. Piot, et al., PRST-AB 9 (2006) 053501.
[19] M. Boscolo, et al., NIM A 593 (2008) 106–110.
[20] M. Bellaveglia et al., EuroFEL-Rep. -2007-DS3-051.
[21] D. Alesini et., Proc. of DIPAC 2009.
[22] L. Poletto et al., Rev. Sci. Instr. 75, 4413 (2004).
[23] S. Reiche, Nucl. Instrum. Methods Phys. Res., Sect. A 429, 243 (1999).

COMMUNICATION and OUTREACH

R. Centioni (Resp.), V. Ferretti (Art.15), L. Sabatini, S. Vannucci (Resp.)
Scientific Information and Documentation Service

From many years, the LNF has been interested in and active in communication in the area of scientific education. Throughout the year they provide basic education in physics by means of a vast outreach program for the general public, teachers and students.

The aims of the program are various: "open the laboratories" inviting general public to be part of INFN "scientific world"; to "stimulate" the curiosity on scientific issues; to offer a more complete view of the scientific institutions operating in the area; to transfer scientific knowledge, methodology and technologies of the research; to inform people about the latest developments in Physics; to enable people to acquire the knowledge and understanding of INFN research activities.

Most of the activities are organized inside the LNF, such as Visits, Scientific Week, Open Days, Physics Lessons, Meetings with the authors of scientific books, Concerts. Special events are dedicated to schools: the "Incontri di Fisica", a course for high school teachers, and Stages for high school students. Other activities are organized outside the LNF such as Seminars at school or at public libraries, and the European Researchers Night.

These activities are made possible by the enthusiastic involvement of INFN-LNF people: graduate students, postdocs, researchers, engineers and technicians.

1. **Visits to LNF** (`www.lnf.infn.it/edu/visite/`) are a well established tradition. They consist of a brief historical presentation of the Laboratories and their activities on site and abroad and of a guided tour to the "open air museum" and to the experimental areas. The visits are organized for high school students (age: 17-19) and for primary and secondary schools (age: 10-14). In this last case a special program is foreseen that includes a first meeting with the students at their school to introduce the world of research and some basic concepts of modern Physics followed by the visit to the LNF in small groups. The visits are requested not only by Italian schools, but also by other countries: Denmark, Austria, Czech Republic, Belgium, Germany, France, Greece, Japan, India, Taiwan, and USA. Each year about 4000 people visit the LNF. It is interesting to remark that about 35 % of schools that visit come back two or more times during the years, a sign of a good performance of LNF dissemination effort.

2. **Scientific weeks and Open Days** (`www.lnf.infn.it/edu/settimana/`) are organized at LNF in collaboration with the other Research Centres located in the Frascati area, Public Institutions, Cultural Associations, and International non-government organizations. This type of event provides guided tours, conferences, public lectures, scientific videos. Most of the LNF employees are in action to present their research centre, answer questions and care for their guests. (LNF, March 28, 2011).

3. **Lessons of Physics** (`www.lnf.infn.it/edu/media/`) *(Care of O. Ciaffoni, G. Di Giovanni and SIDS-Communication and Outreach)* are held by world leading scientists in various fields of science. Students and teachers are invited to attend the lessons which are video-recorded. Slides and videos are available on the LNF website to be used even for lessons at school.2011 Lessons:

   - S. Di Falco, *Dov'è finita l'antimateria? Origini, proprietà e tecniche di rivelazione dei costituenti di un'universo perduto*;

- V. Del Duca, *LHC e il Modello Standard delle particelle*;
- A. Bassi, *Meccanica Quantistica: misteri e paradossi*;
- P. Campana, *LHC: cosa c'insegnano i primi dati raccolti.*

4. **Seminars** (`www.lnf.infn.it/edu/seminaridivulgativi/`) Upon request, LNF researchers give lessons to high school students and the general public. A special program is performed together with public libraries, especially with Frascati town one. The arguments deal with science and society or they take inspirations from scientific or fiction books and theatre.

   - V. Chiarella, *I neutrini*, Lic. Sc. "B. Berto", Vibo Valentia;
   - P. Di Nezza, *Appunti di fisica moderna. La fisica delle particelle elementari*, Lic. Sc. "A. Moro", Margherita di Savoia (FG);
   - A. Paoloni, *I Raggi Cosmici*, Lic. Sc. "P. Levi", Roma;
   - C. Curceanu, *Le basi della Fisica Moderna e la Relatività*, Lic. Sc. "B. Touschek", Grottaferrata (Roma);
   - C. Curceanu, *LHC*, Lic. Sc. "F. d'Assisi", Roma;
   - C. Curceanu, *Fisica Medica*, Lic. Sc. "F. d'Assisi", Roma;
   - S. Bianco, *La velocità dei raggi cosmici*, Lic. Sc. "A. Righi", Roma;
   - C. Curceanu, *Il paradosso di Fermi: dove sono gli extraterrestri?*, Lic. Sc. "Landi", Velletri (Roma);
   - M. Calvetti, *A proposito di scienza*, Biblioteca Comunale Subiaco (Roma).

5. **Incontro con l'Autore** (`www.lnf.infn.it/edu/ica/`) LNF organize meeting with authors who present their scientific books to the general public, students, and teachers.
   B. Arpaia, *L'energia del vuoto*, interview by V. Napolano (INFN Communication Office), March 28, 2011 (see Fig. 5).

6. **European Researchers' Night** (`www.lnf.infn.it/nottedellaricerca/`) has been organized since 2006. The SIDS is involved in this project organizing guided tours at LNF. This event is also performed in other European cities to promote the activities of the main research centers at international level. During all day and night are organized: experiments held by the researchers, games for children, visits to major Italian and European research laboratories, science shows, "scientific coffees", and so on. These initiatives enable dialogue with researchers and help people to discover science through entertainment. (LNF, September 23, 2011).

7. **Incontri di Fisica** (`http://www.lnf.infn.it/edu/idf/`) have organized since 2001. The event is a three-days course for high school teachers and people involved in scientific research dissemination. About 160 teachers from all over Italy attend this event each year. The goal is to stimulate teachers' professional training and provide an occasion for interactive and hands-on contact with the latest developments in physics. The program consists of plenary lessons, presentations of INFN-LNF activities, visits to LNF experimental area and discussions. The peculiarity of this course is that the second day is entirely dedicated to special participation in working groups (8 hours in the laboratory). The working groups concern INFN research topics (nuclear and subnuclear physics, astroparticle physics and technology). They are conducted by INFN researchers, engineers and technicians and they are held in the various experimental LNF laboratories. Each working group consists of a theoretical lesson, hands-on activity or

Figure 1: *"Incontro con l'Autore". The writer Bruno Arpaia (right) interviewed by Vincenzo Napolano from the INFN Communication Office. In the photo also Matteo Palutan (left) that gave a talk about LHC experiments (INFN-LNF Photo).*

data analysis of a real experiment. In this way, teachers have a direct contact with researchers and they can use typical experimental instrumentation employed in contemporary Physics. The lessons are given by speakers from INFN or from other Institutions such as Universities or other Laboratories like CERN. They concern topics on Physics or other scientific matters, application of Physics and more general topics. If we only think that each teacher is in contact with about 120-130 students and their families. "Incontri di Fisica" represents an important occasion for the dissemination of Physics. Moreover, by informing them on cutting-edge Science, it is possible to introduce modern and contemporary Physics in school programs. Teachers can stay in contact with INFN researchers also after the course. The evaluation of the course is performed by a questionnaire. The analysis is very useful for the study of future programs. Teachers, authorized by the Minister of Education, receive a certificate of participation. All the programs are published on the LNF web site (lessons, video, photo). (LNF, October 5-7, 2011).
(Organizing Committee: P. Di Nezza (Chair), M. Calvetti, P. Campana, R. Centioni, C. Curceanu, M. Dreucci, V. Ferretti, S. Miozzi, L. Sabatini, S. Vannucci, G. Venanzoni)

8. **Stages for students** (`http://www.lnf.infn.it/edu/stagelnf/`) have been organized since 2000 for high school students (age 18-19). Students are selected by their teachers on the basis of their curriculum but especially on the basis of their interest and motivation. Tutors are

Figure 2: *The journalist Miriam Mafai with the director of LNF, Umberto Dosselli. (INFN-LNF Photo).*

INFN staff, i.e., researchers, engineers and technicians. They prepare the program with the following goals: to offer a special experience in an important research Institute; to transfer scientific knowledge, methodology and high level research technology; to present INFN-LNF experimental activities; to promote the teaching of modern and contemporary physics; to contact schools from all over Italy and abroad; for student orientation (university or career). In a direct contact with their tutors (1 tutor / 2 students), students are involved in theoretical lessons and practical operations. They acquire knowledge and understanding of INFN research activities in an interactive modality. Curiosity, investigation, hands-on learning, working in a team are the key words of this experience. During their stay at LNF, students are like staff members, working from 8 a.m. to 4 p.m. and they participate in the social events (e.g., lunch at the LNF canteen). At their arrival students receive educational material and general information INFN-LNF and they visit the experimental area. Various types of stages in different periods of the year are organized.

- The Winter stages last 9 days. Students come to LNF once a week from 8 a.m. to 4 p.m. Theoretical lessons and working groups are scheduled. LNF, 7 February - 18 May, 2011. (Scientific Coordinator: C. Curceanu);
- The stage Masterclass is organized on behalf of EPPOG Masterclasses European Project. It lasts 4 full days, usually during February. Students, in a unique group of 41, follow lessons on modern physics and analyze data from an experiment at CERN. LNF, 7 - 10

February, 2011 (Scientific Coordinator: D. Domenici, F. Bossi);

- The stage International Masterclass is open for 20 students in last year(s) of high school/college coming from all European countries. It is organized in lectures on Modern Physics and its applications in Society, and in activities to be performed in laboratories. The participants have, as well, the opportunity to visit the main experiments and accelerating facilities of the LNF. The official language is English. LNF, 7 - 10 February, 2011 (Scientific Coordinator: C. Curceanu);
- The Summer stages are organized in June, at the end of the school year, and last 10 days. LNF, 13-24 June, 2011 (Scientific Coordinator: C. Bloise)

The theoretical plenary lessons are scheduled during the morning. Then, divided in small groups, the students participate in various experimental activities.

At the end of the stages, students make a report of their experience. This report is presented in the LNF main auditorium during a ceremony in the presence of families, teachers and other students. Each student receives a certificate of participation and evaluates the experience of stages by filling out a questionnaire.

Tutors consider the experience of Stage very positively. They think it can also be replicated in other INFN laboratories or research centres.

The project phase of the stage program is very important. Tutors take into account that students belong to various schools of different Italian regions so their school preparation may not be the same. They give particular importance to the use of a scientific/technical language appropriate to the educational preparation of students. Since the scientific language is very particular, tutors recommend that the concepts not included in school programs are explained. Surely, it is extremely important to keep in contact with school teachers in order to better understand the preparation of students. Moreover, tutors take particular care of the experimental activities which represent the real different pedagogical approaches to scientific studies. The Stages are a very special occasion for the students. They can work and study in a big research centre and meet students from other schools. Particularly fascinating is the use of sophisticated instrumentation that is certainly not available in school laboratories. The stages offer the opportunity to learn about physics but also computing and electronics and to be oriented for the university choice or career.

The interaction with the scientists is very stimulating as well as the knowledge of their work and their life. Meeting researchers of different ages, nationalities and experience, the students can understand better the role of the researcher, too often simply considered only as a person who works into a laboratory, far from the real world. Students are curious to ask questions about scientists' experiences and their raesons for becoming a physicist, their hobbies and passions.

Teachers note that at the end of the stage the students are well oriented in a work environment different from school, having had the opportunity to integrate their knowledge on scientific matters. They say that students learn that the research is an enthusiastic adventure made by passion and study realized by working in a team on the solution of problems. Concerning science and scientists students appreciate: the importance of scientific collaboration, being passionate and tenacious to achieve goals, the effort needed in the study, curiosity, and the importance of making sacrifices.

Each school, participating in the LNF Stage program, includes it into their own Annual Training Project. This also means that schools often organize an event during which students make a report on the stage experience to their classmates and parents. From this point of view, stages become a special initiative of diffusion of the scientific culture with a big impact on families, other students, and teachers.

Regarding the university choice students who participate in the LNF stages are oriented to scientific studies in particular Engineering and Physics.

The participation in the stage program has increased over these last 10 years: since 2000, 1235 students have attended the stages. In 2000 LNF hosted 12 students from only one local school, while in 2011, 184 students from 60 different schools all over Italy and abroad came to Frascati.

Table 1: *10 years of Stages.*

Year	**Students**	**Females**	**Males**	**Schools**	**INFN Tutors**
2000	12	1	11	1	7
2001	14	3	11	1	14
2002	57	15	42	8	50
2003	56	11	45	14	22
2004	114	34	80	21	25
2005	154	42	112	29	56
2006	161	48	113	46	58
2007	163	45	118	51	55
2008	161	47	114	51	63
2009	177	40	137	54	67
2010	166	36	130	60	60
2011	184	61	184	60	70

The LNF monitor the success of the various initiatives proposed mostly through questionnaires (each one specific to the event type) and also keep track of the history using dedicated databases by which it is possible to perform simple statistical analysis. The questionnaires are a valid instrument to know the students' evaluation of the stages: general organization, lessons contents and exposition by the tutors, working groups, their personal considerations about the modality and the opportunity of the stages and their idea concerning university or career choice.

9. **Web Page** (`http://www.lnf.infn.it/`) In 2010 the "LNF Web Portal for General Public" project, in Italian and English, was completed. The website is a starting point, a gateway for "non-expert" users to know about modern and contemporary physics in order to fill the gap from Science and Society. People interested in physics can follow the developments and the results of INFN-LNF experiments and international collaborations. Students, teachers and the general public may have access to useful information on educational programs and scientific cultural events (tutor lessons, videos, photos, student reports, information and educational material).

   In Table 2 we report the number of participants for each activity.

10. **From Ada to Super B** (`www.lnf.infn.it/conference/btml2011/`) - LNF and Auditorium Scuderie Aldobrandini Frascati, Decembre 1st

    Fifty years ago, the first electron-positron storage ring in the world, the Anello di Accumulazione (AdA), started operating in Frascati at INFN National Laboratories. AdA had been

Table 2: *Number of participants to LNF events during 2011.*

Events	Participants
Visits	3426
Scientific Week an Open Days	952
Lessons of Physics	170
Seminars	300 (LNF) + 465 (outside)
European Researchers' Night	300
Incontri di Fisica for high school teachers	172
Stages for high school students	184

conceived by the Austrian-born theorist Bruno Touschek, who, in February-March 1960, put forward a project, which had been rapidly approved. Built in less than one year by a team of engineers, technicians and physicists, some of whom had just completed the construction of a powerful electron synchrotron of 1100 MeV, AdA was brought to operation in February 1961.

To celebrate this historic milestone, the Italian Frascati National Laboratories of INFN and the French Laboratoire de l'Accélérateur Linéaire dOrsay, where AdA was successfully operated as a collider for the first time, organized a workshop entitled "1961-2011 from AdA to SuperB" as a special event in the series "Bruno Touschek Memorial Lectures".

The programme was divided in two parts: the first, targeted to the scientific community and dedicated to the history of electron-positron collisions and to the new SuperB project; the second part took place in the beautiful settings of Scuderie Aldobrandini in the town of Frascati where R. Petronzio gave a seminar on SuperB tuned to the general public. Thanks to the Mayors of Frascati and Orsay, a scientific twinning between the two cities will be established.

Acknowledgments

Thanks to the LNF Director, and the heads of Accelerator, Research and Technical Divisions. Special thanks to all INFN-LNF Tutors and Services staff.

CONFERENCES, WORKSHOPS and MEETINGS

International conferences, workshops and meetings hosted and/or organized by LNF:

1. *Two Days in Quantum Field Theory*, LNF, 10-11 January, 2011.
2. Meeting of working group on *Radiative Corrections and Generators for Low Energy Hadronic Cross and Luminosity*, LNF, 28 - 29 March, 2011.
3. Collaboration Meeting *SuperB*, LNF, 4 - 7 April, 2011.
4. *Black Objects in Supergravity School - BOSS2011*, LNF, 2 - 6 May, 2011.
5. ILC GDE Meeting *Damping Ring Technical Baseline Review*, LNF, 7 - 8 July, 2011.
6. *Quantum Field Theory aspects of condensed matter physics*, LNF, 6 - 9 September, 2011.
7. *LC11 Workshop: understanding QCD at linear colliders in searching for old and new physics*, ECT* (Trento), 12 - 16 September, 2011.
8. *N & N 2011 - Nanoscienze e Nanotecnologie*, LNF, 26 - 30 September, 2011.
9. *8th Int. Conf. on Nuclear Physicis at Storage Ring - STORI'11*, LNF, 9 - 14 October, 2011.
10. *TMD Montecarlo*, LNF, 7 - 11 November, 2011.
11. *2nd International Conference Frontiers in Diagnostic Technologies*, LNF, 28 - 30 November, 2011.
12. *BTML2011 - Bruno Touschek Memorial Lectures, 1961-201: from AdA to SuperB*, LNF, 1st December 2011.
13. 2nd Collaboration Meeting *SuperB*, LNF, 13 - 16 December, 2011.

FRASCATI PUBLICATIONS

Available at www.lnf.infn.it

LNF Frascati Reports

LNF - 11 / 1(P)
L. Bonolis, G. Pancheri, *Bruno Touschek: Particle Physicist and Father of the* e^+e^- *Collider*

LNF - 11 / 2(NT)
E. Elsen et al. (Eds.), *The International Linear Collider: A Technical Progress Report*

LNF - 11 / 3(P)
E. N. Tsyganov, *Cold Nuclear Fusion*

LNF - 11 / 4(P)
A. Babaev, S. Dabagov, *Analysis of Relativistic Proton Deflection by Bent Crystals*

LNF - 11 / 5(P)
A. Kashchuk et al., *Measurement of the Absolute Gas Gain and the Gain Variations Study in Straw-Tube Detectors*

LNF - 11 / 6(IR)
AA.VV., *Annual Report 2010*

LNF - 11 / 7(IR)
S. Masi et al., *Report of the INFN - Group 2 Stratospheric Balloons Working Group*

LNF - 11 / 7(IR)
M. Coreno et al., *Collaborative Research for a High-Resolution VUV Free Electron Laser User Facility at SPARC*

LNF - 11 / 9(P)
M. E. Biagini, P. Raimondi, J. Seeman (Eds.), *SuperB Progress Report: The Collider*

LNF - 11 / 10(P)
O. Ciaffoni, M. Cordelli, R. Habel, A. Martini, L. Trasatti, *PORFIDO: Oceanographic Data Sensor for the NEMO Phase 2 Tower*

LNF - 11 / 11(IR)
E. Vilucchi et al., *Il Progetto della Nuova Sala Calcolo e la Farm di ATLAS dei Laboratori Nazionali di Frascati*

LNF - 11 / 12(P)
F. Terranova, *A possible infrared origin of leptonic mixing*

LNF - 11 / 13(P)
A. Casanova Diaz, L. Calero Diaz, G. Conesa Balbastre, L. Cunqueiro Mendez, *Photons and* π^0

discrimination in the electromagnetic calorimeter (EMCal) of the ALICE experiment

LNF - 11 / 14(P)
A. Feliciello, T. Bressani, V. Lucherini, *Production and Study of Baryons with Beauty at the Italian Heavy-Flavor Factory SuperB*

LNF - 11 / 15(IR)
A. La Monaca, D. Nanni, F. Terra, *FastCam Nuova Ultraveloce Streak-Camera: Studio del Trasporto del Fascio di Elettroni in Camera UHV*

LNF - 11 / 16(P)
H. Kozima, F. Celani., *Brief Explanation of Experimental Data Set on Excess Heat and Nuclear Transmutation in Multiplly Nanocoated Ni Wire*

LNF - 11 / 17(P)
F. Celani et al., *Development of a High Temperature Hybrid CMNS Reactor*

LNF - 11 / 18(R)
A. Babaev, S. Dabagov., *On Proton Multiple Inelastic Nuclear Interactions in Bent Crystals*

LNF - 11 / 19(NT)
A. Puri et al., *PRESS-MAG-O: status of the commissioning and of the associated R&D*

LNF - 11 / 20(NT)
S. Fioravanti, *Software per la rilevazione di vibrazioni*

INFN Reports

INFN / CCR_11 / 1
D. Fabiani, E. Mazzoni *Interventi su KERNEL e Microcode per Adeguare il Processore AMD 8356 REV. B2 allAmbiente GRID*

INFN / TC_11 / 1
V. Variale, *Charge Breeding Simulations in a Hollow Gun Ebis*

INFN / CCR_11 / 2
M. Canaparo, C. Galli, E. Ronchieri, C. Vistoli, *A Data Environment for Software Development Process*

INFN / TC_11 / 2
S. Aiola, P. La Rocca, O. Parasole, F. Riggi*Preliminary Tests of a Scintillator-Based Mini-Station for Extensive Air Showers Measurements*

INFN / TC_11 / 3
C. Strizzolo et al., *Riprogettazione del Sito WEB della Sezione di Trieste dell'INFN in Base ad Alcuni Principi del Design Centrato sull'Utente*

INFN / TC_11 / 4
S. Aiello et al., *The Measurement of Late-Pulses and After-Pulses in the Large Area Hamamatsu R7081 Photomultiplier with Improved Quantum-Efficiency Photocathode*

INFN / TC_11 / 5
K. Gracheva, M. Anghinolfi,V. Kulikovskiy, E. Shirokov, Y. Yakovenko, *Down Going Muon Rate Monitoring in the Antares Detector*

INFN / TC_11 / 6
M. Conte, *The Spin Contribution to the Synchrotron Light*

INFN / TC_11 / 7
F. Astuti et al., *Calibrating the Photosensors for the DCAL Extension of the Alice Electromagnetic Calorimeter: An Activity Report*

INFN / TC_11 / 8
G. Alampi, G. Cotto, P. Mereu, D. Gamba, *The Fancy Table, a 5-axis silicon detector beam test bench*

INFN / TC_11 / 9
M. Conte, *Electrostatic Storage Ring*

SEMINARI 2011

20/01/2011	Vittorio Pellegrini	CNR Firenze	Graphene: An electron wonderland
25/01/2011	Gilberto Colangelo	Bern Univ.	Determination of quark masses: the contribution of eta->3 pi
3/02/2011	Francesco De martini	Roma 1 Univ.	Macroscopic Quantum Superpositions Macrorealism and the Quantum to Classical Transition
9/02/2011	Cornelio Sochichiu	Korea Univ	Gauge fields in graphene
1/03/2011	Helmut Satz	Bielefeld Univ.	Quark Gluon Plasma: four lectures
24/03/2011	Koichi Yamawaki	KMI Institute Nagoya	Saga of the Composite Models - A perspective for LHC
28/03/2011	Bruno Arpaia	accordi SIS	L'energia del vuoto
11/04/2011	Joerg Hoerandel	Radbound Univ. Nijmegen	The future of the research on ultra high-energy cosmic rays
15/04/2011	Riccardo Bartolini	Diamond Light Source, UK	Design consideration for state-of-the-art light sources
19/04/2011	Alberto Annovi	LNF INFN	Invariant Mass Distribution of Jet Pairs Produced in Association with a W boson in proton-antiproton Collisions at sqrt(s) = 1.96 TeV
20/04/2011	Giulio Valli	ENEA	Three Mile Island (1979), Chernobyl (1986), Fukushima (2011) - Una riflessione sull'energia nucleare
19/05/2011	Stephan Winkler	Monaco Univ.	Anthropogenic Actinides in the Environment
26/05/2011	Dino Jaroszinski	Univ. Strathclyde, SUPA	Coherent radition from a plasma accelerated beam
7/06/2011	Patric Muggli	Max Planck Institut Munchen	Overview of recent experimental results on Particle Wake Field Acceleration
8/06/2011	Paolo Saraceno	IFSI ROMA	Il mondo fra trent’anni, è possibile uno sviluppo sostenibile?
9/06/2011	Ikaros Bigi	Univ. Notre Dame du Lac	The CKM Triangle(s) -- a Rosetta Stone for Flavour Dynamics
14/07/2011	Andrey Chubukov	Univ. Wisconsin-Madison, USA	Back to the iron age - the physics of Fe-pnictides
21/07/2011	Alex A. Volinsky	Univ. South Florida	Carbon Deposition by Film Delamination and X-ray Mirror Curvatur Control
28/07/2011	Sebastien Buffechoux	Lab. LULI Ecole Polytechnique	Energy enhancement of proton beam driven by ultra high intensity lasers and characterization of proton beams accelerated by ultra short laser pulses
27/09/2011	Alexander W. Chao	SLAC	Gymnastics in Phase Space

29/09/2011	Michael K. Sullivan	SLAC	Interaction Region Designs for Electron Colliders
27/10/2011	Massimo Bottini	Tor Vergata Univ.	PEG-modified carbon nanotubes in biomedicine: current status and challenges ahead
6/12/2011	Claudio Cantone	LNF INFN	ETRUSCO-2: an ASI-INFN project of technological development for Galileo, “the” European Flagship Programme
7/12/2011	Joerg Wotschack	CERN	Development of spark-resistant large-area micromegas detectors for the ATLAS upgrade
14/12/2011	Ian Stuart Anderson	Oak Ridge Nat. Lab.	New Science at the Spallation Neutron Source
20/12/2011	Yogendra Srivastava	Univ. Perugia	Space-Like Motions of Quantum Zero Mass Neutrinos

The General Services and Technical Division

M. Arpaia, F. Angeloni (Art. 15), G. Bernardi, G. Bisogni, F. Bocale, M. Campoli, P. Caponera, B. Casagrande, A. Cassarà, G. Catitti, A. Ceccarelli, P. Celli, O. Cerafogli, A. Chiarucci, A. Clozza, V. Crisanti, A. De Paolis, A. Donkerlo, A. Evangelista, G. Ferretti, M.A. Franceschi, C. Fusco, M. Giorgi, E. Iacuessa, L. Iannotti, M. Marchetti, U. Martini, M. Massimo (borsista), S.G.A. Monacelli, M. Monteduro, L. Musella, T. Napolitano, P. Panattoni, E. Passarelli, L. Pellegrino, R. Ricci, A. Riondino, M. Rondinelli, M. Rossi, U. Rotundo, M. Ruggeri, C. Sanelli (Head, Tech. Div.), F. Sanelli, A. Saputi, A. Sorgi, A. Tacchi, A. Tiburzi, R. Tonus, R. Valtriani

1 Introduction

During 2011, the General Services and Technical Division, created in April 2009, has come into its third year of fully operational activity.
The main task of the Division is the facility management of the Frascati Laboratories, but at the same time the Division must guarantee all the necessary support to research and accelerator activities, mainly in the field of mechanics, electrical systems and HVAC systems. However, the Division can also give support in the fields of vacuum and diagnostics systems, magnets and power electronics for accelerating machines.

During 2011, the Division has been involved in collaborations, support and consultancies with several INFN activities, such as: AMADEUS, BES III, CCR, CED TIER2, CNAO, CUORE, DAFNE, ETRUSCO2, FLAME, ICARUS, JEM-EUSO, KAONNIS, KLOE2, LHCb, MENSA LNF, MOONLIGHT, NA62, PLASMON-X, PRESIDENZA, SIDDHARTA, SPACEWEATHER, SPARC , SPARX, SUPER B, TPS, VIP2.

A special mention must be made of the CNAO project, the hadron-therapy center in Pave, based on a synchrotron accelerator, which is now successfully operating, after an experimental phase, with the treatment of the first batch of patients.

2 General Services Group

The General Services Group of the LNF deals with the organization and management of the general operational activities of the LNF and the Central Administration of the INFN, such as:

1. ENEA Canteen + Bar/Canteen LNF
2. Cleaning Service
3. Guards Service
4. Gardening Service
5. Porterage
6. Purchasing of new furniture and reuse of discarded pieces of furniture
7. Child care center
8. Buses
9. Coffee breaks and lunches
10. Deratization and pest control
11. Purchasing of Hygienic materials and rental of no-dust carpet
12. Purchasing and washing of working cloths
13. Rental of potable water dispensers

14. Microbiological Analysis on food and equipment of LNF bar
15. Leasing, insurances, maintenance and documentation of LNF vehicles
16. Identification badges
17. Liaising with the City of Frascati for licenses, authorizations and taxes
18. Liaising with the ENEA Frascati Center.

In addition to routine activities, in 2011/12 the Service deals with public tender procedures such as:

- Management of the bar and the canteen of LNF;
- Guards Service of LNF;
- Cleaning Service of LNF
- Adjustment works and purchasing of equipment and furniture for the new Canteen of LNF.

Collaboration with the Research Groups in the organization of meetings and conferences (*Comunicare Fisica, Spring School, Microbounching Instability, Lightnet Dissemination, ECFA, SuperB, Incontri di Fisica, LC10* etc)

The General Services Group of the LNF consists of only two persons: the group Head and a collaborator.

3 Central Store and Purchasing Group

During the past year, the Central Stores and Purchasing Group has supervised the purchasing and stocking of goods of the Central Stores as well as those of the Metal Stores, and of all the goods entering and leaving the Central Stores of the Laboratories; development and extension of the stocked articles.

Moreover, the Group has carried out market research upon request of the users to update the collection of stocked goods, and has maintained standards of stocked articles. Maintenance and updating of web pages, including the General Catalog for the general users.

During the 2011 accounting period the Central Stores and Purchasing Group has transferred a total amount of € 200.000,00 for stock materials replenishment as follows:

- € 40.000,00 on Cap. 130110 (standard consumables),
- € 140.000,00 on Cap. 130120 (research consumables)
- € 20.000,00 on Cap. 520110 (inventory – electronic pool set up)

for a total number of about 100 orders for stock replenishment and about 130 orders requested by General Services and Technical Division and other users. In addition, an amount of € 85.000,00 has been spent for the ordinary department activity: mailing services and management of small office devices and lifting machines.

4 Building Management Group

In the course of 2011, fencing and landscaping in the area of the new entrance to the LNF and the adjoining service buildings has been completed.

For the renovation of the roof of the external guesthouse “Villa Laura”, the architectural designs have been completed, and the procedure for the assignment of the contract has been started.

The elaboration of the executive project for the connection of the LNF sewage system to the communal sewage system, which runs under Via E. Fermi, has been assigned.

During the year, routine maintenance and repairs as well as extraordinary maintenance has been executed on the LNF buildings in order to preserve the value of the LNF assets. Other repair and maintenance works involving modifications, adaptations and renovations on LNF buildings have been carried out upon requests of the various LNF experimental groups.

5 Mechanical Design and Construction Group

Five different Units compose the Mechanics Design and Construction Group (SPCM): Mechanical Design, Carpentry and Soldering, Machine Tools, Metrology and Alignment, Material Store.

The SPCM performs the following tasks:

- mechanical design of experimental apparatus and detectors, using CAD/CAE software and FEM analysis;
- construction of prototypes and structures with the support of various soldering techniques and numeric control machine tools;
- production of high precision mechanical components, relying on manual and numeric control machine tools equipped with CAM control;
- high precision dimensional check, material strength test, large structures and apparatus optical alignment;
- acquisition and storing of mechanical components, tooling, metallic and plastic materials of workshop common use.

During 2011 the SPCM supported some experimental activities, playing a role of direct responsibility in the design, production, construction or installation: LHCb at CERN (muon system mechanical structures), CUORE at LNGS (engineering coordination and integration of the whole experimental apparatus), JEM-EUSO to be installed aboard the International Space Station (photo detector module and focal surface mechanics).

Many other activities were supported as well, though with no direct involvement in terms of responsibility: BES III, ETRUSCO2, ICARUS, KAONNIS, KLOE2, MOONLIGHT, NA62, PSUPERB, ROG, SPACEWEATHER, TPS, VIP2 were supported in terms of mechanical design, construction, or dimensional checks and functional tests.

To conclude, more than 40 short-term actions were taken by the SPCM personnel to support experimental activities, in case of unplanned interventions or urgent repairs.

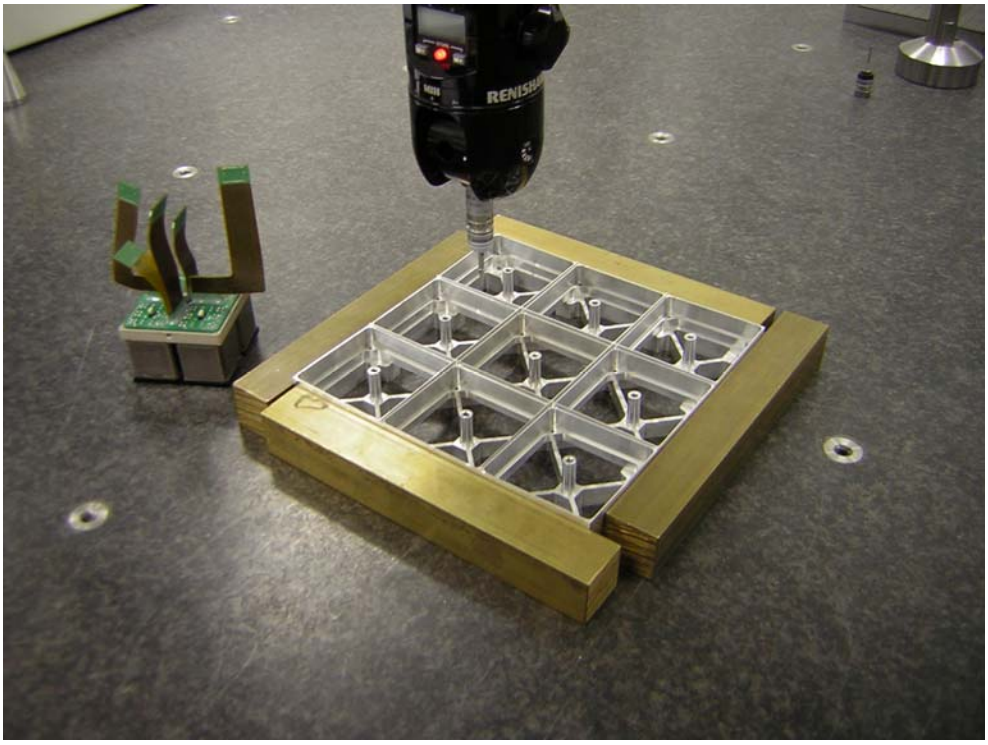

JEM-EUSO: PDM mechanics dimensional check (prototype)

CUORE: Outer Vacuum Chamber top plate

6 Heating, Ventilation and Air Conditioning Group

The group is in charge of the operation and maintenance of the auxiliary plants, comprising water cooling plants, water treatment facilities, compressed air and other gases production and distribution systems, HVAC plants for accelerators, experimental halls and clean rooms.

Within the group scope of work there are the procurements for new installations, from technical specifications definition to the follow-up of tender procedures, construction, start-up, performance tests and standard operation.
In 2011 the group has supported DAFNE, KLOE, BTF, SPARC, FLAME, DAFNE-LUCE and the LNF Data Center.

During the year the invitation to tender for the upgrade of the Frascati Data Center has been issued, and the installation of the cooling water distribution system for the Thomson line of the SPARC upgrade has been completed. Tie in of the magnets is ongoing as they are supplied by the contractor.

7 Electrical Installation Group

The Group manages the LNF electrical installations from the high voltage grid to end users and lighting. The150 kV substation and the 8 cabins are operated by staff, who also cover emergency calls and fault fixing. Routine safety and functional maintenance activities are usually performed by an external firm under the Group's supervision. Maintenance involves several skilled scheduled activities on switchboards, transformers, medium voltage devices, safety lighting, UPS, emergency generating sets and electrical devices of the Dafne cooling system, but also small repairs or changes requested by users.

During the 2011 upgrade of the LNF Data Centre, the electrical installation has been completed, and now the DC can supply 200 kW of IT devices with redundancy. A new main switchboard powers the Computing building. An extension of the substation main switchboard was required in order to get more power from the centralized emergency gen-set that can also supply a backup cooling system. All the existing feeders were reused. A new, double, busbar distribution system supplies the new computing room, and more power is also available in the old one. Activities have been performed during the summer holidays to avoid any inconvenience to the users.

Renewal of the Lighting system of Vacuum and Mechanical workshop of building n. 5 and Dafne was necessary due to age problems.

The Group is also in charge of the INFN Rome Headquarters offices' installation and some maintenance and upgrades were performed in the course of 2011.

Technical support to other INFN sites for Data Centre installation was supplied, through the CCR, specifically regarding the reliability and efficiency of the data centre infrastructure.

The technical management of the electrical power supply contract involves continuous contact with public utility suppliers and ever more accurate forecasts on load and budget. 23 GWh were used in the 2011, with a cost of 3,5 M€.

8 Other Activities

CNAO:
During 2011 the support activity to CNAO has been concentrated on two items: the design of a special spare vacuum chamber to be installed in place of one of the 5 race track ceramic vacuum chambers currently installed on the synchrotron and the setup of the fast closing valves system to be installed on the injection-extraction septa of the synchrotron.

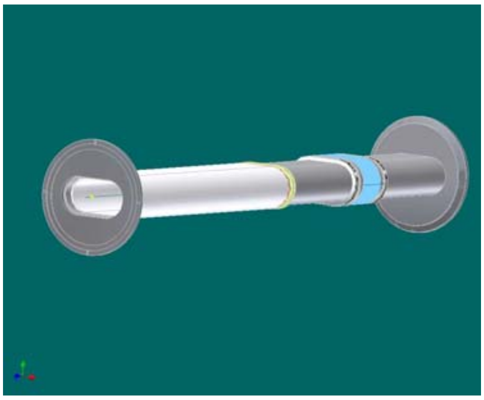

CNAO special spare vacuum chamber

VIP II:
In the last year, the activity concerning the VIP II experiment has been focused on the design of the upgraded version of the apparatus and the realization and testing of a prototype of the water-cooled copper target.

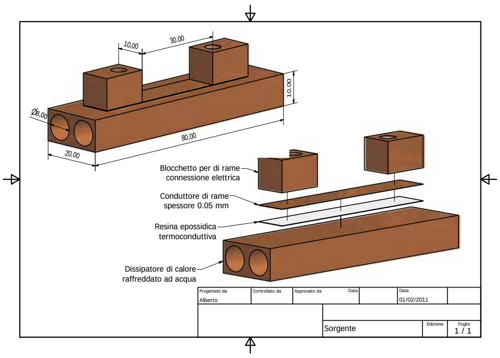

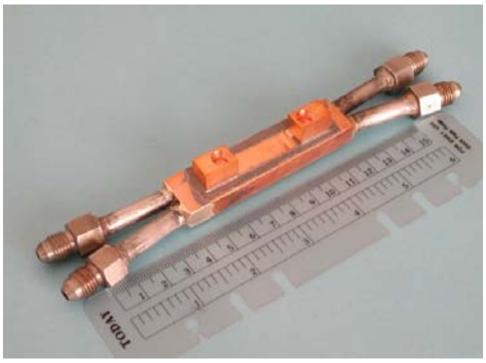

The prototype of the VIP II water cooled copper target

SIDDHARTA II:
The support activity to SIDDHARTA II experiment has been carried out all the year long. The main result is the final design for the vacuum chamber in which the cryogenic target with its detectors will be installed.

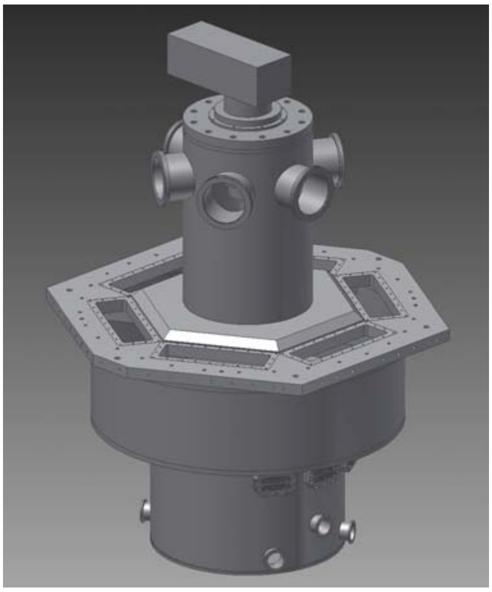

The vacuum chamber for the SIDDHARTA II experiment

Technical Administrative Activity:
The technical-administrative activity carried out as RUP (Project Manager) by the Division Staff during 2011 has mainly been devoted to the setting of the new LNF canteen and secondly to additional works consisting in the consignment and execution of two screening radiation protective walls in the experimental rooms Flame and Plasmon-X.

The protective wall in Flame

The works of renovation of the LNF kitchen.

The renovation work on the kitchen premises have been awarded by competitive tender at an initial amount of € 174.054,54 (VAT excluded) and assigned by contract on 27th July 2011. The work started on 6th September 2011, and are scheduled to be completed by April 2012.
On 19th December, 2011, almost simultaneously with the execution of these works, a competitive tender (starting amount € 418.742,72 +VAT) has been awarded by contract for the supply of most of the canteen equipment.

9 Some Statistics

In April 2011 a separate job request form for the Mechanical Design and Construction Group was put online:
(http://www.lnf.infn.it/dtecnica/SPCM/moduloSPCMRichPiccInterv.htm). This form allows integration of these data into the 2011 statistics for the other Groups, which are collected through the online form of the 'Modulo Unico', inaugurated in 2010 (http://www.lnf.infn.it/dtecnica/MODULOUNICO.pdf).
An automatic email message has been implemented on the General Services homepage, which allowed to collect these data and integrate them into the statistics.

During 2011, a total number of 634 registered requests reached the Technical and General Services Division. Not included in this number are the scheduled maintenance activities on the research and general facilities of the LNF. Of these 634 requests, a total of 618 has been dealt with within the year by the several Technical Division Groups.

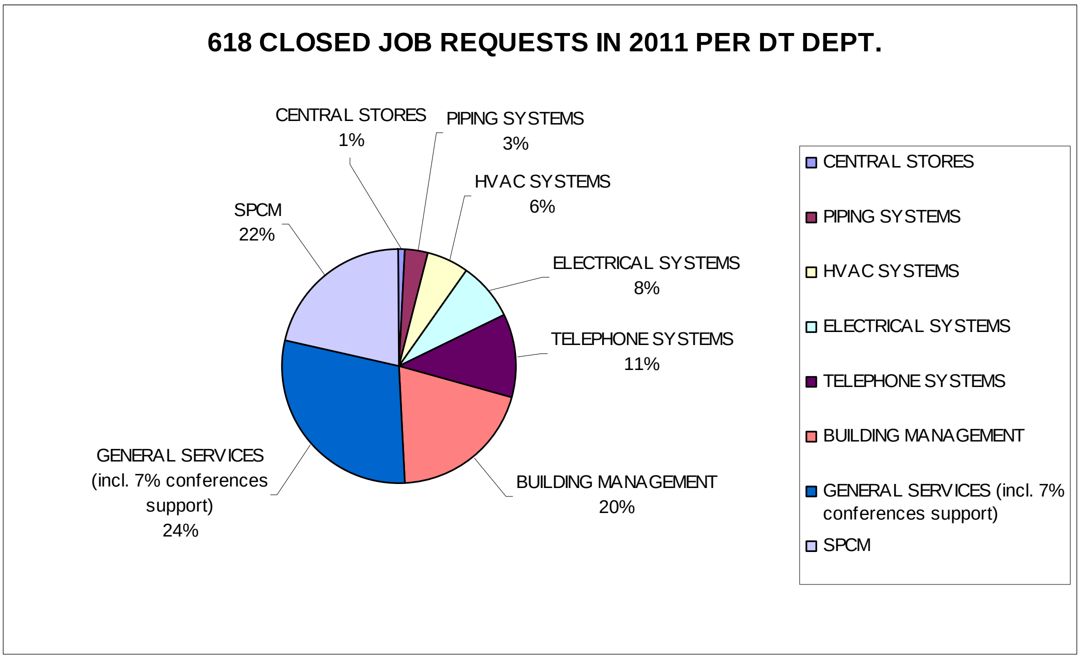

As in 2010, almost half of all requests (48%) were from the Research Division, and about a fifth both from the Accelerator and Technical Divisions:

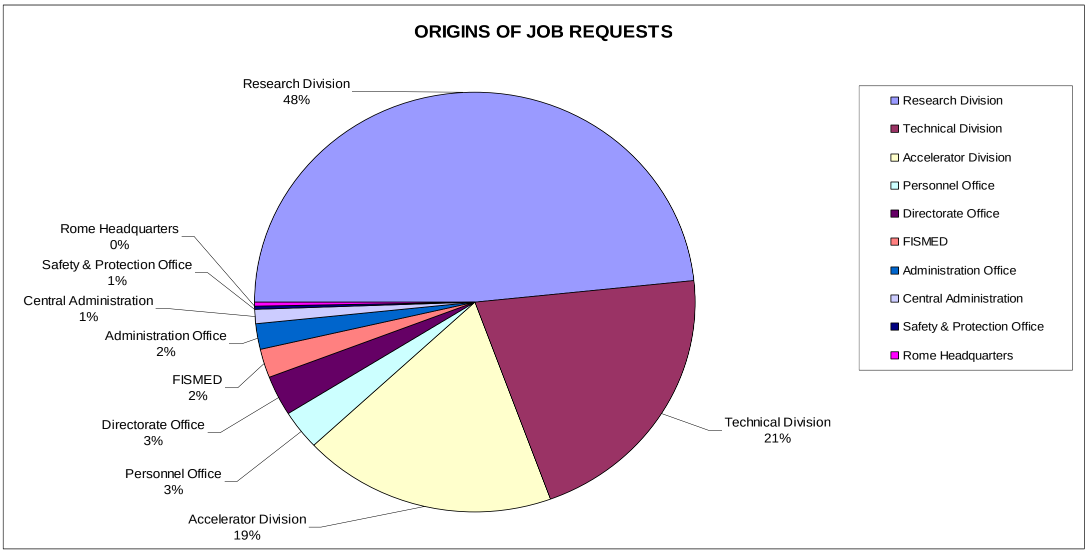

The average time of job completion was 71,94 days. However, since job completion often depends on external factors, one should not interpret the below graphic as an indication of Group efficiency. And again, scheduled maintenance on research and general facilities has not been included in the statistics.